NUREG/CP-0162
Vol. 3
CONF-9710101--Vol.3

Proceedings of the U.S. Nuclear Regulatory Commission

Twenty-Fifth Water Reactor Safety Information Meeting

Volume 3
– Thermal Hydraulic Research and Codes
– Digital Instrumentation and Control
– Structural Performance

Held at
Bethesda Marriott Hotel
Bethesda, Maryland
October 20-22, 1997

U.S. Nuclear Regulatory Commission

Office of Nuclear Regulatory Research

Proceedings prepared by
Brookhaven National Laboratory

AVAILABILITY NOTICE

Availability of Reference Materials Cited in NRC Publications

Most documents cited in NRC publications will be available from one of the following sources:

1. The NRC Public Document Room, 2120 L Street, NW., Lower Level, Washington, DC 20555-0001

2. The Superintendent of Documents, U.S. Government Printing Office, P. O. Box 37082, Washington, DC 20402-9328

3. The National Technical Information Service, Springfield, VA 22161-0002

Although the listing that follows represents the majority of documents cited in NRC publications, it is not intended to be exhaustive.

Referenced documents available for inspection and copying for a fee from the NRC Public Document Room include NRC correspondence and internal NRC memoranda; NRC bulletins, circulars, information notices, inspection and investigation notices; licensee event reports; vendor reports and correspondence; Commission papers; and applicant and licensee documents and correspondence.

The following documents in the NUREG series are available for purchase from the Government Printing Office: formal NRC staff and contractor reports, NRC-sponsored conference proceedings, international agreement reports, grantee reports, and NRC booklets and brochures. Also available are regulatory guides, NRC regulations in the *Code of Federal Regulations*, and *Nuclear Regulatory Commission Issuances*.

Documents available from the National Technical Information Service include NUREG-series reports and technical reports prepared by other Federal agencies and reports prepared by the Atomic Energy Commission, forerunner agency to the Nuclear Regulatory Commission.

Documents available from public and special technical libraries include all open literature items, such as books, journal articles, and transactions. *Federal Register* notices, Federal and State legislation, and congressional reports can usually be obtained from these libraries.

Documents such as theses, dissertations, foreign reports and translations, and non-NRC conference proceedings are available for purchase from the organization sponsoring the publication cited.

Single copies of NRC draft reports are available free, to the extent of supply, upon written request to the Office of Administration, Distribution and Mail Services Section, U.S. Nuclear Regulatory Commission, Washington, DC 20555-0001.

Copies of industry codes and standards used in a substantive manner in the NRC regulatory process are maintained at the NRC Library, Two White Flint North, 11545 Rockville Pike, Rockville, MD 20852-2738, for use by the public. Codes and standards are usually copyrighted and may be purchased from the originating organization or, if they are American National Standards, from the American National Standards Institute, 1430 Broadway, New York, NY 10018-3308.

DISCLAIMER NOTICE

DISCLAIMER

NUREG/CP-0162
Vol. 3

Proceedings of the U.S. Nuclear Regulatory Commission

Twenty-Fifth Water Reactor Safety Information Meeting

Volume 3
– Thermal Hydraulic Research and Codes
– Digital Instrumentation and Control
– Structural Performance

Held at
Bethesda Marriott Hotel
Bethesda, Maryland
October 20-22, 1997

Manuscript Completed: March 1998
Date Published: April 1998

Compiled by: Susan Monteleone

C. Bonsby, NRC Project Manager

Office of Nuclear Regulatory Research
U.S. Nuclear Regulatory Commission
Washington, DC 20555-0001

Proceedings prepared by
Brookhaven National Laboratory

ABSTRACT

This three-volume report contains papers presented at the Twenty-Fifth Water Reactor Safety Information Meeting held at the Bethesda Marriott Hotel, Bethesda, Maryland, October 20-22, 1997. The papers are printed in the order of their presentation in each session and describe progress and results of programs in nuclear safety research conducted in this country and abroad. Foreign participation in the meeting included papers presented by researchers from France, Japan, Norway, Russia, Spain and Switzerland. The titles of the papers and the names of the authors have been updated and may differ from those that appeared in the final program of the meeting.

PROCEEDINGS OF THE
25TH WATER REACTOR SAFETY INFORMATION MEETING

OCTOBER 20-22, 1997

Published in Three Volumes

GENERAL INDEX

Volume 1

Volume 2

Volume 3

REGISTERED ATTENDEES (NON-NRC)
25TH WATER REACTOR SAFETY INFORMATION MEETING

K. ALMENAS
UNIVERSITY OF MARYLAND
COLLEGE PARK, MD 20792 USA
301-405-5213

A. ALONSO
CONSEJO DE SEGURIDAD NUCLEAR
JUSTO DORADO, 11
MADRID, 28040 SPAIN
341-346-0334 341-346-0378
aas@csn.es

R. ANDERSEN
NUCLEAR ENERGY INSTITUTE
1776 I ST., NW
WASHINGTON, DC 20006 USA
202-739-8000 202-785-1898

R. ANDERSON
NORTHERN STATES POWER CO.
414 NICOLLET MALL, RSQ8
MINNEAPOLIS, MN 55401 USA
612-337-2050 612-330-7888

P. ANDRESEN
GE CORP R&D CENTER
1 RIVER RD., K1-3A39
SCHENECTADY, NY 12301 USA
518-387-5929 518-387-7007

T. ANDREYCHEK
WESTINGHOUSE NUCLEAR SERVICES DIVISION
P.O. BOX 355
PITTSBURGH, PA 15230 USA
412-374-6246 412-374-5099
andreyts@wec.com

A. ANKRUM
BATTELLE / ENVIRONMENTAL TECHNOLOGY
PO BOX 999, K8-28
RICHLAND, WA 99352 USA
509-372-4095 509-372-6242
ar-ankrum@pnl.gov

Y. ANODA
JAPAN ATOMIC ENERGY RESEARCH INST.
2-4 SHIRAKATA-SHIRANE, TOKAI-MURA
NAKA-GUN, IBARAKI-KEN, 319-11 JAPAN
81-29-282-5263 81-29-282-6728
anoda@lstf3.tokai.jaeri.go

R. ASHLEY
AIB-VINCOTTE NUCLEAR
AVENUE DU ROI 157
BRUSSELS, B-1190 BELGIUM
32-2-5368342
ray.ashley@ava

G. ASMOLOV
RUSSIAN RESEARCH CENTRE - KURCHATOV INSTIT
MOSCOW, 123182 RUSSIA
7-095-196-93-20 7-095-196-17-02
asmolov@nsi.kige.ru

D. AUMILLER
BETTIS ATOMIC POWER LABORATORY
PO BOX 79
WEST MIFFLIN, PA 15122 USA
412-476-6687 412-476-5151

S. AZUMI
KANSAI ELECTRIC POWER CO., INC.
2001 L ST., NW, STE 801
WASHINGTON, DC 20036 USA
202-659-1138 202-457-0272
sazumi.wdc@kansai.com

T. BALDWIN
PACIFIC GAS & ELECTRIC CO/DIABLO CANYON
PO BOX 56
AVILA BEACH, CA 93424 USA
805-545-4789 805-545-6992
dav1@pge.com

M. BALE
FRAMATOME COGEMA FUELS
3315 OLD FOREST RD.
LYNCHBURG, VA 24506-0935 USA
804-832-2488 804-832-3663
mbale@framatech.com

W. BAMFORD
WESTINGHOUSE ELECTRIC
PO BOX 355
PITTSBURGH, PA 15230 USA
412-374-6515 412-374-6515
bamforwh@westinghouse. com

Y.S. BANG
KOREA INSTITUTE OF NUCLEAR SAFETY
19 GUSUNG-DONG, YUSUNG-GU
TAEJON, 305-600 KOREA
82-62-868-0140 82-42-861-1700
kl64bys@pinpoint.kins.re.kr

R. BARI
BROOKHAVEN NATIONAL LABORATORY
DAT, BLDG, 197C
UPTON, NY 11973-5000 USA
516-344-2629 516-344-5266
Bari@bnl.gov

J. BARON
CUYO UNIV., NRC ARGENTINA
BUENOS AIRES, ARGENTINA

cediac@raiz.uncu.edu.ar

D. BATES
PENN STATE, DEPT. OF NUCLEAR ENGINEERING
231 SACKETT BLDG.
UNIVERSITY PARK, PA 16802 USA
814-863-3251 814-865-8499
dwb136@email.psu.edu

G. BAVA
AGENZIA NAZIONALE PER LA PROFESCIONE DELL'A
VIA VITALIANO BRANCATI 48
ROMA, 00144 ITALY
39-6-5007-2052 39-6-5007-2044
bava@educt4.anpa

R. BEEDLE
NUCLEAR ENERGY INSTITUTE
1776 I ST., NW
WASHINGTON, DC 20006 USA
202-739-8000 202-785-1898

R. BELL
NUCLEAR ENERGY INSTITUTE
1776 I ST., NW
WASHINGTON, DC 20006 USA
202-739-8000 202-785-1898

K. BERGERON
SANDIA NATIONAL LABORATORIES
PO BOX 5800, DEPT. 6421/MS0739
ALBUQUERQUE, NM 87185-0739 USA
505-844-2507 505-844-8719
kdberge@sandia.gov

C. BEYER
PACIFIC NORTHWEST NATIONAL LAB.
PO BOX 999
RICHLAND , WA 99352 USA
509-372-4605 509-372-4439
ce.beyer@pnl.gov

N. BIXLER
SANDIA NATIONAL LABORATORIES
PO BOX 5800
ALBUQUERQUE, NM 87185 USA
505-845-3144 505-844-6466
nbixler@sandia.gov

J. BOCCIO
BROOKHAVEN NATIONAL LABORATORY
BLDG. 197C
UPTON, NY 11973-5000 USA
516-344-7690 516-344-5266
boccio@bnl.gov

B. BOYACK
LOS ALAMOS NATIONAL LABORATORY
P.O. BOX 1663, M/S K575
LOS ALAMOS, NM 87545 USA
505-667-2023 505-665-2897
bboyack@lanl.gov

B. BRADLEY
NUCLEAR ENERGY INSTITUTE
1776 I ST., NW
WASHINGTON, DC 20006 USA
202-739-8000 202-785-1898

J. BRAUN
ARGONNE NATIONAL LABORATORY
9700 SO CASS AVE, BLDG. 208
ARGONNE, IL 60439-4838 USA
630-252-5574 630-252-6690

G. BROWN
AEA TECHNOLOGY
THOMSON HOUSE
RISLEY, WARRINGTON, WA3 1HW ENGLAND
44-1925254473 44-1925254536
geoff.brown@aeot.co.u

W. BRUNSON
FRAMATOME COGEMA FUELS
3315 OLD FOREST RD.
LYNCHBURG, VA 24506-0935 USA
804-832-2687 804-832-3663
wbrunson@framatech.com

R. BRYAN
TENNESSEE VALLEY AUTHORITY
1101 MARKET ST, LP 4J-C
CHATTANOOGA, TN 37402-2801 USA

J. BUTLER
NUCLEAR ENERGY INSTITUTE
1776 I ST., NW
WASHINGTON, DC 20006 USA
202-739-8000 202-785-1898

S. BYRNE
ABB COMBUSTION ENGINEERING
2000 DAY HILL RD.
WINDSOR, CT 06095 USA
860-285-3469 860-285-4232

D. CARUGE
INSTITUT DE PROTECTION ET DE SURETE NUCLEAIR
CE FONTENAY AUX ROSES DPEA/SEAC
FONTENAY AUX ROSES, BP 6, 92265 FRANCE
33146548199 33146548559
caruge.daniel@ipsn.jr

N. CAVLINA
FACULTY OF ELECTRICAL ENG. & COMPUTING
UNSKA 3
ZAGREB, 10000 CROATIA
38516129881 6129880
nikola.cavlina@fer.hr

S. CHAKRABORTY
SWISS NUCLEAR SAFETY INSPECTORATE
PO BOX 5232
VILLIGEN, 5232 SWITZERLAND
4153103936 41563103855
chakraborty@hsk.psi.com

W-W CHAO
ATOMIC ENERGY COUNCIL TAIWAN
67 LANE 144 KEELUNG RD SECT. 4
TAIPEI, 10600 TAIWAN ROC
886-2-3634180-335 886-2-3635377
wwchao@aec.gov.tw

J. CHERRY
SANDIA NATIONAL LABORATORIES
PO BOX 5800, MS0747
ALBUQUERQUE, NM 87185-0747 USA
505-844-0090 505-844-1648
jcherr@sandia.gov

C. CHO
KOREA NUCLEAR FUEL CO.
150, DEOGJIN-DONG, YUSONG-GU
TAEJON, 305-353 KOREA
82-42-868-1840 82-42-862-4790
escho@rdns.knfc.co.kr

W. CHOE
TU ELECTRIC
1601 BRYAN ST., FP15
DALLAS, TX 75201-3411 USA
214-812-4371 214-812-8687

C.K. CHOU
LAWRENCE LIVERMORE NATIONAL LABORATORY
PO BOX 808, MS/L-638
LIVERMORE, CA 94551 USA
510-422-4950 510-423-2157
choul@llnl.gov

B. CHRISTIE
PERFORMANCE TECHNOLOGY
PO BOX 51663
KNOXVILLE, TN 37950-1663 USA
423-588-1444 423-584-3043
103007,3517@compuserve.com

B.D. CHUNG
KOREA ATOMIC ENERGY RESEARCH INST.
DUKJIN-DONG 150, YUSONG-GU
TAEJON, 305-353 KOREA
82-42-868-8312 81-42-868-8990
bdchung@nanum.kaeri.re.kr

H.M. CHUNG
ARGONNE NATIONAL LABORATORY
9700 SO CASS AVE, BLDG. 208
ARGONNE, IL 60439-4838 USA
630-252-5111 630-252-3604
hee-chung@qmgate.anl.gov

G. CLAPISSON
COUNCIL FOR NUCLEAR SAFETY
CENTURION PO BOX 7106
CENTURION, 0046 SO AFRICA
2712663550
gaclapis@cns.co.za

A. COHEN
ARGONNE NATIONAL LABORATORY
9700 SO CASS AVE, BLDG. 208
ARGONNE, IL 60439-4838 USA
630-252-5179 630-252-9232
adam.cohen@anl.gov

R. COPELAND
SIEMENS POWER CORPORATION/NUCLEAR DIV.
2101 HORN RAPIDS RD.
RICHLAND, WA 99352 USA
509-375-8290

K. COZENS
NUCLEAR ENERGY INSTITUTE
1776 I ST., NW
WASHINGTON, DC 20006 USA
202-739-8000 202-785-1898

M. CUNNINGHAM
PACIFIC NORTHWEST NATIONAL LAB.
PO BOX 999
RICHLAND, WA 99352 USA
509-372-4987 509-372-4989
me.cunningham@pnl.gov

G. DAHLL
OEC HALDEN REACTOR PROJECT
PO BOX 173
HALDEN, N1751 NORWAY
476921220 4769212960
dahll@hrp.

A. DANILOV
ATOMIC ENERGY CONTROL BOARD
PO BOX 1046, STA. B, 280 SLATER ST.
OTTAWA, ONTARIO K1P5S9 CANADA
613-992-7227

G. DAVANT
ENTERGY OPERATIONS, INC.
1340 ECHELON PARKWAY
JACKSON, MS 39213 USA
601-368-5756 601-368-5768
davant@entergy.com

L.W. DEITRICH
ARGONNE NATIONAL LABORATORY
9700 SO CASS AVE, BLDG. 208
ARGONNE, IL 60439-4838 USA
630-252-4571 630-252-4780
deitrich@anl.gov

D. DIAMOND
BROOKHAVEN NATIONAL LABORATORY
BLDG. 130
UPTON, NY 11973-5000 USA
516-344-2604 516-344-5730
diamond@bnl.gov

S. DOROFEEV
RUSSIAN RESEARCH CENTRE - KURCHATOV INSTIT
MOSCOW, 123182 RUSSIA
70951969840 70958825801
dorofeev@iaeph.kiae.ru

J. DUNKLEBERGER
NYS HEALTH DEPT.
II UNIVERSITY PLACE, RM. 375
ALBANY, NY 12203 USA
518-458-6461 518-458-6434
jdd08@health.state.ny

B. DUNN
FRAMATOME TECHNOLOGIES, INC.
3315 OLD FOREST RD.
LYNCHBURG, VA 24506-0935 USA
804-832-2427 804-832-3663

J. DUSPIVA
NUCLEAR RESEARCH INSTITUTE - REZ
REZ
NEAR PRAGUE, 25068 CZECH REPUBLIC
420-2-6617-3657 420-2-685-7960
dsp@nri.cz

Z. ELAWAR
PALO VERDE NUCLEAR PLANT
PO BOX 52034, STA. 7527
PHOENIX, AZ 85072-2034 USA
602-393-5328 602-393-5467
zelawar@apsc.com

A. ELKADY
NAT'L CTR FOR NUCLEAR SAFETY-HELIOPOLICE
8 ISMAIL KAMAL ST.
CAIRO, 11351 EGYPT
202-243-0384 202-243-0384

F. EMERSON
NUCLEAR ENERGY INSTITUTE
1776 I ST., NW
WASHINGTON, DC 20006 USA
202-739-8000 202-785-1898

P.O. ERICSSON
SWEDISH NUCLEAR POWER INSPECTORATE
S-10658
STOCKHOLM, SWEDEN
4686988400 4686619086
perolote@ski.se

H. ERIKSON
SWEDISH NUCLEAR POWER INSPECTORATE
S-10658
STOCKHOLM, SWEDEN
4686988424 4686612086
hanse@vkt.se

R. EVANS
NUCLEAR ENERGY INSTITUTE
1776 I ST., NW
WASHINGTON, DC 20006 USA
202-739-8000 202-785-1898

M. EYRE
PECO ENERGY/FUEL & SERVICES DIV.
965 CHESTERBROOK BLVD. (M/C 62a-5)
WAYNE, PA 19087 USA
610-640-6829 610-640-6797

G. FALO
HENRY JACKSON FOUNDATION - USACHPPM
MCHP DC 0, 5158 BLACKHAWK RD
APG, MD 21010-5422 USA
410-671-2670 410-671-5411
gerald.falo@chppm.ccmail.apgea.arwy.mic

I. FIERO
ABB COMBUSTION ENGINEERING
2000 DAYHILL RD.
WINDSOR, CT 06095 USA
860-687-8052 860-687-8051

S. FLOYD
NUCLEAR ENERGY INSTITUTE
1776 I ST., NW
WASHINGTON, DC 20006 USA
202-739-8000 202-785-1898

E. FORD
OAK RIDGE NATIONAL LABORATORY
PO BOX 2008, BLD.G 4500-N, MS 6238
OAK RIDGE, TN 37831 USA
423-574-5272 423-574-9646
wef@ornl.gov

W. FRID
SWEDISH NUCLEAR POWER INSPECTORATE
STOCKHOLM, SE-10658 SWEDEN
4686988460 4686619086
wiktor.frid@ski.se

FRANK FU
TECRO/SCIENCE DIVISION
4201 WISCONSIN AVENUE
WASHINGTON, DC 20016 USA
202-895-1932 202-895-1939

T. FUKETA
JAPAN ATOMIC ENERGY RESEARCH INST.
2-4 SHIRAKATA-SHIRANE, TOKAI-MURA
NAKA-GUN, IBARAKI-KEN, 319-11 JAPAN
81292826386 81292826160
toyo@nsrrsun1.tokai.jaeri.go.jp

J. GALLAGHER
CONSULTANT: NPP 8&C SYSTEMS
1450 NAVAHOE DR.
PEN, PA 15228 USA
412-343-0370 412-343-0370
jang11@tdt.net

G. GARNER
FRAMATOME COGEMA FUELS
3315 OLD FOREST RD.
LYNCHBURG, VA 24506-0935 USA
804-832-5274 804-832-5167
ggarner@framatech.com

R. GAUNTT
SANDIA NATIONAL LABORATORIES
13501 GRAMADA HILLS DR.
ALBUQUERQUE, NM 87123 USA
505-284-3989
rogaunt@sandia.gov

G. GIGGER
WESTINGHOUSE ELECTRIC
P.O. BOX 79
WEST MIFFLIN, PA 15122 USA
412-476-7365 412-476-6924

V. GILBERT
NUCLEAR ENERGY INSTITUTE
1776 I ST., NW
WASHINGTON, DC 20006 USA
202-739-8000 202-785-1898

J. GILMAN
ELECTRIC POWER RESEARCH INSTITUTE
3412 HILLVIEW AVE.
PALO ALTO, CA 94304-1395 USA
650-855-8911 650-855-2774
jgilman@epri.com

B. GITNICK
SCIENTECH, INC.
11140 ROCKVILLE PIKE, STE 500
ROCKVILLE, MD 20852 USA
301-468-6425 301-468-0883
bgitnick@scientech.com

M. GOMOLINSKI
INSTITUT DE PROTECTION ET DE SURETA NUCLEAIR
B.P. 6
FONTENAY AUX ROSES CEDEX, 92265 FRANCE

maurice.gomolinski@ipsn.fr

V. GONZALEZ
COMISION NACIONAL DE SEGURIDAD NUCLEAR
DR. BARRAGAN NUM. 779 COL. NARVARTE
MEXICO, 03020 MEXICO
525-5-90-81-13 525-590-61-03
cnsnsl@servidor.unam.mx

D. GRAY
LOCKHEED MARTIN/KNOLLS ATOMIC POWER LAB
PO BOX 1072
SCHENECTADY, NY 12301 USA
518-395-4763 518-395-6171

G. HACHE
INSTITUT DE PROTECTION ET DE SURETE NUCLEAIR
C.E. CADARACHE - DAT 702
ST PAUL LEZ DURANCE, 13108 FRANCE
33442254657 33442256143
didier.jacquemaim@ipsn.fr

K. HALAC
WESTINGHOUSE ELECTRIC
525 BRINTON AVE. #1
TRAFFORD, PA 15085 USA
412-374-5047 412-374-4011
halack@cecil.pgh.wec.1

A. HALL
HEALTH & SAFETY EXECUTIVE, NII
ST. PETER'S HOUSE, BALLIOL ROAD
BOOTLE, L20 3LZ UNITED KINGDOM
0151-951-4165 0151-951-3942
andy.hall@hse.gov.uk

R. HALL
BROOKHAVEN NATIONAL LABORATORY
ET DIV., BLDG. 130
UPTON, NY 11973-5000 USA
516-344-2144 516-344-3957
rehall@bnl.gov

G. HART
PERFORMANCE CONTRACTING INC.
4025 BONNER IND. DR.
SHAWNEE, KS 66226 USA
913-441-0100 913-441-0953
ghhart@aol.com

J. HART
NETHERLANDS ENERGY RESEARCH FOUNDATION
WESTERDUINWEG 3
PETTEN, NL 1755 LE THE NETHERLANDS
31-22456-4282 31-22456-3490
hart@ecn.nl

E. HARVEGO
LOCKHEED MARTIN IDAHO TECHNOLOGIES CO.
PO BOX 1625
IDAHO FALLS, ID 83415 USA
208-526-9544 208-526-2930
hae@inel.gov

C. HARWOOD
ATOMIC ENERGY CONTROL BOARD
PO BOX 1046, STA. B, 280 SLATER ST.
OTTAWA, ONTARIO K1P5S9 CANADA
613-996-2547 613-943-1292
harwood.c@atomcon.gc.ca

S. HASMAN
CHUBU ELECTRIC POWER CO.
900 17TH ST, NW SUITE 1220
WASHINGTON, DC 20006 USA
202-775-1960 202-331-9256

M. HECHT
SOHAR INC.
8421 WILSHIRE SUITE 201
BEVERLY HILLS, CA 90211 USA
213-653-4717 213-653-3624
myron@sohar.com

R. HENRY
FAUSKE & ASSOCIATE INC.
16W070 W. 83RD ST.
BURR RIDGE, IL 60521 USA
630-323-8750 630-986-5481
henry@fauske.com

L. HERNANDEZ
NATIONAL POLYTECHNIC INSTITUTE, DEPT. OF MEC
EDIFICIO 5, 3RD PISO COL LINDAVISTA UNIDAD PROF
ZACATONCO, MEXICO
5-729-6000 ext. 54586 5-567-0751
luishect@iris.esimez.ipn.mx

K. HIGAR
NORTHERN STATES POWER/NUCLEAR ANALYSIS &
414 NICOLLET MALL (RS-10)
MINNEAPOLIS, MN 55401 USA
612-337-2001 612-330-7671
keith.e.higar@nspco.com

T. HILL
COUNCIL FOR NUCLEAR SAFETY
CENTURION PO BOX 7106
CENTURION, 0046 SO AFRICA
27-12-6635500 27-12-6635513
thill@cns.co.za

K. HO
ATOMIC ENERGY CONTROL BOARD
PO BOX 1046, STA. B, 280 SLATER ST.
OTTAWA, ONTARIO K1P5S9 CANADA
613-995-2908 613-943-8954
ho.k@atomcon.ca

L. HOCHREITER
PENN STATE, DEPT. OF ENERGY
231 SACKETT BLDG.
UNIVERSITY PARK, PA 16801 USA
814-865-0044 814-865-8499
dav1@pge.com

J. HODGES
PACIFIC GAS & ELECTRIC CO/DIABLO CANYON
PO BOX 56
AVILA BEACH, CA 93424 USA
805-545-4622 805-545-6992
dav1@pgd.com

P. HOFMANN
FZK KARLSRUHE
P. O. BOX 3640
KARLSRUHE, 76021 GERMANY
49-7247-82-2517 49-7247-82-4567
peter.hofmann@imf.fzk.de

J. HOLM
SIEMENS POWER CORPORATION/*NUCLEAR DIV.*
2101 HORN RAPIDS RD.
RICHLAND, WA 99352 USA
509-375-8142

H. HOLMSTROM
VTT ENERGY, NUCLEAR ENERGY
PO BOX 1604 (TEKNIIKANTIE 4C)
ESPOO, FIN-02044 VTT FINLAND
358-9-456-5050 358-9-4565000
heikki.holmstrom@vtt.f

W. HOUSTON
SEQUOIA CONSULTING GROUP, INC.
5285 ATLANTIC VIEW
ST. AUGUSTINE, FL 32084 USA
904-461-8774 904-461-8794
whouston@sequoia-cg

D. HOWE
LOCKHEED MARTIN/KNOLLS ATOMIC POWER LAB
PO BOX 1072
SCHENECTADY, NY 12301 USA
518-395-4624

N. HOY
NEW YORK POWER AUTHORITY
PO BOX 41
LYCOMING, NY 13027 USA
315-349-6203 315-349-6148
hoy.n@nypa.gov

J. IRELAND
LOS ALAMOS NATIONAL LABORATORY
PO BOX 1663, MSF606
LOS ALAMOS, NM 87545 USA
505-667-8777 505-665-5204
john.ireland@lanl.gov

M. ISHII
PURDUE UNIVERSITY
1290 NUCLEAR ENGINEERING
WEST LAFAYETTE, IN 47906 USA
765-494-4587 765-494-9570

K. ISHIJIMA
JAPAN ATOMIC ENERGY RESEARCH INST.
2-4 SHIRAKATA-SHIRANE, TOKAI-MURA
NAKA-GUN, IBARAKI-KEN, 319-11 JAPAN
81-292-82-5277

R. ISLAMOV
IBRAE RAN
USACHEVA 29-3-186
MOSCOW, 113191 RUSSIA
7-095-9552655 7-095-9557095
isl@ibrae.ae.ru

B. JACOBS
SOUTHWEST RESEARCH INSTITUTE
6220 CULEBRA RD.
SAN ANTONIO, TX 78238 USA
210-522-2032 210-684-4822
bjacobs@SwRI.edu

K. JACOBS
NEW YORK POWER AUTHORITY
123 MAIN STREET
WHITE PLAINS, NY 10566 USA
914-681-6262 914-287-3710
jacobs.k@nypa

B. JOHNSON
UNIV. OF VIRGINIA
THORNTON HALL
CHARLOTTESVILLE, VA 22903-2442 USA

R. JOHNSON
PACIFIC GAS & ELECTRIC CO.
PO BOX 770000, MC N9B
SAN FRANCISCO, CA 94177 USA
415-973-1784 415-973-0074
rlj3@pge.com

W. JOHNSON
UNIVERSITY OF VIRGINIA
REACTOR BLDG.
CHARLOTTESVILLE, VA 22901 USA
804-982-5464 804-982-5473
wrj@virginia.edu

F. KASAHARA
NUCLEAR POWER ENGINEERING CORP.
4F 17-1, 3-CHOME TORANOMON MINATOKU
TOKYO, 105 JAPAN
81 3 5470 5470 81 3 5470 5454
kasahara@nupec.or.jp

K. KAUKONEN
TEOLLISUUDEN VOIMA OY
OLKILUOTO, 27160 FINLAND
358-2-83813222 358-2-83813209
kari.kaukonen@tuo.tuo.elisz.fi

M. KENNARD
NAC INTERNAT'L-STOLLER NUCLEAR FUEL
485 WASHINGTON AVE
PLEASANTVILLE, NY 10570 USA
914-741-1200 914-741-2093
stollerp@computer.net

H. KHALIL
ARGONNE NATIONAL LABORATORY
9700 SO CASS AVE, BLDG. 208
ARGONNE, IL 60439-4838 USA
630-252-7266 639-252-4500
khalil@ra.anl.gov

M. KHATIB-RAHBAR
ENERGY RESEARCH, INC.
P.O. BOX 2034
ROCKVILLE, MD 20847-2034 USA
301-881-0866 301-881-0867
mkr-eri@radix.net

H. KIM
COMMONWEALTH EDISON
1400 OPUS PL, SUITE 500
DOWNERS GROVE, IL 60517 USA
630-663-3072 630-663-7181
nfshk@ccmail.ceco.com

H. KIM
KOREA INSTITUTE OF NUCLEAR SAFETY
P.O. BOX 114, YUSONG
TAEJON, KOREA
82 42 868 0230 82 42 861 9945
ko98khj@pinpoint.kins.re.kr

H.D. KIM
KOREA ATOMIC ENERGY RESEARCH INST.
DUKJIN-DONG 150, YUSONG-GU
TAEJON, 305-600 KOREA
82-42-868-2664 82-42-868-8256
hdkim@kaeri.re.ler

W. KIM
KOREA INSTITUTE OF NUCLEAR SAFETY
PO BOX 114, YUSUNG
TAEJON, 305-600 KOREA
82-42-868-0327 82-42-861-9945
k095kws@pimpoimt.kims.re.kt

M. KIRK
WESTINGHOUSE ELECTRIC
1310 BEULAH RD.
PITTSBURGH, PA 15235 USA
412-256-1066 412-256-1007
kirkmt@westinghouse.com

R. KIRK
COUNCIL FOR NUCLEAR SAFETY
CENTURION PO BOX 7106
CENTURION, 0046 SO AFRICA
2712663550 27126635513
dkirk@cns.co.za

A. KISSELEV
NUCLEAR SAFETY INST., RUSSIAN ACADEMY OF SCI.
BOLSHAYA TULSKAYA STR. 52
MOSCOW, 113191 RUSSIA
095-955-28-73 095-952-57-01
kso@ibrae.gc.ru

R. KNOLL
FLORIDA POWER CORP.
15760 WEST POWERLINE ST.
CRYSTAL RIVER, FL. 34428 USA
352-563-4543 352-563-4575

D. KOKKINOS
LOCKHEED MARTIN/KNOLLS ATOMIC POWER LAB
PO BOX 1072
SCHENECTADY, NY 12301 USA
518-395-7039

K. KOLLATH
GESELLSCHAFT FUR ANLAGEN UND REAKTORSICH
SCHWERTNERGASSE 1
COLOGNE, 50667 GERMANY
004922a2068-6a9 004922a2068-888

D. KOSS
PENN STATE, DEPT. OF NUCLEAR ENGINEERING
231 SACKETT BLDG.
UNIVERSITY PARK, PA 16802 USA
814-865-5447 814-865-2917
koss@ems.psu.ed

P. KRAL
NUCLEAR RESEARCH INSTITUTE - REZ
REZ
NEAR PRAGUE, 25068 CZECH REPUBLIC
00420-2-66172447 00420-2-6857954
kra@nri.cz

P. KRISHNASWAMY
BATTELLE
505 KING AVE.
COLUMBUS, OH 43201 USA
614-424-5998 614-424-3457
kswamy@battelle.org

W. KUPFERSCHMIDT
ATOMIC ENERGY OF CANADA, LTD.
WHITESHELL LABORATORIES
PINAWA, MANITOBA R0E 1L0 CANADA
204-753-8424 204-753-2455

S. KURATA
CHUBU ELECTRIC POWER CO.
900 17TH ST, NW SUITE 1220
WASHINGTON, DC 20006 USA
202-775-1960 202-331-9256
kurata@chubudc.com

R. KUSHNER
BETTIS ATOMIC POWER LABORATORY
PO BOX 79
WEST MIFFLIN, PA 15632-0079 USA
412-476-5395 412-476-5700

K. KUSSMAUL
UNIVERSITY OF STUTTGART
PFAFFENWALDRING 32
STUTTGART, D-70569 GERMANY
49-711-685-3582 49-711-685-2635
kussmaul@mpa.uni-stuttgart.de

P. LACY
UTILITY RESOURCE ASSOCIATES
SUITE 1600, 51 MONROE ST.
ROCKVILLE, MD 20850 USA
301-294-1941 301-294-7879

J. LAKE
LOCKHEED MARTIN IDAHO TECHNOLOGIES CO.
PO BOX 1625
IDAHO FALLS, ID 83415-3860 USA
208-526-7670 208-526-2930
lakeja@inel.gov

C. LECOMTE
INSTITUT DE PROTECTION ET DE SURETA NUCLEAIR
B.P. 6
FONTENAY AUX ROSES CEDEX, 92265 FRANCE
146547736 014654g5.11
catherine.lecomte@ipsn.fr

G. LEE
KOREA NUCLEAR FUEL CO.
150 DEOGJIN-DONG, YUSONG-GU
TAEJON, 305353 S. KOREA
82 42 868 1832 82 42 862 4790
gwlee@rdns.knfc.co.kr

J-I. LEE
KOREA INSTITUTE OF NUCLEAR SAFETY
19 KUSUNG-DONG, YOUSUNG-KU
TAEJON, KOREA
82 42 868 0143 82 42 861 1700

S. LEE
KOREA ELECTRIC POWER CORP.
150 DUGJIN-DONG, YUSUNG-KU
TAEJON, KOREA
82 42 868 2795

W-J. LEE
KOREAN ATOMIC ENERGY RESEARCH INSTITUTE
DUKJIN-DONG 150, YUSONG-GU
TAEJON, 305-353 KOREA
82-42-868-2895 82-42-868-8990
wjlee@nanum.kaeri.re.kr

Y-W. LEE
KOREA INSTITUTE OF NUCLEAR SAFETY
WANGGUNG APT 4-308
ICHONDONG, YONGSAN, SEOUL, KOREA

S. LEVINSON
FRAMATOME TECHNOLOGIES, INC.
3315 OLD FOREST RD.OF54
LYNCHBURG, VA 24501 USA
804-832-2768 804-832-2683
slevinson@framatech.com

T. LINK
PENN STATE, DEPT. OF NUCLEAR ENGINEERING
231 SACKETT BLDG.
UNIVERSITY PARK, PA 16802 USA
814-863-3251 814-865-8499
tm1110@psu.edu

M. LIVOLANT
INSTITUT DE PROTECTION ET DE SURETA NUCLEAIR
B.P. 6
FONTENAY AUX ROSES CEDEX, 92265 FRANCE
146567179 146549511
michel.livolant@ipsn.fr

A. MARION
NUCLEAR ENERGY INSTITUTE
1776 I ST., NW
WASHINGTON, DC 20006 USA
202-739-8000 202-785-1898

P. MARSILI
AGENZIA NAZIONALE PER LA PROFESCIONE DELL'A
VIA VITALIANO BRANCATI 48
ROMA, 00144 ITALY
39-6-5007-2128 39-6-5007-2044
marsili@edultg.anpant

L. MARTIN
SOUTH TEXAS PROJECT NUCLEAR OPERATING CO.
PO BOX 289
WADSWORTH, TX 77483 USA
512-972-8686 512-972-8577
lemartin@stpegs.com

M. MASSOUD
BALTIMORE GAS & ELECTRIC
1650 CALVERT CLIFFS PARKWAY
LUSBY, MD 20657 USA
410-495-6522 410-495-4498
mahmoud.massoud@bje.com

M. MATSUURA
HITACHI, LTD.
175 CURTNER AVE., MC 725
SAN JOSE, CA 95125 USA
408-925-6151 408-925-4459
matsuuraM@sjcpo5.ne.ge.com

B. MAVKO
JOSEF STEFAN INSTITUTE
JAMOVA 39
LJUBLJANA, 1001 SLOVENIA
386-61-1885330 386-61-188538661
borot.mavko@Js.si

G. MAYS
OAK RIDGE NATIONAL LABORATORY
P.O. BOX 2009, BLDG. 9201-3
OAK RIDGE, TN 37831 USA
423-574-0394 423-574-0382
gtm@ornl.gov

H. McHENRY
NATIONAL INSTITUTE OF STANDARDS & TECHNOLOG
325 BROADWAY
BOULDER, CO 80303 USA
303-497-3268 303-497-5030
harry.mchenry@nist.gov

B. MCINTYRE
WESTINGHOUSE ELECTRIC
P.O. BOX 355
PITTSBURGH, PA 15230
412-374-4334
mcintybh@wesmail.com

J. MEYER
SCIENTECH, INC.
4814 LELAND STREET
CHEVY CHASE, MD 20815 USA
301-468-6425 301-468-0883
jmeyer@scientech.com

D. MITCHELL
FRAMATOME COGEMA FUELS
3315 OLD FOREST RD.
LYNCHBURG, VA 24506-0935 USA
804-832-3438 804-832-3663
dmitchell@framatech.com

S. MIXON
NUS INFORMATION SERVICES
910 CLOPPER RD.
GAITHERSBURG, MD 20878 USA
301-258-2442 301-258-2589
smixon@scientech.com

D. MODEEN
NUCLEAR ENERGY INSTITUTE
1776 I ST., NW
WASHINGTON, DC 20006 USA
202-739-8000 202-785-1898

M. MODRO
IDAHO NATIONAL ENGINEERING & ENVIRONMENTAL
P.O. BOX 1525
IDAHO FALLS, ID 83415 USA
208-526-7402

S MONTELEONE
BROOKHAVEN NATIONAL LABORATORY
BUILDING 130
UPTON, NY 11973 USA
516-344-7235 516-344-3957
smontele@bnl.gov

R. MONTGOMERY
ANATECH CORP.
5435 OBERLIN DR.
SAN DIEGO, CA 92121 USA
619-455-6350 619-455-1094

B. MORRIS
WESTINGHOUSE NSD
PO BOX 355
PITTSBURGH, PA 15601 USA
412-374-4205 412-374-5099
morrisbc@westinghouse.com

D. MORRISON
101 LION'S MOUTH COURT
CARY, NC 27511 USA
919-363-3034

A. MOTTA
PENN STATE, DEPT. OF NUCLEAR ENGINEERING
231 SACKETT BLDG.
UNIVERSITY PARK, PA 16802 USA
814-865-0030 814-865-8499
atm2@pso.edu

M. MULHEIM
LOCKHEED MARTIN ENERGY RESEARCH CORP.
PO BOX 2008
OAK RIDGE, TN 37831 USA
423-574-0386 423-574-0382
m8m@ornl.gov

K. MURATA
SANDIA NATIONAL LABORATORIES
PO BOX 5800
ALBUQUERQUE, NM 87109 USA
505-844-3552

S. NAKAMURA
OBAYASHI CORPORATION
SHINJUKU PARK TOWER, 3-7-1
SHINJUKU-KU, TOKYO 163-10 JAPAN
81-3-5323-3519 81-5323-3550
s.naka@o-net.obayashi.co.jp

R. NANSTAD
OAK RIDGE NATIONAL LABORATORY
PO BOX 2008, 4500S, MS-6151
OAK RIDGE, TN 37831-6151 USA
423-574-4471 423-574-5118
nanstadrk@ornl.gov

A. NELSON
NUCLEAR ENERGY INSTITUTE
1776 I ST., NW
WASHINGTON, DC 20006 USA
202-739-8000 202-785-1898

J. NELSON
ELECTRIC POWER RESEARCH INSTITUTE
3412 HILLVIEW AVE.
PALO ALTO, CA 94303 USA
415-855-2825 415-855-8515
jlnelson@epri.com

M. NISSLEY
WESTINGHOUSE ELECTRIC
P.O. BOX 355
PITTSBURGH, PA 15230 USA
412-374-4303 412-374-4011
nisslem@westinghouse.com

J. O'HARA
BROOKHAVEN NATIONAL LABORATORY
ET DIV., DAT, BLDG. 130
UPTON, NY 11973-5000 USA
516-344-3638 516-344-3957
ohara@bnl.gov

A. ODA
NUCLEAR POWER ENGINEERING CORP.
FUJITAKANKO TROANOMON BLDG. 6F, 17-1
MINATO-KU, TOKYO 105 JAPAN
81-3-5470-5525 81-3-5470-5544

S-H. OH
KOREA INSTITUTE OF NUCLEAR SAFETY
P.O. BOX 114
YUSUNG, TAEJEON 305-600 KOREA
82 42 868 0239 82 42 868 0943
ko67osh@pinpoint.kins.re.kr

A. OHTA
MITSUBISHI HEAVY INDUSTRIES
3-1, MINATOMIRAI 3-CHOME, NISHI-KU
YOKOHAMA, 220-84 JAPAN
81-45-224-9637 81-45-224-9970
ohta@atom.hg.mhi.co.jp

N. ORTIZ
SANDIA NATIONAL LABORATORIES
PO BOX 5800, MAIL STOP 0736
ALBUQUERQUE, NM 87185-0736 USA
505-844-0577 505-844-0955
nrortiz@sandia.gov

D. OSETEK
LOS ALAMOS TECHNICAL ASSOCIATES
BLDG 1, STE 400, 2400 LOUISIANA BLVD NE
ALBUQUERQUE, NM 87110 USA
505-880-3407 505-880-3560
djosetek@lata.com

O. OZER
ELECTRIC POWER RESEARCH INSTITUTE
3412 HILLVIEW AVE.
PALO ALTO, CA 94303 USA
650-855-2089 650-855-2774
oozer@epri.com

J. PAPIN
INSTITUT DE PROTECTION ET DE SURETE NUCLEAIR
C.E. CADARACHE - DAT 702
ST PAUL LEZ DURANCE, 13108 FRANCE
33-4-42253463 33442256143
joelle.papin@ipsn.fr

S-D. PARK
KOREA INSTITUTE OF NUCLEAR SAFETY
19 KUSUNG-DONG, YOUSUNG-KU
TAEJON, KOREA
82 42 868 0003 82 42 861 2653

A. PEREZ-NAVARRO
UNESA/LAESA
PLAZA ROMA, F1,1
ZARAGOZA, 50010 SPAIN
34-976-532614 34-976322956

K. PEVELER
IES UTILITIES/DUANE ARNOLD ENERGY CENTER
3277 DAEC RD.
PALO, IA 52324 USA
319-857-7801 319-857-7678

T. PIETRANGELO
NUCLEAR ENERGY INSTITUTE
1776 I ST., NW
WASHINGTON, DC 20006 USA
202-739-8000 202-785-1898

V. POKROVSKY
INSTITUTE FOR PROBLEMS OF STRENGTH NAN
2 TIMIRYAZEVSKAYA STR.
KIEV, UKRAINE
044-296-25-57 044-296-25-57

A. POOLE
OAK RIDGE NATIONAL LABORATORY
Y-12 PLANT, BEAR CREEK RD.
OAK RIDGE, TN 37831-8038 USA
423-574-0734 423-576-0493
aop@ornl.gov

G. POTTS
GENERAL ELECTRIC NUCLEAR FUEL
CASTLE HAYNE RD
WILMINGTON, NC 28403 USA
910-675-5708 910-675-6966

D. POWELL
PUBLIC SERVICE ELECTRIC & GAS CO.
PO BOX 236, MAIL CODE N21
HANCOCKSBRIDGE, NJ 08038 USA
609-339-2002 609-339-1448

T. PRATT
BROOKHAVEN NATIONAL LABORATORY
BLDG. 130
UPTON, NY 11973-5000 USA
516-344-2630 516-344-5730
pratt@bnl.gov

D. PRELEWICZ
SCIENTECH, INC.
11140 ROCKVILLE PIKE, STE 500
ROCKVILLE, MD 20852 USA
301-468-6425 301-468-0883
damp@scientech.com

J. PUGA
UNESA
FRANCISCO GERVAS 3
MADRID, SPAIN 28020 SPAIN
34-1-5674807 34-1-5674988
unesamuc@dial.eunet.es

C. PUGH
OAK RIDGE NATIONAL LABORATORY
P.O. BOX 2009
OAK RIDGE, TN 37831 USA
423-574-0422 423-241-5005
pug@ornl.gov

R. RANIERI
AGENZIA NAZIONALE PER LA PROFEZIONE DELL' AM
VIA VITALIANO BRANCATI 48
ROMA, 00144 ITALY
39-6-5007-2150 39-6-5007-2941

D. RAO
SCIENCE AND ENGR. ASSOCIATES, INC.
6100 UPTOWN BLVD. NE
ALBUQUERQUE, NM 87110 USA
505-884-2300 505-884-2991
dvrac@seaborse.com

J. RASH
G E NUCLEAR ENERGY
BOX 780
WILMINGTON, NC 28402 USA
910-675-5612 910-675-5879
rashjewlmpo3.wilm.ge.com

J. RASHID
ANATECH CORP.
5435 OBERLIN DR.
SAN DIEGO, CA 92121 USA
619-455-6350 619-455-1094
joe@anatech.com

T. RAUSCH
COM ED NUCLEAR FUEL SERVICES
1400 OPUS PL, STE 400
DOWNERS GROVE, IL 60515 USA
630-663-3020 630-663-7118
nfstr@ccmail.ceco.com

S. RAY
WESTINGHOUSE CNFD
NORTHERN PIKE
MONROEVILLE, PA 15146 USA
412-374-2101 412-374-2045
rays@westinghouse.com

R. REHACEK
STATE OFFICE FOR NUCLEAR SAFETY
SENOVAZNE NAM. 9
PRAGUE, 110 00 CZECH REPUBLIC
420-2-21624729 420-2-21624202
radomir.rehacek@sujb.cz

J. REYES
OREGON STATE UNIVERSITY
116 RADIATION CENTER
CORVALLIS, OR 97331-5902 USA
541-737-4677 541-737-4678
reyesj@cemail.orst.edu

I. RICKARD
ABB COMBUSTION ENGINEERING
2000 DAYHILL RD.
WINDSOR, CT 06095 USA
860-285-9678 860-285-3253

T. RIEKERT
GESELLSCHAFT FUR ANLAGEN UND REAKTORSICH
SCHWERTNERGASSE 1
COLOGNE, 50667 GERMANY
49-224-2068-758 49-224-2068-888
rik@grs.de

J. RIZNIC
ATOMIC ENERGY CONTROL BOARD
PO BOX 1046, STA. B, 280 SLATER ST.
OTTAWA, ONTARIO K1P5S9 CANADA
613-943-0132 613-943-8954
Riznic.j@atomcon.ac.ca

U. ROHATGI
BROOKHAVEN NATIONAL LABORATORY
BUILDING 475B
UPTON, NY 11973 USA
516-344-2475 516-344-1430
rohatgi@bnl.gov

A. ROMANO
BROOKHAVEN NATIONAL LABORATORY
BLDG. 197C
UPTON, NY 11973-5000 USA
516-344-4024 516-344-5266
ramano@bnl.gov

T. ROSSEEL
LOCKHEED MARTIN ENERGY RESEARCH CORP.
PO BOX 2008
OAK RIDGE, TN 37831-6158 USA
423-574-5380 423-574-5118
rosseeltm@ornl.gov

R. ROSTEN
DUKE ENGINEERING & SERVICES
215 SHUMAN BLVD. SUITE 172
NAPERVILLE, IL 60563-8458 USA
630-778-4329 630-778-4444
nwrosten@duke-power.com

J. ROYEN
OECD NUCLEAR ENERGY AGENCY
12 BLVD DES ILES
ISSY LES MOULINEAUX, F 92130 FRANCE
33-1-4524-1052 33-1-4524-1129
jacques.royen@oecd.org

B. RYBAK
COMMONWEALTH EDISON
1400 OPUS PL, SUITE 500
DOWNERS GROVE, IL 60515 USA
630-663-7286 630-663-7155

Y-H. RYU
KOREA INSTITUTE OF NUCLEAR SAFETY
YUSONG-DONG 19
TAEJON, 305-338 KOREA
82 42 868 0228 82 42 861 0943
ko53ryh@pinpoint.kins.re.kr

D. SACCOMANDO
COMMONWEALTH EDISON
1400 OPUS PL, SUITE 500
DOWNERS GROVE, IL 60515 USA
630-663-7283 630-663-7155

M. SAKAMOTO
NUCLEAR POWER ENGINEERING CORP.
4F 17-1, 3-CHOME TORANOMON MINATOKU
TOKYO, 105 JAPAN
81 3 3438 3066 81 3 5470 5544
msakamoto@nupec.or.jp

O. SANDERVAG
SWEDISH NUCLEAR POWER INSPECTORATE
INSPECTORATE
STOCKHOLM, 10658 SWEDEN
4686988463 4686619086
oddbjorn@ski.se

M. SATTISON
IDAHO NATIONAL ENGINEERING & ENVIRONMENTAL
PO BOX 1625, MS 3850
IDAHO FALLS, ID 83415-3850 USA
208-526-9626 208-526-2930
sbm@inel.gov

G. SAUER
TOV ENERGIE UND SYSTEMTECHNIK GmbH
WESTENDSTRESSE 199
MUNICH, D-80686 GERMANY
49-89-5791-1267 49-89-5791-2157
gerhard.sauer@et.tueysued.de

C. SCHLASEMAN
MPR ASSOCIATES INC.
320 KING ST.
ALEXANDRIA, VA 22314 USA
703-519-0200 703-519-0224
cschlaseman@mpra.com

F. SCHMITZ
INSTITUT DE PROTECTION ET DE SURETE NUCLEAIR
CE CADARACHE
ST PAUL LEZ D., 13108 FRANCE
33-442257035 33-442252977
frauz.schmitz@ipsn.fr

S. SCHULTZ
YANKEE ATOMIC
580 MAIN STREET
BOLTON, MA 01740 USA
508-568-2131 508-568-3703
schultze@yankee.com

B.R. SEHGAL
ROYAL INSTITUTE OF TECHNOLOGY
60 BRINELVAGEN
STOCKHOLM, 10044 SWEDEN
011-46-8-790-6541 011-46-8-790-7678
sehgal@ne.kth.se

W. SHACK
ARGONNE NATIONAL LABORATORY
9700 S. CASS AVE. BLDG. 212
ARGONNE, IL 60439-4838 USA
630-252-5137 630-252-4798
wjshack@anl.gov

E. SIMPSON
PUBLIC SERVICE ELECTRIC & GAS CO.
PO BOX 236, MAIL CODE N21
HANCOCKSBRIDGE, NJ 08038 USA
609-339-1700 609-339-5070

B. SINGH
JUPITER CORPORATION
STE 900, WHEATON PLAZA NO.
WHEATON, MD 20902 USA
301-946-8088 301-946-6539
singh@jupitercorp.com

W. SLAGLE
WESTINGHOUSE ELECTRIC / CNFD
161 SAXONBURY ROAD
PITTSBURGH, PA 15238 USA
412-374-2088 412-374-2045
slaglewh@westinghouse.com

A. SMIRNOV
RESEARCH INSTITUTE OF ATOMIC REACTORS
DIMITROVGRAD 10
URYANOVSKI REGION, 433510 RUSSIA
84235-32350 84235-64163
gns@niiar.simbirsk.su

V. SMIRNOV
RESEARCH INSTITUTE OF ATOMIC REACTORS
DIMITROVGRAD 10
URYANOVSKI REGION, 433510 RUSSIA
78923532350 78423564163
gns@niiar.simbirsk.su

M. SOBAJIMA
JAPAN ATOMIC ENERGY RESEARCH INST.
2-4 SHIRAKATA-SHIRANE, TOKAI-MURA
NAKA-GUN, IBARAKI-KEN, 319-11 JAPAN
81 29 282 5815 81 29 282 6147
job916@popsvr.tokai.jaeri.go.jp

J-H. SONG
KOREA INSTITUTE OF NUCLEAR SAFETY
19 KUSUNG-DONG, YOUSUNG-KU
TAEJON, KOREA
82 42 868 0117 82 42 861 2653

K. ST. JOHN
YANKEE ATOMIC ELECTRIC CO.
580 MAIN ST.
BOLTON, MA 01740 USA
978-568-2133 978-568-3700
stjohn@yankee.com

J. STONE
MPR ASSOCIATES INC.
320 KING ST.
ALEXANDRIA, VA 22314 USA
703-519-0200

V. STRIZHOV
NUCLEAR SAFETY INST., RUSSIAN ACADEMY OF SCI.
BOLSHAYA TULSKAYA STR. 52
MOSCOW, 113191 RUSSIA
095-955-28-73 095-952-37-01
vfs@ibrae.ac.ru

K. SUDO
JAPAN ATOMIC ENERGY RESEARCH INST.
2-4 SHIRAKATA-SHIRANE, TOKAI-MURA
NAKA-GUN, IBARAKI-KEN, 319-11 JAPAN
81 29 282 5699 81 29 282 5923

R. SUNDARAM
YANKEE ATOMIC ELECTRIC CO.
580 MAIN ST.
BOLTON, MA 01740 USA
508-568-2125 508-568-3700
sundaram@yankee.com

T. TAIWO
ARGONNE NATIONAL LABORATORY
9700 SO CASS AVE, BLDG. 208
ARGONNE, IL 60439-4838 USA
630-252-7182 630-252-4500
b40364@salt.ra.anl.gov

H. TAMURA
NUCLEAR POWER ENGINEERING CORP.
4F 17-1, 3-CHOME TORANOMON
MINATOKU, TOKYO 105 JAPAN
81 3 5470 5486 81 3 5470 5487
tamura@nupec.or.jp

T. TANAKA
SANDIA NATIONAL LABORATORIES
PO BOX 5800, MS 0747
ALBUQUERQUE, NM 87185-0747 USA
505-844-2981 505-844-3321
tjtanka@sandia.gov

K. TERADA
NUCLEAR POWER ENGINEERING CORP.
SHUWA-KAMIYACHO BLDG, 2F, 4-3-13, TORANOMON
MINATO-KU, TOKYO 105 JAPAN
81 3 3434 4551 871 3 3434 9487

C. THIBAULT
WYLE LABORATORIES
7800 HIGHWY 20 WEST
HUNTSVILLE, AL 35806 USA
205-837-4411 205-837-3363

O. THOMSEN
SOUTHERN CALIFORNIA EDISON
PO BOX 128
SAN CLAMENTE, CA 92674 USA
714-368-8087 714-368-8188
thomscoj@sow65.soe.com

H. THORNBURG
901 S. WARFIELD DR.
MT. AIRY, MD 21771 USA
301-831-7328 301-829-0874
mattt@erols.com

R. TOUZET
AUTORIDAD REGULATORIA NUCLEAR
AV. LIBERTADOR 8250
BUENOS AIRES, 1428 ARGENTINA
541-704-1228 514-704-1188
rtouzet@sede.arn.gov.ar

R. TREGONING
NAVAL SURFACE WARFARE CENTER
9500 MACARTHER BLVD.
WEST BETHESDA, MD 20817 USA
301-227-5145 301-227-5548
tregon.n@metals.dt.navy.mil

H. TUOMISTO
IVO POWER ENGINEERING LTD.
RAJATORPANTIE 8
VANTAA, FIN-01019 FINLAND
358-9-8561-2464 358-9-8561-3403
harri.tuomisto@ivo.fi

R. UHRIG
UNIVERSITY OF TENNESSEE (ACRS MEMBER)
306 PASQUA ENGINEERING BLDG.
KNOXVILLE, TN 37996-2300 USA
423-974-3110 423-974-0668
ruhrig@utk.edu

G. URRIOLAGOITIA
ESIME-I.P.N.
EDIF.5, LINDAVISTA
MEXICO, MEXICO
729-6000 ext. 54586 729-6000 ext. 54588

R. VALENTIN
ARGONNE NATIONAL LABORATORY
9700 S. CASS AVE., BLDG. 308
ARGONNE, IL 60439-4838 USA
630-252-4483 630-252-3250
richv@anl.gov

K. VALTONEN
RADIATION & NUC. SAFETY AUTH, STUK
HELSINKI, FINLAND
358-09-75988331 358-09-75988382
keijo.Valtonen@stuk.fi

W. VAN DOESBURG
SWISS NUCLEAR SAFETY INSPECTORATE
PO BOX 5232
VILLIGEN, 5232 SWITZERLAND
41-56-3103862 41-56-3103854
vandoesburg@hsk.psi.ch

W. VESELY
SCIENCE APPLICATIONS
655 METRO PLACE SOUTH #745
DUBLIN, OH 43017 USA
614-793-7600 614-793-7626

M. VESHCHUNOV
NUCLEAR SAFETY INST., RUSSIAN ACADEMY OF SCI.
BOLSHAYA TULSKAYA STR. 52
MOSCOW, 113191 RUSSIA
095-955-26-18 095-952-5701
vms@ibrae.ac.ru

J. VILLADONIGA
CONSEJO DE SEGURIDAD NUCLEAR
JUSTO DORADO, 11
MADRID, 28040 SPAIN
34-1-3460240 34-1-3460588
jivt@csn.es

K. VINZENS
TOV ENERGIE UND SYSTEMTECHNIK GmbH
WESTENDSTRESSE 199
MUNICH, D-80686 GERMANY
49-89-5791-2317 49-89-5791-2157
kurt.vinzene@et.tuevsued.de

D. VOJNOVIC
SLOVENIAN NUCLEAR SAFETY ADMINISTRATION
VOJKOVA 53
LJUBLJANA, SLOVENIA
386611721147 386611721199
djordje.vojnoric@rujv.sigor.mail.si

K.C. WAGNER
SCIENTECH, INC.
8708 GREENARBOR ROAD
ALBUQUERQUE, NM 87122 USA
505-262-1800

R. WALKER
TU ELECTRIC
PO BOX 1002
GLEN ROSE, TX 76042 USA
254-897-8233 254-897-6573
rwalker5@tuelectric.com

D. WALTERS
NUCLEAR ENERGY INSTITUTE
1776 I ST., NW
WASHINGTON, DC 20006 USA
202-739-8000 202-785-1898

F. WALTHER
BAVARIAN STATE MINISTRY FOR STATE DEV. & ENV.
PO BOX 810140
MUNICH, D-81901 GERMANY
49-89-92142325 49-89-92142286

L. WARD
SCIENTECH, INC.
11140 ROCKVILLE PIKE SUITE 500
ROCKVILLE, MD 20852 USA
301-468-6425

W. WENDLAND
AMERICAN NUCLEAR INSURERS
29 SO. MAIN ST., SUITE 3005
WEST HARTFORD, CT 06107 USA
860-561-3433 860-561-4655
bwendland@amnucins.com

D. WHITEHEAD
SANDIA NATIONAL LABORATORIES
PO BOX 5800, MS0747
ALBUQUERQUE, NM 87185-0747 USA

K. WHITT
SOUTHERN NUCLEAR
40 INVERNESS CENTER PKWY.
BIRMINGHAM, AL 35242 USA
205-922-6396 205-922-6108
kermit.w.whitt@snc.com

F. WINTER
TOV ANLEGEN UND UMWELTTECHNIK GmbH
WESTENDSTRESSE 199
MUNICH, D-80686 GERMANY
49-89-5791-1126 49-89-5791-2070
friedrich.winter@aw.tuevsued.de

R. WOOD
OAK RIDGE NATIONAL LABORATORY
PO BOX 2008, BLDG. 3500 MS 6010
OAK RIDGE, TN 37831-6010 USA
423-574-5578 423-576-8380
woodrt@ornl

G. YADIGAROGLU
SWISS FEDERAL INST. OF TECHNOLOGY (AND PSI)
ETH - ZENTRUM, CLT
ZURICH, CH 8092 SWITZERLAND
41-1-632-4615 41-1-632-1166
yadie@iet.ethz.ch

Y.H. YANG
INSTITUTE OF NUCLEAR ENERGY RESEARCH
PO BOX 3-3
LUNGTAN, TAOYUAN, TAIWAN 325 ROC
886-3-4711400 886-3-4711404

A. YEGOROVA
RUSSIAN RESEARCH CENTRE - KURCHATOV INSTIT
MOSCOW, 123182 RUSSIA
7-095-196-93-20 9-095-196-17-02
asmdov@nsi.kiac.ru

Y.C. YEH
ATOMIC ENERGY COUNCIL TAIWAN
67 LANE 144, KEELUNG RD., SEC 4
TAIPEI, TAIWAN ROC
011-886-2-3634180 011-886-2-3660535
yeyeh@cc22.aec.gov

T. ZAMA
TEPCO
1901 L ST., NW, SUITE 720
WASHINGTON, DC 20036 USA
202-457-0790 202-457-0810
zama@tepco.com

G. ZIGLER
ITS CORPORATION
8015 MOUNTAIN RD. PI NE SUITE 210
ALBUQUEQUE, NM 87110 USA
505-254-1005 505-254-1251
gzigler@itsc.com

Proceedings of the
25th Water Reactor Safety Information Meeting
October 20-22, 1997

Contents - Volume 3

Thermal Hydraulic Research & Codes II
J. Uhle, Chair

Page

Structural Performance
A. Murphy, Chair

THERMAL HYDRAULIC - PROBABILISTIC ANALYSIS (TH-PA) INTEGRATION METHOD AND ITS APPLICATION TO IDENTIFY AP600 BDBA SCENARIOS

Yue Guan and Mohammad Modarres
Material and Nuclear Engineering Department
University of Maryland

Marino diMarzo and David Bessette
Office of Nuclear Regulatory Research
U.S. Nuclear Regulatory Commission

Abstract - *A TH-PA integrated screening method has been developed to identify AP600 beyond design basis accident (BDBA) scenarios in a consistent, systematic and comprehensive fashion. This method is used as a screening tool such that only the scenarios which have reasonable frequency of occurrence and have potential to raise significant safety concerns are identified. The method considers postulated passive safety system failures, thermal hydraulic phenomena and their induced system failures, human actions and their consequences. Results from this research (the identified AP600 BDBA scenarios) provide inputs to further AP600 analysis and experiments and will be used to assess the capability of thermal hydraulic safety analysis computer code RELAP5/MOD3 in addressing scenarios in the BDBA space.*

I. INTRODUCTION

The Westinghouse Electric Corporation has submitted the design for its 600 MWe Advanced Pressurized Reactor (AP600) to the United States Nuclear Regulatory Commission (U. S. NRC) for certification. The AP600 uses many passive safety features not found in conventional operating reactors. Because of these passive safety features, thermal hydraulic (TH) phenomena and certain system behavior which do not raise safety concerns in conventional plant may become important in the AP600 system.

U. S. NRC has previously assessed the TH code RELAP5/MOD3 for conventional reactors. Phenomena important to the AP600 design need to be modeled adequately in the code calculation. U. S. NRC has conducted independent experiments to collect data specifically to assess the adequacy of the TH code in modeling AP600 passive safety systems.

RELAP5 has now been assessed in the design

Most of the AP600 data and its related analysis results are proprietary information. Therefore, in place of such information, either the name of the variable or normalized data is used to show the methodology. The results presented in this paper illustrate the methodology for identifying BDBA scenarios. The application of this method to the AP600 is not yet complete. Its application to other initiating events are scheduled to follow.

basis accident space and is considered adequate. To explore design margins and provide data to assess the TH code's capability to address scenarios in the beyond design basis accident (BDBA) space, U. S. NRC has additionally undertaken the task of performing BDBA code assessment.

Under this task, some selected accident scenarios in the BDBA space have been tested in the experimental facilities. TH code calculations have been completed for some of the accident scenarios and results compared with test data. However, the tests selected may be arbitrary[1] and the scenarios may not cover the whole spectrum of the important phenomena in BDBA space.

Therefore, there is a need to consistently, systematically and comprehensively identify the important scenarios in the BDBA space that have reasonable frequency of occurrence (i.e., probabilistically significant) and have the potential to lead to significant thermal hydraulic concerns (including potential core uncovery) which the code is required to be further assessed and validated. This assessment can provide reasonable assurance that the calculated AP600 response from the computer code is adequate and the assessed code can be used as a basis for the BDBA evaluation.

The plan for code assessment is shown in Figure 1 where flow of information and the decision-making process are presented. In this BDBA plan, a thermal hydraulic-probabilistic analysis (TH-PA) integrated screening method is the starting point. This method uses probabilistic and thermal hydraulic screening criteria to ensure that the identified BDBA scenarios are both probabilistically credible and thermal hydraulically significant.

Once the AP600 BDBA scenarios are identified, a decision must be made whether sensitivity calculations are needed. Based on the results of the sensitivity calculations, a decision will be made on whether additional testing is necessary because there might be phenomena or sequences of events which are identified in these sensitivity calculations that might require experimental confirmation.

The results of sensitivity calculations and/or testing are then evaluated. With this information, a decision will be made on whether to impose additional BDBA requirements on the code. Finally, the code adequacy in the BDBA space is assessed and the relative acceptability for thermal hydraulic uncertainty is determined.

This paper presents the first part of the BDBA code assessment plan, the TH-PA integrated screening method that is specifically developed to identify AP600 BDBA scenarios. The paper gives a brief description of the AP600 passive safety systems in section II. An overall TH-PA integration concept is introduced in section III. In three separate sections, IV, V, and VI, detailed methods are presented for plant state generation and PA screening, TH trajectory prediction and screening, and integration of TH phenomena and human actions, respectively. In section VII, an example will be given to demonstrate the complete process of using TH-PA screening method to identify BDBA scenarios.

II. DESCRIPTION OF AP600 PASSIVE SAFETY SYSTEM

The unique design of AP600 is its passive safety systems which relies on natural circulation and gravity injection to mitigate an accident. A sketch of the passive safety systems is presented in Figure 2. They include two Core Makeup Tanks (CMT), one Passive Residual Heat Removal (PRHR) Heat Exchanger (HX), two Accumulators (ACC), two lines of Automatic Depressurization System 1-3 (ADS1-3), four lines of ADS4, and one In-containment Refueling Water Storage Tank (IRWST).

Both of the CMTs are full of room temperature borated water. Following a CMT actuation

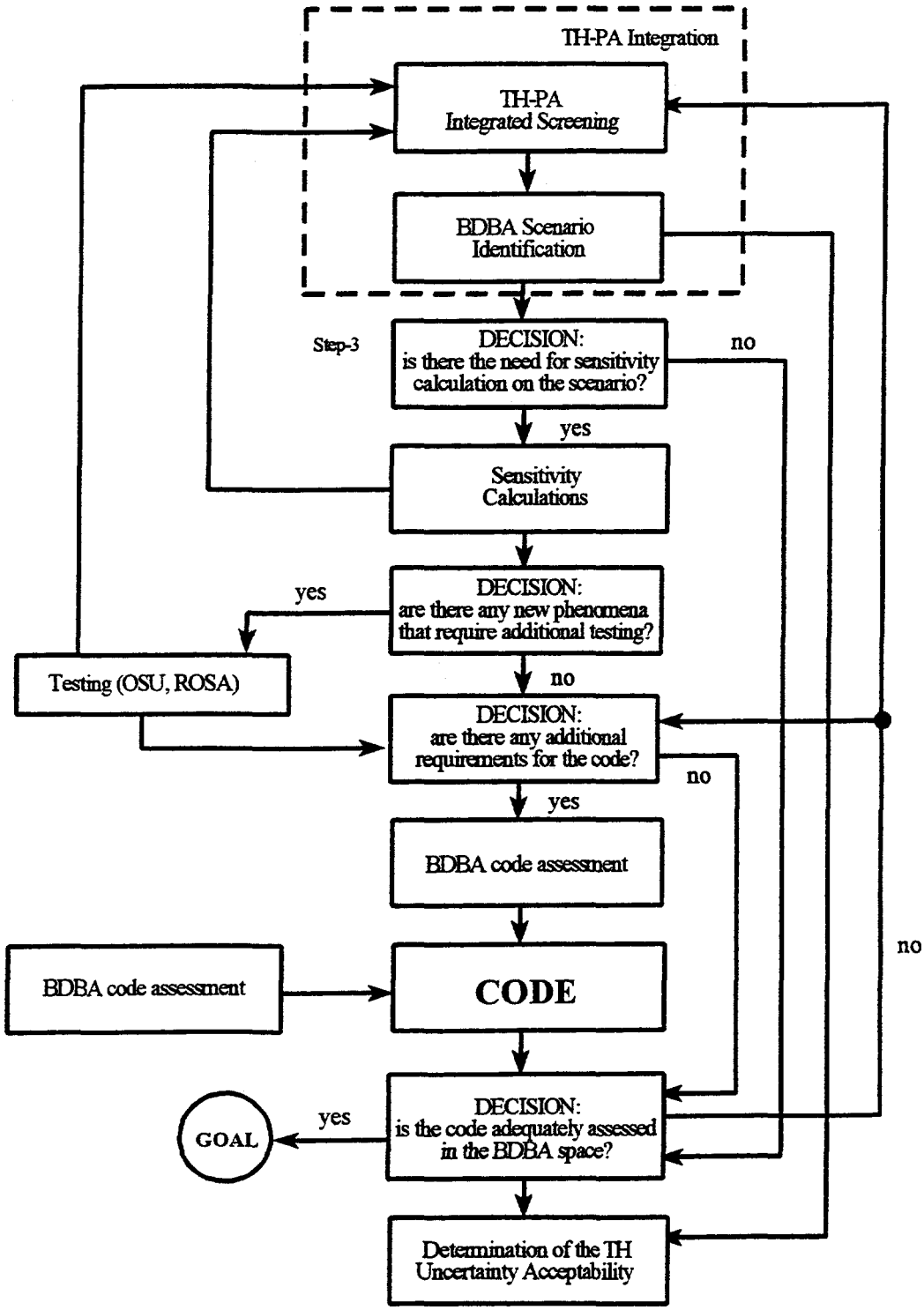

Figure 1. BDBA Plan for Code Assessment

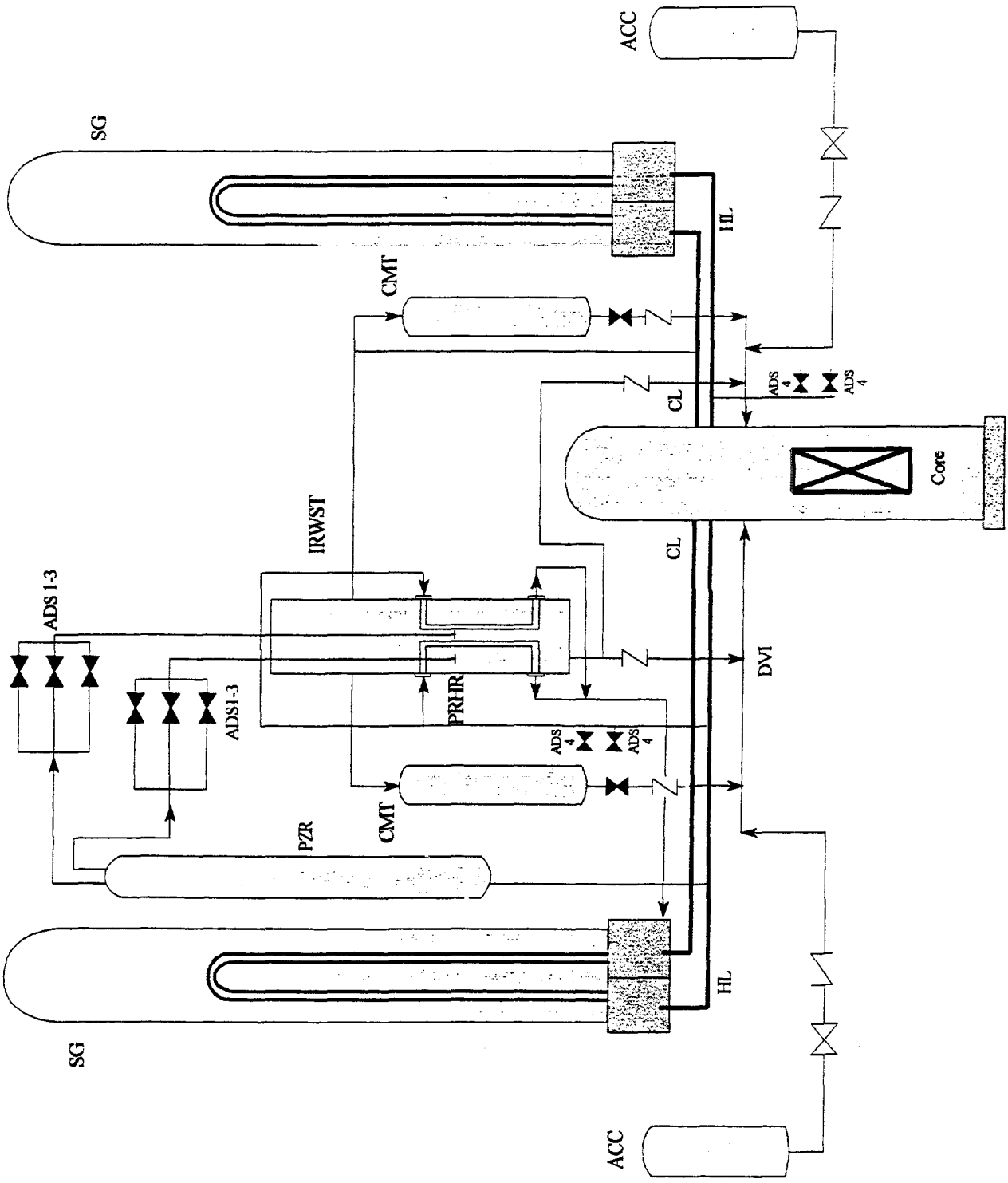

Figure 2. AP600 Passive Safety Systems

signal, the valves on the CMT discharge piping are opened and CMTs begin to provide short-term, liquid circulation to the vessel via Direct Vessel Injection (DVI) line at high system pressure. In the mean time, hot liquid from the cold legs is circulated to the top of CMTs via Pressure Balance Line (PBL). When top portion of the CMTs become saturated and vapor is present, the natural circulation is terminated and CMTs begin to drain. After CMTs begin to drain, the water level in the CMTs decreases. When the water level drops to the first ADS level set point, ADS1 is actuated. ADS2 and ADS3 actuate sequentially based on timing. While ADS4 is actuated on the second ADS level set point and timing.

The PRHR HX is submerged inside the IRWST. The PRHR system is designed to remove 100% of the decay heat in the earlier stage of an accident. It takes the hot fluid from the hot leg and transfers heat into the pool of water in IRWST. The cooled fluid is then returned to RCS via one of the steam generators outlet plenum.

The performance of both the PRHR and CMTs rely on gravity driven natural circulation. Before ACC begins injection to the RCS, PRHR and CMTs are the only means to provide cooling to the RCS and to add water to RCS, compensating the mass loss through the break.

Both of the ACCs are filled with room temperature borated water and are pressurized with nitrogen. When the RCS system pressure drops below the N2 pressure within the accumulators, the accumulators begin to inject water to RCS, via DVI line.

ADS1-4 is designed to depressurize the RCS in a controlled manner. The pressure reduction permits nitrogen pressure driven ACC injection and the gravity-driven safety injection from the IRWST. ADS1-3 takes the hot fluid and vapor from the pressurizer and feeds it into the IRWST. ADS4 takes off from the hot leg and discharges directly into the containment.

The IRWST has three major functions: serves as the heat sink for the PRHR HX; provides the liquid pool for condensing the effluent from ADS1-3; and supplies RCS with long-term gravity-driven injection at low pressure.

III. TH-PA INTEGRATION METHOD

The first step in BDBA plan for code assessment is TH-PA screening using a TH-PA integration method. The general concept of this method is shown in Figure 3.

There are three key elements in the figure: plant state generation and PA screening, TH trajectory prediction and screening, and TH phenomena and human action integration.

Also shown in the figure are the three groups of screening products. The first group are the plant states eliminated after PA screening because the probability of occurrence are below the probability cutoff value. The second group are the plant states eliminated after TH screening because they have no TH significance (will not create a safety concern). The third group are the plant states that have probabilities of occurrence above the probability cutoff value AND has TH significance (i.e., has safety concern or may lead to core uncovery). The third group of plant states and the TH trajectory constitutes the BDBA scenario required by the BDBA plan for code assessment (see Figure 1).

The TH-PA integration method begins with the selection of an accident Initiating Event (IE, e.g., a SBLOCA). Then the plant states associated with the initiating event and their corresponding occurrence probabilities are generated. A probability cutoff value is selected (e.g., 10^{-10}) and will be used as the basis for the PA screening. The plant states with probabilities lower than the cutoff value are automatically eliminated and become the first screening group.

Plant states with probabilities higher than the

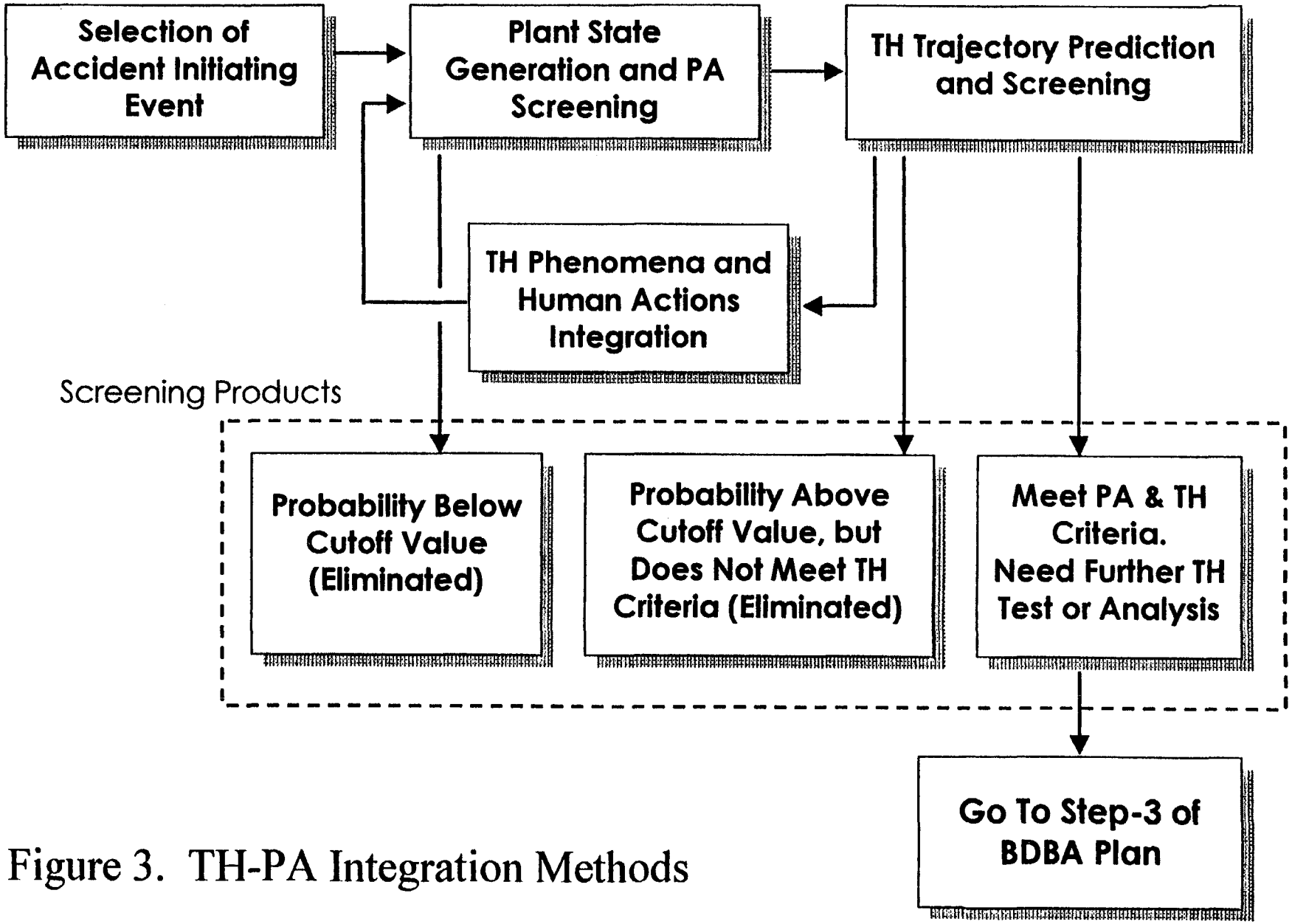

Figure 3. TH-PA Integration Methods

cutoff value are retained after PA screening. Each of these plant states is forwarded to the second key element for TH trajectory prediction and screening. Based on the given plant state which represents the failures of the passive safety systems, TH trajectory prediction is able to capture changes in RCS pressure and RCS liquid volume fraction following the accident initiating event.

TH screening criteria is defined such that if the TH trajectory does not raise a safety concern, such as the RCS pressure will drop to the IRWST injection pressure while the core is still covered, the plant state with this trajectory is eliminated and become the second screening group.

If TH significance can not be determined based on the predicted trajectory, the plant state creating such trajectory is retained and will be integrated with the third key element, TH phenomena and human actions.

If a trajectory raises a safety concern, such as potential core uncovery, the plant state and the trajectory constitute a new BDBA scenario which becomes the third screening group.

In the third key element, TH phenomena and human actions are logically represented in Integrated Behavior Logic Diagrams (IBLDs). Each plant state that survived TH screening and the information from TH trajectory prediction trigger some of the IBLDs and the results are the induced passive safety system failures or changes of system status caused by TH phenomena or human actions. The newly found induced failure and the original plant state form a new plant state. This new plant state will again undergo PA screening (in the first key element). Based on its probability of occurrence, this plant state will be either eliminated or forwarded to the second key element.

Thus, the TH-PA integrated screening method follows an iterative loop "plant state generation and PA screening ==> TH trajectory prediction and screening ==> TH phenomena and human actions integration ==> new plant state generation and PA screening ==>..." An initiating event selected enters this iterative loop and the screening goes on until all the plant states are processed. The plant states are either eliminated or are determined to lead to significant BDBA scenarios and the scenarios are to be further analyzed and tested. Since there are both PA and TH screening criteria built into the process, the plant states not meeting those two criteria are quickly screened out. It only takes a few iteration through the loop to eventually find the BDBA scenarios.

In summary, the TH-PA integrated screening method considers initiating event, postulated passive safety system failures (random failures), system failures or changes in system status induced by TH phenomena and resulted from human actions. This method provides a consistent, systematic, and comprehensive tool to identify important BDBA scenarios that satisfy both probability and TH significance requirements.

IV. PLANT STATE GENERATION AND PA SCREENING

Plant state generation starts with a selected accident initiating event. An AP600 PRA REVEAL-W™,[2] model[3] will be used to comprehensively and rapidly generate all the plant states that are associated with this initiating event. Each plant state generated is a particular plant configuration for which the initiating event has occurred and certain systems have failed.

The AP600 PRA REVEAL-W™ model is based on the event trees and data from Westinghouse AP600 PRA[4]. In this model, logic trees are rebuilt for the AP600 systems (e.g., CMTs, ADS). The failure probabilities of the components and systems and their contributions to core damage are consistent with reference 4. The results from the model have been successfully

validated against the results presented in this reference.

The probability for each plant state is calculated from the AP600 PRA REVEAL-W™ model. A probability cutoff value is defined in the model. Therefore, the plant state with probability lower than the cutoff value is automatically eliminated due to low credibility. The ones with probabilities higher than the cutoff value will be saved as an output.

When a SBLOCA is selected as an initiating event , all the plant states associated with this initiating event are generated. Examples of plant states are :

1. SBLOCA with 1 CMT failure
2. SBLOCA with 2 CMT failures
3. SBLOCA with PRHR failure
4. SBLOCA with PRHR and 1 CMT failure
5. SBLOCA with PRHR and 2 CMT failures
6. SBLOCA with 2 CMT failures and ADS failure

Plant states 4, 5 and 6 have occurrence probabilities lower than the defined cutoff value and therefore are eliminated. Plant states 1, 2, and 3 have occurrence probabilities higher than the cutoff value and are retained after PA screening. Each of these retained plant states is forwarded to the second key element.

For the purpose of screening, plant state at system level is adequate. Since there are much fewer number of systems than components, the number of plant states generated is much less. Therefore, the number of plant states surviving PA screening is limited.

Nevertheless, if there is an interest on certain components (e.g., a specific valve), it is convenient to generate the plant states based on such components and carry out the rest of the process in a similar manner. The number of plant states surviving PA screening will still be bounded, as long as a limited number of components are selected at any one time.

V. TH TRAJECTORY PREDICTION AND SCREENING

The purpose of TH trajectory prediction and screening is to connect the "plant state - system failure" concept used in probabilistic analysis with the "system failure - physical behavior (trajectory)" concept used in thermal hydraulic deterministic analysis. By linking plant state with accident trajectory in a simple method and by applying TH screening criteria on the trajectory, we are able to throw out the plant states and the associated trajectories that do not have TH significance.

Each passive safety system in AP600 design has its role in mitigating an accident. They either add water to the RCS and/or remove energy from the RCS, or relieve RCS pressure. The failure of one or more of the systems alters the accident trajectory, usually to a state with higher system pressure and lower RCS mass. The failure of a passive system, either postulated or induced by TH phenomena or resulted from human actions, is represented by plant state generated by AP600 PRA model and IBLDs. Therefore, by finding the interdependency between accident trajectory and system failure, we are able to link accident trajectory with plant state that represents the failures of passive safety systems.

Accident trajectory is defined as the progressive changes in RCS pressure and liquid volume fraction as a function of passive safety system failures. Since RCS pressure and liquid volume fraction are TH parameters, the accident trajectory is also referred to as TH trajectory.

TH trajectory prediction begins with the identification of the roles of each passive safety system in accident transient. For example in AP600, PRHR removes energy from RCS; ADS relieves RCS pressure through bleeding; CMT adds water to RCS and at the same time removes

energy from RCS (energy reference point is defined as water at saturation at system pressure. Therefore, adding subcooled water to RCS is equivalent to removing energy).

Then, the roles of each system is represented in the mass conservation equations:

$$\frac{dM^{RCS}}{dt}=N^{CMT}(G_o^{CMT}-G_i^{CMT})+N^{ACC}G^{ACC}-G^{Break}-G^{ADS}$$

$$\frac{dM^{CMT}}{dt}=N^{CMT}(G_o^{CMT}-G_i^{CMT})$$

$$\frac{dM^{ACC}}{dt}=N^{ACC}G^{ACC}$$

and in the energy conservation equation:

$$C\frac{dP^{RCS}}{dt}=Q^{Core}+Q^{Mass}+Q^{SG}-Q^{PRHR}-Q^{CMT}-Q^{ACC}-Q^{Break}-Q^{ADS}$$

where
M^X= mass of water in system X (e.g., CMT)
N^X= number of system X available
$G_{i/o}{}^X$= flow rate in/out of system X
G^X= flow rate out of system X or out of a break
P^{RCS}= RCS pressure
Q^X= energy addition/removal by system X
Q^{Mass}= stored energy released from the metal
C= compliance factor

RCS mass conservation equation is also expressed in liquid volume fraction (LVF):

$$LVF(t_2)=LVF(t_1)+\frac{dM^{RCS}}{dt}\frac{(t_2-t_1)}{\rho V}$$

where
$LVF(t_i)$=LVF at time t_i
ρ=average water density
V=total RCS volume above the hot leg

Test data and theoretical calculations provide values for the terms in the equations. For different plant states, the values for each term are different. For a plant state of SBLOCA with PRHR failure, the heat removal rate by PRHR is zero. For a plant state of SBLOCA with two CMTs failures, PRHR heat removal rate has a value that is consistent with the plant state; but, the mass in and out of CMTs are zero and the energy removal by CMTs is also zero.

Figure 4 shows the trajectories predicted for various plant states. The roles played by each passive safety system are clearly presented. For example, failure of one CMT reduces the LVF from 71% to 69% at 0.47 normalized pressure. Failure of PRHR reduces the LVF from 71% to 62% at the same normalized pressure.

Figure 5 shows a comparison between a predicted trajectory with experimental data for SBLOCA with no failure. The two trajectories compare well. Similar comparisons were done for other plant states of SBLOCA with system failures. The results also compare well.

Once the accident trajectory is predicted for the plant states retained after PA screening, TH screening criteria is applied. TH screening looks at the RCS pressure relative to RCS liquid volume fraction and the potential TH phenomena and human actions that can be associated with the trajectory.

Referring to Figure 5, point C is defined as the cross point of two lines: IRWST injection pressure and top of the core. If the trajectory passes through the IRWST injection pressure line above point C, the plant state with this trajectory is eliminated. For the trajectory predicted even before reaching this point, if there are no TH phenomena or human actions that change the course of the trajectory to high pressure and low mass, and the trajectory point to a destiny above point C when it cross the IRWST injection line, the plant state with this trajectory is also eliminated.

If the trajectory raises a safety concern or

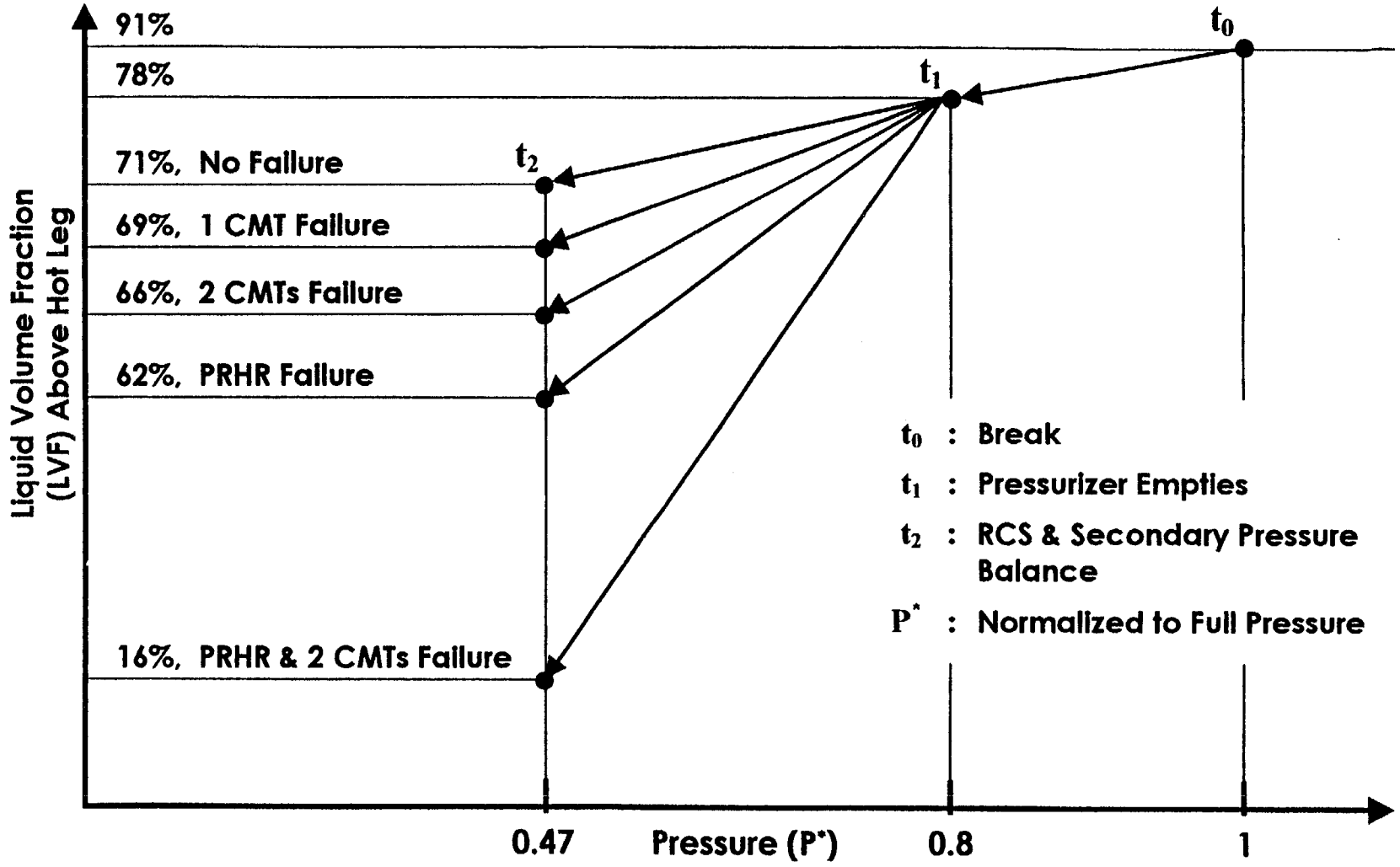

Figure 4. Trajectory Prediction for Different Plant States

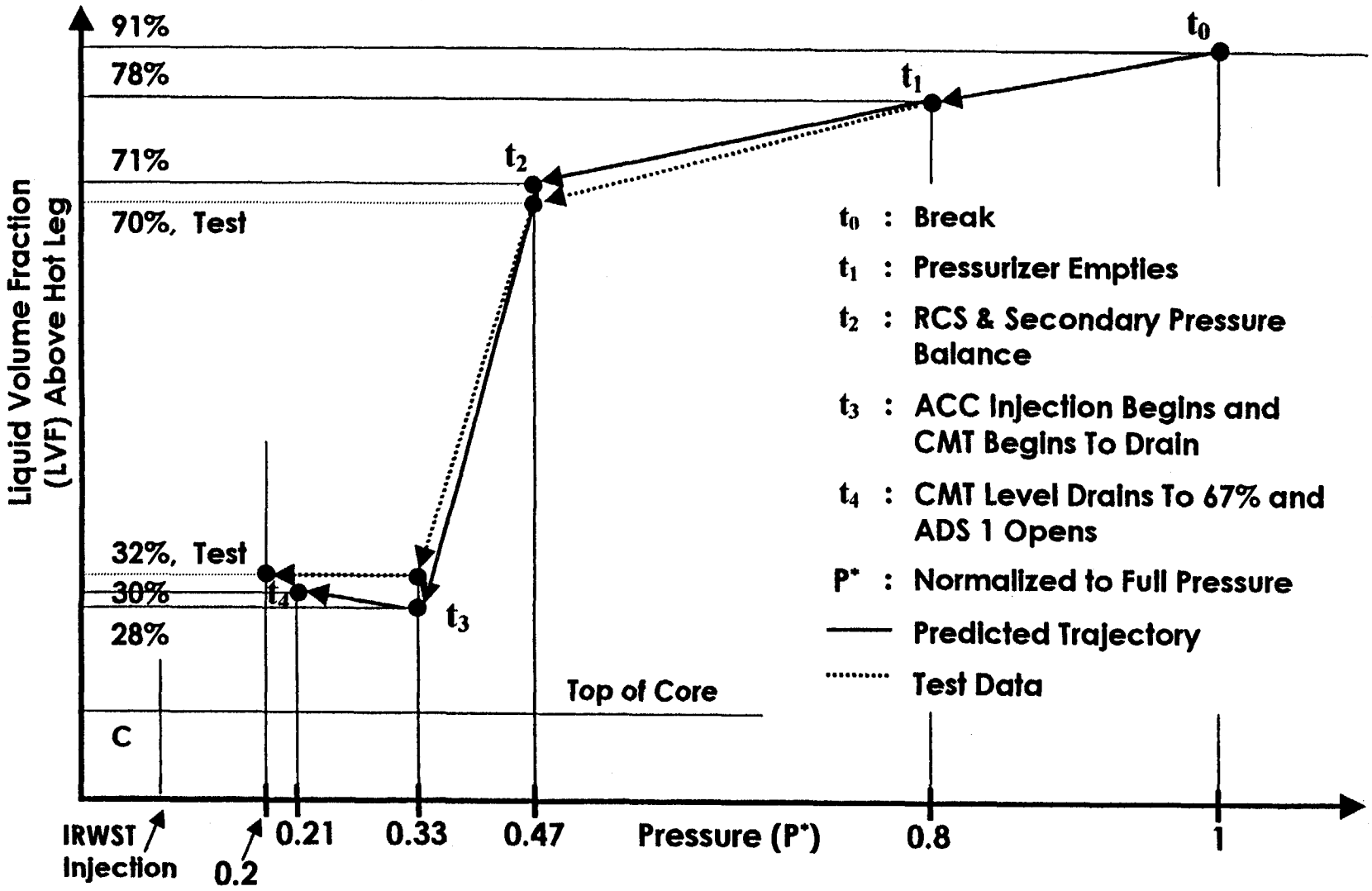

Figure 5. Trajectory Prediction – Comparison With Test Data

already leads to core uncovery (i.e., cross the top of core line when pressure is still above the IRWST injection pressure), the trajectory and the associated plant state constitute an identified BDBA scenario to be further analyzed and tested.

If the TH significance can not yet be determined from the trajectory because it is still premature to make a decision as of if the IRWST pressure line will be crossed above point C, the trajectory and the associated plant state is retained. The retained plant states and the information from the trajectory are combined to form an updated plant state. The updated plant state will be forwarded to the third key element to be integrated with TH phenomena and human actions so that potential new passive safety system failures can be identified

An example of predicting TH trajectory and applying TH screening criteria is given in section VII.

VI. TH PHENOMENA AND HUMAN ACTION INTEGRATION

In this section, the criteria for the selection of TH phenomena and human actions are first presented. Then, TH phenomena and human actions selected for logical representation are provided. The method of forming a logical representations of the TH phenomena and human actions is introduced through developing the Integrated Behavior Logic Diagram (IBLD).

VI.1 TH Phenomena and Human Action Selection Criteria

PIRT report[5] is used as a starting point for generating a list of important TH phenomena. The phenomena in reference 5 that fall into the following categories are not selected:

1. Phenomena that present thermal hydraulic parameters only (e.g., flow, level)
2. Phenomena that are inherent characteristics of design/structure (e.g., flow resistance, loop asymmetry effect)
3. Phenomena that are themselves influenced, or are the results of other phenomena which are modeled (e.g., PZR level swell is induced by flashing)
4. Phenomena that would not affect vessel inventory prior to core uncovery (e.g., CHF/dryout which is related more to the cladding temperature, the level 4 criteria of the Regulatory Guidance for Safety-Related Requirements. In this research, the level 5 criteria, vessel inventory, is used to identify core uncovery scenarios)
5. Phenomena that will not directly lead to system component failure or human action (e.g., thermal stratification, phase separation)
6. Phenomena that are consistently ranked low in reference 5

Westinghouse AP600 Emergency Response Guideline[6] is used to analyze the types of human actions during certain phases of the transient. Human actions having impact on the passive safety systems are considered.

For both TH phenomena and human actions, the following selection criteria apply:

1. Phenomena that potentially affect accuracy of instrumentation (e.g., flashing creates false water level indication)
2. Phenomena that potentially affect system performance (e.g., the presence of N2 degrades PRHR performance)
3. Phenomena that may cause equipment failure or increase hardware failure probability (e.g., condensation induced water hammer can cause pipe break)
4. Phenomena that lead to thermal hydraulic conditions that increase the likelihood of operator errors (e.g., flashing and the

induced swelling may lead to an indication of a solid PZR which may influence an operator to stop the depressurization)

5. Phenomena that influences TH parameters that are important to TH trajectory (e.g., phenomena influencing CMT drainage initiation affects CMT level which in turn affects ADS automatic actuation time. ADS is important to TH trajectory because its opening changes trajectory significantly)
6. System failures that cause failures in other systems (e.g., CMT failure leads to the failure of automatic ADS opening)
7. System failure that requires the operator to take a certain action in which the operator may or may not take such action (e.g., failure of ADS automatic actuation requires the operator to manually open ADS valves)

VI.2 TH Phenomena and Human Actions Selected for Developing IBLDs

Following TH phenomena and human actions are selected for IBLD development. The consequences (resulted from the TH phenomena and human actions) are listed in parentheses :

1. Flashing in CMT and flashing in CMT level sensor (delays automatic ADS actuation)
2. Flashing in PZR (increases water level, causes operator action)
3. Water hammer in ADS1-3 at valve downstream piping (leads to pipe break and redirects ADS1-3 flow into containment, increases ADS1-3 flow rate, elevates containment temperature)
4. Water hammer at ADS 1-3 exit piping and sparger (leads to pipe break, increases flow rate, creates potential blockage of IRWST injection port)
5. Water hammer in DVI line (leads to pipe break and loss of half or all of the passive safety injection)
6. N2 effect on PRHR (degrades PRHR performance)
7. Accumulator effect on CMT (increases CMT water level)
8. CMT drain initiation (controls CMT level and ADS automatic actuation)
9. Thermal stratification on temperature measurement (gives false temperature indication)
10. Thermal binding of valves (leads to valve failure to open)
11. Vessel integrity under rapid depressurization (leads to vessel failure)
12. Containment temperature effect on level measurement (leads to false high level measurement, delays ADS automatic actuation)
13. CMT failure on ADS (leads to ADS automatic actuation failure)
14. Operator actions based on PZR water level (manually closes ADS valves)
15. Operator actions opening or not opening ADS1-3 valves
16. Operator actions opening or not opening ADS4 valves
17. Operator action on temperature measurement (leads operator take actions to prevent vessel failure)

VI.3 Process for Developing an IBLD

The logical representation of the TH phenomena and human actions is achieved through developing an Integrated Behavior Logic Diagram (IBLD). In an IBLD, the causal and logical relationships between cause and consequences of certain phenomena or human actions are presented. This diagram can quantify the severity and frequency of occurrence of certain phenomena under various plant state conditions. Likewise, the probability of passive safety system failure induced by the phenomena or human actions can also be quantified. The

purpose is to use the logical link between the passive safety system, TH phenomena, and human interactions to predict the true system behavior under accident condition.

The principles of developing an IBLD is demonstrated in this section, using water hammer in DVI line as an example. The following is the procedure used to develop an IBLD:

1. First, an important TH phenomena is identified. This phenomena may have the potential to induce passive safety system failure, or to lead to human action which in turn will impact the passive safety system performance. In the example, water hammer in DVI line is identified as the TH phenomena.
2. Second, the causal factors that contribute to the phenomena and human actions are identified. For example, the presence of vapor and cold water in DVI line is part of the causes for water hammer.
3. Third, the plant states that affect these causal factors are identified. For example, plant state for downcomer water level drops to below top of DVI line provides the condition for one of the causal factors, vapor in DVI line, to exist.
4. Next, the logical consequences that can be induced by the phenomena or human action are identified. In the example, the consequence is pipe break.
5. These causal relationships between the cause, the phenomena, and the consequences are formulated into an Integrated Behavior Logic Tree - IBLT, as shown in Figure 6 for the example. This tree provides a simple and clear presentation of the relationships.
6. The details of the relationships in IBLT is captured in an IBLD where they are expressed semi-quantitatively and hierarchically in regard to the severity and likelihood. The IBLD for the example is in Figure 7.

IBLT for water hammer in DVI line is presented in Figure 6. In this figure, the factors that contribute to the phenomena is presented below the phenomena block. The consequence resulted from the phenomena is above the phenomena block. Notice that there are five major factors affecting DVI line water hammer. Thus, co-existence of all five factors provides the stage for water hammer[7]: vapor in DVI line, cold water, flowing through a long horizontal pipe, with low velocity (with low Froude number, Fr. No.), at a relatively high system pressure. For AP600 system design, the cold water coming into DVI line is more than 20°C subcooling. DVI line is horizontal and its length (L) is more than 24 times its diameter (D). Thus, two of the five factors are automatically satisfied.

During a transient, only when downcomer water level drops to below the top of DVI line, can vapor enter the line. Therefore, the water level information from the predicted TH trajectory will determine when this condition exists. The only situation when the DVI line cold water flow rate is low is when either CMT or ACC is injecting water to the DVI line, not both. Therefore, the plant state of having only one of these safety systems functioning during any time is the condition for this factor to be fulfilled. When RCS pressure is higher than 200 psi, damaging water hammer may occur in the DVI line. If the system pressure is lower, water hammer is then mild.

In Figure 7, the same logical relationships that are in Figure 6 are shown in this IBLD, with semi-quantitative values assigned to all the causal factors, the phenomena, and the consequence. This IBLD shows that, when only CMT or ACC is injecting water to the DVI line, DVI line subcooled water flow rate will be less than a critical flow rate Gc. When this is coupled with

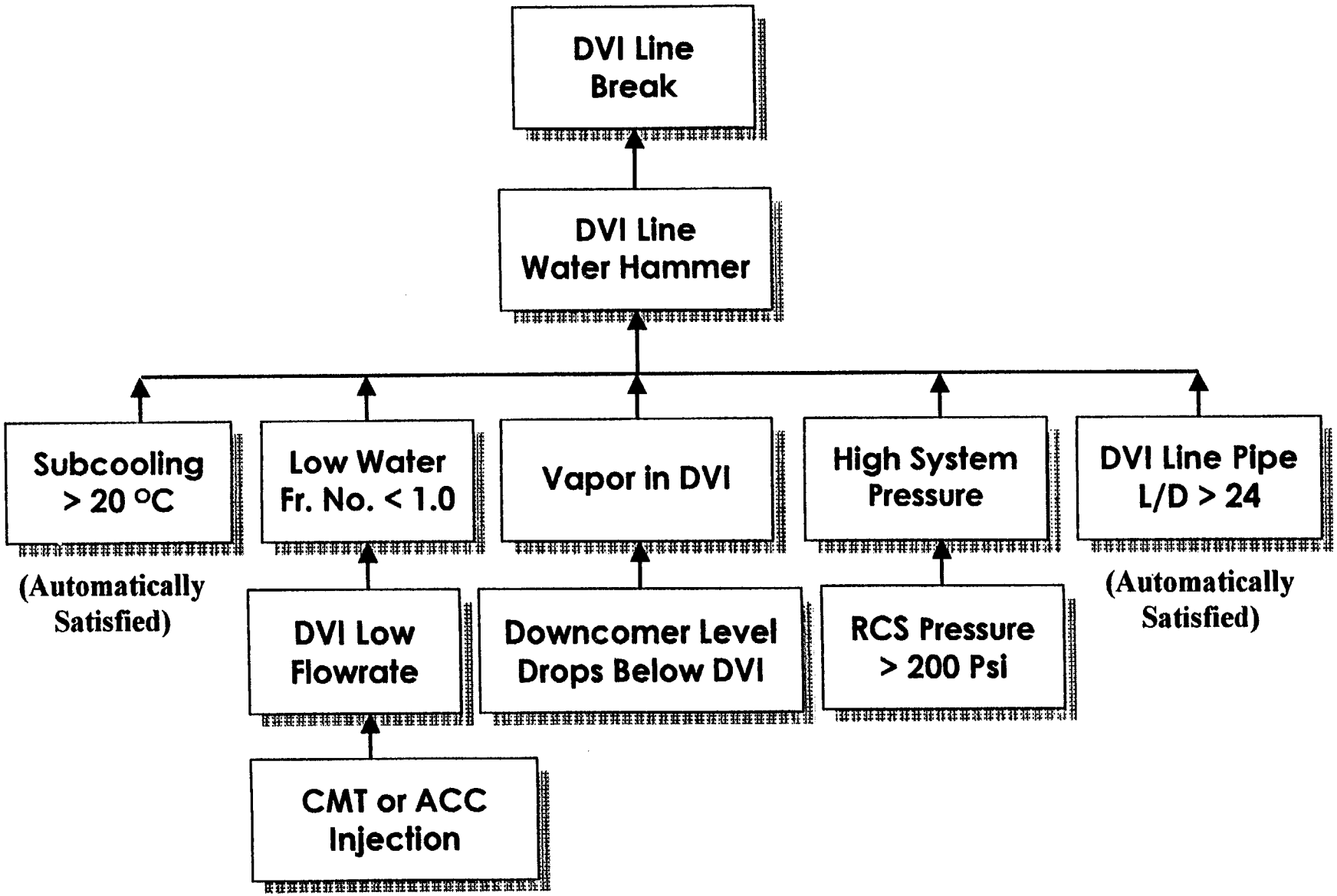

Figure 6. IBLT for DVI Line Water Hammer

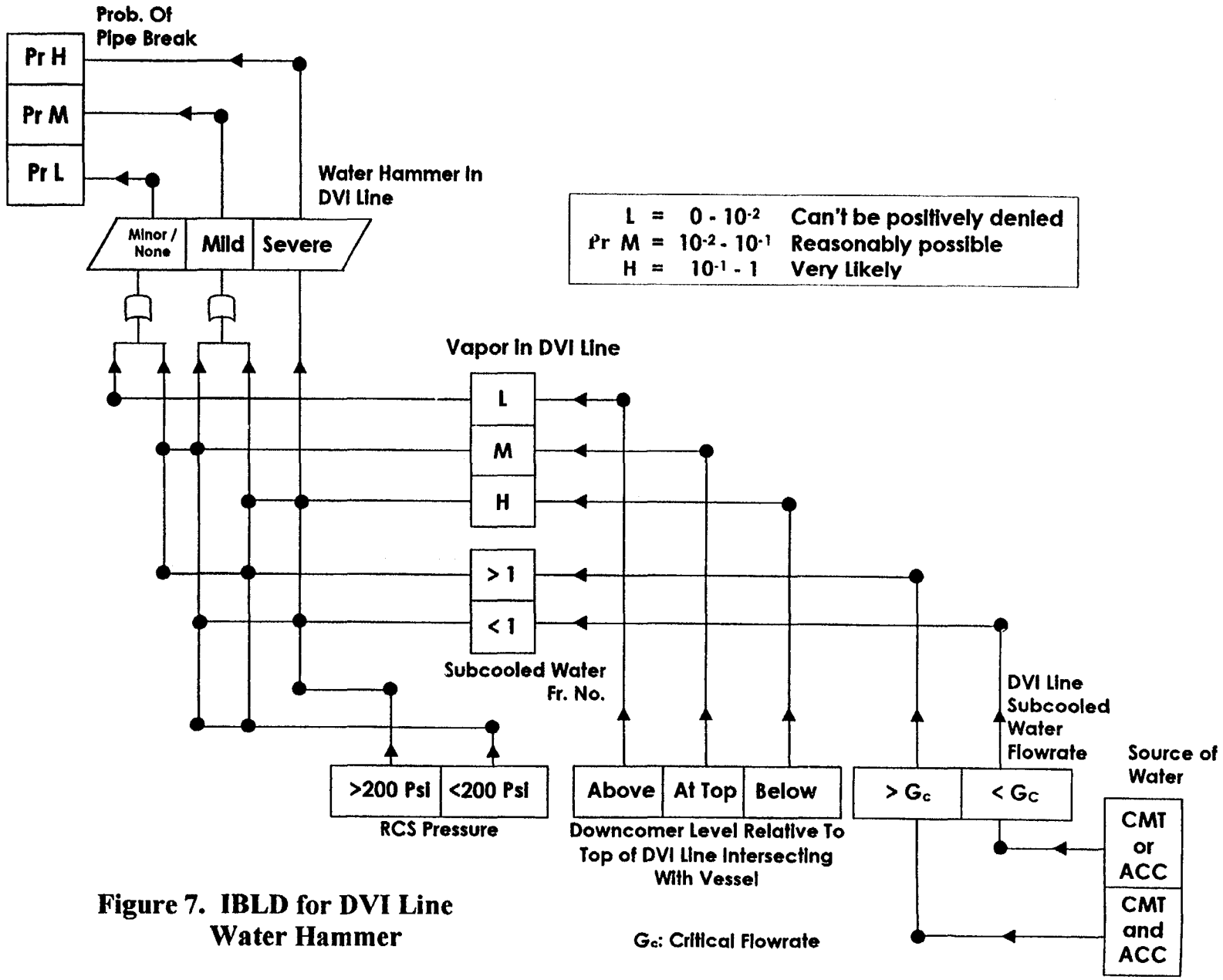

Figure 7. IBLD for DVI Line Water Hammer

downcomer water level below the top of the DVI line and system pressure higher than 200 psi, there is potential for a severe water hammer. Such water hammer is very likely to lead to pipe break (with probability of 0.1 to 1.0).

In the IBLD, the plant states and the information from the trajectory are presented in the lower portion of the diagram (e.g., source of water block and downcomer water level block). The causal factors that are influenced by these plant states and information are presented along left and upward direction (e.g., vapor in DVI line lock). The phenomena of interest is presented in a diamond shape block. The consequences are presented above the phenomena to its left.

In this particular example, if the plant state specifies that both CMT and ACC are functioning and provide cold water to DVI, then the cold water flow rate is higher than the critical flow rate. Thus, the Froude number is larger than 1. If the information from TH trajectory specifies downcomer water level below DVI line, then there is a lot of vapor in DVI line. If the RCS pressure is less than 200 psi, then there will be a mild water hammer in DVI line. The probability of pipe break due to this water hammer is medium. That is, it is reasonably possible that the pipe will break (with the probability of 0.01 to 0.1).

In the IBLD, the likelihood of an adverse consequence is assigned with a probability value. There will be one of three discrete probability values assigned: low, medium, or high. Low probability corresponds to the probability of 0.0 to 0.01 and signifies that the adverse consequence "can't be positively denied." Medium corresponds to a probability of 0.01 to 0.1, and it means the adverse consequence is "reasonably possible." The high probability means the consequence is "very likely" and has the probability value of 0.1 to 1.0.

VII. BDBA SCENARIO IDENTIFICATION PROCESS

In this section, a complete BDBA scenario identification process is demonstrated through an example. Referring to section IV, plant state 2 of SBLOCA with 2 CMT failures has an occurrence probability above the cutoff value. Therefore, this plant state (here referred to as the first generation plant state) is forwarded to TH trajectory prediction and screening.

Figure 8 shows the trajectory prediction for this example. Method presented in section V is used to predict the TH trajectory, shown as the solid line in the figure. The dotted line is obtained from the corresponding AP600 test[8].

The predicted trajectory compares well with the test data up to point t_3. In the AP600 test, since both CMT failed and CMT water level did not decrease, automatic ADS actuation was disabled. Therefore, the test specified that ADS1 was to be manually opened 30 minutes after the CMT actuation signal. When ADS was manually opened, the RCS water was at Cold Leg (CL) level (point t_3). Test trajectory F_0 represents the opening of ADS.

From predicted trajectory, if we visually extend the trajectory from point t_2 to t_3 all the way downward, the pressure at the point where this extended trajectory meets the top of core is higher than the IRWST injection pressure. Therefore, this trajectory points to a high pressure and low mass state and the plant state leading to this trajectory (SBLOCA with 2 CMT failures) is retained after the TH screening. This plant state is forwarded for integration with the IBLDs to identify induced failure and human actions that are associated with this plant state.

The "CMT failure on ADS" IBLD (IBLD #13 in section VI.2) and probability analysis show that ADS1-4 will not automatically actuate because CMT levels do not decrease due to CMT failure; and the probability of this induced actuation

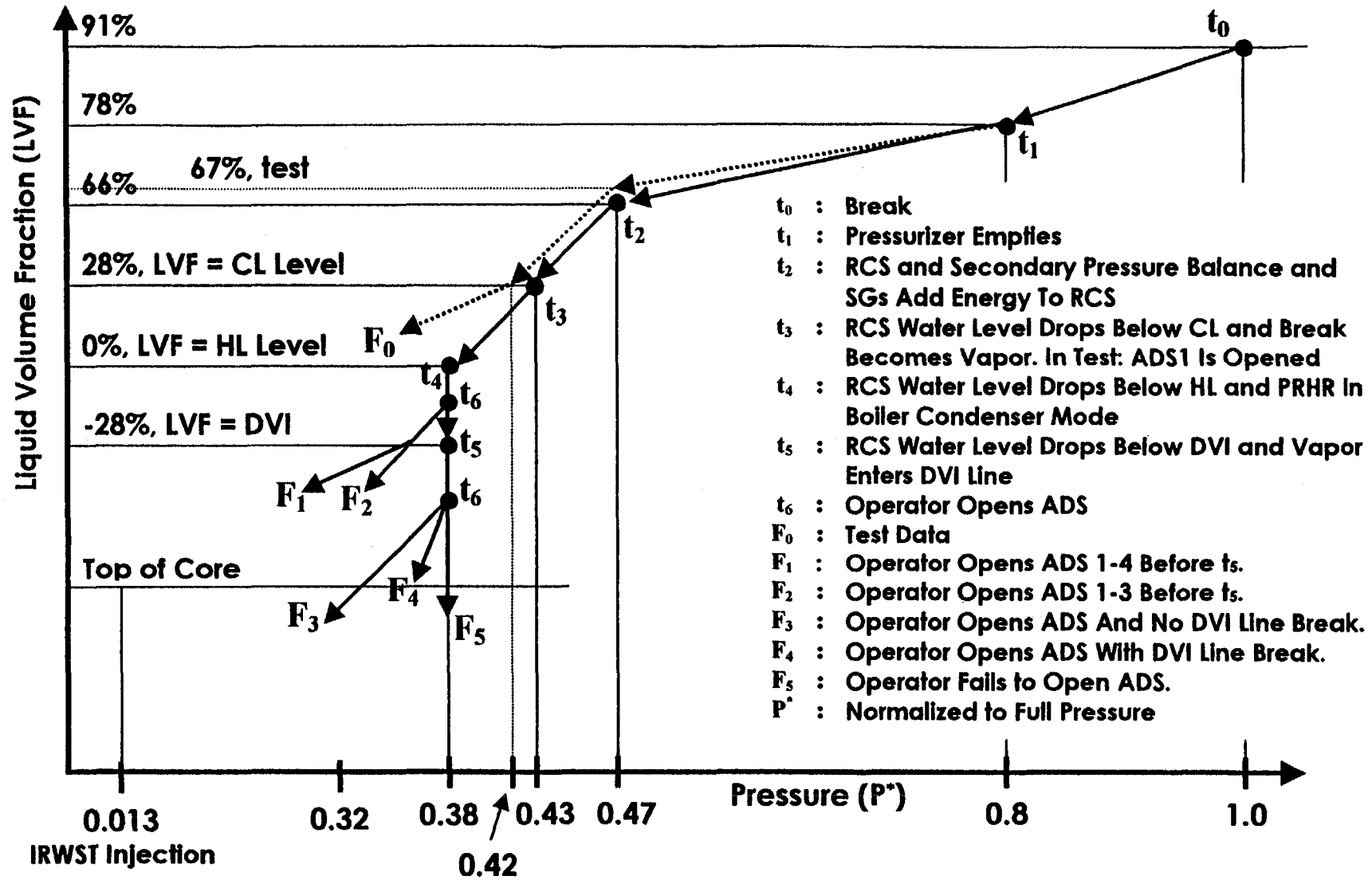

Figure 8. Trajectory Prediction for SBLOCA With Both CMT Failure

failure is 1.0. Therefore, a second generation plant state is identified. It includes SBLOCA, 2 CMT failures, and ADS1-4 automatic actuation failure. The probability of this new plant state is above the cutoff value, and so it is again forwarded for further TH trajectory prediction and screening.

Further TH trajectory prediction shows that, from point t_4 and on, trajectory takes a worsening direction. PRHR heat removal shifts to boiler condenser mode. System pressure reduction is minimized while inventory is continuously lost through the break. The results from TH screening determines that this trajectory and its associated plant state should be retained for further integration with IBLDs.

The "operator actions opening or not opening ADS valves" IBLDs (IBLD #15 and #16 in section VI.2) shows that, once the water level drops below the bottom of Hot Leg (HL), ADS1-4 may be manually opened by the operator. These IBLDs are based on reference 6 which states that if ADS is not opened and CMT level is not below the ADS set point, the operator can open ADS1-4 if the hot leg level measurement indicates low level (at the bottom of the HL). This is the third generation plant state: SBLOCA, 2 CMT failure, ADS automatic actuation failure, and ADS manual opening. The probability of this new plant state is above cutoff value. Therefore it is retained after PA screening. If ADS1-3, then ADS 4 are opened by the operator, the trajectory is F_1. Although ADS1-4 are opened and RCS pressure is relieved, since the opening of ADS1-4 is at a much higher pressure and low inventory state, it is possible that the core may be uncovered at the time the RCS pressure drops to IRWST injection pressure.

IBLDs #15 and #16 also show that, given that ADS automatic actuation has failed, CMT levels remain high, and indicated hot leg level is low, the operator may not choose to manually open ADS1-3, or ADS4 before water level drops to DVI line (point t_5). If ADS1-3 is manually opened but ADS4 is not (which constitutes another third generation plant state), the TH trajectory will follow F_2 which indicates that RCS pressure does not receive adequate relief while inventory is lost from both break and ADS1-3.

Scenarios represented by both TH trajectories F_1 and F_2 and their corresponding plant states represent BDBA scenarios.

If ADS1-4 are not opened, TH trajectory prediction shows that RCS liquid level will drop to below DVI line (point t_5). Since this trajectory represents high pressure and lower system inventory, it is retained for further IBLD integration.

IBLDs #15, #16, and #5 shows that, operator may open ADS during this stage of the transient. And once ADS are opened, the lowered system pressure will initiate ACC injection. The presence of vapor and cold water in DVI line may result in water hammer in DVI line which leads to pipe break. These new failures, plus the second generation plant state forms the third generation plant states. Since the probabilities of these plant states are above the cutoff value, they are retained for TH trajectory prediction.

Trajectories F_3 and F_4 represent ADS opening with and without DVI line break. These two trajectories may have the potential for core uncovery. They are BDBA scenarios.

Trajectory F_5 represents the case when ADS1-4 are not opened. The probability for plant state representing this trajectory is lower than the cutoff value. Therefore, this trajectory is eliminated.

The above example demonstrates the complete process of identifying BDBA scenarios using TH-PA integration method. At least three generations of plant states have been identified and their probabilities calculated. PA screening was applied for each generation of the plant state. The plant states that survived PA screening are forwarded to continue the TH trajectory prediction. During

this process, IBLDs are integrated with the plant state and TH trajectories. Each time the integration is done, new passive system failures or changes in system status are identified. These provide input to the next generation plant state identification.

As a summary of the example, the BDBA scenarios identified are as followings:

1. Trajectory F_1: SBLOCA with 2 CMT failures and with ADS automatic actuation failure, ADS1-4 can be manually opened at high pressure and lower inventory state. AP600 system response with ACC as the only source of coolant make up before pressure drops to IRWST injection pressure is a BDBA scenario.
2. Trajectory F_2: SBLOCA with 2 CMT failures and with ADS automatic actuation failure, when ADS4 is not manually opened by the operator, RCS system pressure may not be able to reach IRWST injection pressure. AP600 system response under such condition is a BDBA scenario.
3. Trajectory F_3: SBLOCA with 2 CMT failures and with ADS automatic actuation failure, opening ADS1-4 at high pressure and at much lower inventory is a BDBA scenario.
4. Trajectory F_4: SBLOCA with 2 CMT failures and with ADS automatic actuation failure, opening ADS1-4 at high pressure and at much lower inventory, combined with one or both DVI line break is a BDBA scenario.

The following additional insights are drawn from the example:

1. Successful ADS functioning has the ultimate effect on AP600 safety. Using CMT level as the sole trigger to actuate ADS disables ADS automatic functioning when CMT level does not decrease to ADS set point for any reason (e.g., CMT failure)
2. When CMT level does not decrease to ADS set point, operator depends on the hot leg level to determine if ADS should be manually opened. Hot leg level measurement is designed for normal cooldown but now is used as the key for emergency RCS depressurization.
3. In reference 4, accident sequence for SBLOCA with 2 CMT failure and with ADS failure was presented. This sequence has very low probability to occur, because the PRA treated the ADS failure as independent of CMT failure, i.e., the PRA did not make the connection between the dependancy of ADS actuation to CMT level and CMT failure. Therefore, this sequence was not probabilistically important in the PRA. In reference 4, sequence of SBLOCA with 2 CMT failure is also presented. Although this sequence has a relatively high probability to occur, since it does not lead to core damage, it has no contribution to the total core damage calculation. From the example presented in this section, it is seen that, if we do not take credit for human action, SBLOCA with 2 CMT failure is equivalent to SBLOCA with 2 CMT failure and with ADS failure which leads to core damage with a relatively high probability.
4. In the SBLOCA with 2 CMT failure sequence, even if we take credit for possible operator action of opening ADS, ADS can be opened at a much higher pressure and at much lower inventory than was tested. This scenario has relatively high probability to occur and may result in core uncovery. Identifying these types of BDBA scenarios are the objectives of this research. It is through the eyes of TH-PA integration where the beauty from both is in one combined, such objective can be sought, and these types of scenarios can be seen.

VIII. CONCLUSIONS

This paper presented the TH-PA integrated screening method that is specifically developed to identify AP600 BDBA scenarios. This integration captures the strength from both deterministic (thermal hydraulic) and probabilistic (probabilistic risk assessment) analysis and creates a fusion process to produce a powerful method. Using this method, the probabilistically credible and thermal hydraulically important AP600 BDBA scenarios can be identified. Currently, this method has been applied for AP600 cold leg SBLOCA. Its application to other accident initiating events will be completed later.

The application of this method goes beyond AP600. Its further development, refinement, and application in other areas of science and engineering will fulfill the purpose of capturing the true dynamics of the systems. With this method, we are able to further understand the underlying reasons that control the dynamic behavior of the systems. Therefore, we are able to design a better system or improve effectively on an existing one so that they can better serve the purpose we set for them.

ACKNOWLEDGMENT

David Meyer of SCIENTECH, Inc. has contributed to the work of IBLD database combination with the PRA model and deserves the recognition and credit. We wish to thank F. Eltawila, G. Rhee, T. Lee, N. Siu of U.S. NRC; P. Griffith of MIT; J. Meyer, B. Youngblood, D. Prelewicz, D. Reeder, H. Wagage, K. C. Wagner of SCIENTECH, INC.; K. Almenas, Y. Y. Hsu, R. Alamsyah of University of Maryland for many helpful discussions. This work was supported by the U.S. NRC, Office of Nuclear Regulatory Research, Reactor and Plant Systems Branch and was subcontracted from SCIENTECH, Inc. We are grateful for this support. Finally, the views expressed in this paper are solely those of the authors and not necessarily those of the U. S. NRC or SCIENTECH, Inc.

REFERENCES

1. D. Bessette, M. diMarzo, P. Griffith, Phenomenology Observed in the AP600 Integral Systems Test Programs Conducted in the ROSA-AP600, APEX, and SPES-2 Facilities, Dec. 1996 (Proprietary)

2. SCIENTECH, Inc., REVEAL-W™, A Modularized Safety & Reliability Analysis System for Windows™, Version 1.0

3. SCIENTECH, Inc., AP600 PRA Model Using REVEAL-W™, 1997 (Proprietary)

4. Westinghouse Electric Company, Simplified Passive Advanced Light Water Reactor Plant Program, AP600 Probabilistic Risk Assessment, Rev. 6, Feb. 12, 1996 (Proprietary)

5. C.D. Fletcher et al., Interim Phenomena Identification and Ranking Tables for Westinghouse AP600 SBLOCA, MSLB, SGTR scenarios, INEL-94/0061, Nov. 1996 (Proprietary)

6. Westinghouse Electric Company, AP600 Emergency Response Guidelines, Rev. 2, Jan., 1997 (Proprietary)

7. P. Griffith, Screening Reactor Steam/Water Piping Systems for Water Hammer, Nov. 1996

8. Japan Atomic Energy Research Institute, Quick Look Reports for ROSA/AP600 Experiments, and Experimental Data Transmitted via Other Form to the U.S. NRC, 1995 - 1997 (Proprietary)

RELAP5 Code Assessment Using AP-600 Test Facility Data

by

D. A. Prelewicz, S. Lucas, H. A. Wagage, SCIENTECH, Inc.
and K. Almenas, University of Maryland

ABSTRACT

The USNRC has sponsored experiments at both the ROSA-AP600 and APEX test facilities. SCIENTECH and the University of Maryland performed a number of post test calculations for experiments from these facilities using RELAP5 version 3.2.1.2, the version of RELAP5 developed specifically for AP-600 analysis. A number of features and modifications were added to this version of the RELAP5 code to address the unique requirements of the AP-600 advanced passive reactor. These features include, an improved critical flow model (Henry-Fauske) for low pressure, several enhancements to improve void modeling, modeling changes to eliminate artificial flow circulation and improvements in the automatic time step algorithm.

Results for several of the post test calculations were compared to previous calculations performed with version 3.1.4, which did not have code features added for AP-600 analysis. The results indicate a major improvement in the RELAP5/MOD3.2.1.2 calculated core level and break flow compared with RELAP5/MOD3.1.4.

Comparison of the calculation results to test data indicate that, while such key results as the core collapsed liquid level are predicted quite well, there remains a need for further improvement in the fine structure of the predictions. This is particularly evident at low pressure and low temperature conditions. Areas identified as needing further improvement in code predictive capability include modeling of thermal stratification, mass error, natural circulation flow, and condensation and escape of vapor in a liquid pool. The needs for improvement are demonstrated by specific responses from ROSA-AP600 tests AP-CL-05, AP-CL-09, AP-AD-01 and AP-BO-01 and APEX tests NRC-10 and NRC-11.

One feature of the AP-600 analysis that is also addressed is the delicate balance of forces which governs the evolution of the later phases of transients during which the passive safety systems are operating to maintain core cooling. Under these circumstances, slight differences in initial conditions and modeling assumptions can result in significant differences in predicted event timing. Overall performance of the safety systems, however, does not appear to be affected by the differences in timing.

1.0 INTRODUCTION

A number of features and modifications were added to version 3.2.1.2 of the RELAP5 code specifically to address the unique requirements of the AP-600. These features include:

- *Critical Flow.* Addition of the Henry Fauske choked flow model to eliminate the artificial choking of ADS-4 at low pressure.

- *Void Oscillations.* An error in the CHF (Critical Heat Flux) low flow interpolation was corrected. Inconsistencies between the RELAP5 flow regime map and the interfacial friction model were corrected. Oscillations that have been caused by the use of an "ad hoc" liquid interfacial heat transfer coefficient have been corrected.

- *Low Pressure Rod Bundle Void Fraction.* Smoothing the transition between the co-current and counter-current flow regimes has been implemented.

- *Flow Circulation.* Artificial flow circulation in the core and lower plenum has been eliminated by not using the momentum flux terms for these regions of the reactor. This is being done until the incorrect differencing and donating of the momentum flux terms is corrected.

- *Time Step.* Invokes a true Courant time step limitation based on over-extraction of the donor phase.

SCIENTECH and the University of Maryland used RELAP5 version 3.2.1.2 to perform post test calculations to benchmark the code against data from test programs sponsored by the US NRC at the ROSA and APEX test facilities. Results for several of the post test calculations were compared to previous calculations performed with version 3.1.4, which did not have code features added for AP-600 analysis. The results indicate a major improvement in the RELAP5/MOD3.2.1.2 calculated core level and break flow compared with RELAP5/MOD3.1.4.

The post test calculations also indicate, however, that there remains a need for further improvement in the fine structure of the predictions, particularly at low pressure and low temperature conditions. Areas identified as needing further improvement in code predictive capability include modeling of thermal stratification, mass error, natural circulation flow, and condensation and escape of vapor in a liquid pool. Comparison of specific system responses to experimental data from ROSA-AP600 tests AP-CL-05, AP-CL-09, AP-AD-01 and AP-BO-01 and APEX test NRC-10 was used to demonstrate the need for code improvements in these areas.

Code comparisons to experimental data are complicated by the sensitivity of the predicted event timings to slight differences in initial conditions and modeling assumptions. This sensitivity is due to the delicate balance of forces which governs the evolution of the later phases of transients during which the passive safety systems are operating to maintain core cooling. One of the significant events which is very sensitive to small changes in modeling is the start of core makeup tank (CMT) draining. For example, a change of a few degrees in initial pressure balance line (PBL) temperature can shift the start of CMT draining by several thousand seconds. Since automatic depressurization system (ADS) actuation is tied to CMT level, the timing of ADS opening is also affected by when the CMTs start to drain. Overall performance of the

Fig. 1. ROSA-Base-Case Nodalization

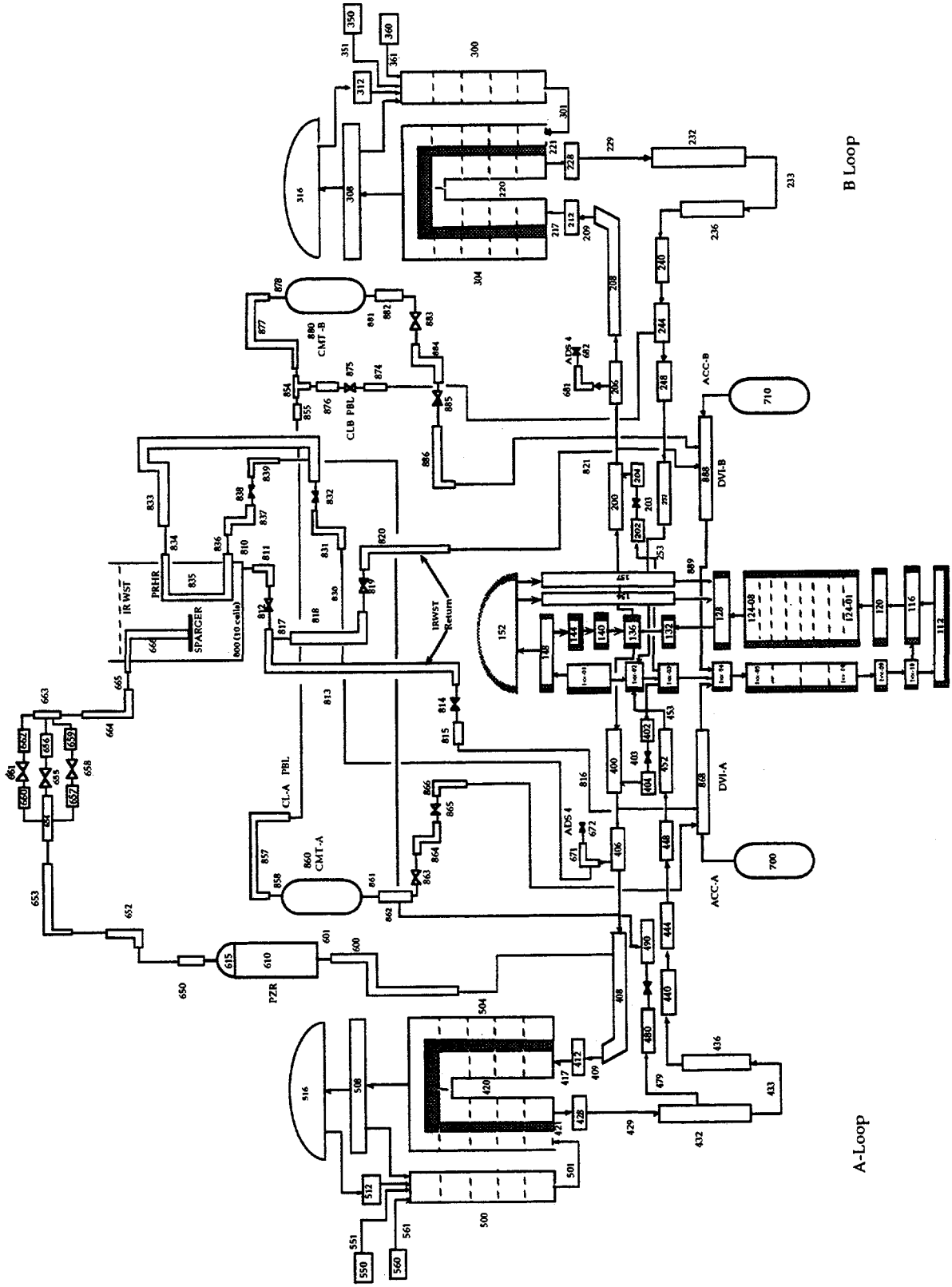

safety systems, however, does not appear to be affected by the differences in timing.

2.0 RELAP5 VERSION 3.2.1.2 BENCHMARK COMPARISONS

Figure 1 shows a nodalization diagram for the RELAP5 model used for the ROSA/AP600 calculations. The model used for APEX calculations is very similar in its level of detail.

2.1 Core Collapsed Liquid Level

The core collapsed liquid level is an important parameter that reflects successful system performance following a small break LOCA since this parameter, in conjunction with the steam flow in the core liquid region, establishes the basic conditions which determine whether the core uncovers and whether heatup will occur. A decrease in the core collapsed liquid level, which reflects an associated decrease in the core two-phase level, can result in core uncovery and fuel heatup. The core collapsed liquid level, in conjunction with the fuel cladding temperature responses, is used to indicate conditions of uncovering the core since there are no measurements of the location of the two-phase level in the core and upper plenum regions.

Figures 2a, 2b, and 2c show the core collapsed liquid level for three ROSA-AP600 tests. For test AP-AD-01, an inadvertent opening of ADS 1-3 valves, the collapsed level predicted by version 3.2.1.2 is slightly improved over the version 3.1.4 prediction. For tests AP-BO-01 and AP-CL-09, predictions of code version 3.2.1.2 are in much better agreement with the data than those of version 3.1.4. For tests AP-CL-09 and AP-BO-01, the model improvements in version 3.2.1.2 were needed to obtain reasonable predictions of core liquid level.

2.2 Critical Flow

Break Flow. Figure 3 compares the break flow calculated for test AP-CL-09 using RELAP5 code versions 3.1.4 and 3.2.1.2. The new break flow model (option 53), which uses the Henry-Fauske critical flow model, shows a distinct improvement compared to the break flow model of version 3.1.4. The version 3.1.4 break flow calculation is consistently low, compared to the data. This contributes to the higher version 3.1.4 calculated pressure when compared to the data and the version 3.2.1.2 pressure calculation. The version-3.2.1.2 calculated break flow is consistent with the data during the subcooled and two-phase portions of the transient.

ADS 1-2-3 Flow. Figure 4 shows ADS 1-2-3 flow which indicates that version 3.1.4 overpredicted the peak flow for test AP-CL-09. There appears to be additional oscillations in the ADS flow in the version 3.1.4 calculation during the low pressure phase of the transient. Apparently, the use of options 55 and 61 in the version 3.2.1.2 calculation has reduced the number of oscillations from the interfacial heat transfer and boiling phenomena. The version 3.2.1.2 calculation captures the peak flow rate in the test, while the oscillations are eliminated during the low pressure portion of the transient.

ADS-4 Flow. Figures 5a and 5b show that version 3.2.1.2 calculated ADS-4 flow is closer to the trends in the data for test AP-CL-09. Because the measured ADS-4 flow was extremely noisy, Reference 1 states that the figures indicate that the comparisons regarding flow are intended for trending purposes only. The magnitudes of the version 3.2.1.2 calculated flow oscillations for ADS-4 are lower than those for the version 3.1.4 calculation which indicates that the new options are contributing to the improved prediction.

Fig. 2a. TEST AP–AD–01: Core Collapsed Liquid Level

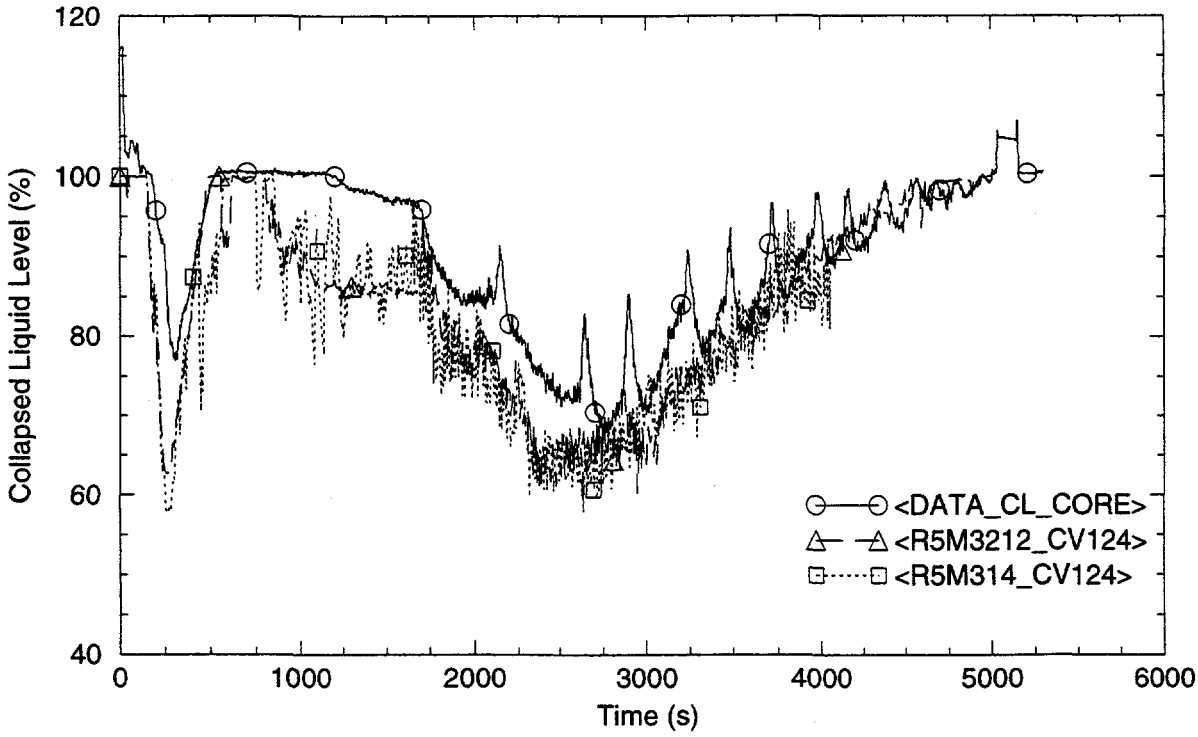

Fig. 2b. TEST AP–BO–01: Core Collapsed Liquid Level

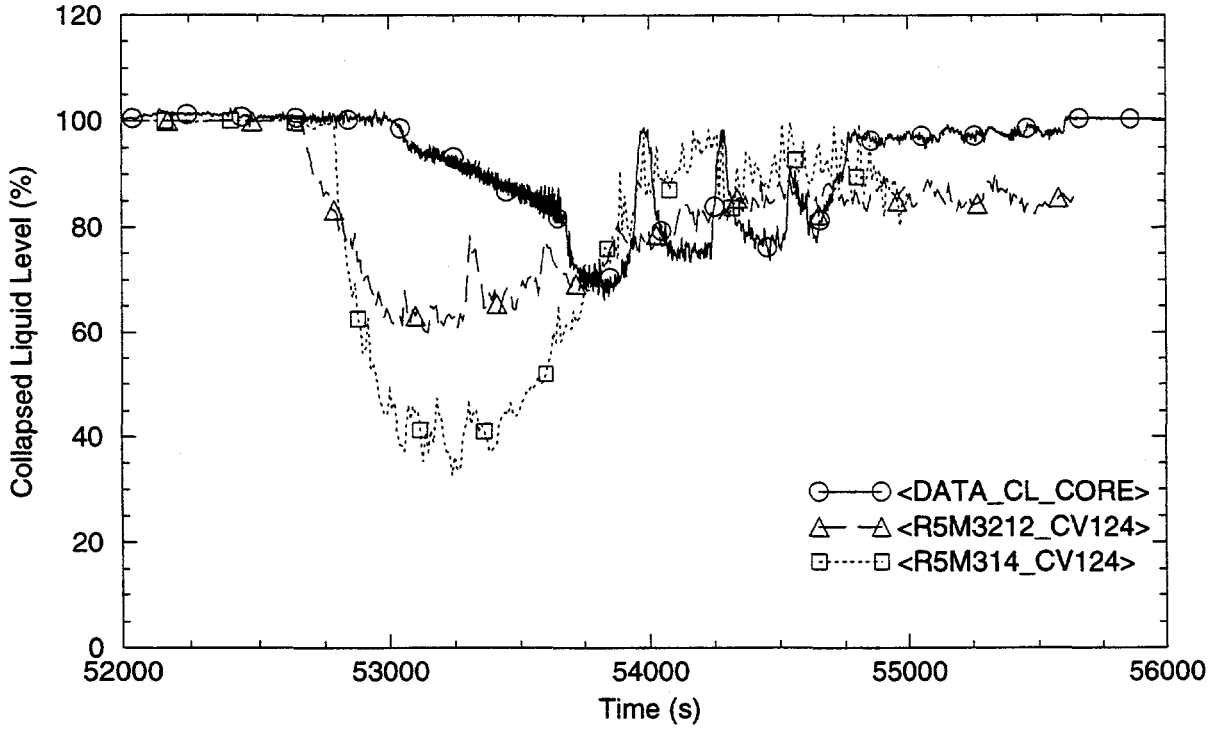

Fig. 2c. TEST AP–CL–09: Core Collapsed Liquid Level

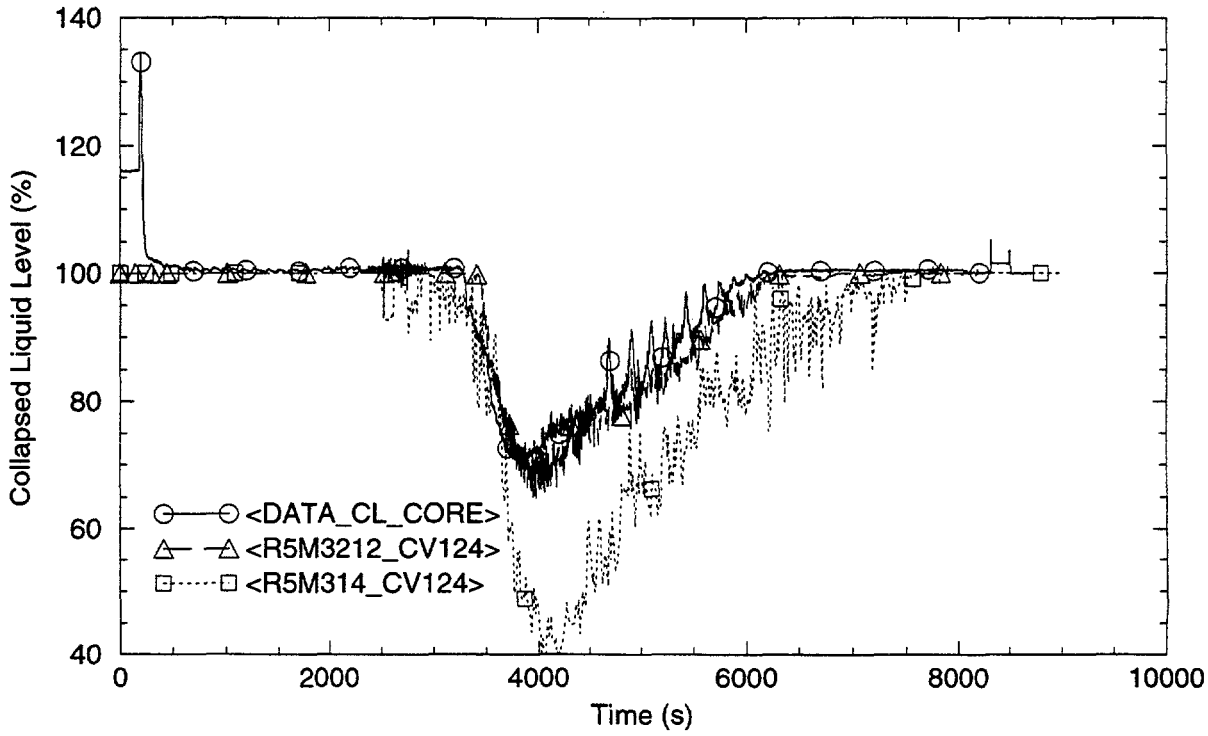

Fig. 3. TEST AP–CL–09: Transient Break Flow

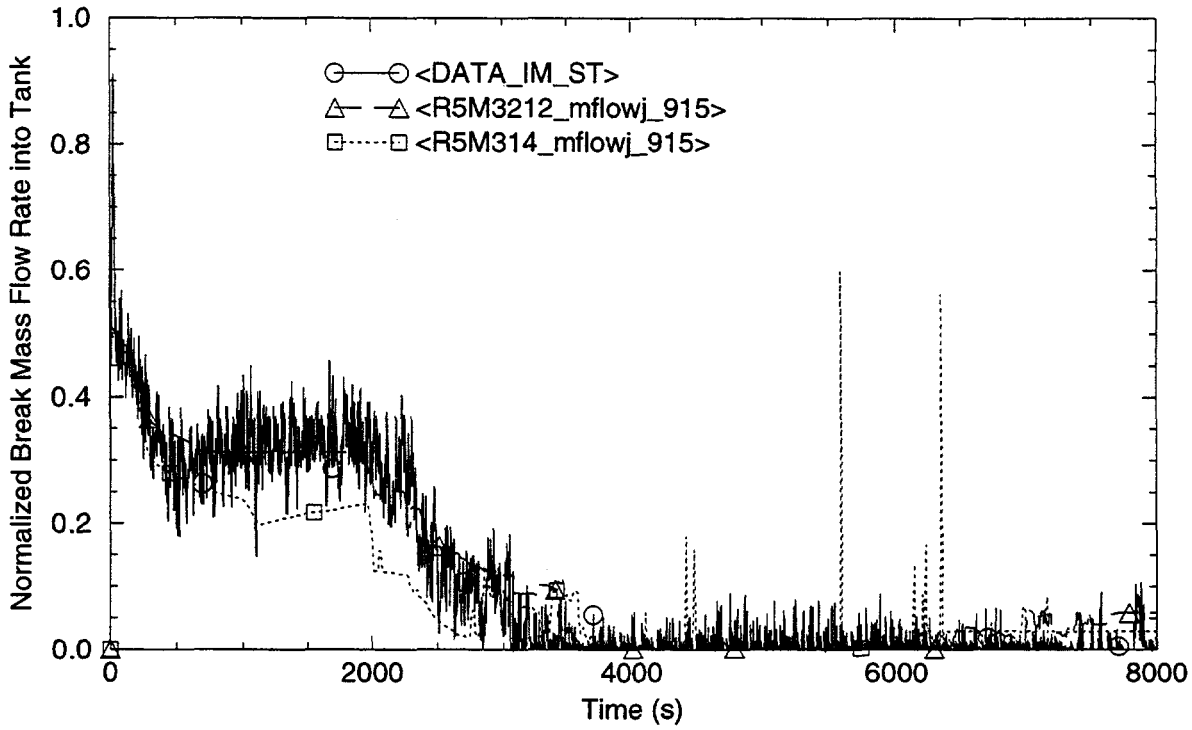

Fig. 4. TEST AP–CL–09: Transient ADS 1–2–3 Flows

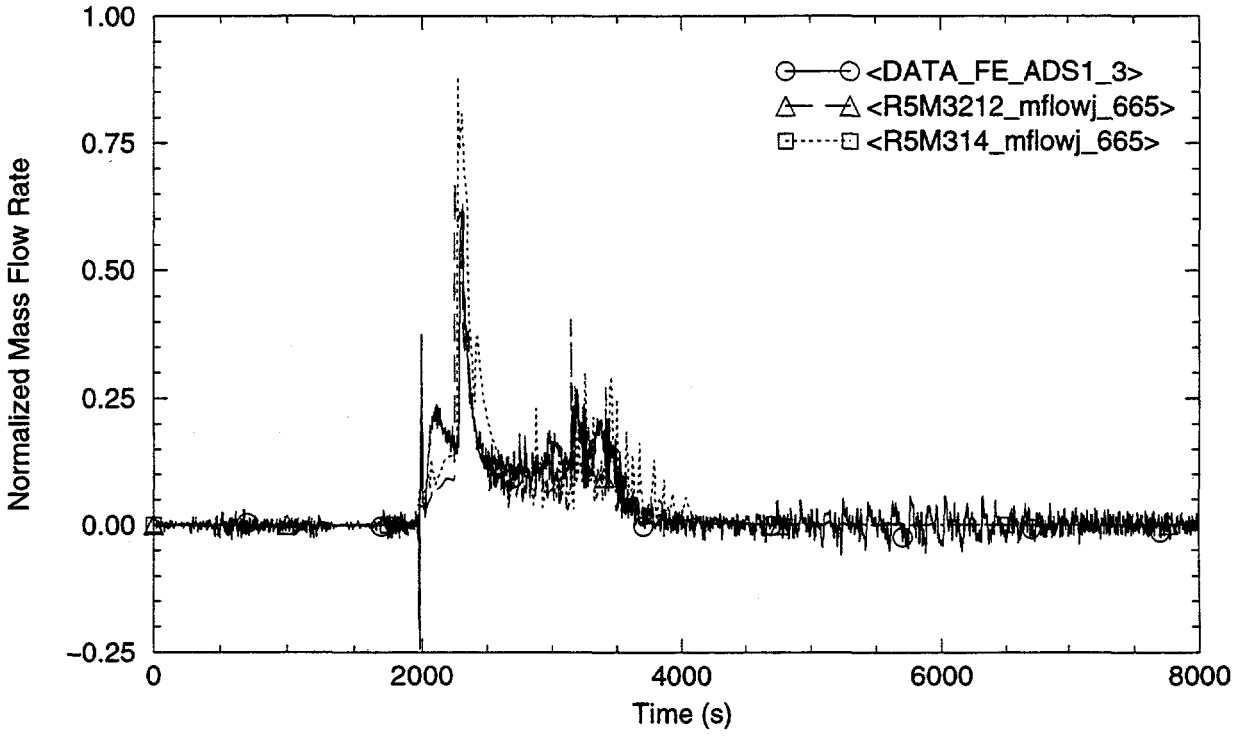

Fig. 5a. TEST AP–CL–09: Transient ADS–4A Flow

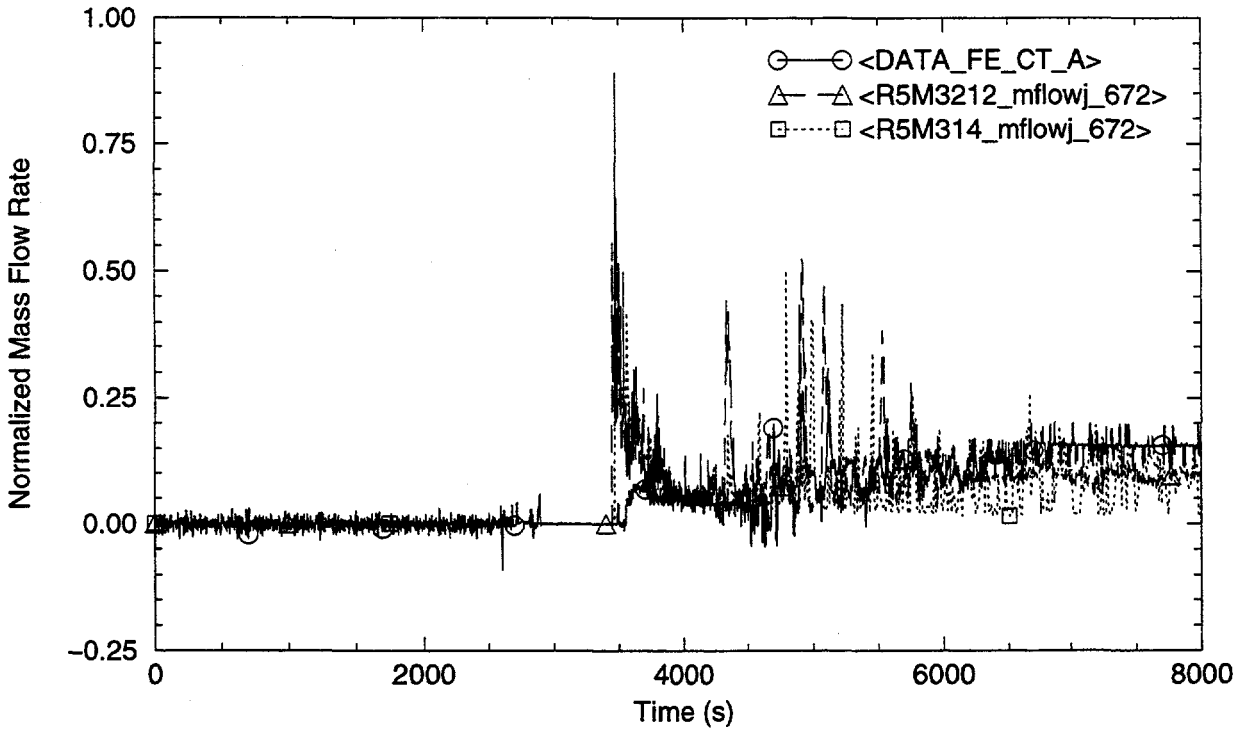

Fig. 5b. TEST AP-CL-09: Transient ADS-4B Flow

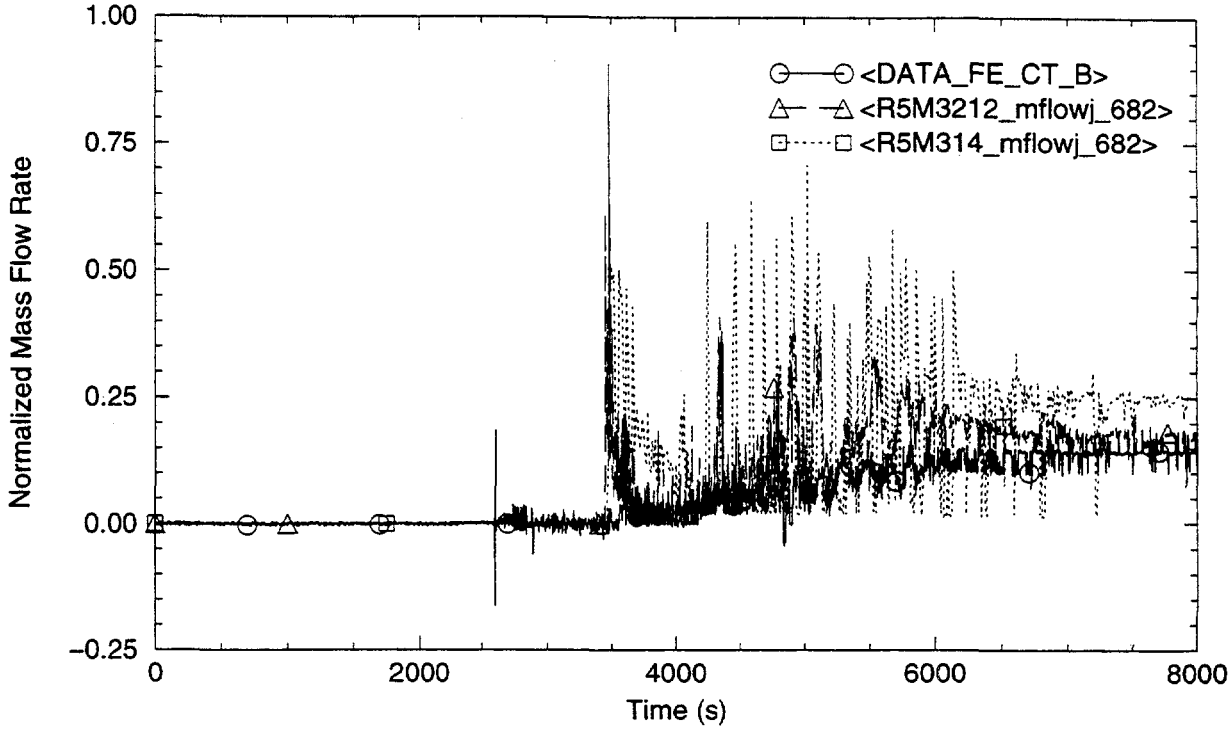

Fig. 6. TEST AP-AD-01: T/C Locations in ROSA P & C Loop Cold-legs

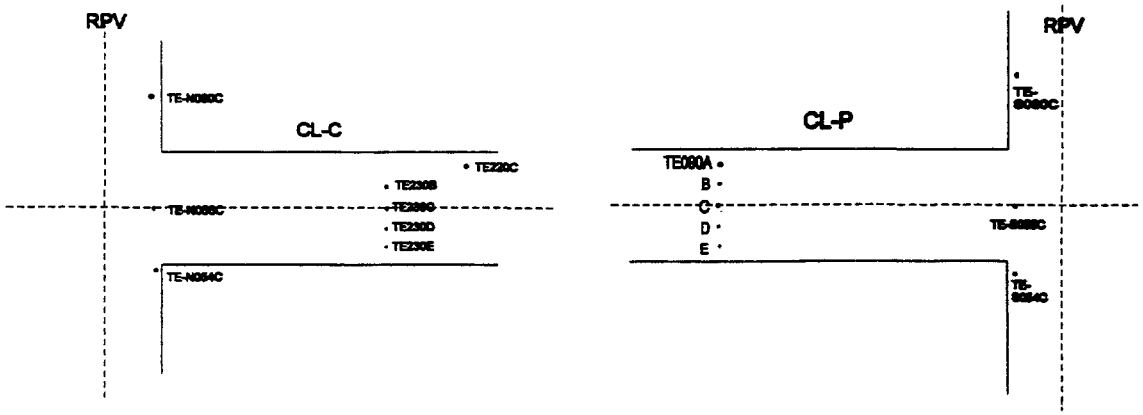

2.3 Code Robustness and Execution Time

Analyses with RELAP5/MOD3.2.1.2 have shown an increased robustness. During the 8,000-second simulation of AP-CL-09 test, RELAP5/MOD3.2.1.2 did not experience a single termination from a property or code failure. The same was true for the 56,000-second simulation of the AP-BO-01 test. Generally, the execution time improved by approximately a factor of five for version 3.2.1.2 compared to earlier code versions such as version 3.2. More importantly, the need for the analyst to coax the run by restarting with a smaller time step following code failures was essentially eliminated, so turn around time was increased by an even larger factor.

3.0 NEED FOR MODELING IMPROVEMENTS

3.1 Cold Leg Thermal Stratification

Thermal stratification in the cold leg can occur either in a liquid solid, a two-phase, or a vapor filled condition. All of these states can occur sequentially over the course of most SB-LOCA transients. In previous assessments most attention has been directed to the liquid-liquid thermal stratification condition.

Thermal stratification in the horizontal sections of the cold leg pipes has been consistently observed in ROSA tests [Ref. 2]. When the measured thermal gradients are large, this is usually an indication that liquid-liquid counter-current flow is present. For example, hot liquid can flow from the downcomer to the steam generator while liquid cooled in the PRHR is flowing counter-currently towards the downcomer in the bottom part of the cold leg. This occurred during test AP-CL-09 but did not occur during test AP-AD-01. Test AP-AD-01 is characterized by an early and rapid depressurization. During depressurization coolant flow velocities are substantial and liquid-liquid stratification in the cold legs did not develop. Within approximately 500 seconds after test initiation primary system inventory decreased sufficiently that vapor penetrated into the cold legs. At this time significant thermal stratification in the cold legs occurred, but it was either two-phase stratification, i.e., vapor-over-liquid or stratification of the vapor phase.

The origin of the fluid within the cold legs can be inferred by observing temperature measurements in the cold leg itself and in the adjacent regions. Figure 6 provides a schematic of thermocouple locations in the cold leg rake and shows the two nearest thermocouples in the adjoining downcomer. Figures 7 and 8 present the measured temperatures in both cold leg rakes for test AP-AD-01. As seen, within approximately 500 seconds the temperature difference between the top and bottom exceeded 100 K and this degree of stratification was maintained for the duration of the test. That this is indeed vapor-liquid (or vapor) stratification can be deduced from the included saturation temperature (the saturation temperature is based on the pressure in the upper plenum) which shows that the vapor phase is in fact significantly super-heated. For selected time segments of the transient, for example 800 to 1,500 seconds and 3,100 to 4,000 seconds, the bottom thermocouples of the P-loop cold leg are covered with liquid. The temperature of the cold leg volume computed by RELAP5 lies at the very bottom of the temperature spread and indicates nearly saturated, or somewhat sub-cooled temperatures. During the periods when sub-cooled temperatures are present, the cold leg is calculated to be liquid filled. The trend of the temperatures in the C loop cold leg (Figure 8) is somewhat different. After approximately 1,900 seconds, liquid did not penetrate into this cold leg and the measured temperatures converged gradually towards a narrower spread of super-heated temperatures. As shown, under these circumstances the RELAP5 calculated temperature diverges even more from the measured values.

Fig. 7. TEST AP-AD-01: CL-P Fluid Temperature

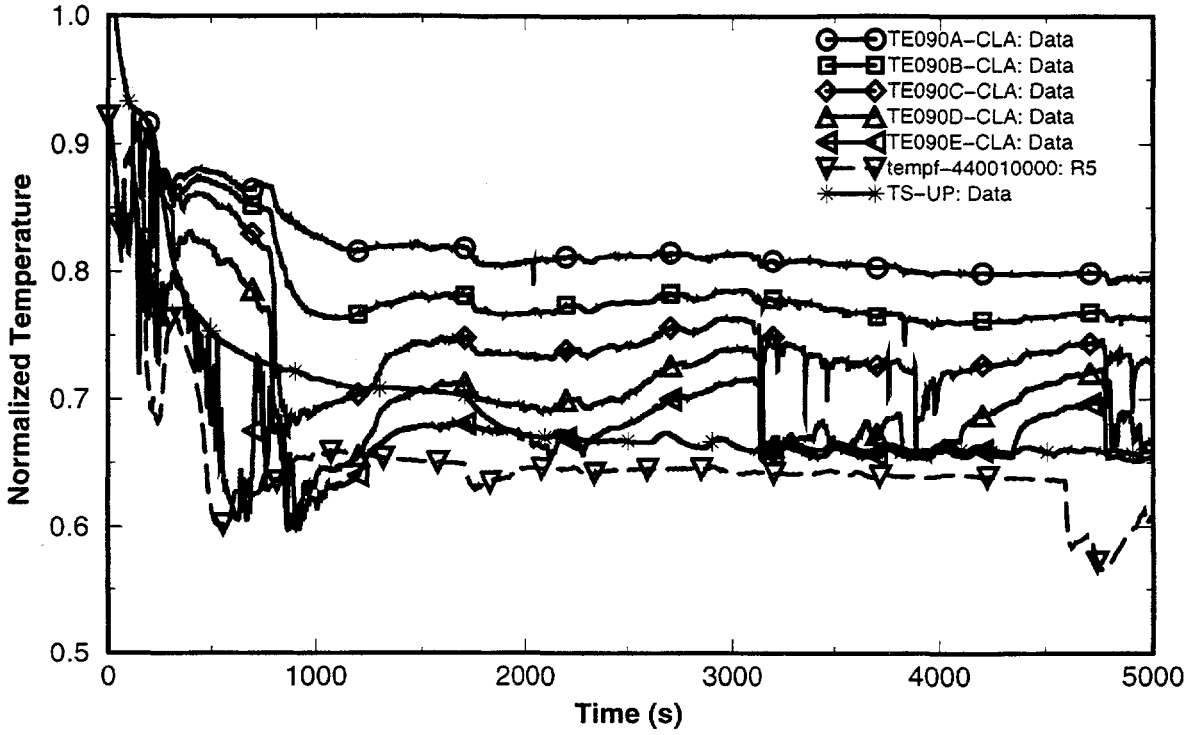

Fig. 8. TEST AP-AD-01: CL-C Fluid Temperature

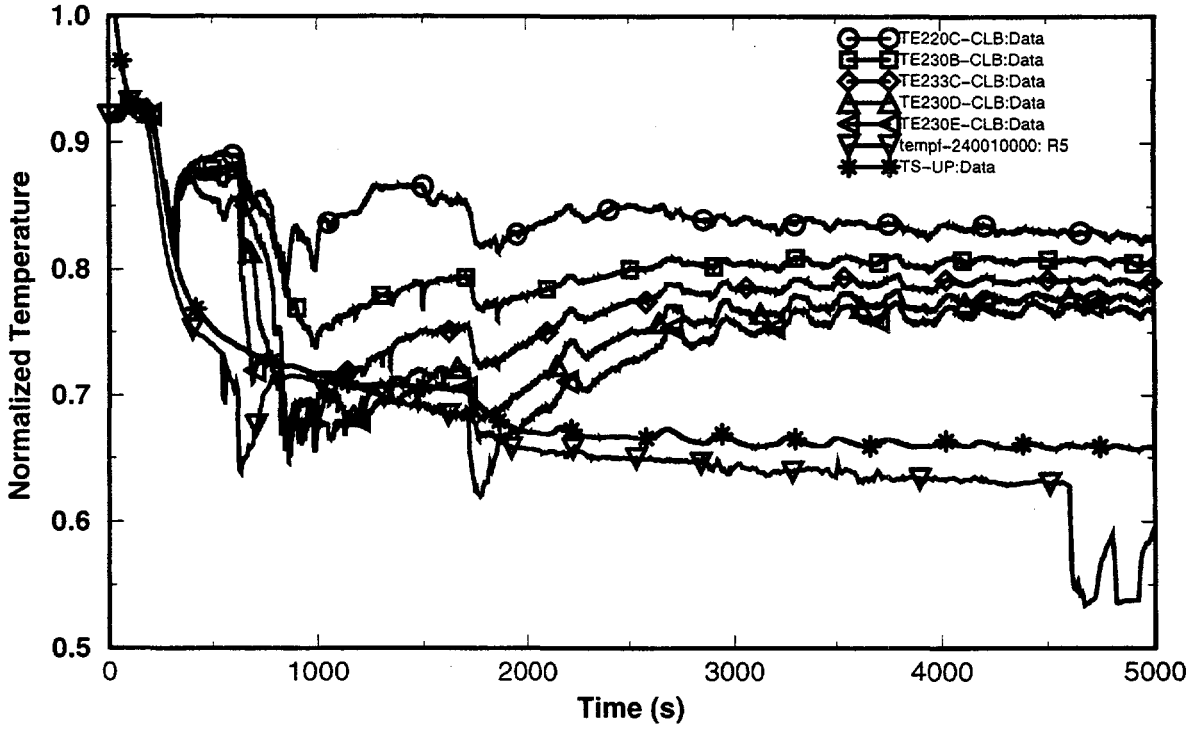

Direct confirmation that the observed temperatures represent either two-phase or pure vapor conditions is given in Figure 9 which shows measured and calculated liquid fractions in both P-and C-loop cold legs. From approximately 200 seconds, experimental coolant density measurements indicate that the cold leg contains predominantly vapor. The calculated trend is qualitatively similar. However, a prominent deviation in the P loop occurs in the 550 to 650 second time frame, caused by a condensation induced pressure perturbation.

The experiment-to-analysis differences documented in the above figures are due to the volume averaged representation of fluid properties by the RELAP5 code and cannot be eliminated. It is therefore appropriate to inquire how large an impact this modeling deficiency has on the key safety related parameters.

Compared to the parameters such as the liquid level and degree of subcooling in the core region, the impact of the failure to model stratification in the cold leg for test AP-AD-01 is secondary. This conclusion is supported by Reference 3 which notes that in spite of the one dimensional representation of the cold leg, evaluation of key performance parameters such as the collapsed liquid level in the core is in general adequate. One reason is that thermal stratification in pipes will develop only for conditions during which flow rates are low. For primary system conditions the densimetric Froude number has to be below unity for liquid-liquid thermal stratification to occur. This implies that for that time segment of the transient during which liquid-liquid thermal stratification is present, the pipes in question do not transfer significant amounts of coolant inventory, and thus do not critically affect the distribution of primary system inventory.

The observations made during RELAP5 predictions of test AP-AD-01 are not typical. In this test coolant loss occurs so quickly that the vapor-steam interface falls to the cold leg entrance level while depressurization is in progress and liquid-liquid stratification never has a chance to develop. For this reason the potential effect of this phenomenon is investigated in more detail by considering two additional ROSA tests, AP-CL-09 and AP-BO-01.

Figures 10 and 11 show the development of stratified temperatures in the cold legs for test AP-CL-09. These figures compare code predictions with the temperatures measured by the cold leg rakes for the entire duration of the test. Two distinct periods of thermal stratification can be observed. The first is a liquid-liquid stratification period which starts around 500 seconds when flows become sufficiently small for stratification to develop and lasts out to about 2,100 seconds when, with the opening of the ADS, depressurization proceeds and the liquid interface decreases to the level of the cold leg entrances. From that time to the end of the test vapor penetrates into the cold legs and vapor-liquid or single phase vapor (in the cold leg of loop C) stratification is present. The two periods can be distinguished by observing the relative position of the saturation temperature line. For the duration of the liquid-liquid stratification period the saturation temperature line is at the top of the temperature spread indicating that the liquid in the pipes is at various degrees of sub-cooling. After depressurization the saturation temperature drops because of the drop in RCS pressure. Figure 10 shows that a stratified vapor-liquid flow regime is present in the P-loop cold leg. In the C-loop (Figure 11) by around 3,000 seconds saturation temperature falls below the measured values indicating that this cold leg is filled with superheated vapor. As the figures show, the RELAP5 computed temperature lies at the bottom of the spread and thus represents either sub-cooled or saturated temperatures.

The analogous measurements obtained for test AP-BO-01 are shown in Figures 12 and 13 which illustrate both similarities and differences. As shown in Figure 12 for this test a pronounced and very long lasting liquid-liquid stratification develops in the P-loop cold leg. As indicated by the superimposed saturation temperature, the temperatures are appreciably subcooled and the RELAP5 computed temperature trace is subcooled to an even

Fig. 9. TEST AP–AD–01: Liquid Fraction in Cold Legs

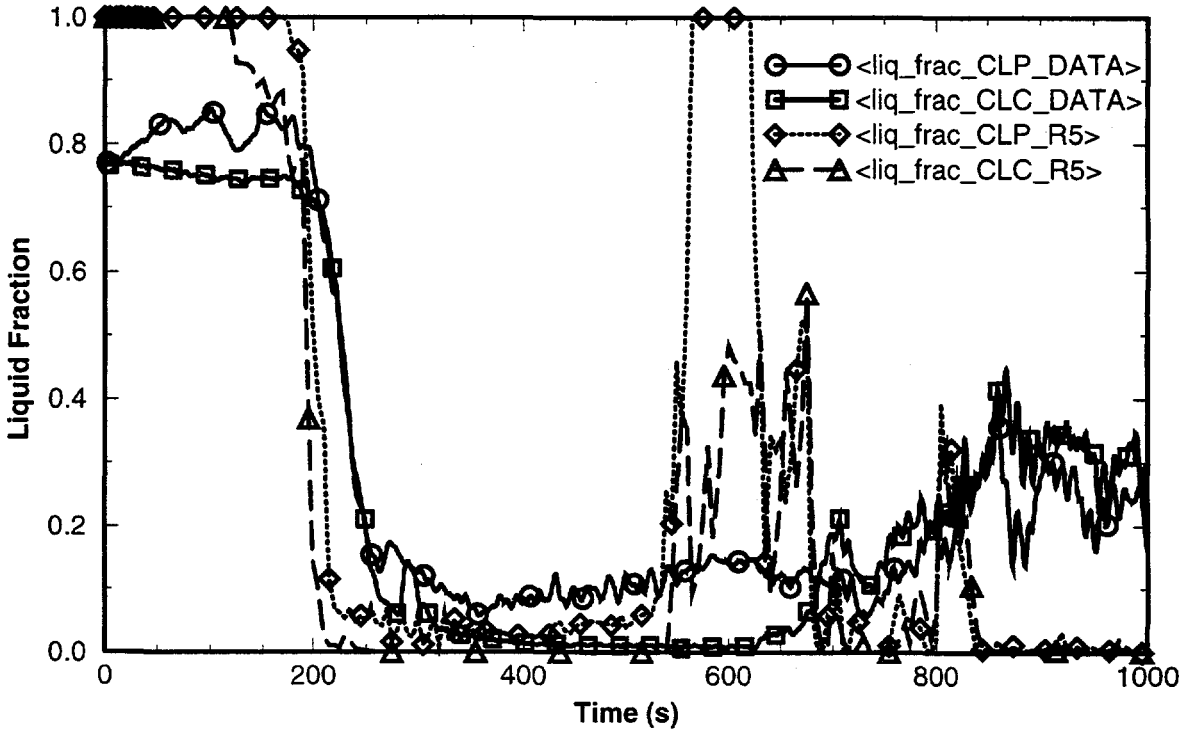

Fig. 10. TEST AP–CL–09: Cold Leg P Temperatures

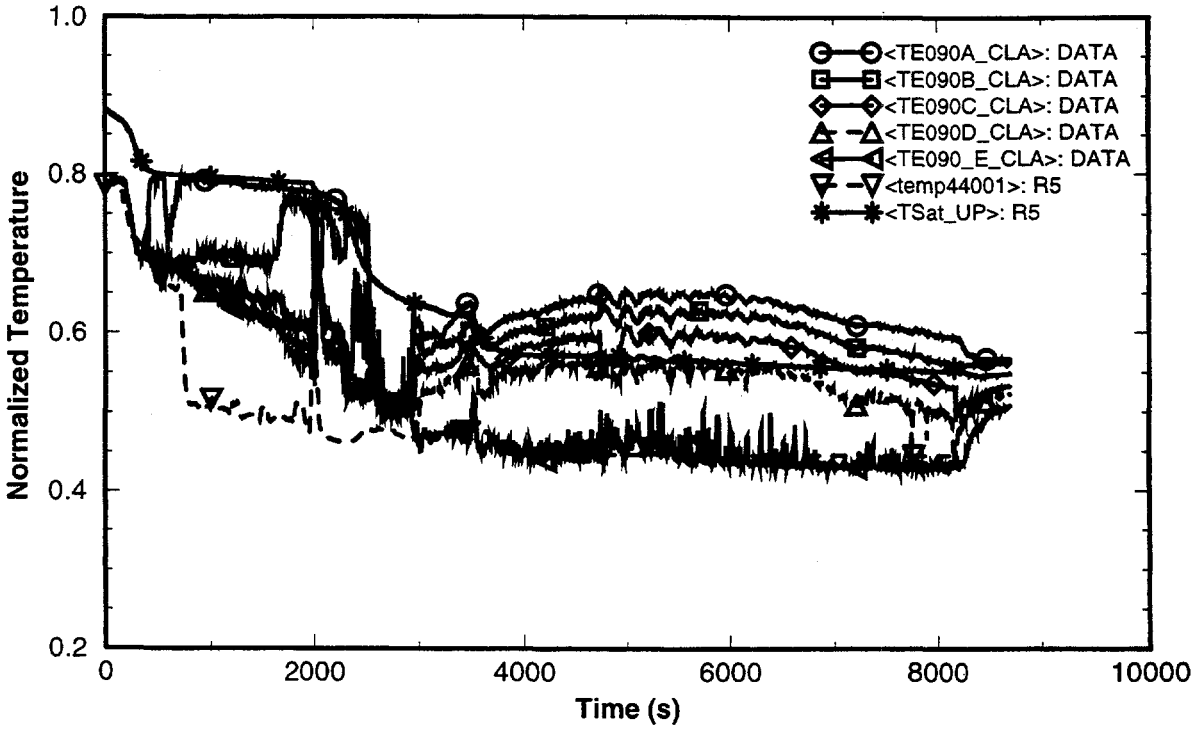

Fig. 11. TEST AP-CL-09: Cold Leg C Temperatures

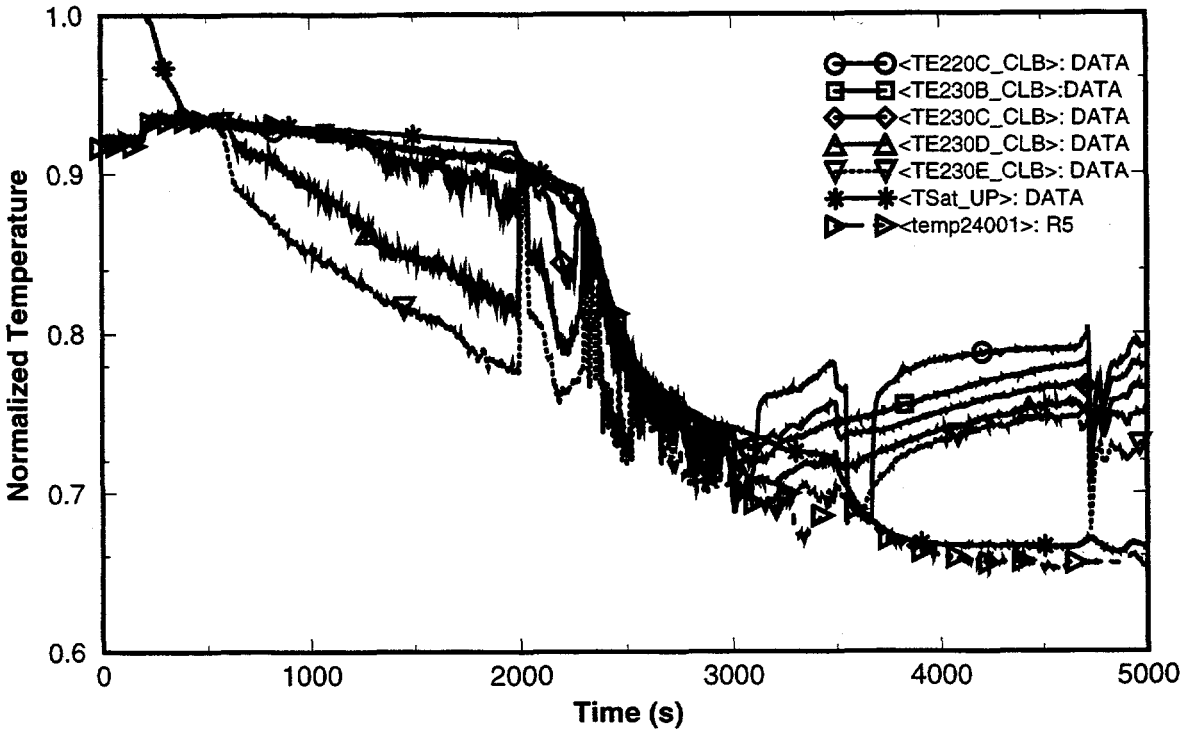

Fig. 12. TEST AP-BO-01: CL-P Fluid Temperature

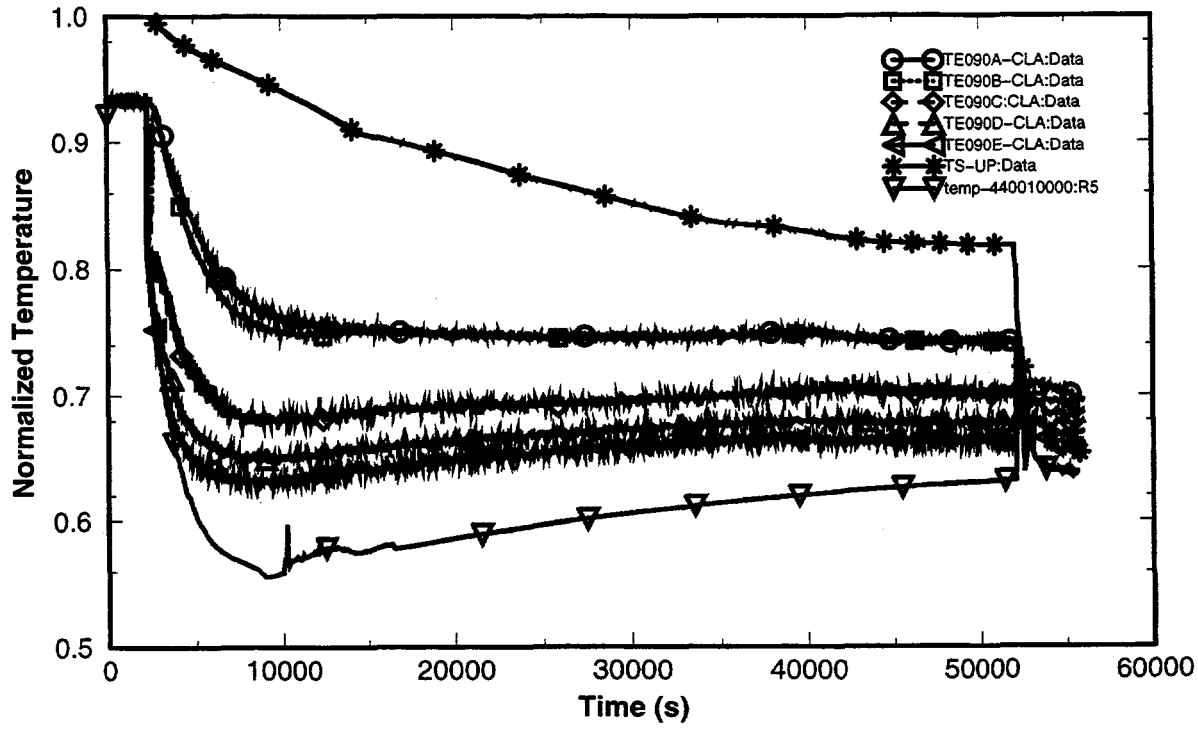

Fig. 13. TEST AP-BO-01: CL-C Fluid Temperature

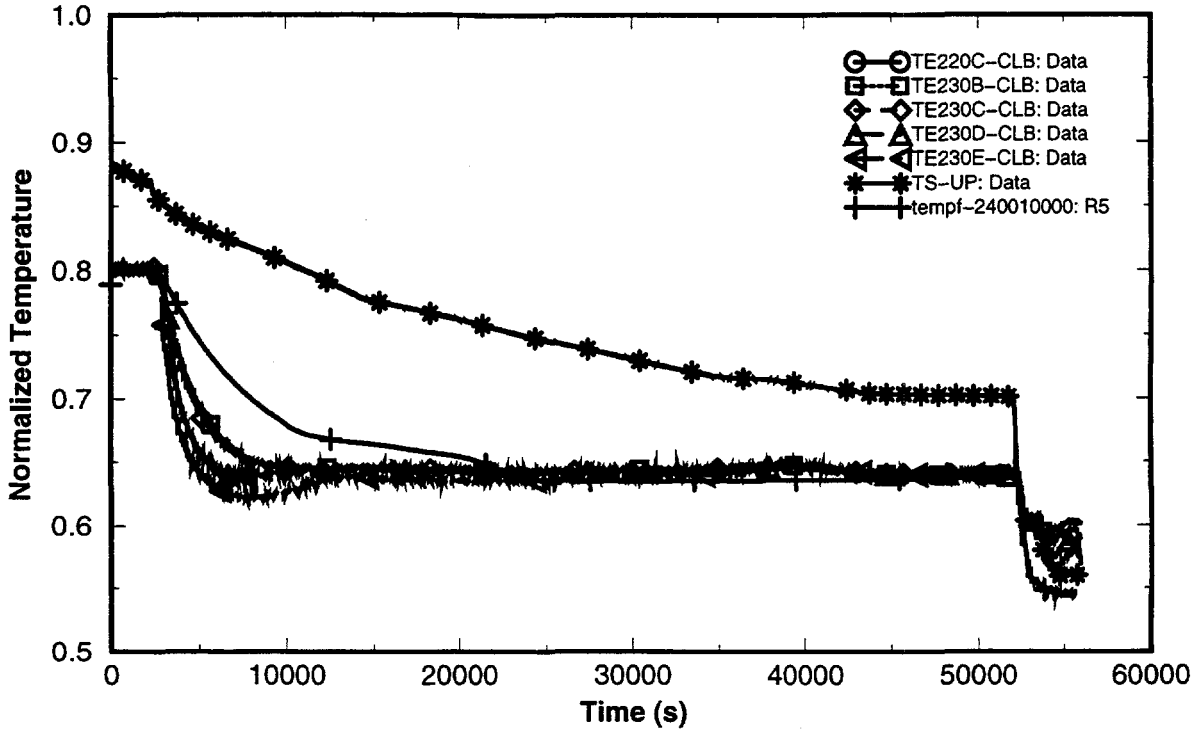

Fig. 14. TEST AP-BO-01: IRWST Collapsed Liquid Level

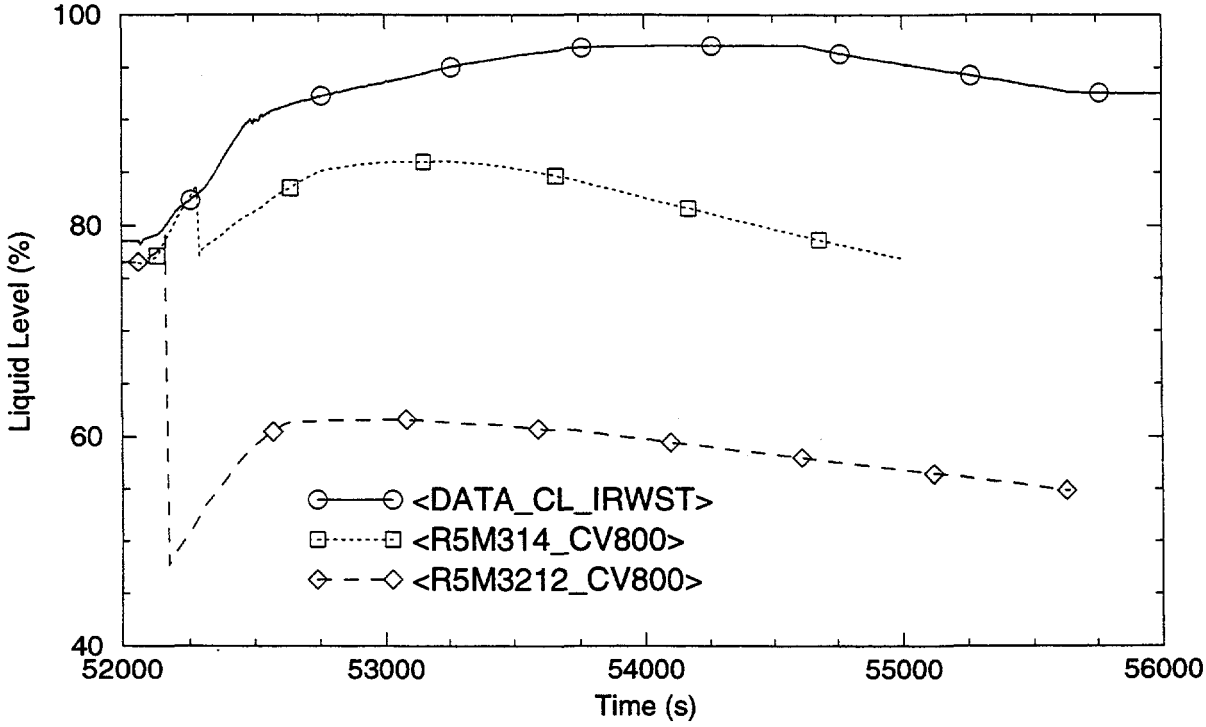

larger degree. On the other hand, the temperature traces for the C-loop cold leg shown in Figure 13 are all nearly coincident indicating that in this loop no temperature stratification developed.

A change in the basic lumped parameter approach used by RELAP5 would be needed to capture the thermal stratification phenomena discussed above. Given that the prediction of key parameters, such as core level and fuel heater temperatures, is not significantly affected by the shortcomings in modeling thermal stratification the need for modeling improvements in this area is of secondary importance.

3.2 Vapor Escape from the IRWST

Both code versions, Mod 3.1.4 and 3.2.1.2, had predicted a rapid mass loss in the IRWST and thus a rapid drop in its collapsed liquid level for test AP-BO-01 as shown by a drop in collapsed liquid level in Figure 14. This was caused by a calculated liquid discharge into the time dependent volume representing the containment. The time dependent volume was intended to receive steam being ejected from the IRWST during boiling and ADS discharge into the IRWST in order to relieve build up of pressure. However, RELAP5 incorrectly predicts that some liquid will be carried with the steam flow. Several sensitivity calculations were performed to find the effect of different RELAP5 models and nodalization on this discrepancy. The RELAP5 models for water packing and choking at the IRWST volume junctions did not have any impact on the above mass loss. However, the RELAP5 model for mixture level tracking adversely affected predictions by increasing the mass loss. Addition of a large volume on top of the IRWST reduced the erroneous prediction of liquid mass discharged into the time dependent volume. Thus a user work around of this basic code limitation is easily implemented.

When the ADS discharges into the IRWST, a large bubble should form, similar to that which occurs in a BWR torus during blowdown. Because the IRWST is modeled with ten nodes, the resulting node size precludes the formation of such a bubble. The bubble is spread out over several volumes and results in the large bubble being characterized by the annular flow regime. RELAP5 does not contain the correct flow regimes nor physics to model this situation. A larger "tank" model is recommended for this situation (i.e., a one node tank with a level tracking capability). This type of model could contain the "bubble" in the tank, rather than spreading it over many volumes and expelling the liquid out of the IRWST to the containment through the vent line at the top of the tank. Alternatively, the interphase drag model could be improved.

3.3 Thermal Stratification in the IRWST

A significant thermal stratification was calculated for the IRWST pool for ROSA test AP-AD-01 as shown in Figure 15. As observed in other analysis to experiment comparisons, the limitations of the RELAP5 code and the highly simplified one-dimensional representation of the IRWST result in the calculation of an unphysical fluid stratification. The figure shows that due to local heating by the ADS1-3 sparger and heating by the PRHR heat exchanger, a "cold-over-hot" water condition is created and subsequently maintained. Thus the highest temperature trace shown in the figure (tempf-80006) represents water in a node slightly below the mid height of the tank, while nodes at higher elevations (tempf-80003, and tempf-80004) show temperatures which are significantly lower. The IRWST model used in this representation consists of a single stack of vertical cells and the calculated results reflect the inability of the model to convect fluid inside the IRWST tank.

Fig. 15. TEST AP-AD-01: IRWST Fluid Temperatures

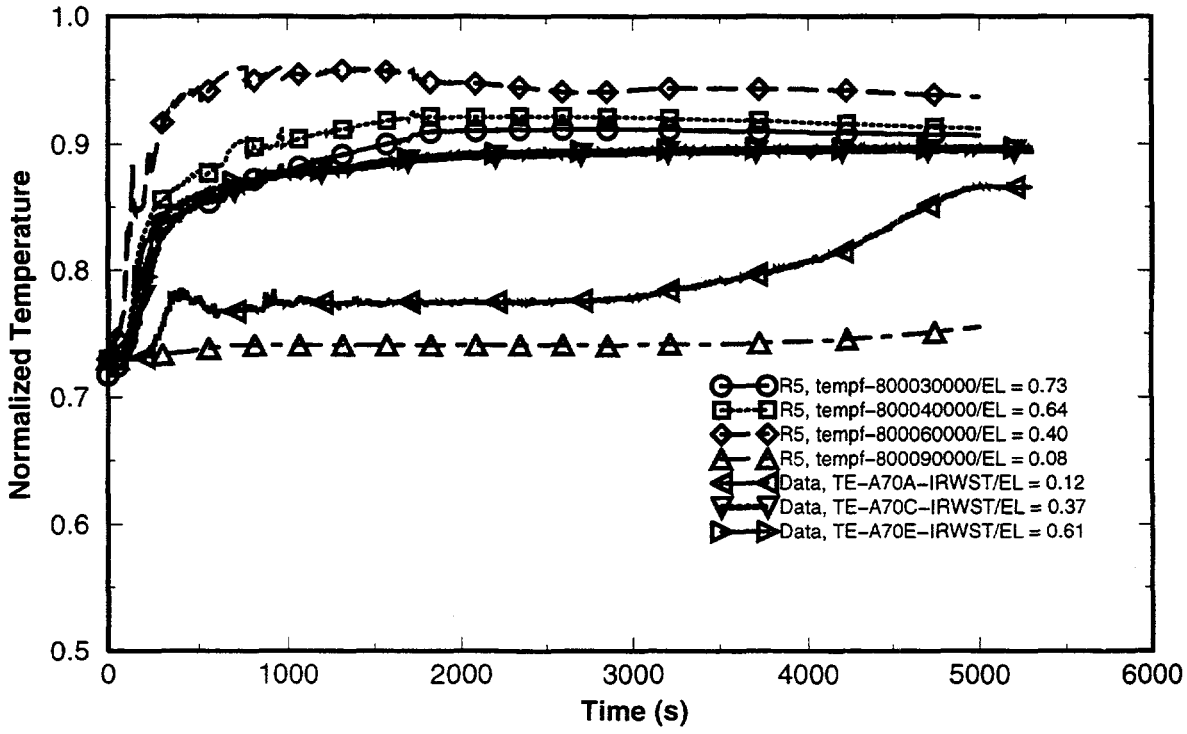

Fig. 16. TEST AP-CL-09: Transient System Mass Error

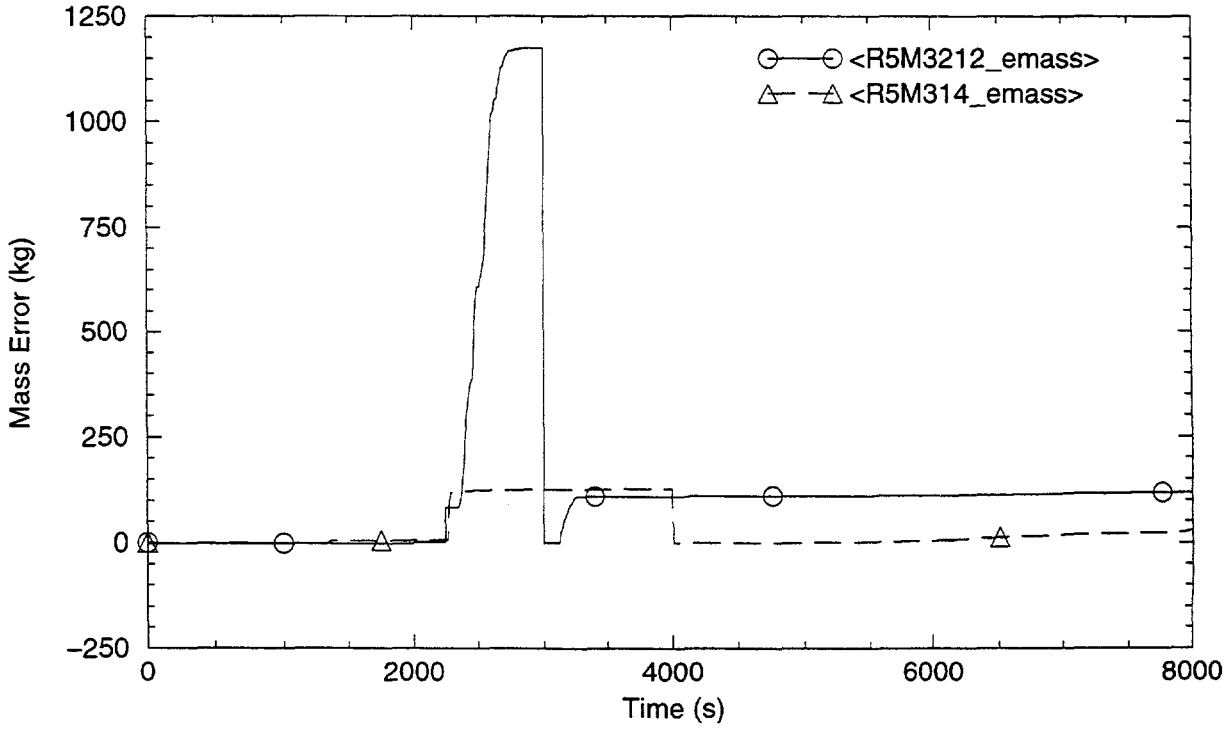

The calculated-to-experiment deviation illustrated above is expected due to the one-dimensional nature of the IRWST nodalization. Potential improvements are theoretically possible if a more detailed nodalization of the IRWST tank is employed. However, modeling is restricted by the inherent limitations of the RELAP5 code.

Thermal stratification in the IRWST can impact the predicted temperature of cooling water which flows to the primary system after the system depressurizes below the static head of the IRWST. However, the effect is minor and can be addressed by performing a bounding calculation.

3.4 Mass Error

Figure 16 shows the system mass error calculated for test AP-CL-09. Both code versions show an increase in mass error which commences when accumulator injection is initiated. The positive mass error is much more pronounced for code version 3.2.1.2. An offsetting negative mass error occurs at the end of accumulator injection and is due to the accumulator component injecting non-existent liquid into the system, resulting in a generation of mass which occurs over a single time step. During the final time step before the accumulator liquid is depleted, a region of the control volume contains gas. However, the value of density donated to the primary system from the accumulator was used as the density of fluid at the interface of the primary system and the accumulator. The fluid at the interface was liquid. Thus, additional liquid was injected into the primary system over a portion of the time step resulting in a system mass error.

There are also additional mechanisms which contribute to the mass error. When steam from ADS 1-3 flow condenses in the IRWST, the steam is most likely being "over-extracted," due to the condensation source term in the mass and energy equations. This over-extraction results in computing a negative vapor (void) fraction which results in a liquid fraction which is greater than unity due to the compatibility condition that the sum of vapor and liquid fractions must be unity. This causes a generation of mass and thus a mass error.

A number of attempts were made to alleviate the mass error that occurred during the calculation for test AP-CL-09. Activating the RELAP5 water packing model for the IRWST component reduced the system mass error, probably by reducing the calculated "over-extraction" of steam described above. Other methods that were examined for the potential reduction of the mass error were use of smaller time steps, option 54, and invoking the level-tracking model. The use of smaller time steps, however, resulted in an increase of mass error during periods of "water-packing" and provided evidence that the water-packing model was not functioning properly or was inadvertently de-activated. Increasing time step and activating the water-packing model decreased the mass error. Option 54 uses implicit ramp functions in the void fraction to anticipate over-extraction of the vapor phase. Use of option 54 resulted in an order of magnitude increase in the mass error. The level model is used to track the two-phase front in a control volume. Activation of the level-tracking model for the IRWST component had no effect on the mass error.

Since the volume of the IRWST is large these calculated mass errors have little effect on the calculation results. Nevertheless, the need for improvement in code performance in this area is indicated. NRC now has a significant effort devoted to resolving mass error problems.

4.0 SENSITIVITY OF EVENT TIMING PREDICTIONS

4.1 PBL Fluid Temperature

The CMTs will begin to empty either when flashing occurs at the top of the tank or when vapor is drawn into the PBL from the C-loop cold leg. Flashing will occur in the CMT when the pressure drops below the saturation pressure corresponding to the temperature of the hottest liquid in the tank. The liquid in the CMT is initially cold. Hot liquid enters the top of the CMT after natural circulation flow through the CMT begins. The temperature of this hot liquid entering the CMT from the PBL and the mixing of this liquid with the cold water in the CMT determines when flashing will occur, and hence when emptying will begin. One would expect the timing of the start of CMT emptying to be sensitive to the predicted temperature of liquid entering the CMT from the PBL, and this is indeed the case.

Figure 17 shows CMT level versus time calculated for APEX test NRC-11 for two different initial PBL average temperatures differing by only a few degrees (approximately 3 K). In this test the PBL was preheated to a temperature slightly above the cold leg temperature. The two cases shown correspond to the PBL at the cold leg temperature and at the slightly higher preheated temperature. The difference in the time when emptying of the CMTs is predicted to begin is around 2,000 seconds. Given this sensitivity, it is not surprising that it is quite difficult to consistently obtain a good prediction of when CMT emptying begins.

4.2 Termination of Natural Circulation Flow

Prediction of when flashing occurs in the CMTs depends not only on the initial temperature of the liquid in the PBL, but also on the temperature of fluid entering the PBL from the cold leg. The temperature of the liquid entering the PBL depends on the flow in the C-loop to which the PBL is connected, and also to a lesser extend on the flow in the P-loop, since this flow can mix with the C-loop flow.

Figure 18 shows predicted versus measured level in the C-loop CMT for APEX test NRC-10. It can be seen that RELAP5 predicts the start of draining about 300 seconds later than occurred in the test. Note that the initial drop in level is due to heatup and reduced liquid density which affects the differential pressure measurement. Start of draining corresponds to the rapid drop in level.

Figure 19 shows predicted and measured fluid temperatures at the entrance and exit of the C-loop PBL. The exit of the PBL is at the top of the CMT. It is apparent that the predicted temperature is generally slightly lower than the measured temperature. This explains the late prediction of flashing and the start of emptying compared to the data.

To predict the PBL inlet temperature correctly, the loop flows and the energy input and output to the primary system must be well predicted. In the APEX tests there was no direct measurement of flow in the primary system loops. However, the magnitude of flow can be inferred from the measured temperatures at different locations around the loop. Figure 20 shows vessel inlet and outlet temperatures for the C-loop. The divergence of the inlet and outlet temperatures for the test data and the lack of divergence for the predictions indicates that natural circulation has ceased in the test at around 600 seconds, while natural circulation is predicted to continue well beyond this time. Hence, the predicted PBL inlet temperature is low accounting for the delayed prediction of flashing.

Fig. 17. TEST NRC–11: C Loop CMT Level

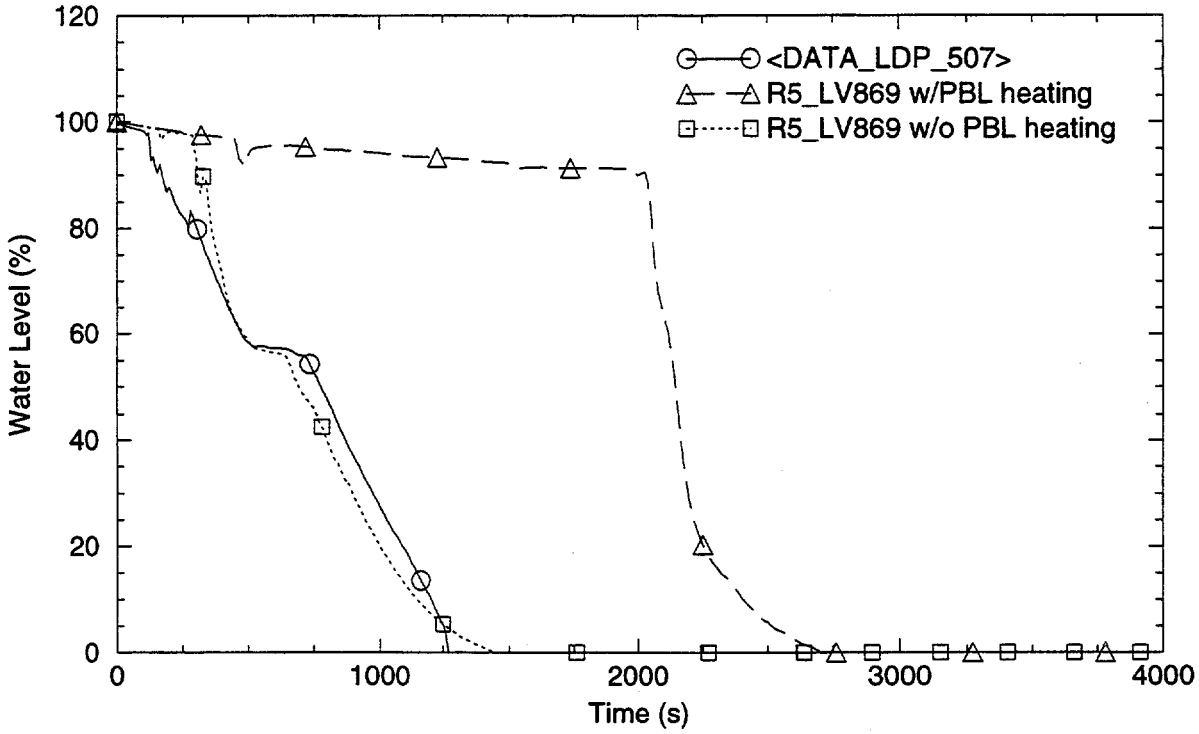

Fig. 18. TEST NRC–10: C–Loop CMT Level

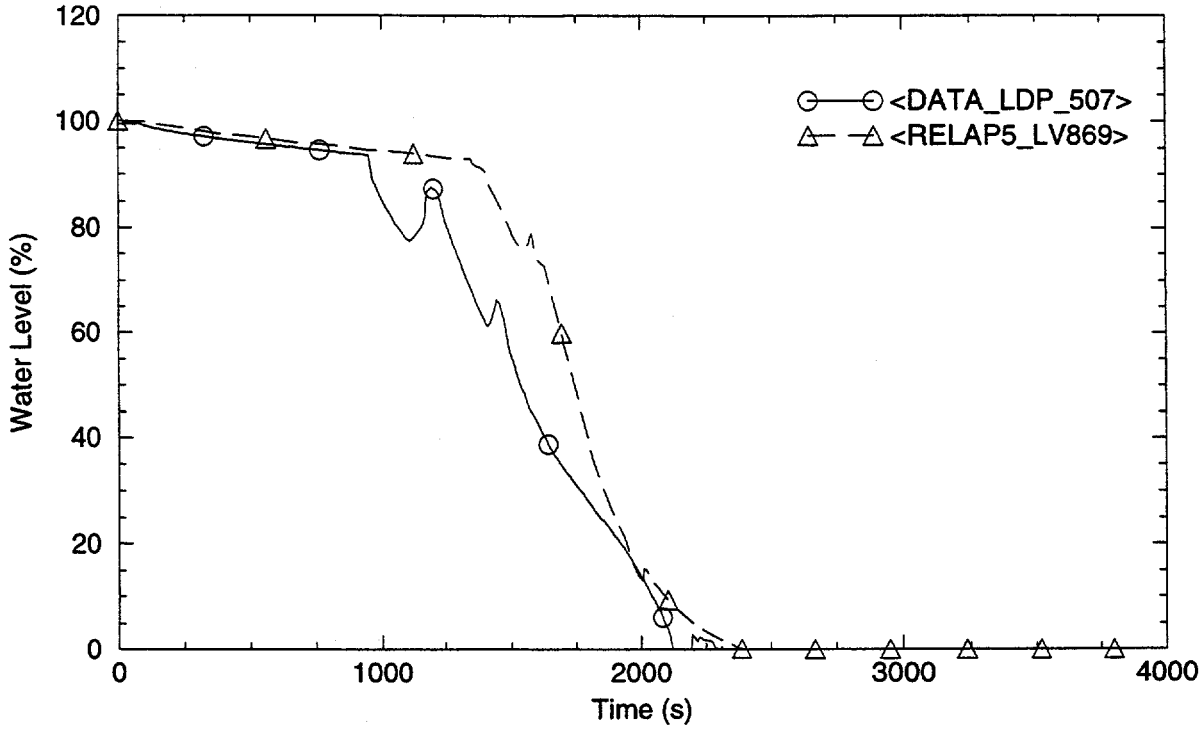

Fig. 19. TEST NRC–10: C–Loop Top of CMT Temperatures

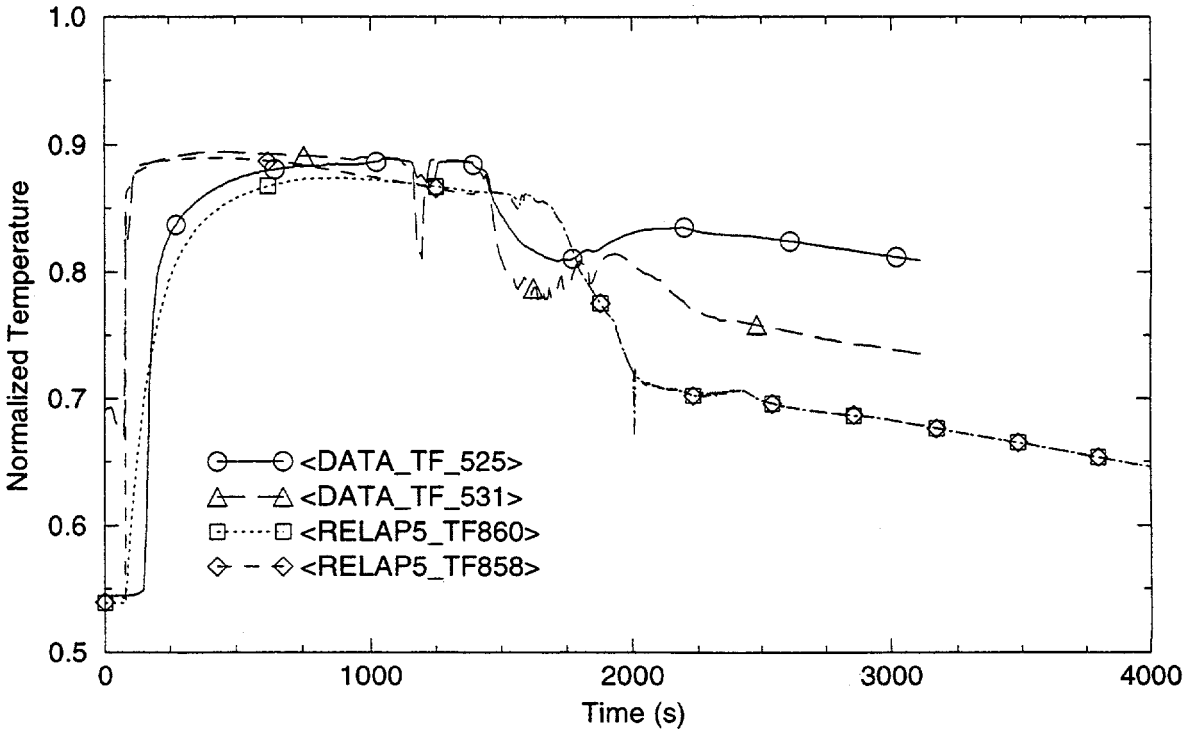

Fig. 20. TEST NRC–10: C–Loop Vessel Inlet & Outlet Temperatures

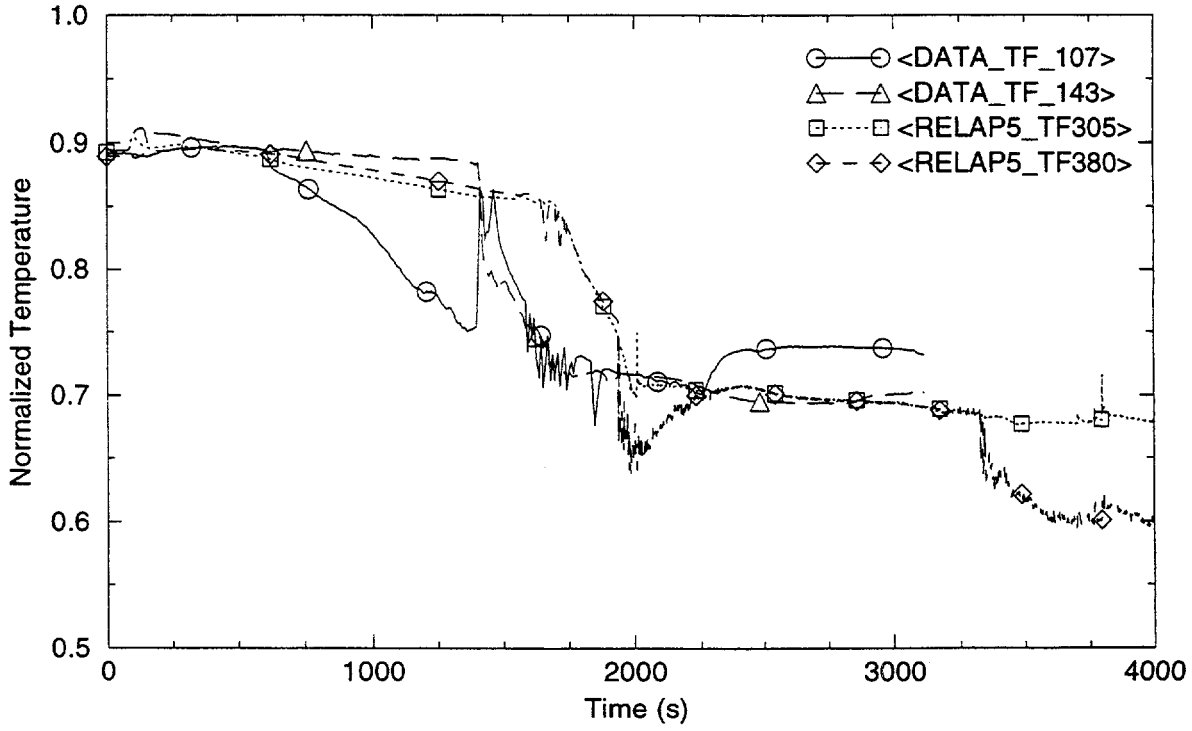

Code limitations in predicting the end of natural circulation flow can significantly affect the timing of events, but the effect on key parameters, such as the core collapsed liquid level, is secondary.

4.3 Condensation on CMT Walls

The computed and measured history of the CMT liquid level for ROSA AP-600 test AP-CL-05 is shown in Figure 21. The figure clearly illustrates that approximately 5,000 seconds into the transient, when both the measured and computed CMT liquid levels reach approximately 40%, a phenomenon occurs in the test facility which is not captured by the model. While the computed draining of the CMTs proceeds at an unchanged rate, the actual CMT draining rate first slows down, then stops entirely. Subsequently, for a time period exceeding an hour the CMT liquid level remains essentially constant. During this time the primary system pressure falls below 1 MPa which triggers the opening of the ADS-4 in the calculation (this is a ROSA test restriction which does not apply for the AP-600 plant). However in the ROSA test, the ADS-4 opening is delayed by the 'hang-up' of the experimental CMT liquid level. The ADS-4 valves are finally tripped when draining resumes and the CMT level in the test facility falls below the setpoint.

The above described phenomenon is caused by a certain mechanical design feature of the test facility CMTs and the approximate manner in which this design feature is represented in the model. This test-to-computation comparison points out the extreme sensitivity of the analytical result to modeling aspects which are usually assumed to be of secondary importance.

Figure 22 shows an approximate schematic of the ROSA CMT and its representation in the RELAP5 model. The ROSA AP-600 CMT is a heavy walled steel cylinder which is bolted together from two unequal height cylindrical sections. As a consequence, at an elevation of around 40% from the bottom there is a quite massive flange and thus a substantial increase in the metal thickness. A thin layer of insulation is added to the walls in order to minimize heat losses. In the RELAP5 model the CMT is represented as an eight segment cylindrical component with two hemispherical ends. The thermal effect of the casing is modeled as a one-dimensional heat structure. This includes the steel wall and the rock-wool insulation. However, the flange located at an elevation approximately 40% of the full height is not modeled.

The mechanism leading to the 'hang-up' of the CMT liquid level was traced to condensation occurring at the CMT flange. As Figure 22 shows, the inlet/outlet taps to the CMTs are at the bottom of the CMT. The entire system thus forms in effect an 'inverted bottle' and the CMTs can drain under two conditions - vapor enters the pressure balance line from the cold leg, or system pressure decreases below the saturation temperature of the liquid in the CMT. In the second case some of the inventory flashes and the generated vapor replaces the draining liquid. If the system is liquid solid up to the cold leg elevation (that is the situation in this case), then only the second mechanism can function. By the time the CMTs start to drain pressure is relatively low and is decreasing slowly. As the CMTs drain down to the level of the flanges, the vapor in the upper half is exposed to a massive, cooler metal structure. At this point the condensation of the vapor on the flange metal leads to a local decrease in pressure that prevents further drainage.

Whether the metal will be able to condense steam depends, of course, on the RCS temperature when the liquid level decreases sufficiently so that it becomes accessible to the vapor. If the thermal time constant of metal is sufficiently small that the hot water preceding the liquid-vapor interface manages to heat it up - no condensation will occur. If the time constant is too large, and the metal remains cool, condensation takes

Fig. 21. TEST AP-CL-05: CMT Liquid Levels
(Nominal RELAP5 Model)

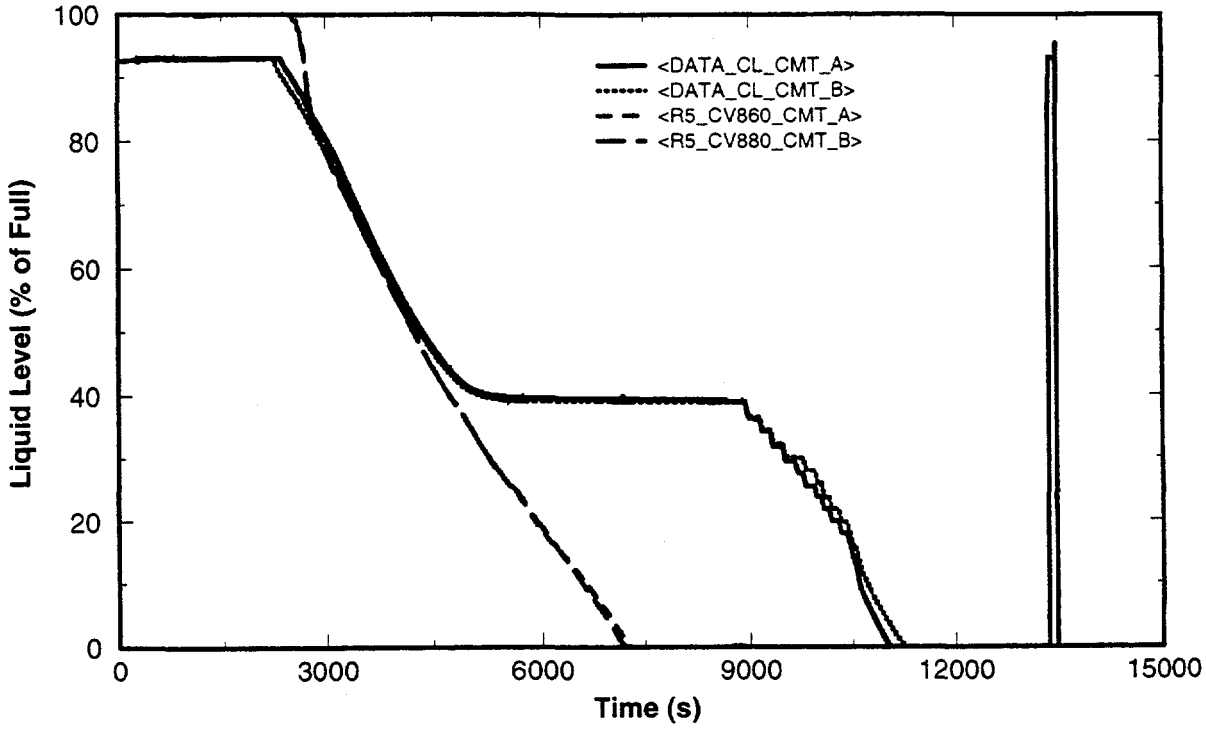

Fig. 22. TEST AP-CL-05: Modified CMT Modeling with the Flange

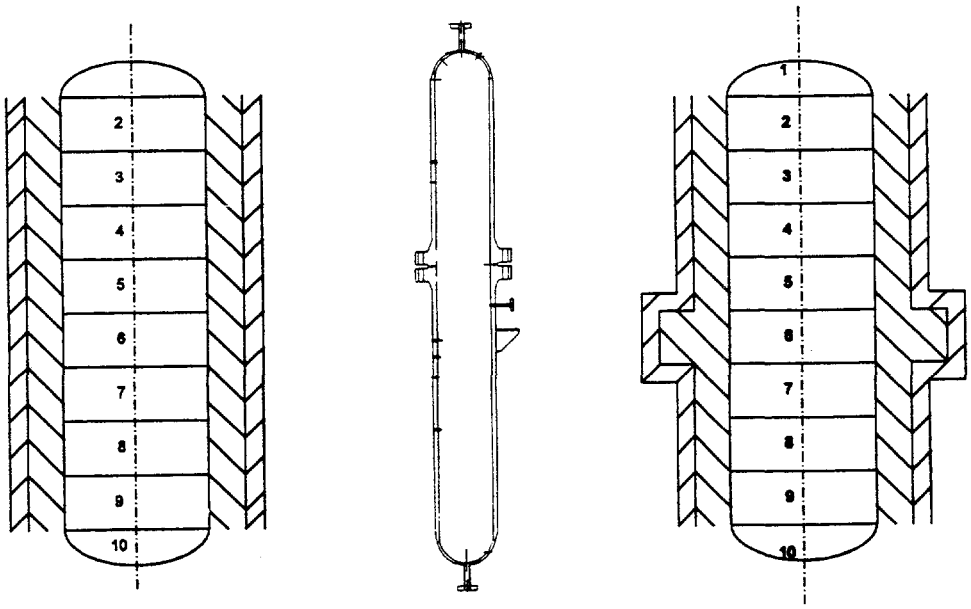

place. In the case of the CMT metal, the shell meets the first criterion, the thick flange meets the second.

The thickness of the metal structure at the flange elevation was parametrically increased by factor of 2 and the code was rerun. The computed results are shown in Figure 23, which shows that when the decreasing liquid level exposes vapor to the thicker flange the computation does indeed generate a short pause in the draining curve. The code is thus able to reproduce this phenomenon. Increasing the metal thickness by a factor of four, however, led to a rapid re-filling of the CMT.

In this example the RELAP5 code is hampered by two opposing limitations. On the one hand, the energy transfer rate into the metal has to be approximated by a model consisting of a one-dimensional metal structure coupled to a 'volume averaged' bulk temperature. Once the vapor level reaches a cool metal structure in this type of a model, the energy transfer to the metal proceeds until the metal reaches thermal equilibrium. As shown in Figure 23, the duration of such a computed condensation transient is limited. In the ROSA AP-600 test facility the condensation rate is controlled by two-dimensional effects. That is, as the liquid-vapor interface exposes cool metal, condensation starts lowering the vapor pressure which in turn increases the liquid level and recovers the cooler metal. This basically two-dimensional effect accounts for the exceptionally long duration of the phenomenon displayed in Figure 21. On the other hand the code can not duplicate these mechanisms since if the metal thickness is increased in order to increase the heat capacity, the increased condensation rate generates motion of both phases and leads to the disruption of the stratified flow regime. This in turn precipitates a bulk condensation event which is terminated only when the steam content is completely exhausted. Thus in one case the model holds up too little water inventory for too short a time, in the second case it leads to a complete refill of the CMT.

This example illustrates the sensitivity of calculated event timing to minor changes in modeling. Again, the time delay only remotely affects the ultimate calculated response. For slowly developing events which characterize the response of passive designs, the criteria for acceptable prediction of system response needs to consider the relative unimportance of shifts in the timing of some events.

5.0 SUMMARY AND CONCLUSIONS

RELAP5 version 3.2.1.2, with modeling features added specifically for the analysis of advanced reactors with passive safety systems, provides improved modeling capability over earlier versions of the RELAP5 code. Comparisons of code predictions with data from various ROSA AP-600 tests shows that version 3.2.1.2 provides improved predictions, particularly for the collapsed liquid level in the core and for critical flow at low pressure. Code robustness and execution time are also significantly improved over earlier code versions.

The need for further improvements in various modeling capabilities is identified by comparison of RELAP5 code predictions with ROSA AP-600 and APEX test cases. Areas in need of improvement include reduction of mass error and improved capability to model thermal stratification, vapor flow and escape from a tank and the termination of natural circulation flow. These improvements are necessary to improve the fine structure of the predictions. Key variables, such as the core collapsed liquid level, are predicted quite well in spite of these code shortcomings.

The sensitivity of calculated results to small changes in initial and boundary conditions was illustrated by

Fig. 23. TEST AP-CL-05: CMT Liquid Levels (with flange*2)

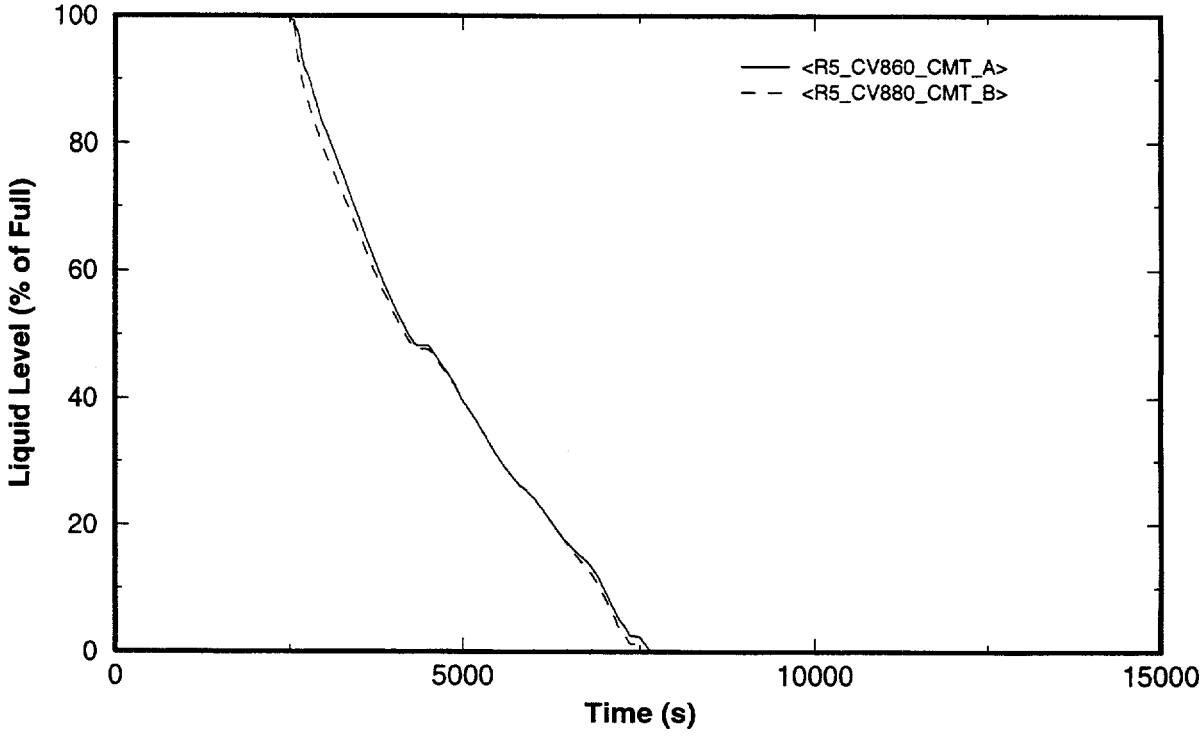

several example calculations for ROSA-AP600 and APEX. Examples shown include sensitivity of the timing of CMT emptying to PBL initial temperature, the time when natural circulation flow in the RCS loops ends and condensation on CMT walls. Overall predicted performance of the safety systems, however, does not appear to be significantly affected by the differences in timing.

6.0 REFERENCES

1. Shultz, R. R., et. al, "RELAP5/MOD3 Code Assessment Analyses Based on the ROSA-AP600 Program: Small Break LOCAs & the Station Blackout Transient," NRC FIN L2644, September 1996.

2. Davis C. B., P. D. Bayless, J. E. Fisher, P. A. Roth, S. T. Polkinghorne, "Evaluation and Assessment of RELAP5/MOD3 Version 3.2.1.2 for Simulating the Long-term Phase of SB-LOCA Accidents in the AP600," INEL-96/0395, October 1996, (Westinghouse proprietary).

3. Kelly, J. M., "Thermal-Hydraulic Modeling Needs for Passive Reactors," OECD/CSNI Workshop on Transient Thermal-Hydraulic and Neutronic Codes Requirements, Annapolis, Maryland, November 5-8, 1996.

Acknowledgments

The authors acknowledge the assistance of University of Maryland graduate students Nadia Ennaciri and Fei Li who performed RELAP5 analyses of ROSA transients AP-CL-05 and AP-AD-01 under the direction of Professor Almenas. Robert Beaton of SCIENTECH performed the calculations for OSU test NRC-11 shown in Figure 17.

An Overview of the FY 97 Test Results from the NRC AP600 Research Program at OSU

José N. Reyes, Jr.

Department of Nuclear Engineering
Oregon State University
116 Radiation Center
Corvallis, Oregon, USA, 97331-5902

Abstract - The Advanced Plant Experiment (APEX) at Oregon State University has been used to study the performance of the passive safety systems of the Westinghouse AP600. Thus far, thirty integral system tests have been performed on behalf of the U.S. Nuclear Regulatory Commission. This includes two parametric series; NRC-13 "return to saturation oscillations" and NRC-25 "no reserve tests," which consist of multiple experiments. In addition, several ROSA-AP600 counterpart tests have also been performed. This paper briefly summarizes the key tests performed in the OSU APEX test facility in FY '97.

1.0 Description of APEX Test Facility

The OSU APEX facility is a one-fourth height scale integral system model of the AP600 primary loop. As shown in Figure 1, APEX includes a reactor vessel, two hot legs, four cold legs, two Delta 75 steam generators, a pressurizer and four reactor coolant pumps. All of the AP600 passive safety systems and actuation logic have been modeled including a Passive Residual Heat Removal (PRHR) system, a four stage Automatic Depressurization System (ADS), two Core Make-up Tanks (CMTs), two Accumulators, an In-containment Refueling Water Storage Tank (IRWST). All of the components are stainless steel and the system's nominal operating conditions are at 400 psia and 420° F. Approximately 750 instruments are used to measure system flow rates, temperatures, pressures, levels, pressure drops and mass.

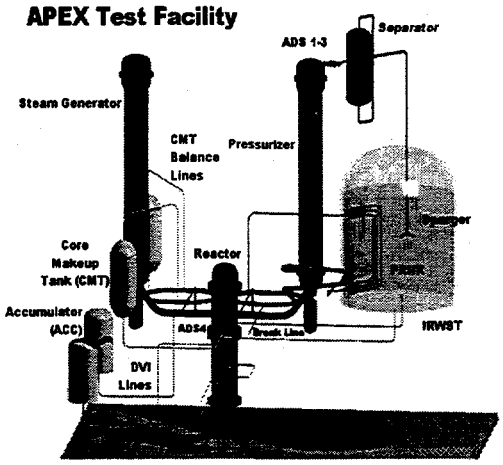

Figure 1. Description of APEX Test Facility

2.0 SUMMARY OF APEX TESTING FOR NRC

A wide range of AP600 operating conditions have been studied in the APEX facility. These range from integral system design basis accident scenarios to separate effect, beyond design basis accident scenarios. Tables 1 and 2 list the APEX matrix tests and parametric test series performed thus far.

*Table 1. Summary of NRC APEX Matrix Testing**

Test Number	Description
NRC-1	1-Inch Cold Leg #3 Break with Failure of ADS 1-3 (ROSA Counterpart)
NRC-2	Station Blackout - ROSA Counterpart
NRC-3	2-Inch Cold Leg #3 Break with Long Term Cooling
NRC-4	2-Inch Cold Leg #3 Break - Flow Oscillation Assessment
NRC-5	1/2-inch Cold Leg#3 Break
NRC-6	1-Inch Cold Leg #3 Break with Full Pressure ADS
NRC-7	1-Inch Cold Leg #3 Break without Accumulator Nitrogen Injection
NRC-10	1-Inch Cold Leg #3 Break with Failure of 3 of 4 ADS-4 Valves
NRC-11	2-Inch Cold Leg #3 with Revised ADS 1-3 Flow Area
NRC-12	2-Inch Cold Leg #4 Break
NRC-14	1-Inch Cold Leg #3 Break with Full Pressure ADS and Failure of 1 of 4 ADS 4
NRC-15	1-Inch Cold Leg #3 Break with Full Pressure ADS with Revised ADS Flow Area
NRC-18	2-Inch Cold Leg #3 with Reactor Pressure Vessel Bypass Holes Plugged
NRC-19	1-Inch Cold Leg #3 with Reactor Pressure Vessel Bypass Holes Plugged
NRC-20	Double-ended DVI Line Break - (W- SB-11 Counterpart)
NRC-21	1-Inch Cold Leg #3 Break, (ROSA AP-CL-03 and W- SB-5 Counterpart)
NRC-22	1-Inch Cold Leg #3 Break, (ROSA AP-CL-03 and W- SB-5 Counterpart)
NRC-23	Inadvertent ADS with Hot CMTs
NRC-24	Inadvertent ADS with Cold CMTs
NRC-26	1-Inch Cold Leg # 3 Break with Core Heat-Up
NRC-27	1-Inch Cold Leg # 3 Break with Degraded Sump (Sump Draining)
NRC-32	1-Inch Cold Leg #3 Break with Failure of PRHR
NRC-34	1-Inch Cold Leg #3 Break with Argon-41 Tracer (Nitrogen Transport Study)

* Repeat Tests are not listed

Table 2. Summary of NRC APEX Parametric Testing

NRC-13 Return to Saturation Oscillations	
Test ID #	**Description**
5013	Steady-State Oscillation Test
6113	Steady-State Oscillation Test with ADS 4 Steam Measurement
6213	Steady-State Oscillation Test with ADS 4 Flow Visualization
NRC-25 No Reserve Tests	
6025	100 psia blowdown, 138 kW, 2 of 4 ADS 4 failed, CMTs isolated
6125	100 psia blowdown, 138 kW, 2 of 4 ADS 4 failed
6225	200 psia blowdown, 120 kW, 2 of 4 ADS 4 failed
6325	200 psia blowdown, 80 kW, 2 of 4 ADS 4 failed
6425	100 psia blowdown, 308 kW, No ADS 4 failures
7525	200 psia blowdown, 0 kW, 2 of 4 ADS 4 failed
7625	100 psia blowdown, 138 kW, No ADS 4 failures
7725	100 psia blowdown, 80 kW, No ADS 4 failures

3.0 SUMMARY OF APEX TEST RESULTS

The test program described in Tables 1 and 2 provide significant insight into AP600 passive safety system operation. This section provides a brief overview of the key test results.

3.1 Design Basis Accident Scenarios

Several confirmatory tests simulating AP600 Design Basis Accidents (DBA) have been performed including breaks ranging from ½ inch cold leg breaks to double-ended DVI line breaks. The key finding from these DBA tests is that none of the tests resulted in uncovering the core.

3.2 Return to Saturation Oscillations (S.C. Franz)

During the IRWST draining phase, periodic oscillations were observed in the ADS 4 flow, DVI flow, system pressure and system temperatures. The onset of these oscillations occurs when the fluid at the core exit reaches saturation conditions. The NRC-13 series of tests (NRC-5013, 6113 and 6013) is a parametric study to investigate these "return-to-saturation" oscillations. The tests were performed under steady-state conditions in which the IRWST liquid level and the core power were incrementally varied. The mechanisms governing the oscillation period and amplitude are highly coupled and directly related to the periodic covering and uncovering of the ADS 4 steam vent path. The tests provided significant insights into the oscillation behavior and were useful in developing the basis for the Advanced Plant Oscillation Simulator (APOS); a

code to predict the oscillation behavior. Figure 2 shows temperature oscillations in the core and a comparison to the APOS predictions. The NRC-13 series included flow visualizations of the ADS 4 vent line flow.

It was determined that the system oscillations terminate when the reactor vessel liquid level remains below the top of the hot leg. This permits a steam vent path to remain open through the ADS 4 line. Thus the process is self-limiting such that the system oscillations cannot lead to core uncovering.

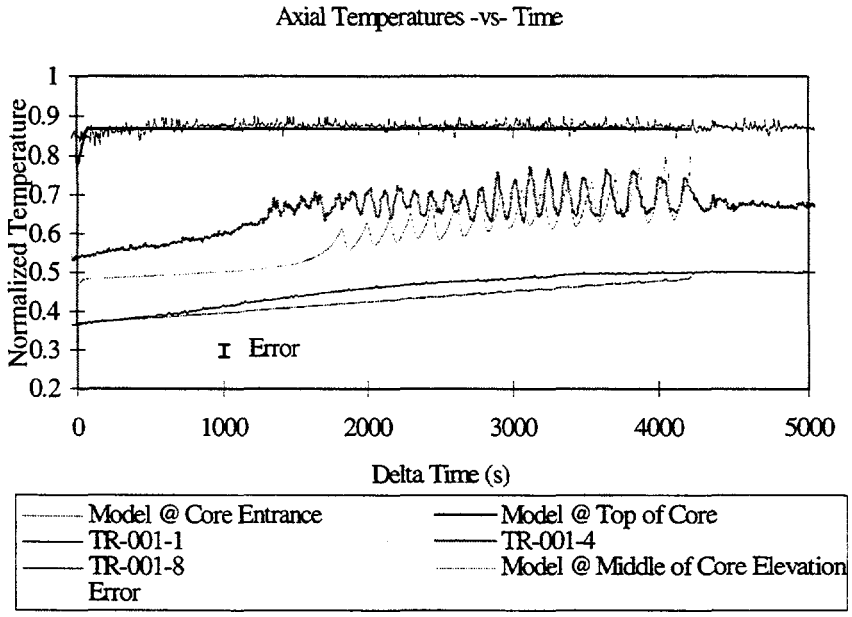

Figure 2. Return to Saturation Oscillations - Core Axial Temperatures

3.3 Primary System Thermal Stratification (D.M. Wachs)

Thermal stratification in the cold legs was observed for a variety of small break LOCA tests. Figure 3 presents an axial temperature trace for cold leg #3 during test NRC-5107. The data indicate that the fluid at the bottom of the cold leg was near injection temperatures while the fluid at the top of the cold leg was near the saturation temperature during the stratification periods. The data from these tests is being used to determine the conditions for the onset of thermal stratification in the primary loops. Modeling with CFX-4 is currently in progress to understand the impact, relative to cold leg thermal stratification, of PRHR coolant mixing in the lower channel head of the steam generator. The CFX-4 code calculations model a negatively buoyant jet from PRHR injection, steady-state primary loop flow from the steam generator tubes, and mixing in the plume falling into the cold legs.

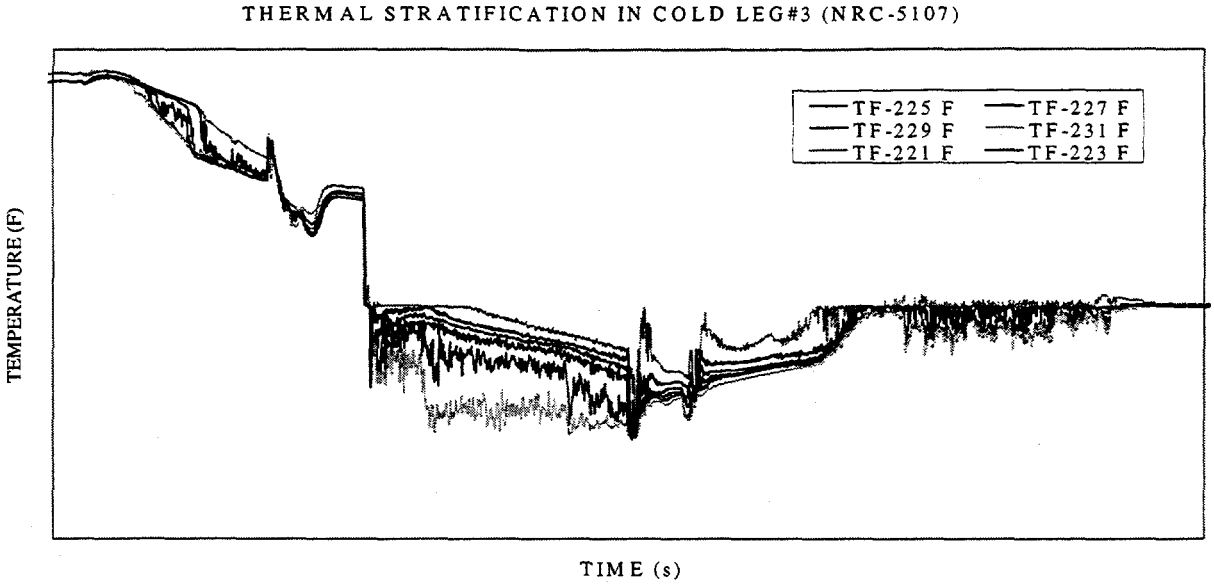

Figure 3. Thermal Stratification in Cold Leg #3 (NRC-5107)

3.4 IRWST Mixing (M.F. Strohecker)

Operation of the Passive Residual Heat Removal (PRHR) Heat Exchanger causes thermal stratification in the IRWST and generates complex circulation patterns when the upper regions become saturated. The fluid circulation patterns impose a feedback on the PRHR heat transfer. In addition, ADS 1-3 sparger operation results in significant mixing of IRWST fluid.

CFX-4 is currently being developed to analyze the mixing behavior in the IRWST caused by operation of the PRHR heat exchanger. Figure 4 illustrates the CFX-4 nodalization of the IRWST, the PRHR heat exchanger and the ADS 1-3 sparger. The model is comprised of 114,000 control volumes arranged in 344 blocks. Initial modeling will be performed for PRHR single phase natural convection. Subsequently PRHR boiling models will be incorporated into CFX.

3.5 Counter-current Flow Limitation (CCFL) in the Pressurizer Surge Line (S.E. Colpo)

Matrix test NRC-10 examined the effects on system depressurization and core liquid inventory caused by a significant reduction in the ADS-4 flow area. During the test, the liquid in the pressurizer did not immediately drain to the reactor vessel because of the high vapor flow rates through the surge line and out the ADS 1-3 vent lines. The onset of this counter-current flow limitation is of significant interest because of the complex geometry of the surge line. Efforts are in progress to assess the adequacy of existing CCFL models for this complex geometry.

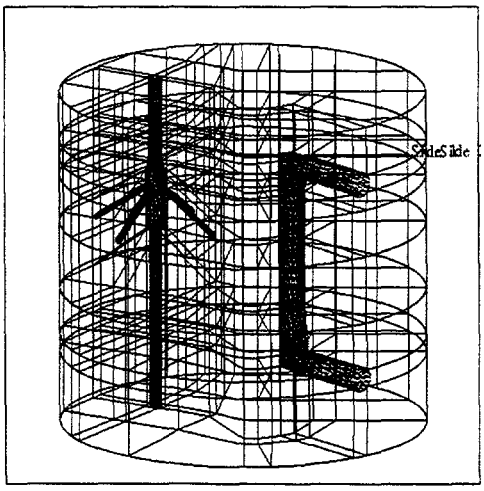

Figure 4. CFX-4 Nodalization of IRWST, PRHR and ADS 1-3 Sparger

3.6 No Reserve Tests (C. Rusher)

The NRC-25 series of tests (NRC-6025, 6125, 6225, 6325, 6425, 7525, 7625, and 7725) represents a parametric study to determine the minimum liquid reserves required to prevent a temperature excursion in the core. The tests are initiated with a failure of all passive safety systems with the exception of portions of the ADS-4 system and the IRWST injection system. The parameters varied were ADS-4 flow area, core power and initial system pressure. The tests were initiated by an ADS-4 blowdown from an initial pressure with the reactor vessel liquid level at the bottom of the hot legs. Power was held constant throughout the test. During the system blowdown, ADS-4 liquid entrainment, core boiling and flashing removed reactor vessel liquid inventory. The only means of refilling the reactor vessel was through IRWST injection. However, IRWST injection could not begin until the system pressure dropped below the gravity head pressure of the IRWST. Unlike previous test, the NRC-25 series was performed at full pressure and time scale. The objective of these tests was to develop a map which identifies the conditions for core uncovering.

Figure 5 presents the normalized temperature at the top of a core heater rod and the normalized reactor vessel liquid level versus normalized system pressure. For test NRC-6425, the core uncovered prior to reaching the IRWST injection pressure for this extreme case.

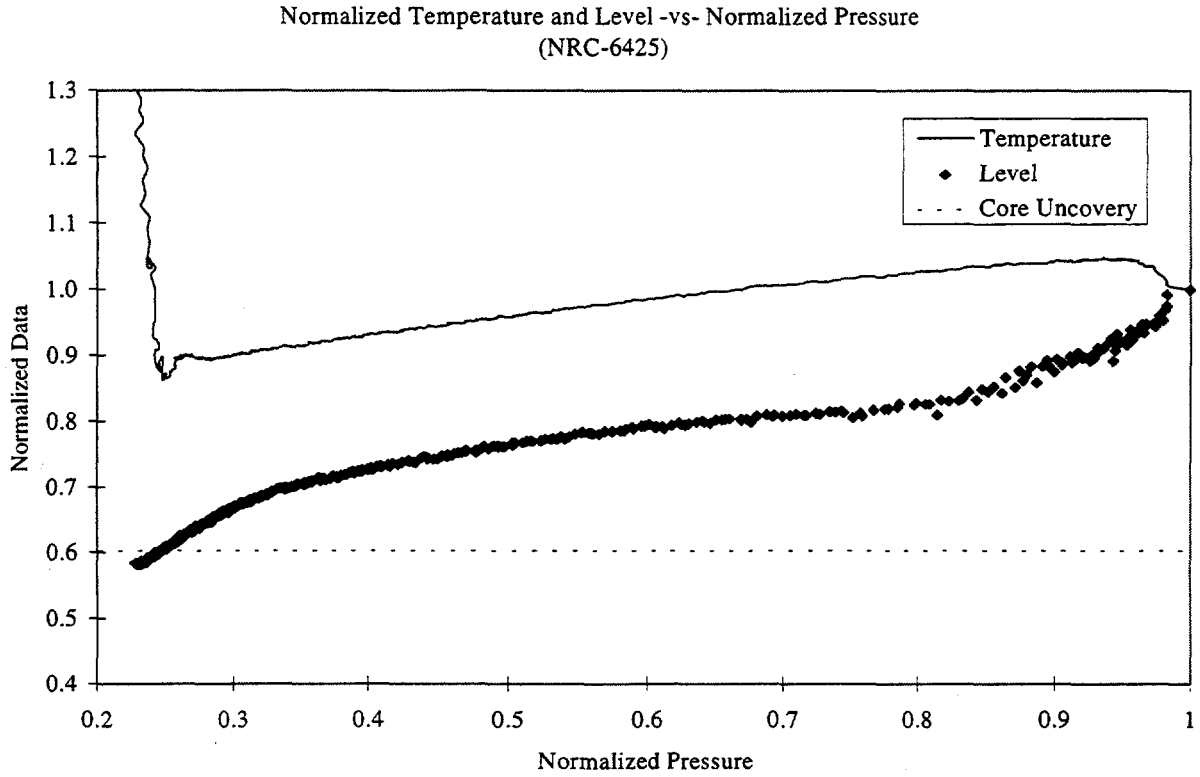

Figure 5. Normalized Reactor Vessel Liquid Level and Core Heater Rod Temperature versus Normalized System Pressure

3.7 Nitrogen Transport in the Primary (Prof. S. Binney)

Tests are presently being performed to determine how nitrogen from the accumulators is transported through the primary system during the course of a LOCA. These experiments implement a radioactive gas, Argon-41, to track the nitrogen throughout the primary system. This phenomena is important to understanding the effects of non-condensible gases in the primary system.

In these tests, a known quantity of Ar-41 is injected into the gas space of a single accumulator. Argon-41 was selected because it is a gamma emitter (thus easily detected through pipe walls) and it has a relatively short half-life (~1.8 hours). Subsequent to charging the accumulators, a small cold leg break is actuated. Detectors were placed at different locations throughout the facility. Significant quantities of Ar-41 were detected in the IRWST head. Trace quantities were detected in the reactor vessel head and the CMT heads.

An initial qualitative assessment suggests that the majority of the nitrogen gas is transported through the DVI, the upper downcomer, the cold legs and the steam generator tubes to the hot legs. The nitrogen gas leaves the primary system through the ADS 1-3 sparger into the IRWST and through ADS-4. These results are preliminary. Quantitative data will be obtained in a future test by "grab" samples at various locations in the facility.

4.0 FUTURE OSU INTEGRAL SYSTEM TEST PROGRAM

In FY 98, the OSU Integral System Thermal Hydraulics Research Program shall focus on developing a fundamental understanding of asymmetric loop interactions under SBLOCA natural circulation conditions. This effort will be applicable to a variety of PWRs including those implementing passive safety systems. Of particular interest are the effects of system "imbalances" caused by asymmetric coolant injection or secondary side heat transfer.

The new program will require instrumentation relocation/upgrades and facility hardware modifications such as core bundle changes and the addition of cold leg safety injection. This data will be valuable for benchmarking advanced thermal hydraulic systems codes.

Two parametric test series are being considered. The NRC-8040 series will focus on the effects of asymmetric steam generator shell side pressure and/or heat transfer on primary loop natural circulation under SBLOCA conditions. The NRC-8041 series will focus on the effects of asymmetric coolant injection in the steam generator lower head (PRHR) or in a single cold leg (safety injection).

Issues to be addressed include:

- Conditions for interruption of natural circulation
- Conditions for onset of flow instabilities
- Effects on core cooling due to natural circulation "stalling" in a single loop
- Effects of asymmetric primary loop void distribution

5.0 SUMMARY AND CONCLUSIONS

In conclusion, thirty NRC matrix tests have been successfully performed in the APEX test facility. Two of these matrix tests are series which include parametric experiments to study oscillation behavior in the primary system and the approach to core uncovering. The experiments have given significant insight into AP600 passive safety system operation. Some key observations are:

- None of the Design Basis Accident Scenarios investigated have resulted in core uncovering.
- Parametric testing has shown that the "Return to Saturation Oscillations" are self-limiting and do not lead to core uncovering.
- Thermal stratification in the cold legs is influenced by the mixing behavior in the steam generator lower head.
- Counter-current flooding limitations can occur in the PZR surge line when the ADS 4 flow is significantly restricted.
- The NRC-25 parametric test series provides data to benchmark a core uncovering map for AP600 worst case Beyond Design Basis Accidents.
- Initial qualitative assessments using an Ar-41 radioactive tracer suggests that a majority of the nitrogen leaves the primary system via the ADS system.

In FY '98, OSU hopes to begin a study of system wide loop interactions under natural circulation conditions. Of particular interest, are the effects of system imbalances on primary loop natural circulation.

SENSITIVITY OF BWR STABILITY CALCULATIONS TO NUMERICAL INTEGRATION TECHNIQUES

Damian Ginestar Peiro
Departamento de Matematica Aplicada; Universidad Politecnica de Valencia
Camino de Vera, 14; 46071 Valencia, SPAIN

José March-Leuba
Instrumentation & Controls Division; Oak Ridge National Laboratory*
P.O. Box 2008; Oak Ridge, TN 37831-6010; U.S.A.

ABSTRACT

Computer simulations have shown that stability calculations in boiling water reactors (BWRs) are very sensitive to a number of input parameters, modeling assumptions, and numerical integration techniques. Following the 1988 LaSalle instability event, a significant industry-wide effort was invested in identifying these sensitivities. One major conclusion from these studies was that existing time-domain codes could best predict BWR stability by using explicit methods for the energy equation with a Courant number as close to unity as possible. This paper presents a series of sensitivity studies using simplified models, which allow us to determine the effect that different numerical integration techniques have on the results of stability calculations. The present study appears to indicate that, even though using explicit integration with a Courant number of one is adequate for existing codes using time-integration steps of less than 10 ms, second-order solution techniques for the time integration can result in significant improvements in the accuracy of linear (i.e., decay ratio) stability calculations.

The problems associated with the numerical solution of oscillatory-type systems can be illustrated by solving the following ordinary differential equation (ODE)

$$\frac{d^2x}{dt^2} + 2\,\sigma\,\frac{dx}{dt} + \left(\sigma^2+\omega^2\right)x = \varepsilon \qquad (1)$$

For this particular simulation, we have used $\sigma = 0.1$ and $\omega = \pi$, which results in an oscillation of frequency 0.5 Hz and DR = 0.82. Following the conventional numerical solution approach, we can convert Eq (1) into two first order ODE's and solve them numerically using different time-integration algorithms and time step. The results are shown in Fig. 1 and indicate that first order integration methods (Euler's method) either overestimate (explicit) or underestimate (implicit) the decay ratio significantly even for reasonable time steps. Second order time-integration methods are very accurate even for large integration time steps. All methods converge to the analytic solution as the time step is reduced (see Fig. 3).

* Managed by Lockheed Martin Energy Research Corp. For the U.S. Department of Energy under contract DE-AC05-96OR22464

By analytically studying the propagation of errors in the numerical solution of Equation (1), it can be shown that the error in the numerically calculated decay ratio, DR_{calc}, is

$$DR_{calc} = DR_{exact}\, e^{\pm \pi\omega\Delta t} \qquad (2)$$

where the plus sign applies to explicit methods and the minus sign applies to implicit methods. For small time steps, Δt (in units of seconds), can be approximated by

$$DR_{calc} \approx DR_{exact} \left(1 \pm 10\ \Delta t \right) \qquad (3)$$

Thus, the percent decay ratio error for first-order integration methods is approximately equal to the integration time step in milliseconds. Most time-domain system codes use integration times of at most 1 to 10 ms; thus, the decay ratio error caused by first-order integration errors should be less than 10% for these codes. Higher-order time integration schemes (e.g., explicit Runge Kutta of second order) result in negligible errors for integration steps of the order of 100 ms or less. Stability calculations are unlikely to use time steps larger than 100 ms due to Courant number constraints; thus, using time-integration schemes of order higher than second for linear stability (i.e. decay ratio) calculations is not likely to result in significant improvements.

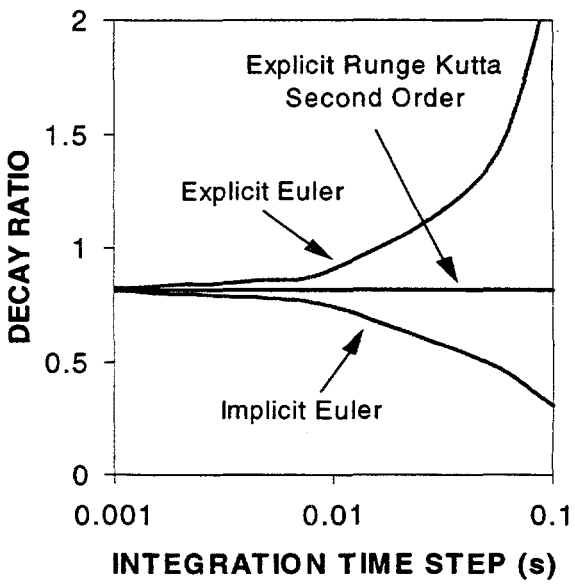

Figure 1. Decay ratio errors induced by first-order numerical integration on Eq. (1)

Even though the partial differential equations (PDEs) that represent BWR stability are significantly more complex than Eq. (1), the qualitative behavior of the solution is similar and one should expect similar behavior. A more complex model of BWR dynamics can be represented by the following equations

$$\frac{\partial \alpha(z,t)}{\partial t} + V \frac{\partial \alpha(z,t)}{\partial z} = Q(t) \qquad (4)$$

$$\frac{dQ(t)}{dt} = -\frac{K}{H} \int_0^H \alpha(z,t)\ dz \qquad (5)$$

where Eq (4) models the convection of the density wave, α, which propagates at constant velocity, V, in this simplified model. The right hand side of Eq (5) models the reactivity feedback, which is proportional to the core-average density, and an approximation to the power, Q, dynamics. The constant K controls the stability of the system and can be thought of as being proportional to the product of the steady-state power times the density reactivity coefficient. For the analysis presented in this paper, the value of the constants are V = 2 m/s, H = 4 m, and K = 3, which result in a decay ratio of 0.41. The boundary conditions are

$$\alpha(z=0,\ t) = 0; \quad \alpha(z,\ t=0) = 0; \quad Q(t=0) = 0 \qquad (6)$$

This model, although simple, captures most of the numerical problems associated with solving the linear BWR stability problem in time and space (i.e., decay ratio of the reactor core-wide mode of oscillation).

The non-linear response (e.g. large-amplitude limit cycles) is beyond the scope of this study. The space dependence of this model can be discretized by defining node-averaged void fractions

$$\boldsymbol{\alpha}_i(t) = \frac{1}{\Delta z} \int_{z_{i-1}}^{z_i} \boldsymbol{\alpha}(z,t)\, dz \tag{7}$$

Integrating Equations (4) and (5) for each node, we obtain the following nodal equations.

$$\begin{aligned} \frac{d\boldsymbol{\alpha}_i}{dt} + V \frac{\boldsymbol{\alpha}(z_i) - \boldsymbol{\alpha}(z_{i-1})}{\Delta z} &= Q\ \Delta z \\ \frac{dQ}{dt} &= -K \sum_{i=1}^{i=N} \boldsymbol{\alpha}_i \end{aligned} \tag{8}$$

We must note that the above equations are exact. The discretization errors occur when we must represent the node boundaries values, $\boldsymbol{\alpha}(z_i)$, as a function of the node-average values, $\boldsymbol{\alpha}_i$. This is accomplished by integrating our approximation for the derivative over each of the nodes. For example, for a first-order up-wind differentiation, we approximate the spatial derivative as

$$\frac{d\boldsymbol{\alpha}}{dz} \approx \frac{\boldsymbol{\alpha}(z) - \boldsymbol{\alpha}(z - \Delta z)}{\Delta z} \tag{9}$$

and we integrate Eq (9) over each node to obtain an approximation for the convective term in Eq (8)

$$\frac{\boldsymbol{\alpha}(z_i) - \boldsymbol{\alpha}(z_{i-1})}{\Delta z} = \frac{1}{\Delta z} \int_{z_{i-1}}^{z_i} \frac{d\boldsymbol{\alpha}}{dz}\, dz \approx \frac{1}{\Delta z} \int_{z_{i-1}}^{z_i} \frac{\boldsymbol{\alpha}(z) - \boldsymbol{\alpha}(z - \Delta z)}{\Delta z}\, dz = \frac{\boldsymbol{\alpha}_i - \boldsymbol{\alpha}_{i-1}}{\Delta z} \tag{10}$$

Thus, to first order in space, our system of partial differential equations becomes

$$\begin{aligned} \frac{d\boldsymbol{\alpha}_i}{dt} + V \frac{\boldsymbol{\alpha}_i - \boldsymbol{\alpha}_{i-1}}{\Delta z} &= Q\ \Delta z \\ \frac{dQ}{dt} &= -K \sum_{i=1}^{i=N} \boldsymbol{\alpha}_i \end{aligned} \tag{11}$$

Using a similar technique, we can develop a second order up-wind approximation for our equations. The second-order up-wind approximation for the spacial derivative is

$$\frac{d\boldsymbol{\alpha}}{dz} \approx \frac{3\boldsymbol{\alpha}(z) - 4\boldsymbol{\alpha}(z - \Delta z) + \boldsymbol{\alpha}(z - 2\Delta z)}{2\Delta z} \tag{12}$$

and the second-order-approximation equations become

$$\begin{aligned} \frac{d\boldsymbol{\alpha}_i}{dt} + V \frac{3\boldsymbol{\alpha}_i - 4\boldsymbol{\alpha}_{i-1} + \boldsymbol{\alpha}_{i-2}}{2\Delta z} &= Q\ \Delta z \\ \frac{dQ}{dt} &= -K \sum_{i=1}^{i=N} \boldsymbol{\alpha}_i \end{aligned} \tag{13}$$

These discretized models, represented by Eqs (11) and (13), allow us to perform a number of analytical

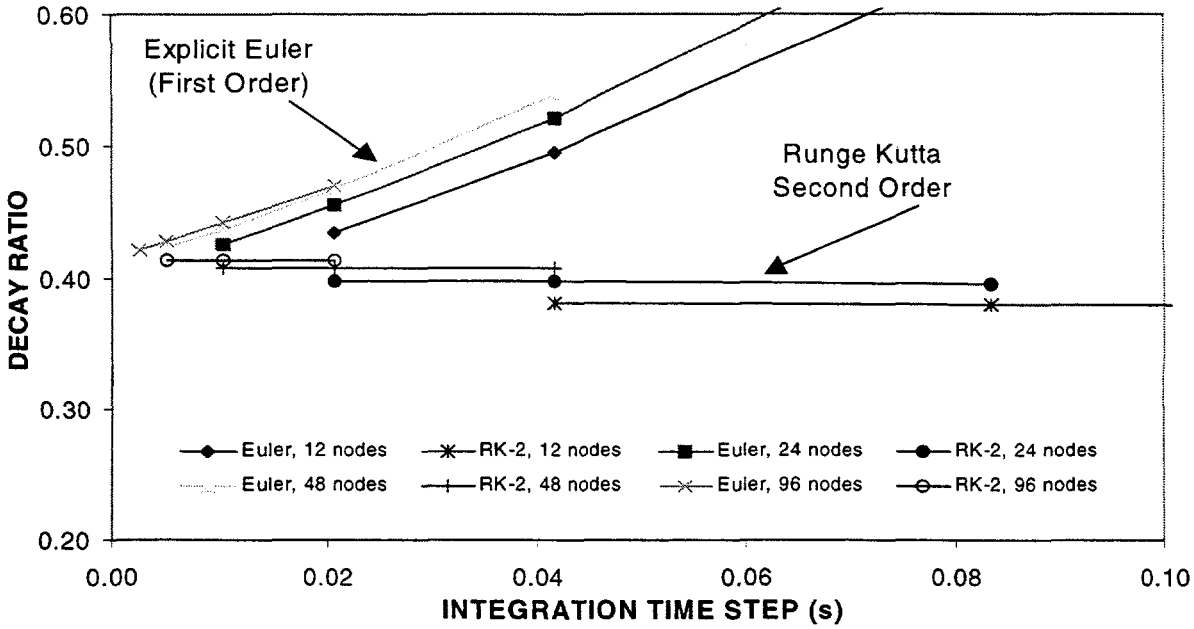

Figure 2. Calculated decay ratios error for Eqs (4) and (5) for different time integration schemes using the first-order explicit space nodalization described by Eq (11).

and numerical simulations to evaluate the error introduced by the spatial discretization and by the time integration. For these analyses, we have assumed that the lower plenum has a constant α=0, so negative indexes in Eq (13) are defined. For example, by integrating the first-order spatial approximation of Eq (11) using different number of nodes and first and second-order time-integration algorithms, we obtain the results shown in Fig. 2.

The numerical-integration results shown in Fig. 2 indicate that space-nodalization errors are not as important as time-integration errors. For example, while the relative error between the 24-node and 96 node case (at constant integration time step) is less than 5%, increasing the time integration step increases the error exponentially to values greater than 50%. It appears from these results that the fact that better results are obtained with larger number of nodes is not because of spatial nodalization errors, but because it forces the integration algorithm to take smaller steps to maintain a Courant limit lower than 1.

Figure 2 indicates that using a higher-order time-integration algorithm reduces the decay ratio error significantly, and the error reduction is independent of nodalization scheme. These results confirm our earlier conclusion that decay ratio errors are controlled by errors in the time integration, and not by spatial discretization errors. Most stability calculations with time-domain system codes are performed with at least 24 axial nodes and the average Courant number in the core is from 0.2 to 0.5, because the controlling Courant number occurs at the core exit where the velocity is highest. The integration time step is smaller than a Courant number of one would require because it is limited by either the smallest node or the node with the fastest velocity. Based on this simulation, we conclude that decay ratio errors induced by first-order explicit integration inaccuracies are expected to be in the order of 10%, which is adequate for stability calculations (all NRC-licensed stability codes are assumed accurate to within 20%).

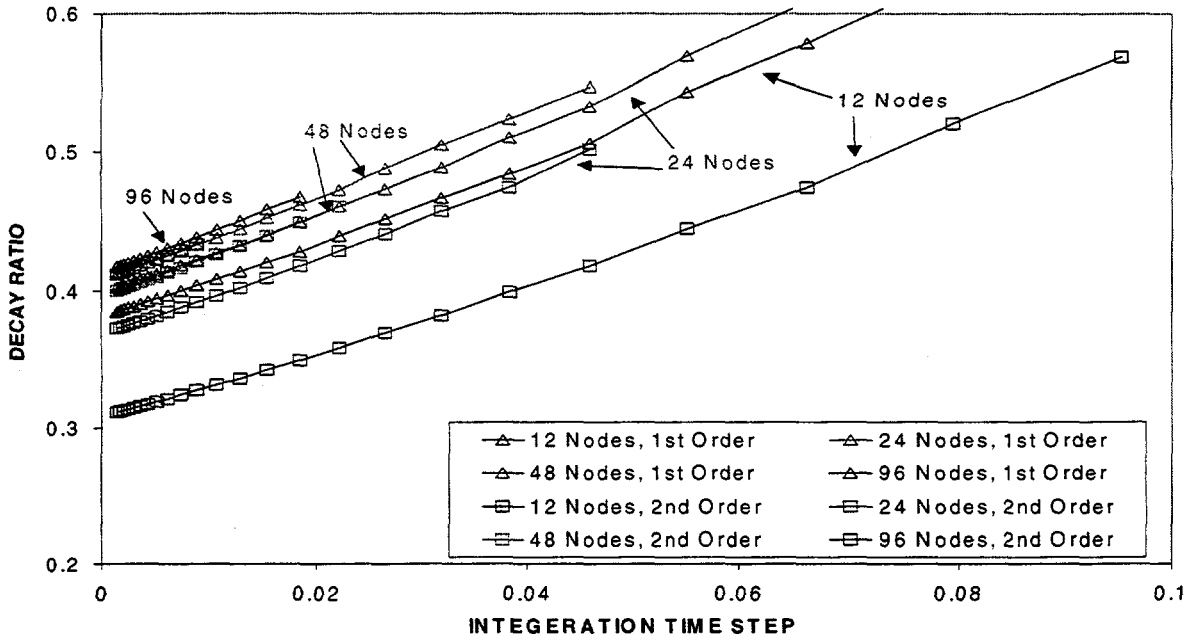

Figure 3. Decay ratio error dependence with time is similar for first- and second-order space discretization.

Using the second-order spatial discretization scheme of Eq (13), we obtain results consistent with the one shown in Figure 2 for the first-order scheme (Eq (11)). These results are shown in Fig. 3 for the first-order explicit (i.e, Euler) time integration scheme. We observe that using a higher-order spatial nodalization does not change qualitatively the error dependence with time step integration, which appears to be completely independent of the space nodalization scheme. A counter-intuitive result from these simulations is that using a higher-order space nodalization scheme actually increases the error when a small number of nodes (e.g. 12) is used. These results are confirmed by an analytical study, where the errors induced by the spacial and time nodalization can be treated separately by calculating the dominant eigenvalues of Eqs (11) or (13). The results of this analysis are shown in Fig. 4. We can conclude form these results that higher-order spatial integration results in better convergence (i.e., lower error) only if the number of nodes is sufficiently large (more than 24 nodes).

We also note in Figs. 3 and 4 that the space-nodalization errors are at least an order of magnitude smaller than the errors induced by the time integration if relatively large time steps are used. For example, even using a coarse 12-node mesh, the space nodalization error is of the order of 10%, while using a time step of 50 ms results in an error of approximately 50%. These numerical results can also be confirmed analytically by calculating the error induced in the dominant system poles by the time discretization. The results of this analytical study are shown in Figure 5. For the results shown in this figure, the following time discretization was used

$$\vec{y}(t+\Delta t) = \vec{y}(t) + \Delta t \left((1-\theta)\frac{d\vec{y}}{dt}(t) + \theta\frac{d\vec{y}}{dt}(t+\Delta t) \right) \qquad (14)$$

which results in explicit first order for $\theta = 0$, implicit first order for $\theta = 1$, and semi-implicit second order for $\theta = 0.5$

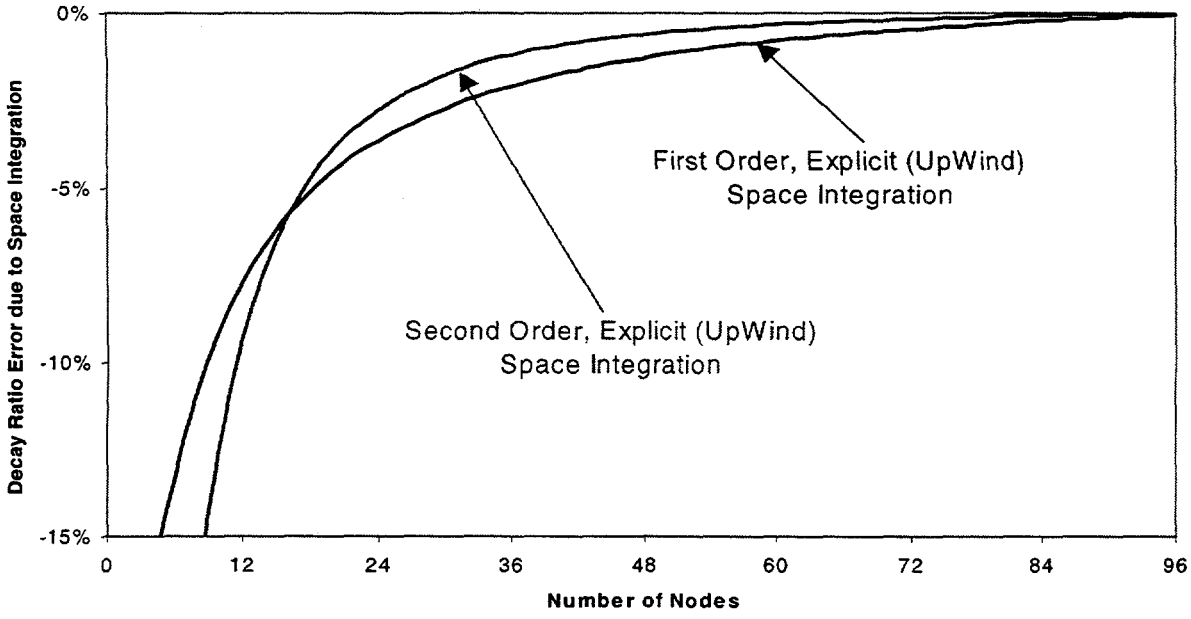

Figure 4. Decay ratio error due to space nodalization, analytical results. Higher-order methods converge faster, but errors can be larger if large nodes are used. For more than 24 nodes, errors are ~5%

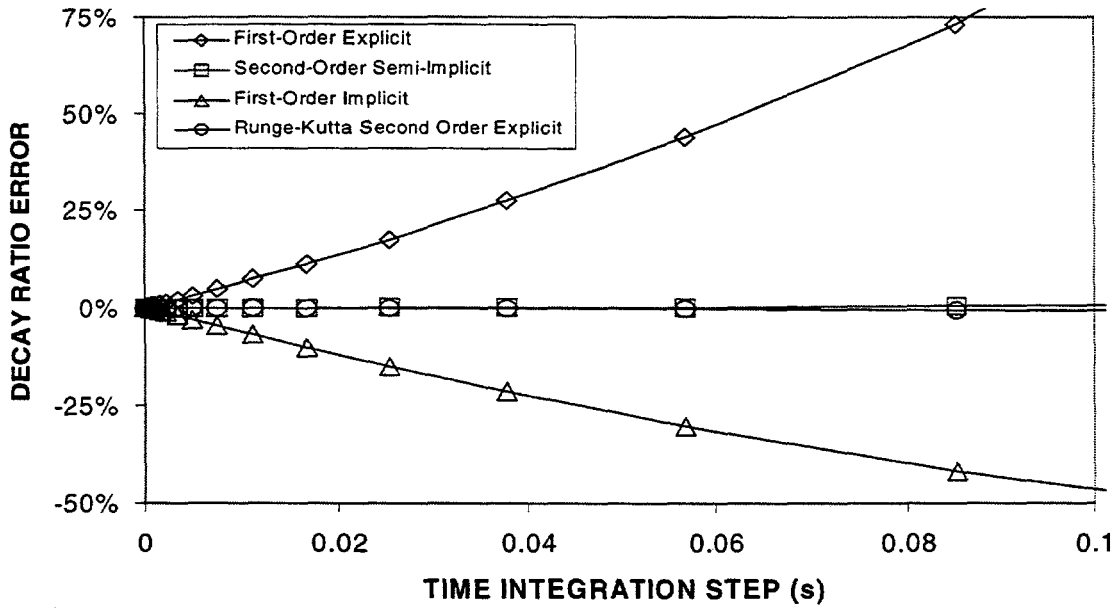

Figure 5. Decay ratio error due to time integration, analytical results. First-order integration errors can be very large. Higher-order time-integration results in negligible errors for time steps up to 100 ms.

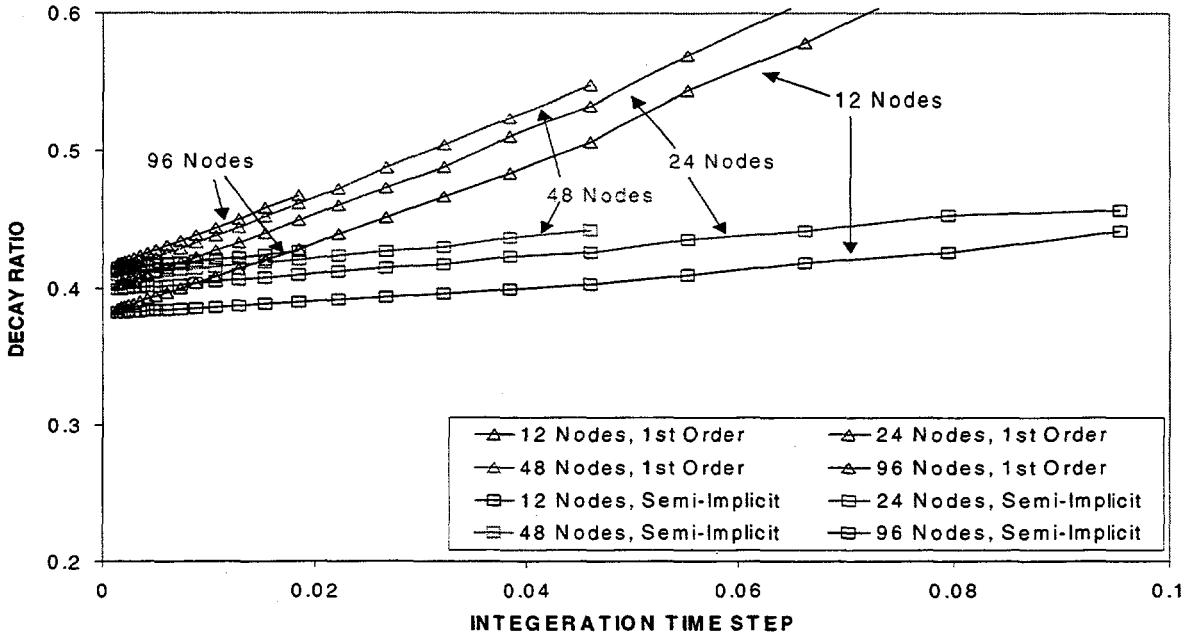

Figure 6. Using a semi-implicit scheme, cancellation of errors appears to increase the accuracy. This method is not recommended.

Large system-type simulation codes rarely use a consistent integration scheme for all state variables. For example, these codes may use an explicit time integration scheme for the energy equation, an implicit scheme for the neutronics, and a semi-implicit scheme for the mass and momentum equations. Under these conditions, the numerical errors are essentially unpredictable, unless the time steps are so small that the errors become negligible. We have attempted to simulate this situation with our simple model by using an explicit scheme for the energy equation [Eq (4)] and an implicit scheme for Eq (5). The numerical implementation consists on simply stepping the α variables in time and then using these new values of α at time t to calculate the power, Q(t). The results of this simulation are shown in Fig. 6. Surprisingly, this unorthodox "mixed" scheme performs better than either fully explicit or fully implicit. The reason for this result is a lucky cancellation of errors. The explicit α integration produces a positive error, which is canceled in part by the negative error introduced by the implicit integration of Q. Although the results shown in Fig. 6 appear to indicate that a semi-implicit method should be the preferred course of action, this method is not recommended unless is thoroughly tested under a wide variety of circumstances. Relying of cancellation of errors to obtain accuracy is extremely dangerous because, under some untested circumstances, the magnitude of errors could change dramatically.

CONCLUSIONS

This paper documents the results of a series of numerical simulations related to the problem of linear boiling water reactor stability (i.e., decay ratio calculations). These simplified simulations indicate that the numerical techniques used to calculate the linear reactor stability introduce two types of errors: (1) time-discretization errors, and (2) space-discretization errors, which are independent of each other. The space-discretization errors are always non-conservative (the calculated decay ratio is lower than the actual), and the time-discretization errors could be conservative (for explicit methods) or non-conservative (for non-explicit methods). This simulations also indicate that the time-discretization errors

can be significantly large for reasonable time steps (e.g., more than 50% error for time steps of 50 ms,) while space-discretization errors are typically small (e.g. less than 5% for 24 or more axial nodes.)

These simulations indicate that, while second-order space discretization errors are more accurate for fine nodalizations, the errors can actually be larger than those of first-order space discretization when coarse nodalizations are used (e.g., 12 or less axial nodes.) For all cases tested, second-order time discretizations decreased the error to insignificant levels (e.g., using a 50 ms time step, the error is reduced from more than 50% with first order to ~1% error if a second order time discretization scheme is used.)

This simulations also indicate that, using mixed semi-implicit methods, one can achieve cancellation of errors that appear to increase the accuracy of the calculation. These methods are not recommended unless they are thoroughly and exhaustively tested, because this cancellation of errors may not be reliable under all circumstances. The preferred course of action is to eliminate the source of the error by using higher-order time-integration and small nodalization schemes.

Based on our simplified simulations, we conclude that detailed numerical simulation studies must be performed to evaluate the particular numerical integration scheme used in each code. It is important that these tests include the complete closed-loop dynamics, as it is clear from these simulations that a feedback loop [e.g., Eq (5)] changes significantly the numerical response.

The PANDA Tests for the SBWR

G. Yadigaroglu*, J. Dreier, M. Huggenberger, C. Aubert, Th. Bandurski,
O. Fischer, S. Lomperski, H.-J Strassberger, G. Varadi†

Paul Scherrer Institute, CH-5232 Villigen PSI, Switzerland

Abstract

The large-scale, integral containment test facility PANDA has been used to examine the behavior of the Passive Containment Cooling System (PCCS) of the General Electric, Simplified Boiling Water Reactor (SBWR). The ten transient system tests discussed here investigated the long-term cooling phase of the SBWR following a Main Steam Line Break. The tests can be grouped as: (1) base-case and repeatability tests, (2) asymmetric tests, (3) other tests.

Uniform or non-uniform Drywell (DW) conditions can be created by varying the split of the steam flow and the number of condensers connected to two PANDA DW vessels. Using this feature, the asymmetric tests established the envelope response of the containment under a very wide range of possible non-uniform conditions. The "startup" test demonstrated PCCS start-up and purge of the air from the DW to the WW. Tests also demonstrated parallel Isolation Condenser and PCCS operation and the effects of leakage from the DW directly to the WW air space. The last test started from initial conditions earlier in the transient and established the link with the actual history of the earlier period of the transient.

The tests demonstrated a favorable overall system behavior due to the "robust" performance of the PCCS. Good understanding of the effects of mixing in the large vessels was obtained.

1. INTRODUCTION: THE PANDA TESTS AND THE SBWR

The ALPHA project was initiated in 1991 at the Paul Scherrer Institute (PSI) in Switzerland (Coddington et al., 1992) to investigate experimentally and analytically two main aspects of containment design for the next-generation of passive Advanced Light Water Reactors (ALWR), namely long-term decay heat removal and fission product retention. Both the dynamic response of passive containment *systems*, as well as detailed understanding of certain key *containment phenomena*, are investigated.

---

main affiliation: Swiss Federal Institute of Technology, ETHZ, ETH-Zentrum, CLT, CH-8092 Zurich, Switzerland.

The ALPHA project has been, in its first phase, directed to the investigation of the General Electric (GE) Simplified Boiling Water Reactor (SBWR) (Shiralkar et al., 1993; Upton et al., 1993) Passive Containment Cooling System (Shiralkar et al., 1997) shown in Fig. 1. This paper summarizes the main findings of the SBWR-related tests that were conducted in the large-scale PANDA integral test facility. The very first results from the PANDA tests were presented at the 23rd Water Reactor Safety Information Meeting (Varadi et al., 1996). The SBWR-related PANDA tests have been successfully completed at the end of 1995; certain results have been already reported (Dreier et al., 1996a,b; Varadi et al., 1996; Fischer et al., 1997; Bandurski et al., 1997).

The PANDA tests were initially expected to bring *only* confirmatory information for the generic certification by the US Nuclear Regulatory Commission (US NRC) of the SBWR. Subsequent developments made, however, these experiments one of the essential elements in this process. As a consequence, they were performed according to the US NRC Quality Assurance procedure NQA-1.

PANDA is a large-scale integral test facility for the investigation of passive ALWR containment phenomena and simulation of system response (Varadi et al, 1996; Dreier et al., 1996a). As shown in Fig. 1, PANDA has a modular structure of cylindrical vessels interconnected by piping. The various mixing and natural circulation phenomena taking place in the containment are complex, depend on the *particular* geometry and dimensions of the containment building, and simple linear geometric scaling would have produced serious scaling distortions. The general philosophy adopted for PANDA was to allow multidimensional effects to take place by dividing the main containment compartments (DW and WW) in two. This allows spatial distribution effects to develop. A variety of controlled boundary conditions can be imposed during the experiments to study mixing phenomena under well-established conditions. Parametric or sensitivity experiments conducted under well-controlled boundary conditions can provide more valuable data for code qualification than experiments where the mixing phenomena are distorted by the scale of the facility or other reasons.

1.1 The SBWR PCCS and Related Tests

Decay heat can be removed from the SBWR via either the Isolation Condenser System (ICS) or the Passive Containment Cooling System (PCCS). The ICS is connected to and condenses steam directly from the Reactor Pressure Vessel (RPV). Decay heat is removed from the SBWR *containment*, namely the Drywell (DW), by the PCCS. The ICS and PCCS condensers are located in interconnected pools on top of the reactor building. The PCCS condensers are permanently connected to the DW. Following system depressurization, the mixture of steam blown into the containment and of nitrogen initially present there during normal operation will enter the PCCS condensers. The steam will condense, while the non-condensable gases must be vented to the pressure suppression pool (SP) in the Wetwell (WW). The DW is connected to the SP via the main pressure suppression vents (MV) as well as through the PCCS condenser vent lines. The path that the steam will follow depends on the pressure differences between the DW and the two possible venting points. During the long-term containment cooling period, direct opening of the main vents and condensation of the steam in the SP is to be avoided since the SP is not provided with a safety-grade cooling system. The steam must be condensed in the PCCS (or ICS) condensers rather than the SP. Fig. 1.

Although the operation of the various components of the PCCS is understood, experimental verification of its integral system behavior under a variety of conditions was performed at two facilities. The GIRAFFE facility, operated by Toshiba in Japan, first provided extensive information about PCCS system behavior

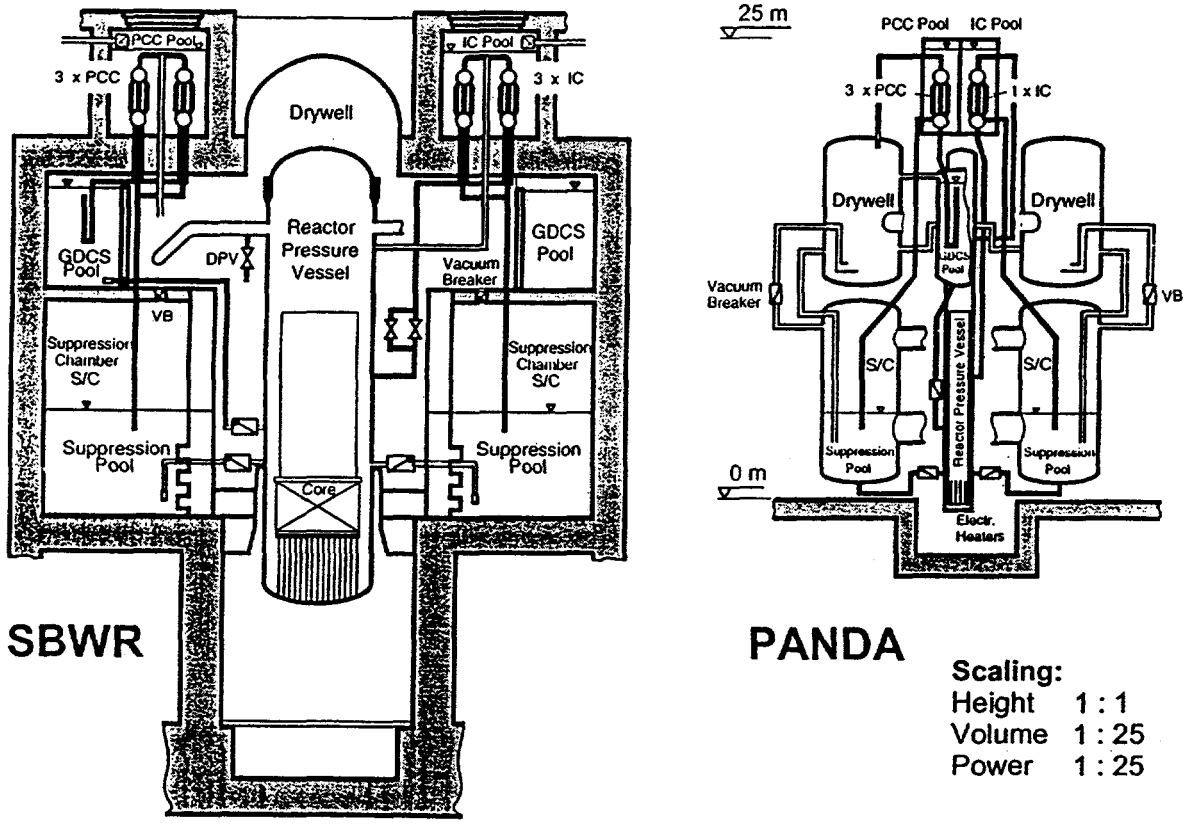

Fig. 1. The SBWR and the PANDA facility

(Yokobori et al., 1991). The much-larger-scale and multidimensional PANDA facility provided additional information.

The objectives of the transient PANDA tests were to demonstrate that:

- The containment performance is similar in a larger scale system to that previously demonstrated with the GIRAFFE tests.
- Any non-uniform distributions in the containment do not create significant adverse effects.
- There are no adverse effects associated with multi-unit PCCS operation and interactions with other reactor systems.

Thus, PANDA tests addressed in detail issues such as the distribution of the constituents (steam and non-condensables) in the large DW volume, and mixing in the containment compartments, PCCS startup, etc. The PANDA tests also extend the data base available for code qualification.

1.2 The PANDA Facility

Following the general experimental design philosophy described by Varadi et al. (1996), the various SBWR containment volumes are simulated in PANDA by six cylindrical pressure vessels. The RPV is equipped with programmable 1.5 MW electric heaters simulating the history of core decay heat generation. Two other vessels may represent the Drywell (DW), another two the Wetwell (WW), and one the Gravity Driven Cooling System (GDCS) pool. Four rectangular pools open to the atmosphere and containing the PCCS and Isolation Condenser System (ICS) condensers are located on top of the facility. The fact that the *three* PCCS condenser units are connected to *two* DW vessels allows asymmetric behavior and creates flows between the two DW vessels. Such an asymmetry occurs also with equal flow resistance from the RPV to the two DW volumes when *all three* PCCS condensers are in operation. The ICS condenser is attached directly to the RPV; it has been connected to the system only for one specific test.

The SBWR DW and WW are connected by vacuum breakers (VB). Their function is not to allow the WW pressure to exceed DW pressure by a certain margin. There are two VBs connecting the two DWs to the two WWs in PANDA, Fig. 1. The operation of the actual VBs is simulated in PANDA by control valves. These are opened and closed by the facility control system when the measured differential pressure between the DWs and the WWs exceeds an upper and a lower limit, respectively.

The PANDA facility was carefully scaled to represent the SBWR (Yadigaroglu, 1996; Gamble et al., 1997). Prototypical fluids under prototypical thermodynamic conditions were used in all tests, except that air has substituted nitrogen. Power, volumes, horizontal areas and flow rates were scaled with the *system* scale of 1:25, while elevations, pressures, and pressure drops were scaled 1:1.

Varadi et al. (1996) and (Dreier et al., 1996a) give additional details on PANDA and its scaling, the various facility characterization tests that were conducted, facility preconditioning for the various tests, instrumentation, etc. These papers also discuss the relation of the PANDA tests to other elements of the SBWR testing program.

2 THE M-SERIES SBWR TRANSIENT CONTAINMENT BEHAVIOR TESTS

The series of ten PANDA transient system behavior tests discussed here examined system response during the long-term containment cooling period. The tests provide a data base for containment PCCS performance and systems interactions. The test matrix was set to investigate parametric variations around a base case that was a counterpart test to one of the GIRAFFE tests (Yokobori et al., 1991). This allowed also to study the effects of system scale, of non-uniform distributions and of parallel operation of units in the system. Figure 2 displays the test matrix. All transient tests considered a Main Steam Line Break (MSLB). With the exception of the "early start" test M9, the initial conditions for these tests were the state of the system one hour after scram, obtained from best-estimate predictions. At that time the DW contains mostly steam and almost all the air has been pushed into the SC. The water in the PCCS and ICS pools was initially always saturated at atmospheric pressure. The power decay curves used for the experiments were those expected during the transient considered and included a small contribution from RPV metal stored heat.

The tests can be divided into three groups: (1) base-case and repeatability tests, (2) asymmetric tests, and (3) remaining tests investigating PCCS start-up, parallel operation of the PCCS and of the isolation condenser (IC), bypass leakage between DW and WW, and "early start."

M3 Series (MSL break LOCA + 1 hr)

M3 Base Case
(3 PCC pools interconnected, no makeup)

M3A Repeatability
(PCC/IC pools isolated, makeup)

M3B Repeatability
(PCC/IC pools interconnected, makeup)

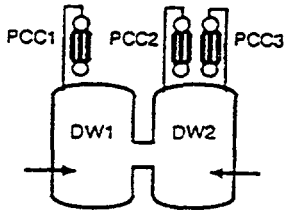

M2 Asymmetric Case 1 (relative to M3 Series)
(Total steam flow to DW2)

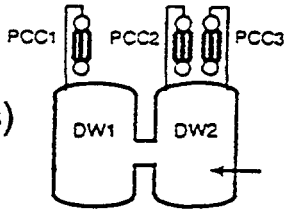

M10 Series: Asymmetric, two PCCs only

M10A Asymmetric Case 2
(DW1 relative isolated, slow gas migration from DW1 to DW2)

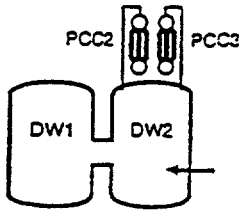

M10B Asymmetric Case 3
(Good mixing in both DWs)

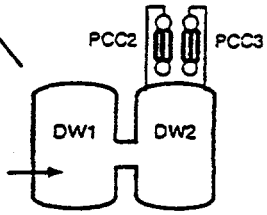

M7 **PCC Startup**
(Bounding n/c gas concentrations)

M6/8 **System Interaction** with IC Operation (M6)
and DW to WW BP Leakage (M8)

M9 **Early Start / GDCS Injection into RPV**
(LOCA + 1040 rather than LOCA +3600s)

Fig. 2 The Test matrix used for the SBWR related PANDA tests

3 BASE-CASE AND REPEATABILITY TESTS

This first series of tests includes Tests M3, M3A and M3B. They are discussed by Dreier et al. (1996b), Fischer et al. (1997) and Bandurski et al. (1997). Their purpose was to prove repeatability and to investigate in depth certain effects related to the mode of interconnection and sequential refill of the condenser pools that were noticed early in the program (Dreier et al., 1996b). Steam was symmetrically discharged to both DW vessels, as shown in Fig. 2. The tests provided good insights into the operation of the system and helped refine the following test matrix.

The PANDA pools have a scaled cross-sectional area about three times smaller than the SBWR pool area. Water can be added to the pools during the tests to provide the missing water inventory. The state of the pools can, however, be modified by such water makeups and affect PCCS operation. To investigate these effects, the M3 series of tests were conducted as follows:

- For Test M3, the three PCCS pools were interconnected and there was no water makeup. At the end of Test M3, the water level in the PCCS pools had dropped to a non-prototypical value of about 0.5 m below the top of the tubes.
- Test M3A was conducted with the three PCC pools isolated; cold water was added from the bottom fill line to each pool individually to keep the nominal water level constant within ± 0.3 m.
- For Test M3B, the PCCS and ICS pools were interconnected and cold water was added simultaneously to all four (using the connecting bottom-fill line) to keep again the nominal water level within ± 0.2 m.

Overall System Behavior: The DW and WW pressures followed very similar global trends in the three tests. The peak DW pressures were very close to one another (Dreier et al., 1996b; Fischer et al., 1997). After an initial pressure increase period that lasted about two hours, the DW pressure stabilized and varied very little thereafter, as shown in Fig. 3 for Test M3. The pressure increase period corresponded roughly to the time needed to practically purge all the air from the DW. Thereafter, the difference between the DW and WW pressures remained essentially constant (except around vacuum breaker openings, as discussed below); the difference represented the submergence depth of the PCC vent in the SP.

Parallel PCC Condenser Operation: The tests showed quite uniform behavior of the three PCC units up to about 35 000 s, as shown in Fig. 3. Then, PCC-2 started absorbing progressively less steam, while slightly more steam was condensed by the other two units (PCC-1 and PCC-3). The reduced performance of PCC-2 could be verified by a number of indicators (Dreier et al. 1996b) and is apparently connected to filling up of the PCC-2 condenser tubes with noncondensables up to a certain level which is significantly higher in the PCC-2 condenser than in the other two condensers. Similar behavior of PCC-2 was observed in certain other tests that followed.

Vacuum Breaker Openings: No VB opening took place in Test M3, and the three PCC units essentially shared the load and condensed the exact amount of steam provided by the RPV.. Vacuum breaker openings *did* take place in Tests M3A and M3B, as discussed below.

One should first note that, most of the time, condensation and significant heat transfer to the pool water takes place only in the upper "active" part of the condenser tubes. The pool water below this active region tends to stratify and may be colder than the saturated water in the well-mixed, upper part of the pool. During Test M3A, the pools were isolated and refilled individually with cold water, as shown in Fig. 4. The cold water was introduced from the bottom of the pools and apparently stratified at the bottom. During each refill, the stratified water front was pushed upwards. Eventually the cold water from the lower layers of the pool arrived at the "active" part of the pool. Some cold water reached then the active, condensing part of the tubes, and/or mixed and reduced the temperature of the well-mixed upper part of the pool (in

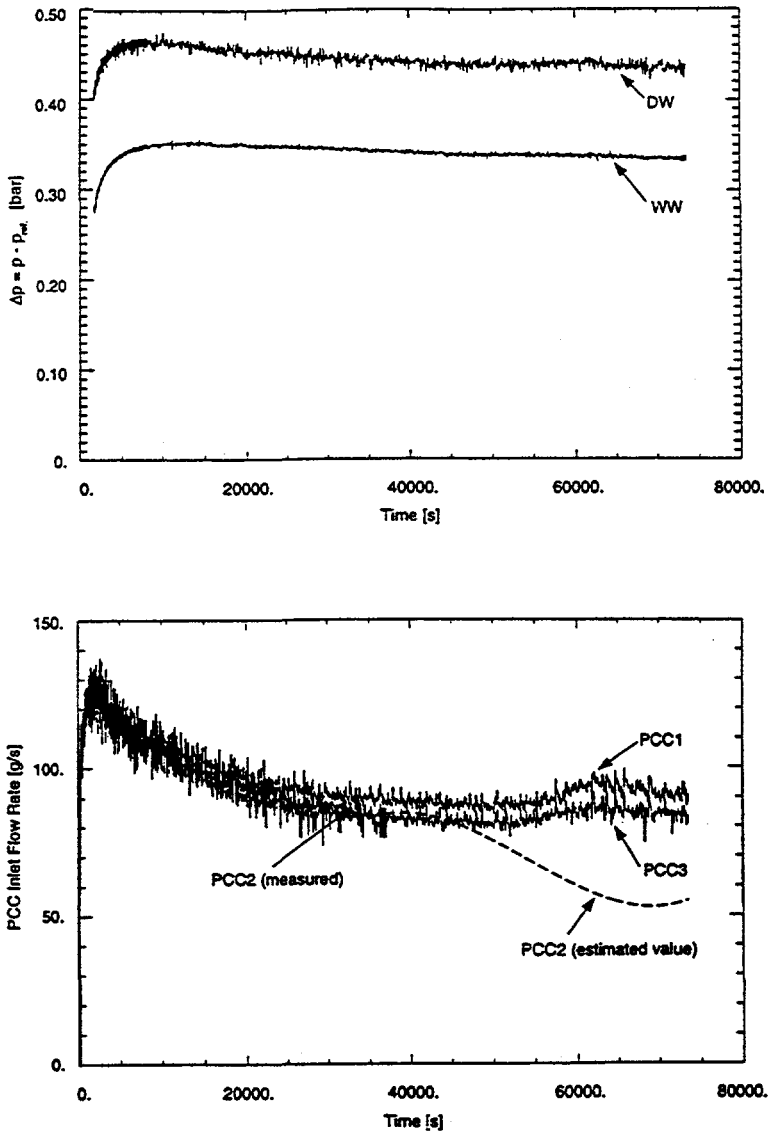

Fig. 3 Test M3: Variation of the DW and WW pressures (top) and of the flow rates received by the three PCC condensers (bottom).

contact with the active part of the tubes). In turn, this produced a significant increase of the heat transfer and condensation rates. The increase in condensation rate has driven the DW pressure below that of the WW and produced vacuum breaker openings.

After vacuum breaker openings, the pressure in the WW dropped slightly also, and the oxygen probes installed in the DW recorded the expected increase in air content. The effect of VB openings did not last long, however, and the DW and WW pressures increased to their pre-VB-opening levels in less then an hour, as shown in Fig. 4.

With or VB breaker openings, the DW pressure decreased slightly after refilling of the pools in both Tests M3A and M3B. The effect was stronger for the later refills (this can be explained by the above discussion of the phenomena taking place during a refill). Vacuum breaker openings were more frequent during Test M3A, where apparently the *individual* refilling of the pools and the larger mass of cold water added during each refill had a stronger effect. Only a single cluster of two VB openings took place late during Test M3B, where apparently the "milder" changes in the pool temperature produced a lesser effect.

Direct measurements of the air partial in the DWs confirm that the air concentration of the DWs increased momentarily following the vacuum breaker openings. The condensation rates of the individual PCC units were affected, but because of the very large margin built into the system, the three PCC units always managed to share the load and the long-term behavior of the DW pressures was not affected.

Recovery of PCCS Operation: Resumption of PCCS operation depended on the concentration of noncondensables in the DW. Recall first that air is back from the WW to the DW after a VB opening. As noted above, filling up of a pool produced a drop in DW pressure. When the DW was full with almost pure steam, the DW pressure tended to remain low and the recovery was slow, as shown following the first two refills and corresponding DW pressure drops in Fig. 4 (that took place without VB opening). This was due to the persisting high rates of condensation in the PCC units due to the fact that a long time was needed to partly fill up again their tubes with air. On the contrary, following a VB opening, when there was more air in the DW , the recovery of the DW pressure was relatively rapid (as shown for the third and fourth DW pressure drop transients in Fig. 4). In this case, air present in the DW could accumulate rather rapidly in the PCC tubes and reduce their heat removal capability.

Conclusions from the M3 Series Tests: The M-3 Series of tests showed very good repeatability of overall system behavior (DW and SC pressures) in spite of :

- perturbations of the secondary, pool-side PCC conditions,
- certain non-uniform sharing of the condensation load among the three PCC condensers, and
- differences in vacuum breaker openings.

Based on these conclusions from the M3 Series tests, it was decided to run all subsequent tests with the pools isolated and without water makeup during the tests. Indeed, the gradual drop by evaporation of the water level in the pools provides a very good measure of the integral power evacuated by the PCC condensers and can be used to confirm other measurements performed. In the following tests, pools had a slightly higher initial water level as a compensation to some extent for the lower water inventory.

There are also interesting findings regarding the distribution of noncondensables and their effects on the PCCS system. Small amounts of noncondensables affect the status of the condensers operating in parallel. The global operation of the PCCS system is not, however, influenced by such possible effects due to non-uniform distribution of noncondensables.

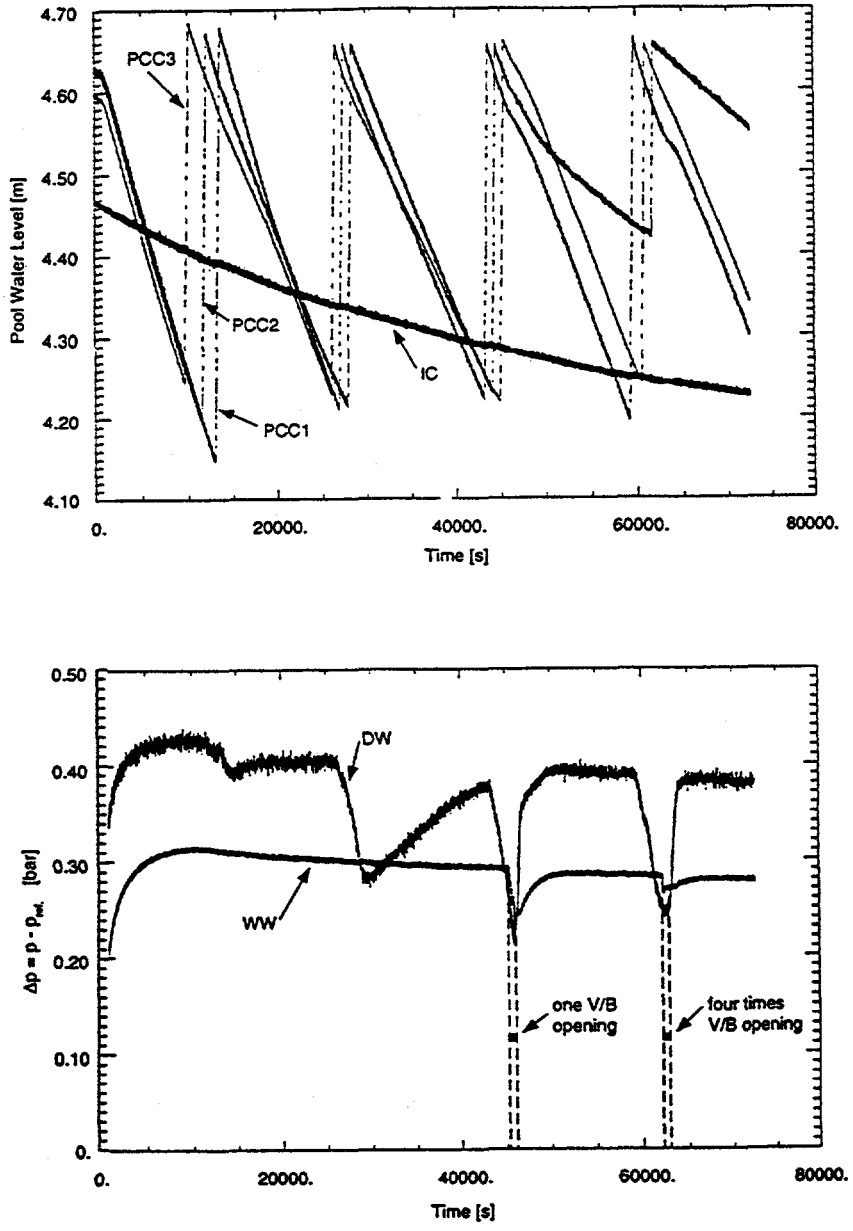

Fig. 4 Test M3A: Recorded PCCS Pool levels showing the procedure followed for maintaining an approximately constant level (top) and DW and WW pressures showing two clusters of vacuum breaker openings (bottom).

4 ASYMMETRIC TESTS

A group of tests can be formed, including the base-case test M3, as well as Tests M2, M10A and M10B. The primary purpose of this group of tests was to examine the influence of an asymmetric distribution of steam and air in the DW on PCCS performance (Fischer et al., 1997; Bandurski et al., 1997). Asymmetries were created in PANDA by varying the number of PCCS condensers connected to the DW vessels, as well as the split of the steam flow from the RPV to the DWs. Tests M10A and M10B were added to provide system response to an overload condition with *only* two of the three PCCs operating. The PANDA configurations for tests M10A and M10B do not represent prototypic SBWR post-LOCA conditions. Comparison of the results from various tests in this group, obtained under well-controlled boundary conditions, establishes the "envelope" response of the containment to non-uniformities in the distribution of noncondensables resulting from a very wide range of mixing conditions and migration and purge rates of noncondensables. Thus, these tests primarily support code qualification work, but also contribute to the assessment of robustness of the system. The large scale of the facility allows mixing and stratification effects to be observed at nearly-prototypical scales. Thus, the test objectives specifically included the study of such mixing of steam and noncondensable gases in the DW and in the WW.

The three asymmetric-configuration tests M2, M10A and M10B were run with single-sided steam feed flow to one of the two interconnected DW vessels, DW1 *or* DW2, as shown in Fig. 2. The global system pressure response of Test M2, as well as those of Tests M10A and M10B were very similar to that of the base-case test M3, in spite of the differences in steam feed (Fig. 2). Fischer et al., (1997) discuss the minor differences observed. For example, the pressure level in Test M2 was lower by 0.04 bar, compared to M3, mainly due to a difference in actual (vs. nominal) *initial* DW air partial pressure and accumulation of some air at the bottom of DW1 during the test. Some noticeable differences that were observed for the gas temperature measurements in the topmost part of the SC are explained by facility design aspects that are specific to PANDA and are not prototypic to the SBWR (Fischer et al., 1997).

4.1 Test M2: Single-Sided Steam Feed

Figure 5 shows the air partial pressure measurements in the top region of the two DW vessels obtained from the group of tests discussed in this section. During Test M2, the air content decreased rapidly in DW2 which was directly supplied with steam and had two PCCs connected. The air partial pressure in the top region of DW1 even *increased* during the first few minutes of the test, and then decreased at a rate about three times slower than in DW2. Apart from the obvious difference in the number of PCC units connected to each of the two DW vessels, the expected carry-over of air from DW2 to DW1 explains this observation. Phase detectors installed in the PCC Vent Lines , as well as temperature readings from these lines indicate that the two PCCs on DW2 vented with significant flow at the beginning of the transient only, while PCC1 was very frequently venting for about 8 hr into the test, and continued to do so with decreasing frequency through the end of the test (Fischer et al., 1997). (In the base-case test, PCC venting virtually came to an end after 2.5 hr since all the noncondensables were purged from the DWs.) Thus, although the mode of steam injection had a noticeable effect at the beginning of the test, the system reached very similar state as soon as the noncondensables were essentially purged from the DW.

All the air was purged from DW2, including its lower parts. However, steam flowing to PCC1, connected to DW1, did not entrain some air that accumulated at the bottom of DW1. Based on temperature and pressure readings from the DWs (Fischer et al., 1997), it is estimated that by the end of the 20 hr test, air at about 0.45 bar partial pressure had accumulated at the bottom of DW1. This can be explained by conden-

sation of steam due to heat loss near the bottom of DW1, as indicated by the lower temperature readings at that location, Fig. 6.

Despite the apparently highly asymmetric purging of air from the DW, hardly any significant differences can be seen between the SC temperatures of test M2 and the base-case test (Fischer et al., 1997). Suppression Pool temperatures showed in both cases a small but steady decrease due to heat loss.

4.2 M10 Tests with Strong Asymmetries and Reduced PCCS Operation

Tests M10A and M10B were conducted with *only* two PCC condensers attached to DW2 and had the steam flow from the RPV directed to only one of the DWs, as shown in Fig. 2. Thus, the heat condensing capacity of the PCCS was exceeded on purpose, as already noted. For Test M10A, DW1 was essentially a dead volume, attached to the system only by means of the large pipe connecting the two DW vessels. All mass transfer to and from DW1 had to rely on natural convection. In Test M10B, all the steam had to

sweep through DW1, the large connecting pipe, and through DW2, to finally reach the two PCCs connected to DW2.

Since the condensing capacity of the PCCS was exceeded during the first hours following Tests M10A and M10B, Main Vent openings did take place and some steam was condensed directly in the suppression pool. In Test M10A these Main Vent openings increased the temperature of the water in the SP above the Main Vent Line submergence by about 1 K (Fischer et al., 1997). Clearly, this is qualitatively different from tests M2 and M3, but is quantitatively negligible. The SP temperature rise in Test M10B was higher, but was due to a non-prototypical peculiarity of the design of the PANDA facility (Fischer et al., 1997). Differences between these two tests in relation to the distribution and mixing of noncondensables are discussed next.

Test M10A: Long-Term Migration of Noncondensables: Both PCC units vented very frequently during the first 3 hr of Test M10A, but then gradually decreased their venting frequency till the end of the test (Fischer et al., 1997). Figure 5 shows the air partial pressure measurements in the top region of the DW vessels. As for the base-case M3, the air partial pressure in the top region of DW2 dropped during the first 0.5 hr at about the same rate as in test M2, but then continued to drop at a much slower rate. In the top region of DW1, the air partial pressure slightly increased during the first 0.25 hr (displacement and pressure rise by steam flowing to DW2) and then steadily decreased by about 0.1 bar in the next 1.5 hr; thereafter the decrease slowed down. The DW1 air partial pressure response in test M10A was the slowest observed in the entire test series, as was to be expected from the test configuration.

Based on temperature and pressure readings from the DWs (Fischer et al., 1997), and assuming saturated steam, it is estimated that air at about 0.35 bar partial pressure accumulated at the bottom of DW1 by the end of the 8 hr test. Air accumulation at the bottom is explained by poor mixing of that region, combined with vessel heat losses depleting the mixture from steam.

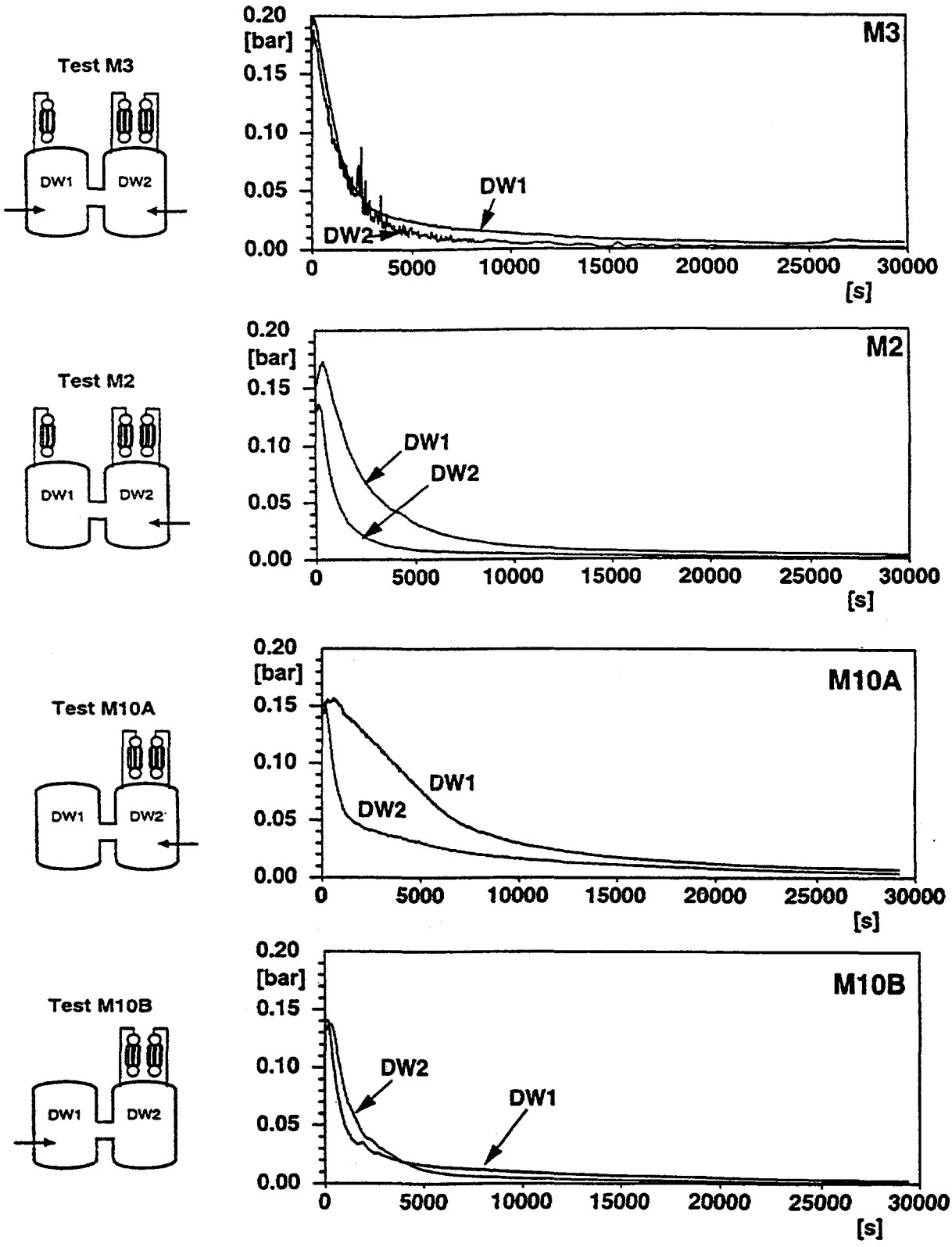

Fig. 5 Variation of the air partial pressure in DW1 and DW2 during the asymmetric test series.

Test M10B: Maximum Noncondensable Purge Rate: During Test M10B the air was purged from both DW vessels at rates similar to those of the base-case Test M3. DW1, which was purged by the steam passing through, showed a lower air partial pressure in the top region during the first hour than DW2 (Fig. 5). Shortly after 1 hr into the test, this situation was inverted and the air partial pressure in the top region of DW2, which had the two PCCs connected, remained lower than in DW1 through the end of the test. Again, based on temperature and pressure readings from the DWs (Fischer et al., 1997) it is estimated that air at 0.25 bar partial pressure had accumulated at the bottom of DW2 by the end of the 8 hr test.

4.3 Conclusions from the Asymmetric Tests

The overall system pressure variation was very similar in all tests. In relation to the concentration of non-condensables, the most important locations are the DW vessel headers from where the PCCS condensers are fed. During the early phase of the asymmetric tests, maximum air concentration ratios of about three developed at these locations in the two vessels.

Perfect mixing was observed when the steam was injected with high momentum directly into a vessel. Air could accumulate at the bottom of the DW1 vessel that was not as well mixed in tests M2 and M10A. The accumulation was due to condensation of the steam by heat loss from the vessel wall combined with insufficient mixing. Thus, stratification was observed in the vessel regions not reached by the main steam flow path when the momentum of the incoming steam was relatively low. However, with higher flow rates through the pipe connecting the two DWs, some mixing below the connecting pipe in the vessel receiving steam through the connecting pipe only *was* possible, as shown by the results of tests M2 and M10B reported by Bandurski et al., 1997.

In test M10B, all steam was transported through the connecting pipe from DW1 to DW2, whereas in M2 approximately one third of the steam flow was transferred to DW1 through the connecting pipe. Consequently, the DW2 bottom gas temperature was higher in test M10B in comparison to the DW1 bottom gas temperature for test M2 (Bandurski et al., 1997).

Although a wide variation of air concentration and air purging patterns were observed, their effects on the global system pressure response were insignificant by engineering standards, particularly when compared to the results of the base-case Test M3.

As expected, for the early part of tests M10A and M10B, the heat removal capacity of only two PCC units was insufficient. Consequently, the Main Vents cleared during the first 1 to 1.5 hr of these tests. However, the corresponding heat input to the SP and SC was insignificant in relation to the system pressure response.

5 OTHER TESTS

The remaining tests grouped in this section, include Tests M7, M6/8 and M9. These tests were run with initial and boundary conditions similar to those of the base-case test M3, except as noted below.

The PCCS-startup Test M7 demonstrated the proper start-up of the PCCS and the purge of the air from the DW to the WW. It was started with practically pure air filling the DWs and PCCS condensers.

Test M6/8 examined and demonstrated parallel IC and PCCS operation and the effects of leakage flow from the DW directly to the WW air space.

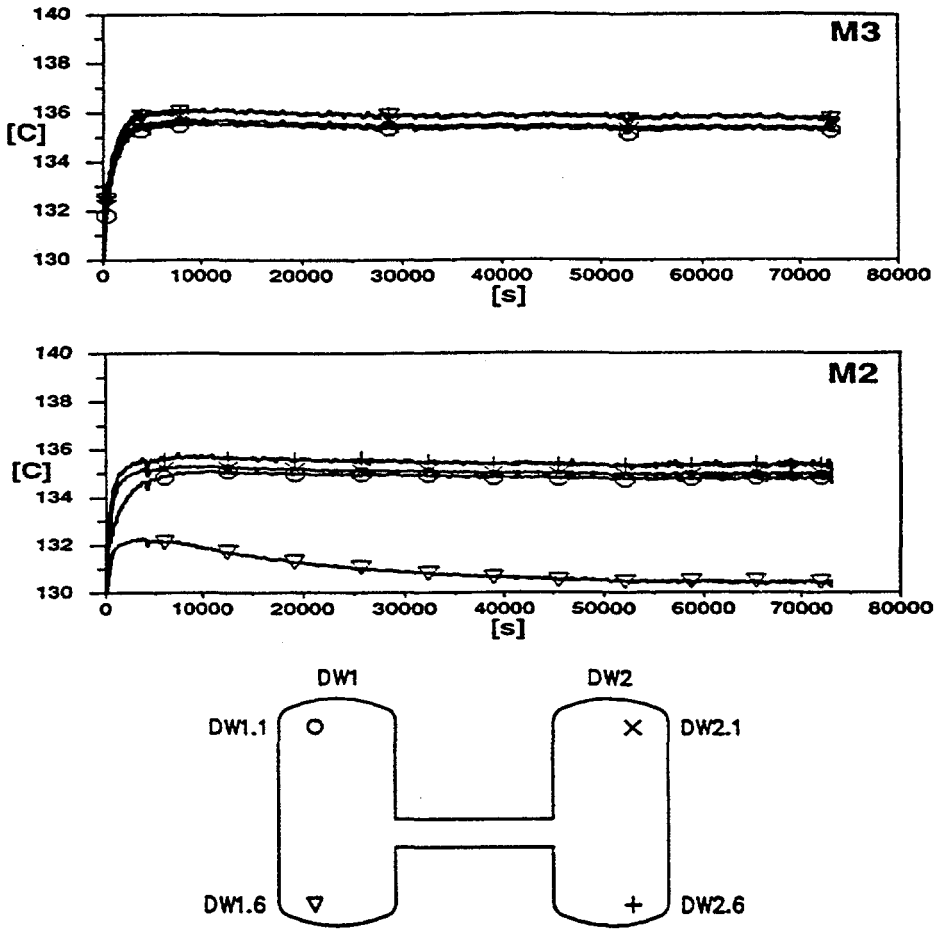

Fig. 6 Comparison of the variations of the axial DW temperatures during tests M2 and M3 (lower figure indicates location of corresponding thermocouples).

The last "early start" Test M9 started from initial conditions earlier in the transient and included the phase when cold Gravity-Driven Cooling System (GDCS) water is discharged into the RPV, thus depressurizing the DWs and causing vacuum breaker openings. This test established the link between the initial conditions calculated for the other tests and the actual history of the earlier period of the transient.

5.1 The PCCS Startup Test M7

The purpose of Test M7 was to demonstrate startup of the PCCS system when the DW and PCCS condensers are filled with air and the RPV starts delivering steam to the DW. To challenge sufficiently the system, the RPV heating power was kept constant at a relatively high value in this test. Figure 7 demonstrates the purging of the air from the DW and its accumulation in the WW. The PCC condensers started

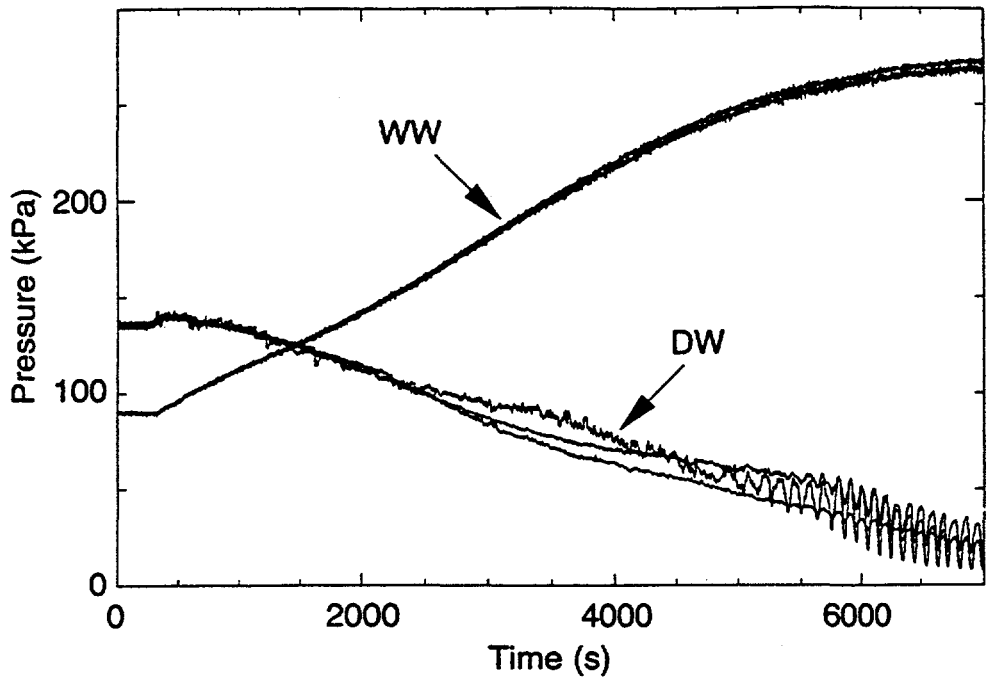

Fig. 7 Startup Test: Measured Drywell and Wetwell partial pressures indicating purging of the air from the DW

purging the DW air to the WW almost immediately after test initiation The condensing load was shared equally by all three PCC condensers.

Starting from non-prototypical pure-air conditions, this process was essentially completed in about 4 hr. The air concentrations, measured by oxygen probes at different elevations in the DW, Fig. 7, show no significant differences, indicating the absence of stratification.

The DW pressure oscillations that appear after 5000 s in Fig. 7 are due to oscillatory steam generation in the PANDA RPV. These are most likely due to particularities of this vessel (that is not a carefully scaled version of the SBWR RPV) and a dropping water level that hampered natural circulation in this vessel.

5.2 The System Effects Tests M6/M8

The goal of this combined test, was to:

- examine the interaction of the ICS operating in parallel with the PCCS,
- study the effect of DW to WW vacuum breaker leakage

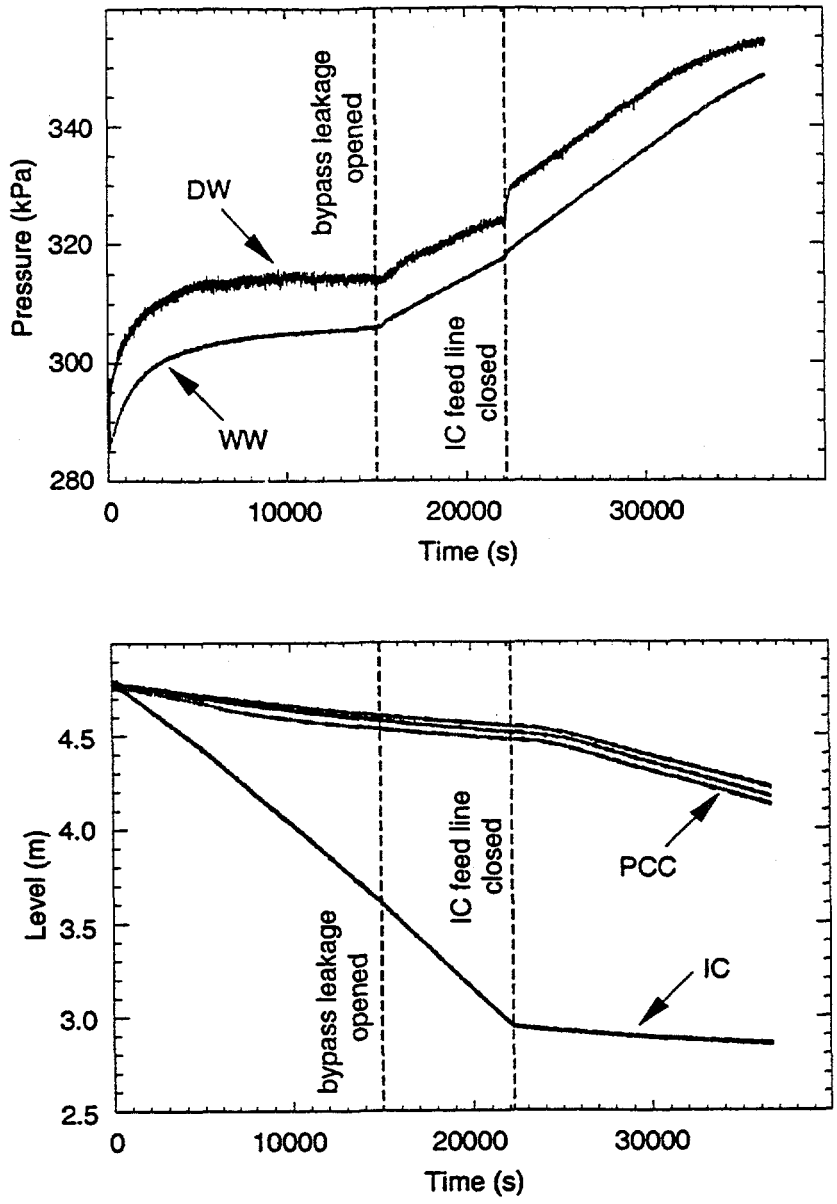

Fig. 8 Test M6/M8: Variation of the DW pressure (top) and of the PCCS Pool levels (bottom).

The DW to WW vacuum breaker leakage flow rate was chosen to be 10 times the SBWR design value. Figures 8 and 9 show system performance during this test. During the first phase of the test (0 to 15 000 s) the PCCS and the ICS operated in parallel and the DW and WW pressures leveled off, as shown in Fig. 8. The DW pressure response in this test was similar to the one in the base-case Test M3.

When leakage was established at 15 000 s, the WW pressure started rising and the DW pressure followed. When the ICS was shut off at about 22 000 s, the PCC vents cleared, as shown by the small jump in DW

pressure. The rate of pressurization of the system now increased, since the DW to WW pressure difference and consequently the leak flow rate had increased. This increased rate of pressurization remained, however, rather modest, especially considering the fact that a leakage flow rate 10 times the SBWR design-value was used in the test.

Figure 8 shows also the water levels recorded in the PCCS and ICS pools. As mentioned above, the rate of evaporation of the pools (reflected in the slope of the levels plotted versus time) gives a good measure of the condensation rate in the corresponding condensers. Figure 8 (bottom) shows that, as long as the ICS was operational, the bulk of the condensation took place in the ICS condenser. When the ICS was shut off, the condensing load was fully picked up by the three PCCS condensers (except for the leak flow rate producing SP and system heat up). Figure 8 shows clearly a increase of the rate of vaporization from their pools. (The small drop of the ICS pool level is due to evaporative heat loss from its top.)

5.3 The Early Start Test

Test M9 was intended to simulate the transition from the GDCS injection phase to the long-term PCCS cooling period. At the beginning of this test, the GDCS tank was filled with cold water, the RPV water level was low but still covering the core, and the DW was filled with pure steam. The test was started by switching on the power, opening the blowdown line valves and the valve in the GDCS return line. The GDCS water was discharged into the RPV within approximately 1000 s. Due to the subcooling of this water, boiling stopped in the RPV. The PCCs continued condensing steam at decreasing rate. Some steam was probably condensed in the RPV. As a consequence, the DW pressure dropped below the WW pressure and the VBs opened repeatedly The DW gas temperature measurements showed stratification during VB openings. At about 2400 s, saturated conditions were reached in the RPV and steam generation resumed.

Forty minutes after test initiation, the vertical distributions of gas temperatures and air concentrations in the DWs were not uniform. There were differences between the two DWs due to the asymmetric vacuum breaker openings -- the two VBs in DW1 and DW2 had different set points. Moreover, the injection of air from the WW to low points in the DWs by the VBs produced vertical stratification. However, after the start-up transient, only minor differences occurred in Test M9 as compared to Test M3 in relation to global system behavior. In Test M9, the WW pressure remained constant, while the DW pressure dropped, and the DW to WW pressure difference decreased significantly, Fig. 9, probably due to the absence of sufficient air in the system (Bandurski, 1997). Indeed, the axial tube gas temperature profiles measured in the condensers indicate some air accumulation in the tubes in Test M9, but less than in Test M3. Obviously, in Test M9 there was less residual air available in the system and, therefore, the heat transfer area available for condensation could not decrease to match the decreasing steam generation. Slightly higher feed flow rates in comparison to Test M3 did cause the slow DW pressure decrease in Test M9 (Bandurski et al., 1997). If the test had lasted longer slow accumulation of noncondensables in the PCC tubes would have stabilized the DW pressure also.

In general, the objective of the early start test was met: after 1 hr from the initiation of the transient, i.e. after about 40 min from the beginning of test M9, the system arrived at conditions very similar to those of the base-case Test M3 (Bandurski et al., 1997).

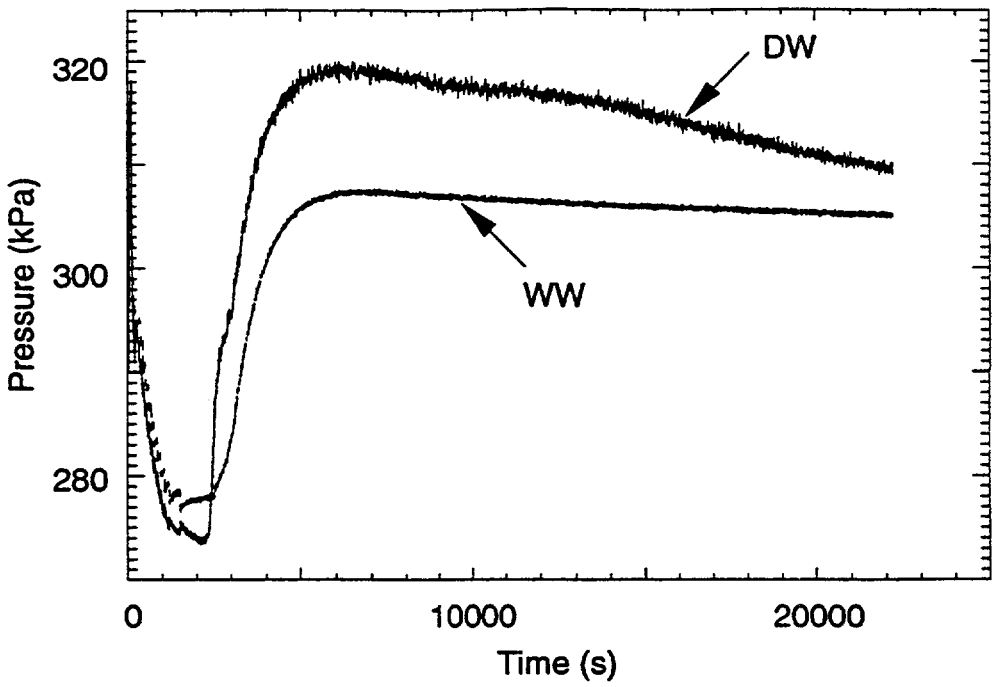

Fig. Test M9: Variation of the Drywell and Wetwell pressures.

6 GENERAL CONCLUSIONS

The M-3 Series of tests showed very good repeatability of overall system behavior (DW and SC pressures). Perturbations induced in the PCCS pools, non-uniform sharing of the condensation load among the PCC condensers, and various vacuum breaker openings produced local system perturbations but did not affect the overall, long-term containment behavior.

Small amounts of noncondensables affected the status of the condensers operating in parallel, but the global operation of the PCCS system was not influenced by any non-uniform distribution of noncondensables.

The asymmetric-configuration tests M2, M10A and M10B, investigated the effects of non-uniform distribution of air under extreme conditions. These tests, and in particular the M10 tests, challenged the system beyond prototypical SBWR operating conditions. They provide bounding conditions for the investigation of system behavior and for code qualification. Thus, the tests further confirmed the favorable and robust overall system response of the SBWR PCCS.

The remaining tests successfully demonstrated several other aspects of PCCS operation, namely:

- PCCS startup with bounding noncondensable gas concentrations in the DW (Test M7)
- the effects of parallel ICS and PCCS operation and of a leak rate (10-times the design value) between DW and WW (Test M6/M8)
- behavior during the transitional period from GDCS injection to long-term PCCS operation (Test M9)

In general, the tests demonstrated a favorable overall system behavior due to the "robust" performance of the PCCS. Good understanding of the effects of mixing in the large vessels was obtained.

Acknowledgments

The first phase of the ALPHA project (ALPHA-I) was conducted at PSI in cooperation with the Electric Power Research Institute (EPRI) and the General Electric Company (GE), and received financial support from the Nuclear Power Committee of the Swiss Utilities (UAK), the (former) Swiss National Energy Research Foundation (NEFF) and GE; these financial contributions are gratefully acknowledged.

This paper results from the collaboration of a large number of persons both inside PSI as well as outside. The authors particularly acknowledge the contributions of PSI collaborators P. Coddington and B. Uebelhart during the early phases of the project, of L. Voser for design, construction and resolution of many instrumentation problems, of J. Healzer for pre-test analyses and general advice, of P. Gritsch, W. Bulgheroni and P. Rasmussen for facility controls and data acquisition systems. The authors are also indebted to J. Yedidia of EPRI who was instrumental in organizing the ALPHA-I program and to their numerous GE colleagues who contributed time and effort, in particular to A. Rao, J. Fitch, B. Shiralkar, J. Torbeck, A. Arretz, B. Usry and B. Wingate.

REFERENCES

Bandurski, Th., Dreier, J., Huggenberger, M., Aubert, C., Fischer, O., Healzer, J., Lomperski, S., Strassberger, H.-J., Varadi, G., and Yadigaroglu, G. (1997) "PANDA passive decay heat removal transient test results,", *Proceedings of the Eighth International Topical Meeting on Nuclear Reactor Thermal-Hydraulics (NURETH-8),* Sept. 30 - Oct 4, 1997, Vol. 1, pp 474-484, Kyoto, Japan.

Coddington, P., Huggenberger, M., Güntay, S., Dreier, J., Fischer, O., Varadi, G., Yadigaroglu, G. (1992) "ALPHA: The long-term decay heat removal and aerosol retention programme," *5th International Topical Meeting on Nuclear Reactor Thermal Hydraulics (NURETH-5),* Salt Lake City, USA, Sept. 1992, pp. 203-211.

Dreier, J., Huggenberger, M., Aubert, C., Bandurski, Th., Fischer, O., Healzer, J., Lomperski, S., Strassberger, H.-J., Varadi, G., Yadigaroglu, G. (1996a) "The PANDA facility and first test results," *Kerntechnik,* 61, 214.

Dreier, J., Huggenberger, M., Aubert, C.,. Bandurski, Th., Fischer, O., Healzer, J., Lomperski, S., Strassberger, H.-J., Varadi, G., Yadigaroglu, G. (1996b) "The first PANDA tests," *Proc. of the ASME-JSME 4th Int. Conf. on Nuclear Engineering, ICONE-4,* A. Rao, R.B. Duffey and D. Elias (editors), New Orleans, Louisiana, March 10-14, 1996, Vol. 1B, pp. 843-851.

Fischer, O., Dreier, J., Aubert, C., Bandurski, Th., Huggenberger, M., Lomperski, S., Strassberger, H.-J., Varadi G., Yadigaroglu, G. (1996) "PANDA asymmetric-configuration passive decay heat removal test results," *Proc. Int. Topical Meeting on Advanced Reactors Safety, ARS'97,* June 1-5, 1997, Orlando, Florida, Vol. I, pp. 431-440.

Gamble, R.E., Hunsbedt, A., Shiralkar, B.S., Yadigaroglu, G. (1997) "Pressure scaling analysis of the SBWR and integral test facilities, Post test review," *Proc. of the Fifth Int. Conf. on Nuclear Engineering, ICONE-5,* ASME/SFEN/JSME, Nice, France, May 25-29, 1997, paper ICONE5-2073.

Shiralkar, B.S., Alamgir, Md., Andersen, J.G.M. (1993) "Thermal hydraulic aspects of the SBWR design," *Nucl. Eng. and Design,* 144, 213-221.

Shiralkar, B.S., Gamble, R.E., G. Yadigaroglu, G. (1997) " Passive Containment Cooling System performance in the Simplified Boiling Water Reactor," *Proc. Int. Topical Meeting on Advanced Reactors Safety,* ARS'97, Orlando Florida, June 1-5, 1997, Vol. I, pp. 478-484.

Upton, H.A., Cooke, F.E., Sawabe, J.K. (1993) "Simplified Boiling Water Reactor passive safety features," *Proc. 2nd ASME JSME Joint Int. Conf. on Nuclear Engineering,* San Francisco, California, 21–24 March 1993, Vol. 1, pp. 705–712.

Varadi, G.,. Dreier, J., Bandurski, Th., Fischer, O., Huggenberger, M., Lomperski, S., Yadigaroglu, G. (1996) "The PANDA tests for SBWR certification," *Proc. Twenty-Third Water Reactor Safety Information Meeting,* October 23-25, 1995, Bethesda, Maryland, NUREG/CP-0149, Vol. 1, p. 225.

Yadigaroglu, G. (1996) "Derivation of general scaling criteria for BWR containment tests," *Proc. of the ASME-JSME 4th Int. Conf. on Nuclear Engineering, ICONE-4,* A. Rao, R.B. Duffey and D. Elias (editors), New Orleans, Louisiana, March 10-14, 1996, Vol. 2, pp. 547-558.

Yokobori, S., Nagasaka, H., Tobimatsu, T. (1991) "System response test of isolation condenser applied as a passive containment cooling system," *1st JSME/ASEM Joint International Conf. on Nuclear Engineering (ICONE-I),* Nov. 1991, Tokyo.

CURRENT U.S. NRC REVIEW GUIDANCE FOR DIGITAL INSTRUMENTATION AND CONTROL SYSTEMS

UPDATE OF STANDARD REVIEW PLAN CHAPTER 7 INSTRUMENTATION AND CONTROLS

Matthew Chiramal
Instrumentation and Controls Branch
Division of Reactor Controls and Human Factors
Office of Nuclear Reactor Regulation
Phone No: 301-415-2845; E-mail: mxc@nrc.gov

October 22, 1997

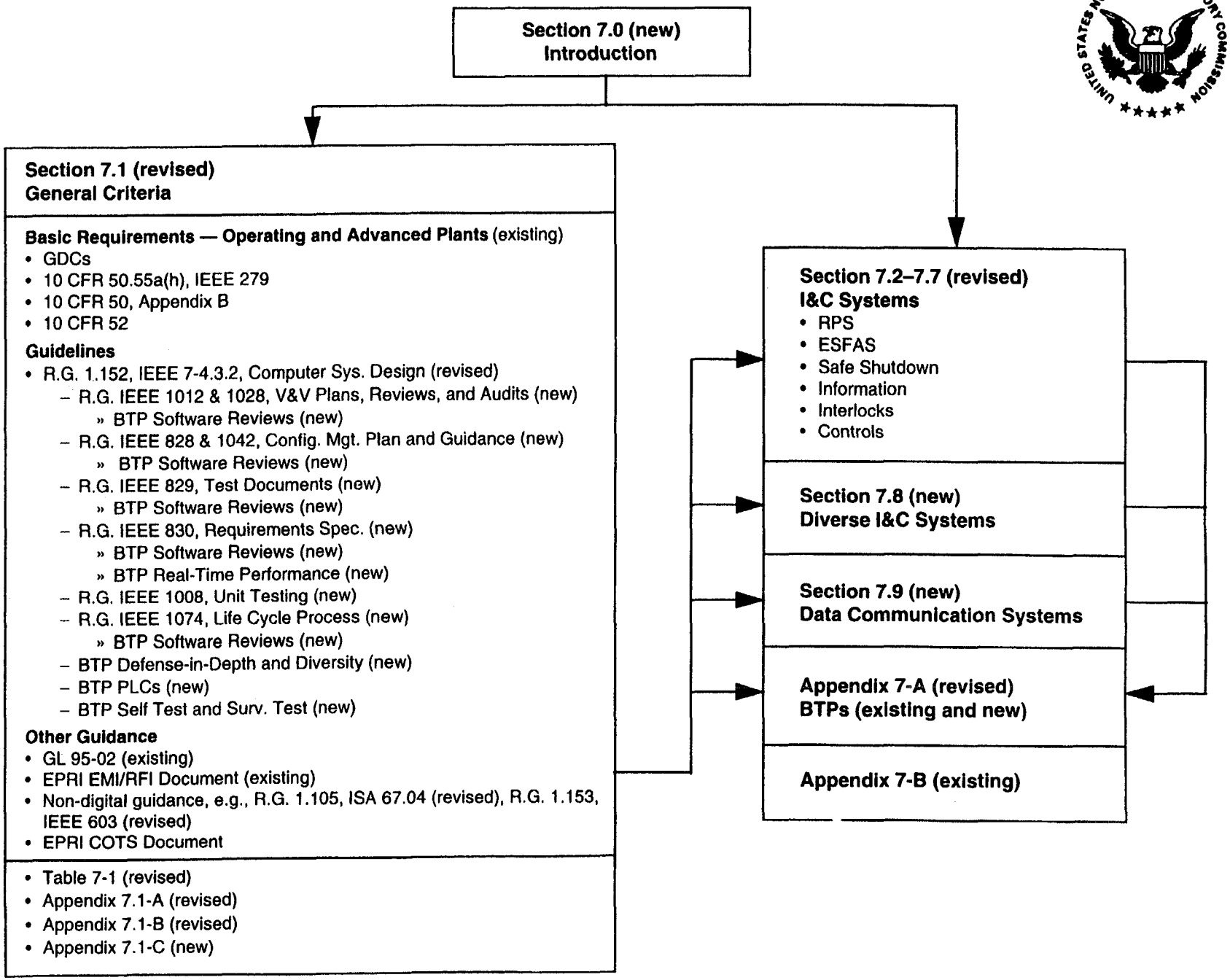
Section 7.0 (new)
Introduction
Section 7.1 (revised)
General Criteria
Basic Requirements — Operating and Advanced Plants (existing)
• GDCs
• 10 CFR 50.55a(h), IEEE 279
• 10 CFR 50, Appendix B
• 10 CFR 52
Guidelines
• R.G. 1.152, IEEE 7-4.3.2, Computer Sys. Design (revised)
– R.G. IEEE 1012 & 1028, V&V Plans, Reviews, and Audits (new)
» BTP Software Reviews (new)
– R.G. IEEE 828 & 1042, Config. Mgt. Plan and Guidance (new)
» BTP Software Reviews (new)
– R.G. IEEE 829, Test Documents (new)
» BTP Software Reviews (new)
– R.G. IEEE 830, Requirements Spec. (new)
» BTP Software Reviews (new)
» BTP Real-Time Performance (new)
– R.G. IEEE 1008, Unit Testing (new)
– R.G. IEEE 1074, Life Cycle Process (new)
» BTP Software Reviews (new)
– BTP Defense-in-Depth and Diversity (new)
– BTP PLCs (new)
– BTP Self Test and Surv. Test (new)
Other Guidance
• GL 95-02 (existing)
• EPRI EMI/RFI Document (existing)
• Non-digital guidance, e.g., R.G. 1.105, ISA 67.04 (revised), R.G. 1.153, IEEE 603 (revised)
• EPRI COTS Document
• Table 7-1 (revised)
• Appendix 7.1-A (revised)
• Appendix 7.1-B (revised)
• Appendix 7.1-C (new)
Section 7.2–7.7 (revised)
I&C Systems
• RPS
• ESFAS
• Safe Shutdown
• Information
• Interlocks
• Controls
Section 7.8 (new)
Diverse I&C Systems
Section 7.9 (new)
Data Communication Systems
Appendix 7-A (revised)
BTPs (existing and new)
Appendix 7-B (existing)

We updated the SRP, we did not rewrite it

- Ground rules
  - Maintain existing regulatory bases
  - Incorporate lessons learned from ALWR reviews
  - Incorporate lessons learned from digital retrofits
  - Incorporate operating experience lessons learned
  - The update will describe I&C system criteria for both operating plants (modifications) and proposed future advanced reactor designs
  - If a topic is already covered, the topic is adequately covered (unless something is clearly wrong)

We made no fundamental changes to the basic architecture of Chapter 7

- General requirements and guidance in 7.1
  - Add references to new regulatory guides and branch technical positions (BTPs) on special digital system issues
  - Highlight review areas, acceptance criteria, and review process for digital systems
  - Add discussion of standard plant reviews
- Remaining sections (7.2–7.9) focus on systems
  - Add references to digital system guidance in Section 7.1

Three new sections were added

- 7.0 — Introduction
  - How to use Chapter 7
- 7.8 — Diverse Actuation
  - ATWS
  - Diverse actuation
    - » Manual system-level initiation
    - » Dedicated displays
    - » Automatic systems that are distinct from traditional protection and control
- 7.9 —Data Communication Systems

Two appendices were added and three revised

- New Appendix 7.0-A describes the overall review process for digital systems
- New Appendix 7.1-C provides guidance with respect to review according to IEEE 603 (Reg. Guide 1.153)
- Revised Appendix 7.1-A addresses rule changes (Part 52 and revisions to Part 50), and new regulatory guides
- Revised Appendix 7.1-B incorporates digital topics into the review of compliance with IEEE 279
- Revised Appendix 7-A includes new BTPs discussed below

A new set of branch technical positions was developed

- Software Reviews
- Defense-in-Depth and Diversity
- Real-Time Performance
- On-Line and Periodic Testing
- Level of Detail for Design Certification Applications
- Programmable Logic Controllers
- Other non-digital system topics

NRC Research developed new regulatory guides

- DG-1054 Verification, Validation, Reviews and Audits (IEEE 1012 and 1028)
- DG-1055 Software Configuration Management (IEEE 828 and 1042)
- DG-1058 Software Requirements Specifications (IEEE 830)
- DG-1056 Software Test Documentation (IEEE 829)
- DG-1059 Software Life Cycle Processes (IEEE 1074)
- DG-1057 Software Unit Testing (IEEE 1008)

The revised SRP and new regulatory guides will aid in future reviews

- There is no impact on existing systems
  - Neither the SRP nor the new regulatory guides are proposed for backfit
- The SRP and regulatory guides are guidance only
- New system developers will benefit from identification of acceptable approaches to designing digital systems
  - Licensees have a clear path to acceptance of modifications
  - Utilities making 10 CFR 50.59 evaluations have more information upon which to base unreviewed safety question determination

Reviewers of license amendment applications will use the revised SRP

- Reviewers will use selected portions of the SRP depending upon the scope of the change
- Depth of review will be determined by the reviewer and will depend upon safety significance and complexity of the change
- For previously approved designs, only the differences identified in the subsequent application and plant-specific issues will be reviewed
- Defense-in-depth and diversity analysis is only applicable to applications involving Reactor Trip Systems or Engineered Safety Features Actuation Systems

Section 7.0 describes the overall review process

- Purpose
  - Describes the overall HICB review process
    - » License applications (including amendments)
    - » Topical reports
- Technical basis
  - Documents existing practice

Summary of Section 7.0

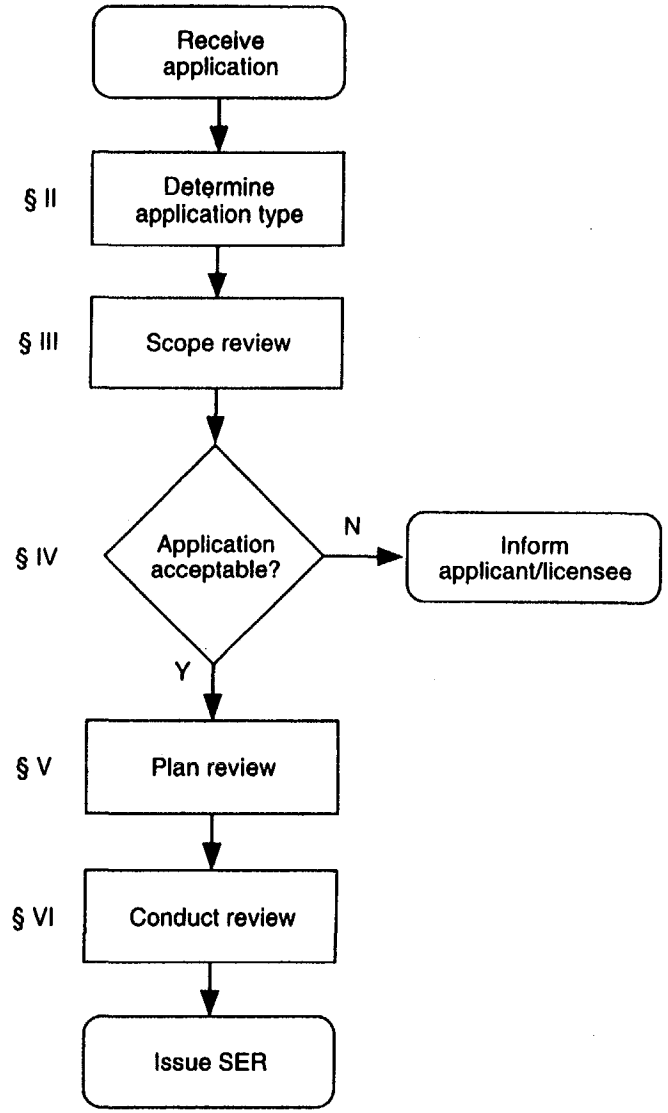

Appendix 7.0-A describes the unique aspects of digital system reviews

- **Purpose**
  - Overview of the process for reviewing the unique aspects of digital I&C
    - » Supplements the description of the process for review of
      - The overall I&C system design described in Section 7.0,
      - Design criteria and commitments described in Section 7.1, and
      - The individual systems described in Sections 7.2 through 7.9.
    - » Illustrates how the review activities interact with each other and with the overall I&C review process

Appendix 7.0-A outlines an overall process for digital system reviews

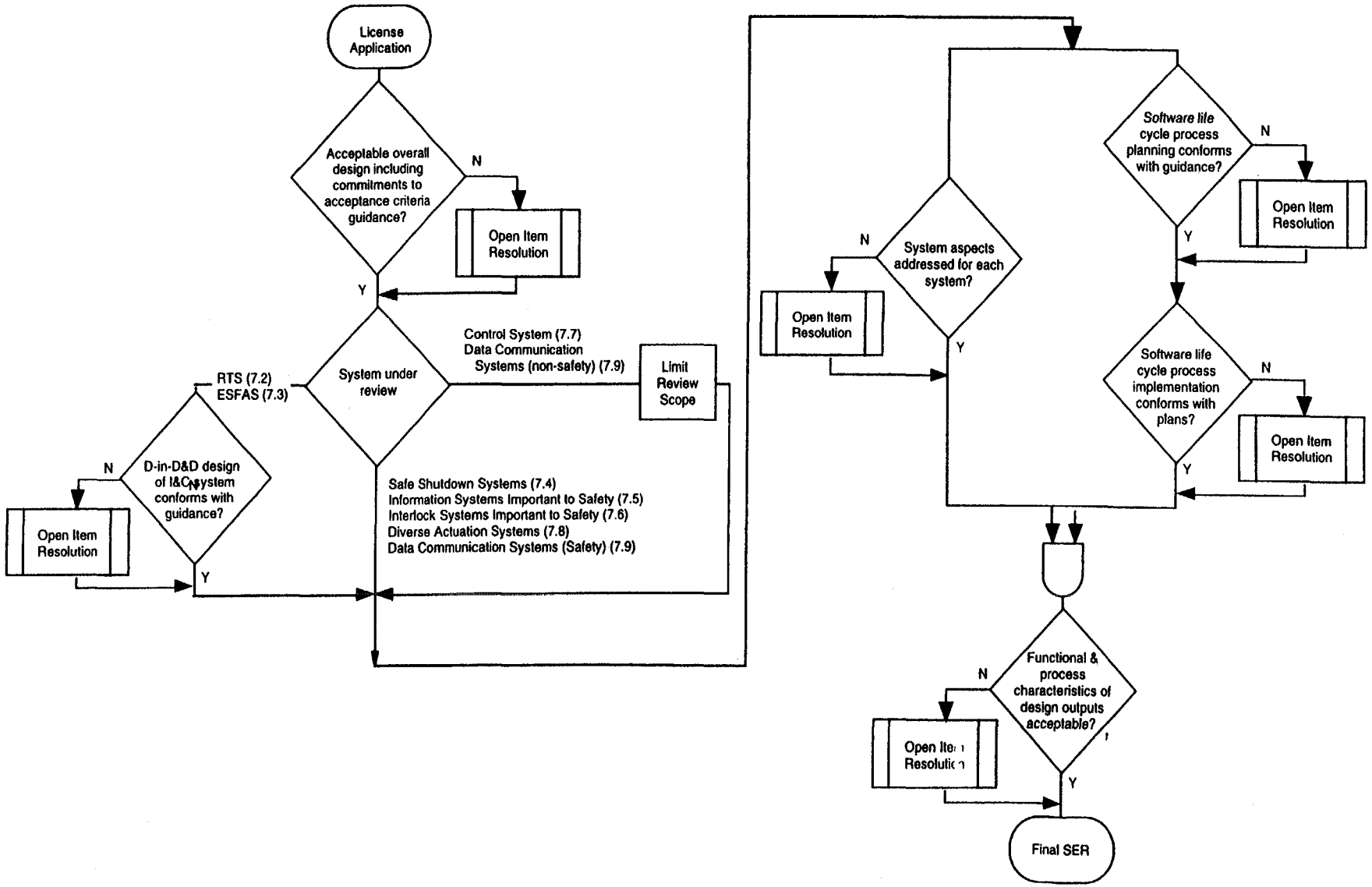

Section 7.1 describes the basic acceptance criteria and guidance for I&C systems

- Purpose
  - Identify systems that should be covered by SAR
  - Identify acceptance criteria applicable to multiple systems
  - Identify regulatory guides and standards for compliance
  - Guide reviewers in evaluating applicant commitments
- Technical basis
  - 10 CFR 50.55a(h) — IEEE Std 279
    - » IEEE Std 603 and IEEE Std 7-4.3.2
  - 10 CFR 50.34(f) — TMI Action Plan
  - 10 CFR 50.62 — ATWS
  - 10 CFR 50 Appendix A — GDC

Structure of Section 7.1

- Section 7.1
  - Review responsibilities
  - Areas of review
  - Acceptance criteria
  - Review process
  - Evaluation findings
  - Implementation
- Appendix A — Acceptance criteria and guidance
  - Summarized in Table 7.1-1
- Appendix B — Evaluation with respect to IEEE 279
- Appendix C — Evaluation with respect to IEEE 603

The review of digital systems follows IEEE Standard 7-4.3.2

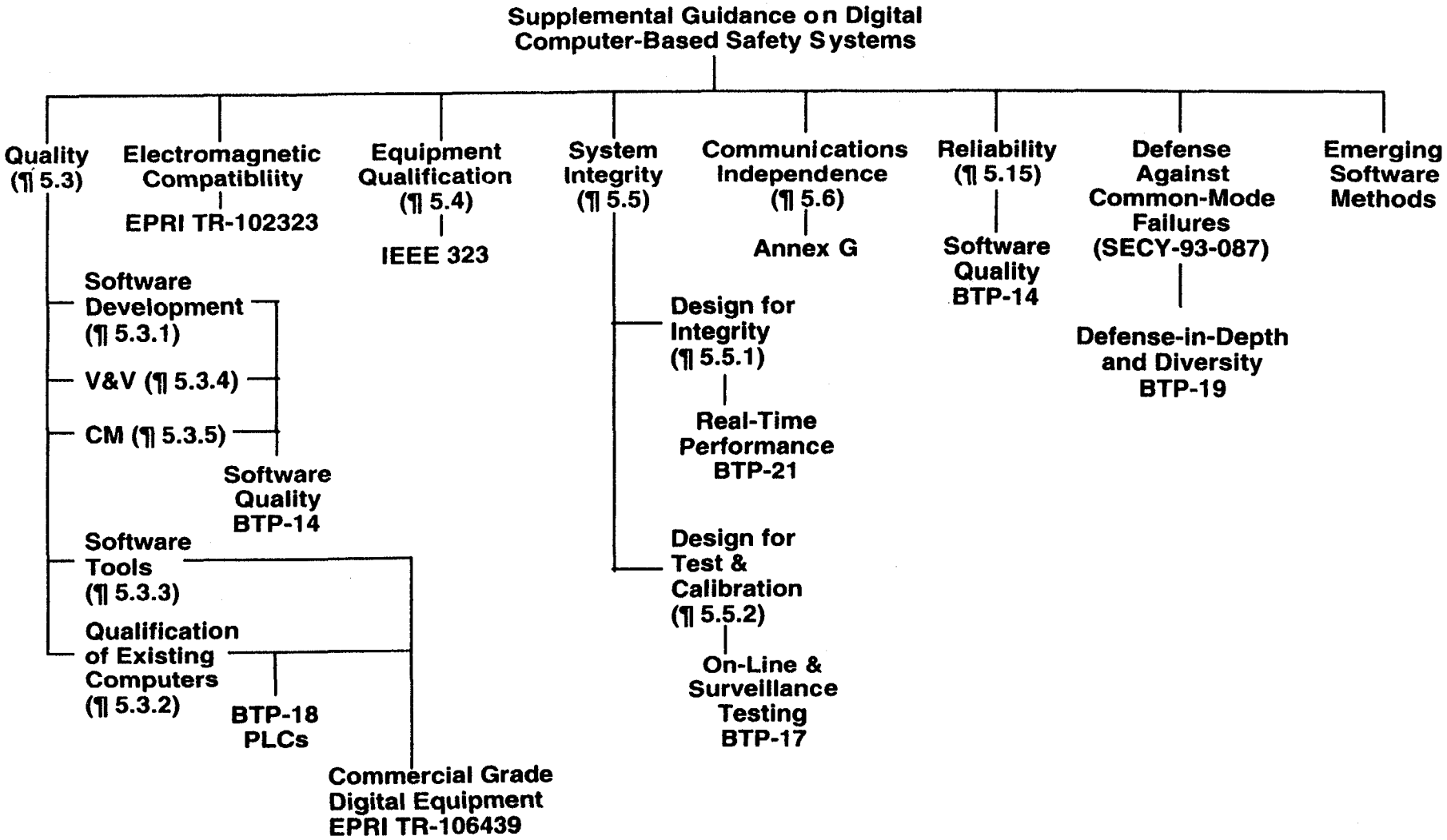

Table 7.1-1 summarizes the acceptance criteria and guidance for each system

- For use as a quick reference by reviewers
- The table is a starting point
  - The criteria and guidance for a specific system may be different depending upon
    - » design characteristics
    - » licensee/applicant commitments

Appendix 7.1-A outlines the review procedures for each acceptance criteria and Reg. Guide

- Sections 7.2 thru 7.9 reference 7.1-A for review procedures
- Reviews start with acceptance criteria
- 7.1-A provides the road map from acceptance criteria to more detailed guidance

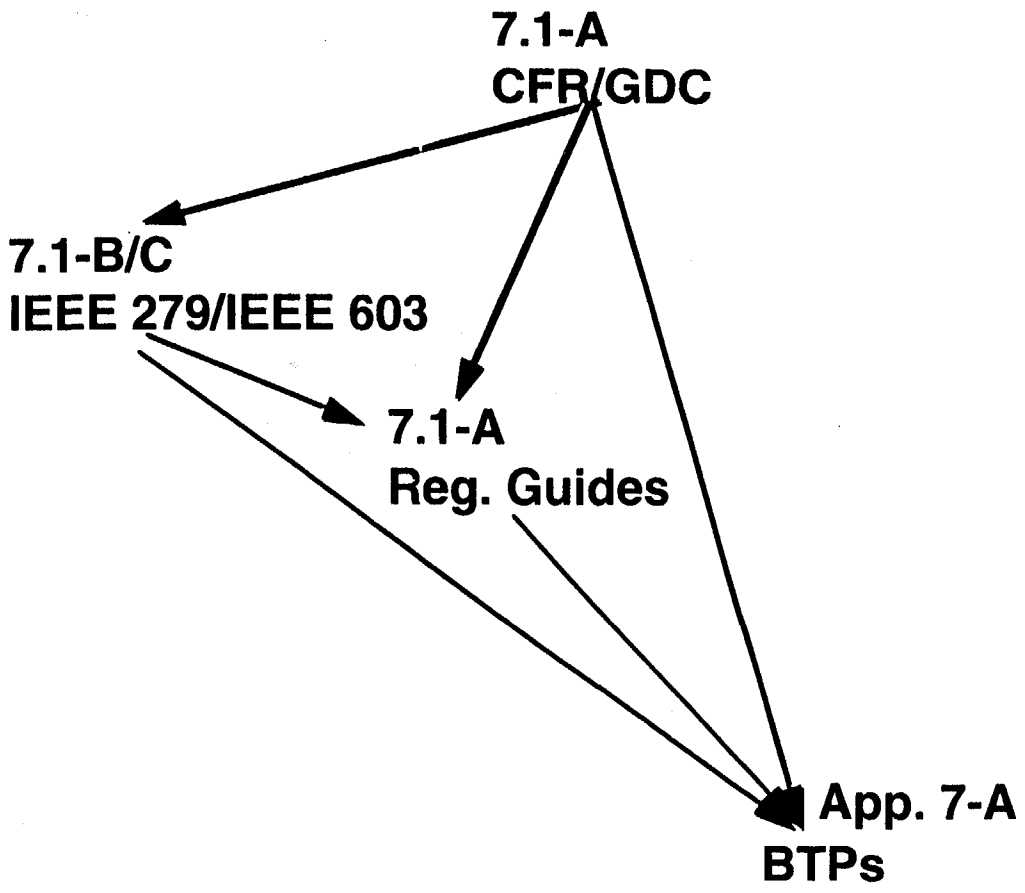

Appendices 7.1-B and C discuss review against 10 CFR 50.55a(h) (IEEE 279)

- The reviewer selects one depending upon the licensee/ applicant's commitments
  - 7.1-B for IEEE 279
  - 7.1-C for IEEE 603
- Compliance with IEEE 279 also satisfies many of the protection system GDC
  - Therefore 7.1-B and C are used in the review process for these acceptance criteria

Sections 7.2 through 7.9 follow a common outline

- Areas of Review
- Acceptance Criteria
- Review Procedures
- Evaluation Findings
- Implementation
- References

Coordination of reviews is similar for all sections

- Reactor Systems Branch
  - Required I&C functions
  - Reactivity measurement and control aspects
- Plant Systems Branch
  - Required I&C functions
  - Supporting systems
- Mechanical Engineering Branch
  - Seismic qualification
- Containment Systems & Severe Accident Branch
  - Required I&C functions
  - Severe accident I&C
- Electrical Engineering Branch
  - Power supply and cable separation
  - Environmental qualification
- Human Factors Assessment Branch
  - User Interface
- ITAAC (Part 52) review described in Chapter 14

Summary of Section 7.2 (Reactor Trip System)

- Scope
  - Automatic initiation of reactivity control
- Acceptance Criteria
  - 10 CFR 50.55a(h)— Codes & Standards (IEEE 279)
  - 10 CFR50.35(f) — TMI Requirements
  - GDC 1 — Quality
  - GDC 2 & 4 — Environmental & Natural Phenomena Hazards
  - GDC 13 & 19 — Instrumentation & Control/Control Room
  - GDC 20-25 & 29 — Protection Systems
  - 10 CFR 52 — Resolution of Safety Issues, ITAAC, Interface Requirements, Level of Detail, Innovative Safety Systems

Summary of Section 7.2 (cont.)

- Review Emphasis
  - RTS design basis
  - Single failure criterion
  - Quality of components and modules (including software)
  - Independence
    - » Between redundant channels
    - » Between control and protection
  - Defense-in-depth and diversity
  - System testing and surveillance measures
  - Use of digital systems
  - Setpoint determination

The evaluation findings describe the conclusions a reviewer should be able to reach

- All acceptance criteria are met
- Typical SER language is provided

This is typical for Sections 7.2 - 7.9

Summary of Section 7.3 (Engineered Safety Features)

- Scope
  - Engineered Safety Feature Actuation
  - Engineered Safety Feature Control
- Acceptance criteria
  - Same as for RTS
  - Also criteria for ESF functions supported
- Review emphasis
  - Same as RTS

Summary of Section 7.4 (Safe Shutdown)

- Scope
  - I&C for safe shutdown from control room or remote location
- Acceptance criteria
  - GDC 2 & 4 — Environmental & Natural Phenomena Hazards
  - GDC 13 & 19 — Instrumentation & Control / Control Room
  - GDC for supported systems (RHR, ECCS, Cont. Heat Removal)
  - 10 CFR 52

Summary of Section 7.4 (cont.)

- Review emphasis
  - Safe & remote shutdown functions
  - Single failure criterion
  - Independence from protection systems
  - Use of digital systems
  - Surveillance test provisions

Summary of Section 7.5 (Information Systems)

- Scope
  - Post Accident Monitoring (PAM)
  - Bypass & Inoperable Status Indication
  - Annunciators
  - SPDS, ERF, ERDS/ protection system independence
- Acceptance criteria
  - 10 CFR 50.34(f) — TMI Requirements
  - GDC 1 — Quality
  - GDC 2 & 4 — Environmental & Natural Phenomena Hazards
  - GDC 13 & 19 — Instrumentation & Control / Control Room
  - GDC 24 — Control/ protection independence
  - 10 CFR 52

Summary of Section 7.5 (cont.)

- Review Emphasis
  - PAM compliance with Reg. Guide 1.97
  - PAM support of EOP actions
  - Severe accident monitoring
  - Scope of bypass and inoperable status indication
  - BISI conformance with Reg. Guide 1.47
  - Annunciator reliability
  - ALWR annunciator requirements
    - » limited redundancy
    - » self-test provisions
    - » safety related annunciators in particular cases
  - Use of digital systems
  - Independence from protection systems

Summary of Section 7.6 (Interlock Systems)

- Scope
  - Interlocks credited for preventing events or maintaining availability of safety systems
- Acceptance criteria
  - 10 CFR 50.55a(h) — Codes & Standards (IEEE 279)
  - GDC 1 — Quality
  - GDC 2 & 4 — Environmental & Natural Phenomena Hazards
  - GDC 13 & 19 — Instrumentation & Control / Control Room
  - GDC for supported systems
  - 10 CFR 52

Summary of Section 7.6 (cont.)

- Review emphasis
  - Interlock functions included
  - Single failure criterion
  - Quality of components and modules
  - Independence from control systems
  - Surveillance testing
  - Use of digital systems

Summary of Section 7.7 (Control Systems)

- Scope
  - Non-safety I&C that can affect performance of safety functions
- Acceptance criteria
  - 10 CFR 50.34(f) — TMI Requirements
  - GDC 1 — Quality
  - GDC 13 & 19 — Instrumentation & Control / Control Room
  - GDC 24 — Control/protection independence
  - 10 CFR 52

Summary of Section 7.7 (cont.)

- Review emphasis
  - Design basis
  - Safety classification
  - Effect of control systems on transients
  - Effect of control system failures
  - Environmental control for safety systems
  - Use of digital systems
  - Control / protection independence
  - Control system functions credited for defense-in-depth and diversity

Summary of Section 7.8 (Diverse I&C Systems)

- Scope
  - ATWS mitigation
  - Systems provided specifically for defense-in-depth and diversity position
    - » Diverse Actuation
    - » Manual Displays and Controls
- Acceptance criteria
  - GDC 1 — Quality
  - 10 CFR 52
  - 10 CFR 50.62 —ATWS

Summary of Section 7.8 (cont.)

- Review emphasis
  - Design basis
  - Quality of components and modules
  - Surveillance test provisions
  - Consistency with defense-in-depth and diversity analysis
  - Power supply availability
  - Environmental Qualification
  - Independence from protection system
  - Manual initiation capability
  - Completion of protective action

Summary of Section 7.9 (Data Communication)

- Scope
  - Communications systems supporting multiple systems
    - » Other than "point-to-point" cables (e.g., multiplexed systems)
- Acceptance criteria
  - Union of acceptance criteria for supported systems
- Review emphasis
  - Quality of components & modules
  - Software quality
  - Performance
  - Reliability

Summary of Section 7.9 (cont.)

- **Additional review emphasis for safety-related data communication**
  - **Single failure criterion**
  - **Independence between redundant channels**
  - **Failure modes**
  - **Surveillance test provisions**
  - **EMI/RFI susceptibility**
  - **Consistency with defense-in-depth and diversity analysis**
  - **Seismic qualification**

Appendix 7.1-A contains the Branch Technical Positions

BTP number	Subject
1	Isolation of Low-Pressure Systems from the High-Pressure Reactor Coolant System
2	Motor-Operated Valves in the Emergency Core Cooling System Accumulator Lines
3	Protection System Trip Point Changes for Operation with RCS Pumps Out of Service
4	Guidance on Design Criteria for Auxiliary Feedwater Systems
5	Spurious Withdrawals of Single Control Rods in Pressurized Water Reactors
6	Design of I&C Provided to for Changeover from Injection to Recirculation Mode
7	Not used
8	Application of Regulatory Guide 1.22
9	Reactor Protection System Anticipatory Trips
10	Application of Regulatory Guide 1.97 (Post Accident Monitoring Systems)
11	Application and Qualification of Isolation Devices
12	Establishing and Maintaining Instrument Setpoints
13	Replacement of Reactor Coolant RTD Bypass Manifold Temperature Instruments
14	Software Reviews for Digital Computer-Based I&C Safety Systems
15	Not used
16	Level of Detail Required for Design Certification Applications Under 10 CFR Part 52
17	Self-Test and Surveillance Test Provisions in Digital Computer-Based I&C Systems
18	Use of Programmable Logic Controllers in Digital Computer-Based I&C Systems
19	Defense-in-Depth and Diversity in Digital Computer-Based I&C Systems
20	Not used
21	Digital System Architecture and Real-Time Performance

There are four groups of BTPs

- BTP 1 - 9 are existing BTPs
  - One BTP deleted because now covered in Chapter 18
  - Others unchanged except for format and reference to IEEE 603
- BTP 10 - 13 reflect lessons learned from operating reactor reviews
- BTP 14, 17, 18, 19, and 21 deal with digital system issues
- BTP 16 discusses level of detail for Design Certification applications

The new BTP's follow a common outline

- Background
  - Regulatory Basis
  - Applicable Guidance
  - Purpose
- Branch Technical Position
  - Acceptance Criteria
  - Review Procedures
- References

BTPs 10 through 13 address operating plant lessons learned

- BTP-10 deals with lessons learned from implementation of Reg Guide 1.97 (PAM)
  - Acceptable deviations for selected variables
- BTP-11 deals with the application and qualification of electrical isolation devices in instrumentation circuits
  - Identifies acceptable design characteristics and test methodologies
- BTP-12 deals with lessons learned from implementation of Reg Guide 1.105 (Setpoints)
  - Adequacy of setpoint calculation methodologies
- BTP-13 documents staff position on cross-calibration of RCS temperature detectors
  - Acceptable methods and impact upon setpoints

BTPs 14, 17-19, and 21 deal with digital topics

- BTP 14 describes the review of software
  - Criteria for planning, process, and design outputs
- BTP 17 discusses self-test and surveillance test features
  - Criteria for types of tests and constraints on tests
- BTP 18 discusses considerations in the use of PLCs
  - The use of PLCs may simplify design activities
- BTP 19 describes the review of defense-in-depth and diversity analysis
  - Key points in evaluating level of diversity provided
- BTP 21 discusses topics for consideration in confirming real-time performance
  - Architectural considerations and timing demonstration

CURRENT U.S. NRC REVIEW GUIDANCE FOR DIGITAL INSTRUMENTATION AND CONTROL SYSTEMS

NEW REGULATORY GUIDES FOR DIGITAL COMPUTER SOFTWARE TO BE USED IN SAFETY SYSTEMS OF NUCLEAR POWER PLANTS

Joel J. Kramer
Control, Instrumentation, and Human Factors Branch
Division of Systems Technology
Office of Nuclear Regulatory Research
Phone.: (301) 415-5891; E-Mail: jjk1@nrc.gov

October 22, 1997

NATURE OF STANDARDS BEING ENDORSED

Consensus Standards on Software Engineering

Overall Software Process

IEEE 1074-1991	Developing Software Life Cycle Processes

Intermediate Software Products

IEEE 830-1994	Software Requirements Specifications

Evaluation of Intermediate and Final Software Products

IEEE 829-1993	Software Test Documentation*
IEEE 1008-1987	Software Unit Testing
IEEE 1012-1986	Software Verification and Validation Plans*
IEEE 1028-1988	Software Reviews and Audits

Control of Intermediate and Final Software Products

IEEE 828-1990	Software Configuration Management Plans*
IEEE 1042-1987	Guide to Software Configuration Management

* These are also products of the software development process

DRAFT REGULATORY GUIDES FOR COMPUTER SOFTWARE USE IN SAFETY SYSTEMS OF NUCLEAR POWER PLANTS

- DG-1054 (Software Verification and Validation)--Proposed Final Regulatory Guide 1.168
- DG-1055 (Software Configuration Management)--Proposed Final Regulatory Guide 1.169
- DG-1056 (Software Test Documentation)--Proposed Final Regulatory Guide 1.170
- DG-1057 (Software Unit Testing)--Proposed Final Regulatory Guide 1.171
- DG-1058 (Software Requirements Specification)--Proposed Final Regulatory Guide 1.172
- DG-1059 (Software Life Cycle Processes)--Proposed Final Regulatory Guide 1.173

PUBLIC COMMENT SOURCES

- Westinghouse
- Commonwealth Edison
- Nebraska Public Power District (Cooper Nuclear Station)
- Capri Technology
- A member of the Atomic Safety and Licensing Board (ASLB)
- (Nuclear Utilities Software Management Group)

SUMMARY OF PUBLIC COMMENTS

- Generally supported use of Software Regulatory Guides as a first step
- Some standards may be too prescriptive
- NRC requirement for "independence"
- Restricting use of Commercial Off-the-Shelf (COTS) Software
- Worthwhile, constructive suggestions for improved wording and clarification
- Need for a software "systems safety model" to provide further assurance of adequacy of software products

PROPOSED CHANGES TO DG-1054 (REGULATORY GUIDE 1.168)
Software Verification and Validation

- Position 3 Independence of Software V+V
  - Proficiency of independent verifiers
  - Responsibility for the adequacy of V+V

- Position 5 Conformance of Materials
  - Acceptance of pre-existing software
  - Regulatory Guide 1.152, Rev. 1, and EPRI T-106439

- Section B Discussion
  - Classification of safety systems software
  - Importance to safety
  - Flexibility in implementation

PROPOSED CHANGES TO DG-1055 (REGULATORY GUIDE 1.169)
Software Configuration Management

- Position 6 Documentation
  - Applicability of guide
  - Software requirements, designs, and code
  - Support software used in development (exact versions)
  - Ensuring that all factors contributing to executable software are understood

- Position 12 Backfit clarification (New Position)
  - Some statements on Section 1.1 of IEEE Std 828-1990 should not be interpreted as a requirement for backfit
  - Section D Implementation contains staff's position

PROPOSED CHANGES TO DG-1056 (REGULATORY GUIDE 1.170)
Software Test Documentation

- NONE

PROPOSED CHANGES TO DG-1057 (REGULATORY GUIDE 1.171)
Software Unit Testing

- Position 4 Independence in Software Verification
    - o Essentially same as with Position 3 for DG-1054 (RG 1.168)

PROPOSED CHANGES TO DG-1058 (REGULATORY GUIDE 1.172
Software Requirements Specification

- Position 6.3 Robustness
    - o Responding to both hardware and software failures vs. handling both
    - o Software requirements for fault tolerance and failure modes be specified for each OPERATING mode
    - o Based on system level hazards analysis or consideration of software internals

PROPOSED CHANGES TO DG-1059 (REGULATORY GUIDE 1.173)
Software Life Cycle Processes

- Position 1.3 Commercial Software
  Essentially same as Position 5 for DG-1054 (RG 1.168)

- Position 1.4 Definitions
  Only definitions for accident and hazard

FUTURE RESEARCH

- Additional research based upon NAS recommendations may lead to an improved technical basis for software evaluation
- We are developing a strategic research plan for digital I&C
- Software reliability
- Total system requirements framework
- Research results to be reflected in future revisions of standards and regulatory guides
- New user needs from NRR

CURRENT RESEARCH RESULTS ON THE TECHNICAL BASIS FOR ENVIRONMENTAL QUALIFICATION OF SAFETY-RELATED DIGITAL I&C SYSTEMS*

K. Korsah, P. D. Ewing, S. Kercel, R. T. Wood, Oak Ridge National Laboratory, Oak Ridge, TN, 37831
Mahbubul Hassan, Brookhaven National Laboratory, Upton, NY, 11973
Tina Tanaka, Sandia National Laboratories, Albuquerque, NM, 87123
Christina Antonescu, U.S. Nuclear Regulatory Commission, Rockville, MD, 20852

ABSTRACT

This paper presents results to date of an NRC-sponsored confirmatory research program initiated at three national laboratories to address environmental compatibility/qualification concerns associated with the use of microprocessor-based safety-related instrumentation and control (I&C) systems in nuclear power plants. The research approach involved evaluating existing military and industrial guidance, identifying the most significant environmental stressors and, for advanced I&C systems in a nuclear power plants, investigating the likely failure modes—both at the integrated circuit and system level—for digital technologies under varying levels of environmental stress (such as smoke exposure and electromagnetic and radio-frequency interference). The insights gained from these studies are being used to recommend appropriate methods for qualifying safety-related digital equipment in nuclear power plants.

1. INTRODUCTION

Distributed computer systems and other advanced digital technologies are being used to upgrade instrumentation and control (I&C) systems in nuclear power plants. One concern with using such systems in nuclear power plants, particularly for safety-related applications, is their potential sensitivities to nuclear power plant environments and the possibility of common cause effects resulting from environmental stress.[1] To properly address the qualification needs for safety-related digital systems, it is useful to more fully understand the response of these technologies to likely environmental stress and to better characterize the environments in which they operate. For example, there is the lack of information on the potential vulnerability of I&C equipment under smoke exposure. As another example, until recently little was known about the prevailing ambient electromagnetic interference (EMI) and radio-frequency interference (RFI) environment in nuclear power plants. This lack of information made it difficult to establish electromagnetic operating envelopes for safety-related I&C systems.

These uncertainties prompted the U. S. Nuclear Regulatory Commission (NRC) to initiate the confirmatory research program, *Qualification of Advanced Instrumentation and Control Systems*, at three U. S. Department of Energy national laboratories—Oak Ridge National Laboratory (ORNL), Sandia National Laboratories (SNL), and Brookhaven National Laboratory (BNL). The objective of this research program is to provide the technical basis for environmental qualification of microprocessor-based safety equipment in nuclear power plants. The research approach involves evaluating existing military and industrial guidance, identifying the

*Research sponsored by the Office of Nuclear Regulatory Research, U. S. Nuclear Regulatory Commission. The opinions and viewpoints expressed herein are those of the authors and do not necessarily reflect the criteria, requirements, and guidelines of the U.S. NRC.

most significant environmental stressors, investigating the likely failure modes for digital technologies under varying levels of environmental stress, and recommending appropriate methods for qualifying safety-related digital equipment. This paper presents a summary of the results to date for the different projects performed under the research program. The program is divided into several projects that are being performed by the national laboratories.

In the first project, BNL conducted a screening study to identify environmental stressors for advanced I&C systems in a nuclear power plant that can be potentially risk-significant. The risk screening was based on estimated risk-sensitivities of the stressors (i.e., relative changes in plant risk caused by the stressors), which are quantified by estimating stressor effects on the occurrences of I&C failure and the consequent increase in risk in terms of relative core damage frequency (CDF). The stressors evaluated for risk effects were temperature, humidity, vibration, EMI from lightning, and smoke.

In the second project, which was performed by SNL, smoke exposure tests were conducted on digital circuit components and circuit boards to determine failure mechanisms and to assess the effectiveness of different packaging techniques. The component tests focused on short-term effects, such as circuit bridging, in typical components and the factors that can influence the degree to which the smoke will affect them. These factors include the component technology and packaging, physical board protection, and environmental conditions such as the amount of smoke, temperature of burn, and humidity level. The likelihood of circuit bridging was tested by measuring leakage currents and converting those currents to resistance.

In the third project, ORNL developed recommendations for endorsing design, testing, and installation practices that contribute to establishing electromagnetic compatibility. As part of the confirmatory research, electromagnetic emission profiles at selected nuclear power plants were characterized through long-term plant measurements. These emission profiles were subsequently used to confirm that the recommended test levels, based on military (MIL-STD-461 and MIL-STD-462) and industrial (IEEE Std C62.41 and C62.45) standards, were appropriately tailored to the nuclear power plant environment (i.e., the recommended envelopes reasonably characterize the ambient electromagnetic conditions as determined from measured data).

In the fourth project, also performed by ORNL, the potential failure modes and vulnerabilities of distributed computer systems under environmental stress were investigated. An experimental digital safety channel (EDSC) incorporating technologies that are representative of proposed advanced light-water reactor (ALWR) safety systems was assembled for the tests. Stressors that were investigated included EMI/RFI, temperature, humidity, and smoke exposure.

The results and insights obtained from all the above studies are being integrated by ORNL to develop the technical basis for environmental qualification of safety-related digital I&C equipment for nuclear power plants. In particular, the technical basis addresses issues including (1) recommended standards for environmental qualification of safety-related digital I&C systems; (2) determination of the appropriate manner in which to address smoke in an environmental qualification program; and (3) resolution of the need to conduct accelerated aging in the qualification of equipment to be located in an environment that is normally considered as mild.

2. SUMMARY OF STRESSOR PRIORITIZATION STUDIES

2.1. Scope of Study

This study was performed to identify environmental stressors for digital I&C systems in a nuclear power plant that can be potentially risk significant.[2] The screening of environmental stressors was based on their risk sensitivities, which are changes in plant risk attributable to the stressors and are quantified by estimating their effects on the occurrences of I&C failure and the consequent increase in risk in terms of relative CDF.

Plant risk sensitivity to an environmental stressor is defined in this study to be the change in risk contributions from plant equipment that can occur due to the detrimental effect of the stressor. The higher the change in risk contributions due to a stressor, the higher is the risk sensitivity of the specific equipment, and consequently the plant, to the stressor. Risk-sensitivity results are obtained by accounting for the effects of the stressor on the equipment's failure occurrences, and then by determining the increase in risk due to those failures. The increase in risk to a plant due to the effect of a stressor depends on four factors:

1. The likelihood of the stressor,
2. The components affected by the stressor,
3. The increase in failure rates of the affected components, and
4. The risk contribution from the affected components.

The risk sensitivity of a stressor can be obtained by quantifying or estimating ranges for these factors. For stressors that can affect safety systems whose function is to prevent core damage, the risk sensitivity is related to the expected increase in CDF. A probabilistic risk assessment (PRA) model of a plant is used to estimate changes in risk due to a stressor.

2.2. Summary of Approach

To identify information on the effects of environmental stressors on digital equipment for this study, an investigation of failure and reliability documentation was performed. Information was sought on stressor effects, system failures, and equipment reliability from several industries to supplement the limited nuclear operating experience with this equipment. Military documents provided information on the performance of digital I&C equipment at the component level. Information at the system level was obtained from nuclear power plant operational experience reported in the Licensee Event Reports (LERs). Experience with digital equipment in nuclear power plant environments reported in the Nuclear Plant Reliability Data System (NPRDS) were analyzed to support the estimation of failure rates. Additional information on the performance of digital systems was obtained from journal publications. Although the information obtained was sparse and uncertainties exist in its adaptation for nuclear power plant applications and environments, the reliability data can be used to broadly compare risks from different stressors based on estimated ranges of, or bounds on, potential effects.

In this study, risk screening for selected stressors was performed using the PRA model of an example plant. The effects of those stressors were introduced into the PRA either by modifying the failure rates of equipment and incorporating the likelihood factors for stressor effects to occur, or by estimating equipment unavailabilities based on frequencies of occurrence of the stressors. The following assumptions are made in estimating the risk sensitivities of stressors: i) assuming the same susceptibility of equipment to environmental stressors at all locations; ii) treating the effects of stressors as the same on all I&C equipment; iii) assuming a likelihood of 1.0 for temperature, humidity, and vibration; and iv) assuming a failure probability of 1.0 for

I&C equipment for potential common-cause events, such as EMI and smoke, to bound the effects of those stressors.

Risk screening using the analysis results from the example plant PRA is based on comparing the CDF contribution for I&C systems subjected to environmental stress to the baseline CDF contribution from I&C systems in general. An order of magnitude increase in the relative I&C risk contribution is considered to be risk significant for this study.

2.3. Results of Risk-Based Stressor Prioritization Studies

Risk-Screening of Environmental Stressors

Figure 1 shows the risk-sensitivities to different environmental stressors for the example plant. The figure represents relative and not absolute contributions to CDF from I&C. The risk-sensitivities of environmental stressors shown in Figure 1 are plotted on a scale (relative CDF contribution) where risk effects from I&C failures equal the baseline total plant CDF when the x-axis value reaches 1.0. Relative CDF contributions from stressors are shown as ranges represented by a bar. These ranges for temperature, humidity, and vibration represent variations in potential risk effects from the stressors for parametric variations in stressor levels. The ranges for lightning-related EMI and smoke represent variations in potential risk effects for average-estimated-occurrence frequencies and assumed periods of detection for failed I&C equipment.

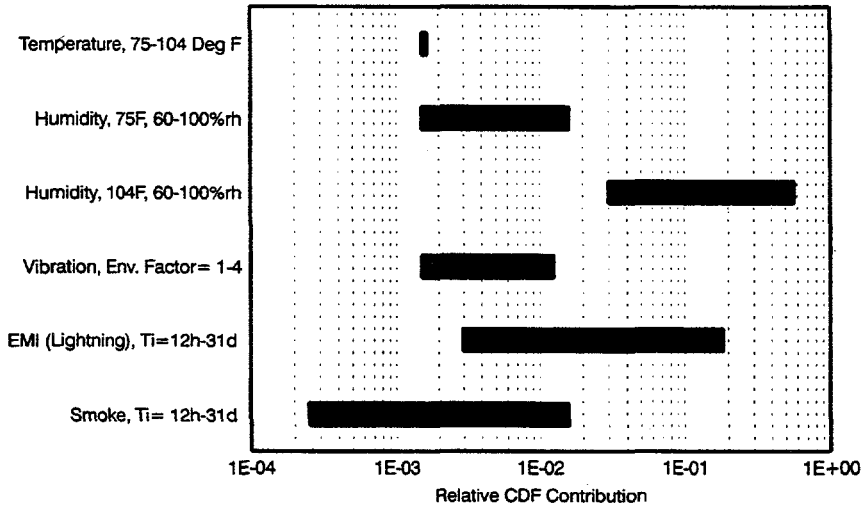

Relative CDF Contribution = CDF Contribution from I&C Cutsets /Baseline Plant CDF.

Figure 1. Risk-Sensitivities of Environmental Stressors in Example Plant

The risk sensitivities to temperature are shown for normal control-room operation (75 ^{o}F maximum, no stressor effect), the cable-spreading room, and switchgear room (104 ^{o}F maximum). Risk-sensitivities to humidity through corrosion are given for two different temperatures, normal temperatures in control room (75 ^{o}F maximum) and in the cable-spreading room/switchgear room (104 ^{o}F maximum), for humidity levels from 60% (maximum under controlled conditions) to a maximum of 100% under uncontrolled environmental conditions. This range in relative humidity represents situations in which air-conditioning is lost in

environmentally controlled areas, such as the control room, and climatic conditions where the plant is located. Risk-sensitivities from humidity are significantly higher at the higher temperature. The results for vibration show the risk-sensitivities from a baseline, where there are no vibrations, to fairly high vibrations, such as would be experienced by equipment mounted on a helicopter.

The risk-sensitivities for lightning-related EMI events are shown for two different periods of detection of equipment failure from these events; shift checks and surveillance-test intervals, 12 hours and 31 days, respectively. Risk-sensitivities to smoke are also shown for the same two periods. In each case, the results show the plant risk-sensitivities for estimated average frequency of occurrences of these events.

Temperature at the I&C cabinet locations in the example plant does not appear to be a risk-significant stressor. Vibration at the levels noted also appears to have no significant risk-effects. Humidity could be a significant stressor at cable-spreading room and switchgear-room temperatures; however, at control-room temperature, humidity does not appear to be potentially risk-significant except at very high levels. EMI from lightning potentially can be a risk-significant stressor for digital I&C systems; however, the risk significance clearly depends on the interval before equipment failure is detected. Under the assumptions made in the study, smoke also appears to have the potential to significantly increase relative risk contributions from digital I&C systems; however, such risk depends on the interval before failure is detected.[2]

The authors caution that bounding assumptions in the BNL study were made in the risk-sensitivity evaluations involving lightning-induced EMI and smoke as stressors. Consequently, the risk-screening results should be interpreted only as potential effects.

3. SUMMARY OF SMOKE EXPOSURE STUDIES ON DIGITAL COMPONENTS

3.1. Scope of Study

This study consisted of smoke exposure tests on digital components and circuit boards, with a focus on short-term effects such as circuit bridging in typical components and the factors that can influence the degree to which the smoke will affect them.[3] These factors include the component technology and packaging, physical board protection, and environmental conditions such as the amount of smoke, temperature of burn, and humidity level. The likelihood of circuit bridging was tested by measuring leakage currents and converting those currents to resistance in ohms. The lower the resistance, the higher the likelihood of shorts. Since circuit bridging by smoke was isolated as one of the short-term or immediate failure mechanisms, the researchers studied factors in smoke generation that affect circuit bridging. Experience with shorts in the SNL preliminary tests indicated that intermittent pathways between exposed contacts develop as a result of smoke. Thus, the objective of the component-level tests was to determine the smoke-related factors that are important in causing failures from shorts. As components were exposed to smoke, loss of function and changes in resistance between contacts were measured. The components tested consisted of seven chip packages, four comb patterns at different voltages, an operating optical isolator chip, and two 16-K memory chips. The chip packages included a ceramic leadless chip carrier (LLCC), a ceramic dual-in-line package (CDIP), a ceramic flat package (CFP), a transistor outline can (TOC), a plastic dual-in-line package (PDIP), a small-outline integrated circuit (SOIC), and a plastic leaded chip carrier (PLCC). The ceramic packages and the TOC were empty packages, while the PDIP and SOIC both contained four hex inverter circuits. These components were chosen because they typify modern microprocessor electronics. They represent both surface and plated-through-hole mounting schemes. The comb patterns represent standard patterns used to measure circuit board process quality and surface insulation resistance. To determine whether coatings or housings had any effect on the

chips or comb patterns, some of these test components were coated with an acrylic spray or housed in a computer case. The factors that were tested included the amount of fuel, the presence of polyvinyl chloride (PVC), the burn temperature, the humidity, the introduction of CO_2, and the presence of galvanic material.

3.2. Summary of Approach and Test Methods

General

The components to be tested were placed in a smoke exposure chamber that was connected by stainless steel chimneys to a combustion chamber (underneath the exposure chamber) where the fuel (pieces of cable) was burned by radiant heat lamps. The smoke was produced over a period of 15 minutes or less and the components were exposed to the smoke for approximately 1 hour. Then the smoke was vented and the exposure chamber was opened, exposing the components to the controlled temperature and humidity of the environmental chamber. (The smoke chamber was located inside this environmental chamber.) The equipment under test remained in the controlled environment for 24 hours from the beginning of the smoke exposure. The components were monitored before each smoke exposure and at least every 5 minutes throughout the test for 24 hours from the beginning of the exposure. This approach simulates exposure of components to a nearby electrical fire and eliminates the heat of combustion from affecting tested components.

Components Tested

Chip Packages

The objective of the chip package experiments was to measure how smoke changes the resistance between exposed contacts in components. A chip mounting board design allowed the leakage current between adjacent conductors to be measured while 5 Vdc was supplied to the contacts. There were between 7 and 44 contacts for the seven chips. Since any pair of these contacts may be bridged, as many contacts as possible were monitored.

Both through-hole and surface-mounted components were represented in the set of chip packages tested. The LLCC, CFP, SOIC, and PLCC are surface-mounted packages and the CDIP, PDIP, and TOC are through-hole-mounted packages. For the empty packages, all of the even-numbered pins were connected to a 5-Vdc supply and all of the odd-numbered pins were connected to ground. For the hex inverters, the power and ground pins were allowed to float, the inputs to the inverters were connected to 5 V, and the outputs were connected to ground. Leakage current measurements were made between the input (5V) and ground (0V). The PLC chip had 11 analog input pins; alternate input pins were connected to 5V and ground while the chip was powered with 5 V. Leakage current measurements were made between the set of inputs connected to 5V and the set of inputs connected to ground. The chip-mounting boards were connected by ribbon cables and card edge connectors to the instrument measuring current leakage, which was located outside of the environmental chamber.

For each smoke exposure, four chip-mounting boards in different configurations were tested. Three boards were mounted inside the smoke exposure chamber; these boards were either bare, coated with an acrylic spray, or housed in a personal computer chassis equipped with an operating fan (i.e., a typical chassis "muffin" fan). A bare board (used as an experimental control) was located inside the environmental chamber, but outside the smoke exposure chamber. The boards were placed in position approximately 1 hour before the test in most cases. The card edge connectors were wrapped in black electrical tape to prevent smoke from corroding the connectors.

Comb Patterns

Surface insulation resistance was measured on comb patterns on Institute for Interconnecting and Packaging Electronic Circuits (IPC) B-24 printed circuit boards. The IPC-B-24 boards contained four identical comb patterns. The comb teeth were 0.4 mm wide with 0.5-mm spaces between opposing teeth. The resistances of the comb patterns were measured similarly to those of the chip packages except that the voltages were different. One comb pattern was biased with 160 Vdc, one with 50 Vdc, one with 5 Vdc, and one was grounded except during measurements, when it was biased with 5 Vdc. (As with the chip boards, measurements with the comb patterns were repeated at approximately 5 min. intervals.) The different voltages allowed evaluation of the effect of electric field strength on circuit bridging during and after smoke exposure. As with the chip boards, four boards were included for each test: a bare board, an acrylic-coated board, a board housed in the PC chassis, and an unexposed control board. The boards were connected to the power and measurement circuit in the same manner as the chip boards and were measured by the same ammeter.

Optical Isolators

A functioning 6N138 optical isolator, which provides a coupling for electrical circuits with a direct electrical connection, was included in all of the smoke exposures. This device operates by using a light-emitting diode and a photodetector that are built into a plastic DIP body. The 6N138 is a low-input current, high-gain optocoupler built for transistor-transistor logic (TTL) applications. The test circuit consisted of a square wave input pulse, and the resistors and capacitors necessary to provide a switching test circuit.

For each exposure, a new optical isolator chip was placed in a socket containing the supporting circuit. The input and output wave form parameters of pulse rise time, amplitude, and delay from the input pulse were measured on a digital oscilloscope. A starting wave form was recorded, and if the values of rise time, delay, or amplitude varied by more than 5% from the starting values, a new wave form was recorded.

Memory Chips

Two package types for 16-K memory chips were exposed for each test: a plastic-packaged commercial chip and a ceramic-packaged chip developed at SNL. The two chips had identical circuitry. They were powered with 5V, but were not operated during the exposure. Standard functional tests were performed on the chips before and after the tests.

Scenarios Tested

The factors varied for the smoke exposures were fuel amount, presence of PVC as part of the fuel, burn temperature, humidity, introduction of CO_2, and presence of galvanic material. Some of the factors that were varied directly affected the smoke production; however, humidity, CO_2, and galvanic metal were included because they were likely to interact with the smoke and affect electronic components. High humidity is known to affect electronics and is commonplace after a fire if sprinklers or water-based fire extinguishers were used. CO_2 is another common fire suppressant. It has been proposed that CO_2 may affect electronics by suddenly cooling the electronics and cracking the bonds. It has been included in some of the smoke exposures to determine the effect it may have on the electronics. Zinc in galvanized metals has been known to combine with chlorides that are frequent components of smoke. $ZnCl_2$ is hygroscopic and will absorb water from the air. The $ZnCl_2$-water mixture forms a syrup, which can drip onto components under the right conditions.

Fuel load, burn temperature, and humidity factors were either at a high or low level. The levels were chosen to span a range for credible fires. For CO_2 and galvanic metal, the material was either present or absent. Because of the high number of parameters, every possible combination was not performed; instead, only conditions that corresponded to likely scenarios in nuclear power plants were produced.

Suppression (CO_2) and Galvanic
Additional effects were added by flooding the exposure chamber with CO_2 from a fire extinguisher and adding a piece of corrugated galvanic roofing material above the test articles. When the CO_2 was added, 60% of the volume of the smoke exposure chamber was filled with CO_2, a standard percentage of the volume that automatic fire suppression systems will flood a room with in case of a fire. This corresponds to 2.5 lb of CO_2 in the smoke exposure chamber.

The galvanized roofing material was included in some of the tests to simulate industrial environments, and provide a source of zinc. In past fires,[4] the presence of galvanic metal has increased damage to electronics because droplets of $ZnCl_2$ and water have deposited on the electronics. The roofing material was cut so that it was above all of the test samples, but did not cover the chimney areas of the chamber. This metal piece was suspended approximately 1 foot above the test samples and covered almost the entire smoke exposure chamber.

Other measurements
Temperature, humidity, smoke deposition, smoke optical density (turbidity), and fuel mass loss were measured, and soot samples were chemically analyzed. Descriptions of the methods used for these measurements can be found in Reference 3.

3.3. Results of Digital Component Smoke Exposure Studies

Figure. 2 shows exposed chip-mounting boards from different test scenarios in the SNL study.

Technology and Packaging
The results of the study of the 16-K memory chips showed that the hermetically sealed ceramic packages were more robust than the plastic packages in a smoke environment. Differences between ceramic and plastic packages were not evident from the resistance measurements; therefore, the higher failure rate encountered for plastic packages might be due to penetration of the plastic by smoke particles or moisture rather than shorting of contacts with soot. Most common digital electronics, however, use less expensive plastic packages. Hermetically sealed ceramic packages are significantly more expensive and are typically only used for military applications.

The voltages at which the digital electronics operate vary according to the digital chip technology. Resistance measurements on the comb patterns indicated that higher voltage patterns are affected by smoke more than lower voltage patterns. The higher voltage lowers the resistance before the smoke is applied and continues to produce more leakage current throughout the exposure. Visually, soot tended to accumulate more around the high voltage patterns. The highest voltage pattern used—a 160-V pattern—was observed to be arcing during the smoke exposure.

Two hex inverter chips were included on the chip mounting board to determine the difference between an SOIC package and a DIP. The statistical analysis, which compared post-exposure averages, showed no appreciable difference between these two packages except with respect to the *rate* of degradation at high fuel loads. When the fuel available for smoke production was high, both packages shorted; however, components with smaller contact spacing shorted earlier. Thus, the more widely spaced contacts of the DIP package resisted shorting longer than the SOIC package. When the available fuel was low, resistance dropped for both resisted shorting longer than the SOIC package. When the available fuel was low, resistance dropped for both packages slightly, and then recovered with little difference observed between the chip packages. A possible

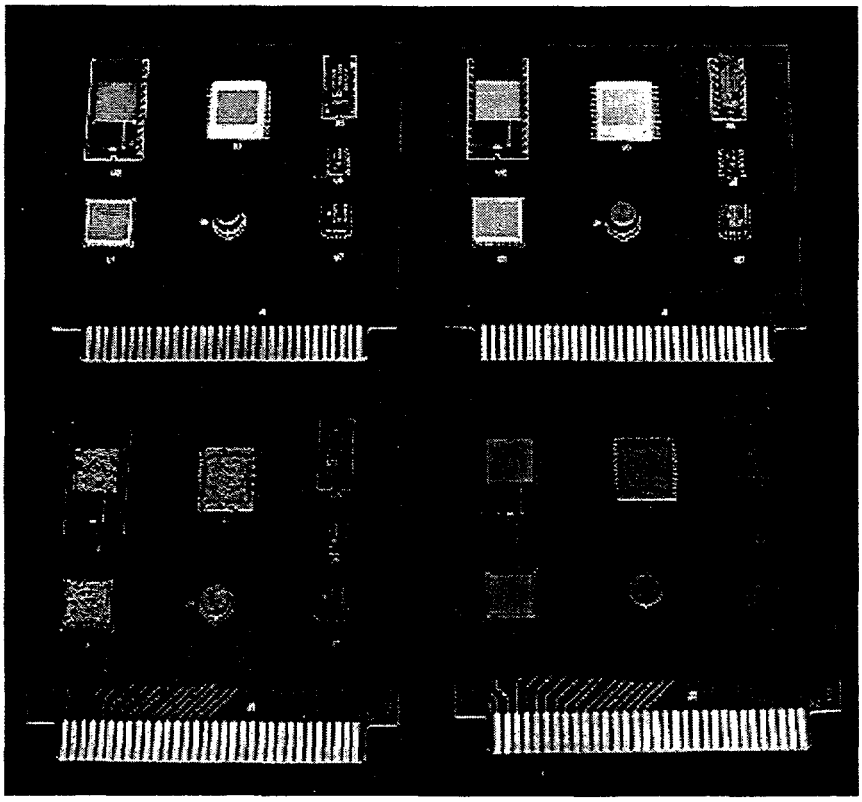

Figure 2. Exposed chip-mounting boards from different tests.

reason for the inability to determine differences may be that the low fuel loads were too low to cause much change in resistance.

Protection

Bare boards were highly affected by smoke while coated boards seemed to be less affected. Housing the boards in a PC chassis, which contained a fan, protected the boards only minimally. Visually, some of the boards that were placed within the chassis looked worse than those that were unprotected because clumps of soot were deposited on the board. For the high fuel load tests, however, virtually all components were shorted in these situations and little difference could be observed in the resistance measurements. Coating the boards with an acrylic spray provided some protection against circuit bridging.

Significant Factors in Determining Circuit Bridging

The most significant smoke-related factors were humidity, fuel level, and burn temperature. High humidity has been shown to affect the surface insulation resistance of printed circuit boards in environmental testing.[5] Other fire corrosivity tests which used comb patterns also showed that the resistance of exposed comb patterns is highly affected by humidity.[6]

As more fuel is burned, resistance drops. Smoke from plastic leaves a film, which is black and powdery if the plastic is burned in the flaming mode with adequate oxygen. The film is white and oily if produced without a flame and black and oily if produced with a flame, but the flame extinguishes due to lack of oxygen. For low

fuel loads, the resistance generally dropped during the smoke exposure but recovered after the smoke was vented. This recovery was not often the case with the high fuel loads; once the circuit was shorted, it never recovered.

The burn temperature (flaming vs. smoldering) did not affect the resistance as much as the humidity or fuel level. The burn temperature would be expected to change the smoke products in two ways: different chemical products can be produced at different temperature, and the mass loss rate of the fuel is slower if the fire is smoldering. Chemical analyses for Cl, Br and SO_4 showed a low correlation between burn temperature and the amount of these chemicals in the soot. Analysis of the amount of fuel that was burned shows that neither the burn temperature nor the fuel level alone determines the percentage of fuel that is burned. If a large amount of fuel was burned at a low temperature, approximately 20% of the fuel was consumed, while if a small amount of fuel was burned at either low temperature or a large amount of fuel was burned at high temperature, approximately 40-50% of the fuel was burned.

The circuit bridging tests showed that the synergistic effects of smoke and humidity are higher than for humidity alone.

PVC (included as part of the fuel load on the high fuel tests only) showed very little effect on resistance. Only a small proportion of the fuel was PVC in these tests and, with the high fuel load, many of the components shorted without PVC. There is also little correlation between the Cl deposition found by chemical analysis and the presence of PVC. Although the other cable materials did not contain PVC, some had high proportions of Cl and Br, which are typically used as fire retardants. No other cable materials were singled out for study in these tests.

The addition of CO_2 as a fire suppressant did not affect the resistance adversely. The addition of CO_2 may be beneficial to the electronics by cooling the room and blowing away some of the soot deposition. These findings are supported by tests on the effect of CO_2 on computers.[7]

The galvanic metal was expected to trap Cl in the form of $ZnCl_2$, form a thick liquid, and drip onto the electronics.[6] Although a greasy film formed on the galvanic metal that was suspended in the smoke exposure chamber, the film never accumulated enough water to drip. Instead, the metal piece formed a surface upon which some of the smoke deposited. The overall effect was to reduce deposition on the surface of the electronics and reduce the negative effect of the smoke. On some high humidity tests, water appeared to be collecting at the base of the PC chassis. This water did not affect any of the components. Overall, these tests were found to be of an inadequate scale to assess the importance of this factor.

4. SUMMARY OF ELECTROMAGNETIC COMPATIBILITY STUDIES

4.1. Scope of Study

The focus of this study was the determination of an approach for addressing the potential vulnerability of safety-related I&C systems to EMI/RFI and power surges in nuclear power plants.[8] The susceptibility of digital technology to EMI/RFI and power surges is of concern to the nuclear industry because faster microprocessor clock rates and lower logic voltage levels can increase the potential for disruption by electromagnetic effects. To minimize the effects of EMI/RFI and power surges, electromagnetic compatibility (EMC) should be established through the application of appropriate design, testing, and installation practices. This study investigated commercial and military standards for EMC to identify those practices that were applicable to

safety-related I&C systems in nuclear power plants. In addition, the ambient electromagnetic conditions that are representative of the nuclear power plant environment were determined through long-term measurements at selected plants.

4.2. Summary of Approach and Test Methods

This research has led to the recommended endorsement of industrial guidance on installation practices to ensure proper grounding, shielding and isolation and to the recommendation of specific test criteria and methods by which to confirm compatibility of equipment with its intended environment.[8,9] IEEE Std. 1050-1996[10] is recommended because it provides well-founded EMI/RFI eliminating practices for design and installation of electronic equipment. Adherence to these practices supports the establishment of a comprehensive electromagnetic compatibility program.

Military standard (MIL-STD) test criteria were selected for recommendation because they provide a well-established, systematic approach by which the susceptibility of equipment to known or expected electromagnetic conditions can be evaluated and by which the contribution of the equipment to the electromagnetic ambient conditions through its own emissions can be determined. These recommended testing practices are based on the military services' considerable experience (almost 30 years) in evaluating EMI/RFI effects. Table 1 shows the recommended EMI/RFI test criteria from MIL-STD 461D[11] and Table 2 gives the corresponding criteria from MIL-STD 461C.[12]

The issue of power surge susceptibility can be addressed through the demonstration of power surge withstand capability (SWC) for electronic equipment. The test criteria and SWC practices in IEEE C62.41-1991[13] are recommended as a means to control the occurrence of upsets in safety-related I&C systems that result from ac power surges. Establishing SWC for safety-related I&C systems through testing is another element of assuring electromagnetic compatibility for I&C systems in NPPs.

4.3. EMI/RFI Site Survey Results

Also relevant to the EMI/RFI qualification of digital safety systems, both for digital upgrades and for advanced reactor designs, is the expected electromagnetic environment in which the systems will operate. Obviously, a system should be made sufficiently resistant to EMI/RFI to perform its required function. (In essence, it should be sufficiently hardened to be compatible with its working environment.) Determining appropriate susceptibility testing levels therefore requires a fairly detailed characterization of ambient conditions at the site of the equipment installation.

To characterize the EMI/RFI environment at current LWRs and to estimate the expected environment at ALWRs, ORNL conducted a long-term survey of ambient electromagnetic conditions at several nuclear power plants.[14] A representative sampling of power plant conditions (reactor type, operating mode, site location) were monitored over extended observation periods (e.g., continuous measurements for up to 5 weeks at a single location) were selected to more completely determine the characteristic electromagnetic environment for nuclear power plants. Observations covered a 14-month period and 8 different nuclear units, representing all U.S. reactor manufacturers. A full range of operating modes—full-power operation, low-power operation, startup, coastdown, plant outage, and an unscheduled event resulting in a plant trip—were observed.

Table 1 Applicable MIL-STD 461D test criteria

Criterion	Description
CE101	Conducted emissions, power leads, 30 Hz to 10 kHz
CE102	Conducted emissions, power leads, 10 kHz to 10 MHz
CS101	Conducted susceptibility, power leads, 30 Hz to 50 kHz
CS114	Conducted susceptibility, bulk cable injection, 10 kHz to 400 MHz
RE101	Radiated emissions, magnetic field, 30 Hz to 100 kHz
RE102	Radiated emissions, electric field, 10 kHz to 1 GHz
RS101	Radiated susceptibility, magnetic field, 30 Hz to 100 kHz
RS103	Radiated susceptibility, electric field, 10 kHz to 1 GHz

C = conducted, E = emissions, R = radiated, and S = susceptibility.

Table 2 MIL-STD 461C counterparts to applicable MIL-STD 461D

Criterion	Description
CE01	Conducted emissions, power leads, 30 Hz to 15 kHz
CE03	Conducted emissions, power leads, 15 kHz to 50 MHz
CS01	Conducted susceptibility, power leads, 30 Hz to 50 kHz
CS02	Conducted susceptibility, power and interconnecting control leads, 50 kHz to 400 MHz
RE01	Radiated emissions, magnetic field, 30 Hz to 30 kHz
RE02	Radiated emissions, electric field, 14 kHz to 1 GHz
RS01	Radiated susceptibility, magnetic field, 30 Hz to 50 kHz
RS03	Radiated susceptibility, electric field, 14 kHz to 1 GHz

C = conducted, E = emissions, R = radiated, and S = susceptibility.

The nuclear units monitored included the following: one Combustion Engineering (CE) pressurized water reactor (PWR), three Babcock and Wilcox (B&W) PWRs, one General Electric (GE) boiling water reactor (BWR), and three Westinghouse (W) PWRs. Participating utility companies included Duke Power, Public Service Electric and Gas, Entergy Operations and the Tennessee Valley Authority.

The electromagnetic measurement system[15] employed consists of two instruments developed by ORNL for long-term, unattended monitoring of ambient electromagnetic emissions. This approach minimized intrusion on the normal day-to-day operation of the plant. The requirements of this survey resulted in several novel instrument developments.[16]

The primary functional requirement for the electromagnetic measurement system (EMS) is to perform long-term, automatic, unattended recording of EMI/RFI levels at nuclear power plant sites. Except for setup and shutdown of the EMI/RFI monitoring instruments, no operator attention is required while the EMS makes its observations. The EMS operates in the presence and plain view of nuclear plant employees; the instruments are unadorned gray boxes, with no external displays, and no external controls except a key lock "off/on" switch whose key can be removed in either setting. The EMS is designed to be sufficiently robust to withstand extended exposure to an industrial environment.

The EMS is designed to be unobtrusive. Other than sensing the ambient levels of electromagnetic fields and taking operating power from the plant electrical power system, it does not interact with the nuclear plant environment. The instruments are EMI/RFI hardened; no radiated energy may enter the EMI/RFI monitors except through the antennas, and no signals generated by the EMS are allowed to escape. The EMS is not intended to be connected to the plant data acquisition system.

The EMS is capable of unattended operation for several months. The instruments include an onboard uninterruptible power supply, and so they can withstand a power interruption of up to 20 minutes. In addition, the recorded data are stored on an onboard floppy disk every six hours. Thus, even in the event of a major failure, most of the recorded data would be preserved.

The overall frequency range is 305 Hz to 8 GHz. This range is derived primarily from MIL-STD 461C[12] requirements RS01 (low end) and RS03 (high end). It was found to be impractical to build a single device to cover the desired frequency range. Accordingly, two devices, the magnetic spectral receiver (covering 305 Hz to 5 MHz), and the electric spectral receiver (covering 5 MHz to 8 GHz), were developed.

The electric spectral receiver is configured to observe high-frequency electric fields (5 MHz to 8 GHz). It uses two resistive taper antennas as broadband electric field probes. The antennas are connected to independent processing circuits, one covering 20 bands of equal width from 5 to 1000 MHz, and the other a single band from 1 to 8 GHz. The electric spectral receiver design uses heterodyne conversion and an analog peak detector.

The other receiver is configured to observe low-frequency radiated magnetic fields or conducted effects. Frequency coverage is from 305 Hz to 5 MHz. The magnetic spectral receiver uses a passive loop antenna as a broadband magnetic field transducer or a current transformer as a transducer for conducted EMI/RFI effects. The 305 Hz to 5 MHz coverage spans 14 octaves, and the receiver simultaneously captures time-localized peak magnetic field strength present in each octave during each sampling cycle. The implementation of the magnetic spectral receiver uses a multiresolution digital filter bank, implemented in dedicated hardware.

The output of each receiver is a two dimensional matrixed histogram. One dimension is band (or bin) of frequency. The other dimension is band (or bin) of peak field strength. The entries in the histogram matrix are the running total of the number of times (i.e., number of receiver operating cycles) that the ambient EMI/RFI level falls within the intersection of a particular strength bin and a particular frequency bin. Resolution is coarse, being limited by the bin width. The cumulative histograms and their individual time tags are stored to disk every six hours as "frames." For considering rates of occurrence, the counts accumulated during any given frame can be determined by subtracting the running total counts at the starting time of that frame from the running total counts at the ending time of the frame.

The survey establishes operating envelopes that bound the observed electromagnetic conditions at the nuclear power plants.[14] Bounding envelopes for the survey are based on the highest EMI/RFI strength observations and the associated expanded uncertainties for the measurements. The expanded uncertainty establishes an interval about the measurement results in which the values of the measured phenomenon can be expected to lie with a high level of confidence (95%). Table 3 presents the bounding observation envelope for radiated electric fields. Table 4 presents the bounding observation envelope for radiated magnetic fields. Table 5 presents the bounding observation envelope for conducted EMI/RFI events. Regarding the confidence that can be placed in the measured data, the ORNL survey generated ~650,000 electric field observations, ~35.7 million magnetic field observations, and ~6.4 million conducted EMI/RFI observations. However, only a few thousand spectra show electromagnetic fields at potentially disruptive levels. Yet, it is the strength and rate of occurrence of these rare higher levels that should determine EMI/RFI susceptibility test levels. A statistical analysis of the data collected in this survey indicates that the probability of observing a significant EMI/RFI event in a random 30-minute spot check is on the order of 0.003. Thus, the results of the survey confirm that long-term monitoring is needed to adequately characterize the electromagnetic environment at a site. Finally, the data from this survey, captured during continuous monitoring for extended periods at each plant location under a variety of operating conditions, provides great confidence that the highest strength EMI/RFI events were captured. The measurement approach and comparative analysis of the survey results are presented in detail in NUREG/CR-6436.[14]

5. SUMMARY OF ENVIRONMENTAL TESTING STUDIES OF A DIGITAL SAFETY CHANNEL

5.1. Scope of Study

An objective of this study[17] was to identify failure modes and vulnerabilities that are associated with digital systems. The study sought to determine experimentally the characteristic effects caused by environmental stressors using a system that is *representative* of digital safety system designs. The tests examined stress levels at which failures began and attempted to quantify the severity of consequences for safety systems.

Ranges of stress were selected at a sufficiently high level to induce errors so that failure modes characteristic of the technologies employed could be identified. Subsystems of the EDSC assembled for the tests included computers, electrical and optical serial communication links, fiber-optic network links, analog-to-digital and digital-to-analog converters and multiplexers. In addition, the trip system design was typical of ALWR and/or some retrofits in the areas of chip fabrication and packaging technology used, temperature ratings and reliability stress tests used during component quality assurance procedures, subsystem functions and communication protocols, and expected memory/board density.

Table 3 Bounding envelope for radiated electric fields

Frequency Band (MHz)	Field Strength (dBμV/m)	Expanded Uncertainty (dB)
5–100	130.7	± 7.8
100–200	132	± 3.5
200–300	109.9	± 3.5
300–400	110	± 3.5
400–500	127.3	± 3.5
500–600	106.2	± 3.5
600–700	108.8	± 3.5
700–800	115.5	± 3.5
800–900	107.6	± 3.5
900–1000	125.1	± 3.5

Table 4 Bounding envelope for radiated magnetic fields

Frequency Band (kHz)	Field Strength (dBpT)	Expanded Uncertainty (dB)
0.30–0.61	107	± 7.5
0.61–1.22	101	± 7.5
1.22–2.44	104	± 7.5
2.44–4.88	104	± 7.5
4.88–9.77	117	± 7.5
9.77–19.53	117	± 7.5
19.53–39.06	106	± 7.5
39.06–78.12	100	± 7.5
78.12–156.25	101	± 7.5
156.25–312.5	102	± 4.9
312.5–625	101	± 4.9
625–1250	101	± 4.9

Table 5 Bounding envelope for conducted EMI events

Frequency Band (kHz)	EMI Strength (dBμA)	Expanded Uncertainty (dB)
0.30–0.61	89.6	± 7.5
0.61–1.22	83.8	± 7.5
1.22–2.44	78	± 7.5
2.44–4.88	78	± 7.5
4.88–9.77	73.2	± 7
9.77–19.53	71.2	± 5.8
19.53–39.06	77.5	± 4.9
39.06–78.12	71.5	± 4.9
78.12–156.25	77.5	± 4.9
156.25–312.5	83.5	± 4.9
312.5–625	83.5	± 4.9
625–1250	77.5	± 4.9

5.2. Summary of Approach and Test Methods

System Description

A block diagram of the EDSC is presented in Figure 3. It consists of two major functional subsystems: the test system (i.e., the equipment under test) and the control system. The test system [process multiplexing unit (PRS/MUX), digital trip computer (DTC), and engineered safety feature multiplexing unit (ESF/MUX)] represents a single channel of an advanced reactor protection system, while the control system (host processor) stimulates the test scenarios (i.e., generates analog signals corresponding to various postulated reactor conditions), simulates the other three channels of a typical reactor protection system (some newer designs include isolated interchannel communication for trip voting), and monitors and logs the performance of the test system during environmental testing.

EMI/RFI Tests

Electromagnetic interference/radio-frequency interference tests were performed on the EDSC according to applicable test criteria and methods stipulated in MIL-STD-461C[12] and MIL-STD-462[18] respectively. MIL-STD-461C establishes the military's emission and susceptibility requirements for electronic, electrical, and electro-mechanical equipment and subsystems. It also provides a basis for evaluating the electromagnetic characteristics of equipment and subsystems by setting operational acceptance criteria. The test methods corresponding to the MIL-STD-461C requirements are described in MIL-STD-462.

The objective of the EMI/RFI tests was to identify/confirm EMI/RFI-induced upsets and failure modes in a microprocessor-based safety system, and also to have a basis for comparing the likely effects of EMI/RFI-related upsets to other environmental effects such as smoke exposure. The tests were *not* intended to ascertain whether the EDSC met emissions criteria. Thus, only susceptibility criteria were used in the tests.

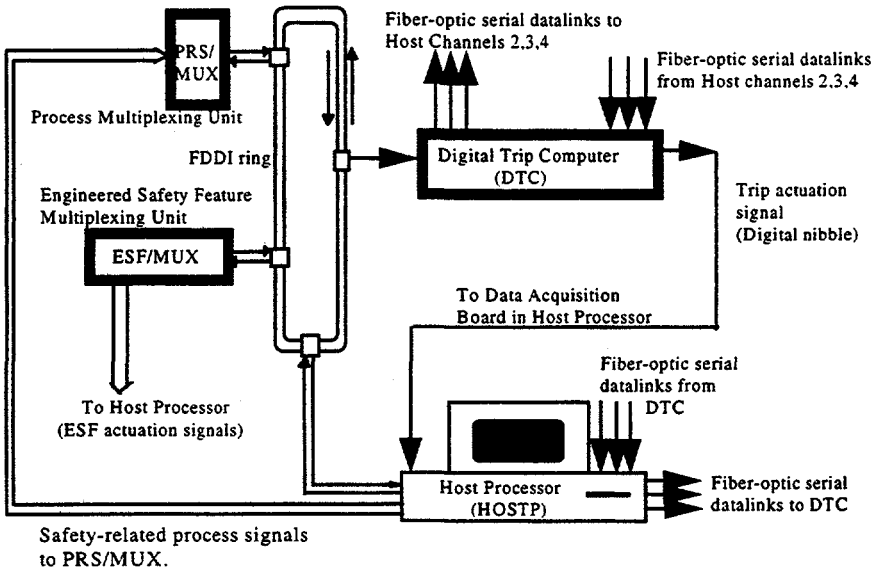

Figure 3. Block diagram of the experimental digital safety channel

The tests performed are the following:

CS01 - Conducted Susceptibility, Low Frequency (evaluates response of equipment to EMI/RFI present on the power leads in the frequency range 30 Hz to 50 kHz).
CS02 - Conducted Susceptibility, High Frequency (similar to CS01 except that it covers the higher frequency range from 50 kHz to 400 MHz).
CS06 - Conducted Susceptibility, Spikes (evaluates response of equipment to spikes on the power leads).
RS01 - Radiated Susceptibility, Magnetic Fields; (evaluates response of equipment to radiated magnetic fields in the frequency range 30 Hz to 50 kHz).
RS02 - Radiated Susceptibility, Spikes (evaluates the response of the equipment to radiated magnetic and electric fields generated by spikes and power line frequency current).
RS03 - Radiated Susceptibility, Electric Fields (evaluates the response of the equipment to radiated fields in the frequency range from 14 kHz to 1 GHz).

Temperature/Humidity Tests
A total of 16 elevated temperature/humidity tests were performed; eight of these were performed with the process multiplexing unit (PRS/MUX) as the Equipment Under Test (EUT) and eight with the digital trp computer (DTC) as the EUT. With the process multiplexing unit as the EUT, temperature tests at 30% relative humidity (RH) were performed at 100°F (38 °C), 120 °F (49 °C), 140 °F (60 °C), and 160 °F

(71°C). The tests were then repeated at the same temperature values, but at a relative humidity of 85%. Both test sequences were then repeated using the DTC as the EUT.

The maximum test temperature of 160°F (71°C) was used for three reasons. First, this value is at a sufficiently high level (taking into account the operating limits of the systems comprising the EDSC) to induce errors so that failure modes, which are characteristic of the technologies employed, could be identified. Second, it is well beyond what the channel is likely to experience in a normal nuclear power plant (control room) environment. Third, it is comparable to the temperature limits used by some manufacturers in qualifying safety equipment for control room environments. [In a typical control room environment, one manufacturer postulates that the loss of heating ventilation, and cooling will increase the temperature in the control room to about 104 °F (40 °C). Qualification testing is performed to about 122 °F (50 °C), while the actual environmental temperature ratings of the system and/or components are typically about 167 °F (75°C). This qualification methodology is typical of reactor manufacturers and suppliers.]

The general procedure followed was to obtain data for about 18 hours at the baseline temperature and humidity, then increase only the temperature to the next test value. The EUT was then monitored at this new steady-state test value for a period of 4 hours. The temperature was then reduced to the baseline value and monitoring was continued for an additional 18 hours, after which the temperature was raised to the next test value. The purpose of running a baseline test before each elevated temperature test was to account for any short-term effects due to the previous elevated temperature tests.

Smoke Exposure Tests

Based on credible smoke exposure scenarios evaluated by Nowlen,[19] three different smoke loads corresponding to three different fire threat scenarios were used for these tests. The smoke loads used are defined as follows:

Small In-Cabinet Fire: In this scenario, only a small fire (confined to 5-15% of the available fuel within the panel) is postulated. In this case, the other non-involved components may not be damaged by the effects of heat and flames but would be exposed to the smoke generated during the fire. The smoke loads for this scenario are most severe because of the relatively small enclosed volume and high fuel loadings found to be typical of nuclear plant control panels. A smoke load of 26-560 g/m^3 was identified for this scenario. For the ORNL tests, a moderate smoke load of 160 g/m^3 was used. Earlier work has shown that through-hole electronics can be reconditioned, with good results, after deposition of up to 100 μg chloride/cm^2 in the surrounding area.[20] The lower limit for when cleaning is needed is often specified to be 10 μg chloride/cm^2. For comparison, analysis of our smoke load of 160 g/m^3 showed the chloride deposition to be 742 μg chloride/cm^2. [The chloride content of smoke from burned cable is significant because when combined with water (from a humid environment), the chloride will form hydrochloric acid, which may dissolve minute, but significant, conducting substrate material.]

Large Control Room Panel Fire: The smallest smoke load postulated by Nowlen is associated with the effects of a large cabinet fire on the general environment within a control room. In this scenario, it is assumed that the fire source is a fully involved electrical panel, and hence it is assumed that all of the components within the burning cabinet would be destroyed by direct thermal effects. This scenario was considered by Nowlen to represent the most severe fire that might be experienced in the main control room. Nonetheless, the relative density of the smoke exposure for this scenario is significantly lower than that of the small in-cabinet fire because it is assumed that the smoke would be distributed throughout the much larger volume of the control room. Based on a consideration of both typical control panel fuel loads

and typical control room air volumes, Nowlen estimated the smoke load for this scenario to be from 2.8-11.2 g/m^3. For the ORNL tests, a smoke load of approximately 3 g/m^3 was used to simulate this scenario. Analysis of the smoke deposition showed the circuit board chloride surface contamination to be about 29 μg chloride/cm^2.

Significant Fires in General Plant Areas: This scenario is intended to be representative of the types of fires that might take place in general plant areas where advanced digital systems might be housed. This would include areas such as relay rooms, cable penetration rooms, cable vault and tunnel areas, etc. It was *not* intended to represent very large plant areas such as the turbine hall. The smoke load for this scenario falls between the two previous scenarios and was estimated by Nowlen to be 14-56 g/m^3. For the ORNL tests, a smoke load of 20 g/m^3 was used to simulate this scenario. Analysis of this smoke load showed the chloride deposition on the boards to be about 57 μg chloride/cm^2.

A total of ten tests were performed on the PRS/MUX and the DTC, which included fiber optic modules for interchannel optical communication. This included three tests designed to simulate and study the short term effects of fire suppression - the increase in humidity (in the presence of smoke) and the presence of carbon dioxide from a fire extinguisher. The general procedure adopted for the tests is as follows:

1. The EUT was placed in the exposure chamber and baseline data was obtained over a period of about 3 hours. The environmental chamber was maintained at 75°F and 30% RH during this time.

2. A predetermined mixture of different types of cables was burned to produce a desired smoke density in the exposure chamber. (NOTE: Experience showed that the cables completely burned in about 5 min.)

3. In the case where the test called for smoke and humidity, a predetermined amount of water was boiled off inside the exposure chamber, 15 min. into the test, to provide 85% relative humidity.

4. The EUT was exposed to the smoke for a total of 1 hour. The smoke was then vented from the exposure chamber.

5. The EUT was left in the exposure chamber and monitoring continued for approximately 20 hours. Chamber temperature was maintained at approximately 75°F and 30% RH.

6. The EUT was examined for damages/malfunctions and thoroughly cleaned. Cleanup consisted of first removing the electronic boards and blowing the deposited, non-sticky soot off with compressed air. The boards were then sprayed with Tech Spray no. 1677-5 Universal Cleaner Degreaser or Chemtronics Electronics Cleaner/Degreaser 2000. The exposure chamber was also thoroughly cleaned and made ready for the next test.

5.3. Results of Environmental Stressor Effects Testing

Interfaces were found to be the most vulnerable elements of the EDSC. The majority of effects resulting from the application of the stressors were communication errors, particularly for serial communication links. Many of these errors were intermittent timeout errors or corrupted transmissions, indicating failure of a microprocessor to receive data from an associated multiplexer, optical serial link, or network node. Because of similarities in fabrication and packaging technologies, other digital safety systems are likely to be vulnerable to similar upsets. As was experienced with the EDSC, intermittent component upsets will

typically impede communication, either on the board level (e.g., during bus transfers of data), or on the subsystem level (e.g., during serial or network data transfers). Thus, qualification testing should confirm the response of any digital interfaces to environmental stress.

Based on incidence of functional errors observed during testing, EMI/RFI, smoke exposure, and high temperature coupled with high relative humidity, in that order, were found to be the most significant of the stressors investigated. The most prevalent stressor-induced upsets, as well as the most severe, were found to occur during the EMI/RFI tests. For example, these tests produced the only permanent failure of the EDSC (i.e., power supply, at an electric field level of 72 V/m).

Although the EDSC test demonstrated system-level effects for both conducted and radiated EMI, the commercial components used exhibited greater susceptibility to conducted EMI. This observation is consistent with general industrial experience voiced by European EMI experts. It should be noted that the relative susceptibility of particular systems can be mitigated by grounding, shielding, isolation, and surge withstand practices.

With regard to temperature and humidity, the study found that the combination of high temperature at high relative humidity was the condition most likely to affect the EDSC, rather than temperature acting alone. High relative humidity is not as likely in a controlled environment such as a control room, but still needs to be considered in qualification, especially for post-accident monitoring equipment.

For smoke exposure, important failure mechanisms are not only long-term effects such as corrosion, but also short-term and perhaps intermittent effects such as current leakage. Smoke can cause circuit bridging and, thus, affect the operation of digital equipment. Because the edge connections and interfaces are typically uncoated, the most likely effect of the smoke is to impede communication and data transfer between subsystems.

During the smoke tests, upsets typically were not encountered until about an hour into the exposure tests. The EDSC did not lose functionality when exposed to smoke equivalent to a large control room panel fire conditions (smoke density of about 3 g/m^3). A large control room panel fire has been postulated by Nowlen[19] as the most likely severe fire which might be experienced in the main control room. In this scenario, a whole panel burns, all equipment within the panel is destroyed, and the smoke from this fire is dispersed throughout the control room. Because of similarities between the EDSC and digital safety systems with regard to circuit board and chip fabrication and packaging, it is reasonable to postulate that commercial digital equipment will likely maintain functionality during its initial period of exposure to smoke equivalent to a large control room panel fire unless any of the equipment is contained in the burning panel or in close proximity to the fire source. Given early detection of a fire and subsequent application of fire suppression measures, digital systems can therefore be expected to maintain functionality (to allow safe shutdown) for as much as an hour or more following exposure, provided that the equipment is not directly exposed to the fire.

The solder mask on commercial electronic boards appear to be effective in preventing catastrophic and/or permanent failure of the board even when they are exposed to a reasonably high level of smoke. The lower limit that necessitates cleaning of circuit boards, due to chloride deposits from smoke, is often specified to be 10 μg chloride/cm^2. For comparison, analysis of the largest smoke load used (160 g/m^3) showed the chloride deposition to be 742 μg chloride/cm^2. (Tests with uncoated boards using comparable smoke loads showed a marked decrease in resistance.[20])

6. CONCLUSIONS

The results for the example plant used in the stressor prioritization study indicated that humidity, EMI from lightning, and smoke can be potentially risk-significant. The risk-significance of EMI from lightning and smoke, however, are sensitive to detection periods for equipment failure following the events. The results also showed that the effects of some stressors, such as humidity, can be sensitive to the location of the equipment. For the levels of the stressors analyzed, risk effects from temperature in digital I&C equipment locations, and from assumed levels of vibrations, appear to be less significant.

The study on the impact of smoke exposure on digital devices found hermetically-sealed ceramic packages to be more resistant to smoke than plastic packages. Coating the boards with an acrylic spray provided some protection against circuit bridging. The smoke generation factors that affected the resistance the most were humidity, fuel level, and burn temperature. The use of CO_2 as a fire suppressant, the presence of galvanic metal, and the presence of polyvinyl chloride (PVC) did not significantly affect the outcome of these results.

Based on the volume of measured EMI/RFI data at nuclear power plants under a wide variety of conditions, the bounding observation envelopes provided a reasonable characterization of the EMI/RFI environment typical of nuclear power plants. Digital I&C equipment hardened to withstand EMI levels greater than those bounding observation envelopes should operate as intended in similar EMI/RFI environments. The EMI/RFI susceptibility of safety-related digital I&C systems with the electromagnetic environment to be expected at nuclear power plants can be determined by applying the recommended MIL-STD test criteria and methods.[8] These EMI/RFI susceptibility tests, when coupled with emissions testing, SWC testing, and well-founded design and installation practices, contribute to the establishment of electromagnetic compatibility for safety-related I&C systems in existing NPPs. Therefore, the results from the EMI/RFI surveys support the determination of a reasonable approach to ensuring electromagnetic compatibility in the safety-related systems of advanced reactors as well.

Results of the environmental testing of a representative digital safety channel showed communication interfaces to be the most vulnerable elements of the EDSC. The majority of effects resulting from the application of the stressors were communication errors, particularly for serial communication links. Many of these errors were intermittent timeout errors or corrupted transmissions, indicating failure of a microprocessor to receive data from an associated multiplexer, optical serial link, or network node. Because of similarities in fabrication and packaging technologies, other digital safety systems are likely to be vulnerable to similar upsets. As was experienced with the EDSC, intermittent component upsets will typically impede communication, either on the board level (e.g., during bus transfers of data), or on the subsystem level (e.g., during serial or network data transfers). Thus, qualification testing should confirm the response of any digital interfaces to environmental stress.

The stressor prioritization study and the environmental study suggest that, in addition to the traditional stressors such as temperature and humidity, EMI is of sufficient risk significance to be included in a qualification program. The findings of the electromagnetic compatibility study establishes the technical basis for evaluating upgrades or new installations of safety-related I&C systems in nuclear power plants.

Although some of the smoke-induced failure mechanisms were identified in the smoke exposure study, the means for addressing smoke susceptibility is still under investigation.

Results from these studies support a recommendation of the applicability of IEEE 323-1983, with some exceptions/clarifications, for qualification of digital safety-related I&C systems. In addition, a general methodology for environmental qualification of microprocessor-based I&C equipment for nuclear power plants is being developed. This methodology will be reported in a forthcoming NUREG/CR report.

7. REFERENCES

1. K. Korsah, R.L. Clark, and R.T. Wood, *Functional Issues and Environmental Qualification of Digital Protection Systems of Advanced Light-Water Nuclear Reactors*, NUREG/CR-5904, Oak Ridge National Laboratory, April 1994.

2. M. Hassan and W. E. Vesely, *Digital I&C Systems in Nuclear Power Plants: Risk-Screening of Environmental Stressors and a Comparison of Hardware Unavailability with an Existing Analog System*, Draft NUREG/CR-6579, Brookhaven National Laboratory, May 1997.

3. T. J. Tanaka, S. P. Nowlen, and D. J. Anderson, "Circuit Bridging of Components by Smoke," NUREG/CR-6476, Sandia National Laboratories, October 1996.

4. B. Reagor, "Smoke Corrosivity: Generation, Impact, Detection, and Protection," *Fire Sciences*, Vol. 10, 1992, pp. 169-179.

5. R. L. Iman, Burress, R. V., Anderson, D. J., et. al., 1995, "Evaluation of Low-Residue Soldering for Military and Commercial Applications–A Report from the Low Residue Soldering Task Force," Sandia National Laboratories, Albuquerque, NM.

6. L. M. Caudill, J. T. Chapin, R. B. Comizzoli, *et. al.*, "Current State of Fire Corrosivity Testing: Preliminary Electrical Leakage Current Measurements," *International Wire & Cable Symposium*, 1995, p. 432-437.

7. M. Arvidson and H. Persson, "Koldioxids (CO_2) paverkan pa elektronik - slackning med laga koncentrationer. [Carbon Dioxide Suppression Systems - Risk of Damage to Electrical Equipment.]," Swedish National Testing and Research Institute, SR Report 1993:20.

8. P. D. Ewing and K. Korsah, *Technical Basis for Evaluating Electromagnetic and Radio-Frequency Interference in Safety-Related I&C Systems*, NUREG/CR-5941, Oak Ridge National Laboratory, April 1994.

9. P. D. Ewing and R. T. Wood, *Recommended Electromagnetic Operating Envelopes for Safety-Related I&C Systems in Nuclear Power Plants*, NUREG/CR-6431 (draft), September 1997.

10. Institute of Electrical and Electronics Engineers, "IEEE Guide for Instrumentation and Control Equipment Grounding in Generating Stations," IEEE Std. 1050-1996, April 4, 1996.

11. U.S. Department of Defense, "Electromagnetic Emission and Susceptibility Requirements for the Control of Electromagnetic Interference," MIL-STD-461D, Jan. 11, 1993.

12. U.S. Department of Defense, "Electromagnetic Emission and Susceptibility Requirements for the Control of Electromagnetic Interference," MIL-STD-461C, Aug. 4, 1986.

13. Institute of Electrical and Electronics Engineers, "IEEE Recommended Practice on Surge Voltages in Low-Voltage AC Power Circuits," IEEE Std. C62.41-1991, Feb. 25, 1991.

14. S. W. Kercel, M. R. Moore, E. D. Blakeman, P. D. Ewing, and R. T. Wood, *Survey of Ambient Electromagnetic and Radio Frequency Interference Levels in Nuclear Power Plants*, NUREG/CR-6436, Oak Ridge National Laboratory, November 1996.

15. S. W. Kercel, "A Confirmatory Research Approach to the Measurement of EMI/RFI in Commercial Nuclear Power Plants," *Proc. Of the USNRC 22nd Water Reactor Safety Information Meeting*, Bethesda, MD., NUREG/CP-0140, Vol. 1, pp. 31-51.

16. S. W. Kercel and W. B. Dress, "A Hardware Implementation of Multiresolution Filtering for Broadband Instrumentation," *Wavelet Applications II*, Harold H. Szu, Ed., Proc. SPIE 2491, Orlando, FL, pp. 1014-1027.

17. K. Korsah, T. J. Tanaka, T. L. Wilson, and R. T. Wood, *Environmental Testing of an Experimental Digital Safety Channel*, NUREG/CR-6406, Oak Ridge National Laboratory, September 1996.

18. U.S. Department of Defense, "Measurement of Electromagnetic Interference Characteristics," MIL-STD-462, July 31, 1967.

19. Steve P. Nowlen, "Defining Credible Smoke Exposure Scenarios," Letter Report to U. S. NRC, Sandia National Laboratories, September 1994.

20. Lennart Cider, "Cleaning and Reliability of Smoke-Contaminated Electronics," *Fire Technology*, Third Quarter, 1993.

Recent Results of an Experimental Study on the Impact of Smoke on Digital I&C Equipment

Tina J. Tanaka*
Sandia National Laboratories
Accident and Consequence Analysis Department
Albuquerque, NM 87185-0748

Christina Antonescu†
U.S. Nuclear Regulatory Commission
Office of Nuclear Regulatory Research
Washington, DC 20555

Abstract

A program to assess the impact of smoke on digital instrumentation and control (I&C) safety systems began in 1994, funded by the US Nuclear Regulatory Commission Office of Research. Digital I&C safety systems are likely replacements for today's analog systems. The nuclear industry has little experience in qualifying digital electronics for critical systems, part of which is understanding system performance during plant fires. The results of tests evaluating the performance of digital circuits and chip technologies exposed to the various smoke and humidity conditions representative of cable fires are discussed. Tests results show that low to moderate smoke densities can cause intermittent failures of digital systems. Smoke increases leakage currents between biased contacts, leading to shorts. Chips with faster switching times, and thus higher output drive currents, are less sensitive to leakage currents and thus to smoke. Contact corrosion from acidic gases in smoke and inductance of stray capacitance are less important contributors to system upset. Transmission line coupling was increased because the smoke acted as a conductive layer between the lines. Permanent circuit damage was not obvious in the 24 hr of circuit monitoring. Test results also show that polyurethane, parylene, and acrylic conformal coatings are more effective in protecting against smoke than epoxy or silicone. Common-sense mitigation measures are discussed. Unfortunately we are a long way from standard tests for smoke exposure that capture the variations in smoke exposure possible in an actual fire.

*Sandia is a multiprogram laboratory operated by Sandia Corporation, a Lockheed Martin Company, for the United States Department of Energy under contract DE-AC04-94AL85000.

†Research sponsored by the Office of Nuclear Regulatory Research, U.S. Nuclear Regulatory Commission. The opinions and viewpoints expressed herein are those of the authors and do not necessarily reflect the criteria, requirements, and guidelines of the USNRC.

1 Introduction

1.1 Purpose of this program

Nuclear power plants are replacing analog instrumentation and control (I&C) equipment with digital I&C equipment; however, there is concern about how these new control systems will be affected by abnormal or severe environments, such as smoke from an electrical fire.[1] In 1994 the U.S. Nuclear Regulatory Commission (USNRC) initiated a program at Sandia National Laboratories (SNL) to determine the impact of smoke on advanced instrumentation and on safety systems. The program was started in response to a user need to determine the impact of smoke on the new digital safety systems, reply to questions posed by the Advisory Committee for Reactor Safeguards, and determine if smoke can cause failures in reactor safety systems. The program is providing information on the reliability of digital I&C systems in a smoke environment. The failure modes of digital I&C caused by smoke have been identified as (1) corrosion of metal contacts and circuit traces, (2) circuit bridging, and (3) an increase in contact resistance. Smoke is expected to cause immediate failures by circuit bridging and an increase in contact resistance, but corrosion is expected to cause long-term failures.

1.2 Background of smoke damage to electrical equipment

At the time this program started, there were little data about how smoke affected active (powered and operating) electronics. Smoke damage in other industries, such as telecommunications, was serious enough to merit detailed analysis of smoke corrosivity and equipment recovery. However, except for the work by Jacobus [2] on relays, power supplies, and switches, no reports have been found in the public literature on active monitoring of electronics in smoke. Since nuclear power plants require continuous control and monitoring of reactor systems, research on the ability to salvage equipment after a fire is not sufficient. It is necessary to be able to determine how smoke affects an active digital system.

The need to protect equipment from smoke has been recognized by the U.S. Navy, the Department of Energy (DOE), the telecommunications industry, and insurance companies. The early studies by the Navy concentrated on the effects of smoke on structural elements in ships.[3] Because of smoke corrosivity, the Navy also created standards for testing the smoke from various cable materials to measure its acidity. Cables that produced less acid when burned were used in ships. Since many of the acidic gases are produced by halogenated compounds (i.e., chlorine and bromine), the Navy has been limiting the use of halogenated materials on ships. Also, the Navy has developed a system by which equipment could be restored to full use by prompt cleaning with detergents and thorough drying [4].

The telecommunications industry has been interested in smoke corrosivity because fires in central offices have disabled service in large areas [5]. Insurance companies are also interested in smoke damage and recovery of electrical equipment. These two groups have contributed to standard testing methods to determine which materials, when burned, would cause the most corrosive smoke. Most

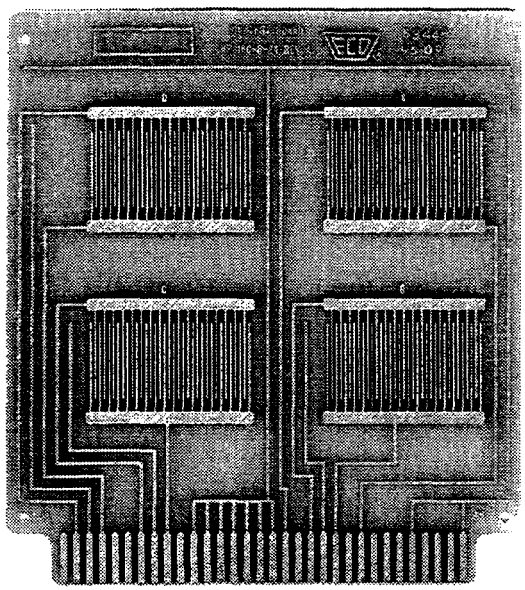

Figure 1: Interdigitated comb board used to measure surface insulation resistance.

of these test methods measure acidity of gases or metal loss. The acidity of the gases is assumed to be directly related to corrosive metal loss. Some of the standards developed for smoke corrosivity testing are ASTM D5485, IEC 754-1, 1994-01, DIN 53436 and CNET(ISO/DIS 11907 part 2). Methods have also been developed to calculate damage probabilities for a given smoke deposition [6]. All of this work is concerned with electronics after the fire, not during the fire.

Degradation of electronics caused by smoke can be similar to degradation from air pollution. Polluted air contains many of the same ionic contaminants as smoke (i.e., chlorides and sulfates); however, the deposition rate of these contaminants is much slower from air pollution.[7] Ionic contaminants increase leakage currents by providing a current path and combining with conductive material to form metal salts. In the presence of ionic contaminants, electrically biased conductors develop metallic dendridic growths that increase leakage currents. Electronics reliability involves both the aging and manufacturing processes. The cleaner the manufacturing process, the more reliable the product. Cleanliness is monitored by measuring surface insulation resistance: interdigitated comb patterns, shown in Figure 1, are biased with dc voltage while the leakage currents are monitored. In order to test how such a pattern would react to pollutants after a long period of time, "accelerated" aging tests are performed at high temperatures and humidity.[8] They also measure surface deposition of ionic contaminants. This particular measurement is now starting to be used for testing smoke corrosivity.[9] The amount of surface deposition of ionic contaminants is used to determine whether smoke-exposed equipment should be reconditioned.

All of this research was focused on damage that measured ionic contamination deposited on surfaces rather than smoke density. Most of these industries are concerned with recovery rather than active control of equipment during the fire; therefore, an important measure is the amount of deposit that remains after the fire. There have been few comparisons to determine what kinds of circuits are

most tolerant of smoke. Knowledge of the mechanisms for smoke damage is important for designing smoke tolerance in electronics and mitigating smoke effects.

1.3 Focus of this research

The research reported here has focused on the impact of smoke on digital I&C equipment. Rather than recovery of equipment, it addresses the need of nuclear power plants to continuously monitor and control a reactor and to determine the immediate effects of smoke on equipment. All of the exposures in our experiments included real-time monitoring to determine what happens as equipment is exposed to smoke. The research has included investigations into the types of failure modes experienced by digital I&C components, exposure of whole computers and digital systems, and possible protection methods. An attempt was made to determine the failure threshold of electronics, but this threshold varies with electronic equipment technology. Three sets of tests have been performed to date: tests on digital systems, measurements of leakage currents, and measurements of the effects of smoke on various circuit types.

Because there are no electronics qualification test standards for smoke, the method of exposure has been based on the draft smoke corrosivity standard for the radiant heat method proposed by ASTM E5.21.70. This method tests different materials and is a static smoke exposure—all of the smoke that is created is contained within an enclosure. The fuel is placed in quartz combustion chambers located underneath an exposure chamber. The fuel is heated and ignited in the combustion chamber. The smoke rises up stainless steel chimneys to the exposure chamber containing the device under test. Two smoke exposure chambers were built—one that is the same size as the draft standard, and a larger one that could hold an entire computer. The larger chamber is shown in Figure 2. The standard exposure time is 1 hr. The radiant heat lamps that heat the fuel are on only for 15 min. The smoke is vented after the 1-hr exposure, and the electronics continue to be monitored for 24 hr after the exposure starts.

2 Summary of Previous SNL Results

2.1 Smoke exposures at SNL

The first set of tests was performed in conjunction with Oak Ridge National Laboratory (ORNL) and its USNRC-sponsored program on advanced I&C qualification.[10] Two digitally based systems were exposed to smoke from cable fires using various plausible scenarios and monitored during the exposure. A multiplexer board that was connected by a serial line to a personal computer outside of the smoke exposure chamber was exposed to three kinds of smoke (cross-linked polyethylene with chlorosulfonated polyethylene, ethylene propylene rubber with chlorosulfonated polyethylene, and polyvinyl chloride). The fuel load provided was equivalent to 75 g of fuel 1 m^3 of air. During the polyvinyl chloride fire, the smoke interrupted the communications between the board and the PC and temporarily stopped the program; however, the program was restarted, and the board seemed to work thereafter.

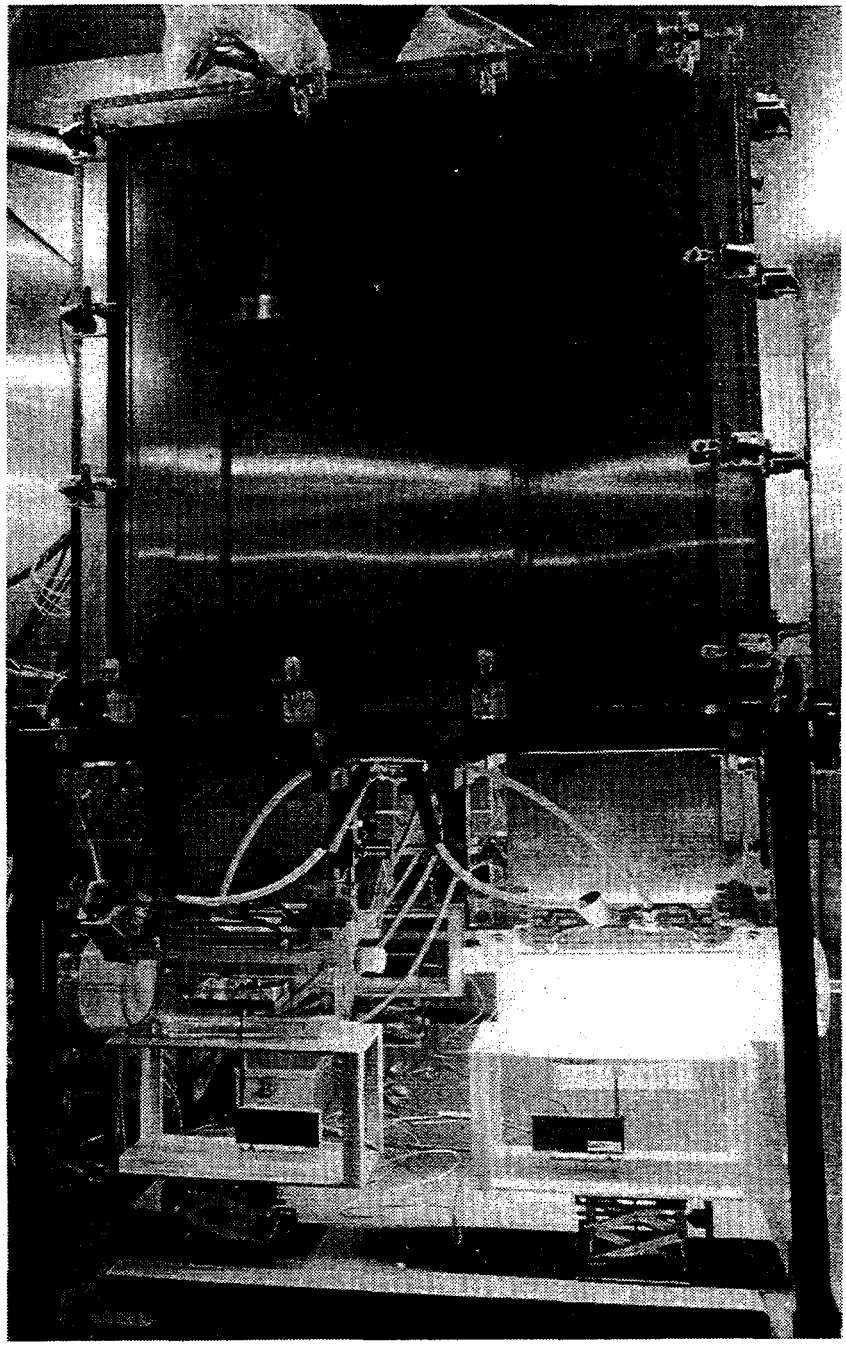

Figure 2: This large smoke chamber was built to expose computers to smoke. It is five times larger in volume than the ASTM draft standard and includes four combustion chambers.

ORNL also designed the second experiment of this set—an experimental digital safety channel where subsystems included computers, electrical and optical serial communication links, fiber-optic network links, analog-to-digital and digital-to-analog converters, and multiplexers. Various subsystems of the safety channel were exposed to smoke of different fuel loads and humidity levels. For these tests, communication upsets were observed at all levels of smoke density, ranging from network retransmissions at low smoke densities to serial link timeout errors at higher smoke densities. Another general observation was that once the various PC units had been exposed to smoke, the baseline tests were no longer upset free. Because these upsets were intermittent, we believe that they were caused by circuit bridging since corrosion and increased contact resistance are not likely to cause only temporary failures.

The second set of tests determined the effect of circuit bridging on component packaging because this was the most likely cause of failure in the first set of tests. Leakage currents were measured between biased pins on empty component packages. Some of the packages were protected with a conformal coating of acrylic or a chassis body equipped with a cooling fan. The tests showed that smoke immediately reduces insulation resistance, but that the resistance may recover if the smoke is vented. The acrylic coating helped reduce circuit bridging, but the cooling fan on the chassis body increased the amount of soot deposited on the components and thus increased circuit bridging. The results of the digital system tests and component packaging tests are reported in NUREG/CR-6476.[11]

The third set of tests was conducted to study the effects of three possible failure modes on a functional circuit board: (1) circuit bridging, (2) corrosion of contacts, and (3) induction of stray capacitance. Stray capacitance can be induced by adding conductive surfaces near high-frequency circuits, and hence is related to circuit bridging. These failures were studied on functional boards containing circuits sensitive to these failure modes. The components on the boards were those commonly used in modern electrical circuits. The boards contained high-voltage (to study circuit bridging), high-current (to study corrosion), high-frequency (to study stray capacitance), and high-speed digital circuits. Circuit performance was measured continuously on bare and conformally coated boards during the smoke exposure and for 24 hr after the start of the exposure. The boards were also subjected to a range of smoke levels to try to determine failure thresholds.

The major results found from all of these tests were that smoke can cause intermittent upsets of digital systems. Smoke increases leakage currents across biased contacts. If leakage currents are increased or shorts occur, the digital systems can receive faulty data that can cause an upset. High smoke density, high humidity, and flaming fires cause more failures than less smoke, low humidity and smoldering fires. Conformal coatings and chip packages with large lead spacing can improve smoke tolerance.

3 Recent Results

Recent results include those for the functional circuit tests, a comparison of chip technologies, and a comparison of conformal coatings. The comparisons of functional circuit tests and chip

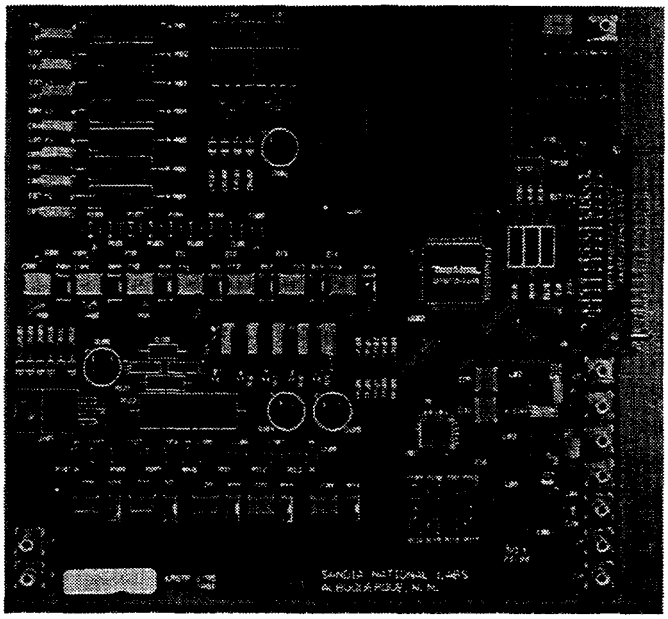

Figure 3: The functional circuit boards allowed testing for different smoke failure modes.

technologies were reported in NUREG/CR-6543 [12]. The comparisons of conformal coatings have been completed and will be included in a results and insights report due in 1998.

3.1 Circuits tested and results

The functional circuit board tests consisted of 12 tests that compared the effect of smoke on different types of circuits. These circuits, listed in Table 1, were designed by the Low Residue Soldering Task Force[1] to determine what particular failure mechanisms would be most likely to happen in electronic circuits. [13] Each circuit displays a different failure. The components of this circuit board include both plated-through hole (PTH) and surface-mounted (SMT) components. In general, SMT components are smaller and easier to install because there is no need to drill holes in printed wiring boards to install them. Thus, more and more digital systems are expected to contain SMT components. When reasonable, the circuits on the functional circuit board contain either SMT or PTH components. Figure 3 shows the functional circuit board. The transmission lines, which are on the reverse side of the functional circuit boards, are shown in Figure 4.

The failures observed during the smoke exposures for the various circuits were as follows:

- High voltage low current—increase in conduction around both PTH and SMT circuits, results in reduced resistance measurement

[1]The Low Residue Soldering Task Force was formed in April 1993 by Sandia National Laboratories and combined the joint efforts of industry, military, and government to evaluate low-residue soldering processes for military and commercial applications.

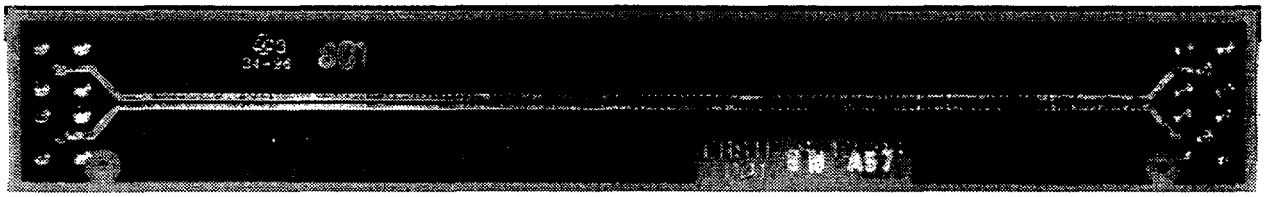

Figure 4: Two 50-Ω transmission lines to measure transmission line coupling.

Table 1: Functional circuits tested and their likely failures.

Circuit	Sensitivity	Package
High voltage low current	Alternative current leakage paths	PTH/SMT
High current low voltage	Increased resistance in solder joints	PTH/SMT
High-frequency transmission line	Coupling between transmission lines	Traces on PWB
High-frequency low-pass filter	Increased inductance or capacitance	PTH/SMT
High-speed digital	Increased pulse rise, fall, or delay times	PTH/SMT

- High current low voltage—increase in resistance for SMT circuit only
- High-frequency transmission line—increase in coupling while smoke in chamber
- High-frequency low-pass filter—very little change from smoke
- High-speed digital—pulse stopped either immediately or after a few hours of exposure, but restarted.

To illustrate the effect of smoke on these circuits, the following three figures plot the response of the circuits to smoke. In general the circuits that responded the most to the smoke were the high-voltage low-current circuits. These circuits had a high potential, 300 Vdc, across a high impedance circuit of 50 MΩ. The measured resistance of the high-voltage low-current circuit depended on the smoke density. Figure 5 shows how the high-voltage low-current circuit reacts to different amounts of smoke. When the smoke density is medium (25 g of fuel per m^3), then the measured resistance falls, but as the smoke clears by deposition and venting, the resistance returns to normal. The circuits tested with a high fuel load (50 g of fuel per m^3) did not recover after venting. The surface deposition was high enough that the current must have passed through the soot on the surface. The resistance of the coated high-voltage low-current circuit did not decrease as much as either of the other circuits. A conformal coating might protect such a circuit.

The high-current low-voltage circuit was a low-resistance circuit that was sensitive to loss of conductivity due to corrosive action of the smoke. Figure 6 shows the reaction of the high-current low-voltage PTH and SMT circuits to smoke (high fuel load, 50 g of fuel per m^3). The resistance of the SMT circuit increases, but does not return to normal after the tests. The PTH circuit seems to be unaffected. The conductive traces or solder joints of the SMT circuit are probably attacked by smoke. Tests with smaller amounts of smoke showed similar but less reaction. The corrosive and

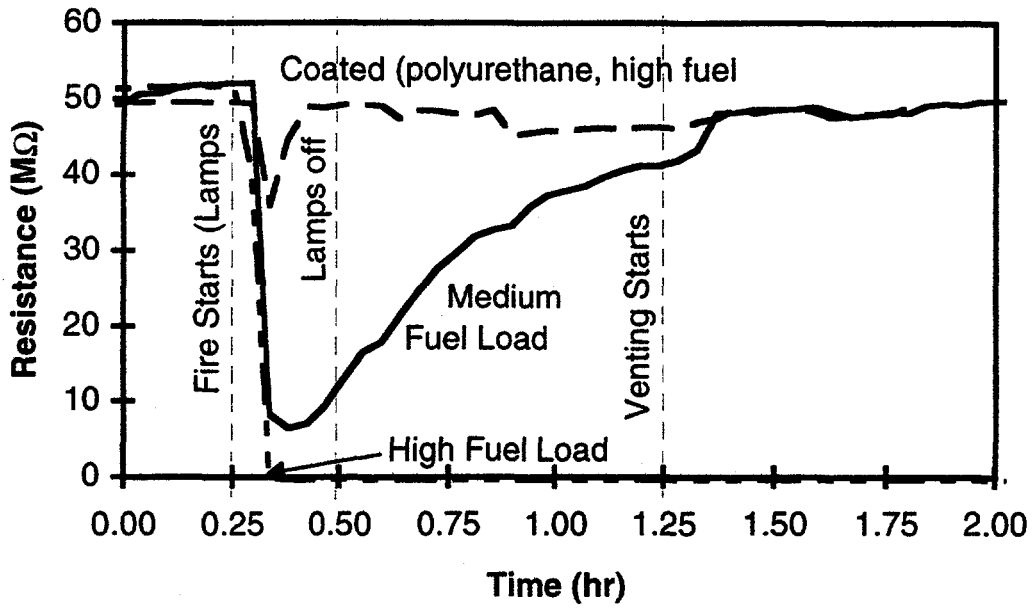

Figure 5: Increased conduction is caused by smoke particles in the air and surface deposition for the high-voltage low-current circuit.

permanent effect of smoke is shown here by this change in resistance. The change is small—only 2%, even for large fuel loads.

The transmission line coupling increased at 50 MHz, as shown in Figure 7. This means that the signal transmitted by one line was picked up on a parallel line. This effect is high while the smoke is in the chamber, but diminishes again once the smoke is pumped out. The smoke seems to act like a conductive layer between the two transmission lines.

3.2 Chip technology comparisons

The component tests and the functional circuit tests showed that smoke can cause circuit bridging. The amount of bridging that is harmful to a particular circuit is dependent on the component technology in the circuit. To determine a failure threshold for logic chips from different chip technologies, a nonsmoke experiment was performed in which the circuit bridging of smoke was simulated with a variable resistor. The concept of this test is illustrated in Figure 8. The normal output of the OR gate at the right of the figure is a high state. The high input to this last gate is connected by a variable resistor to ground, simulating the circuit-bridging effect of smoke. The value of the resistance was lowered to see at what resistance the output of the last OR gate changed to a low state. This was called the critical resistance. The lower the critical resistance, the more tolerant the gate is to smoke, for it would take more smoke to cause a lower resistance.

The critical resistance of a variety of technologies is plotted in Figure 9 against their published switching times. Switching times are indicative of output current drive because the time to switch

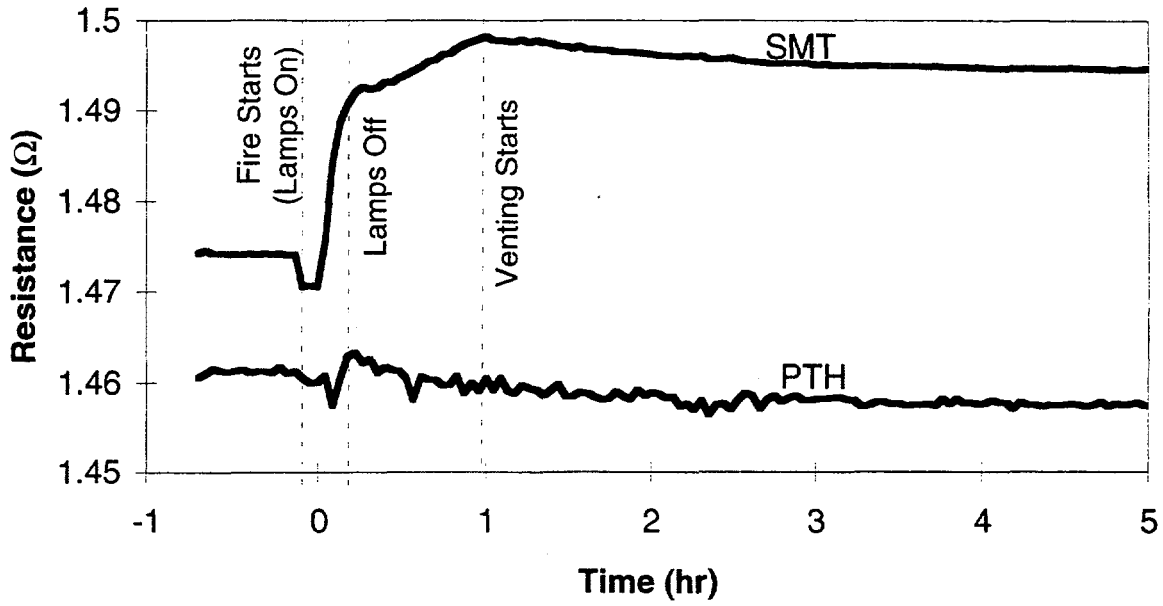

Figure 6: Smoke causes slight increases in resistance of the high-current low-voltage circuit.

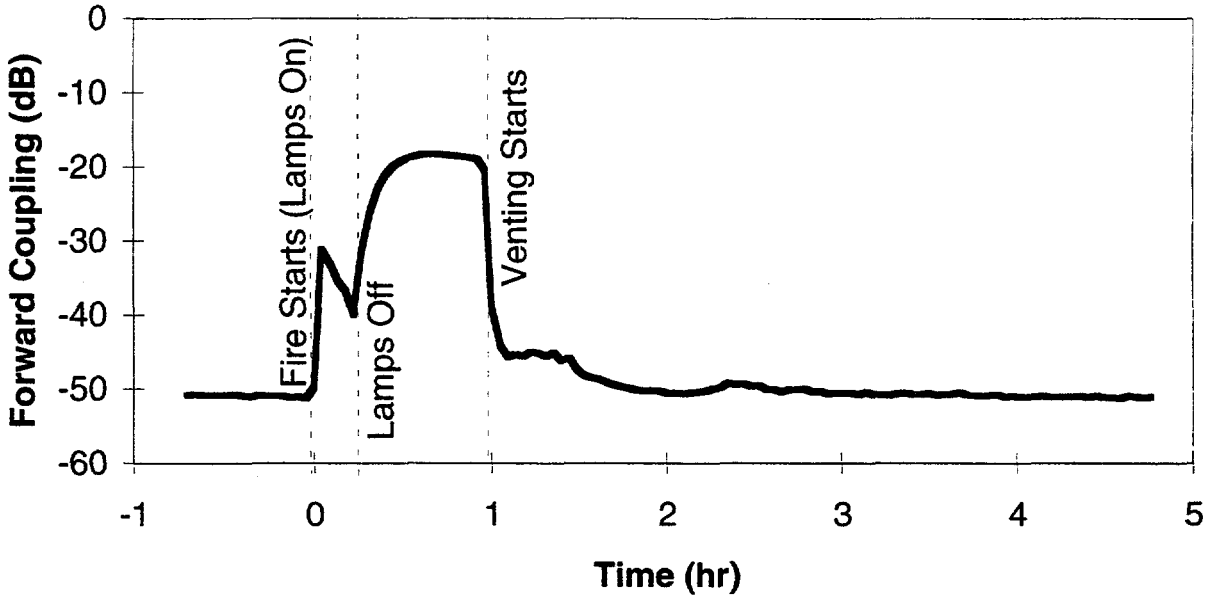

Figure 7: Smoke in the air increases transmission line coupling at 50 MHz.

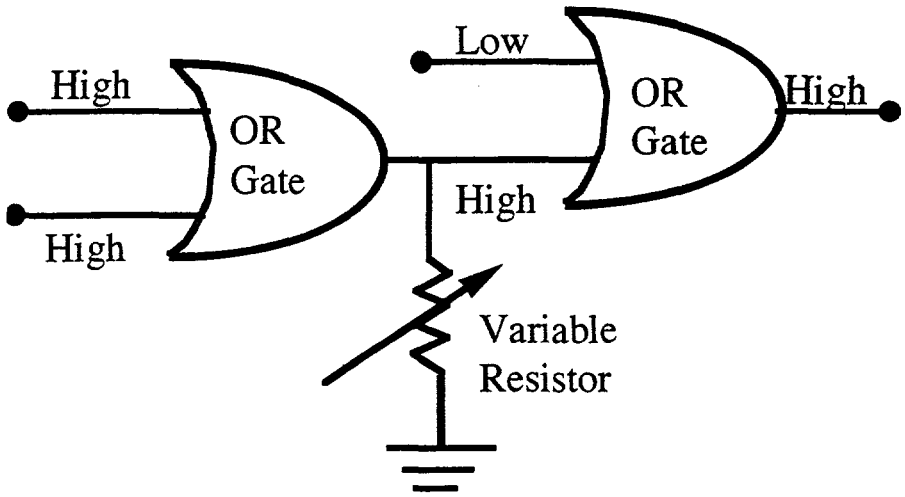

Figure 8: By simulating the circuit bridging effects of smoke with a variable resistor, various logic chip technologies were compared for smoke tolerance.

a state depends on overcoming the RC time constant of the circuit, where R and C stand for the inherent resistance and capacitance of the circuit. The higher the output current and lower the input impedance, the faster the switching time. As seen in the figure, the critical resistance varies approximately with switching time. This means that circuits with faster switching times (high output drive currents) are more tolerant to smoke.

The main component in the high-speed digital circuit tested in the functional circuit board was an advanced transistor-to-transistor logic chip (FAST). This experiment showed that a FAST chip is tolerant to relatively high leakage currents and hence is more tolerant to smoke than other chip technologies. This experiment also showed that technologies with a high output current are more tolerant of smoke. Because standard complementary metal-oxide semiconductor (CMOS) chips have lower output current drive than FAST chips, they are more sensitive to smoke. These tests suggest that CMOS chips would have been affected at lower smoke levels than FAST chips.

3.3 Coating Tests

Conformal coatings can substantially increase the smoke tolerance of both analog and digital circuits. There are more than 75 conformal coatings on the market. In general, there are five types of coatings: polyurethane, epoxy, silicone, acrylic, and parylene. One coating from each of the five types was selected and applied by Specialty Coating, Inc. of Indianapolis, Indiana, to protect the functional boards. These coatings are listed in Table 2. The smoke exposure tests showed that all the circuits performed much better with a conformal coating, although there were minor differences in the performance of the different coatings.

The best circuit to demonstrate differences in coatings is the high-voltage low-current circuit, because it is the most sensitive to smoke. The coatings were expected to provide quite a bit of protection, so a very high fuel level was used—200 g/m^3. Twelve boards remained uncoated, while

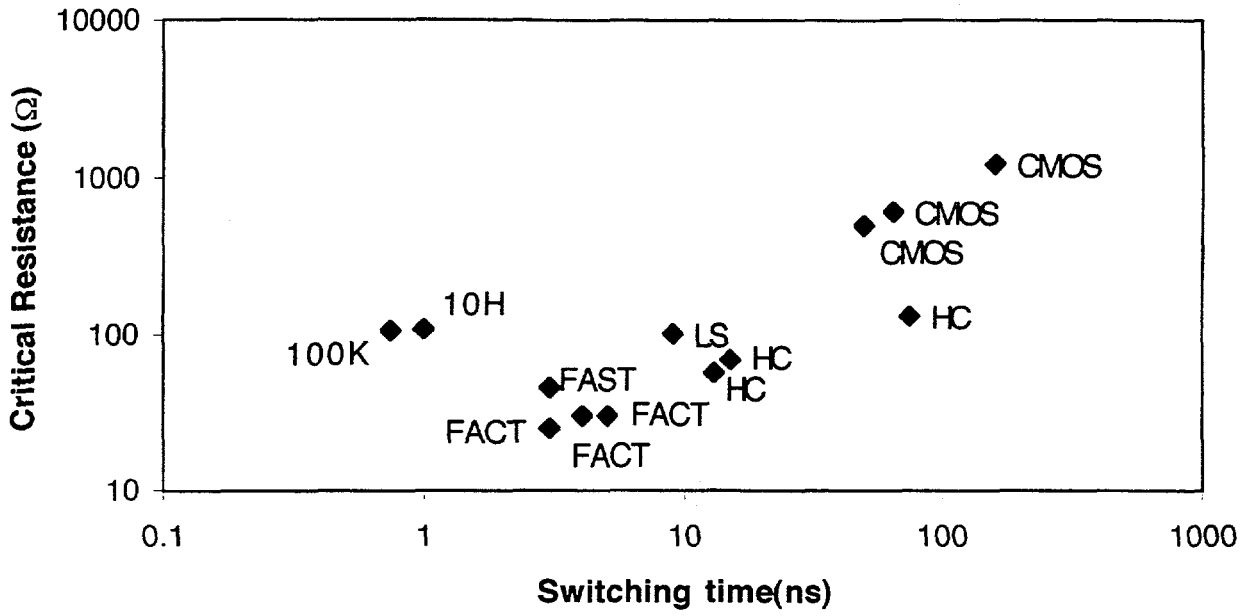

Figure 9: Critical resistance increases with switching time. The technologies with the fastest switching times have more smoke tolerance.

Table 2: Coatings tested.

Coating Types	Brand	Product	Application thickness (nom.)	How applied
Acrylic	Humiseal	1B-31	2.5 mil	Dipped
Epoxy	Envibar	UV1244	2.5 mil	Dipped
Parylene	Union Carbide	Type C	0.75 mil	Vacuum deposited
Polyurethane	Conap	CE-1155	2.5 mil	Dipped
Silicone	Dow	3-1765	5 mil	Dipped

four each of the five conformal coatings were applied to 24 boards. The data from these tests are shown in Figures 10 and 11 for the SMT and PTH circuits respectively. The data are presented as averages of four time periods: preburn (before the fire starts), burn (during the fire), soak (after the fire is out, but before venting), and vent (during venting).

The SMT circuit reacted as expected for the bare boards, as shown in Figure 10. The pretest values were about 50 MΩ. When smoke was added, the resistance decreased. A comparison of the various coatings shows that the best coatings were polyurethane, parylene, and acrylic, and the worst were silicone and epoxy. In fact, the resistance of the silicone-coated board was low during the preburn period.

The PTH circuit displayed two types of failure (Figure 11), one in which resistance decreased as in the SMT circuit and one in which it increased. This increase indicates an open circuit. One explanation of the open-circuit failure is that when the board was heated by the fire during the exposure, the board warped and opened the circuit. We tested the PTH circuits at 75° C (the highest temperature in the exposure chamber that the boards were exposed to) to see if the heat caused the open circuit. However, the circuits that opened during the smoke test did not open at this temperature. Of the uncoated boards, three failed in the open condition while seven failed as if the circuit shorted. The reaction of the coated boards indicates that the polyurethane, parylene, and acrylic coatings protected against the failure where the resistance of the circuit decreased, but did not protect against an open circuit. Again, the epoxy and silicone coatings did not perform as well as the other three.

3.4 Mitigation of Smoke Damage

Smoke damage may be mitigated by controlling the potential fire environment and by designing high smoke tolerance into the electronic systems. Common sense and results from our tests provide several general rules on controlling a fire environment:

- Minimize fire occurrences and quickly detect and suppress fires to minimize smoke exposure.
- Use fire-retardant materials in plants where possible
- Select locations for digital I&C equipment that are:
  - away from areas with a high likelihood of fire, for example, the diesel generator room
  - not equipped with water-based fire suppression systems
  - in controlled, dry environments (<30% RH)
  - protected with smoke removal systems.

Electronic systems should be designed so that they can be tolerant to smoke. Findings from these tests indicate that design elements should:

- be enclosed in a box or conformally coated to protect electronics

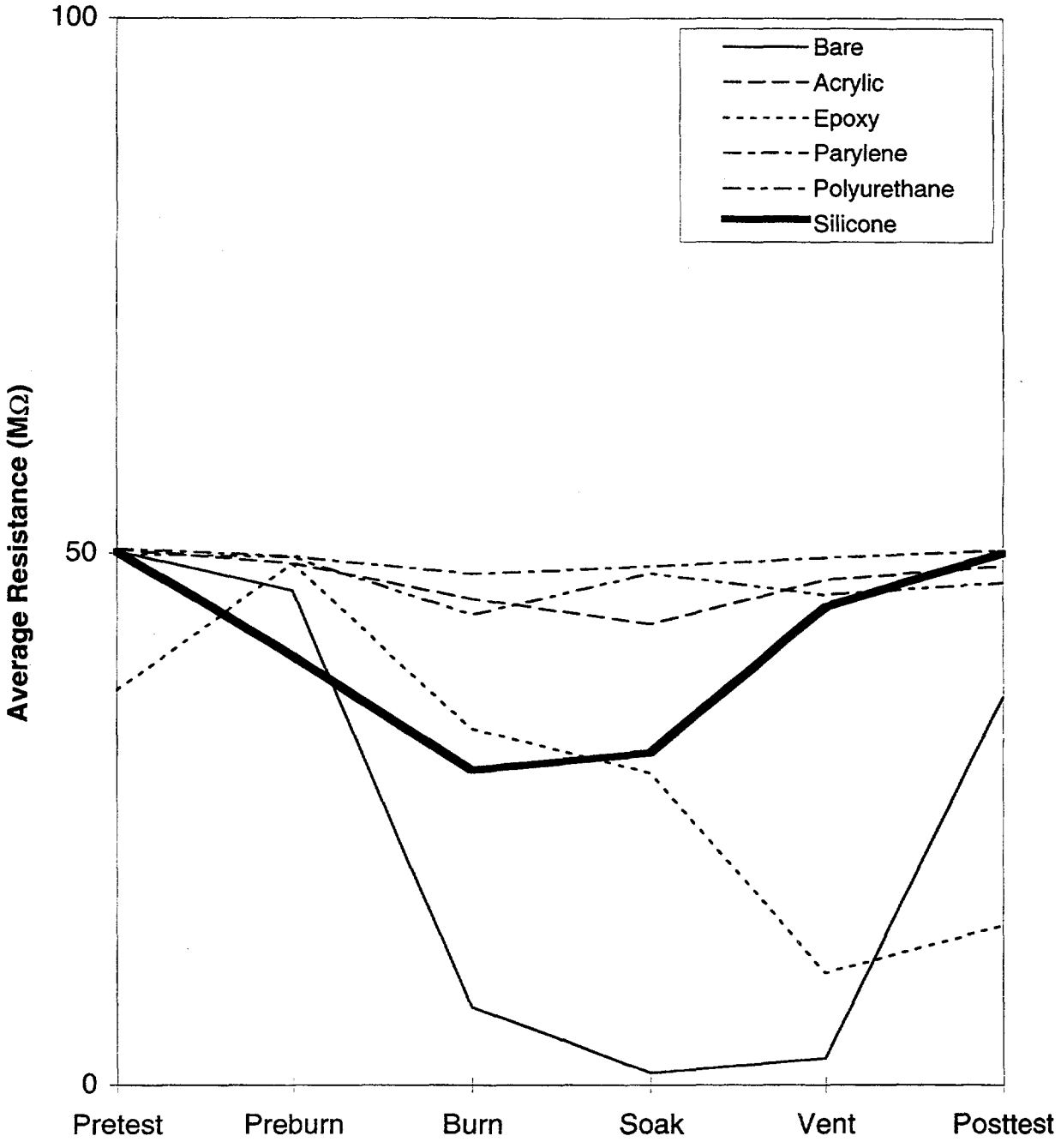

Figure 10: Coating comparison of the high-voltage low-current circuit for the SMT components.

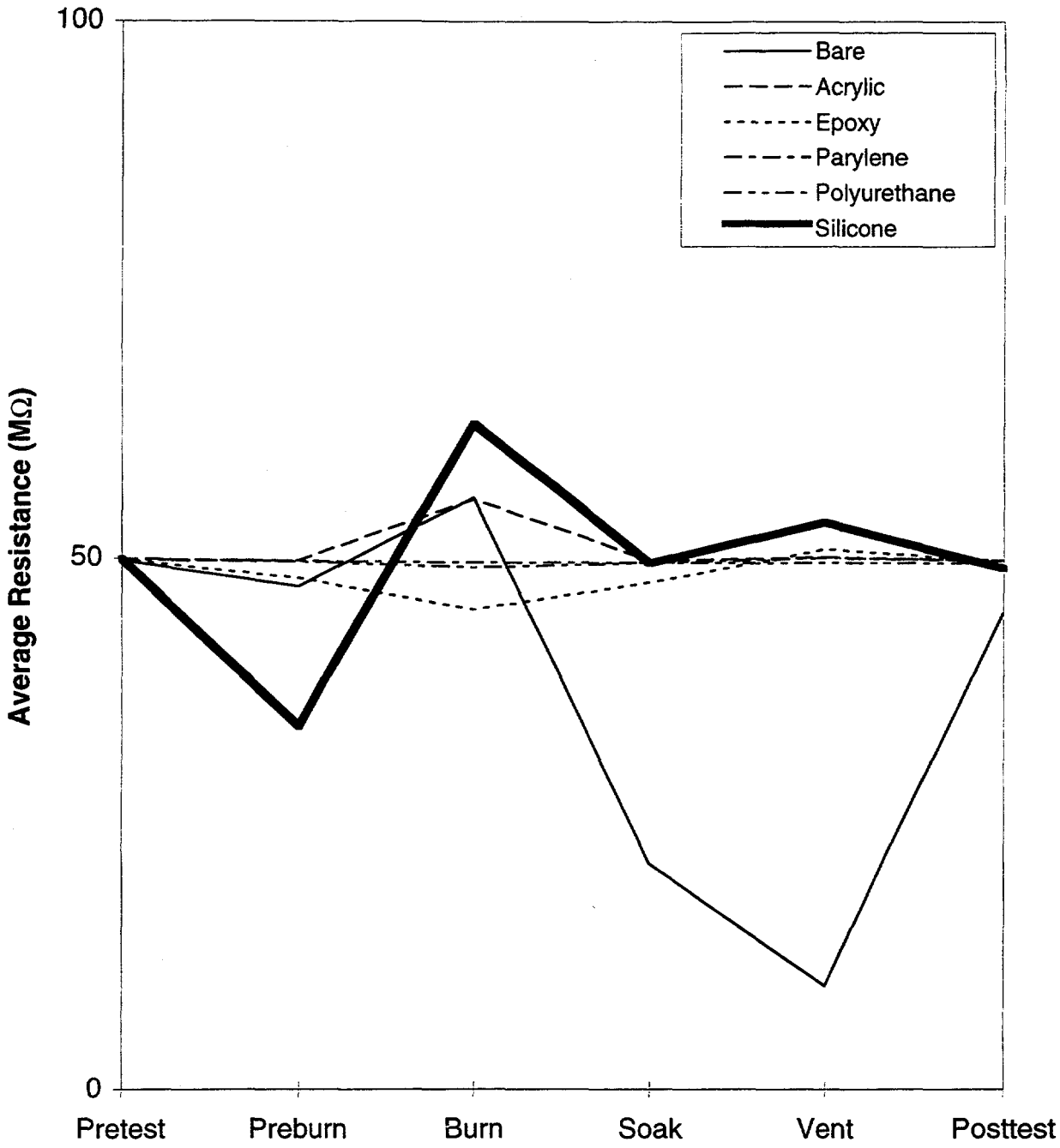

Figure 11: Coating comparison of the high-voltage low-current circuit for the PTH components.

- include electronics with high output current, such as transistor-to-transistor logic (TTL) or advanced CMOS
- include chip packages with widely spaced contacts
- include hermetically sealed packages rather than plastic packages
- avoid ventilation fans that can draw in more smoke
- avoid high voltages because particulates are drawn to strong fields

Beyond protecting the electronics from soot deposition, it is also important to protect them from the charged smoke in the air. At this time it is not possible to predict how any one digital system will react to smoke.

4 Conclusions

Smoke exposure testing is not a well-developed field in terms of an environmental qualification test for any electronic equipment—digital or analog. The program described here has supported some of the first tests of how digital equipment will react to smoke. Smoke causes intermittent upsets of digital equipment by interrupting digital communications. These upsets are caused by circuit bridging; the charged smoke particles act as a bridge for electrical currents. Conductivity is increased both by the smoke and by soot deposits. Smoke can also cause a breakdown in solder joints and increased coupling between transmission lines.

Smoke damage can be minimized by fire awareness, protection and design of digital I&C equipment, and smoke control. Some design elements include the use of types of chips and conformal coatings that can increase the tolerance of electronics to smoke. Chips that have faster switching times tend to be more smoke tolerant. Faster switching times tend to require higher output currents, so any small leakage currents may not be as significant. Conformal coatings such as parylene, polyurethanes, and some acrylics can protect circuits from the effects of smoke.

Smoke qualification testing of digital equipment is not expected to become a standard soon. First, there is no testing standard that can be readily adapted to support the systematic, repeatable assessment of the susceptibility of electronic components to degraded performance due to smoke. Current smoke test methods do not address the question of when a digital I&C system would be upset; rather, they address only the corrosive potential of a given fuel. Second, a smoke-filled environment does not lend itself easily to measurements. For example, the actual smoke density and chemical composition at the time of an upset may be an important parameter, but measurement of this parameter is difficult. Thus, unlike fire temperature tests, where an item is qualified if it can survive exposure to certain time-temperture profiles, it is uncertain how to repeatably create or measure the smoke conditions produced during a test that may be relevant for digital I&C system upset. Third, there is currently no technical basis for establishing bounding smoke conditions for testing purposes that can characterize likely smoke environments in nuclear power plants. We have made estimates based on the type and amount of fuel likely to burn in different environments, but

these estimates do not include smoke transport and evolution, and have provided only minimal indications of the effect of different fuels.

SNL has begun a program to determine how to include smoke in risk assessments. This program will measure the electrical characteristics of smoke, such as conductivity, as a function of smoke density and fuel. In addition to these direct-current measurements, SNL will expose different interfaces (*i.e.*, connectors) carrying digital signals. Connectors are not usually coated, so they may be the most vulnerable region of a digital system. To date, SNL tests have protected the connectors during component and functional board exposures. For the upcoming tests, the connectors will be exposed and bit error rates will be recorded to estimate upset thresholds. Estimates of upset thresholds and failure modes are necessary for risk assessments.

References

[1] K. Korsah, R.L. Clark, and R.T. Wood. Functional issues and environmental qualification of digital protection systems of advanced light-water nuclear reactors. Technical Report NUREG/CR-5904, ORNL/TM-12164, Oak Ridge National Laboratory, Oak Ridge, TN, 1994.

[2] Mark J. Jacobus. Screening tests of representative nuclear power plant components exposed to secondary environments created by fires. Technical Report NUREG/CR-4596, SAND86-0394, Sandia National Laboratories, Albuquerque, NM, 1986.

[3] J.S. Patton. Fire and smoke corrosivity of structural materials. *Journal of Fire Sciences*, 10(4):294–322, 1992.

[4] H.R. Baker and R.N. Bolster. Guide to NRL cleaning and salvaging techniques for reclaiming equipment contaminated with seawater, oil, and smoke deposits. Technical Report NRL Report 7563, Naval Research Laboratory, 1973.

[5] Joint Report of the Office of the State Fire Marshal (Illinois) and the Illinois Commerce Commission Staff. Hinsdale central office fire final report, 1989.

[6] Dimitrios M. Karydas. A probabilistic methodology for the fire and smoke hazard analysis of electronic equipment. In *Interflam '93, Fire Safety International Fire Conference*, 1993.

[7] J.D. Sinclair. Corrosion of electronics: The role of ionic substances. *Journal of the Electrochemical Society*, 135(3):89C–95C, 1988.

[8] Douglas Pauls. IPC cleaning and cleanliness test program. Phase 3: Water soluble fluxes. Technical report, The Institute for Interconnecting and Packaging Electronic Circuits, Lincolnwood, IL, 1992.

[9] J. Thomas Chapin, Loren M. Caudill, Pravin Gandhi, and Robert Backstrom. Leakage current smoke corrosivity testing comparison of cable and material data. In *International Wire and Cable Symposium Proceedings*, 1996.

[10] Kofi Korsah, Tina J. Tanaka, and T.L. Wilson, Jr. Environmental testing of an experimental digital safety channel. Technical Report NUREG/CR-6406, ORNL/TM-13122, Oak Ridge National Laboratory, Oak Ridge, TN, 1996.

[11] T.J. Tanaka, S.P. Nowlen, and D.J. Anderson. Circuit bridging of components by smoke. Technical Report NUREG/CR-6476, SAND96-2633, Sandia National Laboratories, Albuquerque, NM, 1996.

[12] Tina J. Tanaka. Effect of smoke on functional circuits. Technical Report NUREG/CR-6543, SAND97-2544, Sandia National Laboratories, Albuquerque, NM, 1997.

[13] Ronald L. Iman, Robert V. Burress, Dennis J. Anderson, Dennis D. Huffman, Jeffry F. Koon, Barbara M. Waller, Mahendra S. Gandhi, Thomas A. Carroll, Mark J. Shireman, Carol M. Krska, Gary A. Becka, Robin L. Sellers, David P. Carlton, Roger D. Nickell, Mark I. Siewers, Gary S. Falconbury, and Terry L. Munson. Evaluation of low-residue soldering for military and commercial applications: A report from the low-residue soldering task force. Technical Report SAND95-1060, Sandia National Laboratories, Albuquerque, NM, 1995.

Review Guidelines for Software Written in High Level Programming Language Used in Safety Systems

Myron Hecht, SoHaR Incorporated
and Robert Brill, U.S. Nuclear Regulatory Commission

Abstract: This paper provides an overview of the results of a NRC-sponsored research on guidelines for review of software written in high level languages for use in safety systems. These guidelines were developed using a 3-level hierarchical framework consisting of top level, intermediate, and base attributes. The top level attributes of reliability, robustness, traceability, and maintainability were developed in order to define general qualities of software related to safety. Intermediate attributes were then developed to describe the top level attributes in greater detail. At the lowest level are the base attributes which were defined to be sufficiently specific to derive language specific guidelines. These attributes were then used to develop specific guidelines for a total of 9 languages. The resulting guidelines are available in the form of both a NUREG report and HTML files.

Certain programming practices can affect the safety of digital systems, and hence, guidelines can be developed to enhance their dependability. This paper provides an overview of the results of An NRC-sponsored project which identifies such guidelines for safety related software written in the following nine high level languages: Ada, Ada95, C/C++, Pascal, PL/M IEC 1131-3 Ladder Logic, Sequential Function Charts, Structured Text, and Function Block Diagrams. The complete guidelines are described in NUREG CR/6463 Rev. 1 (Hecht, 1997) and in a set of hypertext markup language (HTML) files . The first section describes how the guidelines were developed, the second discusses the generic attributes, and the third discusses language-specific issues for selected languages covered by the guidelines.

1 Methodology

In order to develop a technical basis for the guidelines, attributes of software safety were compiled and classified from a review of the large body of literature in software safety. An initial framework was established and iteratively refined resulting in the 3-level hierarchy described shown in Figure 1. The two highest levels called *top level* and *intermediate level* were used to define broader and narrower categories of attributes. The lowest level, called the *base level,* contains qualities or characteristics of safe programming practices that can then be used to develop language specific guidelines.

These attributes, which are called *generic attributes,* were used by individuals with extensive programming backgrounds in one or more of the 9 languages covered by this project to develop language specific guidelines. The generic attributes and language specific guidelines were then submitted to an independent set of SMEs who served as reviewers. These reviewers provided an initial round of comments, after which the guidelines were revised. The guidelines were then verified by a resubmission to the reviewers for a final round of evaluations. The classification was validated by comparing the attributes with the causes and descriptions of failures in two major air traffic control projects (the Federal Aviation Administration Advanced Automation System and Voice Control Switching System) as well as incident reports from the Eagle 21 reactor protection system upgrades at the Tennessee Valley Authority (TVA) Sequoyah Nuclear Plant. For the C and Ada languages, a total of 150 specific failure reports were associated with specific guidelines. Additional validation came from other published large scale studies of software failures.

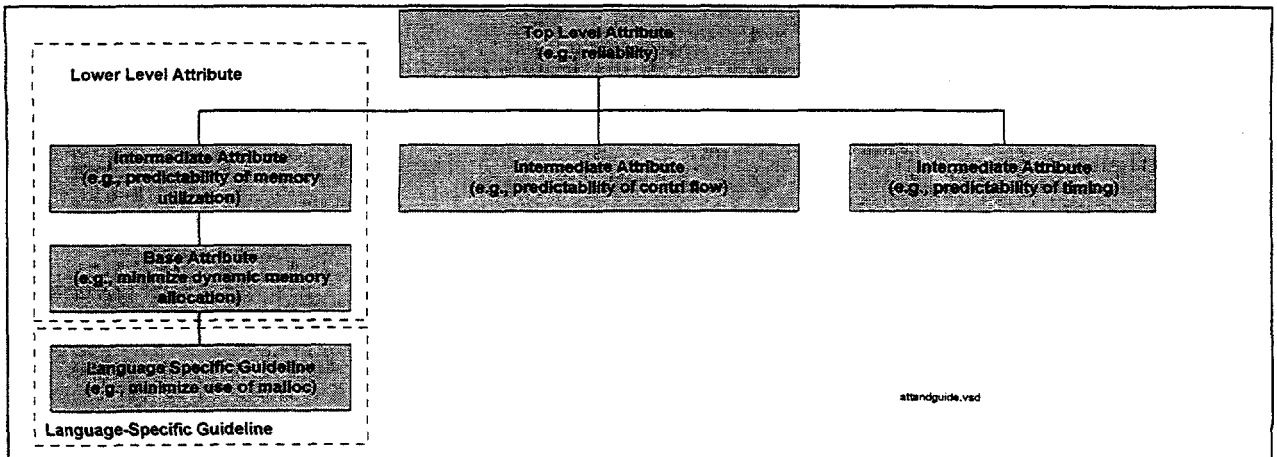

Figure 1. Conceptual Framework for Attributes and Guidelines

2 Generic Attributes

This section describes the generic attributes shown in figure 1. A complete description can be found in Chapter 2 of NUREG/CR 6463 Rev. 1. The top level generic attributes, which define a general quality of software related to safety, are

- *Reliability.* The predictable and consistent performance of the software under conditions specified in the design basis. This top level attribute is important to safety because it decreases the likelihood that faults causing unsuccessful operation will be introduced into the source code during implementation.

- *Robustness.* Robustness is the capability of the safety system software to operate in an acceptable manner under abnormal conditions or events. This top level attribute is important to safety because it enhances the capability of the software to handle exception conditions, recover from internal failures, and prevent propagation of errors arising from unusual circumstances.

- *Traceability.* Traceability relates to the feasibility of reviewing and identifying the source code and library component origin and development processes, i.e., that the delivered code can be shown to be the product of a disciplined implementation process. Traceability also includes being able to associate source code with higher level design documents. This top level attribute is important to safety because it facilitates verification and validation, and other aspects of software quality assurance.

- *Maintainability.* The means by which the source code reduces the likelihood that faults will be introduced during changes made after delivery. This top level attribute is important to safety because it decreases the likelihood of unsuccessful operation resulting from faults during adaptive, corrective, or perfective software maintenance.

2.1 Reliability

In the software context, reliability is either (1) the probability of successful execution over a defined interval of time and under defined conditions, or (2) the probability of successful operation upon demand

(IEEE, 1977). That the software executes to completion is a result of its proper behavior with respect to system memory and program logic. That the software produces timely output is a function of the programmer's understanding of the language constructs and run-time environment characteristics. Thus, the intermediate attributes for reliability are:

- *Predictability of memory utilization.* There is a high likelihood that the software will not cause the processor to access unintended or unallowed memory locations.

- *Predictability of control flow.* There is a high probability that the processor will execute instructions in sequences intended by the programmer.

- *Predictability of timing.* There is a high probability that the software executing within the defined run-time environment will meet its response time and capacity constraints.

- *Predictability of mathematical or logical result.* There is a high probability that the software executing within the defined run-time environment will yield the programmer-intended mathematical or logical result.

Figure 2 shows the reliability hierarchy including base attributes .

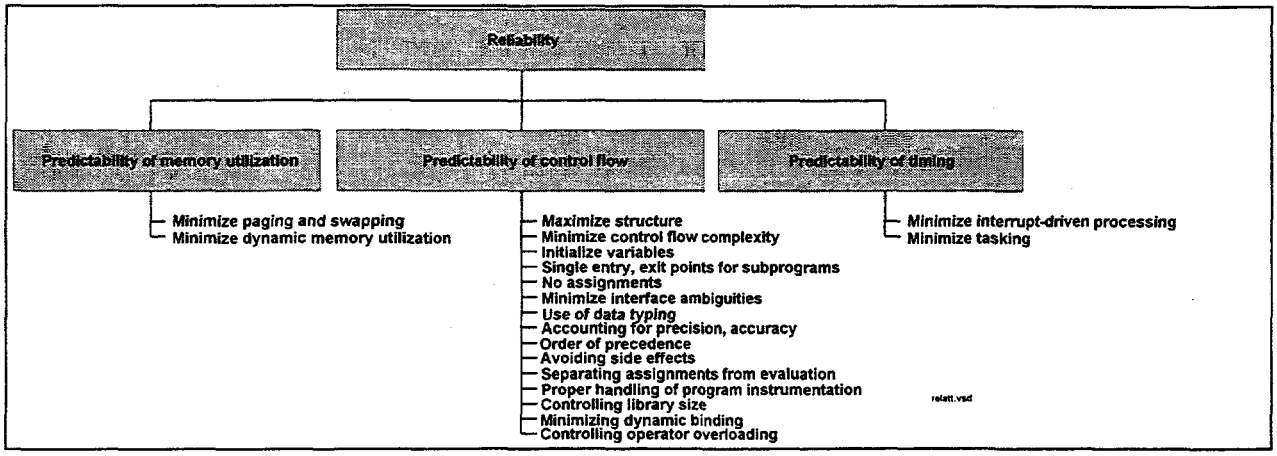

Figure 2. Reliability Attributes

2.2 Robustness

Robustness refers to the capability of the software to continue execution during off-nominal or other unanticipated conditions. A synonym for robustness is survivability (Bowen, 1985; Wigle, 1985). Robustness is an important attribute for a safety system because unanticipated events can happen during an accident or excursion, and the capability of the software to continue monitoring and controlling a system in such circumstances is vital. Figure 3 shows the intermediate and base attributes for robustness

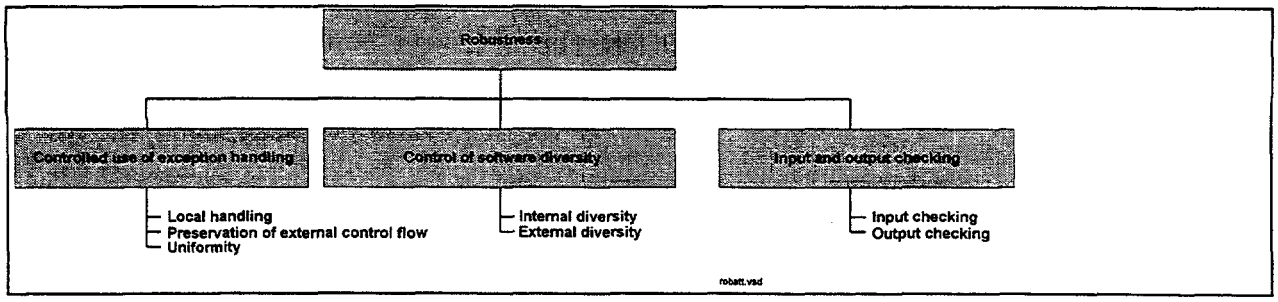

Figure 3. Robustness Attributes

2.3 Traceability

Traceability refers to attributes of safety software which support verification of correctness and completeness compared with the software design. The base attributes for traceability are:

- Readability (also an attribute of maintainability)
- Controlling use of built-in functions
- Controlling use of compiled libraries.

2.4 Maintainability

Software maintainability reduces the likelihood that errors will be introduced while making changes. The intermediate attributes related to maintainability that affect safety include:

- *Readability*: those attributes of the software that facilitate the understanding of the software by project personnel
- *Data abstraction:* the extent to which the code is partitioned and modularized so that the collateral impact and probability of unintended side effects due to software changes are minimized
- *Functional cohesiveness:* the appropriate allocation of design level functions to software elements in the code (one procedure; one function)
- *Portability:* the major safety impact of which is the avoidance of non-standard functions of a language.
- *Malleability:* the extent to which areas of potential change are isolated from the rest of the code

Figure 4 shows these intermediate level and associated base attributes.

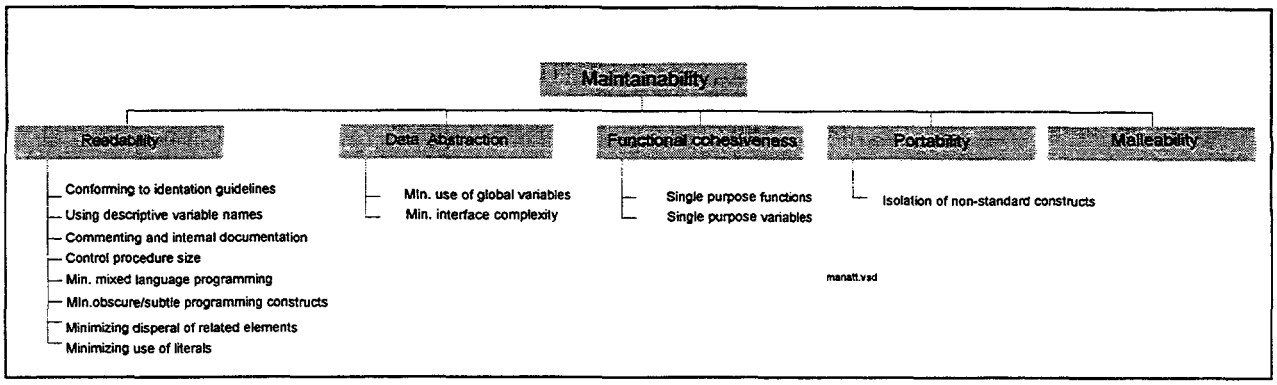

Figure 4. Maintainability Attributes

3 Examples of Language Specific Guidelines

This section provides examples of language-specific guidelines to acquaint readers with what can be found in the full version of NUREG/CR 6463 Rev. 1. The first subsection discusses guidelines on pointer initialization in C; the second discusses timing issues in IEC 1131-3 programming languages used in programmable logic controllers (PLCs).

3.1 C and C++ Guidelines on Pointer Initialization

The C/C++[1] language-specific guideline for pointer initialization was derived from the top level attribute of reliability, the intermediate attribute of the predictability of control flow, and the base attribute of initialization of variables before use.

All variables and pointers should be initialized before use (Porter, 1993; Kernighan, 1978). C supports initialization through the facility of specifying initial values along with declarations. However, it does not require that all objects[2] be initialized (Eckel, 1995). In some cases, the initialization of an object entails not only assigning a specific bit-pattern value to the object location, but also taking special actions to facilitate smooth initialization of the object's life (e.g., allocating corresponding resources to the objects). In C++ it is possible to consider any correlated data set as an object and provide facilities for constructing an instance of the data set and destroying the current instance of the data set in a systematic way. The following are specific guidelines.

- *Do not use pointers to automatic variables outside of their scope.* Pointers to automatic variables should not be used outside of their declared scope. The value stored in a pointer to an automatic variable will contain garbage outside the function scope.

- *Initialize pointers.* Initialization problems can also occur in pointers. In safety systems, all pointer

[1] Guidelines for C and C++ were developed together because of the close relationship between the two languages. In addition, programs written in C++ are also likely to contain C code as well. For C, the guidelines address the problems in memory allocation and deallocation, pointers, control flow, and software interfaces. For C++, the guidelines address additional issues associated with multiple inheritance, late binding, and large class libraries.

[2] That is, variable, structures, or arrays.

variables in C should be initialized to `NULL`, and all pointer variables in C++ language should be initialized to 0 (Plum, 1991). The pointer should then be tested for a valid value before being used. In C and C++, when a pointer is defined, it does not have a memory location associated with it. Using an uninitialized pointer will overwrite an unintended portion of memory. Incorrectly overwriting memory can cause serious problems, including system crashes.

- *Ensure that the indirection operator is present for each pointer declaration.* Each pointer should have an indirect operator (*) when it is declared (Porter, 1993). The following example shows how the C syntax facilitates omitting the indirection operator:

- *Use the ~ operator when initializing to all 1's.* When initializing all bits of an integer type to all 1's, use bitwise `not 0`.

3.2 Guidelines for Timing in IEC 1131 Languages

This subsection summarizes guidelines on timing, fault handling routines, system health monitoring, and watchdog timers and which are relevant across all the IEC 1131-3 languages[3]. These language-specific guidelines are derived from the generic attribute of robustness and the intermediate attribute of exception handling

3.2.1 Fault Routines

Programs should properly account for PLC behavior at shutdown. Generally, all outputs turn off, but this is not always true. The PLC system is designed so that such a shutdown places the system in a fail-safe condition. Some PLCs have the capability to run a subroutine which the processor automatically executes when it encounters a condition that will cause execution of the main Ladder Logic routine to stop. This subroutine is called a "fault routine". It allows the designer to decide on the appropriate action, including shutting down the system in a safe manner. The IEC 1131-3 Programmable Controller Language Specification does not mandate that a compliant PLC system contain a designated hardware fault routine that will execute upon detection of one of a range of fault conditions, similar in concept to the Fault Routine available in current Allen Bradley PLCs (Allen Bradley, 1991). However, a non-periodic task could be set up to trigger appropriate internal diagnostic information to handle particular types of errors (fall-back modes on I/O failures, warnings to operator interfaces, etc). Usage of such a construct should be considered in the design phases of programming for a system of this kind.

The following specific guidelines apply to fault routines:

- *Completeness.* The fault routine cannot be relied on to detect all instances of program crashes. Additional provisions that may be required by the specific safety requirements of the application for PLC major faults must be specified.

- *Observability.* The fault routine should annunciate and log the condition. The execution of the fault routine should not be masked.

- *Validity checking.* The conditions under which the fault routine is running may have corrupted

[3]The International Electrotechnical Commission (IEC) standard 1131-3 has defined standards for a total of five languages for Programmable Logic Controllers (PLCs). Four of the languages were covered by the guidelines (the fifth, Instruction Lists, more closely resembles assembly language)

program memory, data files, or I/O. The fault routine must ensure the validity of its environment before proceeding to execute.

- *Fail safe properties in the absence of the fault routine.* The fault routine cannot be relied upon to operate under every major failure condition. The PLC may be so disabled that this is not possible. Thus, the system design should ensure a safe state in the absence of the successful execution of the fault routine.

3.2.2 System Health Monitoring

PLC systems provide System Health Monitoring information to the application program, usually in the form of designated internal bits and words. Information may include execution times for particular tasks, I/O update information, I/O operating status information, battery state information, and other status information used to determine the proper operating status of a PLC system. Unfortunately, the nature, extent, and type of this information is not covered by the IEC 1131-3 specification. However, the safety program should make use of such information (as available) as part of its health checking and exception processing.

3.2.3 Watchdog Timers

A note in section 2.7.2 (Tasks) of the IEC 1131-3 specification states that "The manufacturer shall provide information to enable the user to determine that all (task) deadlines will be met in a proposed configuration". However, the specification does not mention any form of checks that these deadlines are met at runtime, since this falls into the error-checking category of constructs not covered by the document. Many PLC and PLC-like systems with 1131-3 compliant multitasking capability implement a watchdog timer for each periodic task. Typically, these systems will ignore a single task overrun and flag that an overrun has occurred, but will shut down the system upon N consecutive task overruns, where the value of N will vary from system to system. Where available, programs should monitor the task overrun flag, and react appropriately. It is not appropriate for a safety-critical system of this nature to exhibit regular task overruns — this should be looked for specifically during the check-out phases of development.

4 Conclusions

The guidelines in NUREC/CR 6463 Rev. 1 address a gap in the literature on software safety. Much has been written about the importance of understanding the application, disciplined development, design methodologies, and testing. However, less has been written about language-specific programming guidelines (some examples include Hatton, 1995; Plum, 1993; and Saaltink, 1996) , and even less has on a uniform framework that can be applied across multiple heterogeneous languages. The guidelines developed in this study address programming issues specific to safety. They are not intended as general programming style guidelines; excellent sources already exist for this purpose.

The guidelines are available as both a printed document and in hypertext markup language (HTML) formatted files. As HTML files, they can be particularly valuable because they can be viewed and modified locally, within restricted network domains (such as a development group or organization), or across the entire Internet. For development organizations or groups, they can be customized and enhanced for individual projects based on the experience of the development organization.

References

Allen Bradley, *PLC-5 Programming Software – Programming*, Publication 6200-6.4.7 November 1991.

Bowen, T.P. and G.B. Wigle and J.T. Tsai, "Specification of Software Quality Attributes" Report, 3 Vols. RADC-TR-85-37, available from NTIS, 1985.

Eckel, B., "Exception Handling in C++", *Embedded Systems Programming,* Vol.8, No.1, January, 1995.

Hatton, L. *Safer C,* McGraw-Hill International Series in Software Engineering, Maidenhead, Berkshire, England, 1995

Hecht, H., M. Hecht, S. Graff, *et. al., Review Guidelines for Software Languages for Use in Nuclear Power Plant Systems,* NUREG/CR-6463 Rev. 1, U.S. Nuclear Regulatory Commission, September, 1997

International Electrotechnical Commission (IEC), "Software for Computers in the Safety Systems of Nuclear Power Stations," Standard 880, 1986.

International Electrotechnical Commission (IEC), *Programmable Controllers Programming Languages,* IEC Standard 1131, Part 3, 1993. (Available in the U.S. from the American National Standards Institute, New York.)

Kernighan, B.J and P. J. Plauger, *The Elements of Programming Style, Second Edition*, McGraw-Hill, New York, 1978.

Porter, A., *The Best C/C++ Tips Ever*. Osborne McGraw-Hill, New York, 1993.

Saaltink, M. And Mitchell, S., Ada95 Trustworthiness Study: Guidance on the Use of Ada95 in the Development of High Integrity Systems Version 1.0, (Canada) Department of National Defence contract W2207-5-RC02/01-SV, Document No. TR-96-5499-04, September, 1996.

Spuler, D.A., C++ and C Debugging, Testing, and Reliability, Prentice Hall, Englewood Cliffs, New Jersey, 1994.

Combining Disparate Sources of Information in the Safety Assessment of Software Based Systems

Gustav Dahll

OECD Halden Reactor Project

P.O. Box 173, N-1751 Halden, Norway

E-mail: Gustav.Dahll@hrp.no

Abstract

The OECD Halden Reactor Project (HRP) is an international institution with participation from 19 countries. A main research topic over the last twenty years has been software dependability. Particular emphasis has been placed on software in safety critical systems. The paper starts with a short survey of these activities. However, the main topic of the paper is a discussion on how to combine disparate sources of information in the safety assessment of software based systems. This is based on experience gained through the licensing process of the a programmable system in the Swedish nuclear power plant Ringhals, where a guideline for reviewing and assessing safety critical was applied.

One lesson learned from this activity is that the approval of a programmable safety critical system, in particular one which is based on COTS, is based on a combination of disparate sources of information. This combination of information is made in a diagrammatic framework.

An emerging methodology combine information about disparate evidences in a systematic way is based on Bayesian Belief Networks. The objective is to show the link between basic information and the confidence one can have in a system.

1. Introduction

The use of programmable equipment in safety related systems in NPPs, has many clear advantages compared to conventional equipment. But there has also been a certain reluctance to use programmable equipment in safety critical systems. A reason for this has been the complexity of safety assessment and the licensing of the software in these systems.

The OECD Halden Reactor Project (HRP) is an international institution with participation from 19 countries. USNRC is the main participant from the US. A main research topic over the last twenty years has been software dependability. Particular emphasis has been placed on software in safety critical systems.

There are three complementary principles which should be followed to obtain dependable software. The first principle in this respect is fault avoidance through good software engineering and quality assurance throughout the complete lifecycle of the software. The second principle is fault detection and removal through a thorough validation and verification activity. A third principle, which could also be considered is fault tolerance, i.e. the system should be designed so that a single failure will not jeopardise safety. HRP has made research activities on methods of relevance for all these principles, as formal software development method, static analysis, testing, software diversity etc. Section 2 gives a short survey of HRP activities set in the framework of these principles.

It is, however, not sufficient to produce high integrity software. One must also get confidence in their safe application, and get the regulator's approval for their application in safety critical systems. For this purpose HRP has produced a guideline for reviewing and assessing safety critical software in nuclear power plants for the Swedish Nuclear Power Inspectorate (SKI). These Guidelines were applied in the licensing of the exchange of an analog protection system with a functionally equivalent programmable system (REPAC), in the Swedish nuclear power plant Ringhals. HRP took part as consultants in the licensing process, and some of the experience gained from this work is described in section 3.

One lesson learned from this licensing activity has been that the approval of a programmable safety critical system, in particular one which is based on commercial off the shelf software (COTS), is based on a combination of disparate sources of information. Section 4 discusses how this combination of information about the system into a diagrammatic framework for the safety assessment, and thereby for the final approval of the system. This framework has the form of an 'influence net', i.e. a directed graph where each node represents an aspect in the total assessment process. The top nodes in the graph represent the basic information sources which are used in the acceptance process. This information is penetrated through the net down to the bottom node which represents the final acceptance of the system.

Bayesian Belief Networks (BBN) is a methodology to combine such evidences in a systematic manner, based on Bayes probability methodology. The objective is to show the link between basic information and the confidence one can have in a system. Although this application of BBN is still rather premature, and has not yet been applied in real safety cases, there is a certain research activity on this topic, and this will be presented in section 5.

2. Halden Reactor Project Activities on Software V&V.

As stated above, there are three complementary principles which should be followed to obtain dependable software. The first principle, fault avoidance, can be obtained through good software engineering and quality assurance. However, to obtain extra high integrity the use of *Formal software development methods* has been advocated. These are methods which provide a mathematically based framework within

which specification, development and verification of software systems can be done in a systematic and precise way. The use of formal specification and design makes it possible to discover many errors which might otherwise very easily be overlooked.

Following the principles behind formal software development, the Halden Project has developed a methodology based on algebraic specification and a proof tool, the *HRP Prover*. One of the virtues of this methodology is that the same language, tool and proof techniques can be used both in specification and design, even down to a "concrete" specification which can be automatically translated into code. In the specification phase, the theorem prover is used to verify and validate the specification, while in the design phase the same tool is used to verify the correctness of the design steps.

There is, at the market, a variety of commercial tools supporting formal development methods. An ongoing activity at HRP is to investigate the applicability of such tools. Based on a comparative review of a large number of systems four were selected for a closer evaluation. Of these, one system has been selected for an experimental investigation, by application on a subsystem in a new experimental control room (HAMMLAB 2000) which is being developed at HRP.

The methods for fault detection can be divided into two main categories: *Static analysis* and *testing*. Static analysis is defined as the process of evaluating a computer program without executing it. The main objective of the static analysis is to check that the final program conforms with the specification or design documents, but it is also used to reveal defects in the program. These defects may be direct faults, but they may also be violation of coding standards.

The Halden Project has in the SOSAT (SOftware Safety Tools) project, a joint project with TüV-Nord and GRS/ISTec in Germany developed a set of tools which can assist in the safety analysis of computer programs /DaS90/ It is based on a memory dump of the host computer, i.e. the computer where the analysed program is implemented. One reason for basing the analysis on the machine code representation of the program is to reveal potential faults introduced through the compiler and other programming aids. A disassembler extracts the part of the memory content which constitutes the program(s) and translates it into a processor independent language, which is the basis for the further analysis.

An ongoing activity at HRP on software analysis is, in co-operation with GRS/ISTec, to develop tools which check high level language programs against a variety of coding standards and guidelines.

Testing a program means to execute it with selected test data to demonstrate that it performs its task correctly. Ideally the test data should be selected so that all potentially residual faults should be revealed. The Halden Project have performed several investigations of testing methodologies (/Bis87/, /Dah91/). An ongoing activity at HRP on testing is an experimental evaluation of a method, the PIE (Propagation, Infection, Execution) method suggested by Dr. Jeff Voas /Voa92/.

The third principle, fault tolerance, can be obtained in different ways, e.g. through diversity and/or safety checks. A project on diverse software (PODS) was performed as a joint project between the Safety and Reliability Directorate (SRD), Central Electricity Research Laboratory (CERL), The Technical Research Centre (VTT) of Finland and HRP (/Bis86/, /DBB90/). The main objective of the project was to provide a measure of the relative merits of using diverse programs, as compared with any one of the programs replicated in all channels, in a 2-out-of-3 majority voting protection system. To achieve the objective, an experiment was mounted which simulated a normal software development process to produce three diverse programs to the same requirement. The requirement was for a reactor over-power protection system. After careful independent development and testing the three programs were tested back-to-back against each other to locate residual faults. The three development teams were allowed to discuss problems with the

requirement specifiers, but not with each other. All phases of the project were carefully documented for subsequent analysis.

3. Application of Guidelines in the licensing of REPAC.

As stated above, a guideline for reviewing and assessing safety critical software in nuclear power plants has been written for the Swedish Nuclear Power Inspectorate (SKI). This section describes some experience gained from application of the Guidelines in the licensing of a computer based protection system (REPAC) in the Swedish nuclear power plant Ringhals.

The Guidelines can conceptually be divided into following topics:

- Safety analysis
- Program development: specification, design and coding-
- Safety assessment

They are based on accepted standards and guidelines, in particular /IEC880/ and /EWICS/.

- Safety analysis.

An identification and analysis of all aspects with potential safety consequences should be made before one starts to develop, as well as to assess, a safety related system. This includes aspects which are of general nature with respect to safety, as well as aspects of the particular system which shall be implemented.

Questions which may be raised are

- Which hazards or accidents may occur?
- Are there some superior plant protection system, which acts as a last defence if the target system should fail?
- Is it possible to bring the plant into a safe state, or to a state of reduced risk, in case of a hazard situation?
- Are there any general safety principles which is applicable to the system?

REPAC is a one-to-one exchange of old analogue equipment in an existing plant. All information about the plant was therefore thoroughly documented in advance, including a safety analysis. A set of initiating events lead to reactor trip or other protective functions by a set of activated protection channels. A substantial part of the initiating events which activates the REPAC system, in particular the most critical ones, is also activating protective functions in a protection system based on neutron flux measurements, using analog technique. An 'umbrella' is thus given by signals from the analogue equipment as back-up for the REPAC system. A shut down will bring the plant in a safe state if a hazardous failure in the protection system occurs. The REPAC system is classified in the highest safety class (1E).

- The specification.

The functional specification is a document stating what the target system is intended to do, and what it actually does if it contains no faults. However, even if the system does not contain any faults, it is not necessarily correct nor safe. The system may be incorrect if the functional specification is faulty. It may be based on a wrong process model, it may contain internal inconsistencies or ambiguities, or it may contain direct (clerical) faults. Even if the specification is correct, in the sense that it correctly expresses the intention of the specifier, it needs not be safe. It may contain inadvertent side effects which may jeopardise safety. A thorough analysis of the specification is thus necessary for the safety assessment.

As REPAC is a one-to-one exchange of an existing safety critical system, the definition of this system also represents the specification of the new. It is made in a combination of graphical description, mathematical formula and text. The functions and interface to the plant is the same The safety analysis of the existing system is also valid for REPAC

A particular problem to consider is whether a digital and a analog system based on the same specification are functionally equal.

- Design and Coding

The REPAC system is developed in what can be called a *configurable software system.* This means that the program is build up by an application program and a set of standard modules. The application program usually have a form similar to the graphical representation of a corresponding analog system, whereas the software modules are commercial off the shelf software (COTS) which are used in a broad application area, and not particularly for nuclear or safety relevant applications.

The whole program consists fairly simple modules, like e.g. limit checks, lead-lag filters etc. This would have been easy to make in a general language, but the diagrammatic form is closer to what an engineer is accustomed to, so the use of configurable software is probably more comprehensible to them. The standard software modules are often the same as a corresponding hardware component in traditional systems.

It is typical for configurable systems that, in order to limit the number of standard modules, there are various options connected to each of them. A number of input parameters is typically used to characterise the different modes of operations. F.ex. a simple limit checker module uses 14 input parameters to identify the different options.

- Programming related recommendations.

The Guidelines states that the use of high level languages is recommendable, but that low level languages are acceptable if properly verified. However, the specific language in which REPAC is coded can neither be considered high nor low level.

The Guidelines also recommend that the coding is made according to a generally accepted standard or guideline (e.g. /IEC880/) Encouragement should be given to provide

- easily understandable code
- use of strict naming conventions for variables
- modularity (small modules appreciated)
- initiation of all variables
- sufficient program comments

Tricky and fancy programming, code compression etc. should be avoided.

However, many of these recommendations are made with general programming languages in mind, and are difficult to follow for the particular programming style used in the configurable software system. E.g.

- Naming convention is impossible
- Initiation of variables are implicitly set to 0.
- In-line code commenting is impossible

However, fancy programming is impossible in this programming system, and modularity is natural

4. Safety Assessment Based on Multiple Evidences.

The approval of a programmable safety critical system, in particular one which is based on COTS, is based on a combination of disparate sources of information. This acceptance process is illustrated in Fig.1 in the form of an 'influence net', i.e. a directed graph where each node represents an aspect in the total assessment process. The top nodes in the graph (rectangles) represent the basic information sources which are used in the acceptance process. This information is penetrated through the net down to the bottom node which represents the final acceptance of the system. The latter is mainly influenced by the safety assessment of the system, although there may also be other acceptance criteria. The safety assessment is influenced by a reliability assessment of the of the system, as well as by an evaluation of whether a failure in the system will jeopardise safety. This can be achieved through a hazard analysis of potential risks to plant and environment. Safety defences (both against hardware and software failures) may be implemented as an additional barrier against consequences of failures. A commonly used principle in this respect is diversity, i.e. the same functional goal is obtained through different means. The highest degree of diversity can be obtained if the same functional goal can be reached with completely different functions. This is essential to reach the safety goals of a safety critical system. For example, the REPAC protection system is divided into a number of protection channels which each performs a protective function, as e.g. a reactor trip, triggered by an initiating event, like e.g. loss of feedwater. The system is designed so that each initiating event is handled by at least two protection channels. As each protection channel is performed by a distinct processor one has obtained a complete functional diversity.

4.1 Information About Producer and Development Process.

The avoidance of faults in the program is clearly related to the quality of the development process of the software system. A lousy made program can of course be correct, but a well documented production procedure, in accordance with accepted standards, enhances the assessor's confidence in the reliability of the product. This confidence is also enhanced if the producer can document a history of producing high quality products.

To obtain a sufficiently high confidence in the quality, one should require that all parties involved in the development follow a quality assurance policy based on well-known standards for safety related systems (e.g. /IEC 880/). This may, however, be difficult when the COTS software modules are concerned, since they are often delivered without appropriate information on the development process as well as on the final product itself. It may thus be difficult to assess whether the system has been developed according to the standards required for safety critical software. The experience from the REPAC project was that the system used was a fairly old system, which were developed before the presently available standards for safety related software were established. The development procedure was, however, documented, and a retrospective comparison of this procedure with several standards was documented, although the conformance with IEC-880, which is very detailed, is hard to obtain in a retrospective analysis.

4.2 Information About the Programs.

Detailed information about the software is needed to assess the reliability of its application. One aspect is to identify structural properties of the program which makes it vulnerable to programming errors. Complexity is obviously one of these, i.e. the more complex a module is, the more likely it is that it contains coding faults. A main source of information about complexity can be gained through an analysis of the program listing. However, for COTS software such listings are in general not available. It may

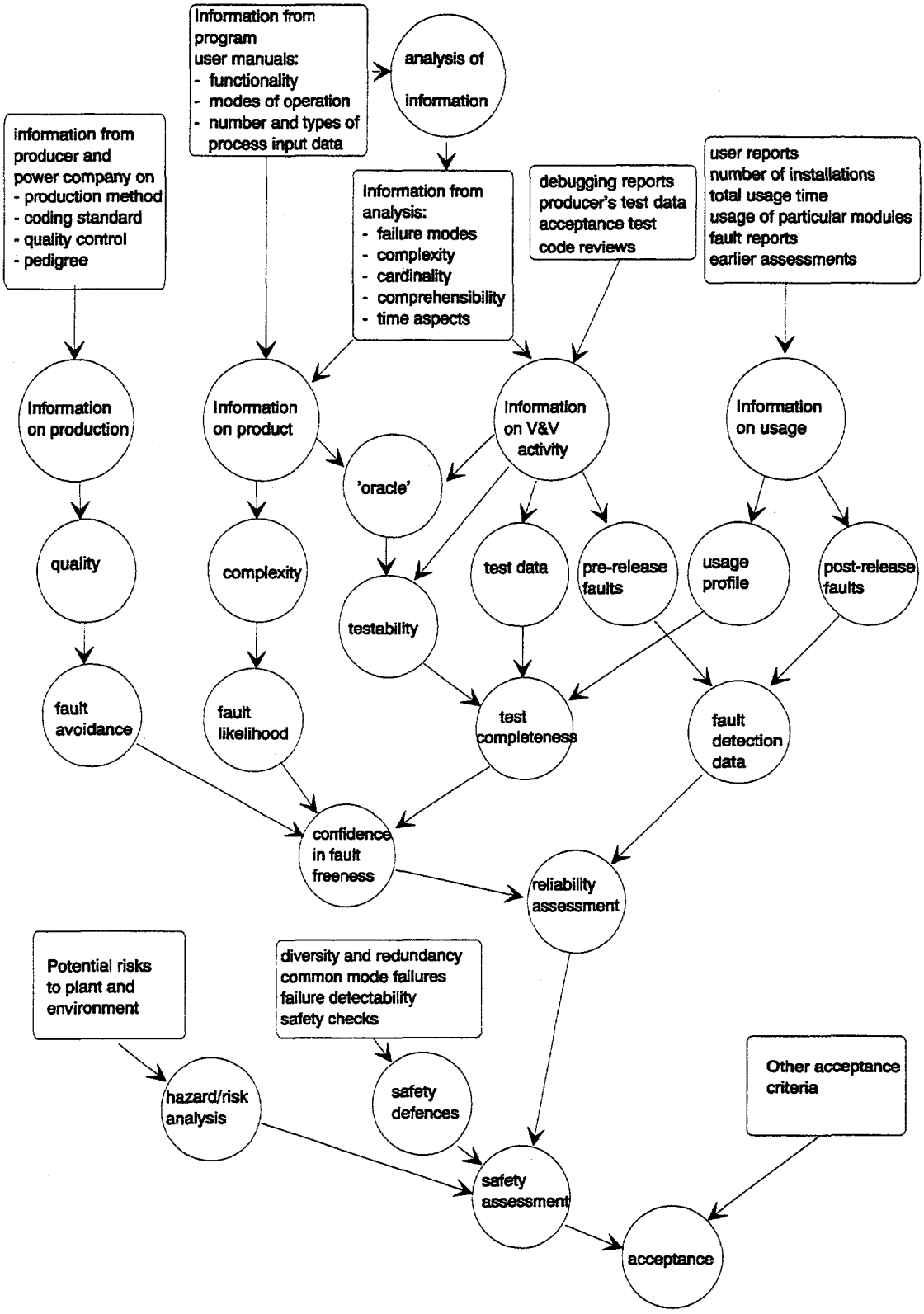

Fig. 1 Influence graph of a safety assessment and acceptance process.

be difficult to assess the complexity without this, but an indication on the complexity of the module can be seen from the complexity of the specification. A well structured and comprehensible explanation of the use of the module is also an indication of a well structured program.

A characteristic for the COTS modules in a configurable software system is that they often have several modes of operation. A large number of operation modes will increase the complexity of the module as a whole. However, in an actual application only one operation mode is used, so one could ask whether only the complexity of the used mode is relevant. This depends upon how the selection of operation modes are coded in the module. Since one does not know the code it is difficult to know how it is done, but information about the producer's coding standard could be used in this respect.

A third aspect is the inherent complexity of the actual function itself. It is intuitively obvious that an adaptive controller is more complex to make, and therefore more error prone, than an AND gate, to take two extremes. One way to measure the inherent complexity of a module where one does not have access to the source code is to write it in a formal way, either as a program in high level language, or as a formal specification, and define a metric to measure the complexity.

Another way to analyse COTS modules is to apply FMECA (Failure Mode, Effect and Criticality Analysis) on them. An IEC standard for FMEA and FMECA is given in /IEC812/. The basis for an FMECA analysis is a functional description of the analysed system, in terms of its components. For each of the components in the system all potential modes of failure are identified. Then, for each failure mode one makes an evaluation with respect to:

- the *failure mode*, i.e. how the failure manifest itself.
- the *failure cause*, which includes both immediate causes and more basic causes, as e.g. design errors.
- the *failure mechanism*, i.e. the mechanism which leads from the cause to the failure.
- the *failure effect*. One can here distinguish between *local effect*, which is the effect on the component in question and its immediate surroundings (e.g. failure mode: pump stop, effect: no flow), and the *end effects*, which are the effects the failure may have at the highest system level, i.e. on the plant and its environment.
- *failure detection*, i.e. the way the failure can be detected and the likelihood it will be detected.
- *failure probability*. This can be stated in qualitative terms (e.g. high, medium, low), or quantitative as probability of occurrence per time unit or per demand.
- *mean time to repair*.
- *failure criticality, i.e.* the consequences the failure may have on the safety at the plant or potential harm in the environment. One can also here distinguish between immediate consequences (e.g. radioactive release after a tube rupture), and more indirect consequences which are consequences of the end effects.

Traditionally FMECA has been considered for hardware components where failures occur randomly during operation, although design faults also are considered. As the components considered here are realised in software, only potential design (programming) errors which results in faults in the programs are taken into account in this connection. However, such faults can result in stochastic failures during program execution, due to randomness in the input data.

One problem in the application of FMECA to COTS modules is the lack of detailed information. In particular one needs a more or less detailed functional specification of each module. One available source of information can however be found in the set of user manuals. These contain descriptions of how each

module is working, and from this it should be possible to deduce some kind of functional specification. In addition, one has some knowledge about the general characteristics of programmable systems. Altogether this should make it possible to perform, at least partially, a FMECA on the COTS modules.

4.3 Information about V&V and testing.

A thorough V&V and testing activity, at the module level as well as on the program as a whole, will increase the confidence in the program, and thereby its reliability. Information about the V&V activities can be obtained from various sources, as debugging reports, factory acceptance tests, site acceptance tests etc. For COTS systems an important information source is test data compiled during the development of the system, and during modifications before new releases.

To generate test data for a relevant and sufficiently complete test, a fairly detailed knowledge about the tested system is necessary. In this connection one should distinguish between the testing of the COTS modules and of the application program. There are two types of data used by a COTS software module, viz. the configuration data, which decide the mode of operation, and the variable input data (process data, operator input etc.). If one should test a standard software module as such, a coverage of both configuration data and variable input data must be obtained. In an actual application, however, testing is only needed for the operation modes which are used, and only the variable input data need to be covered.

An additional simplification of the testing can be obtained by utilising the result from the FMECA and fault tree analysis. From these one can identify the critical failure modes of each software module, and concentrate the testing with respect to these.

To measure statement and path coverage for a test, one needs to know the program code in the software module. For a COTS module, however, the code is in general not available. An alternative is to make a coverage measure based on the specification, e.g. to measure the number of properties, or combinations of properties, which are checked by a certain test. If an oracle program has been made, an alternative is to instrument this with counters, and perform the coverage measurement on this.

During testing it is necessary to test the correctness of the output. If this is done manually, it is laborious and error prone. The use of an 'oracle' would simplify the testing procedure considerably. Based on the functional specification given in the user manual, it might be possible to make an executable specification, or a program with the same function, and use this as an oracle. Even if this program of course could be incorrect, it can be considered a diversely developed program. Any discrepancy between the software module and this program must therefore be analysed carefully.

A complementary activity to testing is static analysis. In general, static analysis is based on the code listing, which is not available for configurable software. A possibility, however, is to perform reversed engineering on the memory dump of the software module, e.g. with the use of the SOSAT tools /DaS90/. This can be used to identify undesired properties and potentially dangerous code (e.g. interrupts and undetermined loops).

The verification of the application program is similar to the verification of an ordinary program. However the application program in a configurable software system is in general much simpler than an ordinary program, and therefore also simpler to verify. If the configurable software program is based on a graphical depiction, this could also be utilised both for a static analysis, and to define a coverage metric (coverage of lines in the graph). Some configurable software systems are also equipped with the possibility for reversed engineering, in the way that it produces a graphical representation based on the final program, and this could then be manually checked against the graphical specification.

4.4 Information About Usage

'Proven design' is often used as an argument for high reliability by the producers of COTS system. This means that the system has been used by a wide range of users over a long period, with no, or few, reported faults. The idea behind this claim is that long user experience should reveal all inherent faults, if they exists. So if no faults have been reported over a long period, this should be a strong indication on error freeness. It is questionable, however, whether this argument is sufficient. A configurable software system has often a quite general purpose, and consists of many standard modules, each of which has many modes of operation. To claim general high reliability of the system based on user experience, it is necessary to show the experience with all modes of operation of all software modules. This requires information about all installations of the system.

Another aspect is the configurator, i.e. the program which is used to generate the application program and include the COTS modules. These are used only once per installation. To get a broad user experience with these programs it is necessary to have many installations. Information about the number of installations is therefore important for the reliability assessment of the configurator.

The number of versions of the COTS system which are released is also relevant information. A new version implies changes in the system, and changes may have influence on its reliability. It is therefore relevant to know which changes have been made, or at least where the changes are made. In an actual application one should know whether any changes have been made in the software modules which are used in the application.

4.5 Reliability Assessment.

Reliability is according to standard terminology defined in probabilistic terms as the probability of failure free operation of a system over a specified time period. This definition may be adequate for hardware systems, where it can be estimated on the basis of statistical failure data of the components of the system. For software, however, such an estimation method is conceptually more complicated. A simple estimate of the reliability could be based on a program test by dividing the number of failed tests with the number of executed tests. However, if a fault is revealed, the program would probably be corrected, and thus the reliability changed. And if no faults are found, such an estimate would not differentiate between no failures in 10 tests and no failures in a million tests.

There are, however, developed a variety of *reliability growth models*, which, based on the sequence of times between observed and repaired failures, calculate the reliability and current failure rate, and predict the time to next failure and required time to remove all faults. The general assumption of these models is that a single system is followed chronologically with recording of times to failure, and that the faults are corrected. This may be easy to achieve in the debugging and testing phase. However, the reliability figure obtained in this way estimates the failure probability if the real input profile is the same used in the testing. It is questionable, however, whether this gives a realistic estimate of the reliability in real applications, with a different input distribution.

A more realistic estimate is obtained if the data are collected during real operation. This could be obtained from user experience and failure reports on standard software modules in the post release period. A problem is that it is difficult to identify the chronological order of failures from such reports. Different faults are found by different users, who report them back to the producers. The same faults may also be found by different users. The producers will then usually collect the error reports and correct all the reported faults in the next program release, whereas the users will continue to use the faulty program, and

possibly find new faults, until they get a new program release. None of the models take into account this realistic scenario.

Another problem with these methods is that they do not distinguish between different types of faults, e.g. between real faults and more cosmetic faults. It is of course a possibility to only take into account a particular class of faults. In this case, however, one may easily get an insignificant number of faults, in particular when one only takes into account critical faults. An alternative way to measure the reliability of a program with respect to a certain class of faults is to perform the reliability estimation with all types of faults and multiply this with the ratio between the number of faults in the particular class and the total number of faults.

A computer program implemented in a safety critical system contains presumably no known faults. There is, however, a possibility that it contain unknown faults, and an alternative reliability measure is the confidence in fault freeness of the program, or more generally in the upper limit of the 'bug-size'. Such a measure can be made on statistical basis from data obtained during testing of the complete program, as well as of the different modules. One set of data can be gained through a controlled testing combined with a coverage measure. The latter requires a fairly detailed knowledge about the program structure, which is not always available when COTS modules are used. For these, however, there may be an additional large set of 'test' data obtained from information about the usage of the system (see below).

5. Bayesian Belief Networks

A more qualitative type of reliability measure is expressed as a subjective judgement, as a 'belief' in fault freeness. A methodology which has been proposed is to use Bayesian Belief Networks (BBN) and engineering judgement to combine evidences from different information sources for a quantitative assessment of this belief.

A literature survey on this methodology showed that it has mainly been developed and applied in the AI society. More recently, however, it has been proposed to apply it to software safely assessment (/NeF96/, /DMS97/). Ongoing work on this is performed in two ESPRIT projects: SERENE and DeVa, and at the Centre for Software Reliability at City University in London. There are, however, no description of, or reference to, any application of BBNs in real (or realistic) safety cases. It thus seems that this methodology is at an early stage, but that there is a clear tendency to develop it further.

The objective of using BBNs in software safety assessment is to show the link between basic information and the confidence one can have in a system. A BBN is a connected and directed graph, consisting of a set of nodes and a set of directed links between them. Associated to each node is a variable which can be in a set of states, and a probability density function over this states which expresses the probability (or belief, confidence etc.) that the variable is in a particular state. This probability depends on the status of the variables represented by the start nodes at the incoming edges to the variable (the parent nodes). The edges represents conditional probabilities The name Bayesian is used for the network, because these conditional probabilities is used to update the probability function based on the probability functions of the parent nodes, using Bayes theorem.

The nodes and associated variables can be classified into three groups:

1. *Target nodes* - the node(s) for which the objective of the network is to make an assessment about. This assessment is expressed with a quantifiable *target variable*. Typical examples of such nodes are "No faults in a program" or "No failure on demand for a trip"

2. *Observable nodes* - nodes which can be directly observed. Some examples are: "No failures during N test", "No reported failures during previous usage of modules", "All quality requirements are fulfilled" etc. The associated *observable variable* should be or measurable or at least quantifiable.
3. *Intermediate nodes* - nodes for which one have limited information, or only "beliefs". The associated variables are the *hidden variables*. Typical hidden variables are development quality, producer's pedigree etc.

The application of BBNs in safety assessment of a system consists of three tasks:

- construction of the BBN
- assigning probabilities to nodes and edges
- computations with BBNs

The construction of the BBN is made gradually, by combining the target nodes with the observable nodes and the intermediate nodes. The aim is to combine all available relevant information into the net. A way to do it is to start from a target node and draw edges to nodes influencing this. Then from these nodes draw edges to new nodes etc. In this way one will gradually build up a large BBN. This is similar to construct a fault tree from a critical top event. And as for fault trees, there is a problem when to stop, i.e. how much details does one want to have in the BBN. That is often a more iterative procedure. I.e. one starts with constructing a (simple) BBN. Then one tries to assign probabilities and make computations. Through this process one may identify conditions which are assumptions for the probability estimates, and information which can be used to confirm these assumptions.

The next task is to assign probability density functions (pdf) to the nodes and conditional probabilities to the edges. The pdfs to the target nodes and intermediate nodes are considered prior distributions. For the observable nodes we would expect exact values, and therefore no pdf. However, for some observables the quantification is somewhat fuzzy, and so a pdf might also be the appropriate representation of these. Both the prior distributions and the conditional probabilities must to a large degree be based on expert judgement and experience.

An alternative to using continuous pdfs and conditional probabilities is to discretise them. The variables associated with the node can be in a finite number of states with a probability associated with each state. The conditional probabilities associated with the edges are expressed as correlation matrices between the states of the variables associated with the start node respectively the end node of each edge. One advantage of this method is for expert judgement based assignment of probabilities to variables which are not by nature numeric. If f.ex. a node variable associated with a quality attribute could be represented by the four states 'bad', 'acceptable', 'good' and 'excellent'. And if the BBN contained an edge between the nodes 'development method quality' and 'product quality', the edge would be assigned a matrix representing the influence the quality of the development method has on the quality of the final product.

To make computations with BBNs, even simple ones, using Bayes theorem on continuous pdfs is actually very complicated, in particular to compute backwards on the edges,. The use of simplification methods and tools are therefore necessary for computations of a realistic BBN. An advantage of the use of variable with a finite (not too large) set of states is that this simplifies the computation. A reference to computational methods and associated tools is /Jen93/ with the associated tool HUGIN /AJN93/.

6. Conclusions.

The objective of this paper has been to utilise the experience gained during the licensing process of a computer based protection system to formulate a framework for the assessment process. The licensed

system was implemented with a configurable software system, i.e. a program is build up by an application program and a set of COTS modules, and emphasis has been made on particular aspects related to the assessment of the COTS modules.

The framework is made in the form of an influence net, i.e. a directed graph where each node represents an aspect in the total assessment process. The top nodes in the graph represent the basic information sources which are used in the acceptance process, whereas the bottom node represents the final acceptance of the system. The paper discussed how the various sources of information about these modules can be utilised through the net.

One aspect which was particularly emphasised was the possibility to apply Bayesian Belief Networks computations as a support for a decision of approval or disapproval of a software based system with safety relevant application. This is a promising, although still immature, methodology to combine information from disparate evidences about the system into a reliability figure for the total system. This method could be particularly useful when a configurable software system is used, and information is collected both on the system itself and on the applied COTS modules. HRP has, together with ABB-Atom in Sweden and VTT in Finland, initiated a project (Reliability Assessment of Programmable Protection Systems, RAPPS) for an experimental investigation of this methodology by applying this on a realistic test case.

References

/AJN93/. S.H. Aldenryd, K.B. Jensen, L.B. Nielsen: 'Hugin Runtime for MS-Windows', Tool made by Hugin Expert a/s, Aalborg 1993.

/Bis86/ P. Bishop, D. Esp, M. Barnes, P. Humphreys, G. Dahll, J. Lahti: "PODS - The Project on Diverse Software." IEEE Transactions on Software Engineering, SE-12, no. 9 1986

/Bis87/ P. Bishop, D. Esp, F. Pullen, M. Barnes, P. Humphreys, G. Dahll, B. Bjarland, J. Lahti, H. Välisuo: "STEM - A Project on Software Test and Evaluation Methods" Paper presented at SARSS'87, Manchester 1987

/Dah91/ G. Dahll. "Software Safety Checks Using Stored Tested Paths." Proceedings from IFAC conference SAFECOPM'91, Trondheim Oct. 1991

/DaS90/ G.Dahll and J.E. Sjøberg: "SOSAT - a Set of Tools for Software Safety Assessment" Paper presented at Second European Conference on Software Quality Assurance, Oslo 1990.

/DBB90/ G. Dahll M. Barnes, P. Bishop: "Software Diversity: way to Enhance Safety." Information and Software Technology, vol. 32 no. 10, 1990.

/DMS97/ Delic K, Mazzanti M. and Strigini L.: "Formalising Engineering Judgement on Software Dependability via Belief Networks". Paper submitted to DCCA'97. Garmisch-Partenkirchen, Germany March 5-7, 1997

/EWICS/ Dependability of Critical Computer Systems", vol 1 (1988) and vol 2 (1989) edited by F. Redmill, vol. 3 (1990) edited by P. Bishop. Elsevier Applied Science.

/IEC812/ "Analysis Techniques for Systems Reliability - Procedures for Failure Mode and Effects Analysis (FMEA)", IEC publication 812, 1985.

/IEC880/ "Software for computers in the application of industrial safety related systems." IEC-publication 880, 1986.

/Jen93/. Finn Jensen: 'Introduction to Bayesian networks', Hugin Expert a/s, Aalborg 1993.

/NLF96/ Neil M., Littlewod B.and Fenton N.: "Applying Bayesian Belief Networks to Systems Dependability Assessment" in Proceedings of the Fourth Safety-Critical Systems Symposium, Leeds, U.K., 6-8 February 1996, pp. 71-94. Published by Springer-Verlag.

/Voa92/ J.M. Voas: "PIE: A Dynamic Failure-Based Technique," IEEE Trans. Software Eng., 18 (8), 717-727, 1992

Safety-Critical Digital Systems

Paul J. Perrone and Barry W. Johnson

Center for Semicustom Integrated Systems
Department of Electrical Engineering
University of Virginia
Charlottesville, Virginia 22903-2442

Abstract

The use of computers in systems which have a direct or indirect effect on human, environmental, and equipment safety is prevalent. This paper presents an overview of the problems encountered by those designing safety-critical systems along with the fundamental definitions and concepts employed by their design. A survey of such designs is also presented along with a generic safety-critical system design model. Finally, a taxonomy of safety-critical system designs is presented which classifies the known design solutions. It is the authors' hope that this information will aid current and future designers of safety-critical systems to understand their design choices and to quickly assemble candidate solutions for their particular problem.

1. Introduction

It is a common, modern fact that computers have been and are assuming more and more control of physical world functions which affect the safety of our lives. The informational universe and the physical universe have collided. Be it indirect (e.g., computers control power plants which deliver energy to hospitals and subsequently consumed by life-critical respirators) or direct (e.g., computers control life-critical respirators), the control that computers are consigned over life-critical systems is ubiquitous. Broadly stated, computers are given powers to control and protect the physical world in ways which are critical to human safety. Furthermore, computers are also given powers to control and protect the environment and valuable equipment from hazardous situations.

This paper describes the problems encountered by those involved in the development of a safety-critical system. The context in which a system operates that makes it "safety-critical" and the safety assurance lifecycle are both described here. Fundamental definitions and concepts employed by those involved with the safety assurance lifecycle are also described. A survey of safety-critical system designs is presented and used to form the basis of a generic model for safety-critical system designs. Finally, a taxonomy of safety-critical system designs is presented which classifies the known design solutions.

2. The Safety-critical system problem

Safety-critical systems (Figure 1) are systems whose input-to-output behavior monitors and controls some external process which has direct or indirect control over human or economic safety. The external process referred to herewithin describes the combination of human operator(s) and a controlled physical system (the plant) wielding the ability to cause loss. Loss typically involves death, injury, financial damage, or environmental damage. The outputs from a safety-critical system thus have an effect on the state of the external process which in turn has a direct or indirect effect on the safety of human beings, other biological beings, an economic system, or an environmental system. The outputs can directly control plant actuators or devices used by human operators to convey safety-critical information to the senses (visual displays, audible alarms, or stored information to be retrieved). The inputs from this external process to the safety-critical system can come directly or indirectly from the plant sensors or in the form of operator commands.

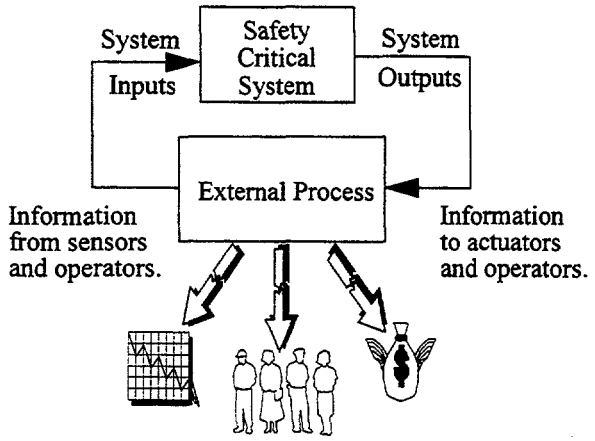

Figure 1: Safety-critical system context

The entering of human operators into the external process of the control loop thus adds some level of indirect control over safety. For example, a locomotive computer may be designed to assume that operator information regarding the state of a locomotive (such as its current movement authority) is correct and base control calculations on this information. While the safety of the onboard computer may be demonstrable, the overall safety of the system is dependent on this information's completeness and correctness. Additional measures may be necessary to account for any unsafe scenarios that could result from this particular system design.

Furthermore, sub-systems within the safety-critical system which do not directly control plant actuators or provide information to an operator may interact with other sub-systems which can affect the safety of the external process. Thus, when considering the safety-critical monitoring and control of a safety-critical process, one must consider the safety-critical system as a whole and the operator-machine interface to this system. Interfaces between these subsystems must be examined in detail and assumptions made about these interfaces should be made explicit. Leveson [1] discusses the problems of considering the

man-machine interface and safety as a systems problem in more depth.

When examining Figure 1 we can see that there are three primary system components and relations that exist outside of the external process that need to be considered by the designers of a safety-critical system. These are the system inputs, the system outputs, and the safety-critical system itself. The safety-critical system designer is concerned with three corresponding high-level issues:

- The correct and complete monitoring of all external processes.
- The correct and complete control and protection of all external processes.
- The correct and complete input-to-output behavior of the safety-critical system.

The actual extent to which a particular development process concerns itself with these issues varies greatly. These issues persist throughput the entire lifecycle of the safety-critical system development, operational, and post-development process and filter down from high-level issues to lower-level issues. The lifecycle involving the resolution of these safety-critical system issues is the safety assurance lifecycle. Safety assurance may be defined as the set of qualitative and quantitative measures taken to assure the safety of a system. The safety assurance lifecycle is depicted in Figure 2. Figure 2 depicts the fact that safety assurance processes must attempt to verify (prove correctness) and validate (prove completeness) a safety-critical system throughout its life-cycle.

The *a priori* phase (sometimes referred to herewithin as the "offline" phase) concerns itself with three primary sub-phases: the concept formation phase, the design phase, and the test, integration, production, and deployment phase. The concept formation phase concerns itself with safety planning, safety concept development, and domain concept development. Safety planning involves the establishment of a safety organization and system safety plan. Some of the root causes of accidents are the result of a safety organization's limited authority or responsibility [1]. The roles, goals, and responsibilities of a safety organization within an organization responsible for any aspect of a safety assurance lifecycle must be clearly defined and to a certain extent verified and validated for their ultimate effects on safety. Safety planning also involves the establishment of a written formal system safety program plan.

Safety concept development involves the establishment of safety-related definitions and concepts, as well as the establishment of safety assurance concepts and assumptions. Typical safety-related concepts involve system, information, correctness, error, failure, hazard, accident, and checking models. Domain concept development involves the formation of concepts about a particular safety-critical problem domain and the hazards associated with the external process. Safety assurance must be provided during these activities via verification and validation of concept assumptions to a confidence level considered acceptable.

The design phase involves the verification and validation of specifications, specification analyses, designs, and implementations of primary and redundant systems. Test, integration, production, and field deployment of a system must also be verified and validated to ensure that the required safety mechanisms have been incorporated into actual fielded systems.

Post-development *a posteriori* demonstration of safety and testing of safety features should be provided to verify the safety requirements of the system. Demonstration via inspection, mathematical analysis, modeling, or simulation are typical demonstration methodologies.

Finally, on-line *a posteriori* safety assurance verifies and validates a system during operation of safety-critical behaviors as well as during start-up and shutdown modes. Furthermore, assurance of system safety must also be provided during on-line test and maintenance, as well as during the switching between these non-standard modes and standard operational modes.

While realistic lifecycles iterate over these various stages, safety assurance strives for verification and validation of each stage before proceeding to the next stage. Again, the extent to which a particular organization or project provides verification and validation during each of the stages varies greatly. This paper will consider some of the design products from the different approaches and attempt to derive a unified, underlying safety-critical system design model. It is the desire of the authors that future safety-critical system designs can thus benefit from using

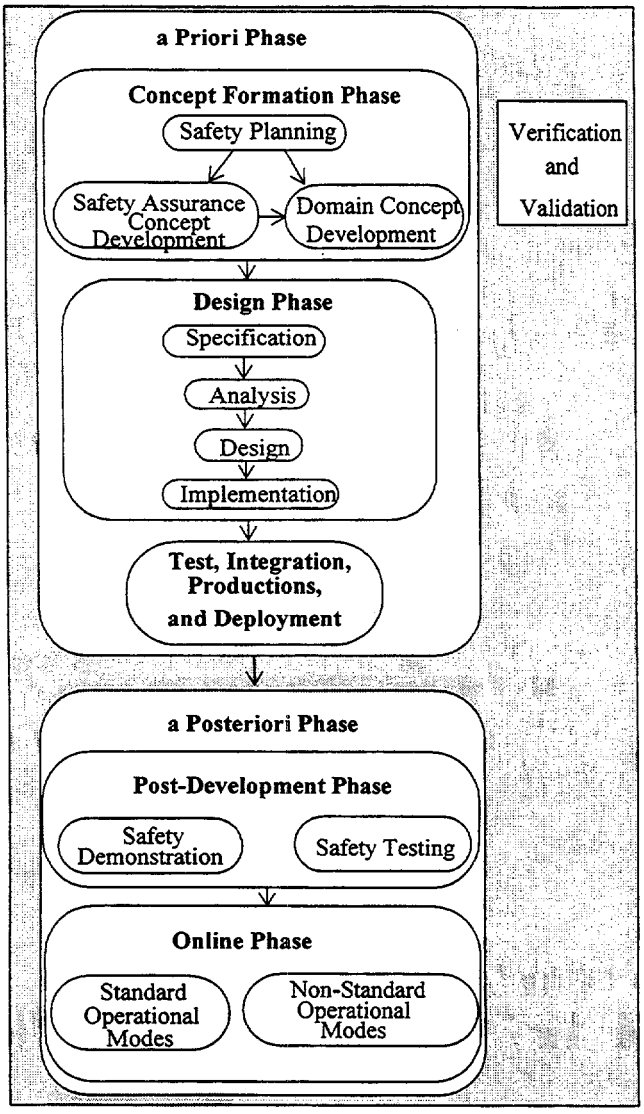

Figure 2: Safety assurance life-cycle

this generic model which attempts to summarize and envelope the efforts of those pioneering work in this area.

3. Conceptual foundations

The various approaches to safety assurance considered in establishing the generic safety assurance model by this paper employ a base set of concepts from system theory, systems engineering, and control theory as well as a set of their own definitions and rules. These concepts and definitions help define safety-critical systems and are presented in this section.

Two generic representations for any system are presented in this section. Many safety-critical system designs employ concepts from control and logic theory when describing a safety-critical methodology. Other designs employ concepts from automata or systems theory, especially when describing and defining "fail-safety" in sequential machines.

Many systems which are safety-critical will involve the control of processes capable of exerting energy on their environment which could cause injury or death to human beings. These systems may thus be classified as control systems. A common way to represent a digital control system is shown in Figure 3 (modified from [3]). Direct inputs from the plant (process under control) may need to be converted using analog-to-digital (A/D) conversion before being processed by the digital controller. Similarly, the system outputs may need to be converted using digital-to-analog (D/A) conversion before being submitted to the plant. Some system outputs may be fed back directly to the digital controller. These fedback inputs and the digitally coded inputs from other systems may act as control commands to help stabilize or keep the control algorithm in check. The digital code inputs may also be commands from a user, such as altitude control in an avionics application, or maximum allowable velocity in a train control application.

There are a wide variety of applications to which control theory has been applied. The controlled processes may be chemical processing plants, robotic manipulators, nuclear reactors, lighting, ground transport, actuators on airplanes, medical devices, or other examples. Some parameters are associated with the controlled process which model the behavior of the plant under exertion of external forces. These control process parameters are incorporated within the control algorithm running on the digital computer as the model-based portion of the system controller. The servo portion of the system controller is used to modify the behavior of the plant in a desired fashion. The digital computer running the control algorithms is typically a special-purpose microcontroller, a more general-purpose microprocessor, or a digital signal processor.

Another way to represent systems comes from the discipline of automata theory. Automata theory attempts to describe the behavior of information systems via mathematical models. These models can also be used by designers of safety-critical systems to analyze the behavior of a system under the influence of errors, and to analyze how these errors might produce unsafe outputs in a system. The system models from automata theory are also referred to as: sequential machines, finite state automaton, or finite state machines.

A system can be defined as an entity comprised of a related set of components. Any system can be mathematically represented

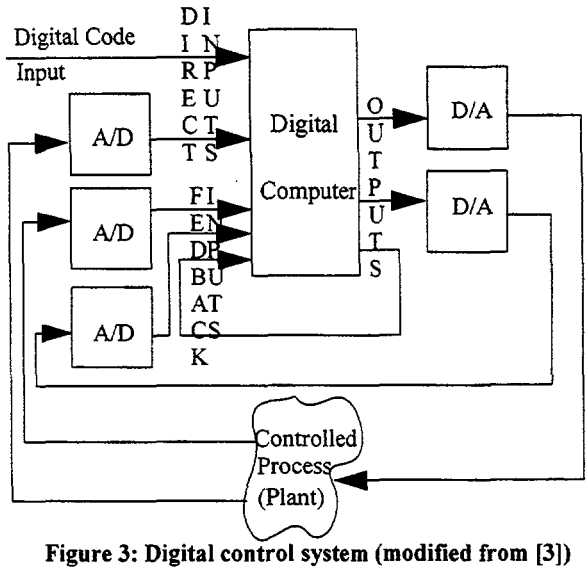

Figure 3: Digital control system (modified from [3])

as an automaton M(X, Q, Z, S, O) [4], [5], [6], [7]. As shown in Figure 4: X = set of system input symbols, Q = set of system states, Z = set of system output symbols, S = system state transition function defined as the relation {S: X x Q --> Q}, and O = system output function {O: X x Q --> Z}.

There have been a wide range of demands from various safety-critical applications that industry and academia have attempted to address. Efforts to fulfill these demands from those in industry have provided us with a very large set of definitions, concepts, and design rules. Some representatives from industry and academia have attempted to formulate a popular consensus of these terms and practices as derived from safety-critical applications. Others in academia have attempted to generate more formal definitions and concepts which may extend correctness and completeness verification and validation techniques to applications outside the typical safety-critical realm. The remainder of this section will discuss the consensus of definitions, concepts, and design rules derived from pre-existing safety-critical applications, and the more formal approach from certain academic circles.

Safety-critical applications typically attempt to protect people, the controlled process, or the environment from hazards

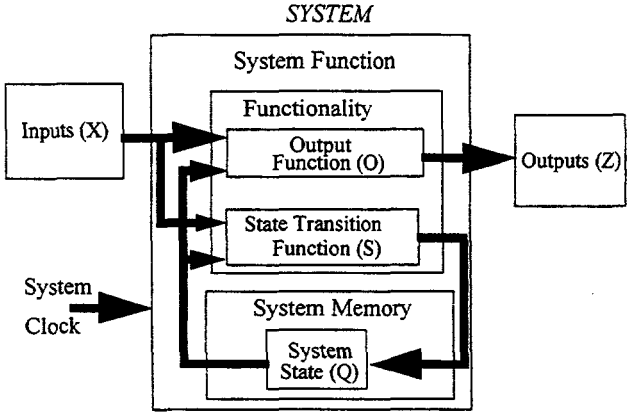

Figure 4: Generic system model

that inevitably lead to accidents. These hazards are eliminated or controlled by the safety-critical control behaviors. One sub-class of the control behaviors which are implemented on computers in a safety-critical application may be in the form of "interlocking" or "safety-enforcement" equations. Many interlocking equations use Boolean expressions to ensure that an output to the plant will not assume unsafe values. For example, in the railway switching and signalling application shown in Figure 3.3, a light on track segment B which signals whether or not a train on segment B can enter track segment A is controlled by the following algorithm:

IF (TRACK A IS UNOCCUPIED AND TRACK B IS OCCUPIED) THEN (SIGNAL GREEN)

The default (safe) condition is a red light. Thus, if there is a train on segment A, or if there is no train on either track, the light will be red.

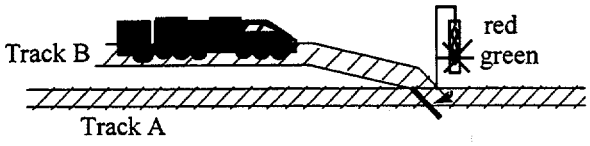

Figure 5: A simple control algorithm example

McCarthy [8] provides the following definitions in an attempt to summarize industry's thoughts on computer control and safety:

- **Accidents** - An undesired release of energy causing injury or loss (human).
- **Risk** - The quantitative measure of safety. Accounts for both frequency and severity of accidents.
- **Safe System** - A machine posing an acceptable risk of injury or loss (of human life) in use by society.
- **Acceptable Risk** - A risk level of one in a million chance of fatality per hour or unit of participation is amazingly recurrent in risk research, and represents a good "rule of thumb" as to what risk level people will voluntarily accept if the risk is of their election.

McCarthy's definition of safety-critical systems limits the risk of injury or loss to that related to humans. Not all those wanting their systems to fail in a safe manner, however, are wanting to protect just humans. This added demand is evident in Magison's [9] definition of safety in a system as "an acceptably low risk that a system will injure workers, destroy the plant, or function in some other socially, economically, or legally unacceptable way."

Others have kept their definitions of safety-critical systems more generic and somewhat loosely defined. Gruhn [10] defines safety systems as those designed to:

- Respond to conditions of the plant which are hazardous or which could eventually become hazardous.
- Generate correct outputs proactive to prospective hazardous outputs.

The United States Department of Defense MIL-STD-882C [18] provides perhaps some of the most encompassing definitions related to safety-critical systems:

- **Mishap** - An unplanned event or series of events resulting in death, injury, occupational illness, or damage to or loss of equipment or property, or damage to the environment.
- **Hazard** - A condition that is prerequisite for a mishap.
- **Risk** - An expression of the possibility/impact of a mishap in terms of hazard severity and hazard probability.
- **Safety** - Freedom from those conditions that can cause death, injury, occupational illness, or damage to or loss of equipment or property, or damage to the environment.
- **Safety-Critical** - A term applied to a condition, event, operation, process or item of whose proper recognition, control, performance or tolerance is essential to safe system operation or use.

In some safety-critical applications, the control algorithm is subdivided according to criticality of control. Levels of hazard severity dictate appropriate methods to implement safety features at these levels. Murphy and Humphrey [11] categorize the control algorithm for a nuclear power plant into three sets: (1) the entire process control algorithm, (2) the interlock algorithm which is a subset of the entire process control algorithm, and (3) the hard-wired interlock algorithm which is a subset of the interlock algorithm. The hard-wired interlock algorithm is the most critical partition of the control algorithm controlling various alarms regarding safety levels of the plant. The interlock algorithm implements control of the outputs to the plant which are safety-critical. Each algorithm is implemented differently with the more critical functions implemented using more reliable methods.

Zodeh and Sikora [12] categorize the control algorithms for petroleum and chemical processing plants into regulatory, operator and interlock control. The regulatory control system keeps the process variables within a desired range. The operators take corrective control measures whenever alerted. The interlock control system is the fail-safe aspect of the entire control process which should fail the system safely.

Ghosh [13] points out that "safety interlocking systems in process control applications are frequently used as backup systems that are responsible for detecting unsafe failures and bringing the system to a safe state." These safety interlocking functions are frequently independent of the control algorithm actually controlling the process. Ghosh makes use of the definition of an interlocking system used by the National Fire Protection Association: "a device or group of devices that are arranged to sense an off-limit condition or improper sequence of events and to shut down the offending or related piece of equipment, or to prevent proceeding in an improper sequence in order to avoid a hazardous condition" [14].

Balls and Gruhn [15] point to four levels of activities contributing to safety in processing plants: (1) plant design; (2) process management and control; (3) emergency shutdown

(interlocking systems); and (4) fire and gas monitoring and control.

Moldoveneu [16] believes that safety in process control must be a systems approach: "All components must work together to have a truly safe environment." He argues that although a programmable logic controller (PLC) may detect an abnormal condition via its control algorithm, hazardous conditions within the plant actuators may still exist: "A common need is immediate and positive removal of the energy source from the prime motion actuator, typically a motor or piston." Moldoveneu makes the point that not only safety interlocks and stop switches are responsible for fail-safety, but that power controls such as contactors, actuators and motor starters are also important for safe control of the plant.

The definitions of safety-critical systems encountered imply that the process apparatus must enter a "safe" state in the event of a safety-critical component failure. The "safe" state of process apparatus must be the "fail-safe" position. Fail-safe implies that control of the output in the event of a safety-critical system component failure will render that output to the plant in a safe state.

Murphey and Humphrey [11] provide examples illustrating two different situations needed for safe control of outputs to a nuclear power plant. The output to a valve which allows small quantities of air into a low-pressure chamber containing the nuclear-reaction process must fail in the closed state in the event of a system component failure. Too much air allowed into the chamber will render the reaction process unstable and therefore unsafe. The output to a valve controlling the amount of cooling water allowed into various parts of the reactor to remove excess heat from the process must fail in the open state. If this valve were to fail in any other fashion, then not enough water would cool the reactor and excess heat might render the plant unsafe.

With the growth of sophisticated combinations of computer hardware and software components in safety-critical systems to implement safety-critical functions, academia [6], [17] has attempted to provide more formal and mathematical definitions of fail-safety in sequential machines.

Figure 4 depicted a generic representation of a sequential machine. The input code space is denoted as {X} and the output code space is denoted as {Z}. Let the output of a circuit under fault free operation given some $x \in X$ be denoted as z(x). Under the influence of some fault $f \in F$ (the set of all prescribed faults), denote this output as $z_f(x)$. Denote the set of safe outputs for the system as Z_s which may or may not be a subset of Z. Pradhan [6] defines a circuit to be fail-safe with respect to F if and only if: $\forall f \in F; \forall x \in X; z_f(x) = z(x)$ or $z_f(x) \in Z_s$

Note that this definition is extended here to apply to sequential machines in general (hardware/software) and not just sequential circuit hardware.

Pradhan goes on to describe a methodology for designing sequential circuits to be fail-safe. Safe-side outputs using the above definition are guaranteed with respect to a prescribed set of faults. The derivation of a prescribed set of faults for complex VLSI circuits is not an easy problem, however, and is often impossible.

A unified theme underlies all of the above definitions. This theme is cast into the following problem statement for those involved in the safety assurance lifecycle:

> ***Find qualitative and quantitative techniques for assuring that safety-critical computer hardware and software systems control hazards, do not induce hazards, and fail-safe in the event of detected errors that can lead to hazardous events which can cause accidents associated with the external process.***

Various parties are typically involved with determining what is "acceptable" and what is not. Acceptability may be measured in terms of quantifiable safety requirements, qualitative requirements, or assumptions made in using a particular technique. The end-user may be a company or organization employing the safety-critical product. Sometimes, society may be affected by the safety-critical product (e.g. nuclear power plant), and may or may not have a say in the level of risk acceptability. Often a government or industrial standards committee will be involved with determining acceptable risk levels as well.

4. Safety-critical system model and survey

This section presents a generic model and survey of safety-critical system designs. A scheme for classifying safety-critical hardware and software is first presented. A generic safety-critical system is then described in terms of its basic safety-critical components. A few of the basic component types are then described in more detail. These designs need only be employed for the safety-critical behaviors that the system exhibits. The determination of what behaviors are safety-critical and techniques for verifying and validating the specification of these behaviors (e.g. formal methods) is beyond the scope of this paper.

4.1. Hardware and software classifications

The hardware for the basic components of safety-critical systems have been designed using two general component types which can be categorized as either class I, or class II hardware [19]. There is also a third class of hardware which is defined as that which implements only non safety-critical functions.

Class I hardware has failure modes and characteristics which can be analyzed using standard Failure Modes and Effects Analysis (FMEA) techniques. FMEA must show that no single failure mode produces an unsafe condition, classify failure modes as revealing or non-revealing, and provide the confidence that the probability of unsafe failure is low enough to be acceptable. Typical class I hardware components include discrete components (transistors, resistors, four terminal capacitors), current threshold detectors, electro-mechanical relays, and discrete rate-decoding filters. Typically, there is no statistical measure of fail-safety associated with class I hardware. A circuit either passes or fails FMEA.

Class II hardware includes more complex circuits which are not directly analyzable using standard FMEA techniques, but are used to implement safety-critical functions. These may be processors, memories, address logic, or any integrated circuit within a safety-critical system implementing safety-critical functions. The failure modes within these components are very often infinite.

Software components may be categorized according to their effect on safety-critical functions. Some applications have required multiple categories of safety-critical software components, but in general software may be classified as safety-critical or non-safety-critical. Rutherford [19] defines vital (safety-critical) software as "software required for the implementation of a vital function. In addition, vital software is any software whose execution could affect the implementation of a vital function."

While different levels of safety for a component may be achieved within the safety-critical category, the safety-critical designs employed by all safety-critical levels are considered in the generic design model presented in this paper.

4.2. Safety-critical system components

The large-scale use of class I hardware in safety-critical system designs is often economically impractical. However, the use of safety-critical software and safety-critical class II hardware components in modern safety-critical systems requires additional measures to ensure system safety. On-line system checking mechanisms which check that the class II hardware or software is operating correctly are needed. A generic safety-critical system design model is depicted in Figure 6.

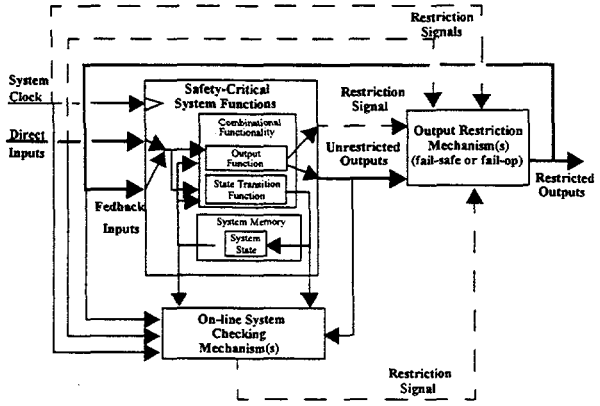

Figure 6: A generic safety-critical system

Here, only the safety-critical functions, inputs, and outputs of a system are shown. The safety-critical system functions are represented using the generic system models presented in Section 3. Inputs, safety-critical system functions, or outputs that are not implemented using class I hardware are checked during on-line system operation by the on-line system checking mechanisms. Inputs, safety-critical system functions, or outputs implemented using class I hardware need not be checked by an on-line checking mechanism and are not explicitly indicated here for simplicity of representation.

Safety-critical system outputs from software or class II hardware implemented components are considered unrestricted controlling outputs. An output restriction mechanism is usually employed to ensure that no unsafe output state will be delivered to the external process. A restriction signal from the on-line checking mechanisms will determine whether or not the unrestricted output will be permitted to be delivered to the external process. In the event of a detected error which could lead to a hazardous event (errors in the safety-critical behavioral processing), the system outputs will be restricted to a fail-safe state to assure safety.

Finally, restriction information from other parts of the system may be used to control the restriction mechanism(s). The frequency of a system clock may be considered vital to system operation and perhaps be used as a restriction signal. If the clock deviates from its specified frequency, for example, power to the outputs may be cut-off. An over-riding restriction command from an operator may also be communicated to the restriction mechanism(s) via a direct input channel. Also, the system itself may be responsible for computing a restriction signal. For example, in the event that some output from the system does not alternate according to some specified frequency such as an I/O cycle, the outputs may be required to go to their restricted state.

4.3. On-line checking mechanisms

Perhaps what differentiates various solutions to safety-critical systems the most is their methodologies for checking for faults or errors. Many of these solutions will employ a mixture of on-line checking techniques. In addition to the use of on-line checking mechanisms for achieving safety in various parts of the system, some safety-critical system solutions will also use class I hardware to implement parts of the system not easily checked with an on-line system checking technique.

Watchdog timers are used to indicate the failure of a system to adhere to a pre-determined timing paradigm. Watchdog timers guaranteeing safe time-out bounds must be reset on a repetitive basis based on the completion of some safety-critical function(s). These safe time-outs are used to indicate whether or not a safety-critical output is computed within a bounded time interval. Watchdog timers have been used to check the safe timing paradigms of control systems in applications such as the railway [21], [22], as well as in chemical and petroleum processing plant applications [12].

The outputs submitted to the external process from the system are sometimes fed back to the control system in the form of fedback inputs. These fedback inputs may be used in computation of the control algorithm or as part of a checking scheme known as command feedback or closed-loop feedback. Command feedback ensures that the outputs submitted to the external process from the system during a previous I/O cycle are either in the safe state or are what the control algorithm computed them to be.

A redundant hardware or software scheme may compare the previously computed outputs stored in the system with the actual submitted outputs. The "checking" of the fedback outputs may also be accomplished within the state equations representing the control algorithm. That is, the control algorithm may use the fedback outputs along with a read in or stored safe threshold to derive a compensation value which will drive the output to a safe state within a pre-determined time delay. This algorithm-based fault tolerant technique uses redundancy of software (extra equations) to implement closed-loop feedback.

While redundant hardware and software may be used to do the actual comparison of delivered information with fedback information, another redundant aspect of this methodology comes from the fact that a device within the system or some mechanism outside of the system receives some information and must feedback the delivered information. The redundancy is in this delivery/feedback mechanism in the form of information

redundancy. This mechanism is akin to a request/acknowledge process.

Hardware redundant schemes are perhaps the most popular methodology for on-line checking in safety-critical systems [23]. Dual processors for on-line checking compare the processing activity at the algorithmic or bus-level. These processors may be diverse or duplicated. Diverse implementations attempt to reduce the likelihood of common-mode failures between compared processes. However, duplicated implementations have the advantage of not requiring added design overhead and expertise required with diverse implementations. Also, validation of one process implementation will often be easier than for two different implementations. Memories, I/O ports, PLCs and other system components also may employ such redundant configurations.

Railcar control applications abroad [24] and by ITT SEL of Canada [23], subway applications such as in the Bay Area Rapid Transit (BART) District in the San Francisco Bay area [25], the Airport PeopleMover station controller at Walt Disney Productions in Burbank, CA [23] all use dual microprocessors as an on-line checking scheme. Railway switching and signalling applications are also popular users of dual processors such as the Indian Railway's FIRM architecture [26] and British Rail Research's dual processor modules [27]. Aircraft flight controls by Rockwell [23], chemical processing by DuPont [12], and the real-time classification of railroad track flaws [28] are all other examples of dual processing applications for checking a safety-critical system. Organizations within the process control industry also often use dual PLC configurations to check the processing of interlocking and control algorithms [29], [30], [31], [11], [32].

Triplicated and quadruple processing elements have been used to help mask errors from propagating to other parts of the system. Voting via triplicated inputs, processing elements, memories, and outputs all preclude the need for immediate fault detection, location, and configuration perhaps required by some systems. In cases where an immediate backup operator interface is required to be switched into the control loop in the event of a detected fault, a voting configuration will be able to account for possible human delay in taking control. Voting concepts have been used by Westinghouse in Pittsburgh, PA for railcar control using three processors [23], by British Rail Research [27] in Derby, England in the form of triplicated interlocking modules for solid-state interlocking, by Japanese National Railways [21] for railway switching and signalling, for nuclear reactor control [11] in the form of triplicated diverse modules, and by many processing control applications [30]. NASA's space shuttle flight controls are protected via a configuration of four similar processing devices and one diverse processor [23].

Hardware and information redundant checking at the circuit level allows for very small fault detection latencies. The VIPER microprocessor [30] is one example of a processing device specifically designed to be used in a safety-critical system and whose on-line detection capabilities lie within self-checking. Illegal operations, faulty ALU operations, and illegal addressing modes are all examples of faulty behaviors which are detected at the circuit level within the VIPER processor. Another safety-critical system for safe control of chemical and petroleum processes [12] employs circuit-level techniques to check ROMs on power-up using memory checksums.

On-line software diagnostics are used in many safety-critical systems as checking methodologies in addition to other schemes. Some applications, however, heavily rely on software diagnostics to assure global system safety. Examples of which are present in railway switching and signalling applications [27], [22], subway railcar control applications [25], and space system control applications [34]. These diagnostics may be in the form of data consistency checks, memory read, write and addressing tests, I/O port read and write tests, operation checks, etc.

Diverse or N-version programming techniques require that N versions of a particular safety-critical software component be coded, compiled, assembled and used to compare results generated from all N modules. This scheme is thought to help protect against software design errors. It is thought unlikely that different designers and compilers will make the same mistake in generating different software modules. Often, these different versions are implemented on different processors to further protect against common mode failures. Rockwell Collins, for example, has employed the concepts of diverse programming in their aerospace and astrospace applications [23].

Coding theory has provided some safety-critical system designers with yet another on-line checking option. The inputs to a system are encoded through some coding function. This coding function may be a checksum over the input bits, a cyclic redundancy code, a Hamming code, or some other function mapping a k-bit input to an m+k-bit output. Any initial data which reside within the system *a priori* may also be encoded using the same scheme (e.g. database information). Inputs and state variables are processed within the system using these coded formats for operands. The final outputs are considered safe only if the received output codewords are still valid. Corruptions within the system will produce invalid codewords according to some calculable probability as a function of the particular code chosen.

Rutherford [35], [36] uses coding concepts for a railway switching and signalling application. The inputs are encoded using a cyclic code. Operation inputs and results are compressed along with a precomputed seed in a linear feedback shift register (LFSR), and all final equation results are compressed along with another precomputed seed in a LFSR. The final output from this LFSR is some predetermined "signature" which is presumed to be uniquely generated with some probability only if there were no errors within the system.

The French company C.S.E.E. has also placed a coded processing approach to on-line system checking into operation in a train control system [37]. Here arithmetic as well as Boolean operands are encoded using a residue number coding scheme. Operation signatures are compressed as part of the codeword to assure that the predetermined correct operation was performed. Timestamps are also compressed into the codewords to ensure freshness of data throughout the system. A scheme of final signature generation similar to the previously mentioned technique is also used here to determine the probability that no error has occurred.

4.4. Output restriction mechanisms

The output restriction mechanism prevents unsafe outputs from entering the external process based on restriction information from the on-line system checking mechanisms employed, the

system clock, direct operator inputs, or from the system finite state machine itself. Restriction information from on-line checking mechanisms may be redundant outputs from redundant hardware or software, a signature from a scheme using coding theory, or a signal from a watchdog timer. The output restriction mechanism will use some *decision logic* to determine the *action* it should take based on the received restriction information.

How this *decision logic* "decides" depends on the restriction signal itself. The decision logic may simply vote on the received information in a triplicated hardware configuration. Outputs from dual redundant processors may be compared and action will be taken in the event of a disagreement. Any pattern deviating from a specified signature in a code-based scheme may warrant action. This signature may also be required to vary from cycle to cycle. A signal from a watchdog timer indicating failure will require action on the part of the output restriction mechanism as well.

The *action* taken by the restriction mechanism may be to: (1) cause the outputs to go to a predetermined safe state, (2) allow operator inputs to directly control the outputs, or (3) allow another operational device to take over control of that output. Turner [23] refers to these three respective action types as (1) fail-safe, (2) fail-passive, and (3) fail-operational.

In all cases, the output restriction mechanism is often the critical point for assuring safe control of the outputs. If this mechanism fails, then regardless of all measures taken elsewhere throughout the system, safe control of the outputs is in jeopardy. For this reason, output restriction mechanisms are often implemented using class I hardware whose failure modes are well known. Rutherford [36] discusses the use of an LFSR whose final signature after equation evaluation drives a relay which will sustain power to the output cards only if the correct signature is received. If power is removed, then the outputs fail to the safe state for this railway switching and signalling application. Correct operation in [21] is assured when two squarewaves out of phase by 90 degrees sustain power to its vital relay configuration.

5. Taxonomy of safety-critical designs

Section 4 presented a generic model of safety-critical system designs. The efficient implementation of class I hardware, the designs of on-line checking mechanisms, the designs of output restriction mechanisms, and the designs of safety-critical system functions for safety checkability are all features that fundamentally distinguish the various approaches to safety-critical system designs. Certain application design decisions can preclude the efficient and satisfactory design and implementation of online safety checking mechanisms. It can thus be very important to consider the ***design for safety checkability*** early on in the safety assurance lifecycle. This section further classifies specific online safety-critical system checking designs with a top-level design taxonomy. It is hoped that this top-level checking design taxonomy will aid the designers of safety-critical systems in identifying candidate checking approaches early in the design lifecycle.

Cost, flexibility, performance, and functionality enhancement goals have caused designers to use class II hardware and software computer components as a replacement for much of the expensive electro-mechanical and class I hardware components used in safety-critical systems. The use of class II hardware and software in the implementation of safety-critical functions and online checking mechanisms makes for a very difficult design problem due to the complexity of these functions in modern system designs.

The good news is that the on-line checking problem is not unique to safety-critical system designs. Most fault tolerance techniques must employ some concurrent detection scheme to assure other system requirements such as reliability, availability, or maintainability. Thus, we may look to on-line checking techniques developed for other fault-tolerance requirements as candidate solutions to be employed by an online safety-critical system checking design. With a suitable set of on-line checking mechanisms chosen to satisfy system requirements, particular output-restriction mechanism designs and the design of safety-critical system functions for safety checkability may follow.

On-line system checking mechanisms can be divided into two classes [39]: circuit-level techniques and system-level techniques. On-line system checking mechanisms are also sometimes referred to as concurrent error detection (CED) or implicit error detection techniques. Single error correcting and double error detecting Hamming codes for memories, data bus parity checking techniques, residue arithmetic codes for ALUs, and totally self-checking circuits are some examples of checking techniques at the circuit-level. N-version programming, duplication with comparison, voting, watchdog timing, and closed-loop feedback are all examples of system-level checking techniques. All techniques at both the circuit and system level use some redundant aspect of the system to check for faults or errors during on-line operation.

At the circuit-level, concepts of hardware, information and time redundant checking are often used to check a low-level system component such as a combinational function or memory element. Hardware redundant schemes use additional hardware in replicating or inverting some combinational or sequential function of the system at the logic level. These techniques include replication of multiple buses [21], replication of logic functions [32], replication of processors [26], [40], replication of memories [21], and self-checking circuits [41], [17]. Information redundant schemes add extra information to a symbol of information (i.e. user data) and use this added information to check that the originally unencoded symbol is correct. Information redundant schemes at the circuit-level include parity codes [42], m-of-n codes [41], replicated codes [43], or cyclic codes to check memories, buses, or other communications paths [42]. Residue codes [44], [17], AN codes [44], and Berger Check Prediction [45] are all examples of codes used to check combinational functionality. Time redundant schemes such as recomputation with shifted operands [46], recomputing with swapped operands [47], and recomputing with duplication with comparison [48] are all examples of schemes which are used to check combinational functionality using the same hardware, but doing the same or different operation at a later time for comparison.

System level techniques can also be partitioned according to redundant checking concepts. Redundancy at the system level in hardware, software, information and time is used to check higher level abstractions of system behavior or information, such as operations, operands, program control flow, memory access behavior, and data reasonableness.

Many of basic ideas behind techniques used at the circuit-level may often be applied to higher-levels of system operation as well. For example, in an algorithm-based fault tolerant technique, the functionality of a control algorithm may be expressed as a combinational logic function and techniques used to check circuits at the logic level may be applied to this higher level representation. Thus, concepts such as hardware replication, information coding, and recomputation with comparison all may be applied to a higher level system representation. Concepts more unique to system level checking via redundancy come from software-based redundant techniques and algorithm-based fault tolerant techniques. These methodologies include n-version programming concepts [49], [50], capability checks [51], data reasonableness checks [43], matrix computation checking [53], [54], and control flow checking [52], [39], [55], [56], [57].

A safety-critical system design may be fully described by its components and their relations, and the implementation type of each system component. Figure 7 presents a taxonomy of safety-critical system designs. The general implementation types were discussed in Section 4.1, the components and relations composing a safety-critical system design were discussed in Section 4.2, and the specific on-line system checking methodologies were considered in this section and section 4.3.

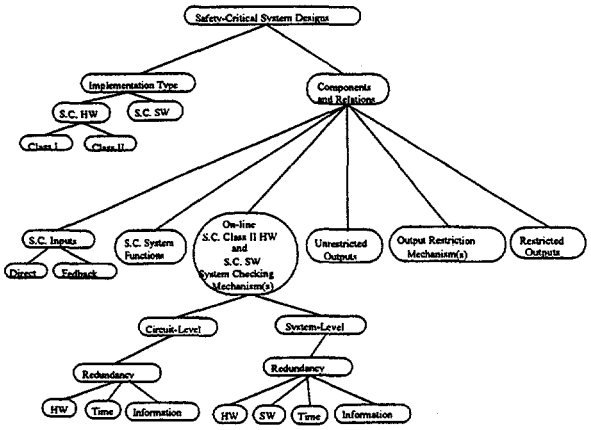

Figure 7: Taxonomy of safety-critical system designs

Three categories for describing how a particular safety-critical function is implemented are: (1) use of class I hardware, (2) use of class II hardware, or (3) use of software. If a safety-critical component is implemented using software or class II hardware, some on-line checking mechanism is used to verify the correct behavior of its functionality.

The on-line checking mechanisms used throughout the system may be categorized by one of the techniques described in this section. The checking mechanisms may be physically distributed or centrally located in a system and check aspects of system behavior not confined to the mechanism's physical location. This is especially true for system-level checking techniques.

6. Conclusions

This paper described the results of a survey of safety-critical systems in general. The common problems of those involved with the safety-critical system development process were highlighted along with associated fundamental safety-related concepts and definitions. A survey of safety-critical system designs was presented along with a generic model capturing the common underlying principles and features of all safety-critical system designs. A taxonomy that classifies the design solution space for safety-critical systems was also presented. It is the authors' hope that this information will aid current and future designers of safety-critical systems to understand their design-space and to quickly assemble candidate solutions for their particular problem.

7. References

[1] Leveson, N, *Safeware: System Safety and Computers*, Addison-Wesley, Reading, Massachusetts, 1995.

[2] Perrone, Paul J., *Global Safety Assurance: Concepts and Application to Train Control Systems*, University of Virginia Master's Thesis, August 1995.

[3] Kuo, Benjamin C., *Digital Control Systems*, Saunders College Publishing, A Harcourt Brace Jovanovich College Publisher, Ft. Worth, TX, Second Edition, 1992.

[4] Booth, Taylor L., *Sequential Machines and Automata Theory* John Wiley and Sons, INC., New York, 1967.

[5] Gluskhov, V.M., and A.A. Letichevskii, J.T. Tou, Editor, *Advances in Information Systems Science*, Volume 1, Plenum Press, New York, NY, 1969.

[6] Pradhan, D.K., *Fault-Tolerant Computing* Prentice-Hall, Englewood Cliffs, NJ, 1986.

[7] Robach, C., and G. Saucier, "Dynamic Testing of Control Units", *IEEE Transactions on Computers*, Volume C-27, Number 7, July 1978, pages 617-623.

[8] McCarthy, Roger L., "Present and Future Safety Challenges of Computer Control", *IEEE Proceedings of COMPASS 1988*, pages 1-7.

[9] Magison, E.C., "Make Sure Your System Is Safe", *Instruments and Control Systems*, December 1979.

[10] Gruhn, P., "The Pros and Cons of Qualitative & Quantitative Analysis of Safety Systems," *ISA Transactions*, Volume 30, Number 4, pages 79-86.

[11] Murphy, K.J., and J.A. Humphry, "A Highly Reliable Computer-Based Interlock and Alarm System," *ISA Transactions*, Volume 24, Number 1, pages 47-52.

[12] Zodeh, Oli M., and Donald S. Sikora, "Self-Checking Safety Interlock System," *IEEE Transactions on Industry Applications*, Volume 25, Number 5, September/October 1989, pages 851-854.

[13] Ghosh, Anup K., *Distributed System for Train Control*, Master's Thesis, University of Virginia, Charlottesville, Va, May 1993.

[14] Nair, V.S.S., Y.H. Hoskote, and J.A. Abraham, "Probabilistic Evaluation of On-Line Checks in Fault-Tolerant Multiprocessor Systems", *IEEE Transactions on Computers*, Volume 41, Number 5, May 1992, pages 532-541.

[15] Balls, B.W., and P. Gruhn, "Design Considerations for High-Risk Safety Systems," *ISA Transactions*, Volume 30, Number 4, pages 71-77.

[16] Moldoveanu, Andrei, "Key to Safety? Systems Approach to Safety Interlocking", *Automation*, September 1991, pages 28-30.

[17] Wakerly, J.F., *Error Detecting Codes*, Elsevier North-Holland, New York, 1978.

[18] U.S. Department of Defense, *System Safety Program Requirements*, MIL-STD-882C, January 19, 1993.

[19] Rutherford, D.B., "Evolving Standards for the Evaluation of Fail-Safety in Processor-Based Vital Control Systems", *American Public Transit Association 1991 Rapid Transit Conference*, Philadelphia, PA, June 9-13, 1991.

[20] Rutherford, D.B. "Evaluating Fail-Safety in Processor-Based Vital Control Systems", *American Public Transit Association 1990 Rapid Transit Conference*, Vancouver, B.C., June 2-7, 1990.

[21] Akita, K. T., T. Watanabe, H. Nakamura, and I. Okumura, "Computerized Interlocking System for Railway Signalling Control: SMILE", *IEEE Transactions on Industry Applications*, Volume 1A-21, Number 4, May/June 1985, pages 826-834.

[22] Disk, D., "A Unique Application of a Microprocessor to Vital Controls," *Proceedings of the International Conference on Railway Safety Control and Automation*, 1984, pages 97-104.

[23] Turner, David B., Roger D. Burns, and Herebrt Hecht, "Designing Micro-based Systems for Fail-Safe Travel", *IEEE Spectrum*, February 1987, pages 58-63.

[24] Bordenave, Henri, "Fault-Tolerant Computing Architecture for MF 88 and MP 89 Rolling Stock", *Transportation Technologies Applications*, pages 419-422.

[25] Kravetz, Gary A.,"Fail-safe Rapid-transit Engineering Ensures Reliability, Passenger Safety," *Electronics*, May 17, 1984, pages 152-154.

[26] Chandra, Vinodi, and M.R. Verma, "A Fail-Safe Interlocking System for Railways", *IEEE Design & Test of Computers*, March 1991, pages 58-66.

[27] Cribbens, A., "The Solid State Interlocking System",*Proceeding of the International Conference on Railway Safety Control and Automation*, Institute of Railway Signalling Engineers, London, September 1984, pages 24-29.

[28] Sholl, Howard, Kevin Morris, and James Norris, "A Multicomputer for Real-Time Classification of Railroad Track Flaws", *IEEE Transactions on Computers*, Volume C-31, Number 10, October 1982, pages 1009-1017.

[29] Fisher, Thomas G., "Are Programmable Controllers Suitable for Emergency Shutdown Systems?", *ISA Transactions*, Volume 29, Number 2, 1990, pages 1-22.

[30] Frederickson, T. and L.V. Beckman, "Comparison of Fault Tolerant Controllers Used in Safety Applications,"*ISA Transactions*, Volume 30, Number 4, 1991, pages 97-106.

[31] Lewinski, A., "Fail-Safe Control Method for Programmable Electronic Systems in Railway Applications", pages 440-442.

[32] Sikora, D.S. and R.L. Jones, "Emergency Shutdown System,"*IEEE Transactions on Industry Applications*, Volume 27, Number 2, March/April 1991, pages 254-256.

[33] Cullyer, W.J., "Implementing High Integrity Systems: The VIPER Microprocessor",*IEEE COMPASS Proceedings 1988*, Gaithersburg, MD, June 27-July 1 1999, pages 56-66.

[34] Wunram, Jurgen, "A Strategy for Identification and Development of Safety Critical Software Embedded in Complex Space Systems", *Acta Astronautica*, Volume 29, Number 3, 1993, pages 213-221.

[35] Rutherford, D.B., "Fail-Safe Microprocessor Interlocking with Safety Assurance Logic: Establishing a Vital Benchmark," *Proceedings of the International Conference on Railway Safety Control and Automation*, 1984, pages 1-5.

[36] Rutherford, D.B., "Fail-safe Microprocessor Interlocking - An Application of Numerically Integrated Safety Assurance Logic," *Proceedings of the Institution of Railway Signal Engineers*,London, September 1984.

[37] Koursi, M. El, and A. Stuparu, "Safety Microprocessors in Guided Ground Transport", pages 428-432.

[38] Sha, Lui, John Lehoczky, and Marc Bodson, "The Simplex Architecture: Analytic Redundancy for Software Fault Tolerance", *Proceedings of the 1rst International Workshop on Responsive Computer Systems*, Nice, France, October 1991.

[39] Mahmood, Aamer, and E.J. McCluskey, "Concurrent Error Detection Schemes Using Watchdog Processors - A Survey",*IEEE Transactions on Computers*, Volume 37, Number 2, February 1988.

[40] Verma M.R., and Vinod Chandra, "The Design and Development of a Fail Safe Interlocking System Using Microprocessors for Indian Railways", *IEEE TENCON 1989*, April 1989, pages 511-514.

[41] Lala, Parag K., *Fault Tolerant and Fault Testable Hardware Design*, Prentice/Hall International, Englewood Cliffs, NJ, 1984.

[42] Lin, S., and D.J. Costello, *Error Control Coding: Fundamentals and Applications*, Prentice-Hall, Englewood Cliffs, NJ, 1983.

[43] Johnson, B W, *Design and Analysis of Fault Tolerant Digital Systems*, Addison-Wesley, Reading, MA, 1989.

[44] Rao, T.R.N., *Error Coding for Arithmetic Processors*, Academic Press, New York, NY, 1974.

[45] Lo, J-C, S. Thanawastien, and T R N Rao, "An SFS Berger Check Prediction ALU and its Application to Self-Checking Processor Designs", *IEEE Transactions on Computer-Aided Design of Integrated Circuits and Systems*, Volume 11, April 1992, pages 525-540.

[46] Patel, J.K., and L.Y. Fung, "Concurrent Error Detection in ALUs by Recomputing with Shifted Operands", *IEEE Transactions on Computers*, Volume C-31, Number 7, July 1982, pages 589-595.

[47] Hana, H.H., and B.W. Johnson, "Concurrent Error Detection in VLSI Circuits using Time Redundancy", *Proceedings of the SOUTHEASTCON '86*, Richmond, Va., March 23-25, 1986, pages 208-212.

[48] Johnson, Barry W., J. H. Aylor, and H.H. Hana, "Efficient use of Time and Hardware Redundancy for Concurrent Error Detection in a 32-bit VLSI Adder.", *IEEE Journal of Solid-State Circuits*, Volume 23, Number 1, February 1988, pages 208-215.

[49] Chen L., and A. Avizienis, "N-version programming: A Fault Tolerant Approach to Reliability of Software operation", *Proceedings of the International Symposium on Fault Tolerant Computing*, 1978, pages 3-9.

[50] Miremadi, G., J. Karlsson, U. Gunneflo, and J. Torin, "Two Software Techniques for On-Line Error Detection", *22nd Fault Tolerant Computing Symposium*, July 1992, pages 328-335.

[51] Gunneflo, U., J. Karlsson, and J. Torin, "Evaluation of Error Detection Schemes Using Fault Injection by Heavy-Ion Radiation", *Proceedings of the 19th International Symposium on Fault-Tolerant Computing*, June 1989, pages 340-347.

[52] Delord, X., and G. Saucier, "Control Flow Checking in Pipelined RISC Microprocessors The Motorola MC88100 Case Study", *Euromicro 1990*, pages 162-169.

[53] Huang, K-H, and J.A. Abraham, "Algorithm-Based Fault Tolerance for Matrix Operations", *IEEE Transactions on Computers*, Volume C-33, Number 6, June 1984, pages 518-528.

[54] Jou, J-Y, and J.A. Abraham, "Fault-Tolerant Matrix Arithmetic and Signal Processing on Highly Concurrent Computing Structures", *Proceedings of the IEEE*, Volume 74, Number 5, May 1986, pages 732-741.

[55] Michel, T., R. Leveugle, and G. Saucier "A New Approach to Control Flow Checking Without Program Modification",*21rst IEEE Fault Tolerant Computing Symposium*, June 1991, pages 334-341.

[56] Shen, J.P. and S.P. Tomas, "A Roving Monitoring Processor for Detection of Control Flow Errors in Multiple Processor Systems", *Microprocessing and Microprogramming*, Volume 20, May 1987, pages 249-269.

[57] Sosnowski, J., "Detection of Control Flow Errors Using Signature and Checking Instructions", *1988 International Test Conference*, September 1988, pages 81-88.

NRC Thermal-Hydraulic Code Consolidation and Improvement Program

J. L. Uhle
USNRC

ABSTRACT

NRC currently maintains four distinct thermal-hydraulic codes including: TRAC-P, TRAC-B, RELAP5 and RAMONA. These codes have similar but not identical capabilities. The existence of the four separate codes dilutes the NRC resources, as effort must be expended in quadruplicate to support code improvement, assessment, analysis and maintenance. Additionally, the collective expertise is also diluted as the user community is distributed amongst the four codes. To alleviate these problems, NRC plans to consolidate the codes into a single state of the art code. The consolidated code will incorporate all of the capabilities embodied in the separate codes, so that the user needs will not be compromised.

The NRC codes will be maintained for a period during the consolidation process, so that user needs are accommodated. These versions will not be static, but will be aggressively maintained and improved throughout the effort. Concurrently, NRC will work to develop innovative code numerics and physical models that, when completed, will be merged with the consolidated code, either during the consolidation program or upon its conclusion. Additionally, a GUI will be developed to aid in the use of the code and to provide an input deck translator so that previously constructed input decks will not become obsolete.

NRC will not discontinue support of any code until all capabilities are recovered, their functionality well assessed and users are familiarized with the use of the consolidated code. In summary, the NRC plan consists of both recovering all capabilities of the current suite of codes and making substantial improvements.

1 INTRODUCTION

The NRC currently relies on four different thermal-hydraulic system analysis codes to audit vendor or licensee analyses of new or existing designs, to establish and revise regulatory requirements, to study operating events and to anticipate problems of potential significance. NRC plans to consolidate all functionality embodied in the suite of codes into one code. Since each of the four codes serves a particular function, the codes will be maintained for a period during the consolidation process, so that user needs are accommodated. These versions will not be static, but will be aggressively maintained and improved throughout the effort. Concurrently, NRC will work to develop innovative code numerics and physical models that, when completed, will be merged with the consolidated code, either during the consolidation program or upon its conclusion. This paper summarizes the NRC thermal-hydraulic code consolidation program.

2 BACKGROUND

The NRC currently maintains 4 distinct thermal-hydraulic codes including: TRAC-P, TRAC-B, RELAP5 and RAMONA. These codes have similar but not identical capabilities. For pressurized water reactors (PWRs), the RELAP5 code is primarily used for simulation of small break LOCA and plant transient analyses and provides a one-dimensional (1D) representation of the flow field. RELAP5 lacks the models required for large break LOCA analyses, such as a three-dimensional (3D) vessel component and has not been assessed against data for this particular application. TRAC-P has the capability to model multi-dimensional flows and is therefore utilized for large break LOCA analyses. Generally, RELAP5 was developed as a fast running, more simplistic code for long term transients, whereas TRAC-P provides a more detailed description of the flow field in faster transients. More recently, this distinct separation of functionality has eroded and the present capabilities of the two codes overlap. However, the codes often model the same phenomena with different constitutive packages and also employ different numerical schemes. The reactor physics capabilities of both codes are limited to point kinetics.

For boiling water reactors, the situation is comparable. The RAMONA code treats the flow field as 1D but incorporates a 3D kinetics package. A 3D representation of the flow field is provided by the TRAC-B code, but the neutronics models are limited to either point or 1D kinetics. TRAC-B stemmed from the TRAC-P code and was developed in parallel specifically for BWRs. It incorporates BWR specific models such as the jet pump and also utilizes a different constitutive package and numerical scheme than TRAC-P. The development of both TRAC codes has proceeded independently.

The NRC thermal-hydraulic codes were developed in the 1970s and therefore do not take advantage of today's abundant supply of inexpensive, fast memory. In addition, older programming languages did not readily provide a means for dynamic memory allocation. As a result, creative programming styles (such as "bit packing" and "container arrays") were invoked to overcome these limitations. Unfortunately, these techniques produced cryptic coding and compromised readability, maintainability and portability. Presently, a great deal of effort is vested in deciphering these codes in order to improve the numerical techniques or physical models.

User friendliness is associated with the difficulty one encounters when using the code. This hardship arises from the laborious task of input deck preparation and the equally daunting task of interpreting the output. Since using the code is a complex task, different users will generate different results. This notion is deemed the user effect. One method employed to minimize the user effect and to generally facilitate the use of the code is a graphical users interface (GUI). Traditionally, users have relied on command line input through the terminal as the primary means of interaction with the thermal-hydraulic codes, and therefore each code would benefit by the development of a GUI.

Since each code requires modernization, an improved user interface and would benefit from upgrades in physical models and numerics, NRC plans to consolidate the suite of codes into one, with an aim of minimizing the dilution of the resources that are dedicated to development and maintenance of the four codes. As a result, user needs will be accommodated more expediently, since effort will not be distributed amongst the four codes. Additionally, the consolidation will enhance analysis capabilities, as the NRC and the user community can focus attention on one code, thereby developing the collective expertise far more efficiently than is possible when four codes are utilized. Input deck construction would not be duplicative, as all transients for a plant design would be performed with one code instead of two.

3 GOAL

It is evident that the existence of the four separate codes dilutes the NRC resources, as effort must be expended in quadruplicate to support code improvement, assessment, analysis and maintenance. To alleviate this problem, NRC plans to consolidate the codes into a single state of the art code. The consolidated code will incorporate all of the capabilities embodied in the separate codes, so that the user needs will not be compromised. TRAC-P will serve as the basis for the consolidation process, since it contains a 3D hydraulic vessel component, utilizes a network solution procedure, which enhances extendibility (the ability to add components), and is more modular (the database structure and first steps in the solution procedure are component specific).

The NRC codes will be maintained for a period during the consolidation process, so that user needs are accommodated. These versions will not be static, but will be aggressively maintained and improved throughout the effort. Additionally, a GUI will be developed to aid in the use of the code and to provide a tool which will assist the user with the conversion of input decks, so that previously constructed input decks will not become obsolete. Consolidation of TRAC-B and RAMONA (3D kinetics) capabilities is scheduled to begin upon completion of the modernization. During this time, RELAP5 will be improved, since work to recover its capabilities will not begin until the TRAC-B and 3D kinetics consolidation is complete. These improvements are further described in section 7. Once the consolidation is completed, NRC will support a transition period during which the code will be further tested and NRC will provide training for use of the code. NRC will not discontinue support of any code until all capabilities are recovered, their functionality well assessed and users are familiarized with the use of the consolidated code.

Throughout the consolidation, NRC will work to develop innovative code numerics and physical models that, when completed, will be merged with the consolidated code, either during the consolidation program or upon its conclusion. NRC has just organized an Institute of Thermal-Hydraulics, comprised of a consortium of universities, with Purdue University serving as the lead contractor. In conjunction with NRC, the Institute will perform research and development in the following areas to eradicate deficiencies in the current codes' capabilities:

designing and performing two-phase flow experiments
development of constitutive models, component models and correlations
development of numerical methods
development of a graphical user interface
applications of computational fluid dynamics codes to simulate reactor components

These capabilities will be developed for incorporation into the consolidated code and small scale fundamental experiments will be run to generate a database that can be used in future code development endeavors. NRC staff will participate in and guide the research activities of the Institute to ensure that NRC needs goals are realized. In summary, the NRC plan consists of both recovering all capabilities of the current suite of codes and making substantial improvements.

4 APPROACH

4.1 Introduction

The consolidation will not involve simply lumping the codes together, developing a generic input processor and renaming the code, as this approach would not eradicate any of the difficulties associated with the maintenance of four distinct codes. Instead, TRAC-P will serve as the framework into which the other codes' models will be incorporated.

As previously mentioned, TRAC-P was chosen as the base for the consolidated code for three reasons:

- 3D vessel

A 3D thermal-hydraulic component may be required for transients that involve asymmetric behavior, such as large break LOCA and localized reactivity insertions.

- component based structure

Each component (ie, pipe, vessel, etc...) has its own data structure, which heightens the potential for limiting access to a component's data and also tailoring components' storage needs. Additionally, the initial steps of the solution procedure are component specific, which promotes the options of evaluating component specific constitutive packages and formulations of the conservation equations.

- network solver

The TRAC-P solution scheme is based on a network solver concept. Essentially, the internal junction variables of a component (internal junctions connect the individual control volumes that comprise the component) are solved for in terms of the variables at the external junctions, which link the component to the other adjacent components. This scheme reduces the inter-component communication inherent in the solution procedure and facilitates the addition of components.

Before the capabilities of the other codes are incorporated into TRAC-P, the code will first be modernized, employing Fortran 90 as the coding language and restructured into a more modular design. Modernization will facilitate the code consolidation activities and long-term code improvements.

4.2 TRAC-P Modernization and Modularization into TRAC-M

Presently, the TRAC-P code is being modernized in two steps. First, non-standard Fortran 77 is being replaced with standard coding that is supported by all Fortran 77 compilers. The database is then being restructured using Fortran 90 to allow for dynamic memory management without the use of a container array and also to utilize object-oriented principles that enhance all levels of code modularity, extendibility and readability.

Effort will also be vested in increasing the high level functional modularity of TRAC-M. High level functional modularity means that the functions of the code will be done in sections of the code. This distinct zoning of functions makes the code easier to develop. Three tasks will be performed to enhance the high-level functional modularity of the TRAC-P code.

The solution procedure of the code will be modularized, so that the building of the matrix will be separated from the solving of the matrix (no subroutine will develop the terms of the finite volume equation matrix and also proceed with the matrix solution), thereby enhancing the ability to implement various differencing schemes or matrix solution techniques. The component communication will be modularized so that boundary information will be provided to each component by a communication manager without the use of pointers embedded in a variety of subroutines. NRC plans to separate the input processing from the computational engine (those subroutines that perform the solution based on the geometry set up and the values initialized by the input processor). This separation of functionality will aid the consolidation, since as models are incorporated, the input deck must be modified accordingly. During this stage, the input deck will be bullet-proofed to aid the user in diagnosing fatal errors in the input deck. The consolidation will involve a great deal of assessment and bullet proofing the input will expedite the work considerably.

Consolidation of the other codes' capabilities will begin upon the completion of the modularization. To promote clarity of this paper, at this stage of the effort, the code will be referred to as TRAC-M.

4.3 Developmental Assessment

To ensure that the consolidated code will have all the capabilities of the suite of codes, NRC is developing developmental assessment (DA) matrices for each code based on the philosophy embodied in the Phenomena Identification and Ranking Tables (PIRTs). The matrices are based on the CSNI integral effects tables and supplemented with other applicable transients if necessary. Since the tables break down each transient into phenomena, existing PIRTS can be used to supplement the list of phenomena.

The integral effects test (IET) matrix can be developed from this finalized list of transients and phenomena. Development of the separate effects test (SET) matrix will require additional work. System code results and scaled test data will be used to further narrow the range of parameters over which the phenomena occur. With this information, the SET matrix will be constructed.

The finalized PIRTs will identify all phenomena the code is required to model. This information can then be used to identify phenomena that are not represented by code models and can also divulge cases where a model's range of validity does not encompass the range over which the identified code applications will exercise the model. These identified deficiencies will be eradicated by the NRC experimentation and model development efforts (section 7).

Code assessment plays a vital role in NRC thermal-hydraulic code improvement efforts. A great deal of effort is spent comparing the results of the code predictions to test data to determine the accuracy of the code. NRC has just initiated an effort to produce and document a set of numerical techniques to rate code assessment results. For example, these techniques may include; root mean squared comparison and Fast Fourier Transform techniques to evaluate the frequency components of the shape of the data. Since the technique will be used to ensure that the code predicts all the dominating phenomena, the technique will provide quantitative measures of the simulation fidelity by comparing the magnitudes of the parameter, the slopes and inflection points of the curves that represent major changes in the trends of the parameters and timing of events. Therefore, rating the simulation fidelity of the code as excellent, reasonable, minimal and insufficient will be based on the results of the numerical techniques. To set numerical standards that correspond to the qualitative labels (excellent, reasonable, ...), a peer review process will be used. This numerically based rating system will ensure consistency throughout the project and will facilitate full automation of the developmental assessment activities.

4.4 RAMONA

To recover the capabilities of the RAMONA code, NRC plans to couple the PARCS 3D neutronics code to TRAC-M. The kinetics will be internally coupled to TRAC-M, so that TRAC-M thermal-hydraulics will be used to model the fluid conditions in the core. The required properties will then be passed to the kinetics routines that provide the core power. The codes' databases will not be mixed to limit the required maintenance in the kinetics routines stemming from modifications to the thermal-hydraulics coding. Essentially, an interface will be generated to read the required thermal-hydraulics code variables, map them to the meshing of the kinetics code, rename them to be consistent with the labeling convection of the kinetics code and finally pass them to the kinetics routines. The power would then be passed in the other direction. Improvements can be made to the kinetics code without involving the thermal-hydraulic code. These modifications can then be implemented by changing the interface accordingly. The development of this interface is the first step in the incorporation of 3D kinetics into a thermal-hydraulic code. NRC also plans to couple PARCS to RELAP5 (section 4.6) using this same coupling technique.

NRC is currently investigating wether or not the ability to model stability will require additional work, such as higher order differencing of the momentum and energy equations (or other techniques to minimize unphysical damping). Future work will also entail determining and developing the required capabilities to model high burnup and MOX fuels.

4.5 TRAC-B

To consolidate the models of TRAC-B into TRAC-M, the following strategy has been planned.

- Each of the TRAC-B BWR components are based upon pipe and tee components. The BWR components, such as CHAN (the core rod bundles and channel boxes) and the jet pump, will be built from the TRAC-M components in the form of a module that is consistent with the TRAC-M Fortran 90 data structure.

Since the numerical scheme of TRAC-M differs from that of TRAC-B, this effort does not entail simply cutting and pasting TRAC-B coding. Since the physical models of TRAC-M and TRAC-B are different, the TRAC-M physical models may yield unsatisfactory results for the TRAC-B developmental assessment matrix. The term common models will be used to refer to physical models used in the two, such as interfacial heat transfer and drag in a pipe.

- To then ascertain the impact of the TRAC-M common models on the capability to simulate a BWR, the TRAC-B SET matrix will be run with TRAC-M to determine the BWR simulation fidelity of the modules in TRAC-M.

- If TRAC-M common models are deficient in modeling the BWR components, then TRAC-B common models will be coded into TRAC-M and used only for the BWR components. These models are now referred to as BWR component specific models. The models will then be assessed against the TRAC-B SET matrix.

Therefore, the BWR components will either use the models of TRAC-B or TRAC-M, but the remainder of the system will use TRAC-M models. For example, if TRAC-B models are used for the BWR components, then for a jet pump component, which is comprised of a generic tee component with an additional momentum

source term, the jet pump would use the TRAC-B wall drag correlation but all other generic tee components (not part of jet pumps) would use the TRAC-M correlation.

The last two steps will assess the accuracy of the BWR components in the TRAC-M code against SET data, which will determine the ability of the code to model a few phenomena but not the complete system.

- To determine the ability of the code to model the complete BWR system, the TRAC-B IET matrix will be run with TRAC-M and the deficiencies noted.

This DA activity will determine if any TRAC-M common models used for the generic components are not appropriate for BWR applications. It is likely that the common model selection for the generic components will be done simultaneously with RELAP5 DA, so that the common models will not improve the simulation fidelity of one code application at the expense of the others. These models will be chosen at this stage based not only on overall accuracy but also on parameter range and the degree of documentation that exists in literature. Common model selection will involve running SET matrices with a driver code or pilot code, if a two-fluid formulation is required, as well as coding them into TRAC-M and running the IET to determine how TRAC-M numerics and other models affect their performance. For the purpose of clarity in this paper, at the stage when the BWR components and 3D kinetics capabilities are incorporated, the code will be referred to as TRAC+, and TRAC++ when the common model selection for generic components is completed.

4.6 RELAP5

Once the common models are selected, then the RELAP5 specific models can be incorporated, such as thermal front tracking and the accumulator component. At this point, the code will embody all capabilities of the suite of codes and is now referred to as ARC (Advanced Reactor Code).

Concurrent with the consolidation effort, RELAP5 will be improved since its capabilities will not be recovered until the later stages of the consolidation program. Improvements include:

- Development of a GUI
- Removing bit packing (a technique used to save memory) to enhance readability;
- Modularizing excessively large subroutines to enhance readability;
- Incorporating 3D kinetics;
- Improving the non-condensible numerics;
- Improving mass conservation and robustness;
- Converting the code into F90 to provide dynamic memory allocation while enhancing readability and maintainability.

5 TRANSITION

As part of the consolidation effort, a full DA of ARC will be run for all the code applications. Once the consolidation is completed, NRC will support a transition period during which the code will be further tested and NRC will provide training for use of the code. NRC will not discontinue support of any code until all capabilities are recovered, their functionality well assessed and users are familiarized with the use of ARC. Additionally, NRC will provide users with the capability of translating input decks from those of TRAC-B, TRAC-P and RELAP5 to the consolidated code, so that previously constructed input decks will not become obsolete. Throughout the consolidation program, all development efforts will adhere to NRC Software Quality Assurance.

6 SOFTWARE QUALITY ASSURANCE

NRC has developed a Software Quality Assurance (SQA) program for the code consolidation effort. SQA will ensure that what is in the code has been developed in accordance with SQA procedures, has been authorized by the NRC and the documentation associated with the modifications are sufficient so that future code users and developers will understand the bases for the changes, and through assessment results, be assured of the operability and accuracy of the modifications. Therefore, the SQA program will oversee areas of documentation of code, assessment and configuration control.

7 CODE IMPROVEMENTS

Concurrent with the consolidation, NRC will work to improve the capabilities of the code. These improvements may involve modifying the numerics, creating a parallelized version of the code, developing a GUI, improving the constitutive packages, developing new components, such as a Lagrangian based accumulator or CMT and in the longer term, incorporating links to a stand-alone code, such as a CFD code. Programs currently underway to develop these improvements are discussed in the following sections.

7.1 Parallel Version

NRC plans to develop a coarse grain parallelized version of the consolidated code to increase both the speed of the code and the memory available for each simulation. Essentially, the parallelized code will operate like there is a version of the code on each processor (CPU) but the database specific to each CPU is only available to that CPU. Information on each processor will act as boundary conditions to the other processors. The matrix solver will function on another CPU and will feed information back to the other processors. The option of implementing a data distribution algorithm that performs automatic data decomposition or process mapping may be considered. Load balancing or dynamic data decomposition is also an option for long term.

7.2 Graphical User Interface

The Graphical User Interface (GUI), which has been named the Symbolic Nuclear Analysis Package (SNAP). SNAP development is currently focusing on a RELAP5 preprocessor interface. Future versions will provide fuller RELAP5 deck modification and preprocessing capabilities and will include expert systems (wizards) as well as runtime and postprocessing enhancements. A concurrent effort will be undertaken to assist the user in the translation of RELAP5 to TRAC-P input decks. Once developed for RELAP5, the full capabilities of the

GUI will be available for the consolidated code.

7.3 Interfacial Area Transport

For predicting the thermal-hydraulic behavior of two-phase flow, the interfacial structure is one of the most important parameters, since all the transfers of mass, momentum and energy occur at the interface. Traditionally, the effects of interface structure have been analyzed using flow regimes and transition criteria that do not dynamically represent the changes in interfacial structure. To better represent the effects of interfacial structure and regime transition, the use of a first order equation to characterize interfacial area transport has been recommended. The equation is in the form of a conservation equation of interfacial area concentration with the right hand side that represents the sources and sinks due to the physical processes that govern the creation and destruction of interfacial area. NRC is sponsoring research to determine the constitutive relations for the source and sink terms over the range of conditions and flow geometries prototypic of nuclear reactor designs.

7.4 Reflood

Reflood has been extensively studied. However, parameters such as local void fraction, droplet diameter, phasic temperatures and velocities have not been measured in detail precluding the development of a model that predicts detailed behavior, which is thought to be necessary for this phenomenon. Therefore, the previous work has not yielded an accurate predictive capability. NRC is investigating methods to perform more fundamental experiments with an aim of allowing more physical, accurate modeling of low pressure boiling and heat transfer, axial void profile (particularly interfacial area and drag), and reflooding of rod bundles (particularly precursory cooling above the quench front).

7.5 Phase Separation

Accurate modeling of phase separation is vital to reactor safety analysis. For either a postulated break, a relief valve or an automatic depressurization system, the fluid quality of the effluent is a critical parameter--the higher the quality the more rapid the depressurization, and the lower the quality, the greater the inventory loss. If the phase separation model over-predicts the phase separation at the break or off-take, the plant depressurization rate is enhanced while the liquid inventory in the core is maximized. Therefore, an inaccurate phase separation model can result in non-conservative predictions of core liquid inventory, the key figure of merit used in analyzing reactor safety. Therefore, NRC plans to develop a set of suitable correlations for modeling phase separation at the break in SBLOCA conditions in the AP600 and conventional plants and for the hot leg off-take geometry for all ADS stages in the AP600.

8 SUMMARY

NRC currently utilizes four separate thermal-hydraulic codes. In an effort to minimize the dilution of resources and expertise associated with the maintenance, development and use of these codes, NRC plans to consolidate all functionality embodied in the suite of codes into one code. Since each of the four codes serves a particular function, the codes will be maintained for a period during the consolidation process, so that user needs are accommodated. These versions will not be static, but will be aggressively maintained and improved throughout the effort. Concurrently, NRC will work to develop innovative code numerics and physical models that, when completed, will be merged with the consolidated code, either during the consolidation

program or upon its conclusion. Once the consolidation is completed, NRC will support a transition period during which the code will be further tested and NRC will provide training for use of the code. NRC will not discontinue support of any code until all capabilities are recovered, their functionality well assessed and users are familiarized with the use of ARC. Additionally, NRC will provide users with the capability of translating input decks from those of TRAC-B, TRAC-P and RELAP5 to the consolidated code, so that previously constructed input decks will not become obsolete.

NRC Generic Graphical User Interface Development for RELAP5

B. J. Gitnick
Scientech, Inc.

S.G. Smith
U.S. Nuclear Regulatory Commission

Introduction

The United States Nuclear Regulatory Commission (NRC) is sponsoring the development of a generic tool to assist in the construction and evaluation of nuclear safety analysis models for simulation codes such as RELAP5 and TRAC-P. This code is referred to as SNAP, for Symbolic Nuclear Analysis Program. SNAP is being developed to meet the special requirements of the nuclear safety analyst, whose task is to evaluate complex system models composed of many components (See Table 1).

Creating, modifying and verifying system models is difficult, yet these are tasks that the safety analyst must perform frequently. Poor documentation and confusing input syntax makes these codes difficult and inflexible to use. Typically, runs must be coaxed through several restarts to reach the desired problem end time. Users must manipulate numerous large files to plot and analyze the results.

SNAP will contain four modules designed to help users build, modify, submit, monitor, inspect, and visualize analytical results:

1) A preprocessor to aid in developing and modifying input models.
2) A runtime processor for problem submission and initialization, reporting and plotting of results for runs in progress and job status monitoring and control.
3) The post-processor includes those functions required to analyze the results of a calculation, including plotting and animation tools for visual presentation of model information and calculated results.
4) An interface to a database management system (DBMS) for organizing, searching and storing project, plant, and model information. The database also will contain libraries of models and model parameters, such as material properties and pipe schedules, to assist users constructing simulation models.

SNAP will also provide expert assistants to assist users through complex modeling tasks such as problem nodalization, initialization, as well as pump, valve, heat structure and break component setup. The expert assistants ("Wizards") are being developed (Table 2) based on the knowledge base of experienced engineers, the user guidelines and the developmental assessment results.

A preliminary version of the SNAP preprocessor is in Beta Test at the NRC. Currently, only the RELAP5 computer code is supported in this initial implementation of the SNAP user interface. The other modules are still in the design stage or early in the implementation stage of the development process.

Intelligent and Intuitive User Interface Approach

The SNAP preprocessor provides a Graphical User Interface — a GUI — which allows the user to assemble a complex facility model by manipulating symbols and icons. The SNAP interface makes interrelationships (flow paths, heat transfer paths, reactivity feedbacks, and controller loops) between components clear both at a logical and a physical level.

There have been several previous GUIs developed for safety analysis codes. Unlike these earlier codes, SNAP does more than convert the existing card deck format into a series of graphical dialogs. SNAP dialogs and diagrams typically provide descriptive text and a units field for each variable. Generally, inputs appear on dialogs only if they needed. In some cases, where these inputs are optional, unavailable inputs are made are uneditable ("grayed out") when an option is selected, and only made editable again when those inputs options are re-activated by user input. More advanced features and options are on separate dialogs, which users need not generally invoke. Brief help and full help messages will be available, as are hypertext links to the RELAP5 guidelines documents.

Systems analysis codes generally represent a hydraulic system by dividing it up into "cells" which are joined together by "junctions". Some of the cells may be specialized representations of other components such as pumps, and some of the junctions may be specialized representations such as valves, but the use of cells and junctions to model a hydraulic network is fairly standard. The way the cells and junctions are interconnected defines a flowing system as much as the physical characteristics of the individual components: piping, valves, pumps, fills, breaks and tees, etc. The cell and junction representation has stood the test of time, and the SNAP interface adopts it too.

The SNAP interface allows the user to build and edit input models by manipulating icons and through user friendly interactive commands. SNAP icons have a recognizable shape and scaleable proportion, so that they can represent reactor system and containment components in the familiar nodalization diagram format. These icons behave like real components, e.g., users can connect these icons only if RELAP5 allows these components to connect. Users construct a flow network by connecting component icons with junctions. (See Figure 1). Some icons represent single volumes, while other components, such as pipes and branches, contain multiple volumes and junctions. SNAP also allows composite components, which may contain other components, including composites (i.e., nesting is allowed). These composites can be code specific (e.g., a RELAP5 pipe), or selected from a library of components (listed in Table 1) or user defined.

Editing functions are provided to allow users to easily access and change model inputs, add or delete components, and define component groups. Component properties are input or modified for individual components using tabbed dialogs (Figure 2), or globally using the "component navigator" feature, which lists all components' properties using a spreadsheet-type interface (not yet implemented). In the future, these libraries of components

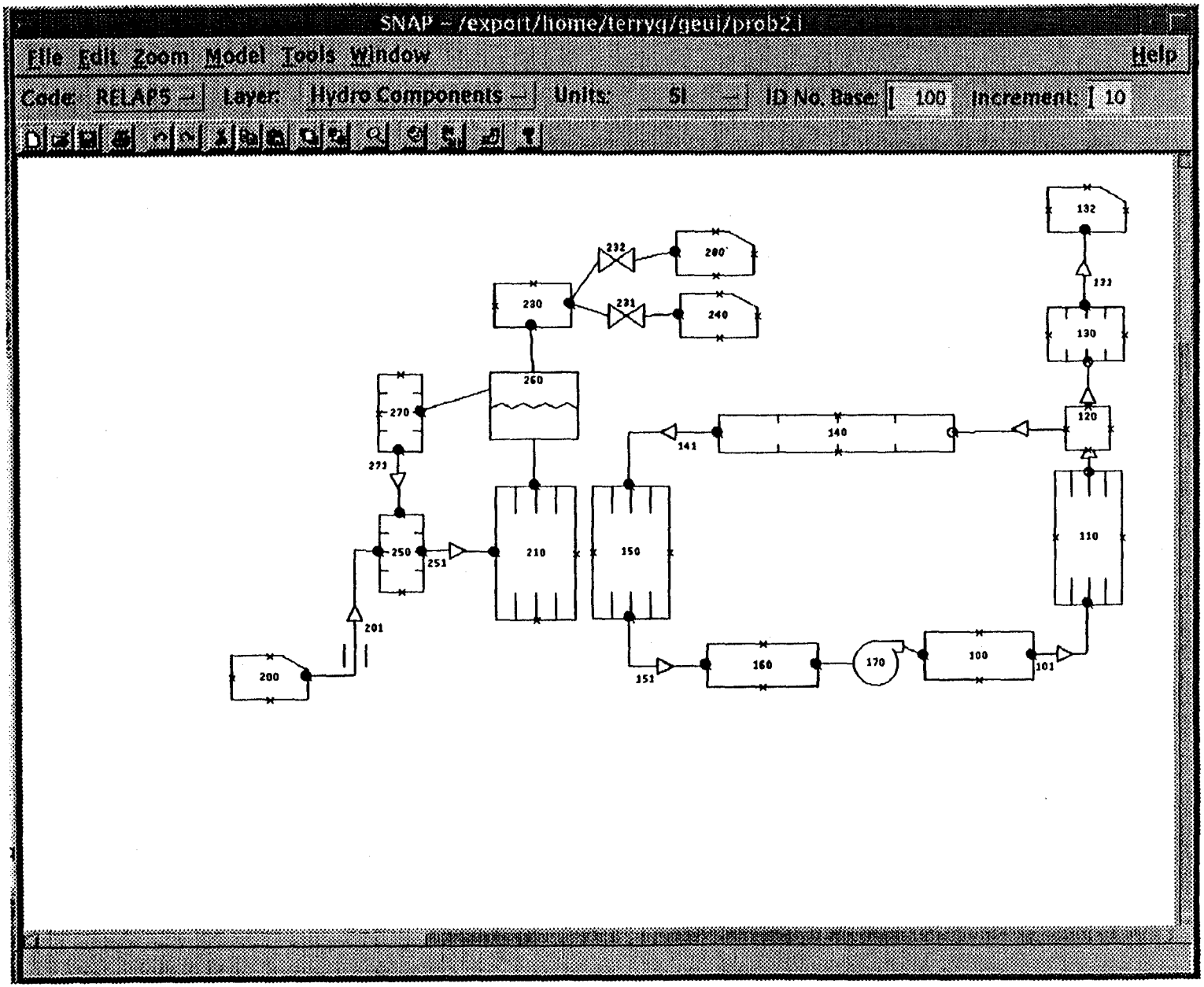

Figure 1. SNAP User Interface

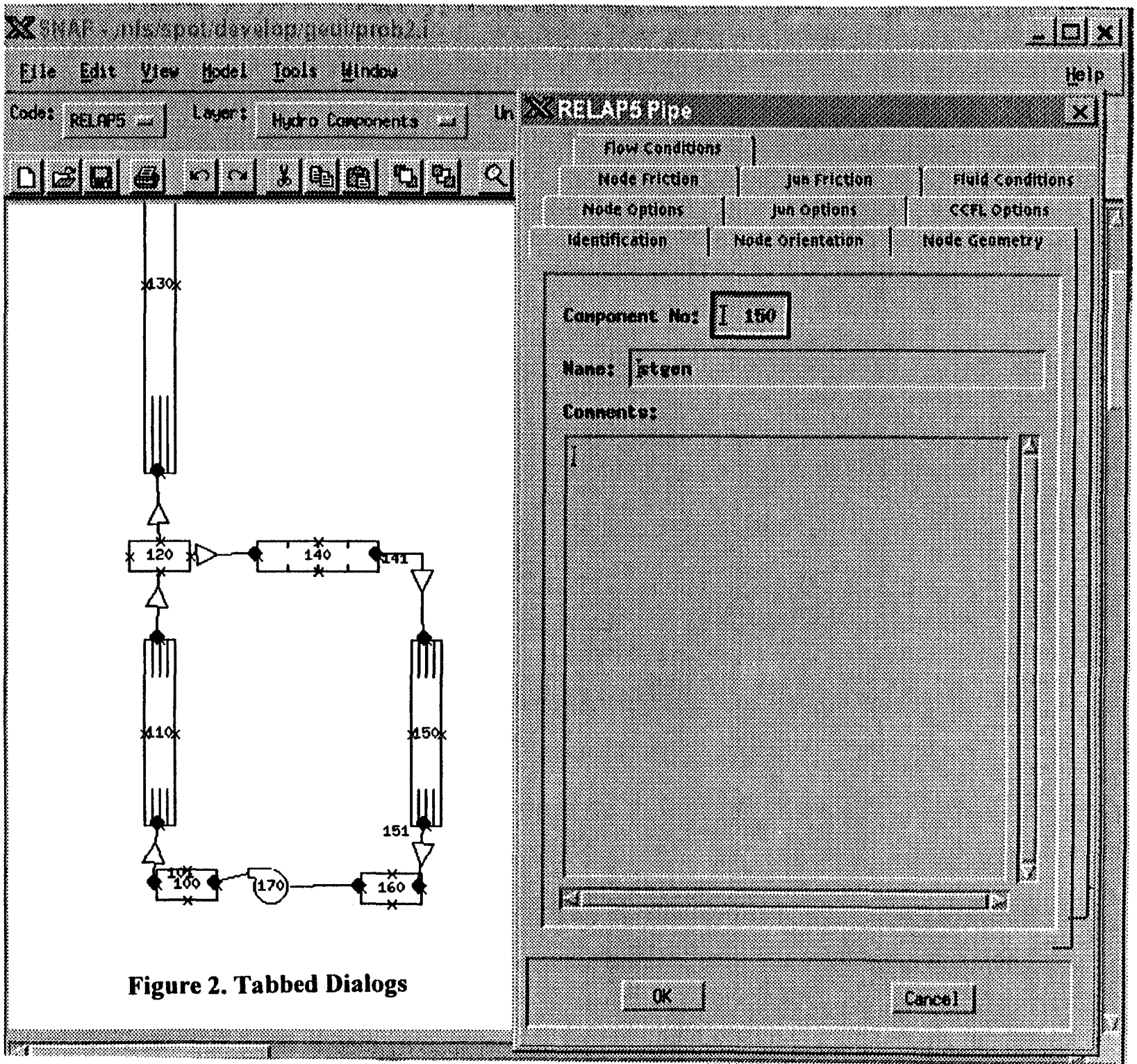

Figure 2. Tabbed Dialogs

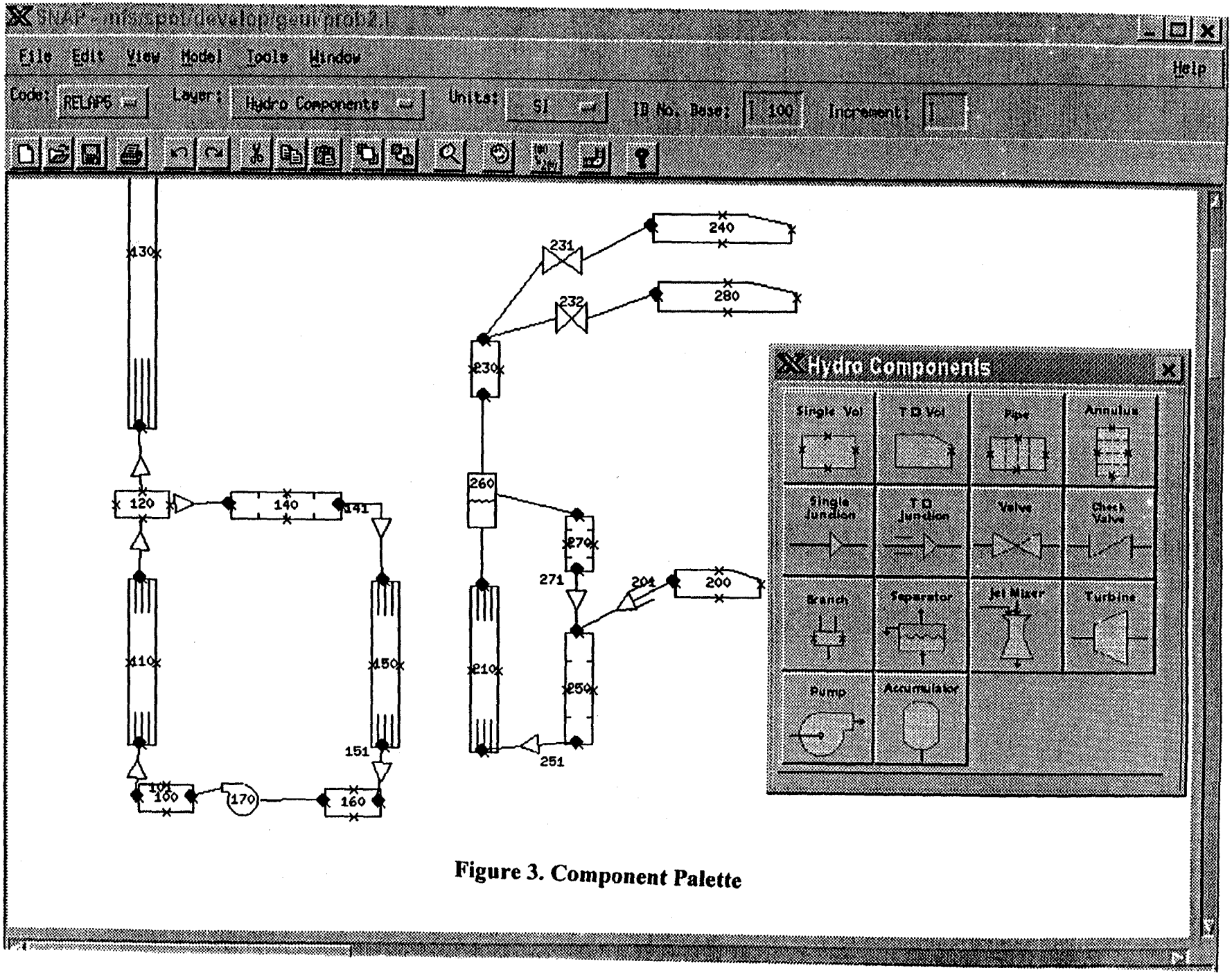

Figure 3. Component Palette

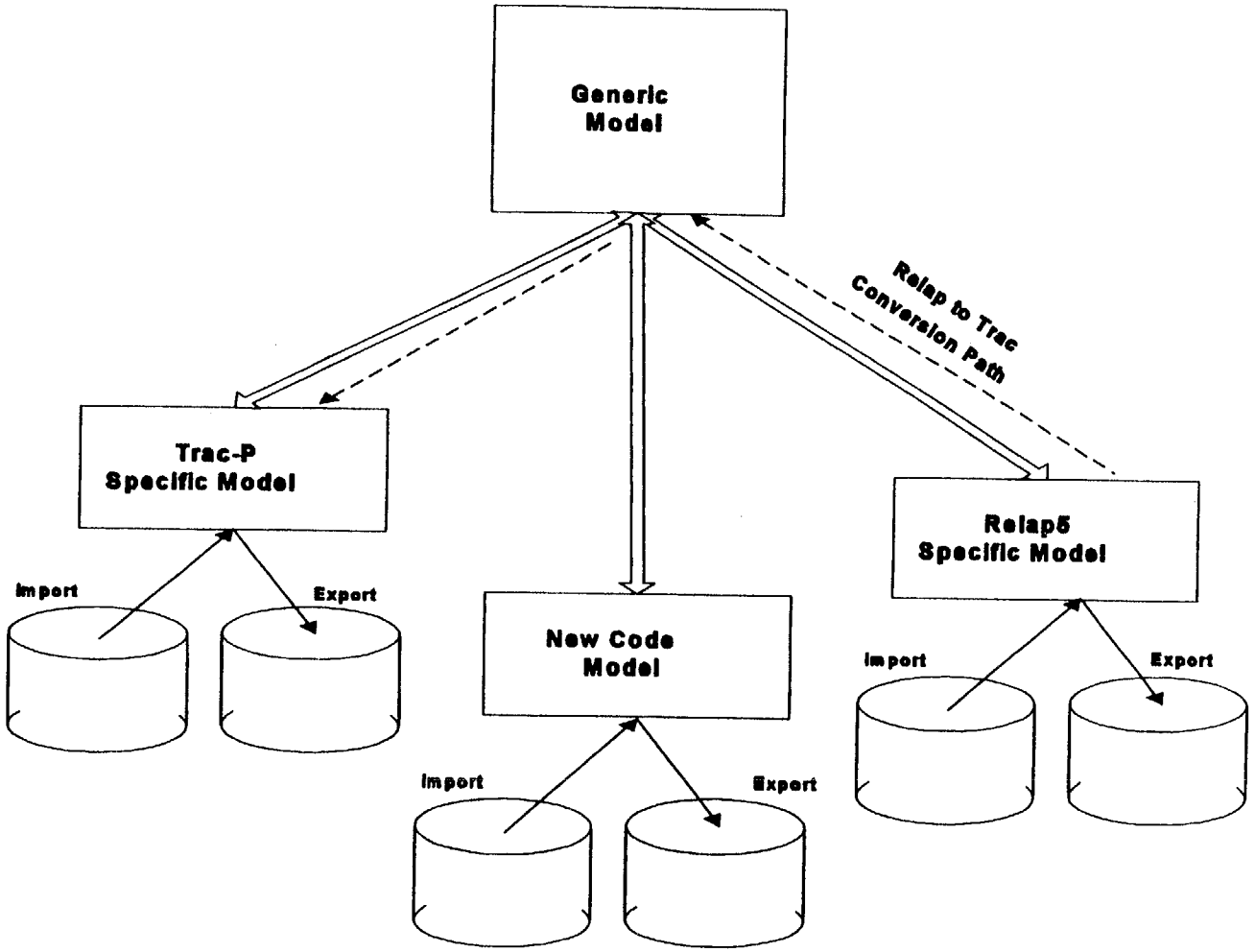

Figure 4. Design for Extensability

("Templates") typically used in nuclear power plants to facilitate the modeling development process, will be contained in the SNAP DBMS as discussed in the data storage section below.

SNAP can import previously developed models (i.e. existing plant decks) and display the resulting input model. Whether creating or modifying an existing model, users may add, delete, connect or disconnect junctions, and add or delete components using interactive (mouse and/or keyboard) commands. Junctions and components can be copied, grouped, pasted and renumbered. One of the expert assistants ("Wizards") will assist in renodalization. New components are selected from a palette. (Figure 3). Palettes are organized in a four-tier hierarchy: hydrodynamic components, heat structures, heat sources, trips and controls. This representation is flexible and applicable to all of the analysis codes under consideration, and provides a convenient means to organize the physical data necessary to create the model specific input files — with data provided either by the user or extracted from libraries of component templates and previous designs stored on the database. SNAP provides visualization and error checking tools help to locate and correct errors in models earlier in the model building procession.

Generic Basis for Code-to-Code Model Translation

The SNAP design provides a foundation and framework to support other existing NRC safety analysis codes, such as TRAC-P, MELCOR, CONTAIN, and new codes which may be developed in the future. For example, RELAP5 and TRAC-P are both systems transient codes. Yet these codes are based on philosophical models which are sufficiently different that highly experienced users have a hard job adapting a model from one code to the other.

A unique feature of the SNAP its capability to translate from one simulation code to another. SNAP stores both generic and code specific model information. Generic information includes geometric and performance data for physical pieces of equipment, such as pumps, pipes, elbows, reducers, tees, valves, tanks, etc. Code specific information is used to supplement the generic information for input data items specific to each code, such as model options and flags. SNAP translates most input parameters, such as model components, geometric information, etc., to a common reference "generic" representation, ignoring only code-related options and switches. SNAP translates the model from this "generic" format to a "code specific" format at "export time", as shown in Figure 4. In the future, users will be encouraged to enter physical information, and let the SNAP translate this generic information to code specific information as much as possible.

This design has numerous advantages. One advantage is that whenever a new code is added to SNAP, only translators to and from the new code to the generic mode are needed. These translators (actually C++ Classes) need to be developed to handle the unique features and procedures for input and output processing for all of the specific codes to be supported. These code specific functions translate to and from "code specific" input deck formats to SNAP "generic" information on import and export of analytical models. Without the generic

intermediate step, the addition of a new code would require the addition of translators to and from each of the existing analysis codes.

Database Storage

SNAP will read and write all model information to/from a Structured Query Language (SQL) Database Management System (DBMS), such as Sybase or Oracle. SNAP will use an ODBC (Open Database Connectivity) driver to allow the code to connect to many SQL database clients. An OBDC intermediary will allow greater flexibility by shielding the application from the differences between Database Management Systems.

The SNAP DBMS will contain libraries of components ("Templates") typically used in nuclear power plants to facilitate the modeling development process. These libraries of component templates and design parameters needed for the online expert systems will also be stored in DBMS files. Information contained in the DBMS will be used to support both input preparation and post-calculation analysis of results.

SNAP communicates with the DBMS through a separate access process which will run on the DBMS server. The main SNAP modules which contain the iconic interface and the expert guides ("Wizards") will run on each user's workstation (the "clients"). It will be possible to co-locate the client and server processes on the same workstation, however, best performance will be available if multiple processors are available.

SNAP will be capable of keyword search and retrieval of component parameters, such as pipes, pumps, valves, fuel designs, and steam generators from other reactor models previously entered in the DBMS.

Component Navigator

In addition to the iconic interface the SNAP will allow the user to view and change properties of the components through an alternate interface tool, referred to as the "component navigator". Upon initiation, the component navigator tool opens a separate window to display the top level component categories contained in the model.

These component groups can be "expanded" when clicked on by the mouse. The expanded view shows all the members of the component group. The expansion process continues until the lowest level is reached, the user may view and/or change information for a single item or groups of items. For example, the initial view may contain volumes and junctions. If volumes are expanded, the new view will may contain single volumes and time dependent volumes. Single volumes can be expanded to produce a list of all the single volumes and their properties.

Runtime and Postprocessor

The Runtime and Postprocessor modules of SNAP, which are currently in the design stage, will provide methods to control job execution, monitor the status of jobs in progress, and view and/or plot results of code calculations. Initially, information will be available as x-y plots for the variables associated with each component. Plans for later versions of SNAP call for more visualization aides, such as animation tools, instrumentation mimics, and three dimensional plotting.

Programming Language and Operating System Requirements

The SNAP was designed as an object-oriented method and constructed in a modular fashion. The preprocessor was developed in C++ for the UNIX/X/Motif environment since this system is supported on all engineering workstations that run the NRC safety analysis codes of interest. X/Motif system libraries include many of the programming tools needed for the SNAP development. Other tools include the Standard Template Library (STL), a library donated to the public domain by SGI and HP, and proposed for adoption in the draft ASNI standard for C++, and wxWindows, a free, publicly available cross-platform GUI toolkit developed by the Artificial Intelligence Institute of the University of Edinboro. (*http://www.aiai.ed.ac.uk/*). UNIX shell script, GNU configure and PERL will be used for installation and linking scripts. HTML documents and web browsers may be included for the help system. These tools are all system and platform independent. All machine dependencies are identified and isolated in a specific group of functions.

Conclusions

SNAP preprocessor should greatly improve ease-of-use and reduce the potential for user error and the "User Effect", e.g., the undesirable variation in the results of RELAP5 and TRAC-P input models constructed by different users. SNAP has tools to insure data integrity, retrievability, and traceability. SNAP should significantly improve consistency in modeling approach and assumptions. Over time, use of the SNAP will result in an improvement in the quality of the developmental assessment database and more accurate simulations using RELAP5 and other codes.

SNAP gives the NRC safety analysis community (NRC staff, consultants and contractors, university researchers, and staff from participating international organizations) a common graphical/iconic user interface, capable of handling a wide variety of pre- and post-processing tasks related to analysis of nuclear reactor and containment accident and transients.

Table 1. Components To Be Included In SNAP Libraries

Basic Components	Composite Components
Single Volume	PWR Core/15x15, 16x16, 17x17
Time Dependent Volume	PWR Reactor Vessel
Single Junction	PWR Pressurizer
Time Dependent Junction	PWR U-Tube Steam Generator
Pipe	PWR Once Through Steam Generator*
Annulus	AP600 Core Makeup Tanks*
Branch	AP600 IRWST*
Separator	BWR Core/7x7, 8x8, 9x9, 10x10*
Jet Mixer*	BWR Separator/Dryer*
Turbine*	BWR Jet Pump*
ECC Mixer*	BWR Jet Pump Reactor Vessel*
Valves	BWR Non-Jet Pump Reactor Vessel*
Pumps	BWR Water Level Controller*
Multiple Junction	BWR Pressure Controller*
Accumulators	BWR Recirculation Pump Speed*
Breaks	Heat Exchanger*
	BWR MK I Containment*
Heat Structures	BWR MK II Containment*
Kinetics Data*	BWR MK III Containment*
Trips and Controllers	
	Large Dry Containment*
	AP600 Containment*

* Future Items

Table 2. Expert Guides ("Wizards")

Preprocessor

Centrifugal Pump
Control Systems*
Heat Conductor
Heat Exchanger*
Jet Pump*
Steam Generator*
Nodalization
Reactor Kinetics*
Separator*
Valve*

Runtime

Initialization*

* Future Items

THREE-DIMENSIONAL SPATIAL KINETICS FOR COUPLED THERMAL-HYDRAULIC/NEUTRONICS SYSTEMS ANALYSIS CODES

T. Downar **D. Barber**
School of Nuclear Engineering
Purdue University

D. Ebert **V. Mousseau**
Division of Systems Technology
Office of Regulatory Research
US NRC

Abstract

A three-dimensional spatial kinetics capability within a thermal-hydraulic systems code provides an analysis tool that more correctly describes the core physics during reactor transients which experience significant variations in the neutron flux distribution. This paper addresses some of the important issues related to the development of a spatial kinetics capability in a coupled systems code. These issues include the development of methods for coupling a systems thermal-hydraulics and spatial kinetics code, the development of advanced spatial kinetics methods for more accurately modeling a reactor core with advanced fuel types, and a discussion of the issues related to the application of high performance computing to the coupled code.

I. INTRODUCTION

A three-dimensional spatial kinetics capability within a thermal-hydraulic systems analysis code is important for reactor transients which experience significant variations in the core power distribution. In both the U.S. and abroad, there has been considerable progress in recent years in the development of coupled thermal-hydraulics/spatial kinetics systems codes. This work has been motivated primarily by the prospects of improved nuclear power economics and reactor safety.

Recent initiatives to reduce plant operating costs at U.S. nuclear utilities include further extensions of the fuel cycle length and plans to increase the plant power rating. As an example, this past year GPU nuclear analyzed the Main Steam Line Break transient in support of their uprate analysis of the Three Mile Island plant using TRAC-PF1 coupled with a three-dimensional spatial kinetics code [Ivanov, 1996]. The analysis with point kinetics predicted a return to power during the transient, whereas there was no return to power predicted when the same analysis was performed with three-dimensional spatial kinetics.

This provides strong evidence that best estimate analysis of certain reactor safety events with a coupled code can provide increased safety margin through reductions in the conservatisms incurred with lower dimensional kinetics calculations [Diamond, 1996]. Furthmore, transients such as BWR flow stabilities and PWR boron dilution events, can only be properly analyzed with multi-dimensional spatial kinetics. This paper will address some of the important issues related to the development of a spatial kinetics capability in a coupled systems code.

II. METHODS FOR COUPLING THERMAL-HYDRAULICS AND NEUTRONICS CODES

One of the most basic issues regarding the implementation of spatial kinetics into a thermal-hydraulics systems code is the **integration method** which determines whether the core simulator should have thermal-hydraulics separate from the systems code. In an "external" integration the core simulator provides its own TH and the systems and core simulator codes are coupled at the inlet and outlet plenums. Conversely, in an "internal" integration the systems code solves the temperature and fluid fields for both the core and ex-core. There have been implementations of spatial kinetics in systems codes using both methods [Hagrman, 1997, Judd, 1996, Paulsen, 1996]. Perhaps the greatest disadvantage of the external integration is that generally, the thermal-hydraulic models in systems codes are more complete and detailed than those of core simulators. Some limitations on phenomena such as counter current flow or high void content could possibly be encountered in the core simulator and not the systems code. For this and other reasons, the work here was based on an internal integration approach.

The most general approach for coupling a thermal-hydraulics and a spatial kinetics code would be to use a separate "interface" code for transferring data between calculational modules that is independent of the specific structure of the thermal-hydraulics or spatial kinetics module. This would minimize the modifications necessary when using different TH or neutronics modules. An interface code was designed based on this concept and is described briefly in the following section.

II.A. General Design

The implementation of a thermal-hydraulic/neutronic interface for the reactor vessel is depicted in Figure 1. The design is based on an internal integration approach in which the neutronics code solves for

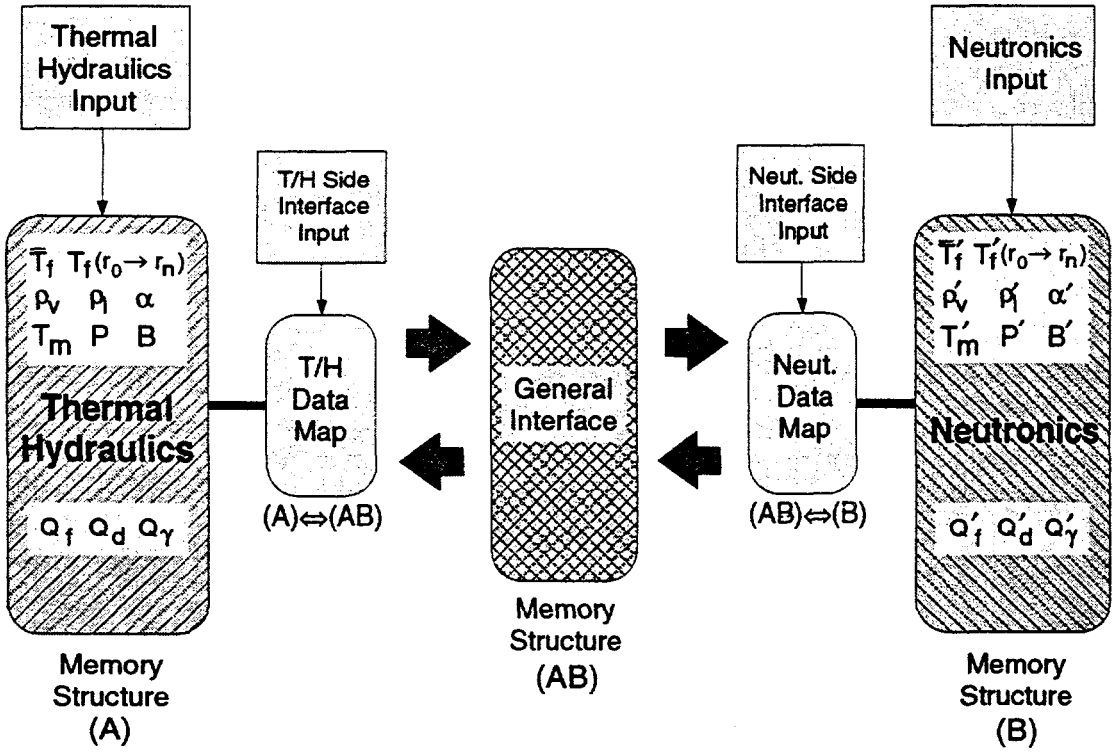

Figure 1. Diagram of Interface Implementation

the neutron behavior only, and the system code solves for both the system and the core thermal-hydraulics. This concept utilizes independent input processing for the thermal-hydraulic and neutronic codes, which insures that modifications to existing input decks will be minimal. In addition, the input for the interface is processed separately by the code-specific mapping routines. This provides flexibility for inputting code-specific mapping and calculational control information separately.

The basic design of the interface includes an immutable generalized interface unit which provides the mapping of property data between thermal-hydraulic ***zones***, neutronic ***nodes***, and heat structure (HS) ***components***. Memory mapping between the interface module and the thermal-hydraulic and neutronic modules is accomplished with customized mapping routines which are specific to the thermal-hydraulic and neutronic codes used in the coupled code system.

II.B. Variable Transfer

The coupling of the spatial kinetics module to the thermal-hydraulics module is accomplished via the incorporation of thermal-hydraulic feedback effects into the cross sections. For an explicit coupling approach, the fuel and moderator temperature and moderator density from the end of the time step, along with all reference temperatures and densities, are passed through the interface to the spatial kinetics module. The coupling of the thermal-hydraulics module to the spatial kinetics module is achieved with the node-averaged *fission*, *decay*, and *gamma powers* (Q_f , Q_d , Q_γ), which are used in the heat transfer calculation. For transient control in the coupled code, *time-dependent information*, such as the logic for control rod movement and the time step data, are also passed through the interface.

In an effort to fully generalize the treatment of the fuel temperature feedback, the space- dependent *average fuel temperature* ($\bar{T}_f$) and *radial fuel temperature profile* in the pin ($T_f(r_0 \text{-} r_n)$) are transferred to the interface, as shown in Figure 1. This provides flexibility for the spatial kinetics codes which vary in the method of calculating doppler temperature for feedback into the cross sections. To describe the radial profile, space will be allocated for ten fuel pin temperatures. The treatment of the moderator density feedback is generalized to allow the use of mixture density and/or void density correlations. This is accomplished by transferring the space-dependent *liquid and vapor densities*, along with the *void fraction* (ρ_l , ρ_v , α), from the thermal-hydraulics module to the interface. Finally, the space-dependent *moderator temperature* (T_m), *pressure* (P), and *Boron concentration* (B) are also passed through the interface.

II.C. Design of the Mapping Function

The mapping function between thermal-hydraulic zones and neutronic nodes used by the General Interface is represented as a single permutation matrix, $\boldsymbol{P}$, composed of variable-dependent submatrices of either size n-by-m or size n-by-m', where n is the number of neutronic nodes, m is the number of thermal-hydraulic zones, and m' is the number of heat structure components. In practice, a different submatrix is employed for each of the variables passed from the thermal-hydraulics code to allow for separate averaging techniques. The submatrices for the fuel temperatures, which correspond to heat structure components, have dimension n-by-m', and the six submatrices for the moderator temperature and pressure, moderator liquid and vapor densities, void fraction, and boron concentration have dimension n-by-m. In an effort to ease the input requirements, the user should be given the option of assigning an input permutation submatrix to multiple state variables. In addition, the mapping function between neutronic nodes and heat structure components is represented as a single permutation matrix, $\boldsymbol{P'}$, composed of three submatrices of size m'-by-n for each power (i.e. fission, decay, and gamma), and a submatrix of size m-by-n, which will be used to map a fraction of the node-wise gamma powers directly to the thermal-hydraulic zones.

The use of the permutation matrix, P, in mapping zone-wise and component-wise thermal-hydraulic variables to neutronic nodes is given by:

$$P\, x^{HS+TH} = x^{Neut.} \; ; \; x^{HS+TH} \in \mathbb{R}^{11m'+6m} \; , \; x^{Neut.} \in \mathbb{R}^{17n} \tag{1}$$

where the dimension of the vector, x^{HS+TH}, is based on 11 component-wise variables (i.e., 1 average fuel temperature and 10 fuel temperatures describing the radial pin profile) and the six zone-wise variables ($6m$). Conversely, the use of the permutation matrix, P', in mapping neutronic nodal powers to corresponding heat structure components and thermal-hydraulic zones is given by:

$$P'\, x^{Neut.} = x^{HS+TH} \; ; \; x^{HS+TH} \in \mathbb{R}^{3m'+m} \; , \; x^{Neut.} \in \mathbb{R}^{4n} \tag{2}$$

where x^{HS+TH} consists of fission, decay, and gamma powers for the heat structures ($3m'$) plus the fractional gamma power for the thermal-hydraulic zones (m) to account for direct heating to the coolant.

The form of these permutation matrices is easily demonstrated with the simple thermal-hydraulic and neutronic planar nodalizations shown in Figure 2.

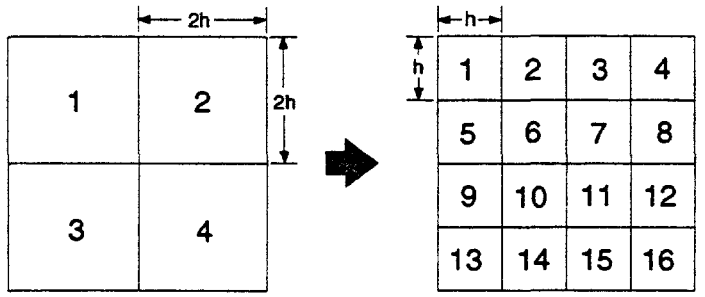

Figure 2. Cartesian Thermal-Hydraulic to Neutronic Mapping

The corresponding permutation for a single thermal-hydraulic variable would be,

$$x^{Neut.} = \begin{bmatrix} 1&0&0&0 \\ 1&0&0&0 \\ 0&1&0&0 \\ 0&1&0&0 \\ 1&0&0&0 \\ 1&0&0&0 \\ 0&1&0&0 \\ 0&1&0&0 \\ 0&0&1&0 \\ 0&0&1&0 \\ 0&0&0&1 \\ 0&0&0&1 \\ 0&0&1&0 \\ 0&0&1&0 \\ 0&0&0&1 \\ 0&0&0&1 \end{bmatrix} x^{TH} \; ; \quad \begin{matrix} x^{Neut.} \in \mathbb{R}^{16} \\ x^{TH} \in \mathbb{R}^{4} \end{matrix} \tag{3}$$

This example assumes that the boundaries of the thermal-hydraulic zones and neutronic nodes are congruent, which is the case for most practical applications. However, when the boundaries are not congruent, resulting in overlapping thermal-hydraulic and neutronic regions, the user is responsible for incorporating appropriate weighting factors (e.g., volume fractions) into the permutation matrix. The general form of the permutation matrix is now given as:

$$P_i = \sum_{k(i)\in j} w^i_{k(i)}\, e_{k(i)} \;\; ; \;\; e_{k(i)} \in \mathbb{R}^{1,j} \; ; \;\; for \; i=1\cdots n \tag{4}$$

where $k(i)$ designates the thermal-hydraulic zone(s) belonging to neutronic node i, and $e_{k(i)}$ is a row vector with 1 in the $k(i)$-th position, and zeros everywhere else. The dimension represented by j corresponds to either m or m', depending on the variable-dependent submatrix. The weighting factor, $w^i_{k(i)}$, is a scalar which represents the weighting of the $k(i)$-th thermal-hydraulic zone on the i-th neutronic node. The restriction on the weighting factor, is given as

$$\sum_{k(i)\in m} w^i_{k(i)} = 1.0 \tag{5}$$

It should be noted that for P, Eq. (5) represents the summation of elements in *row* i, and for P', Eq. (5) represents the summation of elements in *column* i. An example which would require the use of weighting factors is shown in Figure 3, where a planar mapping from cylindrical thermal-hydraulic coordinates to cartesian neutronic coordinates is required.

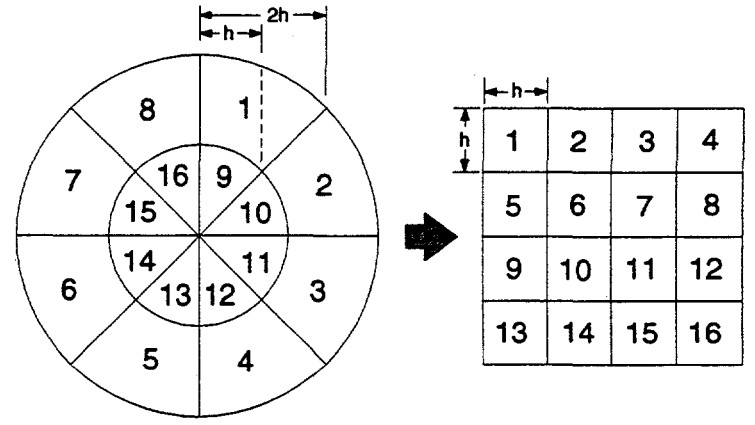

Figure 3. Cylindrical to Cartesian Mapping

By taking the weighting factors for this example to be simple area fractions, the permutation submatrix for a single thermal-hydraulic variable would be of the form:

$$P = \begin{bmatrix}
0 & 0 & 0 & 0 & 0 & 0 & 0.5 & 0.5 & 0 & 0 & 0 & 0 & 0 & 0 & 0 & 0 \\
0 & 0 & 0 & 0 & 0 & 0 & 0 & 0.7146 & 0 & 0 & 0 & 0 & 0 & 0 & 0 & 0.2854 \\
0.7146 & 0 & 0 & 0 & 0 & 0 & 0 & 0 & 0.2854 & 0 & 0 & 0 & 0 & 0 & 0 & 0 \\
0.5 & 0.5 & 0 & 0 & 0 & 0 & 0 & 0 & 0 & 0 & 0 & 0 & 0 & 0 & 0 & 0 \\
0 & 0 & 0 & 0 & 0 & 0 & 0.7146 & 0 & 0 & 0 & 0 & 0 & 0 & 0 & 0.2854 & 0 \\
0 & 0 & 0 & 0 & 0 & 0 & 0 & 0 & 0 & 0 & 0 & 0 & 0 & 0 & 0.5 & 0.5 \\
0 & 0 & 0 & 0 & 0 & 0 & 0 & 0 & 0.5 & 0.5 & 0 & 0 & 0 & 0 & 0 & 0 \\
0 & 0.7146 & 0 & 0 & 0 & 0 & 0 & 0 & 0 & 0.2854 & 0 & 0 & 0 & 0 & 0 & 0 \\
0 & 0 & 0 & 0 & 0 & 0.7146 & 0 & 0 & 0 & 0 & 0 & 0 & 0 & 0.2854 & 0 & 0 \\
0 & 0 & 0 & 0 & 0 & 0 & 0 & 0 & 0 & 0 & 0 & 0 & 0.5 & 0.5 & 0 & 0 \\
0 & 0 & 0 & 0 & 0 & 0 & 0 & 0 & 0 & 0 & 0.5 & 0.5 & 0 & 0 & 0 & 0 \\
0 & 0 & 0.7146 & 0 & 0 & 0 & 0 & 0 & 0 & 0 & 0.2854 & 0 & 0 & 0 & 0 & 0 \\
0 & 0 & 0 & 0 & 0.5 & 0.5 & 0 & 0 & 0 & 0 & 0 & 0 & 0 & 0 & 0 & 0 \\
0 & 0 & 0 & 0 & 0.7146 & 0 & 0 & 0 & 0 & 0 & 0 & 0 & 0.2854 & 0 & 0 & 0 \\
0 & 0 & 0 & 0.7146 & 0 & 0 & 0 & 0 & 0 & 0 & 0 & 0.2854 & 0 & 0 & 0 & 0 \\
0 & 0 & 0.5 & 0.5 & 0 & 0 & 0 & 0 & 0 & 0 & 0 & 0 & 0 & 0 & 0 & 0
\end{bmatrix} \quad (6)$$

II.D. Calculational Control

The coupling of the thermal-hydraulic, neutronic, and interface modules can be accomplished with either a single process for the entire coupled code, or independent processes for each module. The **single process** option requires an additional driver routine which controls the flow into each module, as depicted in Figure 4. This strategy also requires modification to both the thermal-hydraulic and neutronic codes to set the entry points into each module.

For the single process approach shown in Figure 4, the driver controls the flow to the input processing units of the individual modules. Once the permutation matrices have been processed in the code-specific data mapping routines, these matrices are passed to the initialization unit of the General Interface routine to be stored for future use. Following the input processing, the neutronics code calculates the steady-state power distribution based on the initial thermal-hydraulic condition of the core. Using this power distribution, either the steady-state initialization or the transient calculation can be performed.

The decision of whether to use point or spatial kinetics during the steady-state initialization is left to the user. However, to avoid a non-initialized core condition, the kinetics used in the transient calculation should be consistent with that employed for the steady-state initialization.

The flow through the interface routines is the same regardless of whether a steady-state or transient calculation is being performed. As shown in Figure 4, this flow proceeds in two directions, dictated by the integer flag *imapdir*. Specifically, when *imapdir* equals zero, the flow is coming from the thermal-hydraulic module, and when imapdir equals one, the flow is coming from the neutronics module. This implies that each of the three modules, the T/H Data Map, General Interface, and Neutronics Data Map, contains two functional units corresponding to the mapping direction.

When *imapdir* equals zero in the code-specific T/H Data Map, the corresponding variables contained in the T/H data structure, denoted by (*A*) in Figure 1, are mapped to the data structure used by the General Interface, denoted by (*AB*). This requires that the T/H Data Map routine contain information on the memory structure utilized by the thermal-hydraulic and General Interface modules. In addition, this routine performs conversion of the data to the units utilized by the interface. Conversely, when *imapdir* equals one, and the flow is proceeding from the General Interface to the thermal-hydraulic module, the component powers for the heat structures are placed in the thermal-hydraulic array structure, and all necessary unit conversion and normalization is performed.

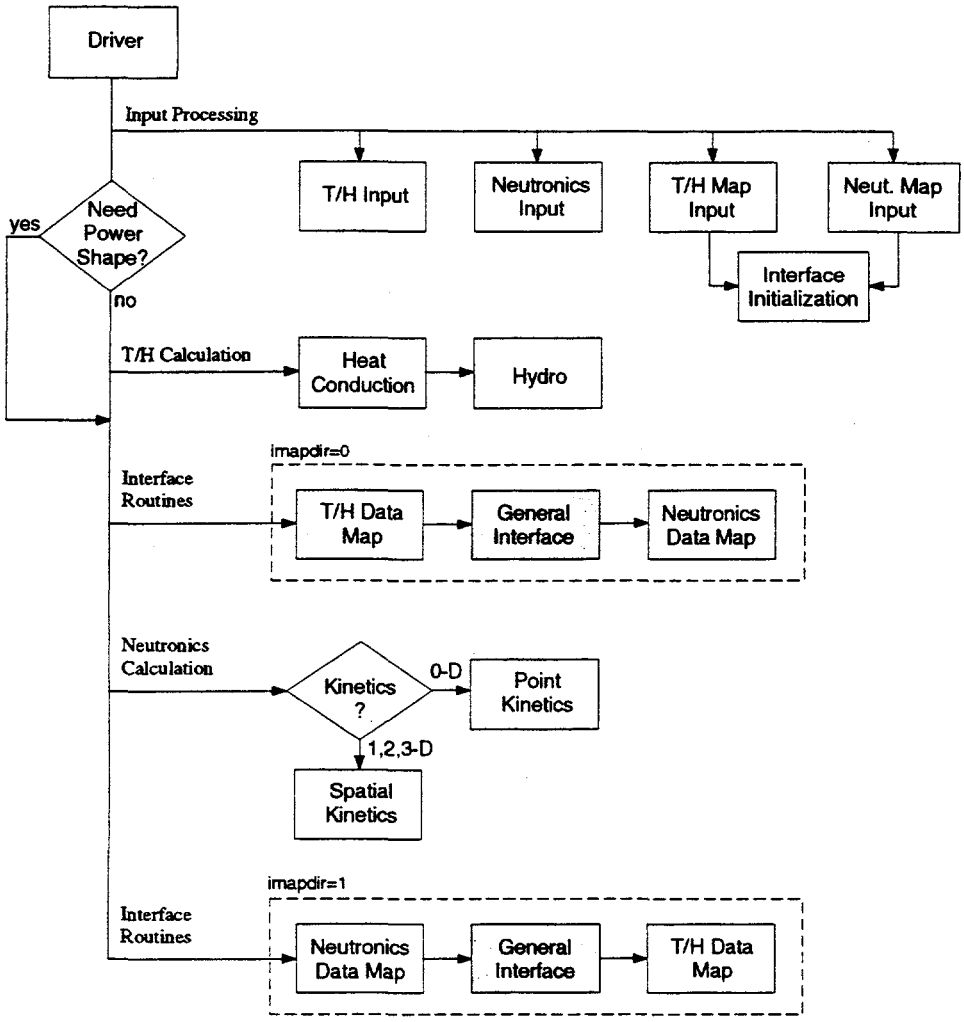

Figure 4. Single Process Flow Control for Coupled Code

The General Interface module performs all data mapping from both thermal-hydraulic zones and heat structure components to neutronic nodes when *imapdir* equals zero. When *imapdir* equals one, all neutronic powers are mapped from neutronic nodes to heat structure components and thermal-hydraulic zones. As described in Section II.C, this results in one matrix-vector multiply for each mapping direction.

When *imapdir* equals zero in the code-specific Neutronics Data Map routine, all thermal- hydraulic data that is stored in the interface array is mapped to the data structure utilized by the neutronics module (*B*), which implies that this routine contains the memory structure for both the general interface and the neutronics code. This functional unit also performs all necessary unit conversion for consistency in the neutronics routines. Finally, when *imapdir* equals one, the nodal powers are mapped to the interface data structure, and any required normalization and unit conversion is performed.

For a **multiple process** coupling approach, the flow through the interface routines is roughly the same. The difference is seen in the management of entry points in the interface routines, where the coupling of the modules is now achieved by the use of either the Parallel Virtual Machine (PVM) or Message Passing Interface (MPI) packages. Specifically, the entry points into and out of the interface would be controlled

with *sends* and *receives*, as shown in Figure 5. This coupling strategy appears to be more efficient than the single process approach, however the user would be required to maintain an additional coding package for either PVM or MPI.

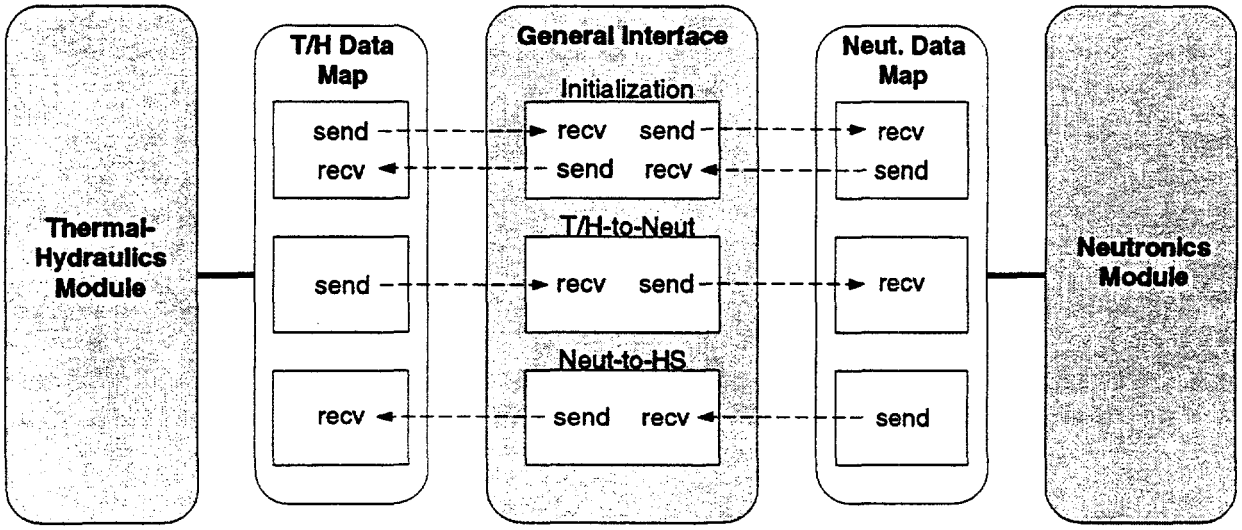

Figure 5. Coupling with PVM or MPI

II.E. Time Step Control

Time step control for the coupled code is handled by the T/H Data Map routine and is based on the control information passed through the interface from the thermal-hydraulics and neutronics modules. Because of the difference in characteristic times between the thermal-hydraulics and neutronics during severe transients (e.g. super-prompt critical events or events involving a phasic transition), the flexibility exists to allow either module to subcycle the time step. However, following a time step subcycling, it is necessary to re-synchronize the time steps, and this is controlled by the T/H Data Map routine. In addition, if the time step size sent to the neutronics is such that the change in the core condition is too large, logic control is provided for the neutronics code to reject the time step data, and request a new thermal-hydraulic calculation at a finer time step size.

II.F. Interface Summary

The coupling of a thermal-hydraulics and neutronics code described here is accomplished with the use of an immutable generalized interface unit. To accommodate this design, it is necessary to utilize code-specific data mapping routines for both the thermal-hydraulics and neutronics codes. This allows the two modules to be coupled with only minor programming modifications to each.

The interface design employs a basic internal coupling strategy, and the calculational control is explicit in nature. However, the design is flexible enough to accommodate more sophisticated thermal-hydraulic/neutronic coupling strategies (e.g. implicit, semi-implicit). In addition, this coupled code will have the capability to accurately predict a wide range of transient scenarios, including BWR stability problems.

III. ADVANCED SPATIAL KINETICS METHODS

Among the issues in the use of spatial kinetics in a systems code is the ability of existing neutronics methods to model accurately the physics behavior of new fuel types. During the past few years there has been some concern about limitations with existing methods [Taiwo, 1997], particularly for applications such as the use of mixed oxide (MOX) fuel with standard UO_2 fuel at high burnups in LWRs. Severe flux gradients which are difficult to model can occur between a fuel assembly with standard uranium fuel and one with high concentrations of plutonium. Part of the solution to this modeling problem was to develop a nodal coupling technique to replace the existing polynomial expansion method. The following section discusses the development of the analytic nodal coupling technique within the framework of the nonlinear nodal method.

III.A Advanced Nodal Methods

Nonlinear nodal methods [Smith, 1984] in which higher order coupling is imposed at the level of a "two-node" problem have been widely used to solve static and transient reactor physics problems. A well known advantage of the nonlinear method is the reduction in computer storage that results from not having to save the expansion coefficients. However, an equally important advantage is a reduction in execution time because the solution variables in the global CMFD portion of the algorithm are only the node averaged fluxes for which efficient solution schemes have been developed. Furthermore, the two-node portion of the algorithm lends itself naturally to parallel solution and when solved in conjunction with a parallel CMFD method, significant execution time reductions can be achieved with the nonlinear nodal method on multiprocessors [Joo, 1996].

One of principal issues in the implementation of the nonlinear nodal method is the interface current technique used in the two node coupling relation. As discussed in the review by Lawrence [Lawrence, 1986], two principal classes of transverse integrated methods have been developed over the years, the polynomial and the analytic methods. In the polynomial nodal expansion methods (NEM), the transverse integrated equations are solved by approximating the transverse integrated flux with a truncated polynomial expansion, whereas in the analytic nodal methods (ANM) an analytic solution is used in some portion of the procedure to solve the transverse integrated equations.

During the 1980's, most neutronics codes based on the nonlinear nodal method employed a two node coupling based on NEM [Turinsky, 1994, Aviles, 1993, Smith, 1992]. This was largely because of its superior computational efficiency compared to ANM. In recent years there has been interest in "semi-analytic" two node kernels that employ a combination of NEM and ANM [Esser, 1993]. These efforts have been motivated in part by concerns with NEM for applications such as the use of mixed oxide (MOX) fuel in LWRs. In the following section some of the fundamental issues of accuracy and computational efficiency regarding the use of NEM and ANM two node kernels are discussed.

III.A.1 The Analytic Nodal Method

The distribution of the neutron flux in a reactor can be obtained by solving the multi-group neutron diffusion equation. Since the primary focus of the work here is the Light Water Reactor the following development will be simplified by using two energy groups. Using standard notations and the eigenvalue defined as $\lambda = 1/k_{eff}$, the discretized form of the multi-group diffusion equation can be written for node "m" in terms of the node-average flux (ϕ_g^m) and the surface average net currents (J_{gw}):

$$\sum_{w=xyz} \zeta_w^m \, (J_{1w}^{m+} - J_{1w}^{m-}) + \Sigma_{r1}^m \, \phi_{1m} = \lambda \sum_{g=1}^{2} \nu \Sigma_{fg}^m \, \phi_g^m \qquad (6)$$

$$\sum_{w=xyz} \zeta_w^m \, (J_{2w}^{m+} - J_{2w}^{m-}) + \Sigma_{r2}^m \, \phi_{2m} = \Sigma_{12}^m \, \phi_1^m$$

where the plus and minus superscripts of J represent the positive and negative side surfaces of the node m in the w-direction and ζ_w^m is the surface area to volume ratio. In the nonlinear nodal method, the net surface averaged current on the interface is represented by the following equation in terms of the node average fluxes of the left and right nodes:

$$J_g = D_g^F \, (\phi_g^r - \phi_g^l) + D_g^N \, (\phi_g^r + \phi_g^l), \qquad (7)$$

where D_g^F is the coupling coefficient determined by the finite difference approximation of the neutron current and D_g^N is the correction term to the coupling coefficient, which is determined by the two-node nodal solutions and is updated during the nonlinear iteration. The method used here to update the coupling coefficient is described in section III.A.2.

The derivation of nodal kernels for the nonlinear nodal method begins with the transverse-integrated form of the neutron diffusion equation. The static transverse integrated one dimensional two group diffusion equations can be written:

$$-D_1 \frac{d^2 \phi_1}{dx^2} + \Sigma_{r1} \phi_1 - \lambda \, (\nu \Sigma_{f1} \phi_1 + \nu \Sigma_{f2} \phi_2) = - L_1(x) \qquad (8)$$

$$-D_2 \frac{d^2 \phi_2}{dx^2} + \Sigma_{r2} \phi_2 - \Sigma_{12} \phi_1 = - L_2(x)$$

where: $L_g(x) \equiv \frac{1}{h_y} \, [J_{gy}^+(x) - J_{gy}^-(x)] + \frac{1}{h_z} \, [J_{gz}^+(x) - J_{gz}^-(x)]$.

Similar equations are written for the y and z directions.

The objective of a two-node kernel for the nonlinear nodal method is to express the current at the interface of two nodes in terms of the group constants, the node average fluxes, and the transverse leakages. The NEM and ANM coupling relations differ primarily in the functions used to describe the one-dimensional fluxes. The following sections outline the development of the ANM and NEM coupling kernels.

Henry and Smith [Smith, 1979] used analytic solutions of the transverse integrated equations as the basis for the Analytic Nodal Method (ANM). The general development of the ANM for the core wide implementation is somewhat complicated and is given in [Smith, 1979]. A simpler formulation based on the work of Henry and Smith can be derived for the two node problem and is outlined below.

Homogeneous Solution

The analytic solution of the transverse integrated equations is constructed from separate homogeneous and particular solutions. The homogeneous solution begins by finding the eigenvalues of the homogeneous differential equations. Let:

$$- \frac{d^2 \phi_g^H}{d x^2} = B^2 \phi_g^H \qquad (9)$$

which can be used in Eq.(8) to provide the homogeneous system:

$$\begin{bmatrix} D_1 B^2 + \Sigma_{r1} - \lambda \nu \Sigma_{f1} & -\lambda \nu \Sigma f 2 \\ -\Sigma_{12} & D_2 B^2 + \Sigma_{r2} \end{bmatrix} \begin{bmatrix} \phi_1^H \\ \phi_2^H \end{bmatrix} = \begin{bmatrix} 0 \\ 0 \end{bmatrix} \tag{10}$$

For a nontrivial solution, the determinant of the coefficient matrix must be zero, or:

$$(B^2)^2 + \left[\frac{\Sigma_{r2}}{D_2} \frac{\Sigma_{r1}}{D_1} - \lambda \frac{\nu \Sigma_{f1}}{D_1} \right] B^2 + \left[1 - \lambda k_\infty \frac{\Sigma_{r1}}{D_1} \frac{\Sigma_{r2}}{D_2} \right] = 0 \tag{11}$$

where: $k_\infty = \dfrac{\nu \Sigma_{f1}}{\Sigma_{r1}} + \dfrac{\Sigma_{12}}{\Sigma_{r1}} \dfrac{\nu \Sigma_{f2}}{\Sigma_{r2}}$.

The roots of Eq.(11) depend on the sign of B^2 and can be written as:

$$\hat{\kappa}^2 \equiv b \left[-1 + \sqrt{1 - \frac{c}{b^2}} \right], \text{ and } \hat{\mu}^2 \equiv b \left[-1 - \sqrt{1 - \frac{c}{b^2}} \right] \tag{12}$$

where the constant b is the coefficient of the first order term divided by two and the constant c is the zeroth order term in Eq.(11). The second root, $\hat{\mu}^2$, is always negative, but the first root, $\hat{\kappa}^2$, can be either positive or negative depending on whether the node k_∞ is greater or less than the k_{eff} ($= 1/\lambda$) of the reactor.

By defining,

$$\kappa \equiv \sqrt{|\kappa^2|}, \text{ and } \mu \equiv \sqrt{|\mu^2|}$$

the four roots of Eq.(11) can be obtained as:

$$\kappa_\pm = \pm \begin{cases} \kappa & , \lambda k_\infty > 1 \\ 0 & , \lambda k_\infty = 1 \\ i\kappa & , \lambda k_\infty < 1 \end{cases}, \qquad \text{and } \mu_\pm = \pm i\mu \tag{13}$$

The homogeneous solution can then be constructed by solving Eq.(9) with the four roots, or equivalently using trigonometric and hyperbolic functions:

$$\begin{bmatrix} \phi_1^H(x) \\ \phi_2^H(x) \end{bmatrix} = \begin{bmatrix} r & s \\ 1 & 1 \end{bmatrix} \begin{bmatrix} a_{21} sn(\kappa x) + a_{22} cn(\kappa x) \\ a_{23} sn(\mu x) + a_{24} cn(\mu x) \end{bmatrix} \tag{14}$$

where

$$sn\,(j, \lambda k_\infty, x) = \begin{cases} \sin(x), & \text{if } \lambda k_\infty > 1 \text{ and } j = 0 \\ x, & \text{if } \lambda k_\infty = 1 \text{ and } j = 0 \\ \sinh(x), & \textit{otherwise} \end{cases}$$

and a similar expression can we written for cn, with $cn(j, \lambda k_\infty, x) = 1$ when $\lambda k_\infty = 1$. The fast to thermal flux ratios r and s are given by:

$$r \equiv \frac{a_{11}}{a_{21}} = \frac{a_{12}}{a_{22}} = \frac{\pm D_2 \kappa^2 + \Sigma_{r2}}{\Sigma_{12}} \begin{cases} + \text{ if } \lambda k_\infty > 1 \\ - \text{ otherwise} \end{cases} \tag{15}$$

and

$$s \equiv \frac{a_{13}}{a_{23}} = \frac{a_{14}}{a_{24}} = \frac{-D_2 \mu^2 + \Sigma_{r2}}{\Sigma_{12}}$$

Particular Solution

For a given quadratic transverse leakage approximation:

$$L_g(x) = \overline{L_g} + b_{g1} f_1(\xi) + b_{g2} f_2(\xi) \tag{16}$$

where $\xi \equiv x/h_x$, the particular solution would have the form:

$$\phi_g^P(x) = \sum_{n=0}^{4} c_{gn} f_n(\xi) \tag{17}$$

where the polynomial basis functions are given in [Turinsky, 1994].

The constants are determined by substituting Eq.(17) into Eq.(8) and equating coefficients of the same order terms. The results are shown here only for the case with $k_{eff} \neq k_\infty$, for which the expansion coefficients corresponding to the third and fourth order terms are zero: $c_{g3} = c_{g4} = 0$ (These coefficients are nonzero when $k_{eff} = k_\infty$). The other three expansion coefficients are given by the following equations:

$$\begin{bmatrix} \Sigma_{r1} - \lambda\nu\Sigma_{f1} & -\lambda\nu\Sigma_{f2} \\ -\Sigma_{12} & \Sigma_{r2} \end{bmatrix} \begin{bmatrix} c_{1p} \\ c_{2p} \end{bmatrix} = \begin{bmatrix} -b_{1p} \\ -b_{2p} \end{bmatrix}, \quad p = 0,1,2 \tag{18}$$

where b_{g1} and b_{g2} are given by Eq.(16) and b_{g0} is a function of $\overline{L_g}$ and D_g. Thus the particular solution is determined solely by the transverse leakage and is not affected by the any other constraints.

Final Solution

For the case of $k_{eff} \neq k_\infty$, the final solution becomes:

$$\begin{bmatrix} \phi_1(x) \\ \phi_2(x) \end{bmatrix} = \begin{bmatrix} \phi_1^H(x) + \phi_1^P(x) \\ \phi_2^H(x) + \phi_2^P(x) \end{bmatrix} = \begin{bmatrix} r & s \\ 1 & 1 \end{bmatrix} \begin{bmatrix} a_{21} sn(\kappa x) + a_{22} cn(\kappa x) \\ a_{23} sn(\mu x) + a_{24} cn(\mu x) \end{bmatrix} + \begin{bmatrix} c_{10} + c_{11} f_1(\xi) + c_{12} f_2(\xi) \\ c_{20} + c_{21} f_1(\xi) + c_{22} f_2(\xi) \end{bmatrix} \tag{19}$$

Since the coefficients in the particular solution are determined by Eq.(18), there are now four unknown coefficients in each node and the eight unknown coefficients in the two-node problem are determined using constraints on the node average flux (4) and the continuity of flux (2) and current (2) at the two-node interface. This results in two 2x2 and a 4x4 system for each interface which must be solved in addition to the three 2x2 systems of Eq.(18).

III.A.2 The NEM Coupling Kernel

In the Nodal Expansion Method (NEM), the one-dimensional fluxes in Eq.(8) are described by fourth order polynomial expansion functions. The detailed derivation of the NEM equations are provided in several references and the exact form used in the work here is given in [Turinsky, 1994]. For every interface, the NEM two node problem results in a system of 16 equations for the 2 energy group problem. It is interesting to note that the size of the linear systems to be solved for the NEM two node problem are larger than for the ANM two-node problem. However, as will be seen in the applications, the computational time for the NEM two-node solution is smaller.

The implementation of the NEM or ANM two node kernels within the framework of the nonlinear nodal method is straightforward and has been described in numerous references [Sutton, 1996]. The corrective nodal coupling coefficient, D_g^N, in Eq.(7) is updated during the course of the nonlinear iteration using the interface current determined from the two node solutions and the relationship given in Eq.(7). The nonlinear iteration is terminated when a user specified tolerance is achieved on the eigenvalue, fission source, and doppler temperature. Both an ANM and NEM coupling kernel were implemented within the framework of the nonlinear nodal method using the PARCS code [Joo, 1997] and tested using various benchmark problems. In the following section, results of these benchmarks are presented and analyzed.

III.B ASSESSMENT OF NEM AND ANM KERNELS

The ANM and NEM kernels were applied to several NEACRP benchmark problems using the spatial kinetics code PARCS [Joo, 1997]. Comparisons of ANM and NEM are first provided for one and two dimensional NEACRP L336 MOX benchmark problems. A detailed analysis is then performed for one of the configurations of the NEACRP PWR spatial kinetics benchmark.

III.B.1 Benchmark Problem Descriptions

The primary objective of NEACRP benchmark L336 [Lefebvre, 1991] is to compare different techniques for the fine flux distribution assessment within assemblies. The core model of these problems is two-dimensional and consists of both UO-2 and MOX fuel elements which poses a severe test for coarse mesh nodal methods. Among the five core configurations the most challenging configuration is reproduced in Figure 6 and will be analyzed here. Each fuel assembly is 21.42 cm in width and various mesh sizes are used in the analysis. A one-dimensional variation of the two-dimensional problem (also shown in Figure 6) was also performed because it demonstrates some of the important issues regarding ANM, NEM, and the transverse leakage approximation.

The second benchmark problem analyzed here is the 3-D NEACRP PWR spatial kinetics problem [Finnemann, 1992] which has been widely analyzed by modern nodal codes. The results of the eigenvalue and transient problems for the first two core configurations will be analyzed here: a hot zero power (HZP) case A1, and a hot full power (HFP) case A2. The boron concentrations used for the A1 and A2 problems are 561.3 and 1159.4 ppm, respectively. Several radial meshes were examined, keeping the axial mesh nodalization constant as given in the specifications (18 planes). All benchmark problems here were executed on a single processor of the Sun UltraSparc II computer with double precision arithmetic and the eigenvalue calculation is accelerated using the Weilandt shift method.

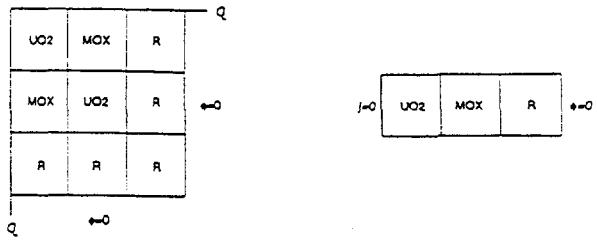

Figure 6 Configurations of the NEACRP L-336 Case 5 and the 1D Benchmark Problem

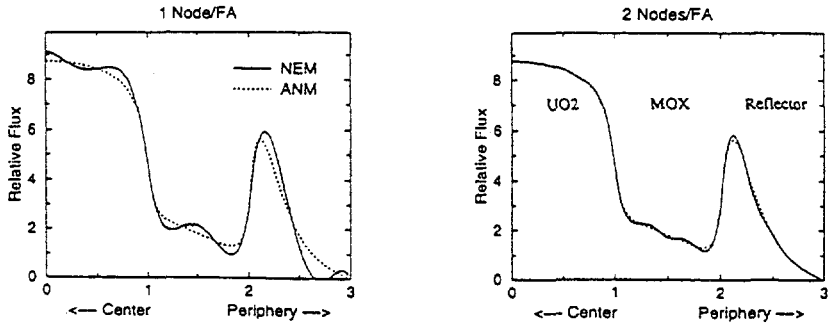

Figure 7 Comparison of the Thermal Flux Distributions Obtained for the 1D MOX Problem

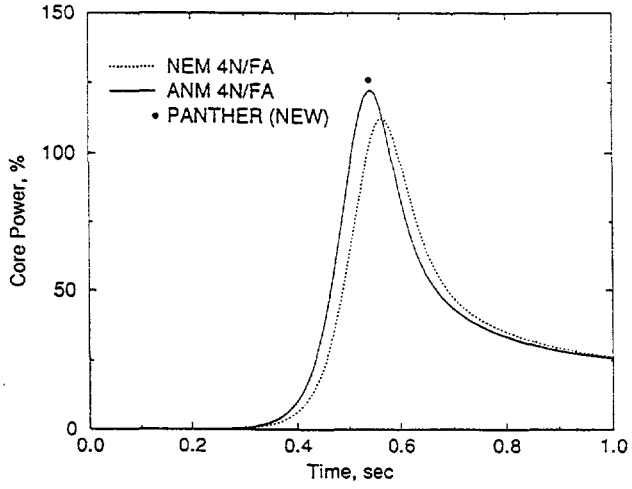

Figure 8 Comparison of ANM and NEM Solutions to NEACRP Problem A1

III.B.2 One-Dimensional MOX Benchmark Analysis

The primary purpose of the one-dimensional benchmark problem was to analyze the performance of ANM and NEM without introducing the transverse leakage approximation and the assembly discontinuity factors (ADFs). The one dimensional thermal flux for this problem is shown in Figure 7 for discretizations of 1 and 2 nodes per assembly. Because there is no transverse leakage in this problem, the ANM solution is exact and as shown in Figure 7, the solutions for ANM are identical for the both nodal discretizations. The plots in Figure 7 clearly demonstrate shortcomings in the NEM solution. The quartic polynomial basis functions introduce a nonphysical curvature in the one-dimensional flux and for the 1 node assembly NEM calculation, the 1-D flux becomes negative in the reflector region. The maximum error in the intranodal flux for the 1 and 2 node(s)/assembly NEM cases is 27% and 12%, respectively. This distortion of the 1-D flux also leads to a significant misprediction of the interface currents and consequently the NEM solution underestimates the k-effective by 178, 36, and 2 pcm for the 1, 2, and 4 node solutions, respectively.

III.B.3 Two-Dimensional MOX Benchmark Analysis

The MOX NEACRP L336 problem was then analyzed in two dimensions as specified in the original problem statement and results are shown in Table 1. The ANM and NEM solutions were performed with increasingly finer nodalizations (i.e. 1, 4, 16, and 64 mesh per fuel assembly). As indicated in Table 1, both solutions converge to the same k_{eff}, however, the ANM solution converges much sooner with errors of only 6 pcm in the k_{eff} and 0.1% in the relative power distribution (RPD) for the most commonly used 4 node/assembly mesh. The error in the NEM solution for the same nodalization are about 50 pcm and 0.7% for the k_{eff} and RPD, respectively. For the 1 and 4 node(s)/assembly cases, the NEM solution error is consistently an order of magnitude larger than the ANM error.

This problem also provides insight regarding the validity of the transverse leakage approximation, since the errors in the ANM coarse mesh solutions are attributable directly to the quadratic transverse leakage approximation. Some researchers have questioned the accuracy of the transverse leakage approximation for problems with severe gradients such as experienced in MOX fueled cores. However, as shown in Table 1, the error introduced in the ANM solution by the transverse leakage approximation is only 6 and 24 pcm for the 4 and 1 node/assembly cases, respectively.

III.B.4 Three-Dimensional NEACRP Benchmark Analysis

The final NEACRP benchmark problem used in this analysis is more practical since it is based on an actual 3-D PWR core. The results of the eigenvalue calculation at HZP conditions is shown in Table 2 for three different spatial meshings. Similar to the results of NEACRP MOX problem, both ANM and NEM provide essentially the same solution with a fine spatial mesh (i.e. 16 nodes/assembly), however ANM provides a more accurate solution than NEM at the coarser mesh of 1 and 4 nodes/assembly which are typically used in reactor analysis. The results of the radial power distribution comparison are also shown in Table 2. The maximum RPD error of NEM is about 2% for 4 nodes/assembly and it occurs at the periphery of the core. There is a global tilt in the NEM solution such that the flux in the peripheral region is overpredicted and the flux in the central region is underpredicted. This is primarily because NEM can potentially cause large errors at the fuel-reflector interface where steep flux gradients are most likely to occur. Although errors in the NEM solution are not large, the misprediction of the flux distribution can significantly impact the prediction of core transient behavior for events such as a control rod ejection from hot, zero power conditions.

Table 1. Comparison of the ANM and NEM Results for the NEACRP L-336 Case 5 Problem

Nodes/FA	k_{eff} Error pcm		Error in Relative Assembly Power, %					
			Central UO_2		MOX		Peripheral UO_2	
	NEM	ANM	NEM	ANM	NEM	ANM	NEM	ANM
1	-254	24	4.05	-0.03	-1.81	0.12	-0.42	-0.20
4	-49	6	0.71	-0.08	-0.33	0.08	-0.04	-0.08
16	-2	2	0.03	-0.02	-0.01	0.03	-0.01	-0.02
64	-0	0	0.01	0.00	0.00	0.00	0.00	0.00
Reference[a]	0.93813		1.3569		1.0830		0.4770	

[a] Based on homogenized assembly cross sections and discontinuity factors.

Table 2. Comparison of the NEM/ANM Eigenvalue Calculations for two NEACRP Cases

Case	A1 (561.3 ppm)					A2 (1259.4 ppm)				
Nodes/FA	1		4		16	1		4		16
Method	NEM	ANM	NEM	ANM	NEM	NEM	ANM	NEM	ANM	NEM
k_{eff} Error[a], pcm	83	43	14	3	1	140	57	37	4	6
Pos. RPD Err., %	-3.88	-2.02	-0.72	-0.16	-0.07	-3.39	-1.32	-0.92	-0.10	-0.16
Neg. RPD Err., %	9.07	4.25	1.96	0.40	0.23	5.98	1.63	1.85	0.13	0.33
CPU Time, sec	NEM		ANM		Ratio	NEM		ANM		Ratio
Nodal Calc. Only	1.73		2.09		1.21	1.97		2.39		1.21
Total	4.41		4.78		1.08	4.77		5.18		1.09

[a] The 16 Nodes/FA case is taken as the reference. The reference k_{eff}'s are 0.99996 and 1.00023 for A1 and A2, respectively.

Results are also shown in Table 2 for the eigenvalue calculation of problem A2 which is at hot, full power conditions. As indicated, the discrepancies in the ANM and NEM prediction of the k_{eff} and the relative power distribution are larger than A1 for both the 1 and 4 node/assembly calculations. This is because the the power in the peripheral assemblies is higher in A2 which accentuates limitations in NEM in predicting the flux at the core/reflector interface. The execution times for the ANM and NEM solutions to the eigenvalue problems are also compared are in Table 2. As indicated, the ANM two-node portion of the nonlinear nodal calculation for the eigenvalue problem exceeds the NEM time by 20% because the evaluation of the transcendental functions is more computationally expensive than polynomials. However, because the "two-node" calculation is not a large fraction of the overall solution time, the total execution time for the nonlinear nodal calculation with ANM exceeds the total time with NEM by only about 10%.

Finally, the results of the transient solution of problem A1 are shown in Figure 8. As indicated the transient solution with the ANM coupling kernel more closely matches the reference solution than the solution with the NEM coupling kernel. The nodal expansion method overpredicts the flux at the core/reflector interface which leads to an underprediction of the power in the core interior. This leads to an underestimatation of the central rod worth and therefore as shown in Figure 8, the NEM solution underpredicts the core power response for problem A1 by about 8% and mispredicts the peak time by about 20ms. Conversely, the ANM predictions closely match the reference solution and reinforce the decision to replace NEM with the ANM two node kernel.

IV. HIGH PERFORMANCE COMPUTING

The computational burden can be large for a coupled spatial kinetics and thermal-hydraulics calculation. While the numerical methods described in the previous section are highly efficient, it is important to take advantage of recent advances in high performance computing to minimize the execution times for the coupled field calculations.

The concept of gaining performance improvement through utilization of multiprocessors is very alluring since it appears to be a simple and cost effective manner of achieving additional performance. However, the incorporation of parallelization in a production computer code can impact many aspects of the code, such as data structures and numerical solution algorithms. Furthermore, the parallel computer architecture can influence the type of parallelization used in a code [Liebrock, 1996]. Parallel computing on a distributed memory machine or on a network of workstations requires explicit message passing between processors and therefore high efficiencies are achievable only with coarse grain parallelism. Conversely, parallel processing on a Shared Address Space (SAS) does not require message passing since processors can share common memory address space. High efficiencies on an SAS can be achieved with finer granularity than distributed memory implementations.

Generally, the constructs necessary to achieve the best multiprocessing performance are different for shared and distributed memory machines. Standard implementations of message passing libraries such as MPI and PVM are generally less efficient on shared memory machines since communication between processors must proceed through the TCP/IP protocol. However, good parallel performance with message passing on shared address space machines was demonstrated with the CATHARE code and its implementation on the SGI multiprocessor workstation [Bestion, 1996, Brun, 1996]. Generally, the best parallel performance on shared address space machines is achieved with threads programming in which some local variables may be defined, but the majority of memory address space remains global. This is an area for continuing research which will impact the choice of parallel methods used in the coupled

code.

Spatial reactor kinetics has much in common with TH computations with respect to parallel computing. Similar to solving the state equations for a control volume in a thermal hydraulics code, a substantial fraction of the grind time in a spatial kinetics code is associated with evaluating cross-sections at local node conditions. This implies a substantial fraction of the code is naturally parallel. It is more problematic to introduce parallelization into the sparse matrix iterative solver. Fortunately, the applied mathematics community has done substantial work in this area. Preconditioned Krylov iterative solvers lend themselves easily to domain decomposition techniques which have been shown to be efficient for the neutron diffusion problem and such a method has been incorporated into the PARCS spatial kinetics code [Joo, 1996]. While some results have been reported with the parallelization of spatial kinetics codes [Joo, 1996], current efforts are underway to perform consistent demonstrations of both threaded and message passing versions of the PARCS code on both shared and distributed memory machines.

V. CODE VALIDATION

The choice of benchmarks is important for code **validation and verification**. Numerous computational and experimental benchmarks are available to provide sufficient breadth and depth to the assessment of both the spatial kinetics methods and the coupled reactor systems / spatial kinetics capability. One of the important benchmarks for assessment of the coupled code is the recently proposed OECD/NEA Steam Line Break benchmark developed by Penn State University [Ivanov, 1996]. This problem will include three-dimensional core modeling for both neutronics and thermal-hydraulics and is particularly timely because best estimate analysis of the main steam line break event can play an important role in future utility initiatives such as cycle length extension and plant uprate. Similar benchmark problems for the Boiling Water Reactor are currently being assessed and include the OECD BWR Stability benchmark which employs measured data from the Ringhals 1 reactor [Lefvert, 1996].

VI. SUMMARY AND CONCLUSIONS

There are strong economic and safety incentives for pursuing the integration of full physics, three-dimensional spatial kinetics in reactor systems codes. While the coupled field calculation is currently computationally feasible, important issues remain concerning the method of integrating separate thermal-hydraulics and spatial kinetics codes, as well as the adequacy of current spatial kinetics methods in light of the recent use of mixed oxide and high burnup fuels.

This paper described the development of a general interface method for coupling a systems thermal-hydraulics and spatial kinetics code and the development of advanced spatial kinetics methods for more accurately modeling a reactor core with advanced fuel types. Also, some of the issues concerning the application of high performance computing to the coupled code were briefly addressed.

In general, the technology appears to be available today for the nuclear industry to realize the economic and safety benefits from reactor analysis with coupled spatial kinetics and thermal-hydraulic field calculations.

Acknowledgement

The authors would like to acknowledge the valuable contributions of Jennifer Uhle and Undine Shoop in the preliminary discussions of the code interface design.

VII. REFERENCES

1. Aviles, B., "Development of a Variable Time Step Transient NEM Code: SPANDEX," Trans. Am. Nucl. Soc., 68, 1993, 425-427.
2. Diamond, D., "Multidimensional Reactor Kinetics Modeling," Proceedings of OECD/CSNI Workshop on Transient Thermal/Hydraulics and Neutronic Code Requirements, Annapolis, MD, 5-8 November, 1996.
3. Esser, P. and Smith, K., "A Semianalytic Two-Group Nodal Model for Simulate-3," Trans. Am. Nucl. Soc., 69, 1993, 220-222.
4. Finnemann, H., NEACRP-L-335 (Revision 1) January, 1992 and H. Finnemann, et al., "Results of LWR Core Transient Benchmarks," Pro. Int. Conf. Math. and Supercomp. in Nuc. App., Vol. 2, 243, Karlsruhe, April, 1993.
5. Finnemann, H., et al., "Interface Current Techniques for Multidimensional Reactor Calculations," Atomkernenerie, 30, 123-128.
6. Hagrman, D., et al., "SIMULATE-3K RETRAN-3D Coupled Systems Calculations," Proceedings on Advances in Nuclear Fuel Management II, Mrytle Beach, SC, March, 1997.
7. Ivanov, K., et al., "TMI MSLB Analysis Using TRAC-PF-1 Coupled With Three-Dimensional Kinetics," ASME-JSME 4th Int. Conf. on Nuclear Eng., No. 10389C, pp. 33-40, 1996.
8. Ivanov, K., et al., "OECD PWR MSLB Benchmark Specifications," DRAFT, PSU/OECD/NRC, MSLB Benchmark Workshop, April 23-25, 1997, Washington, D.C.
9. Joo, H., et al., "PARCS: A Multi-dimensional Two-Group Reactor Kinetics Code Based on the Nonlinear Analytic Nodal Method," Purdue University, PU/NE-97-4, August 1997.
10. Joo, H., et al., Pro. Int. Reactor Physics Conf., Mito, Japan, September 1996.
11. Joo, H. and T. Downar, "Incomplete Domain Decomposition Preconditioning for Reactor Spatial Kinetics," *Nuclear Science and Engineering*, July 1996.
12. Judd, J., et al., "High-Fidelity Real Time Simulation with RELAP5/NESTLE," ANS Trans., Vol. 75, 321-322, Nov. 1996.
13. Lawrence, R., "Progress in Nodal Methods for the Solution of the Neutron Diffusion and Transport Equations," Progress in Nuclear Energy, Vol. 17, No. 1, pp. 271-301, 1986.

14. Lefebvre, J., et al., "Benchmark Calculations of Power Distributions within Assemblies," NEACRP-L-336, October 1991.

15. Lefvert, T., "Ringhalls 1 Stability Benchmark," NEA Nuclear Science Committee, NEA/NSC/DOC(96)22, November,1996.

16. Liebrock, L., "Parallelization and Automatic Data Distribution for Nuclear Reactor Simulations," Proceedings of OECD/CSNI Workshop on Transient Thermal/Hydraulics and Neutronic Code Requirements, Annapolis, MD, November 5-8, 1996.

17. Paulsen, M., et al., "Application of RETRAN-3D for Nuclear Power Plant Transient Analysis," ANS Trans., Vol. 75, 325-327, Nov. 1996.

18. Smith, K., "An Analytic Nodal Method for Solving the 2-Group, Multi- dimensional, Static and Transient Neutron Diffusion Equations," Nuc. Eng. Thesis, Dept. of Nuc. Eng., MIT, 1979.

19. Smith, K., "SIMULATE-3 Methodology." Studsvik Report SOA-92/02, 1992.

20. Smith, K., "Nodal Method Storage Reduction by Nonlinear Iteration," Trans. Am. Nucl. Soc., 44, 1984, 265-266.

21. Sutton, T. and Aviles, B., "Diffusion Theory Methods for Spatial Kinetics Calculations," Progress in Nuclear Energy, Vol 30, pp. 119-182, 1996.

22. Taiwo, T., et al., "Need for Higher-Order Polynomial Basis for Polynomial Nodal Methods Employed in LWR Calculations," ANS Trans. Vol. 76, Orlando, FL, June, 1997.

23. Turinsky, P., et al., "NESTLE: A Few-Group Neutron Diffusion Equation Solver," North Carolina State University, Electric Power Research Center, June 1994.

Interfacial Area Measurement and Transport Equation

M. Ishii and Q. Wu
School of Nuclear Engineering
Purdue University
West Lafayette, IN 47907-1290

Abstract

The importance of the interfacial area in two-phase flow formulation is explained. The use of the interfacial area transport equation to model the dynamic structure changes in two-phase flow is proposed. This transport equation requires several constitutive relations to model the fluid particle coalescence and disintegration. The local interfacial area and interfacial velocity measurements are reviewed. The use of these measurements for the development of the interfacial constitutive relations is discussed.

I. Introduction

Two-phase flow is characterized by the existence of the interface between phases and discontinuities of properties associated with them. The internal structures of two-phase flow are identified by two-phase flow regimes. Various transfer mechanisms between the mixture and wall as well as between phases strongly depend on these two-phase flow regimes. This leads to the use of flow regime dependent correlations and closure equations together with appropriate flow regime transition criteria. The basic structure of flow can be characterized by two fundamental geometrical parameters. These are the void fraction and interfacial area concentration. The void fraction expresses the phase distribution whereas the interfacial area describes available area for the interfacial transfer of mass, momentum and energy. Therefore, an accurate knowledge of these parameters is necessary for any two-phase flow analysis. This fact can be further substantiated with respect to two-phase flow formulation.

In order to analyze the thermal-hydraulic behavior of two-phase flow, various formulations such as the homogeneous flow model, drift-flux mode (Ishii, 1975; Zuber and Findley, 1965; Wallis, 1969; Ishii, 1977; and Chawla and Ishii, 1980), and two-fluid model (Ishii, 1975; Vernier and Delhaye, 1968; Kocamustafaogullari, 1971; Boure, 1978; Ishii and Mishima, 1980; Chawla and Ishii, 1978; Delhaye and Achard, 1977; Sha et al., 1983) have been proposed. As suggested by Ishii and Kocamustafaogullari (1982), among these models the two-fluid formulation can be considered the most accurate model because of its detailed treatment of the two-phase interactions at the interface.

The two-fluid model is formulated by considering each phase separately in terms of two sets of conservation equations which govern the balance of mass, momentum and energy of each phase. These balance equations represent the macroscopic fields of each phase and are obtained from proper averaging methods. Since the macroscopic fields of each phase are not independent of the other phase, the phase interaction terms which couple the transport of mass, momentum and energy of each phase appear in the field equations. It is expected that the two-fluid model can predict mechanical and thermal nonequilibrium between phases accurately. However, it is noted that the interfacial transfer terms should be modeled accurately for the two-fluid model to be useful. In the present state of the arts, the closure relations for these interfacial terms are the weakest link in the two-fluid model. The difficulties arise due

to the complicated transfer mechanisms at the interfaces coupled with the motion and geometry of the interfaces. Furthermore, the closure relations should be modeled by macroscopic variables based on proper averaging.

In general, the interfacial transfer terms are given in terms of the interfacial area concentration a_i and driving force (Ishii, 1975; Ishii and Mishima, 1980) as

$$\text{(Interfacial Transfer Term)} \sim a_i \times \text{(Driving Force)}$$

The area concentration defined as the interfacial area per unit volume of the mixture characterizes the first order geometrical effects; therefore, it must be related to the internal flow-pattern of the two-phase flow field. On the other hand, the driving forces for the interfacial transport characterize the local transport mechanisms such as the turbulence, molecular transport properties and driving potentials. In two-phase flow systems, the void fraction and interfacial area concentration are two of the most important geometrical parameters. The interfacial area concentration should be specified by a closure relations, or by a transport equation. The above formulation indicates that the knowledge of the interfacial area concentration and the interfacial structure classified as the flow regimes are indispensable in the two-fluid model.

Various transfer mechanisms between phases depend on the two-phase flow interfacial structures. The geometrical effects of interfacial structure can be modeled in a macroscopic field by the interfacial area and void fraction. In order to take into account the effect of entrance, developing flow, coalescence and disintegration, and wall nucleation source, an introduction of the interfacial area transport equation is recommended (Ishii, 1975; Kocamustafaogullari and Ishii, 1995).

The development of the source and sink terms in the transport equation heavily depends on understanding the mechanisms of particle coalescence and disintegration as well as accurate experimental data for the changes in the interfacial area in two-phase flow. The paper discusses the local measurement methods of interfacial area and the development of the area transport equation.

II. Importance of Modelling Interfacial Area Transport

In nuclear reactor systems, numerous practical thermal hydraulic phenomena are dominated by the interfacial transport. In Table 1, a brief summary of the LOCA PIRT is presented for different types of nuclear reactors in the United States, with the emphasis on some SBLOCA cases relevant to interfacial transport processes. Lack of proper mechanistic models for the interfacial transfer processes, these identified phenomena are not well understood, and thus become the major concern in the current two-phase flow modeling practice. Generally, the interfacial transfer rates can be considered as the product of the interfacial flux and the available interfacial area. The difficulty arises in the treatment of the interfacial area concentration because of the complicated interfacial structure, especially when subjected to two-phase flow regime transitions. In the present system codes like RELAP5 and TRAC, the interfacial area concentration is given by empirical correlations that are based on two-phase flow regimes and regime transition criteria (Kelly, 1997; Mortensen, 1995).

(1) The flow regime transition criteria are algebraic relations for steady-state, fully developed flows. They do not fully reflect the true dynamic nature of changes in the interfacial structure. Hence the effects of the entrance and developing flow cannot be taken into account correctly, nor the gradual transition between regimes.

(2) The method based on the flow regime transition criteria is a two-step method which requires the regime dependent closure relations for the interfacial area effects. The compound errors from the transition criteria and area correlations can be very significant.
(3) The existing flow regime dependent correlations and criteria are valid in limited parameter ranges for certain specific operational conditions. Most of them are obtained from simple experiments and phenomenological models. Often the scale effects of geometry and fluid properties are not taken into account correctly. When applied to high pressure steam-water transients, these models may cause significant discrepancies, artificial discontinuities and numerical instability.

These shortcomings have also been noticed by some European researchers (Grand, 1997; Städtke, 1997) in developing their next generation codes for reactor safety analysis. Their representative proposals related to the study of interfacial area transport phenomena are listed in Table 2.

In reality, flow regime transition in two-phase flow is a gradual evolutional process, rather than sudden switching of flow characteristics, except for certain transitions such as CHF. For instance, the transition from bubbly flow to slug flow occurs mainly due to agglomeration and coalescence of smaller bubbles into cap bubbles. Once a cap bubble is formed, further coalescences follow in the wake region of a cap bubble. These observations indicate that for good mechanistic modelling, it is necessary to study bubble coalescence and breakup criteria. The latter will give information on the maximum bubble size and bubble size distribution. These are important in the formation of a link between the flow-pattern transition and the characteristics of the interfacial structure, such as interfacial area concentration and void fraction distributions. In terms of heat transfer, the nucleation phenomena are important.

Since the flow regime dependent models have the inherent shortcomings, for complicated transient reactor thermal hydraulics analysis, it is recommended to use an appropriate model which can characterize changes in the interfacial structure. Based on the current development in multi-phase studies, most researchers agree that interfacial area transport equation is a rational choice for such a purpose. This model, the interfacial area transport equation in principle, closely models the two-phase flow evolution across flow regime transition boundaries, and thus prevent artificial discontinuities. The elimination of artificial bifurcation in a mathematical formulation of the of the two-phase model is highly desirable in terms of computational efficiency and numerical stability. It is expected that the interfacial area transport equation can expand the current capability of the two-fluid model from both scientific and practical point of view. The effective use of a similar approach has been demonstrated for the analysis of a choked flow by Riznic and Ishii (1989). They used the bubble number transport equation, wall nucleation source based on the nucleation site density model and bubble expansion model which has a memory of where bubbles are generated.

With the interfacial area transport equation, the two-fluid model is formulated based on seven balance equations. In this model, the change in the interfacial area is dynamically predicted by the transport equation. This equation, which has a built-in mechanism to predict the development of the interfacial structure, can properly propagate the boundary condition downstream in terms of the available surface area. Therefore, the artificial bifurcation related to the flow regime transition in the conventional model can be eliminated. However, in order to develop a proper transport equation, the closure relation for the source and sink terms should also be established. To address the feasibility of the approach, the

Table 1. LOCA PIRT relevant to interfacial area transport process for different types of reactors

High Ranked Phenomena from AP600 SBLOCA PIRT (NUREG/CR-6541)		
COMPONENTS	PHENOMENA	TRANSIENT PHASE
Reactor Core	Flashing	Short term
	Subcooling Margin	Short term
	Two-phase Mixture Level	Short term and long term
Cold Leg	PBL to Cold Leg Tee Phase Separation	Short Term
Hot Leg	Phase Separation in Tees	Short Term
Upper Head/UP	Two-phase Level in Upper Plenum	Long Term
High Ranked Phenomena from B&W SBLOCA PIRT (NUREG/CR-5818)		
COMPONENTS	PHENOMENA	TRANSIENT PHASE
Vessel	Natural Circulation	Blowdown, Natural Circulation and Loss of Natural Circulation
Steam Generator	Natural Circulation	Natural Circulation
U-Bend	Phase Separation in U-Bend	Natural Circulation
High Ranked Phenomena from BWR-5 ATWS PIRT (NUREG/CR-6200)		
PHENOMENA	TRANSIENT PHASE	
Two-phase Flow Dynamics	Power Oscillation Growth and Suppression Pool Heat-up	
Phase Change Process	Power Oscillation Growth and Suppression Pool Heat-up	
Pressure Drop	Power Oscillation Growth and Suppression Pool Heat-up	
Energy Transfer	Power Oscillation Growth and Suppression Pool Heat-up	
High Ranked Phenomena from SBWR LBLOCA PIRT (BNL)[2]		
COMPONENTS	PHENOMENA	
Core (Vertical Channel and Rods)	Low Pressure Boiling	
	Flashing and Void Fraction Distribution	
Chimney (Vertical Channel)	Flashing, Level, and Void Fraction Distribution	
Downcomer (Annulus)	Flashing, Level, and Void Fraction Distribution	
Lower Plenum (Vessel)	Flashing, Level, and Void Fraction Distribution	
Suppression Pool	Direct Contact Condensation with NC gases	
ICS (Vertical Downflow Tube Submerged in Pool)	Direct Contact Condensation with NC gases	
PCCS (Vertical Downflow Tube Submerged in Pool)	Direct Contact Condensation with NC gases	
Near Break Pipe (Horizontal and Vertical)	Liquid Entrainment from Separator or Downcomer	

Table 2. Studies relevant to interfacial area transport process proposed by Grand and Städtke

Thermal Hydraulic Modeling Requirements (D. Grand, DRN/DTP, CEA-Grenoble, France)[5]		
PROPOSED TOPICS	PHENOMENA	MODEL NEEDS
• CHF in Core • 2Φ Heat Transfer in SG • Erosion in Condenser • LBLOCA Oscillatory Reflooding	• Nucleate Boiling. • 2Φ natural circulation • Particle deposition • Droplet induced erosion • Inverted annular flow • Droplet formation during quenching • Droplet Entrainment and re-entrainment	• Multifield models. • Interfacial area transport. • Interface velocity. • Source/sink terms for interfacial area transport. • Interfacial area evolution in tee pipe conjunction.

Future Perspective of Thermal Hydraulic Codes for LWR Safety Analysis(H. Städtke, CEUJRC, Italy)[6]	
POTENTIAL IMPROVEMENTS	PHENOMENA
Multifield Model for Specific Flow Regimes	• Two-phase Annular-mist Flow • Two-phase Intermittent Flow
Interfacial Area Transport Equation	• Interfacial Transfer Phenomena • Flow Regime Transition

following proposed theoretical and experimental studies outline the overall strategy of the development of the interfacial area transport equation. Eventually, the research will include not only the development of the interfacial area transport equation but also a pilot code which can demonstrate these advantages mentioned above.

II. Two-fluid Model and Interfacial Transfer

A three-dimensional two-fluid model has been obtained by using temporal or statistical averaging, Ishii (1975). For most practical applications, the model developed by Ishii can be simplified to the following forms:

Continuity Equation

$$\frac{\partial \alpha_k \rho_k}{\partial t} + \nabla \cdot \left(\alpha_k \rho_k \vec{v}_k\right) = \Gamma_k \tag{1}$$

Momentum Equation

$$\frac{\partial \alpha_k \rho_k \vec{v}_k}{\partial t} + \nabla \cdot \left(\alpha_k \rho_k \vec{v}_k \vec{v}_k\right) = -\alpha_k \nabla p_k + \nabla \cdot \alpha_k \left(\tau_k + \tau_k^t\right)$$

$$+ \alpha_k \rho_k \vec{g} + \vec{v}_{ki} \Gamma_k + \vec{M}_{ik} - \nabla \alpha_k \cdot \tau_i \tag{2}$$

Enthalpy Energy Equation

$$\frac{\partial \alpha_k \rho_k H_k}{\partial t} + \nabla \cdot \left(\alpha_k \rho_k H_k \vec{v}_k\right) = -\nabla \cdot \alpha_k x$$
$$\left(q_k + q_k^t\right) + \alpha_k \frac{D_k}{Dt} p_k + H_{ki} \Gamma_k + \frac{q_{ki}''}{L_s} + \Phi_k \tag{3}$$

Here Γ_k, M_{ik}, τ_i, q_{ki}'', Φ_k are the mass generation rate, generalized interfacial drag, interfacial shear stress, interfacial heat flux, and dissipation, respectively. The subscript k denotes k phase, and i stands for the value at the interface. α_k, ρ_k, v_k, p_k and H_k denote the void fraction, density, velocity, pressure and enthalpy of k phase, whereas τ_k, τ_k^t, q_k, q_k^t and g stand for average viscous stress, turbulent stress, mean conduction heat flux, turbulent heat flux and acceleration due to gravity. H_{ki} is the enthalpy of kth phase at the interface, thus it may be assumed to be the saturation enthalpy for most cases. L_s denotes the length scale at the interface, and $1/L_s$ has the physical meaning of the interfacial area per unit volume a_i. Thus,

$$\frac{1}{L_s} = a_i = \frac{Interfacial\ Area}{Mixture\ Volume} \tag{4}$$

The above field equations indicate that several interfacial transfer terms appear on the right-hand sides of the equations. Since these interfacial transfer terms also should obey the balance laws at the interface, interfacial transfer conditions could be obtained from an average of the local jump conditions (Ishii, 1975). They are given by

$$\sum_k \Gamma_k = 0 \tag{5}$$

$$\sum_k \vec{M}_{ik} = 0 \tag{6}$$

$$\sum_k \left(\Gamma_k H_{ki} + q_{ki}''/L_s\right) = 0 \tag{7}$$

Therefore, closure relations, for M_{ik}, q''_g/L_s, and q''_f/L_s are necessary for the interfacial transfer terms. The enthalpy interfacial transfer condition indicates that specifying the heat flux at the interface for both phases is equivalent to the closure relation for Γ_k if the mechanical-energy transfer terms can be neglected (Ishii, 1975). This aspect greatly simplifies the development of the closure relations for interfacial transfer terms.

By introducing the mean mass transfer per unit area, m_k, defined by

$$\Gamma_k \equiv a_i m_k \tag{8}$$

the interfacial energy transfer term in Eq. (3) can be rewritten as

$$\Gamma_k H_{ki} + \frac{q_{ki}''}{L_s} = a_i \left(m_k H_{ki} + q_{ki}''\right) \tag{9}$$

The heat flux at the interface should be modeled using the driving force or the potential for an energy transfer. Thus,

$$q''_{ki} = h_{ki}\left(T_i - T_k\right) \tag{10}$$

where T_i and T_k are the interfacial and bulk temperatures based on the mean enthalpy and h_{ki} is the interfacial heat transfer coefficient. A similar treatment of the interfacial momentum transfer term is also possible (Ishii and Mishima, 1980). In view of the above, the importance of the interfacial area concentration, a_i, in developing closure relation for this term is evident. The interfacial transfer terms are now expressed as a product of the interfacial area and the driving force. It is essential to make a conceptual distinction between the effects of these two parameters. The interfacial transfer of mass, momentum and energy increases with an interfacial-area concentration toward the mechanical and thermal equilibrium.

IV. Local Measurement of Interfacial Area

A theoretical study carried out at Argonne National Laboratory (Kataoka et al., 1984) gives a method of using electrical resistance probe technique to measure the local interfacial area concentration. Using this theoretically supported method Kataoka et al. (1984, 1986, 1984), Wang and Kocamustafaogullari (1990) and Revankar and Ishii (1992) studied the local interfacial area concentration in air-water bubbly flow using a two-sensor resistivity probe. When using the two-sensor probe to measure the local interfacial area, it is necessary to make certain statistical assumption on bubble parameters. The ANL study (Kataoka et al., 1984) also proposed a four-sensor probe to measure the local interfacial area concentration. This method using a four-sensor probe does not require any statistical assumptions. Multi-sensor probes have been used by Burgess and Calderbank (1975, 1975a, 1975b), and Buchholz et al. (1983) to measure the bubble size and velocity in bubble columns of interest to chemical engineering. These authors used the average void fraction and the mean Sauter diameter measured from these multisensor resistivity probe to find the average interfacial area concentration in bubbly flow. Recently Kataoka and Serizawa (1990) have proposed a correlation method for the four-sensor probe to measure the interfacial area and presented some preliminary measurements on air-water bubbly flow using this method. In this method, the interfacial area is obtained from the measured correlation function of the characteristic functions at two different positions by probe sensors.

The four-sensor probe method for measuring the actual vectorial interfacial velocity to obtain the area has been applied by Ishii and Revankar (1993) and Revankar and Ishii (1993) to cap bubbly and slug flow regimes. It was possible to measure the local void fraction, interfacial area and interfacial velocity from a single probe. Furthermore, the contributions of large bubbles and smaller follow-up bubbles can be measured separately. Such a detailed measurement method for the local structures of the two-phase flow has never been developed previously. The probe also can give some statistical information such as the Sauter-mean diameter, bubble cord length probability density, number of particles and velocity fluctuation of the interface. The reliability of the data is confirmed by comparing them to direct photographic data as well as to the global data from the pressure transducers through the void fraction.

The axial development of the transverse void fraction and interfacial area concentration have been measured (Leung et al., 1995). This type of data can easily be used to determine the rate of coalescence or disintegration of fluid particles.

V. Interfacial Area Transport Equation

The geometrical relations developed for the interfacial area concentration (Ishii and Mishima, 1980) show the importance of the existence and size of small fluid particles for all flow regimes. This implies that the number density of small bubbles is important in bubbly, slug, and churn flows, whereas in annular-mist, dispersed droplet, or inverted annular film boiling flows, the droplet size distribution (Kataoka et al., 1983; Ishii and DeJarlais , 1987) and amount of entrainment (Ishii and Grolmes, 1975; Ishii and Mishima, 1982; Kataoka and Ishii 1982) are important in determining the interfacial area. The entrainment data at higher pressure or for viscous fluids are not sufficient to develop a reliable correlation for these cases. The droplet size distributions and interfacial characteristics in inverted annular film boiling (Ishii and DeJarlais, 1987; Obot and Ishii, 1988) are the key parameters for determining the heat transfer and the relative velocity between phases.

For bubbly, slug and churn flow, the maximum stable bubble size, mechanisms of bubble coalescence, disintegration and nucleation are important. In order to accurately predict the interfacial area concentration for these flow regimes, it may be necessary to introduce a transport equation for the interfacial area (Ishii, 1975). For example, for a boiling flow, a bubble number transport equation can be written in terms of the bulk liquid bubble nucleation rate, the bubble number density sink rate due to coalescence and collapse and generation rate due to bubble disintegration (Kocamustafaogullari and Ishii, 1983). This equation is equivalent to the interfacial area transport equation. The bubble number transport equation and bubble growth model have been applied to predict flashing flow (Jones and Shin, 1984; Riznic et al., 1987).

Since the interfacial area concentration changes with the variation of the particle number density due to coalescence and breakage, analogous to Boltzman's transport equation, a Population Balance Approach (PBA) was recently proposed by Reyes (1989) to develop a particle number density transport equation for chemically non-reacting, dispersed spherical fluid particles. A similar method was employed in combustion theory, known as the spray-equation (Williams, 1965). For the purpose of interfacial area transport, Kocamustafaogullari and Ishii (1995) generalized Reyes' model, then taking a moment of number density with interfacial area, they obtained the interfacial area transport equation based on statistical mechanics. It is given by

$$\frac{\partial a_i}{\partial t} + \nabla \cdot a_i \vec{v}_i = -\sum_j \phi_j + \phi_{ph} \tag{11}$$

where a_i is the local interfacial area concentration in the macroscopic field. ϕ_j denotes the various source or sink terms due to particle coalescence and disintegration. The last term ϕ_{ph} is the source due to nucleation, phase change at the interface and compressibility of fluid particle. The development of these source and sink terms are the most important problems.

The parameters involved in the break-up components of the source term are the maximum fluid particle volume, the average daughter particle size distribution at the break-up, and the frequency of the break-up. For the coalescence sink term, the major parameters are the collision frequency and the coalescence probability.

IV. Major Break-up and Coalescence Mechanisms

In any two-phase flow field, the initial bubble or drop size is determined in terms of the mechanism of fluid particle generation such as the formation of bubbles at an orifice or bubble entrainment mechanisms and generation of droplets by shearing off of roll waves in separated two-phase flow patterns such as annular and stratified-wavy flows. However, in forced convective pipe flow or

mechanically agitated systems, the initial fluid particle size may be too large or too small to be stable. In these cases, the fluid particle size is further determined by a break-up and/or coalescence mechanism. In boiling systems, in addition to the break-up and coalescence mechanisms, the growth rate should also be considered.

When a fluid particle exceeds a critical value, the particle interface becomes unstable and break-up is likely to occur. Similarly, when fluid particles are smaller than some critical dimension, the coalescence is likely to occur on a series of collision events. Therefore, the particle break-up can be related to the maximum attainable size of the particle; whereas particle coalescence can be related to the minimum size. The literature contains several models for determining the maximum and minimum sizes of fluid particles. These models have been developed from first principles and have been used to develop break-up and coalescence criteria. These criteria, however, do not treat a distribution of fluid particles. Rather, they describe the particle size limits of break-up and coalescence.

The fluid particles can break-up due to collisions with turbulent eddies, shearing force in viscous layer or interfacial instabilities such as the Raleigh-Taylor and Kelvin-Helmholtz instabilities.

In the case of turbulent flow, particle break-up is caused by fluctuating eddies resulting in the pressure variation along the particle surface. In laminar flow, viscous shear in the continuous phase will elongate the particle and cause break-up. However, even in the absence of net flow of continuous phase such as rising bubbles in a liquid and rising and falling drops in a continuous gas or immiscible liquid, the fluid particle break-up is caused by interfacial instabilities due to the Raleigh-Taylor and Kelvin-Helmholtz instabilities.

Aside from the break-up mechanism caused by interfacial instabilities, basically there are two external forces that are involved in the breaking-up of fluid particles, namely turbulence induced inertial forces. In most applications, the Reynolds numbers that are characteristic of the flow field are so large that viscous effects are negligible. In other cases, however, inertial effects play a minor role and may be neglected. Existing experimental and theoretical information can, therefore, be classified into two categories, namely, in which surface tension and viscous forces interact, and another in which surface forces and turbulence induced dynamic pressure forces are dominant.

Kocamustafaogullari and Ishii (1995) reviewed the existing criteria and mechanisms in detail.

The coalescence of fluid particles is dominated by the two major mechanisms. These are the random collision induced by local turbulence and entrainment of fluid particles in a wake of other particles. By combining various effects into three major effects, the interfacial area transport equation can be expressed as

$$\frac{\partial a_i}{\partial t} + \nabla \cdot a_i \vec{v}_i = \phi_{dis} - \phi_{co} + \phi_{ph} \tag{12}$$

The various local mechanisms affecting the break-up and coalescence terms have been discussed above. Here we study the general functional dependence of these two terms. The fluid particle disintegration occurs mainly due to the turbulent fluctuation and interfacial stability. Therefore, locally it should depend on the particle size, r_d, turbulent intensity, $\overline{v'^2_c}$, and local relative velocity, v_r. Hence:

$$\phi_{dis} = \phi_{dis}\left(\overline{v_c'^2}, r_d, We\right) \tag{13}$$

where the Weber number is given by

$$We \equiv \frac{2\rho_c r_d v_r^2}{\sigma} \tag{14}$$

which scales the interfacial instability.

The coalescence process depends on the random collisions and the systematic wake entrainment. The collision is a strong function of the inter-particle distance and the amplitude of the fluctuating particle velocity. The latter depends on the continuous phase turbulent fluctuations. The wake flow structure depends on the particle Reynolds number, Re_d, and the particle size. The coalescence probability after a collision depends on the particle sizes and fluctuating velocity components. Thus:

$$\phi_{co} = \phi_{co}\left(\alpha_d, r_d, \overline{v_c'^2}, \mathrm{Re}_d\right). \tag{15}$$

The turbulence intensity in dispersed flow may be related to the continuous phase Reynolds number, Re_c, and a distance from a wall.

The simplest form of the interfacial area transport equation can be obtained by applying the cross-sectional area averaging and reducing it to a one-dimensional form. This form of the interfacial area transport equation may have the most useful and practical applications in the existing one-dimensional two-fluid model. It can replace the traditional flow regime maps and regime transition criteria. The changes in the two-phase flow structure are predicted mechanistically by introducing the interfacial area transport equation. The effects of the boundary conditions and flow development are efficiently modeled by this transport equation. Such a capability does not exist in the current state-of-the-art. Thus a successful development of the interfacial area transport equation can make a quantum improvement in the two-fluid model formulation.

By applying the cross-sectional area averaging, the one-dimensional area transport equation becomes:

$$\frac{\partial\langle a_i\rangle}{\partial t} + \frac{\partial}{\partial z}\langle a_i\rangle\bar{v}_{iz} = \langle\phi_{dis}\rangle + \langle\phi_{co}\rangle + \langle\phi_{ph}\rangle\langle\phi_w\rangle \tag{16}$$

where $\langle\phi_w\rangle$ is the wall nucleation source. By using the local interfacial area measurement methods, the following parameters can be measured simultaneously:

$$a_i = a_i(r, z) \tag{17}$$

and

$$v_{iz} = v_{iz}(r, z) \tag{18}$$

Under the adiabatic and steady conditions, there are no effects of phase changes; thus:

$$\frac{d}{dz}\langle a_i v_{iz}\rangle = \langle\phi_{dis}\rangle - \langle\phi_{co}\rangle \tag{19}$$

which shows the way to measure the right-hand side source and sink terms. First, two limiting cases are studied to isolate the break-up source term and the coalescence sink term. It is considered that there is a

critical Reynolds number, Re_c^*, for a break-up process. Below this value, the break-up of fluid particles becomes insignificant. Hence, for $Re_c << Re_c^*$, the coalescence process dominates.

Thus by performing experiments at relatively low Reynolds number and at high Reynolds number, and measuring the changes of the interfacial area along a channel, the data for the source $\langle \phi_{dis} \rangle$ and sink $\langle \phi_{co} \rangle$ can be measured separately. The Thermal-hydraulics and Reactor Safety Laboratory at Purdue University is performing a large number of such experiments and developing the constitutive relation for these terms (Wu et al., 1997).

Conclusion

The importance of the interfacial area concentration in two-phase flow formulation is discussed in detail. The void fraction and the interfacial area concentration characterizes the macroscopic effects of the interfacial geometry. In the two-fluid model formulation, the interfacial area should be specified either by a constitutive relation or a transport equation which describes its evolution. Both approaches are discussed in detail. The local interfacial area measurement methods are reviewed. The special highlight is given to the very recent development of the multi-sensor local probe technique and its theoretical background. Both the double sensor and four-sensor methods appear very promising.

The interfacial area transport equation is obtained and its significance is explained. The constitutive relation development for the transport equation is reviewed in terms of the physical mechanisms and then the major parameters characterizing them are identified. The relation to the local measurements of the interfacial area and interfacial velocity and the data base for the constitutive relations for the transport equation is explained.

Acknowledgment

This work was performed under the auspices of the U.S. NRC. The authors would like to express their sincere appreciation to Drs. J. Uhle and F. Eltawila.

References:

1. Ishii, M., *Thermo-Fluid Dynamic Theory of Two- Phase Flow*, Eyrolles, Paris (1975).
2. Zuber, N. and Findley, J.A., "Average Volumetric Concentration in Two-Phase Flow Systems," *J. Heat Trans.*, Vol. 87, pp. 453-468 (1965).
3. Wallis, G.B., *One-Dimensional Two-Phase Flow*, McGraw-Hill Publishing Co., New York, pp. 261-263 (1969).
4. Ishii, M., "One-Dimensional Drift-Flux Model and Constitutive Equations for Relative Motion Between Phases in Various Flow Regimes," Argonne National Laboratory Report, ANL-77-47 (1977).
5. Chawla, T.C. and Ishii, M., "Two-Fluid Model of Two-Phase Flow in a Pin Bundle of a Nuclear Reactor," *Int. J. Heat Mass Transfer*, Vol. 23, pp. 991 (1980).
6. Vernier, P. and Delhaye, J.M., "General Two-Phase Flow equations Applied to the Thermohydrodynamics of Boiling Nuclear Reactor," *Energ. Primaire*, Vol. 4, No. 1, pp. 5 (1968).
7. Kocamustafaogullari, G., "Thermofluid Dynamics of Separated Two-Phase Flow." Ph.D. Thesis, Georgia Institute of Technology (1971).
8. Boure, J.A., "Mathematical Modeling of Two-Phase Flows," *Proc. of CSNI Specialist Meeting*, Banerjee, S., and Weaver, K.R., Eds. A.E.C.L., Vol. 1, August 3-4, Toronto, pp. 85 (1978).
9. Ishii, M. and Mishima, K., "Study of Two-Fluid Model and Interfacial Area," Argonne National Laboratory Report, ANL-80-111 (1980).

10. Chawla, T.C. and Ishii, M., "Equation of Motion for Two-Phase Flow in a Pin Bundle of a Nuclear Reactor," *Int. J. Heat Mass Transfer*, Vol. 21, pp. 1057, (1978).
11. Delhaye, J.M. and Achard, J.L., "On the Use of Averaging Operators in Two-Phase Flow Modeling," *Thermal and Hydraulic Aspects of Nuclear Reactor Safety*, Vol. 1, Light Water Reactors, Jones, D.C. and Bankoff, S.G., Eds. ASME, New York, pp 289 (1977).
12. Sha, W.T., Chao, B.T. and Soo, S.L., "Time Averaging of Local Volume Averaged Conservation Equations of Multiphase Flow," NUREG/CR-3434, ANL-83-49 (1983).
13. Ishii, M. and Kocamustafaogullari, G., "Two-Phase Flow Models and Their Limitations," *NATO Advanced Research Workshop on Advances in Two-Phase Flow and Heat Transfer*, Spitzingsee, BRD, August 31-September 3 (1982).
14. Kocamustafaogullari, G., and Ishii, M., "Foundation of the Interfacial Area Transport Equation and It's Closure Relations," *Int. J. Heat Mass Transfer*, Vol. 38, pp. 481-493 (1995).
15. Kelly, J.M., "Thermal-hydraulic modeling needs for passive reactors," OECD/CSNI Specialist Meeting on Advanced Instrumentation and Measurement Techniques, Santa Barbara, CA, USA, March 17-20 (1997).
16. Mortensen, G.A., "Long-term plan for NRC thermal-hydraulic code development," Report to U.S. NRC under contract DE-AC07-94IDI3223, March (1995).
17. Rohatgi, U.S., et al., Presentation at the First SBWR PIRT Meeting, Brookhaven National Laboratory, May 12-13 (1994).
18. Grand, D., "Thermal-hydraulic modeling requirements for next generation reactor safety analysis codes," OECD/CSNI Specialist Meeting on Advanced Instrumentation and Measurement Techniques, Santa Barbara, CA, USA, March 17-20 (1997).
19. Städtke, H., "Thermal hydraulic code for LWSR safety analysis: Present status and future perspective," OECD/CSNI Specialist Meeting on Advanced Instrumentation and Measurement Techniques, Santa Barbara, CA, USA, March 17-20 (1997).
20. Riznic, J.R. and Ishii, M., "Bubble number density and vapor generation in flashing flow," *Int. J. Heat Mass Transfer*," Vol. 32, pp. 1821 (1989).
21. Kataoka, I., Ishii, M. and Serizawa, A., "Local Formulation of Interfacial Area Concentration and its Measurements in Two-Phase Flow," Argonne National Laboratory Report, ANL-84-68, NUREG/CR-4029 (1984).
22. Kataoka, I., Ishii, M. and Serizawa, A., "Local Formulation of Interfacial Area Concentration," *Int. J. Multiphase Flow*, 12, pp. 505-529 (1986).
23. Kataoka, I. and Serizawa, A., "Averaged Bubble Diameter and Interfacial Area in Bubbly Flow," *Proc. 5th Two-Phase Symp. Japan*, Kobe, Japan, Nov. 28-29, pp. 77-80 (1984b).
24. Wang, Z. and Kocamustafagullari, G., "Interfacial Characteristic Measurements in a Horizontal Bubbly Two-Phase Flow," *ANS Trans.*, 62, pp. 712-713 (1990).
25. Revankar, S.T. and Ishii, M., "Local Interfacial Area Measurement in Bubbly Flow, " *Int. J. Heat Mass Transfer* (To be published) (1992).
26. Burgess, J.M. and Calderbank, P.H., "The Measurement of Bubble Parameters in Two-Phase Dispersions - I. The Development of an Improved Probe Technique," *Chem. Eng. Sci.*, 30, pp. 743-750 (1975)
27. Burgess, J.M. and Calderbank, P.H., "The Measurement of Bubble parameters in Two-Phase Dispersions - II. The Structure of Sieve Tray Froths," *Chem. Eng. Sci.*, 30, pp. 1107-1121 (1975a).
28. Burgess, J.M. and Calderbank, P.H., "The Measurement of Bubble Parameters in Two-Phase Dispersions - III. Bubble Properties in a Freely Bubbling Fluidized-Bed," *Chem. Eng. Sci.*, 30, pp. 1511-1518 (1975b).

29. Buchholz, R., Tseptonides, J., Steinemann, J., and Onken, U., "Influence of Gas Distribution on Interfacial Area and Mass Transfer in Bubble Columns, " *Ger. Chem. Eng.*, 6, pp. 105-113 (1983).
30. Kataoka, I. and Serizawa, A., "Interfacial Area Concentration in Bubbly Flow," *Nucl. Eng. Design*, 120, pp. 163-180 (1990).
31. Ishii, M. and Revankar, S.T., "Four Sensor Conductivity Probe Application to Two-Phase Flow," *Proc. Int. Conf. Multiphase Flow*, 91 - Tsukuba, Sep. 24-27 Vol. (1991).
32. Revankar, S.T. and Ishii, M., "Local Interfacial Area Using Four Sensor Probe in Two-phase Flow," *Int. J. Heat & Mass Transfer*, Vol. 36, pp. 2997-3007 (1993).
33. Leung, W.H., Revankar, S.T., Ishii, Y., and Ishii, M., "Axial Development of Interfacial Area and Void Concentration Profiles Measured by Double-sensor Probe Method," *Int. J. Heat Mass Transfer*, Vol. 38, pp. 445-453 (1995).
34. Reyes, J.N., Statistically Derived Conservation Equations for Fluid Particle Flows," Proc. ANS-THD, 1989 ANS Winter Meeting, San Francisco, CA, pp. 12 (1989).
35. Williams, F.A., "Combustion Theory," Addison-Wesley Publishing Co., Reading, MA (1965).
36. Kataoka, I., Ishii, M., and Serizawa, A., "Local Formulation of Interfacial Area Concentration," *J. of Fluid Engr.*, Vol. 105, pp. 230-238 (1983).
37. Ishii, M. and DeJarlais, G., "Flow visualization Study of Inverted Annular Flow of Post Dryout Heat Transfer Region," *Nucl. Eng. And Design*, Vol. 99, pp. 187-199 (1987).
38. Ishii, M. and Grolmes, M.A., "Inception Criteria for Droplet Entrainment in Two-Phase Concurrent Film Flow," *AIChE.J.*, 21(2), p. 308 (1975).
39. Ishii, M. and Mishima, K., "Liquid Transfer and Entrainment Correlation for Droplet-Annular Flow," *7th Int. Heat Trans. Conf.*, Munich (Sept. 1982).
40. Kataoka, I. and Ishii, M., "Mechanism and Correlation of Droplet Entrainment and Deposition in Annular Two-Phase Flow," NUREG/CR-2885, ANL-882-44 (1982).
41. Obot, N.T. and Ishii, M., "Two-Phase Flow Regime Transition Criteria in Port Dryout Region Based on Flow Visualization Experiments," *Int. J. of Heat Mass Tr.*, Vol. 31, pp. 2559-2570 (1988).
42. Kocamustafaogullari, G. and Ishii, M., "Interfacial Area and Nucleation Site Density in Boiling Systems," *Int. J. of Heat Mass Trans.*, Vol. 26, pp. 1377-1387 (1983).
43. Jones, Jr., O.C. and Shin, T.S., "Progress in Modelling of Flashing Inception and Critical Discharge of Initially Subcooled Liquids Through Nozzles," *Joint Japan-U.S. Seminar on Two-phase Flow Dynamics*, Lake Placid, NY, July 29-Aug. 3 (1984).
44. Riznic, J., Ishii, M., and Afgan, N., "Mechanistic Model for Void Distribution in Flashing Flow," *Proc. Transient Phenomena in Multiphase Flow*, ICHMT Seminar, May 24-30, Dubrovnik, Yugoslavia (1987).
45. Wu, Q., Kim, S., Ishii, M., and Beus, S.G., "One-Group Interfacial Area Concentration Transport in Vertical Air-Water Bubbly Flow," submitted to 1997 NHTC, Baltimore, August 10-12 (1997).

Aspects of Reflood Heat Transfer Modeling

L.E. Hochreiter
Dept. of Nuclear Engineering
Pennsylvania State University

Introduction/Background

With the approval of the Appendix K rule revisions, vendors are starting to utilize "Best-Estimate" safety analysis thermal-hydraulic methods to perform large-break LOCA analysis to evaluate the allowable core thermal limits. Even with the application of best-estimate methods, the large-break LOCA still is the most limiting transient and results in establishing the maximum allowable fuel rod linear power level (kw/ft). Typically what has occurred is that as Best-Estimate analysis methods have identified peak linear heat rate margin; this margin has been used by the utility or the vendor for power up- ratings, longer fuel cycles, low leakage core loadings and advanced fuel designs to improve the economics of the nuclear power plant. All of these economic improvements result in the need for higher operating kw/ft values (1). This is true for both BWR and PWR designs. When the best-estimate methods are applied with the higher linear heat rates, the resulting calculated peak cladding temperatures are nearly the same as those previously calculated using the original Appendix K requirements as seen in Figure 1. However, the difference is that the allowable linear heat rate, (kw/ft) is now higher.

The best-estimate calculations indicate that for nearly all PWR designs the peak cladding temperatures are reached during the reflood portion of the transient at low pressures, typically one to three bars. A similar situation also occurs in the hot channel for the more modern BWR designs (BWR5 and 6), as well. The flow pattern in the BWR hot channel is co-current upflow during reflood similar to a PWR (2).

In either case and for all designs, the thermal-hydraulic heat transfer phenomena which dominates the reflood transient is dispersed flow film boiling. When the rod surface reaches T_{min}, the quench rate on the fuel rods progresses and causes, liquid entrainment at the quench front which determines the convecture and radiation heat transfer above the quench front. All these different heat mechanisms have been lumped together and called "Reflood Heat Transfer" The heat transfer rates during this period are very low , and several different mechanisms are responsible for the total wall heat flux. No single mechanism dominates the reflood heat transfer process such that several different mechanisms must be predicted by the best-estimate calculational tool with roughly equal precession. Those mechanisms include:

- Convection to superheated vapor,
- Surface radiation to vapor and droplets,
- Interfacial heat transfer between droplets and superheated vapor,
- Direct contact heat transfer between the wall and entrained liquid,
- Convective enhancement of the vapor by the entrained droplets

- Impact of structures (grids) in the rod bundle causing flow acceleration and droplet break-up,
- Rewetting and development of quench fronts at the top and bottoms of the rods,
- Liquid entrainment at the quench front due to the heat release.

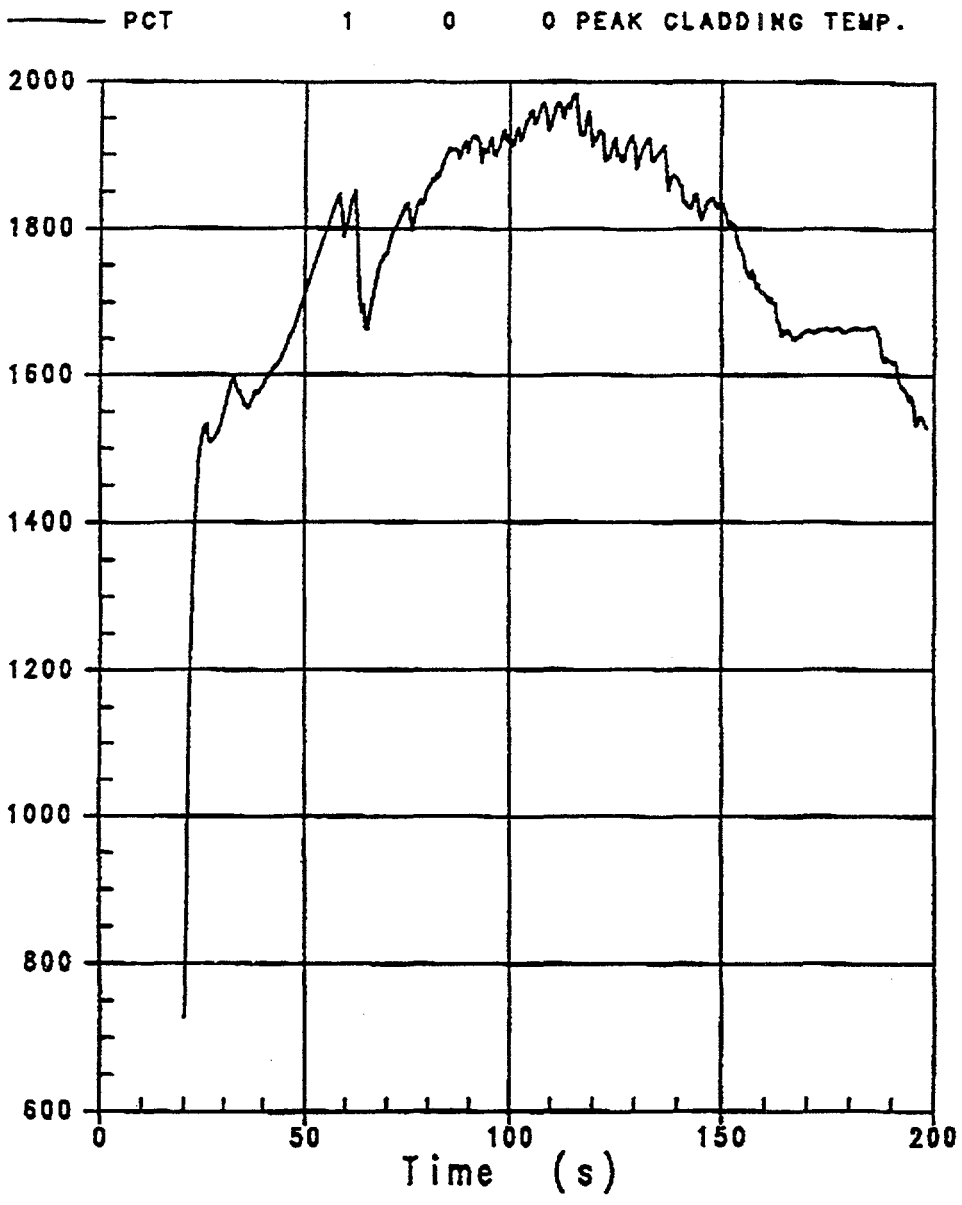

Figure 1. Best Estimate Calculate Peak Clad Temperature at 15.4 kw/ft

Also, since the different mechanism are of comparable magnitude, improving one particular model is difficult since very little data is available to isolate its particular contribution to the total wall heat flux. Therefore, compensating errors can result as the code's predictive capabilities are improved.

Figure 2 shows the different heat transfer mechanisms which are present in the high temperature potions of the rod bundle where the peak cladding temperatures are calculated. This figure is taken from the work of Andreani and Yadigaroglu (3) who have published several excellent review papers and reports on dispersed flow film boiling. The heat transfer process is a combination of a "two-step and three-step " dispersed flow film boiling process. A "two-step" dispersed flow film boiling process consists of heat transfer from the wall to the vapor flow by convection as well as by radiation. There is also wall-to-wall radiation heat transfer and wall to entrained droplet heat transfer. The vapor is the heat sink and quickly reaches superheated conditions as it receives energy from the wall. The second step of the "two-step" process is the heat transfer between the superheated vapor and the entrained droplets. The interfacial heat transfer between the drops and the vapor result in a lower vapor temperature which is the fluid heat sink for the wall heat transfer. The "two-step" film boiling process becomes a "three-step" process as the wall temperature decreases such that there can be intermittent direct (or near direct) droplet-wall contact heat transfer. It is believed that the direct wall contact heat transfer component occurs within and just above the transition region which results in improved heat transfer. The improved heat transfer in this region can be seen from the FLECHT-SEASET test data.(4)

Dispersed flow film boiling also dominates the downflow period of the PWR blowdown transient as well as the reflood transient. Similar heat transfer mechanisms are present for the blowdown downflow period as well as the reflood period. The primary difference is that the vapor convection term is more dominate for the blowdown situation as compared to the reflood phase, and the vapor has less super heat.

The single largest uncertainty in predicting the dispersed flow film boiling heat transfer in reflooding rod bundles is the liquid entrainment at the top of the transition region just above the quench front. Figure 3 shows the quench front data from a low flooding rate FLECHT-SEASET test with the transition region location indicated. Figure 4 indicate is a schematic of the flow regime just above the quench front within the transition region. In this region, the steam generation from the quenching of the fuel rods results in a very large vapor velocities which entrain and shear liquid filaments into droplets which are then swept into the upper regions of the rod bundle. The entrained droplets provide cooling by several different mechanisms in the upper regions of the rod bundle where the resulting peak clad temperatures are calculated.

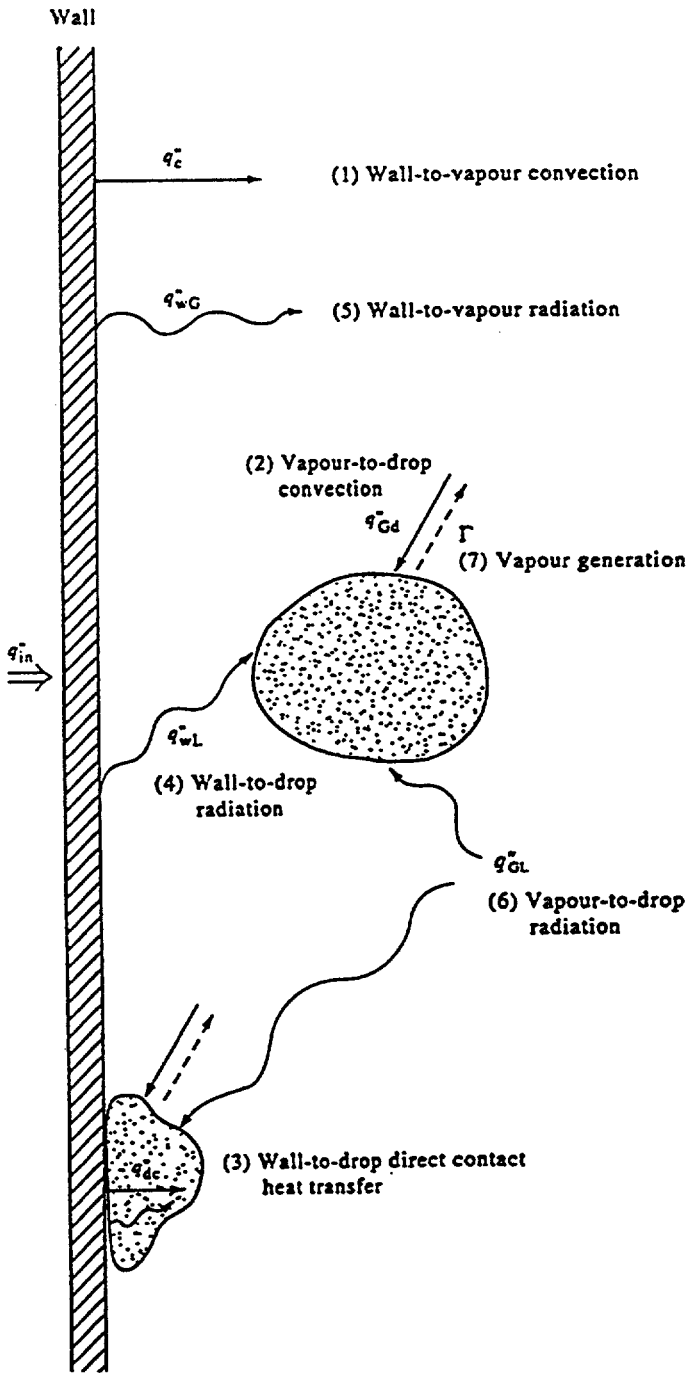

Figure 2. Heat and Mass Transfer Phenomena For Dispersed Flow Film Boiling. (From Reference 4)

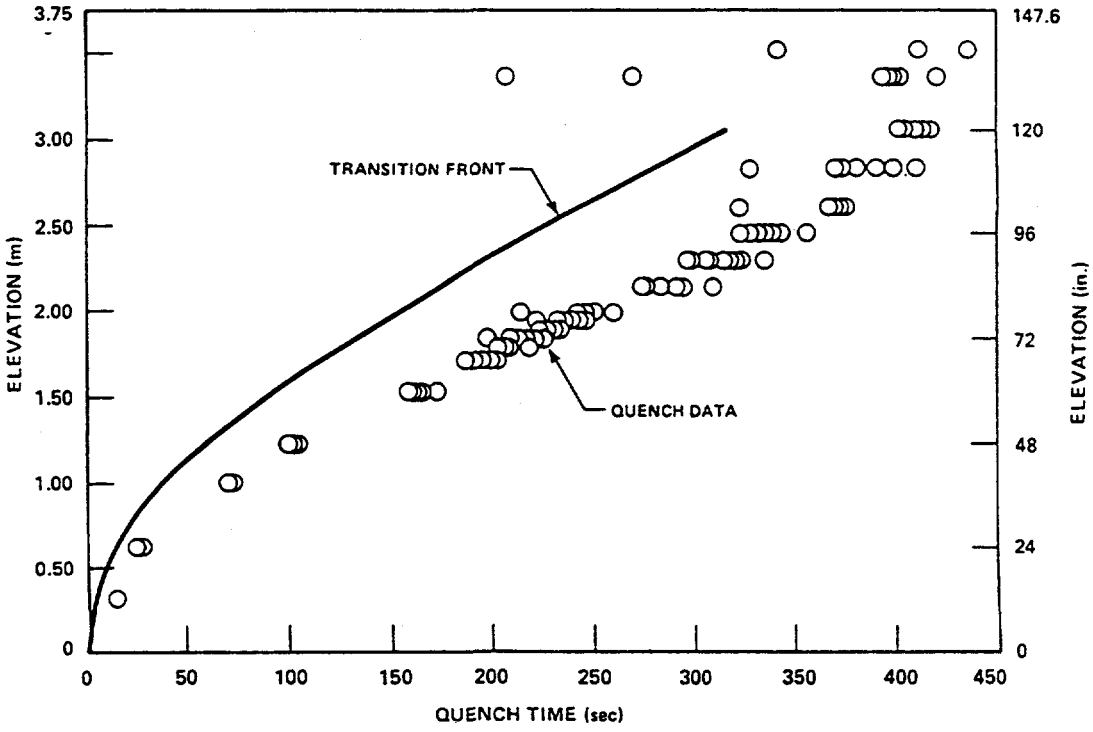

Figure 3a. Transition Front Curve, Run 31203

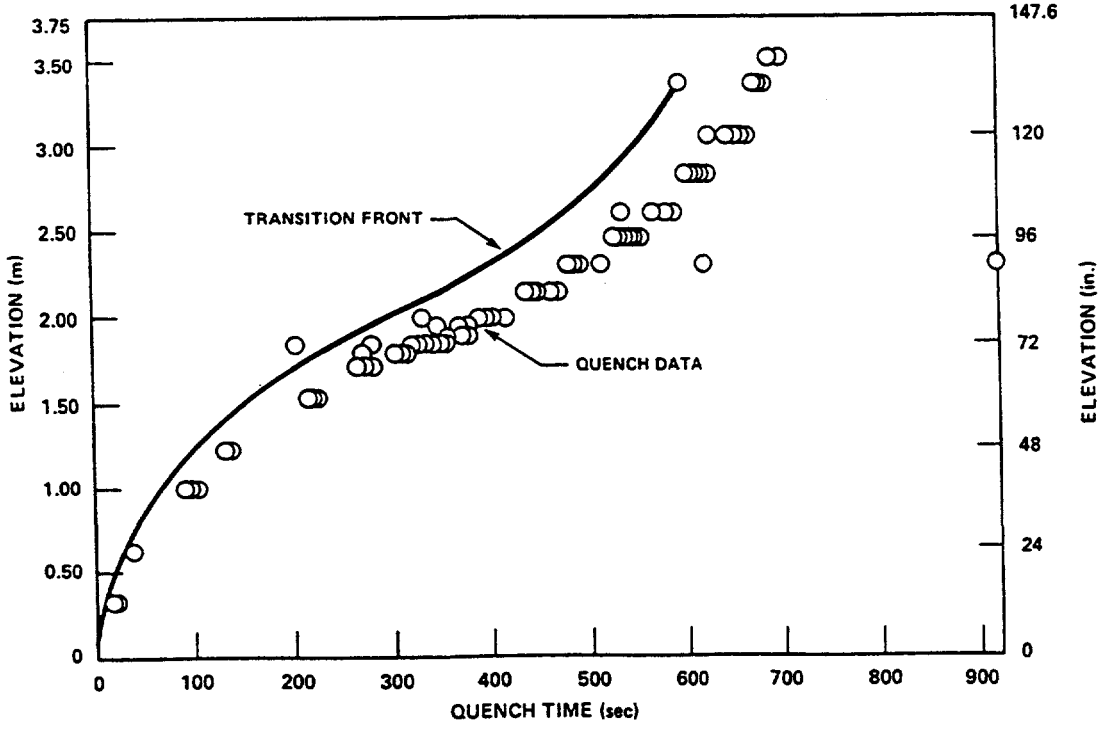

Figure 3b. Transition Front Curve, Run 31805

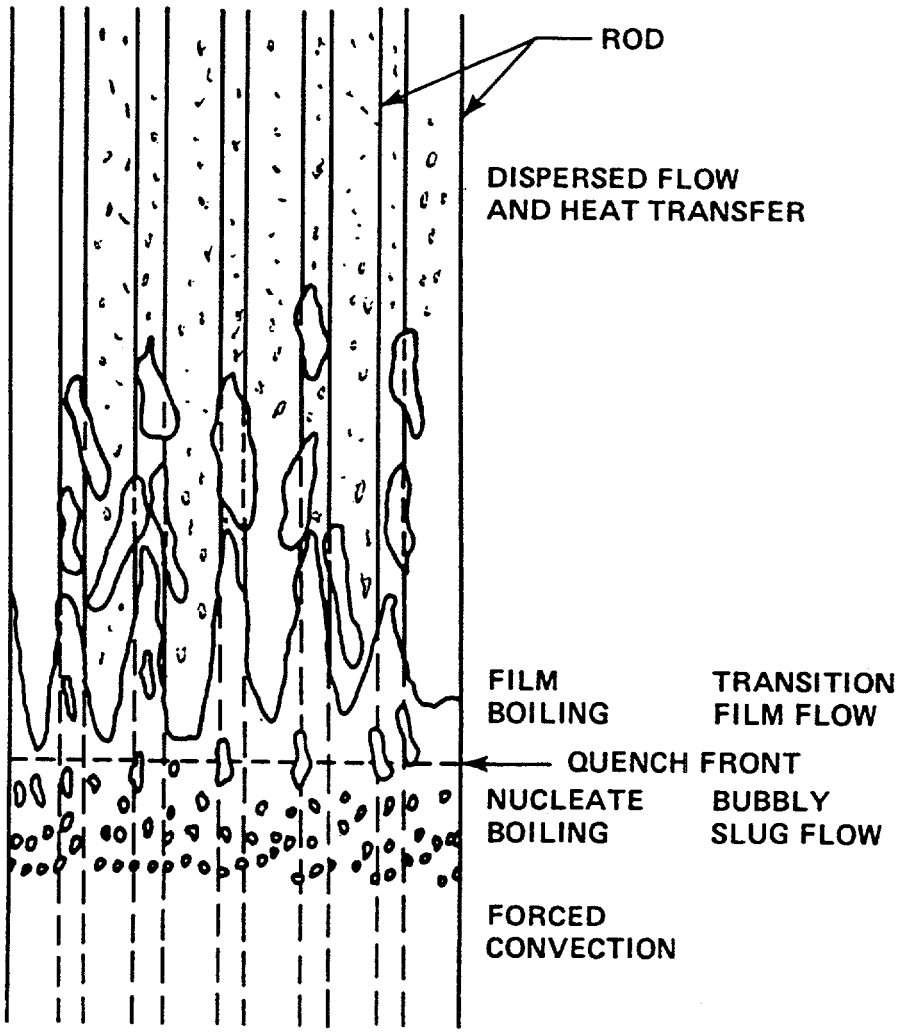

Figure 4. Typical Conditions in Rod Bundle During Reflood

Previous Studies, Reflood Data Base

The dispersed flow film boiling reflood period has long been the most limiting heat transfer period for the large break LOCA. Several experimental programs have been performed over the years to provide the data needed to develop models for this portion of the LOCA transient. For PWRs, the most significant program was the Nuclear Regulatory Commission and Westinghouse sponsored Full Length Emergency Core Heat Transfer (FLECHT) Program which was completed in 1973 (5 ,6). This initial program provided experimental data for the industry such that empirical correlations could be developed to predict heat transfer and entrainment using simple thermal-hydraulic models which would conform to the Appendix K rules as given in 1974.

More recently, the Nuclear Regulatory commission, Westinghouse and Electrical Power research Institute sponsored the FLECHT-Separate Effects and Systems Effects Tests FLECHT-SEASET program which was completed in 1985 (3, 7, 8, 9, 10). There were a total of 16 reports written as part of the FLECHT-SEASET program. The objectives of this program were to quantify the conservatism in the Appendix K rule for the reflood portion of the transient and to provide experimental data which could be used to validate a PWR Best-Estimate thermal-hydraulic computer code. The FLECHT and FLECHT-SEASET programs provided a portion of the data base which was used by the NRC to revise the Appendix K rule (11).

One of the more interesting rod bundle reflood experiments was the FEBA (12, 13) experiments performed at the Karlsruhe Research Center. These experiments examined the effects of spacer grids on dispersed flow film boiling by performing tests with and without a spacer grid located at the center of the bundle. These tests clearly showed the beneficial effects of spacer grids in promoting improved heat transfer downstream of the spacer by shattering entrained droplets, enhanced convective heat transfer, and the quenching effects of the grid. Similar heat transfer effects have been observed in the ERSEC (14), PERICLES, and the Westinghouse G-2 experiments. The spacer grids effects were also seen in the FLECHT-SEASET experiments. The ERSEC, PERICLES and G-2 experiments used mixing vane spacer grids more typical of current vendor fuel assembly designs. Mixing vane grids have a higher rod bundle subchannel flow area blockage and result in even greater heat transfer improvement downstream of the spacer grid.

There were also comparable Nuclear Regulatory Commission and General Electric sponsored spray cooling and reflood experimental programs (15, 16) for the BWR design which also provided data for, first empirical heat transfer correlation development and later as part of the BWR refill and reflood program (17) using the Two Loop test Apparatus (TLTA), data to validate a Best-Estimate BWR thermal-hydraulics computer code

In addition to these programs, the Nuclear Regulatory Commission has sponsored higher pressure rod bundle film boiling, steam cooling, and level swell experiments at the Oak Ridge National Laboratory on a full length 8 x 8 rod bundle (18) (19). These tests also examined dispersed flow film boiling conditions, however, the pressure was much higher, more characteristic of a PWR or BWR blowdown situation. These experiments also confirmed the beneficial heat transfer effects of spacer grids for higher pressure blowdown situations as well as for reflood heat transfer.

There were also intermediate to low (0.28 to 7.1 Mpa) pressure, single tube experiments performed at Idaho Nuclear Engineering Laboratory to evaluate the post CHF heat transfer models in the TRAC code (20, 21). These single tube experiments were performed over a range of pressures, flows, wall superheats, and qualities which would be expected for a PWR or BWR higher pressure film boiling situation.

There were also 3 by 3 rod bundle experiments performed at Lehigh University which examined dispersed flow film boiling up to pressures of approximately 100 psia. These experiments used directly heated fuel rod simulators at the experimenters attempted to "freeze" the quench front to study the flow in a near quasi-steady state manner (22) (23).

There have also been a number of smaller scale, single tube experiments using water as the working fluid as well as refrigerants to shed light on the different mechanisms of dispersed flow film boiling (24, 25, 26, 27, 28, 29). The models which have been developed from these experiments have also been used in the best estimate computer codes and later validated against larger rod bundle data using water as the working fluid (see the TRAC- PF1/Mod1 Models and Correlations Document, Reference (30)).

All the experiments discussed above measured the temperature transient of a fuel rod simulator tube wall, and for most of the tests, the total wall heat transfer could be calculated from the data. The INEL single tube experiments performed some limited measurements of vapor superheat but the probe caused a significant blockage in the bundle which was reflected in the down stream wall temperature measurements. The Lehigh experiments also measured selected vapor superheat, but the vapor probe was also large relative to the bundle size. The FEBA experiments measured vapor superheat using bare thermocouples mounted on the spacer grids.

Only the FLECHT-SEASET experiments attempted to measure the details of the heat transfer and non-equilibrium flow such that a best-estimate computer code could be assessed against the test data. In the FLECHT-SEASET experiments, vapor superheat was measured at several axial locations, wall temperatures were measured for the housing, and guide tube thimbles and the heater rods. Limited data of droplet diameters and velocities were obtained for a few selected tests using high speed photography. The heater rod total heat flux was calculated using an inverse conduction technique using the heater rod thermo couples and measured power. With these measurements, the heat transfer due to radiation could be calculated and separated from the total wall heat transfer as shown in Reference 4. The convective portion of the heat

transfer, droplet evaporation, and droplet enhancement of the convection heat transfer were also calculated. Figure 5 shows the measured wall temperatures and vapor temperature for a reflooding test with a flooding rate of one-inch/second (a typical PWR value). Figure 6 shows the radiation network used to solve for the radiation heat transfer within the test bundle. Figure 7 shows the percentage of the total wall heat flux which is due to radiation and convection as a function of time at two elevations in the bundle. As the figure indicates there is significant non-equilibrium in the flow, although the flow quality is approximately 50 percent. With the instrumentation, mass and energy balances could be calculated for the test bundle such that the axial behavior of the flow quality could be calculated. Also the void fraction was measured along the bundle with the most accurate measurements at or near the quench front. The calculated radiation heat transfer was subtracted from the total measured heat flux to obtain the convective portion, the heat transfer. Figures 8 and 9 indicate that the convective heat transfer is enhanced by the entrained droplets as compared to fully developed convectives.

Dispersed Flow Film Boiling Phenomena to be Modeled

With the revision to the Appendix K rule, there have been four computer codes which have been developed within the United States as "Best-Estimate" thermal-hydraulic codes for LOCA analysis. They are the TRAC-P, TRAC-B codes which are used for three-dimensional analysis of PWRs and BWRs respectively. The RELAP-5 code, which was initially developed as a best-estimate small-break code, has been improved and can be utilized as a one-dimensional large-break code. The COBRA/TRAC code was developed for detailed LOCA analysis of reactor systems. Different versions of each of these codes exist, with differing levels of detail for the film boiling models and the treatment of the dispersed flow film boiling region for rod bundles. All the codes use correlations which have been developed from simple geometries for the different heat transfer regimes during the film boiling process and use the void fraction to transition from one flow regime into another. The void fraction weighting is a method of indicating the amount of liquid in the flow as well as the amount of liquid-to-vapor interfacial area available for interfacial heat, momentum and mass transfer. The greatest uncertainty in this approach is the characterization of the flow and heat transfer for the different regimes. There are specific void fraction limits which can lead to abrupt heat transfer regime changes in the heat removal capabilities of the fluid. As a result, the calculated temperature response of the fuel rods can display heat-up and cooldown periods which are discontinuous and are not observed in the data. Specific ranges are imposed on the codes to minimize these effects.

As mentioned above, dispersed flow film boiling process is a two-step process above the quench front alone the heat transfer rates are low; and a three-step process near the quench front or transition region alone the heat transfer rates are higher. The phenomena which must be calculated for the dispersed flow film boiling period include:

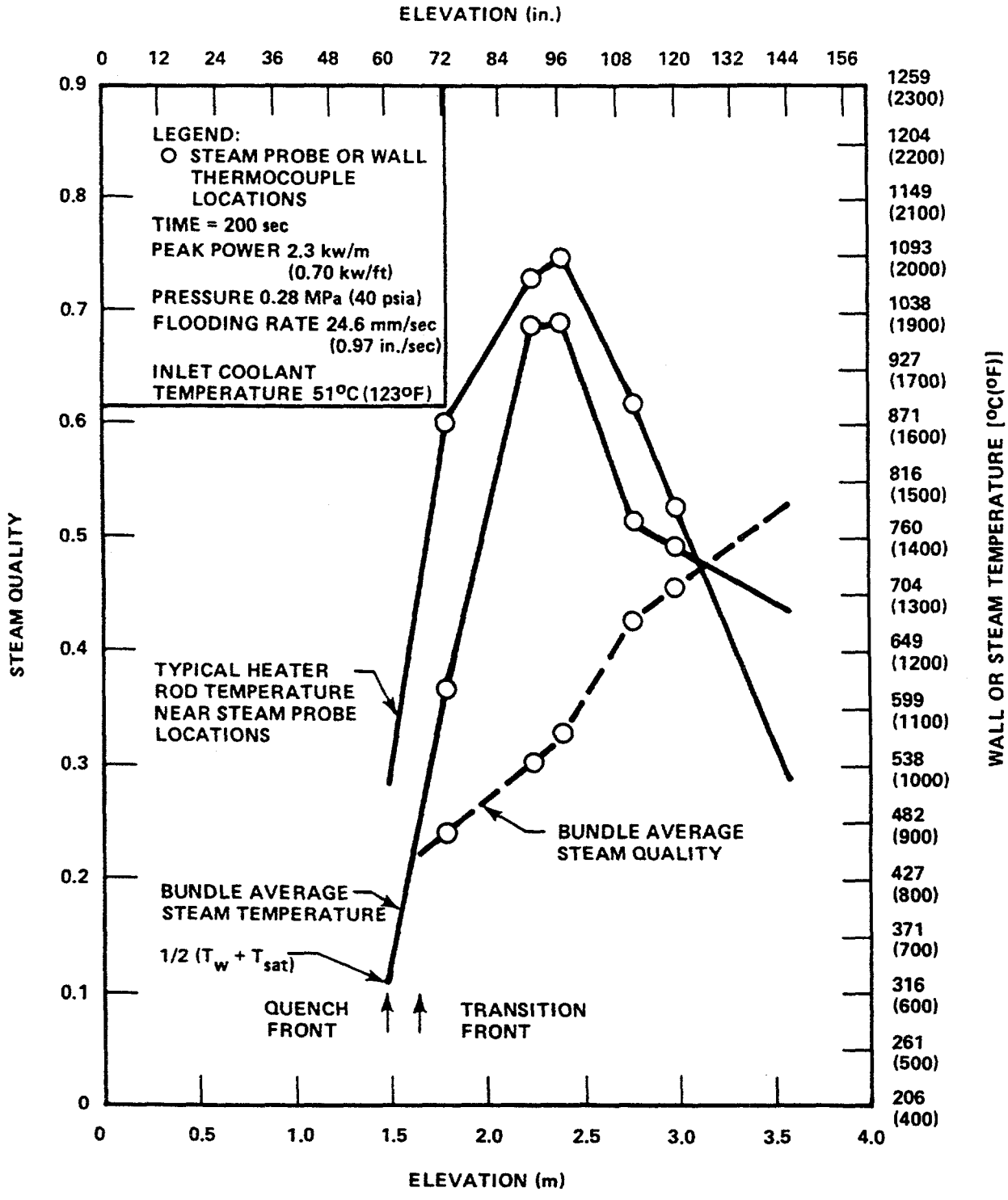

Figure 5. Data-Based Wall Temperature, Steam Temperature, and Steam Quality

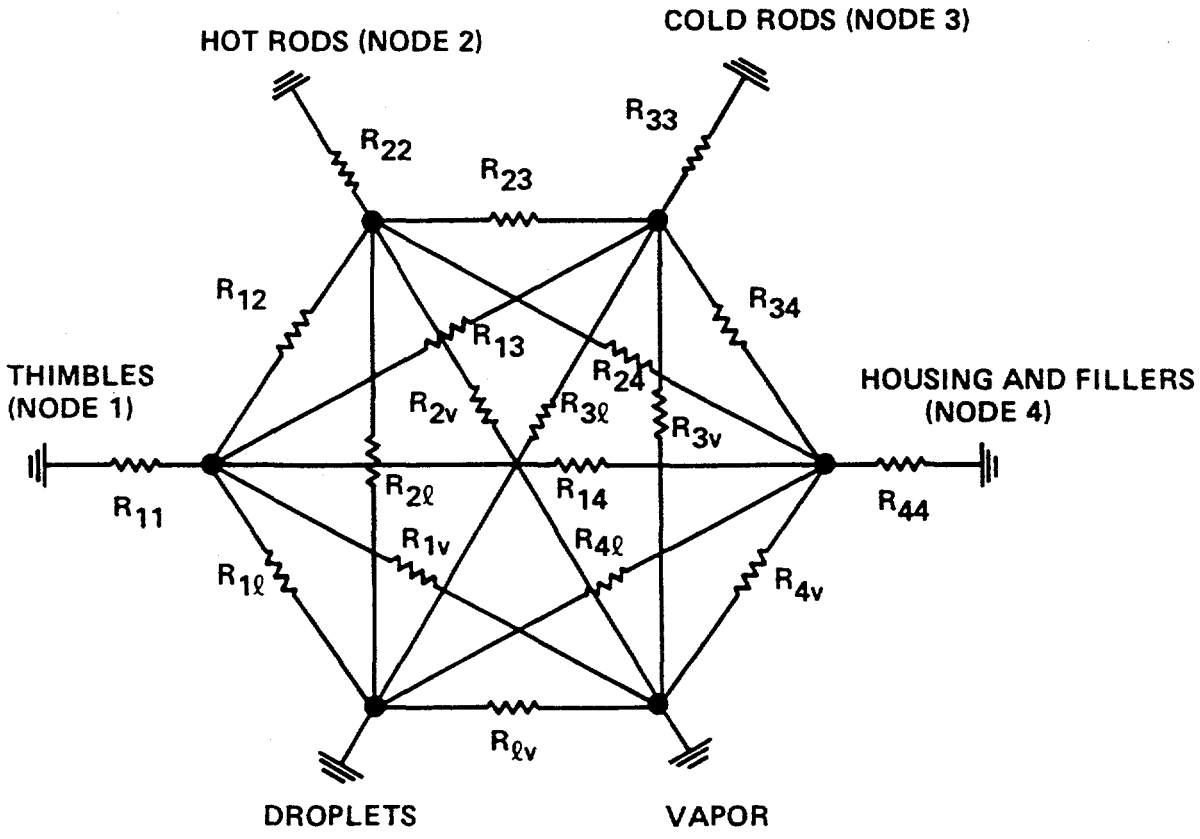

Figure 6. Radiation Network for Calculating Radiation Heat Transfer in FLECHT SEASET 161-Rod Bundle

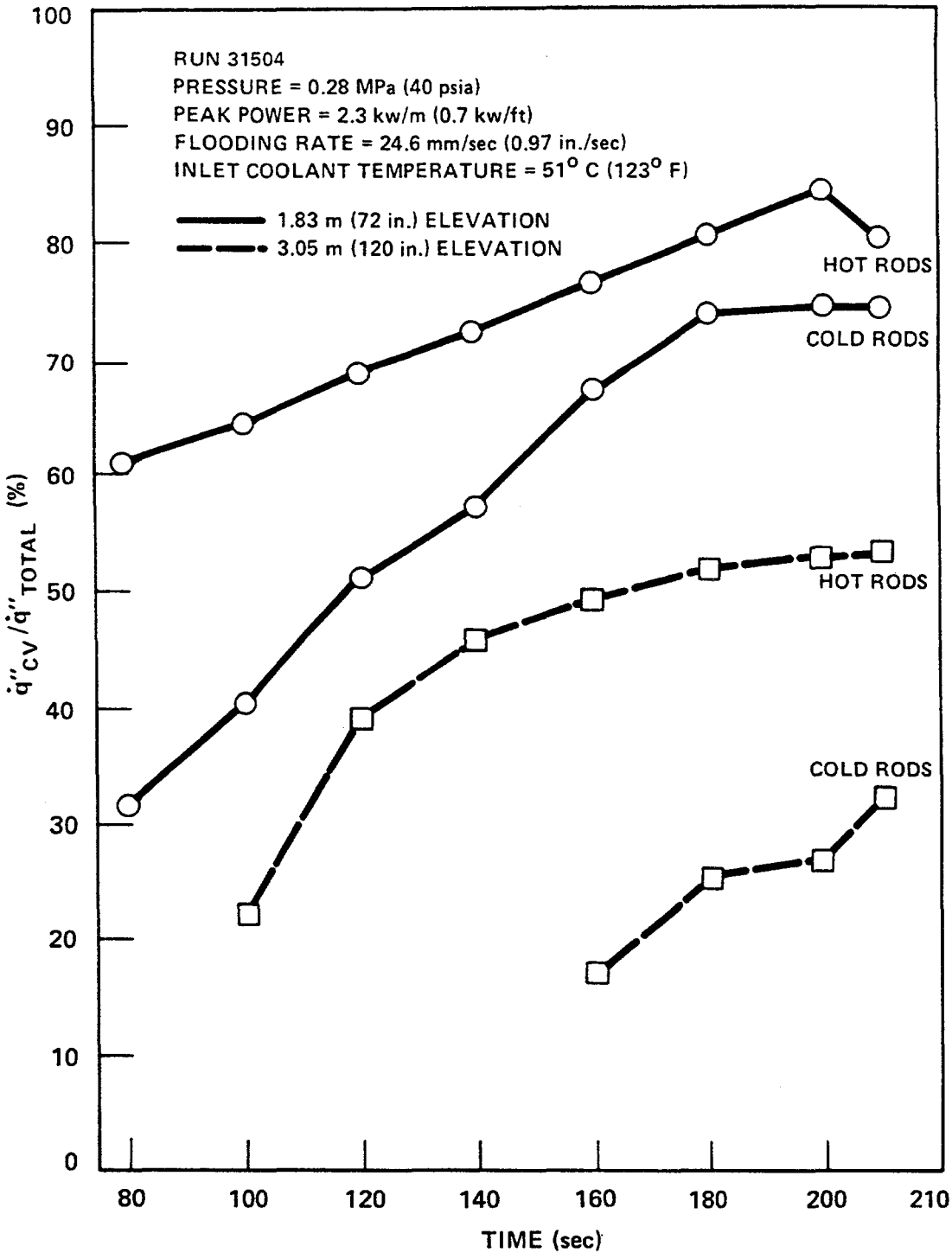

Figure 7. Relative Contribution of Convective Heat Flux During Reflood at 1.83 m (72 in.) and 3.05 m (120 in.) Elevations

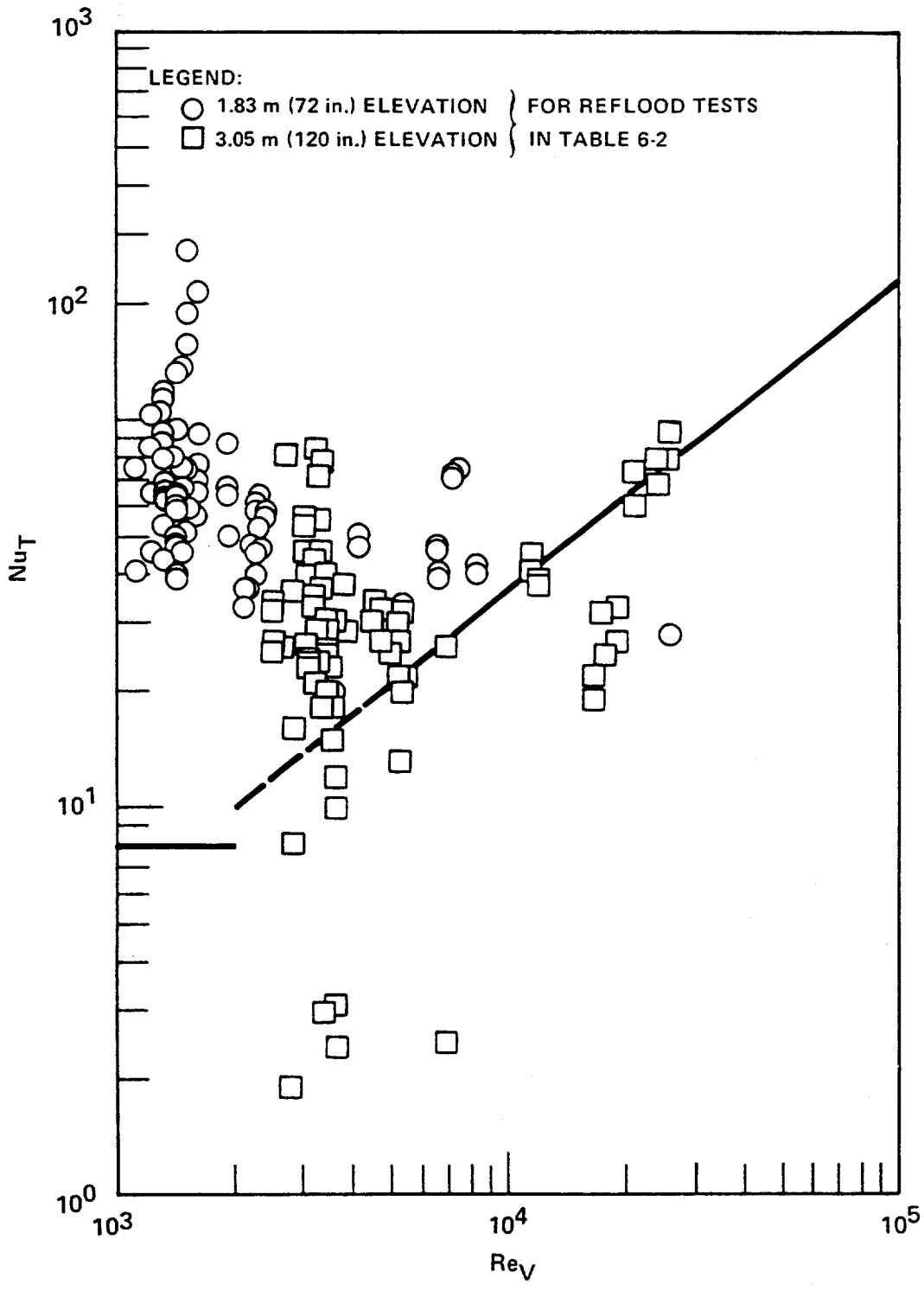

Figure 8. Calculated Nusselt Number (Based on Heater Rod Total Heat Flux) Versus Vapor Reynolds Number

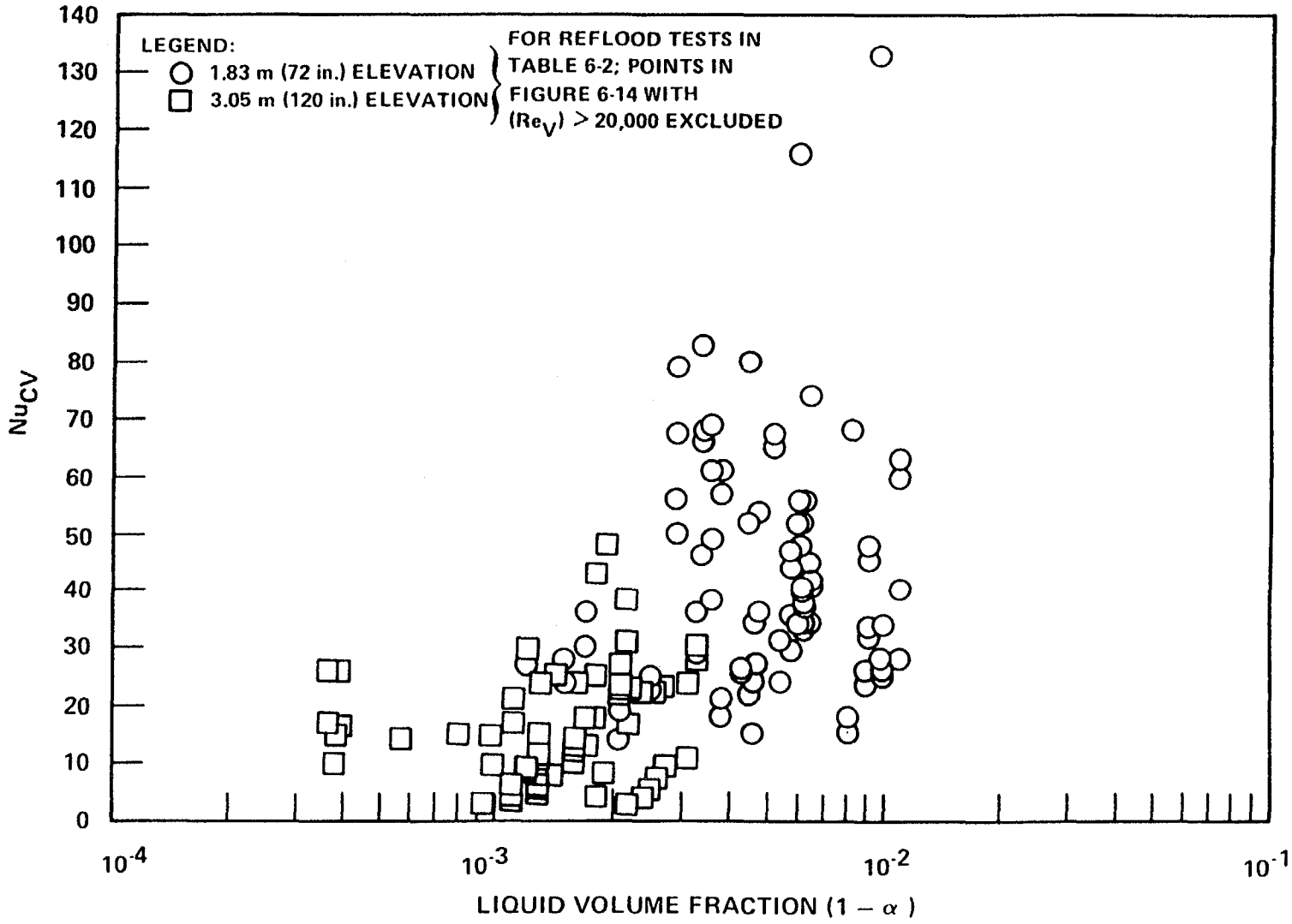

Figure 9. Calculated Nusselt Number (Based on Heater Rod Convective Heat Flux) Versus Liquid Volume Fraction

The transition region flow and heat transfer characteristics which includes

- flow regime characteristics, with estimates of the interfacial area
- quench front velocity and transition region liquid and vapor velocities
- entrained drop size, number density, and velocity at the top of the transition region
- vapor temperature
- void fraction
- flow quality
- convective enhancement of spacer grids
- wall temperature
- wall heat flux
- droplet shattering effects caused by spacer grids

In the dispersed flow film boiling region above the transition region which includes:

- vapor temperature and velocity
- droplet shattering effects of spacer grids
- drop size, velocity, and number density
- spacer grid convective enhancement
- void fraction
- spacer grid rewetting
- flow quality
- wall temperature
- temperature of structures for surface-to-surface radiation heat transfer
- wall heat flux

One of the important aspects in modeling rod bundles during the reflood (and blowdown) transient is modeling the thermal-hydraulic behavior of the spacer grids used to support the fuel rods. Spacer grids are designed by the vendors to enhance the mixing within the rod bundle such that higher allowable critical Heat Flux (DNB) margins can be obtained. The improved critical heat flux limits, are directly used in the evaluation of the Class II Plant Transient Analysis in which departure from nucleate boiling is the evaluation criteria. If spacer grids improve the heat transfer in bubbly flow, it is expected that would also improve the heat transfer in dispersed flow film boiling. There are three main heat transfer improvements caused by the spacer grids:

1) Enhanced convective heat transfer immediately downstream of the grid due to the flow acceleration through the grid and the reestablishment of the velocity and temperature boundary layers.

2) Rewetting of the unheated spacer grid which then acts to de-superheat the steam flow through the grid. A spacer grid has a large surface area, which is at rest

relative to the flow, such that the resulting interfacial heat transfer is large and the continuous vapor field is de-superheated.

3) Entrained droplet breakup due to contact with the spacer grids which mechanically reduces the droplet size and increases the liquid surface area for interfacial heat and mass transfer.

The spacer grids are generally all at the same elevations within the reactor core such that there is no significant assembly-wide flow redistribution. If however, the grids become located at different elevations or off-set, there can be additional flow redistribution from the fuel assembly with the higher grid pressure drop to the assembly with the lower grid pressure drop. The cross-flow will compound the difficulty in modeling the effects of the spacer grids and can lead to a heat transfer decrease in the affected assembly if the crossflow is significant. If the assembly with the higher pressure drop grids is the "hot assembly" there can be an additional heat transfer penalty.

In a similar fashion, for the limiting large-break LOCAs, the highest powered fuel rods are calculated to swell and burst even with a best-estimate model. The effects of the swelled and burst fuel rods within the rod bundle on the heat transfer in the coolant channels is similar to the effects of the spacer grids. The fuel rod blockage causes local flow acceleration through the restricted channels which acts to locally improve the convective heat transfer portion of the dispersed flow film boiling. Also, droplets which are entrained in the vapor flow can impact and shatter on the blocked rods particularly if they have burst and the cladding penetrates into the subchannels. Both of these mechanisms will act to improve the heat transfer in blocked bundle arrays relative to unblocked bundles. There is also one potential heat transfer penalty associated with flow blockage within the reactor core. The higher power rods are calculated to balloon and burst while the lower powered rods may just swell a little or not at all. Therefore, there is higher hydraulic resistance in the blocked portions of the core and flow by-pass will occur such that there is less fluid which passes through the blockage region such that the temperature rise of this fluid is more severe resulting in poorer heat transfer downstream of the blockage.

There have been rod bundle flow blockage experiments performed as part of the FLECHT-SEASET program (9) which indicated that for the flow rates of interest for PWR reflooding; the local heat transfer improvement with convection enhancement and droplet shattering, off-set the loss of flow through the blocked region such that the net heat transfer increased.

Current Computer Code Capabilities for Modeling Reflood Heat Transfer

Most of the current generation of best estimate safety analysis computer codes use a two field (liquid and vapor), separated flow model for the two-phase flow. They can have an additional field if the effects of non-condensible gases are explicitly modeled. A specific flow regime map and logic is used to specify the interfacial constitutive relationships between the

phases which determine the heat, mass and momentum transfer at the phase interface. There are also constitutive packages of models and correlations which are used for predicting the wall pressure drop and the wall heat transfer. These codes also include specific models for reactor system components such as the reactor coolant pumps, steam generators, jet pumps, steam separators, and the reactor control systems, core and vessel. The codes which fit this brief description are the TRAC series of codes, RELAP -5, CATHARE and ATHLET. These codes all have problems in predicting accurately the dispersed flow film boiling heat transfer typical of reflood conditions for a limiting large break LOCA in which the peak cladding temperature is near the acceptance limit. When these codes are validated against the test data, only the six-foot peak power location, for symmetrical cosine power shapes, is examined in detail and for this location some of the comparisons are good. However, a reactor can have many power shapes which have the possibility of being limiting such that the evaluation model must be able to predict the different elevations in a fuel rod from two-foot to the ten-foot equally well. In fact, usually the most limiting power shapes have a peak at eight-foot. One of the difficulties for these series of computer codes for modeling reflood is that there is no natural evolvement of the dispersed liquid phase into the continuous vapor phase. As a result the interfacial area, which changes in the dispersed flow film boiling portion of the transient, is only approximately modeled.

One code which was developed at the same time as the TRAC series of computer codes which accounts explicitly for the dispersed phase is the COBRA-TF code and its system counterpart, COBRA/TRAC(31, 32, 33). In addition to being used as part of a system code, COBRA-TF can also be used as a subchannel code such that individual subchannels within a rod bundle can be modeled. COBRA-TF has a vapor field, similar to TRAC, but includes two liquid fields; continuous liquid, to better model film flows and bubbly flow, and entrained droplet flow to better model liquid entrainment in the continuous gas phase. COBRA-TF also has specific flow regimes for 'cold walls", where the wall temperature is below the CHF point, and "hot walls" when the wall is in film boiling. The additional flow regime flexibility allows for accurate modeling of both situations. COBRA-TF also includes an interfacial area transport equation to track the interfacial area between the phases in a dispersed flow. Items such as droplet break-up are specifically modeled in the interfacial area equation as sources while deposition and evaporation are sinks of interfacial area. The more accurate field formulation allows the user additional flexibility in modeling the dispersed flow film boiling heat transfer regime and the effects of spacer grids and flow blockages.

COBRA-TF was extensively tested and used as part of the FLECHT-SEASET rod bundle flow blockage heat transfer program. Models which captured the phenomena given earlier, for the dispersed flow film boiling phase of the transient, and the effects of spacer grids and fuel rod blockages, were incorporated into COBRA-TF. Several comparisons were made with bottom reflood data, with and without simulated flow blockage (9); and for top down spray cooling situations typical of a BWR(34, 35). Comparisons of COBRA-TF predictions and experimental data for both reflood and top down spray cooling are shown in Figures 10 to 19. As these comparisons indicate, COBRA-TF does a creditable job of predicting the rod temperatures as

well as the measured vapor superheat temperatures. It was also found that COBRA-TF also would predict approximately the mean droplet diameter of the measured droplet distribution which was measured in the experiments.

Desired Code Features for Best Estimate Modeling of Dispersed Flow Film Boiling

Many of the desired code features for modeling the dispersed flow film boiling phenomena all ready exist in the existing computer codes, such as multiple fields, modeling of non-equilibrium in the flows and the models for the reactor system components. However, in order to improve the modeling of the dispersed flow film boiling heat transfer regime , it is recommended that at least three fields be used; vapor, continuous liquid, and entrained liquid. It would be preferable if four fields could be used with two different entrained liquid droplet fields such that the shattering effects of spacer grids and blockages, which generate a population of smaller droplets, could be modeled explicitly rather than combining their heat transfer effects with the larger unshattered drops.

Along with the features of additional fields for the entrained flow; an interfacial area transport equation is needed to track the changes of the interfacial area along the rod bundle, due to evaporation and or condensation, as well as in other components. Using this approach, phenomena such as droplet shattering, deposition, evaporation, and generation (at orifice plates or other reactor hardware) can be more explicitly modeled.

Reflood is more of a lagrangian process, with different "fronts" moving through the core as the fuel rods cool and quench. Currently, most computer codes use a coarse mesh for the eulerian hydraulic cell representation of the core or a rod bundle. There is an extremely sharp gradient in the void fraction at the quench front in the transition region where the flow transitions from a liquid inlet flow to a dispersed droplet flow regime. Usually this region is contained in a single hydraulic cell in the code. As a result, the prediction of the void change and the resulting liquid entrainment, and the vapor superheat in this region, is something less than perfect. It is believed that the use of finer hydraulic noding (three-inch cells or less) for the entire transition region would help resolve the void gradients in the flow as well to more accurately model the entrainment. The entrainment which is generated at the quench front and the transition region is the source of entrained liquid for the dispersed flow film boiling region downstream of the quench front where the peak cladding temperature is calculated. The entrainment at the top of the transition region as well as the vapor superheat are boundary conditions for the dispersed flow heat transfer region. The use of smaller cells would result in sufficient cells in which an individual void fraction can be calculated as the void changes from nearly zero at the quench front to nearly 100%

It is this authors opinion that it is very desirable to have a best-estimate code which can represent both lumped fuel assemblies as well as having the ability to model rod bundles on a subchannel basis. This combination provides the user with greater flexibility for modeling and he can better isolate the hot assembly and if necessary, the hot rod. One can also model more precisely the effects of other fuel assembly structures such as the guide tube thimbles, which are a radiation heat sink during the reflood process.

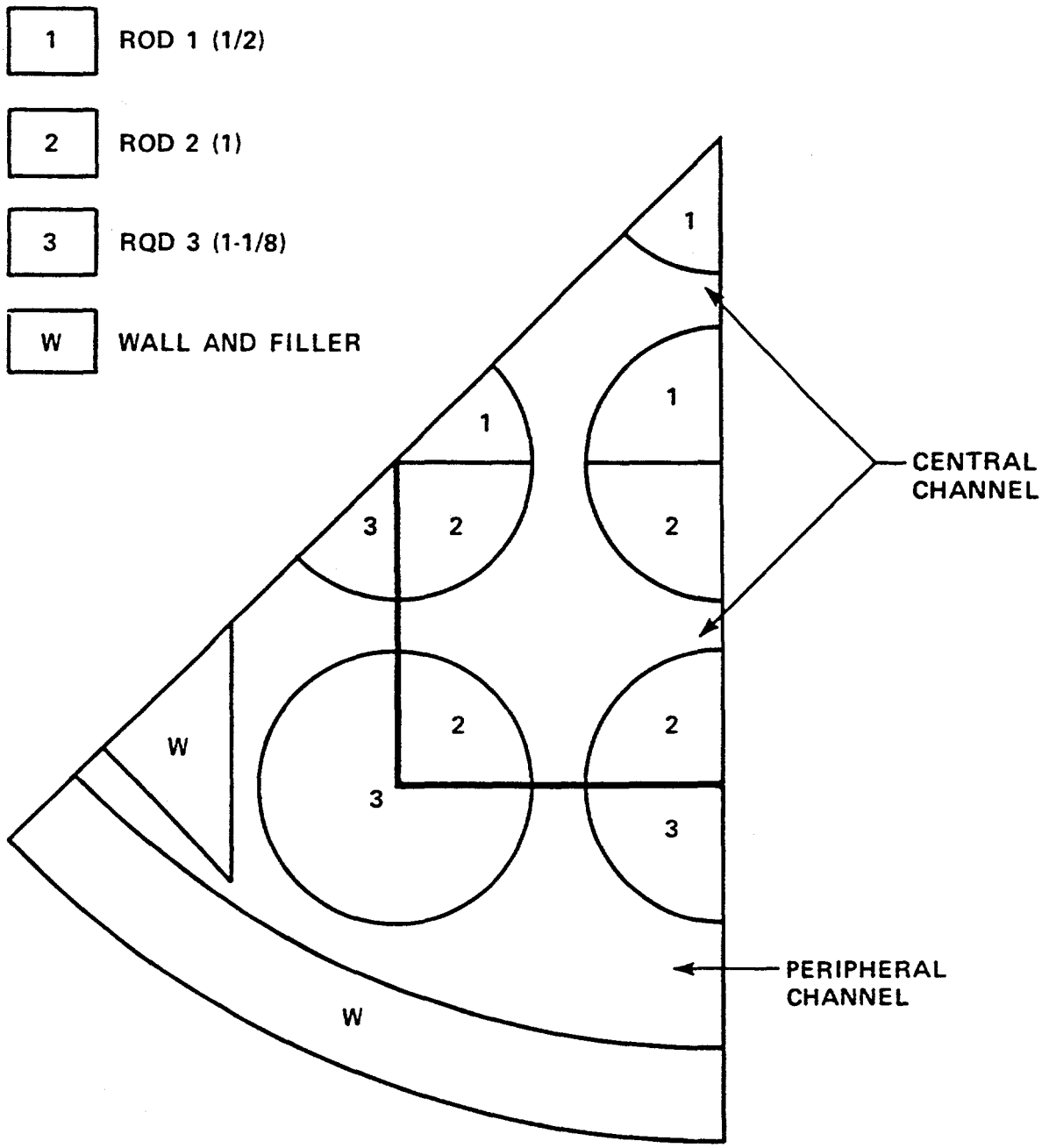

Figure 10. Radial Noding for FLECHT SEASET 21-Rod Bundle Test Data Comparisons

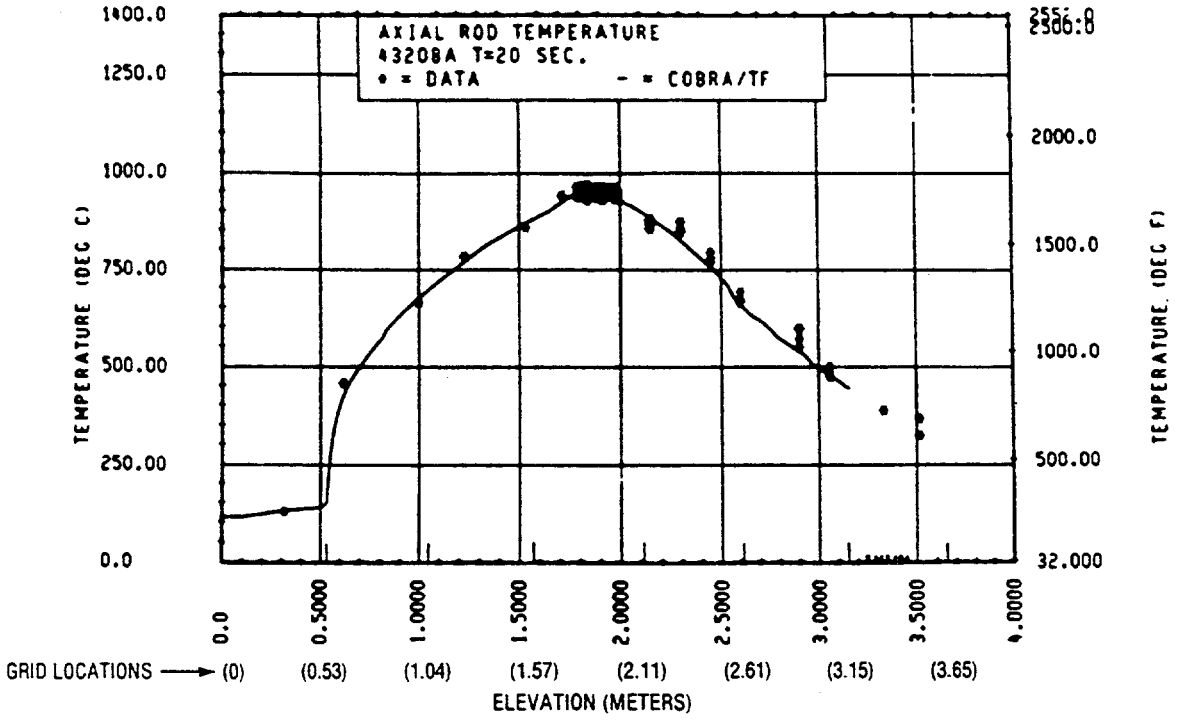

Figure 11a. Comparison of COBRA-TF-Calculated Axial Rod Temperature Versus Elevation With FLECHT SEASET 21-Rod Data, Test 43208A, t = 20 Seconds

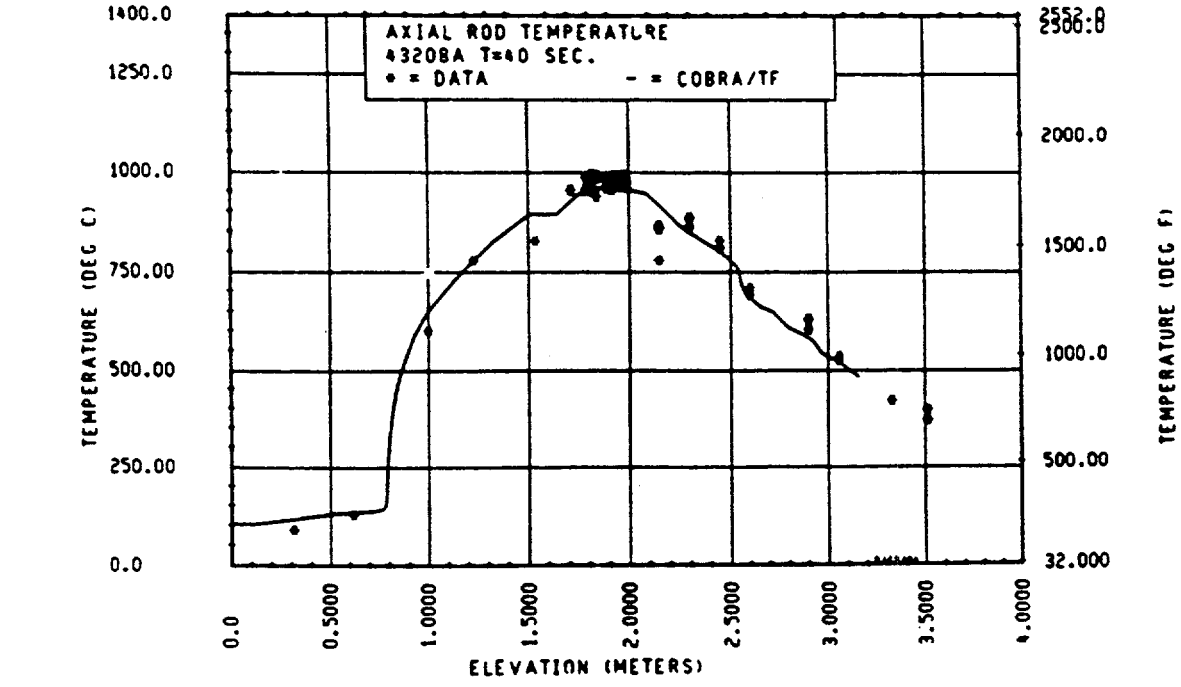

Figure 11b. Comparison of COBRA-TF-Calculated Axial Rod Temperature Versus Elevation With FLECHT SEASET 21-Rod Data, Test 43208A, t = 40 Seconds

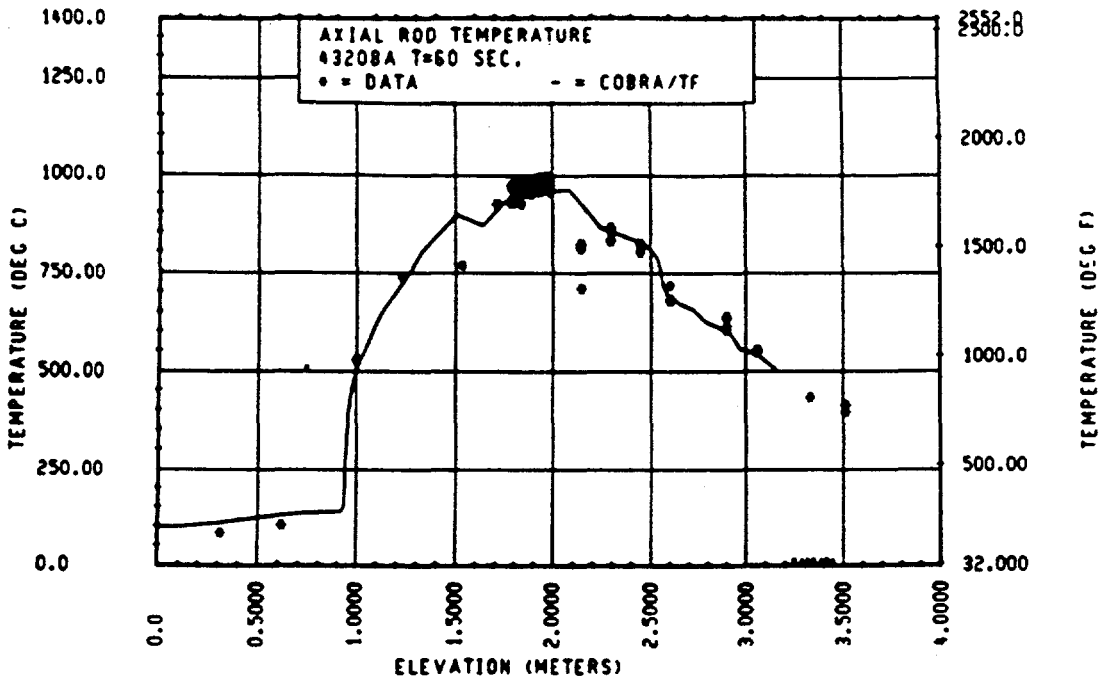

Figure 12a. Comparison of COBRA-TF-Calculated Axial Rod Temperature Versus Time With FLECHT SEASET 21-Rod Data, Test 43208A, t = 60 Seconds

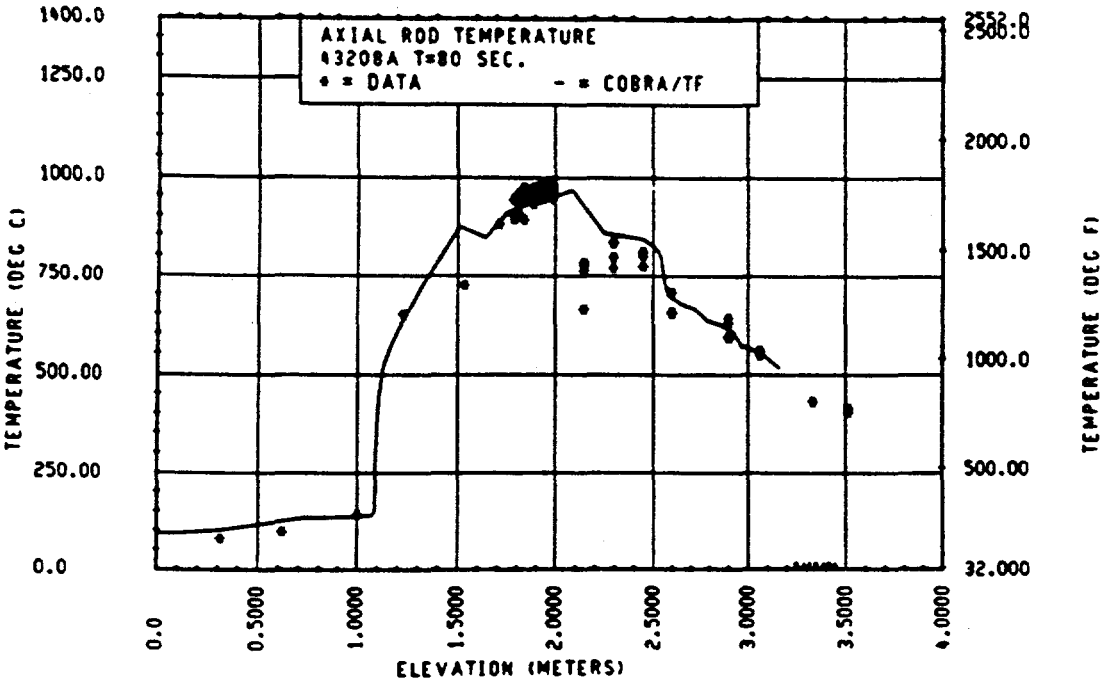

Figure 12b. Comparison of COBRA-TF-Calculated Axial Rod Temperature Versus Time With FLECHT SEASET 21-Rod Data, Test 43208A, t = 80 Seconds

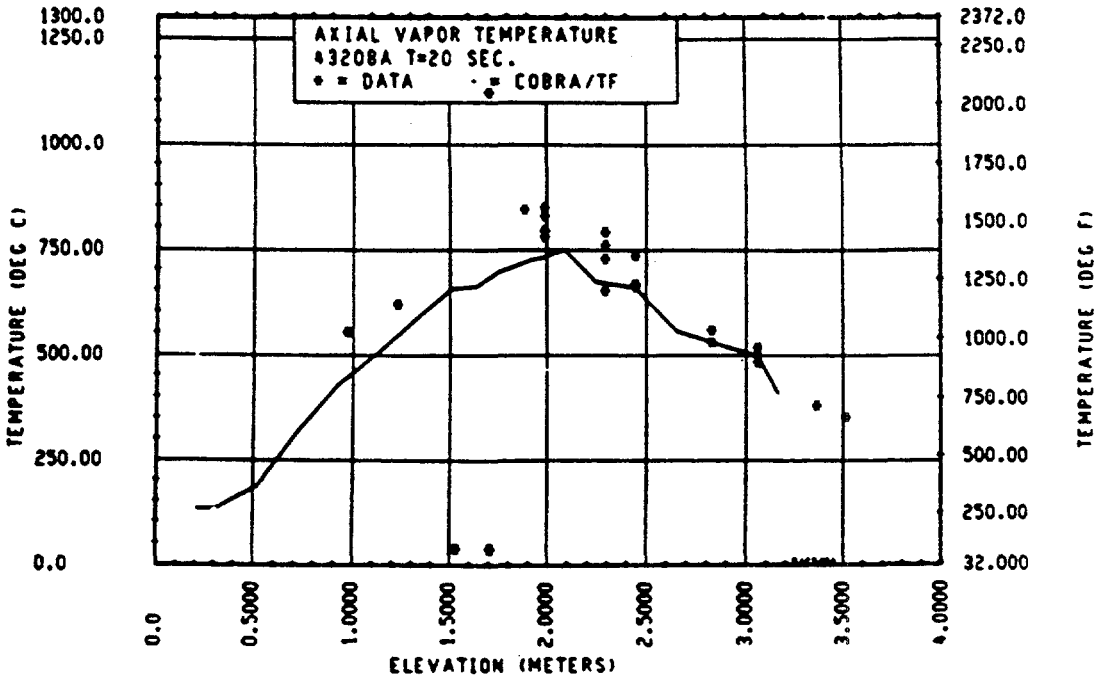

Figure 13a. Comparison of COBRA-TF-Calculated Axial Vapor Temperature Versus Elevation With FLECHT SEASET 21-Rod Data, Test 43208A, t = 20 Seconds

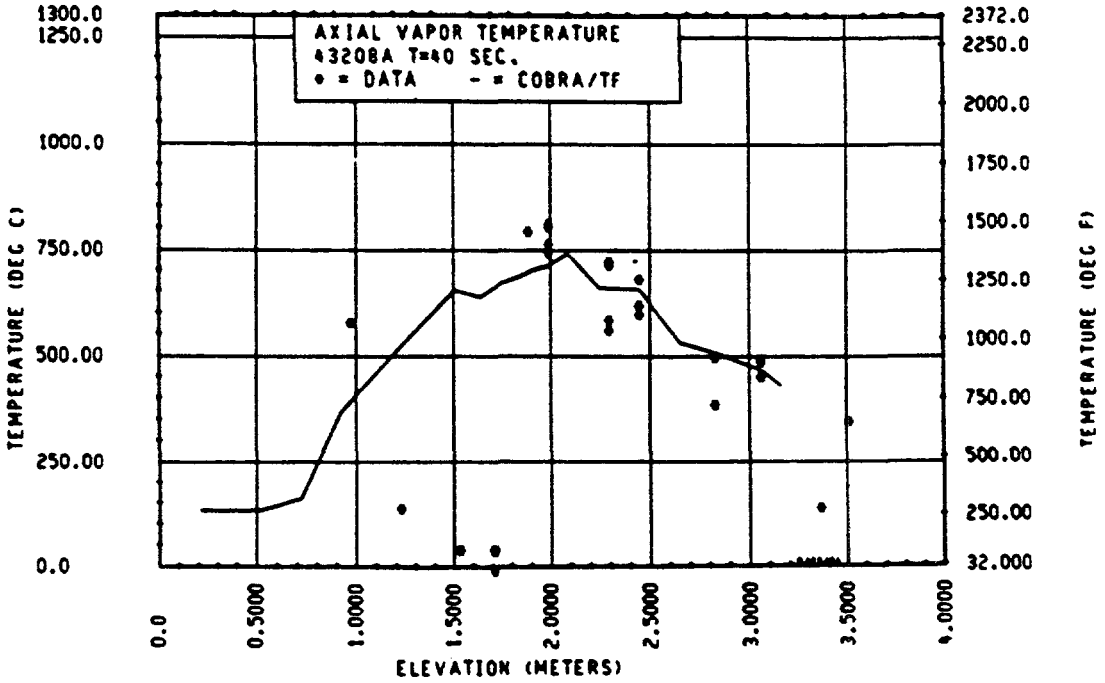

Figure 13b. Comparison of COBRA-TF-Calculated Axial Vapor Temperature Versus Elevation With FLECHT SEASET 21-Rod Data, Test 43208A, t = 40 Seconds

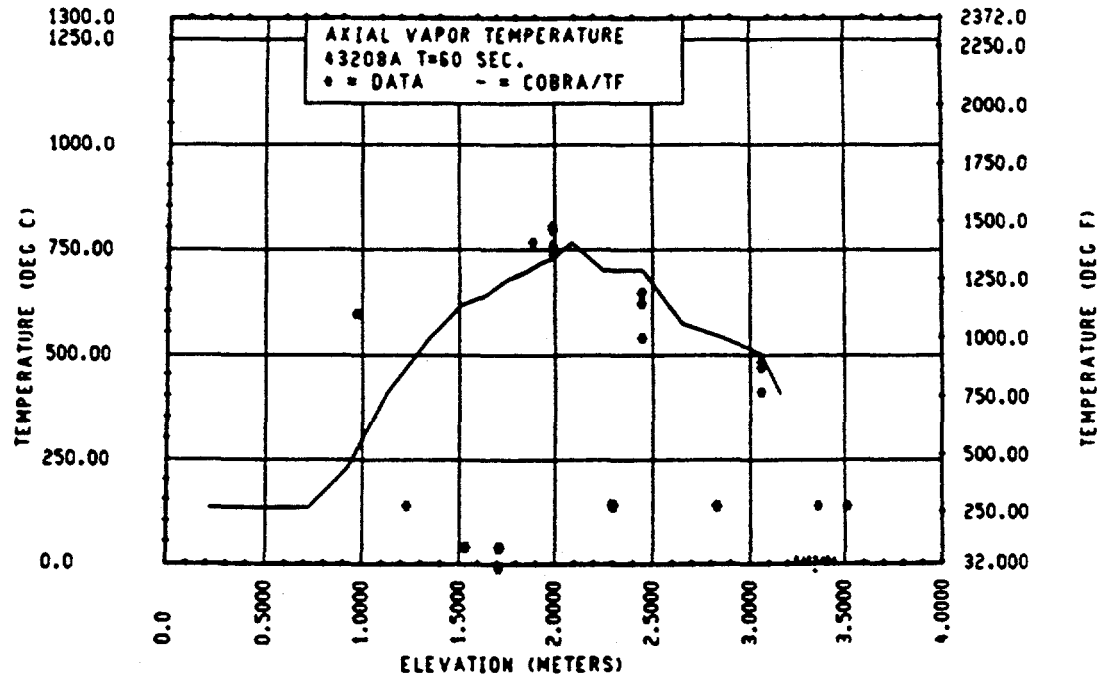

Figure 14a. Comparison of COBRA-TF-Calculated Axial Vapor Temperature Versus Time With FLECHT SEASET 21-Rod Data, Test 43208A, t = 60 Seconds

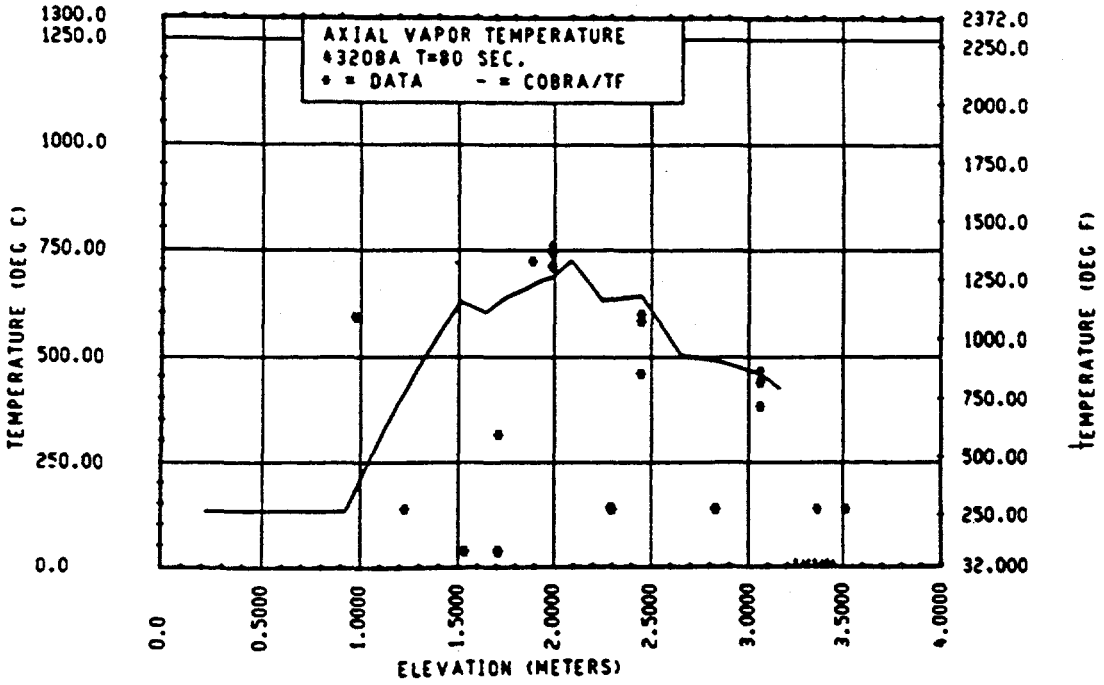

Figure 14b. Comparison of COBRA-TF-Calculated Axial Vapor Temperature Versus Time With FLECHT SEASET 21-Rod Data, Test 43208A, t = 80 Seconds

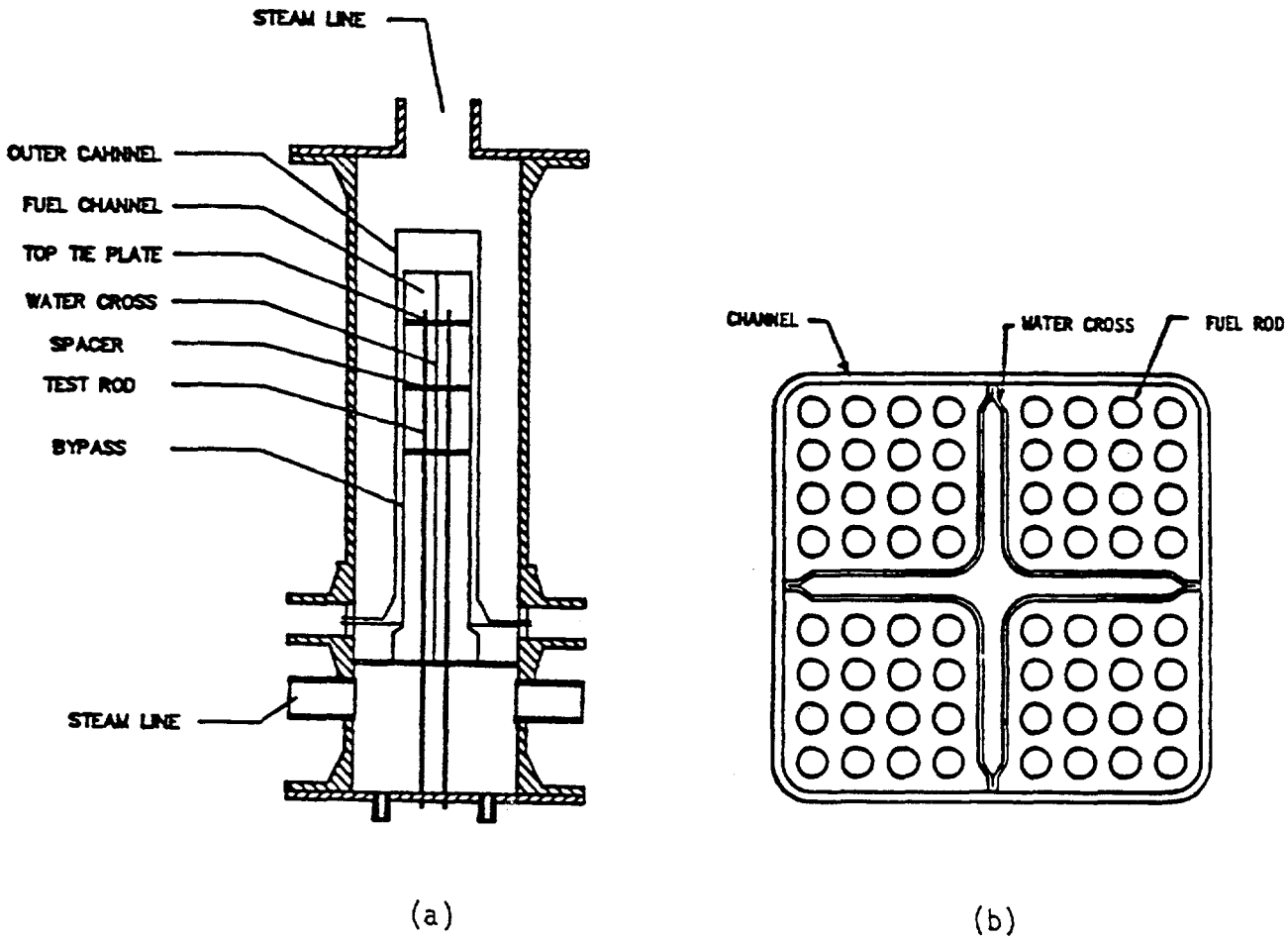

Figure 15. The Test Section of SVEA Spray Cooling Experiments

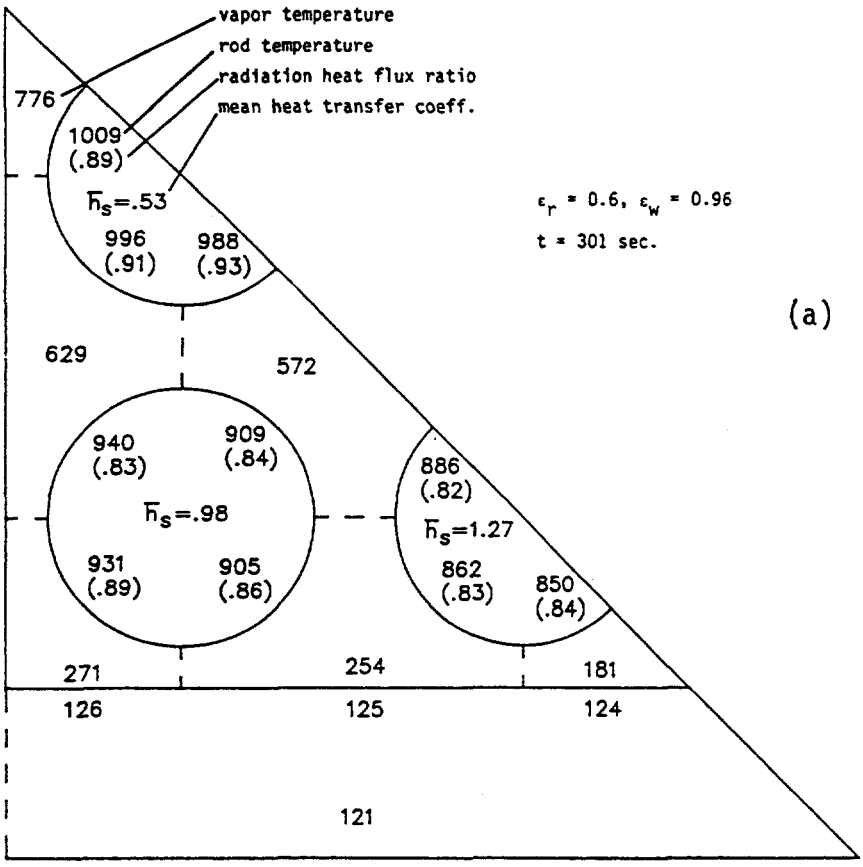

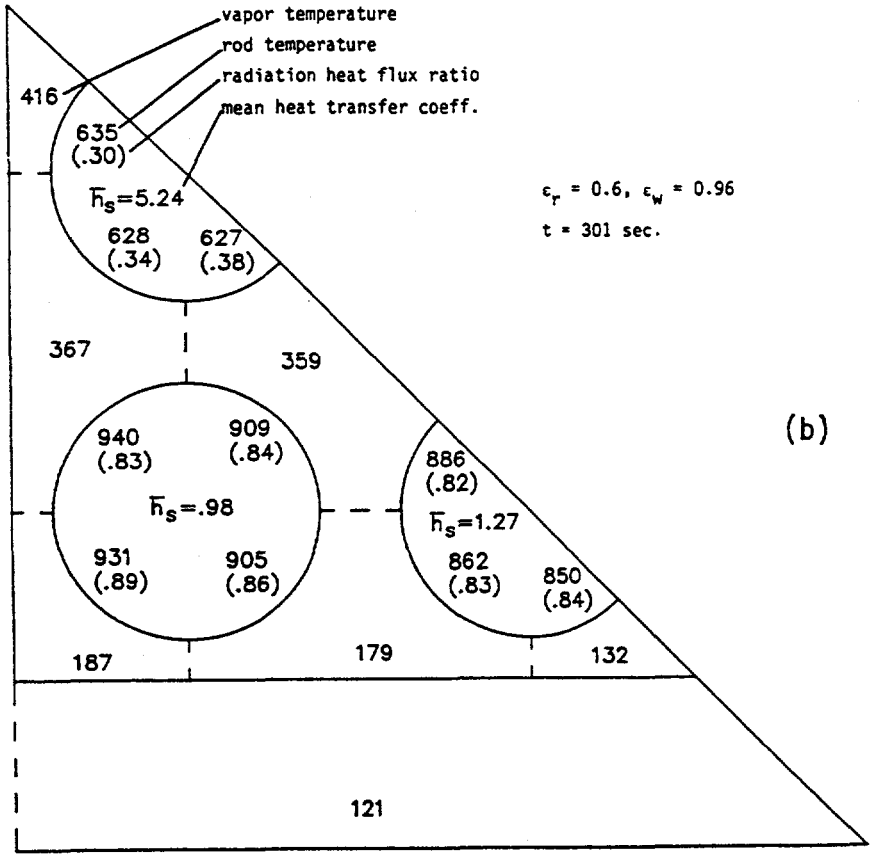

Figure 16. Predicted Vapor and Surface Temperatures (a) Level 4, (b) Level 7 for Uniform Spray, Test 44

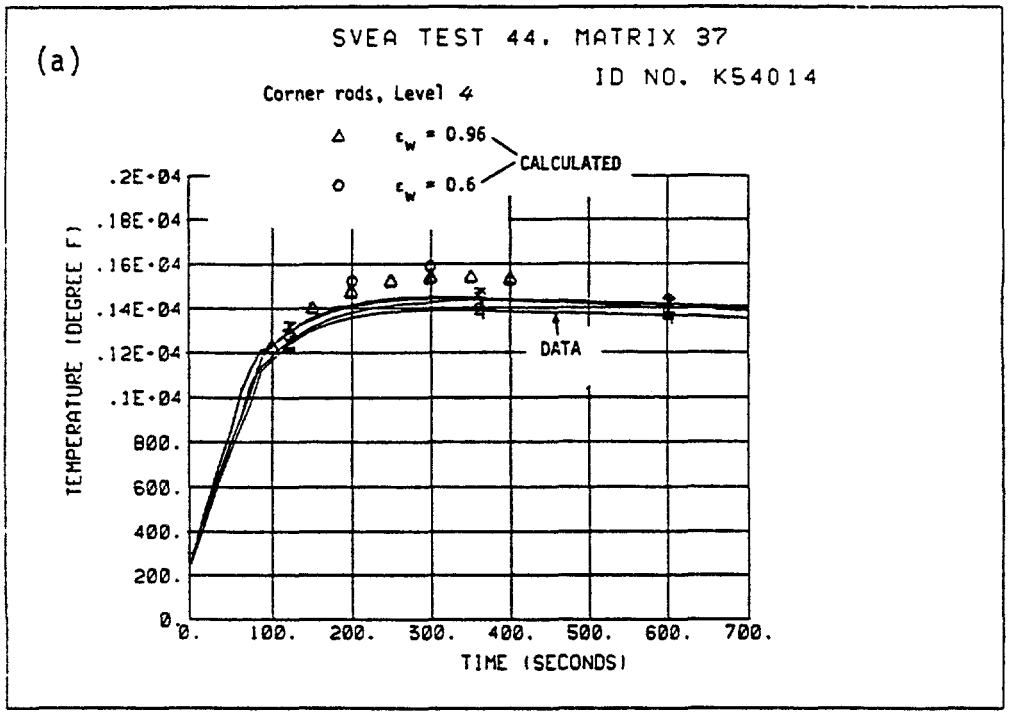

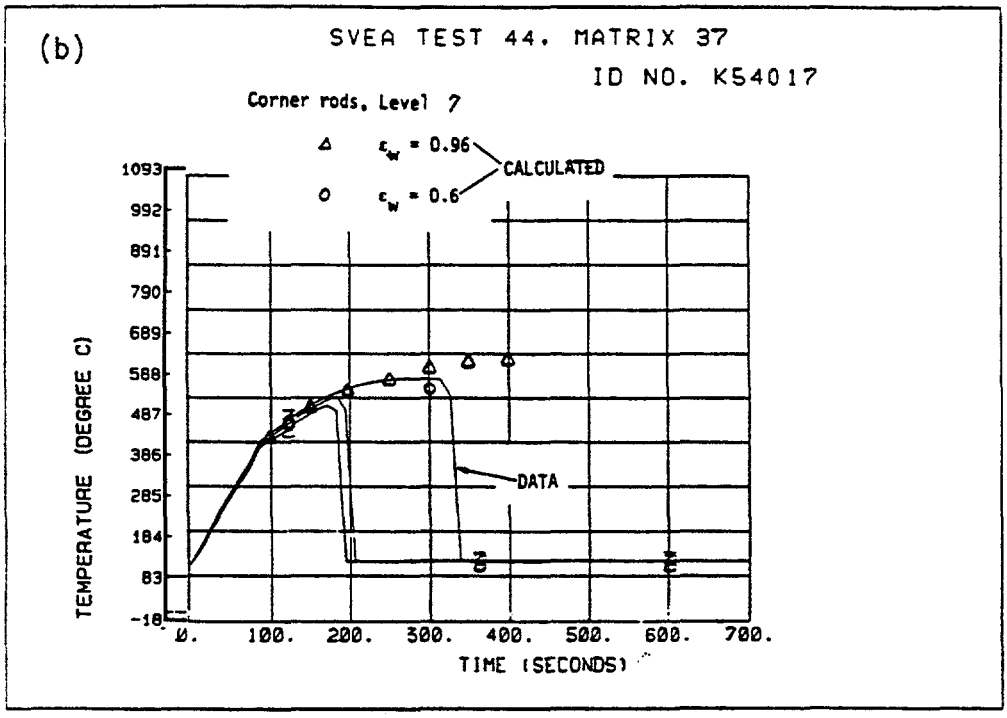

Figure 17. Comparison of Corner Rod Temperature at (a) Level 4, (b) Level 7 for Uniform Spray, Test 44

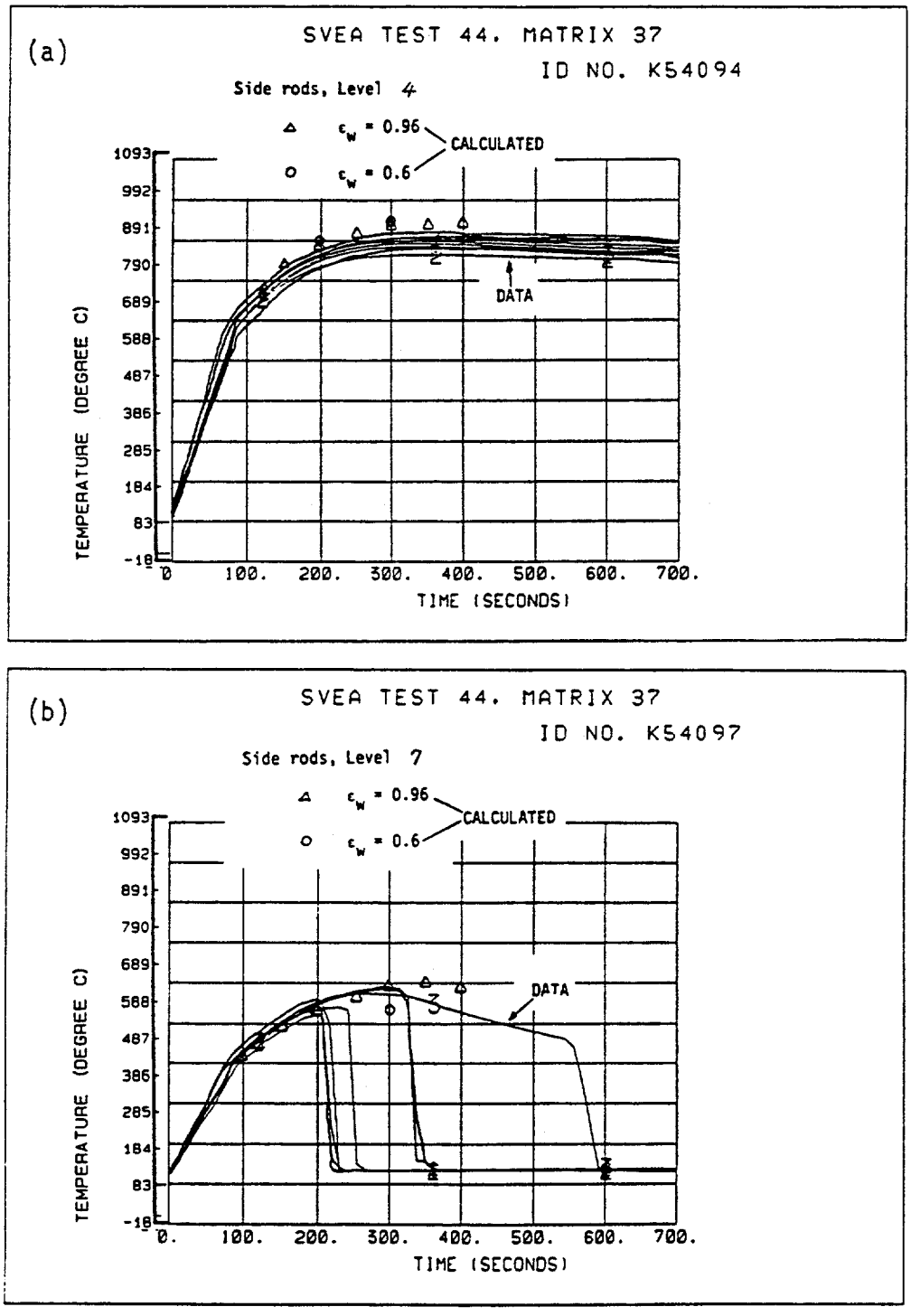

Figure 18. Comparison of Side Rod Temperature at (a) Level 4, (b) Level 7 for Uniform Spray, Test 44

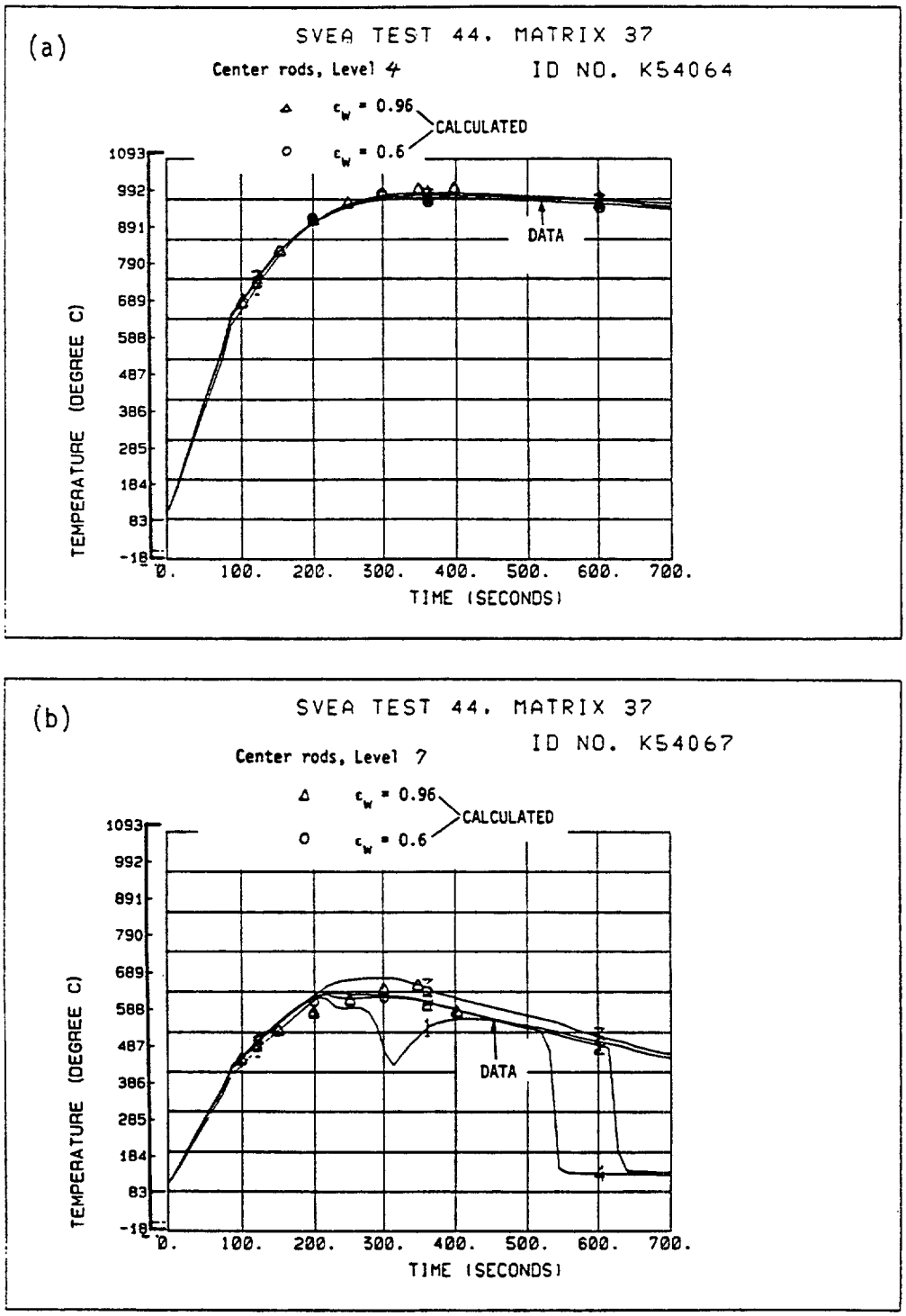

Figure 19. Comparison of Center Rod Temperature (a) Level 4 (b) Level 7 for Uniform Spray, Test 44

References

1. Hochreiter, L.E., Ankney, R.D., Young, M.Y., and Kalra, S.P., "Application of PWR LOCA Margin with the Revised Appendix K Rule," Nuclear Engineering and Design, Vol. 132, No. 3, pp. 437-447 (1992).

2. Wheatley, P.D., "Analysis of a BWR/6-218 During a Large Break Loss of Coolant Accident Using Evaluation Model Type Boundary Conditions," EGG-SAAM-6519, (1984).

3. Andreani, M., and Yadigaroglu, G., "Prediction Methods for Dispersed Flow Film Boiling." Int. J. Multiphase Flow, Vol. 20, Suppl., 1-51, 1994.

4. Lee, N., Wong, S., Yeh, H.C., and Hochreiter, L.E., "PWR FLECHT-SEASET Unblocked Bundle, Forced and Gravity Reflood Task Data Evaluation & Analysis Report," NRC/EPRI/Westinghouse Report No. 10, WCAP-9891, NURG/CR-2256, EPRI NP-2013, November (1981).

5. Lilly, G.P., Yeh, H.C., Hochreiter, L.E., and Yamaguchi, N., "PWR FLECHT Cosine Low Flooding Rate Test Series Evaluation Report," WCAP-8838 (1977).

6. Lilly, G.P., Yeh, H.C., Hochreiter, L.E., and Yamaguchi, N., WCAP-9183, PWR FLECHT Skewed Profile Low Flooding Rate Test Series Evaluation Report.

7. Conway, C.E., Hochreiter, L.E., Krepinevich,, M.C., Massie, H.W., Jr., Rosal, E.R., and Howard, R.C., "PWR FLECHT Separate Effects and System Effects Test (SEASET) Program Plan," NRC/EPRI, Westinghouse Report No. 1, December (1977).

8. Howard, R.C. and L.E. Hochreiter, "PWR FLECHT-SEASET Steam Generator Separate Effects Task Data Analysis and Evaluation Report," EPRI NP-1461, Project 959-1, Topical Report No. 9, NURC/CR-1534, WCAP-9724, February (1982).

9. Paik, C.Y., Hochreiter, L.E., Kelly, J.M., and Kohrt, R.J., "Analysis of FLECHT SEASET 163-Rod Blocked Bundle Data Using COBRA-TF," NUREG/CR-4166, WCAP-10375, October (1985).

10. Hochreiter, L.E., "FLECHT-SEASET Program Final Report," NUREG/CR-4167, WCAP-10926, November (1985).

11. USNRC, "Compendium of ECCS Research for Realistic LOCA Analysis, NUREG-1230, (1988).

12. Ihle, P., and Rust, K., "Influence of Spacers on the Heat Transfer During the Flood Phase of a Pressured Water Reactor Loss of Coolant Accident," Nuclear Research Center, Karlsruhe, KFK Report 3178. September 1982.

13. Ihle, P., Rust, K., and Lee, S.L., "Experimental Investigation of Reflood Heat Transfer in the Wake of Grid Spacers," presented at NRC/ANS Meeting on Basic Thermal-Hydraulic Mechanisms in LWR Analysis, September 1982, published in NUREG-CP-0043.

14. Clement, P., Deruazz, R., and Veteau, J.M., "Reflooding of a PWR Bundle Effect of Inlet Flow Rate Oscillations and Spacer Grids," presented at European Two-Phase Flow Group Meeting, Paris, June 1982.

15. Yamanouchi, A., "Effect of Core Spray Cooling in Transient State After Loss of Coolant Accident," Nucl. Appl., 5 (1968).

16. Slifer, B.C., "Loss of Coolant Accident and Emergency Core Cooling Models for General Electric Boiling Water Reactors", NEDO-10329, (April 1971).

17. Schumacher, D.G., "BWR Refill-Reflood Program, Task 4.4-CCFL Refill Systems Effects Tests," GEAP-24893, April 1981).

18. Yoder, et al., "Dispersed Flow Film Boiling in Rod Bundle Geometry - Steady State Heat Transfer Data and Correlation Comparisons, NUREG/CR-2435, ORNL-5822, March 1982.

19. Zhang, J., Hochreiter, L.E., Bajorek, S.M., and Kemper, R.M., "WCOBRA/TRAC Analysis of ORNL High Flow Rod Bundle Film Boiling Tests," to be presented at the National Heat Transfer Conference, Baltimore, MD, August 1997.

20. Gottula, R.C., Condie, R.G., Sandaram, R.K., Neti, S., Chen, J.C., and Nelson, R.A., "Forced Convective, Nonequilibrium, Post-CHF Heat Transfer Experiment Data and Correlation Comparison Report," Idaho National Engineering Laboratory Report EGG-2245, NUREG/CR-3193 (March 1985).

21. Katsma, K.R., Hall, D.G., Shaw, R.A., Fletcher, C.D., and K.S. Boodry, Nuclear Regulatory Commission, "Quantifying Reactor Safety Margins, Appendix O," NUREG/CR-5249 EGG-2552 R4, 1989.

22. Chen, J.C., "A Short Review of Dispersed Flow Heat Transfer in Post-Dryout Boiling," Nuclear Engineering and Design, 95, 375-383, 1984.

23. Unal, C., "An Experimental Study of Thermal Nonequilibrium Convective Boiling in Post-Critical-Heat-Flux Region in Rod Bundles," Ph.D. Dissertation, Lehigh University (1985).

24. Forslund, R.P., and Rohsenow, W.M, ."Dispersed Flow Film Boiling," J. Heat Trans. 90 (6), 399-407 (1968).

25. Hynek, S.J., Rohsenow, W.M., and Gergles, A.E., "Forced-Convection Dispersed-Flow Film Boiling," Massachusetts Institute of Technology Report 70586-63 (April 1969).

26. Dougall, R.S., and Rohsenow, W.M., "Film Boiling on the Inside of Vertical Tubes with Upflow of the Fluid at Low Qualities," MIT Report 9079-26.

27. Ganic, E.N., and Rohsenow, W.M., "Dispersed Flow Heat Transfer," Int. J. Heat and Mass Transfer, Vol. 20, pp. 855-866 (1977) .

28. Iloeje, O.C., Plummer, D.N., Rohsenow, W.M., and Griffith, P., "A Study of Wall Rewet and Heat Transfer in Disposed Vertical Flow," MIT Report 72718-92 (1974).

29. Iloeje, O.C., Plummer, D.N., Griffith, P., and Rohsenor, W.M., "An Investigation of the Collapse and Surface Rewet in Film Boiling in Vertical Flow," J. Heat Trans., Vol. 97, pp. 166-172 (1975).

30. Liles, D.R., et al, "TRAC-PF1/MOD1 Correlations and Models," NUREG/CR-5069 LA-11208-MS, September 1988.

31. Hochreiter, L.E., Kelly, J.M., Kohrt, R.J., Paik, C.Y., and Utton, D.B., "Reflood Heat Transfer Models for Rod Bundles with Flow Blockage," Proceedings of the 1987 ASME/AIChE National Heat Transfer Conference, Pittsburgh, PA, August (1987).

32. Kelly, J.M., Hochreiter, L.E., Loftus, M.J., and Paik, C.Y., "COBRA-TF Grid Spacer Heat Transfer Models," ANS Transactions, Vol. 46, pp. 842-844, New Orleans, LA, June 3-7 (1984).

33. Hochreiter, L.E., Kelly, J.M., Paik, C.Y., and Young, M.Y., "Improved Analytical Models for PWR Safety Analysis," Proceedings at the Transient Phenomena in Multiphase Flow Meeting, Dubrovnik, Yugoslavia (1987).

34. Chiou, J.S. and Hochreiter, L.E., "Combined Radiation and Dispersed Flow Film Boiling in BWR Rod Bundles with Top Spray," Proceedings of the 26th National Heat Transfer Conference, Philadelphia, PA, August (1989).

35. Hochreiter, L.E. and Chiou, J.S., "COBRA/TF Analysis of SVEA Spray Cooling Experiments," Proceedings of the 26th National Heat Transfer Conference, Philadelphia, PA, August (1989).

BORON-MIXING CODE ASSESSMENT TESTS AT THE UMCP 2X4 LOOP

Prepared for the 25th Water Reactor Safety Meeting
October 22, 1997

M. Gavrilas, G. Pertmer, K. Kiger*,
K. Almenas, M. DiMarzo*, Y.Y. Hsu,
B. Woods, and F. Gavelli*

Department of Materials and Nuclear Engineering
*Department of Mechanical Engineering
University of Maryland
College Park, MD 20742

Abstract

The potential reactivity insertion caused by the transport of a boron-dilute water volume to the core region has been an active area of research in the past years. The University of Maryland at College Park (UMCP) 2x4 Loop has been involved in a three year study of boron-dilution related reactivity transients. This program investigated the means of formation of a boron-dilute slug in the steam generator, the transport of the slug through the system and the predominant mixing mechanisms that will affect the boron-dilution of this slug as it enters the core region.

The concomitant review of literature on the subject revealed limitations of current computer codes in simulating phenomena associated with boron-dilute volume reactivity transients. This paper describes a series of tests that will assess code performance in such transients. The tests are devised in the context of the current UMCP boron mixing experimental program. The tests employ the integral test facility configuration of the Loop, but are proposed with more controlled initial conditions than would be expected in a prototype. This compromise preserves the test realism, while providing an assessment problem that can be more clearly evaluated.

Introduction

The reactivity insertion caused by the transport of a boron-dilute water volume to the core region has been shown to depend on the location where the volume forms, and the means by which it forms and is transported to the core. As expected, specific plant design features that enhance or limit the mixing of the boron-dilute volume as it travels to the core affect the reactivity insertion.

A boron-dilute slug can accumulate in either the vessel lower plenum or the steam generator. The formation in both these places can be due to unborated water ingress from an interfacing system. In the steam generator, a boron dilute volume can also form as a result of operation in boiling/condensing mode (BCM). The inadvertent actuation of primary coolant pumps can transport the boron-dilute slug to the core. When the slug is formed during BCM operation, refilling the primary system can lead to the resumption of natural circulation which also transports the slug to the core region.

The University of Maryland Loop experimental program was devised to investigate the formation of the slug during BCM operation and its transport to the core through pump actuation or resumption of natural circulation.

The University of Maryland 2x4 Thermal-hydraulic Facility

The 2x4 Loop is a scaled integral model of a Babcock and Wilcox (B&W) lowered-loop PWR system; it is a reduced-pressure and reduced-height facility. B&W pressurized water reactors (PWRs) are unique in using once-through steam generators (OTSGs); the other PWR vendors use U-tube steam generators (UTSGs). In B&W lowered-loop configuration plants, the elevation of the horizontal portion of the hot legs is at about the mid-plane elevation of the steam generators (SGs).

The UMCP 2x4 loop facility has two OTSGs connected to the reactor pressure vessel (RPV) via two hot legs and four cold legs. Figure 1 is a top-view schematic. There are four reactor coolant pumps (RCPs) at the top of the four cold leg risers. The vessel internals of the downcomer region and the upper plenum are also representative of the prototypical configuration.

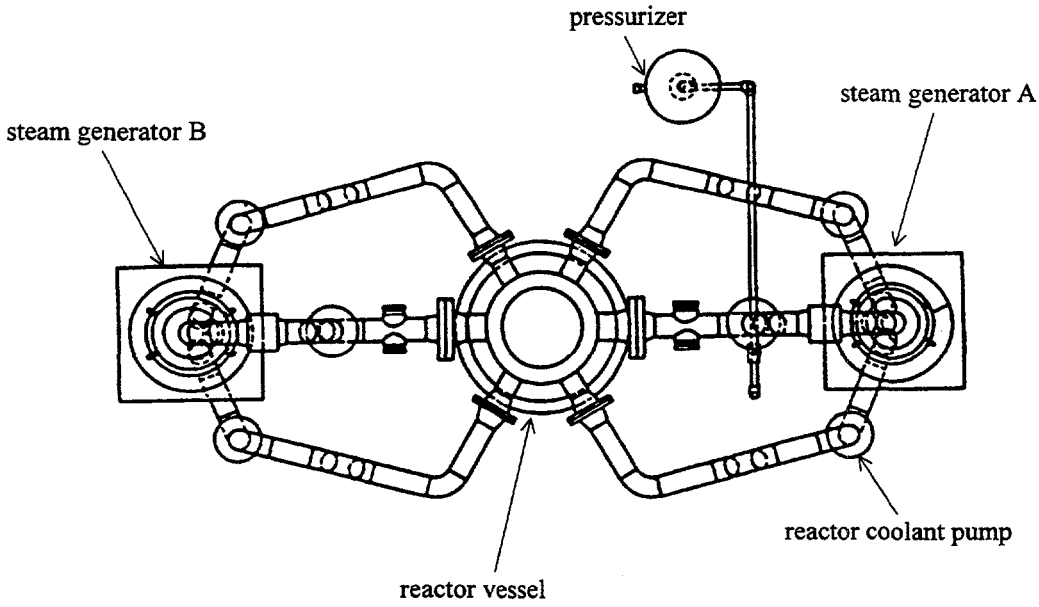

Figure 1. Schematic of the UMCP 2x4 loop facility

Auxiliary systems such as high-pressure safety injection, auxiliary feedwater, etc. are all represented in the facility and can be readily modified to accommodate the desired experimental boundary conditions. The facility is rated for a maximum core power of about 200 kW. In the present configuration the power input is limited to 110 kW. The facility design pressure is 2 MPa at saturated steam conditions. The proposed program will be executed at low temperature and low pressure that are well within these design boundaries.

The Loop thermal-hydraulic facility is well suited for boron-mixing investigations because the lowered-loop OTSG configuration makes possible the accumulation of a large boron-dilute volume.

Fundamental Concepts in the Design of the Tests

Table 1 summarizes mechanisms and phenomena relevant to the amount of reactivity that follows the entrance of a boron-dilute volume into the core region. The bolded items will be the focus of code assessment runs described in this paper. The regular font items have been part of our current test efforts and are already documented in the literature. [Gavelli et al., 1997; Almenas et al., 1997]

Table 1. Mechanisms Relevant to Boron-mixing Investigations

Stage	*Mechanisms*	*Comment*
generating the boron-dilute volume	**flow from an unborated interfacing system**	**new UMCP test**
	boiling-condensation mode coolant accumulation in the steam generator (SG)	
transport of the boron-dilute volume	**actuation of primary coolant circuit pumps**	
	resumption of natural convection (BCM only)	
mixing of the boron-dilute volume along its way to the core	molecular diffusion	insignificant
	axial turbulent diffusion	not a principal player
	entrainment	
	geometric-discontinuity induced	**including pump impellers**

The next series of tests does not only allow rigorous code assessment, but it also expands experimental investigations into boron-mixing for an interface ingress type transient. The primary system is assumed full at the beginning of the transient. The pressure in an interfacing system (e.g., the secondary) is higher than that of the primary system and a leak develops. Unborated water enters the steam generator and accumulates at the bottom. Five Nuclear Power Experience precursor events have been recorded between 1976 and 1982. [Jacobsen, 1989]

Blayais (France) had a significant ingress of secondary coolant into the SG in March 1990. [INPO, 1990]

The fact that the tests simulate a plausible transient contributes to their value as benchmarking exercises. However, to provide good initial and boundary conditions for code input, one must optimize the realism built into the transient with the control of test parameters.

Boron-mixing Tests

In experimental investigations, the boron-dilute volume is represented by a volume of water of a different temperature than the coolant in the primary system. The tracking of the slug along its path and the mixing of the slug with primary coolant are both monitored by temperature readings. Care has to be exercised to minimize heat losses, because in the interpretation of data they are equivalent to overestimating the mixing between the slug and the coolant. Previous experience has shown that the largest heat losses occur between the fluid in the downcomer and that in the core region. Effectively, a countercurrent flow heat exchange path forms through the core barrel. To minimize this heat exchange, the core barrel will be insulated with epoxy resins.

The maximum possible amount of unborated coolant will be allowed to accumulate. The slug will fill the lower part of the steam generator and the vertical sections of the two adjacent cold legs up to the level of the horizontal section of the cold legs. Figure 2 illustrates the status of the system at the beginning of the transient.

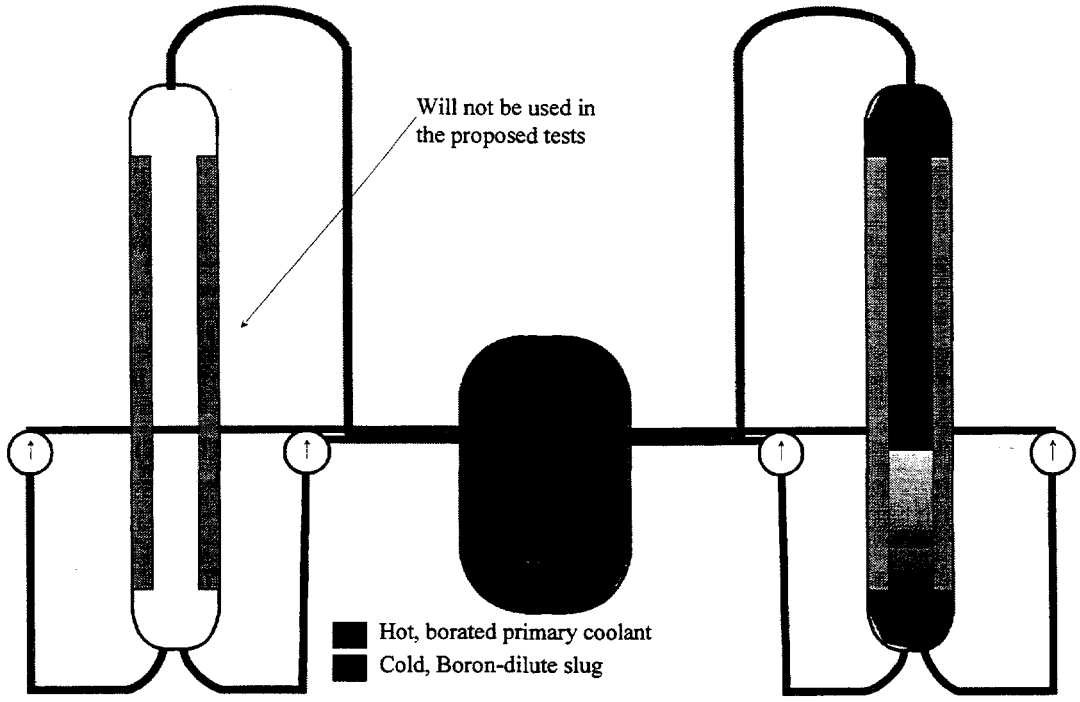

Figure 2. Schematic of initial test conditions for boron-mixing investigations of interfacing system ingress

Two essential characteristics of boron-mixing transients in the Loop require special attention. The first is consistent with prototype behavior: over the duration of the transient, the flow is developing. The second is that the flow field and mixing up to the entrance into the lower plenum is sufficient to result in a nearly uniform azimuthal concentration at the downcomer outlet. Furthermore, the largest fraction of the mixing occurs in the downcomer region.[1]

Unlike a pressurized thermal shock investigation in which buoyancy plays a major role, the boron-mixing transient is far less sensitive on Fr number scaling. This conclusion was verified experimentally in a series of tests in which the slug ranged from negatively buoyant, to neutral and then positively buoyant. A Fr number,

$$Fr = \dot{m}/A_{DC}\sqrt{gL\rho_{slug}\Delta\rho},$$

of 0.333 (with the slug at 0 °C and the primary at 95 °C) can be reached for the downcomer. This value is larger than that postulated for the prototype B&W PWR during resumption of natural circulation transients.

The dominant dimensionless number is the Re number, which can be simulated sufficiently well in the Loop. At full pump speed, the Re number in the cold leg is approximately 150,000 and in the downcomer 18,000.

The fact that the transient occurs during the flow development period poses extra challenges to code simulations; a flow-field is difficult to identify. However, the second factor can be used to simplify the posed problem. The fact that most of the mixing occurs in the downcomer suggests that modeling efforts should be focused on this region. The test series will have boundary conditions and data will be collected to permit the separate modeling of the downcomer and/or lower plenum.

Code Features Tested—Required Data

Reactivity insertion caused by the transport of a boron-dilute volume to the core depends on the spatial and temporal boron-concentration distribution of the volume at the core inlet. The transient has characteristics that make it suitable for both system and CFD code simulations. Specifically, the complexity of the primary system does not lend itself to CFD computations, thus a system code must be employed to evaluate the transport of the slug to the downcomer entrance. The required details of spatial and temporal boron-concentration distribution are best obtained from CFD code simulations. This detail is essential in a system where uneven mixing is expected to occur in the downcomer and lower plenum, which may lead to portions of the slug reaching the core unmixed. CFD codes can also aid in devising/evaluating features that enhance the mixing of the slug along its path.

---

[1] Geometric discontinuities prior to the downcomer inlet—including pump impeller motion—have however a role in that the turbulent structures they create are transported into the downcomer.

Table 2 lists code features challenged by boron-mixing transient simulations; the challenges are listed separately for system and CFD codes. Note that it is assumed that system codes will model the entire active part of the primary system, while CFD codes will only focus on the downcomer and lower plenum regions.

Table 2. Code Features Challenged by Boron-mixing Transient Simulations

System codes	CFD codes
transport of the slug through the cold leg—pump effects	flow field development
mixing through the cold leg	geometric discontinuity induced mixing
cold leg bypass*	lower plenum curvature effects
distribution along the downcomer	nonparticipation of fluid
entrainment/nonparticipation of lower plenum fluid	

* The cold leg bypass is flow that will enter neighboring cold legs instead of traveling through the downcomer.

The Specific Code-assessment Test Series

Three tests are proposed: one open test and two closed (blind) tests. To narrow the focus, a single-SG configuration (one hot leg, one or two cold legs) will be used for the blind tests.

To assure the proper modeling of Loop-specific parameters, *a simple open test* will be made available for input deck preparation. The open test will only provide cold leg inlet and downcomer information during gravity-driven injection. The system is solid, and the simulated boron-dilute slug is injected from an external tank. The slug will be injected from a fixed-liquid-level tank; this maintains a constant flow rate. Figure 3 shows the schematic of the Loop setup for the open test.

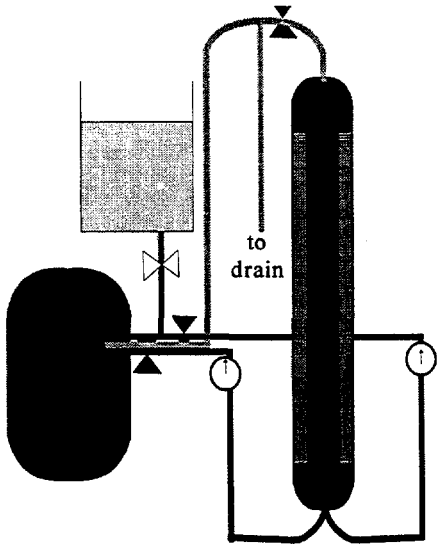

Figure 3. Experimental setup for the open test

Several factors differentiate the open test from the blind tests:

- only the cold leg inlet and the vessel participate,
- the slug injection rate is lower than in blind tests,
- the injection is gravity-driven, and
- only quasi-steady state data will be provided to analysts.

The open test will thus allow the proper setup of an input deck regarding inlet and downcomer geometry information.

The description of the value of this test, as described above, is limited. However, this test will also be used by Loop experimentalists for a final examination of the suitability of the instrumentation for the closed tests. Also, because of the larger slug volume that can be accommodated in an external tank (vs. that which can accumulate in the steam generator) the test will provide further information about the system response.

The single loop is well suited for blind tests because it is relatively easy to instrument and the boundary conditions can be well defined. Using two cold legs increases the realism of the test by opening a path for potential downcomer flow bypass.

The *first blind test* is an approximation of the steam generator in-leakage (Swedish) scenario:

- Reactor shut down,
- (RHR cooling is on, but it will not be included in the test of added complexity,)
- Secondary water enters the primary system and collects in the lower part of the SG and cold leg; the boron-dilution remains undetected because it is remote from the sampling site, and
- RCPs are actuated.

For the test, the system is filled and conditioned (heated and mixed) prior to test initiation. The slug is inserted from an external supply into the bottom of the steam generator. A single pump is used to initiate slug motion. Figure 4 shows the schematic initial conditions for the first blind test.

The following will be provided for code input preparation:

- primary system temperature (and approximate distribution if appropriate),
- the slug temperature and level (volume),
- the flow velocity in the cold legs as a function of time, and
- the temperature in both cold legs at the downcomer inlet

The required code predictions are the average temperature at select levels in the downcomer, and the core inlet spatial and temporal temperature distribution (see instrumentation section).

The *second blind test* is a pseudo-BCM boron dilution scenario:

- Reactor in BCM mode,
- Primary coolant inventory is just under the cold leg,
- (SI on will be ignored because of added complexity, and)
- RCP inadvertently actuated.

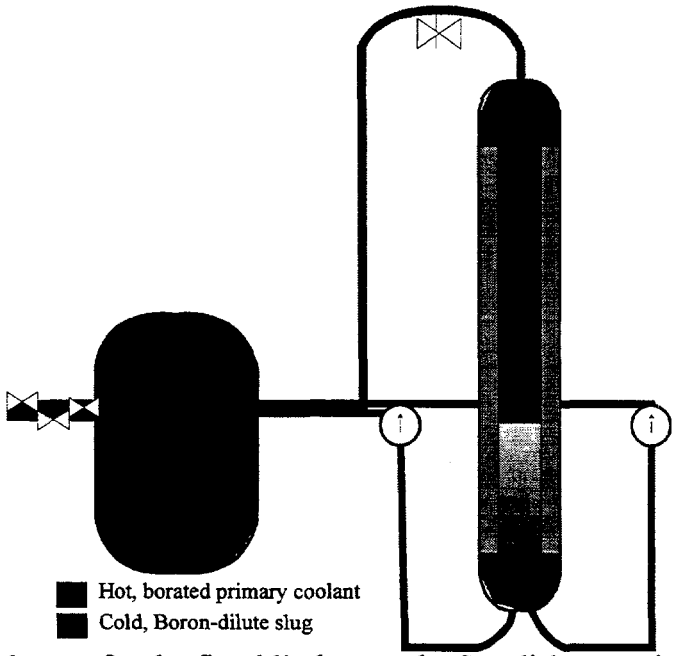

Figure 4. Experimental setup for the first blind test—the Swedish scenario

During the test, the slug is injected into a partially voided system, as in a LOCA recovery scenario. The primary system is initially filled to approximately cold leg elevation level. The boron-dilute slug is injected from the steam generator by the pump. Figure 5 shows the initial test configuration. The input data is the same as for the first blind test, but the vessel and steam generator liquid levels are monitored by differential-pressure (DP) cells. The mass flow rate of the slug will be calculated from the SG liquid-level drop. The second blind test requires minimal effort not just from an experimentation point of view but also for code modeling because it is very similar to the first blind test. It does, however, extend the challenge to codes into the multi-fluid area.

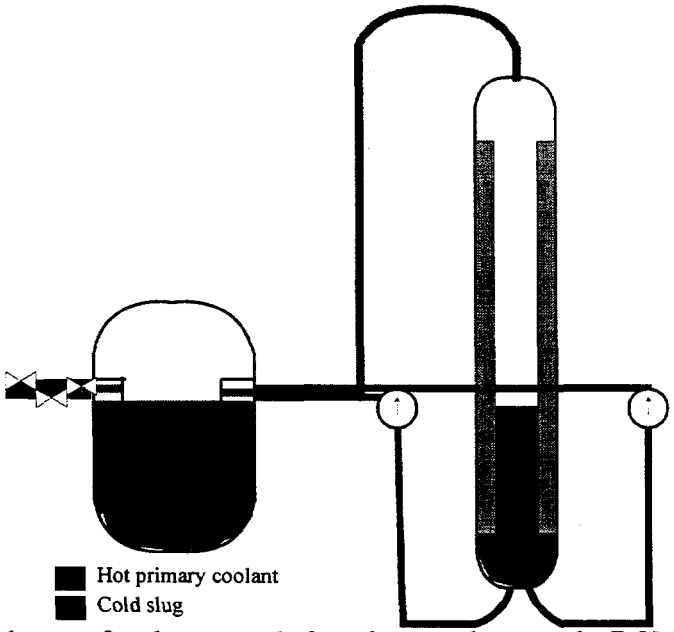

Figure 5. Experimental setup for the second closed test—the pseudo-BCM scenario

Three additional factors will be considered in the facility modification and running of these tests. The most important is minimizing heat losses through the core barrel, which is accomplished by coating it with epoxy resins. The coating will also serve to fasten the thermocouples that will protrude from the core region through the core barrel into the downcomer.

The second factor is streamlining the flow into the downcomer. Because the eddies introduced as the slug travels through the system prior to entering the downcomer (especially those created by pump impellers) cannot be quantified in an integral test facility they will be reduced to negligible levels through a honeycomb structure and several screens.

And finally, the tests will each be repeated several times. While the flow is developing for the entire relevant part of the transient and a flow field is hard to identify, a series of repetitions will assure the completeness and proper functioning of instruments.

Instrumentation

To characterize the slug behavior in the Loop, the following instrumentation will be used:

- for transport—flow measurement in the cold legs,
- for mixing—temperature measurement in cold legs and downcomer,
- for slug volume—DP or temperature measurements, and
- for heat losses—temperature measurement in the core and downcomer.

A schematic of the instrumentation is shown on figure 6.

The location and number of instruments is selected so that the boundary and initial conditions are provided as accurately as possible. Furthermore, the test data acquired has to be sufficient to establish that code predictions are correct for the right reasons. In the alternative, the data has to be sufficiently detailed to point towards code models that need improvement.

Initial conditions data have to include the temperatures in the steam generator and the vertical section of the cold legs—figure 7, and in the rest of the primary circuit; the transition between the slug and the primary coolant has to be evident. For CFD simulations the temperature as a function of time at the downcomer inlet is needed as a boundary condition. The slug velocity through the cold leg must also be prescribed.

Code predictions will be compared to temperature traces obtained along the path of the slug. Past experience suggests that most mixing measurements have to be focused on the downcomer. Specifically, the loci of greatest mixing are at the cold leg inlet into the downcomer and the downcomer expansion (which is effectively a backwards-facing step). [Gavelli et al., 1997] The instrumentation will be placed at levels that will evidence the relative impact of these large contributors to mixing. Figure 8 shows the levels at which thermocouples will be placed in the downcomer and lower plenum; figure 9 shows the horizontal placement of thermocouples at the levels depicted on figure 8. Two factors make it possible to enhance the downcomer instrumentation relative to that used in the current program. First, the thermocouples will be inserted into the downcomer through the core barrel wall. The leads will thus occupy core-region space rather than downcomer space. This is essential for CFD calculations; where the

obstruction posed by thermocouple leads would lead to large uncertainties. And second, the disabled hot leg will be adapted into an instrumentation port, which will eliminate the current limitation due to insufficient vessel penetrations.

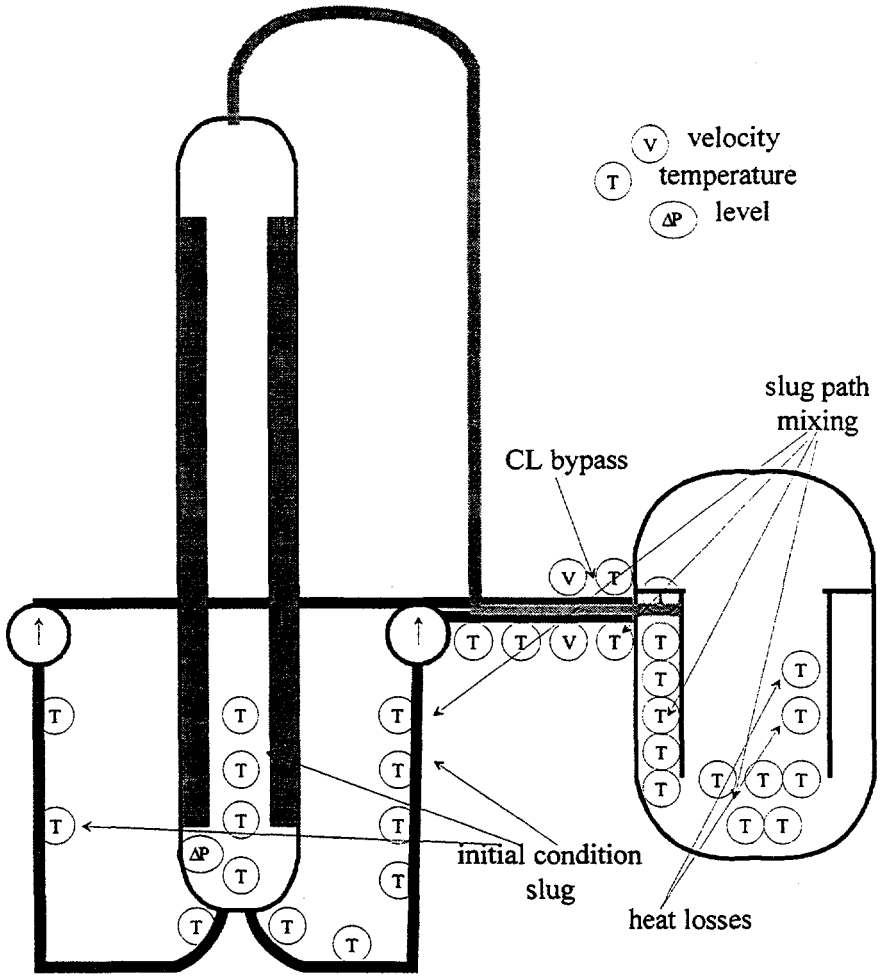

Figure 6. Instrumentation schematic for blind tests

Mixing in the lower plenum has also been shown to be significant. The presence of instrumentation ports challenges computer simulations beyond just the representation of a hemispherical surface. The possibility of removing the tubes that now simulate instrumentation ports in the loop will be evaluated. The proposed thermocouple arrangement for the lower plenum is depicted on figure 10.

The current data acquisition system—figure 11—will be optimized to accommodate the number of readings necessary to obtain a good mapping of the slug path. Hewlett Packard estimates that the 3852 unit can acquire 168 channels in 0.28 s. Because the 3497 unit is used as a controller in our current test series, we are yet unable to verify the maximum speed attainable. Routing through all channels in about a third of a second is our goal for these tests, because the thermal inertia of the thermocouples is of the same order.

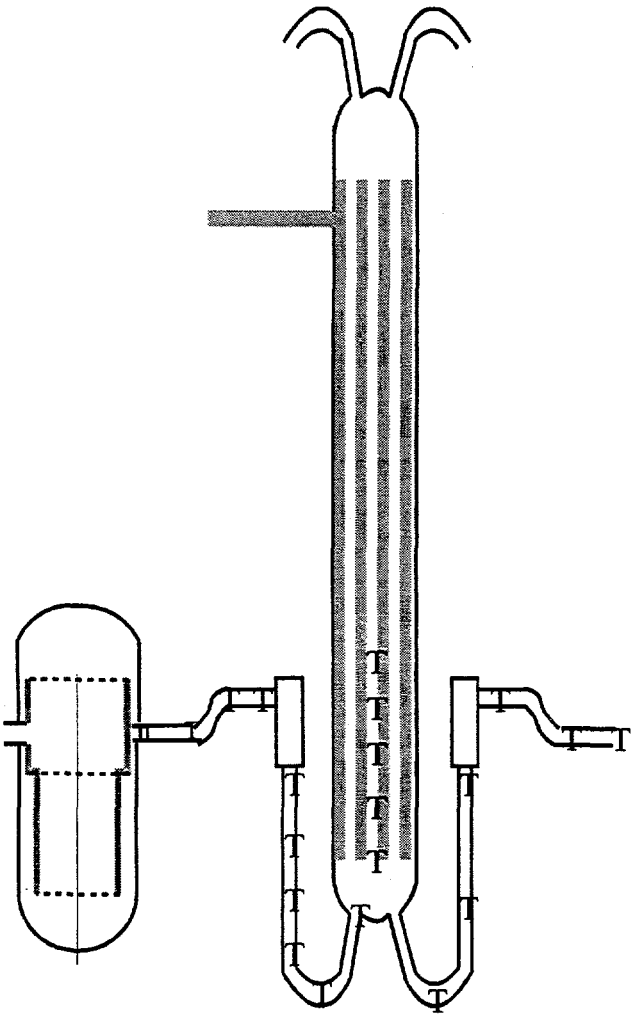

35 TCs in the SG and CLs

Figure 7. Temperature measurements to determine slug volume.

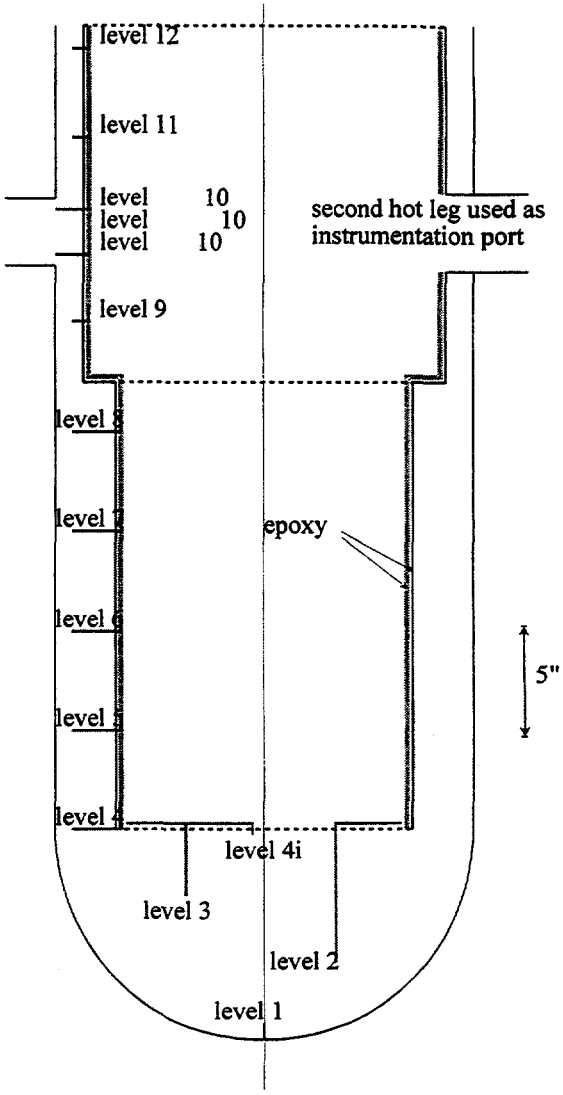

Figure 8. Levels for thermocouple-placement in the vessel

Flow Visualization

In order to supplement the data provided by the integral tests, a transparent replica of the Loop reactor vessel downcomer will be constructed to provide a detailed flow visualization of the diluted slug insertion. Using dye tracer studies and laser Doppler velocimetry, such an experimental set-up will be able to provide a spatially resolved temporal evolution of the slug concentration as it moved through the downcomer, local mean flow measurements of the axial and circumferential velocities, and some indications of the turbulence intensities within the downcomer. These detailed measurements will provide a clear physical picture of the dominant phenomena which determine the mixing within the downcomer.

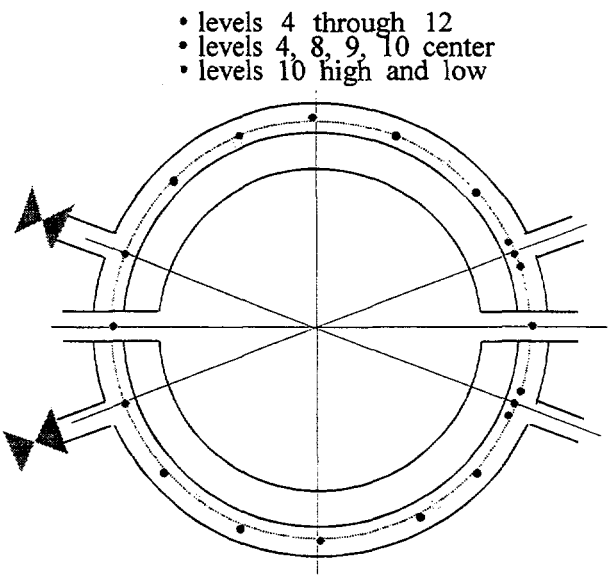

Figure 9. Horizontal arrangement of thermocouples at various levels in the reactor vessel

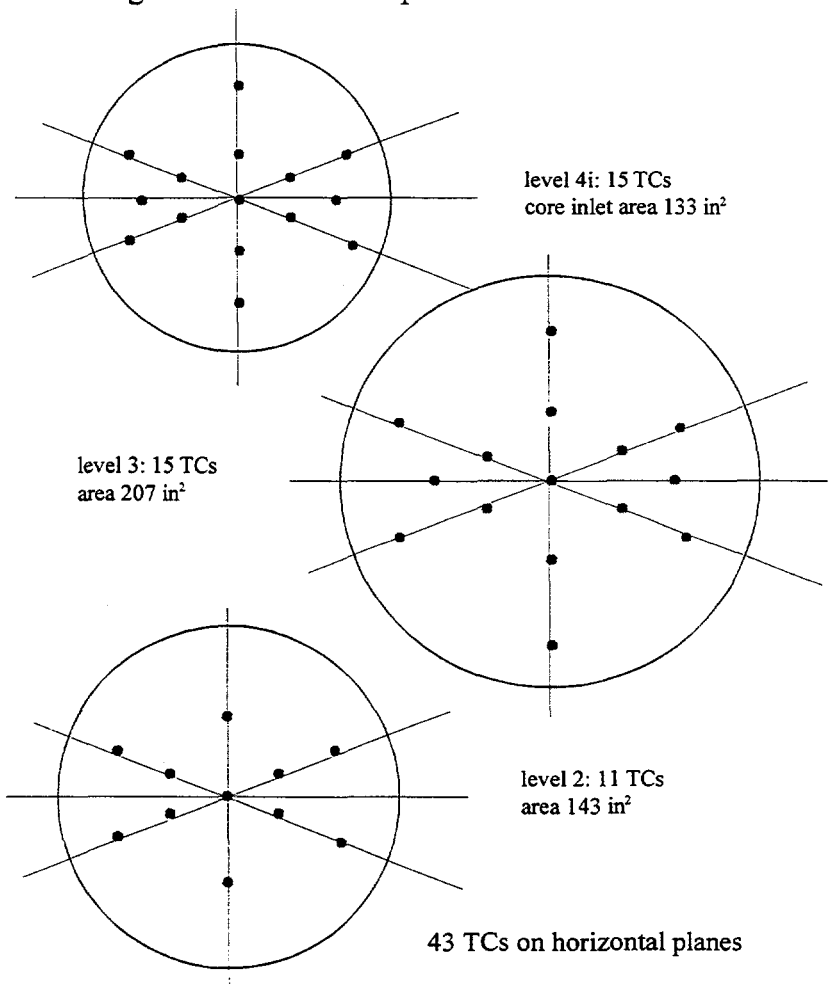

Figure 10. Horizontal arrangement of thermocouples at various levels in the lower plenum

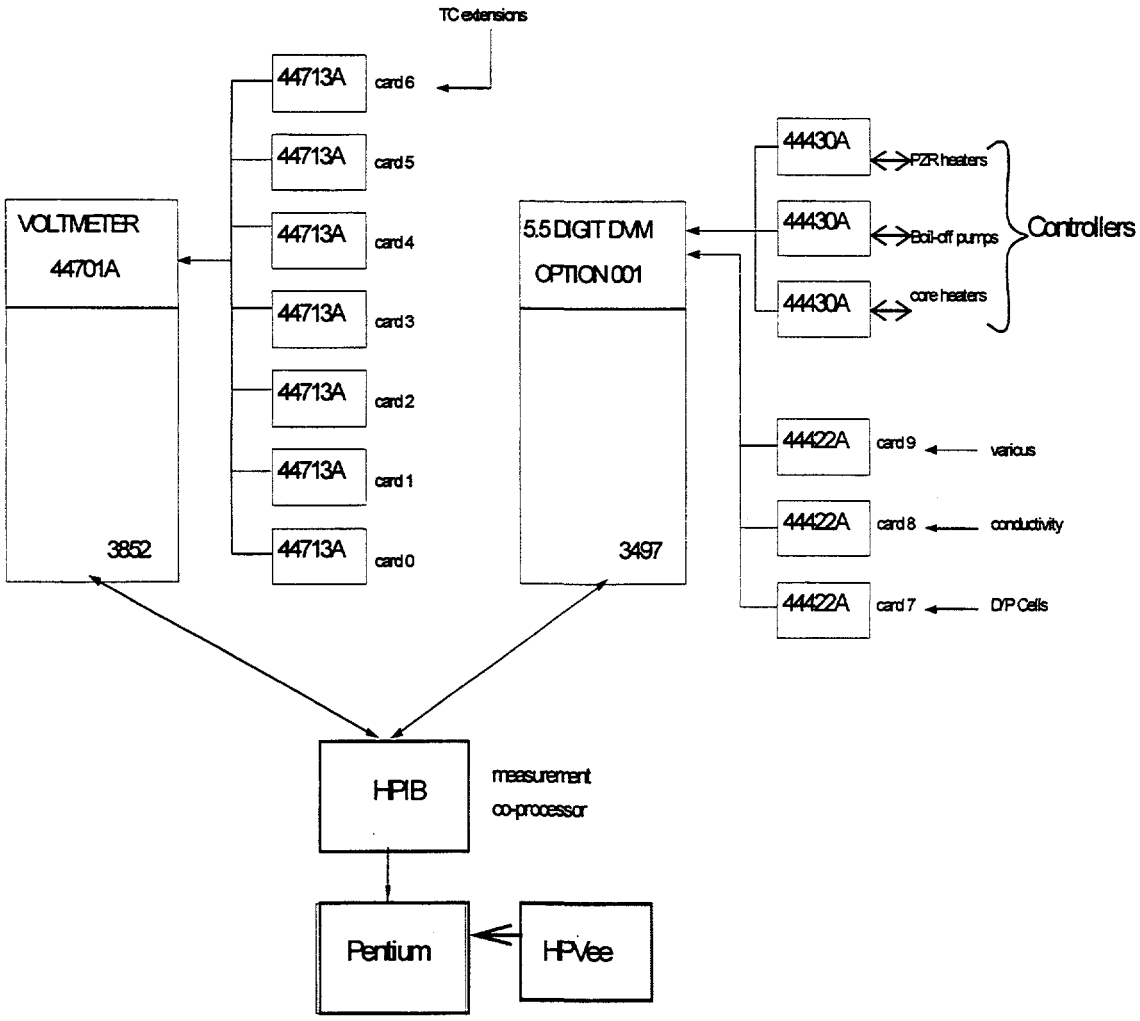

Figure 11. Loop data acquisition system

The flow visualization facility will consist of a cold-leg entrance pipe connected to a transparent annular replica of the reactor downcomer (see figure 12). The relevant entrance and bypass pipes will be retained to allow for the reproduction of the actual flow conditions of the integral loop facility. The time dependent, spatial concentration measurements will be performed through the use of laser induced fluorescence (LIF). In this technique, the slug is seeded with a fluorescent dye, and is subsequently illuminated by a thin, directional laser sheet [Nash et al., 1995]. The laser induces the dye to fluoresce with an intensity proportional to its concentration. A radially averaged concentration profile will be produced by scanning the downcomer with radially oriented light sheet projected from a rotating table within the center of the vessel (see figure 1), which would allow for temporal reconstruction with a minimum of optical distortion.

In addition to the concentration measurements, velocity information can be obtained through the use of laser Doppler velocimetry (LDV). This non-intrusive measurement technique will provide a temporal point measurement of the fluid velocity components in the axial and azimuthal directions. The point measurements can be averaged to provide mean velocity components, and also turbulence quantities such as r.m.s. disturbance levels stresses.

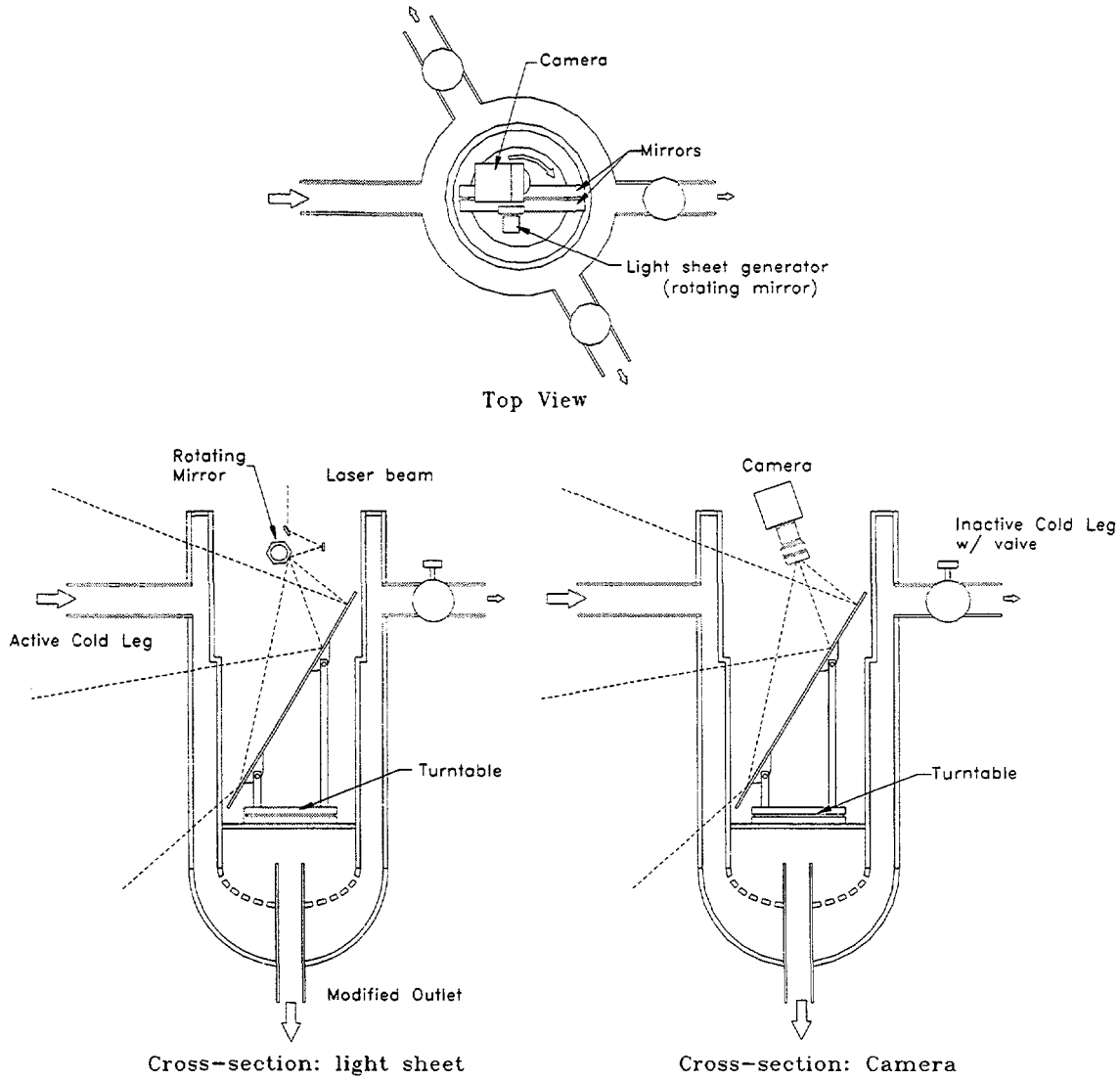

Figure 12. Conceptual sketch of annular downcomer visualization facility and scanning LIF concentration probe

Conclusions

The new tests that will be performed at the University of Maryland will provide insight into boron-transients initiated by the ingress of unborated water from an interfacing system. The tests are designed specifically for code assessment. In addition to the experience brought by the University of Maryland team involved in the current program, consultations with Swedish and French experimentalists led to further improvements in the design of the tests and associated instrumentation. Most significant among these is the simplification of the domain that results from employing a single steam generator loop. The focused placement of instrumentation based on previous data that show that most mixing occurs in the downcomer is another such improvement.

A series of three basic tests will be carried out; each of the tests will be repeated several times to gain knowledge about expected experimental uncertainties. The first test, while most removed from a realistic simulation of a boron-transient, will provide a set of ideal data for simulations. The open test has the cleanest boundary and initial conditions, and will be performed over a duration that exceeds a typical boron-mixing transient. This test will permit the specification of geometric code input parameters that affect mixing.

The two blind tests, one devised to approximate the Swedish in-leakage scenario and the other a pseudo-BCM test, will provide data for both system and CFD code analysis. Information regarding flow field characteristics and turbulent parameters will be augmented by visualization studies. The challenges posed to models by the tests described in this paper qualify the data for the highest and most complex level of code verification.

References

Almenas K., M. diMarzo, M. Gavrilas, A. Tafreshi, Gavelli, F., "Scaling of Thermally Differentiated Flows in Primary System Flow Geometries," *1997 National Heat Transfer Conference*, Baltimore, Maryland, August 10-12, 1997

Gavelli F., M. diMarzo, K. Almenas, "Resumption of Natural Circulation during Post-BCM Refilling in a B&W PWR," *1997 National Heat Transfer Conference*, Baltimore, Maryland, August 10-12, 1997

Gavelli F., M. diMarzo, K. Almenas, M. Gavrilas, G. Pertmer, B. Woods, "Boron-mixing Experiments Final Report Task 3: Boron-free Water Transport and Mixing," Report ND-NUME-97-006, University of Maryland College Park, October 1997

INPO Significant Event Report 13-90, "Unplanned Boron Dilutions from Shutdown Conditions," August 1990

Jacobson Sven, "Some Local Dilution Transients in a Pressurized Water Reactor," LIU-TEK-LIC-1989: 11, Linkoping University, Sweden, 1989

Nash J. D., G. H. Jirka, and D. Chen, "Large scale planar laser induced fluorescence in turbulent density-stratified flows," *Exp. in Fluids*, 19, pp. 297-304, 1995.

Preliminary Results of Steel Containment Vessel Model Test[1]

V. K. Luk[a], M. F. Hessheimer[a],
T. Matsumoto[b], K. Komine[b], S. Arai[b], and
J. F. Costello[c]

[a] *Sandia National Laboratories, Albuquerque, NM, USA*
[b] *Nuclear Power Engineering Corporation, Tokyo, Japan*
[c] *United States Nuclear Regulatory Commission, Washington, D.C., USA*

Abstract

A high pressure test of a mixed-scaled model (1:10 in geometry and 1:4 in shell thickness) of a steel containment vessel (SCV), representing an improved boiling water reactor (BWR) Mark II containment, was conducted on December 11-12, 1996 at Sandia National Laboratories. This paper describes the preliminary results of the high pressure test. In addition, the preliminary post-test measurement data and the preliminary comparison of test data with pretest analysis predictions are also presented.[1]

1. Introduction

The Nuclear Power Engineering Corporation (NUPEC) of Japan and the U.S. Nuclear Regulatory Commission (NRC) have been co-sponsoring and jointly funding a Cooperative Containment Research Program at Sandia National Laboratories. The purpose of the program is to investigate the response of representative models of nuclear containment structures to pressure loading beyond the design basis accident and to compare analytical predictions with measured behavior. This is accomplished by conducting static, pneumatic overpressurization tests of scale models at ambient temperature. One of the tests was a test of a mixed scaled model with 1:10 in geometry and 1:4 in shell thickness of a steel containment vessel (SCV), representing an improved boiling water reactor (BWR) Mark II containment.

This paper describes the preliminary results of the high pressure test of the SCV model. The preliminary post-test measurement data for the gap between the SCV model and the contact structure and the preliminary comparison of test data with pretest analysis predictions are also included. The pretest preparations and the summary of the conduct of the tests are described in Reference 1.

---

[1] *This work is jointly sponsored by the Nuclear Power Engineering Corporation and the U.S. Nuclear Regulatory Commission. The work of the Nuclear Power Engineering Corporation is performed under the auspices of the Ministry of International Trade and Industry, Japan. Sandia National Laboratories is operated for the U.S. Department of Energy under Contract Number DE-AC04-94AL85000.*

2. Test Objectives

The SCV model test was intended to accomplish the following specific test objectives:

1) to provide experimental data for checking the predictive capabilities of analytical methods to represent some aspects of the static internal pressure response of a steel containment,

   a) beyond the elastic range, without consideration of contact with a surrounding shield structure or thermal effects, and

   b) after contact with a surrounding shield structure,

2) to investigate the failure mode of the SCV model, and

3) to provide experimental data useful for the evaluation of actual steel containments.

To meet these objectives, the high pressure test was conducted using a monotonic pressure rise and the cycle of unloading and reloading was not desirable.

3. High Pressure Test

The high pressure test of the SCV model was conducted on December 11-12, 1996 at Sandia National Laboratories. The actual conduct of the test was described in detail in Reference 1. Briefly, after approximately sixteen and a half hours of continuous monotonic increase in pressure by pumping nitrogen gas into the SCV model, the test was terminated when the pressure in the model dropped very rapidly, even with the pressurization system operating at its maximum flow rate of 1300 scfm (standard cubic feet per minute). The cause of failure of the SCV model was a tear resulting in leakage; the failure mode was not catastrophic. The maximum internal pressure achieved during the test was 4.66 MPa, which is 5.97 times the design pressure.

4. Preliminary Instrumentation Data

Post-test inspection of the SCV model revealed a large tear, approximately 230 mm long, along the weld seam at the edge of the equipment hatch reinforcement plate. The tear was found on the left side of the equipment hatch (from an interior view, as shown in Fig. 1a) and preliminary inspections suggest that the tear may have initiated at a point roughly 30 mm below the material change interface and propagated in both directions before it stopped. In addition, a small meridional tear, approximately 55 mm long, was found next to a semi-circular hole (situated at about 200^0) in the stiffening ring above the equipment hatch. The cause of this tear has not been determined.

More than 97 % of the instruments on the SCV model survived the high pressure test and recorded information on deformation behavior of the model during the test. This paper provides a summary of the preliminary raw data from the test. These data have not been compensated for temperature variations. In addition, the strain data have not been adjusted for cross-axis compensation, and the displacement data for interior transducers have not been adjusted due to the movement of the central support column that was installed inside the model to anchor the displacement transducers.

4.1 Strain gage data around equipment hatch reinforcement plate

A network of strip, rosette, and single strain gages was installed around the equipment hatch. Some of these gages recorded very high strain readings. Figure 1a shows the locations of a few critical strain gages around the equipment hatch. The strip gage (STG-I-EQH-16) installed adjacent to the upper end of the large tear registered 4.35 % strain and a rosette gage (RSG-I-EQH-12) slightly above it had a reading of 3.7 %. However, the highest strain reading of 8.7 % was recorded on the right side (an interior view), the non-torn side, by a strip gage (STG-I-EQH-37) above the material change interface. A strain reading of 1.53 % was recorded at the top of the equipment hatch (STG-I-EQH-2) and a very low strain reading of 0.10 % was found at its bottom (STG-I-EQH-28). Figure 1b shows the strain data recorded by these gages around the equipment hatch.

4.2 Free field strain gage data

Free field hoop strain data ranging from 1.8 to 2.1 % were recorded by the exterior strain gages at the upper conical shell section above the equipment hatch. The narrow range of strain variations around this section suggests that the SCV model experienced axisymmetric expansion there.

4.3 Horizontal and vertical displacement data

The interior displacement transducers in the middle conical shell section at the elevation directly above the material change interface recorded the highest horizontal displacements, ranging from 19 to 27 mm. A plot of these horizontal displacement data is shown in Fig. 2. The transducer at the top head region recorded a vertical displacement of 17.3 mm and that at the center of the equipment hatch had a vertical displacement reading of -2.8 mm at the end of the test.

4.4 Round Robin analysis output location data

A set of pretest analytical predictions, euphemistically referred to as a Round Robin analysis, was conducted by analysts from eight organizations in Germany, India, Italy, Japan and the U.S. The Round Robin analysis participants were requested to provide pretest analysis predictions at 43 strategically chosen standard output locations throughout the SCV model. Data were recorded at every one of these locations. The Round Robin pretest analysis predictions will be compared with the test data at a later date.

4.5 Acoustic emission data

There were twenty-four acoustic emission sensors installed on the model: eighteen interior and six exterior. The preliminary analysis of data collected by these sensors indicated two regions with high acoustic emissions during the test. One region was located just below the equipment hatch. It had most of the emission occurring at 4.25 MPa. The close proximity of this region to the equipment hatch suggests that the large tear might have initiated at this pressure. Another region had a significant increase of emission at 3.75 MPa. However, this region is not very close to the small tear, therefore it is not clear whether the initiation of the small tear is related to this pressure.

5. Post-Test Measurement Data

A steel contact structure was installed over the SCV model prior to the pressure tests to represent some features of the reactor shield building in the actual plant. There are 70 holes

drilled on the contact structure in four arrays, 90^0 apart. The locations of these holes are shown in Fig. 3. The purposes of these holes were 1) to facilitate the positioning of the contact structure with respect to the SCV model during its installation, and 2) to provide access for installing the contact detection devices to monitor gap closing during the high pressure test.

The gap size at every hole location was measured before and after the high pressure test. Table 1 shows these measurements. The equipment hatch is situated at 90^0. As shown in Fig. 3, hole # 2 is located close to the bottom of the contact structure and hole # 19 is at its top. Holes # 7 and 8 are at the elevation of the equipment hatch. As seen from Table 1, the top of the contact structure came in contact with the SCV model, and the gap around the equipment hatch and the region above it closed during the test. In addition, pretest measurement data of the fabricated SCV model indicated that the local areas around the equipment hatch reinforcement plate were pulled inward during welding of this section onto the model. The extent of this out-of-roundness of the SCV model seemed to be decreased when the model underwent outward expansion under internal pressurization.

6. Comparison of Test Data with Pretest Analysis Predictions

There was a locally thinned section, very close to the large tear at the equipment hatch reinforcement plate, where reduced shell thickness was detected and measured before the pressure tests. Pretest analysis results [2] predicted that the SCV model would fail around this section at a pressure of 4.50 MPa. Test data indicate that the model failed at a pressure of 4.66 MPa during the high pressure test. Therefore, the pretest analysis gave a good prediction of the failure pressure, but was based on a different response mode.

Post-test inspection of the equipment hatch and the strain gage data around this area indicate that the model might have had a very steep strain gradient near the weld seam on the edge of the equipment hatch reinforcement plate where the large tear was detected. The pretest analysis results predicted much lower strains and strain gradients around the equipment hatch, and a higher strain at the locally thinned section, very close to the large tear, where thinner shell thickness was used in the analysis to simulate local shell thickness variations.

As mentioned in Section 4.2, the highest free field hoop strain data were recorded at the upper conical shell section, ranging from 1.8 to 2.1 %. The pretest analysis predictions on free field hoop strain data at this section are approximately 25 % below the test data. Close comparison between the two sets of plots indicate a reasonably good agreement at low pressure range, up to approximately 3.5 P_d, but the pretest analysis results on strains did not increase as fast as the test data at higher pressure ranges.

7. Conclusion

The high pressure test of the SCV model was conducted at Sandia National Laboratories on December 11-12, 1996. The cause of failure of the SCV model during the high pressure test was a tear in the model wall resulting in leakage; the failure mode was not catastrophic. The maximum internal pressure achieved during the test was 4.66 MPa which is 5.97 times the design pressure. Most of the instruments on the SCV model survived the test and recorded data that will be extensively analyzed to examine the deformation behavior of the model during the test.

A preliminary comparison of the test data with the pretest analysis predictions was performed. A detailed evaluation will be conducted to provide guidance for the post-test failure analysis and inspection. Metallurgical evaluation of the two tears is also planned.

8. References

1. Luk, V.K., et al. 1997. Testing of a Steel Containment Vessel Model Test. SMiRT 14, Lyon, France, August 17-22, 1997.

2. Porter, V.L., Carter, P.A. and Key, S.W. 1996. Pretest Analyses of the Steel Containment Vessel Model. NUREG/CR-6516, SAND96-2877, Sandia National Laboratories, Albuquerque, New Mexico.

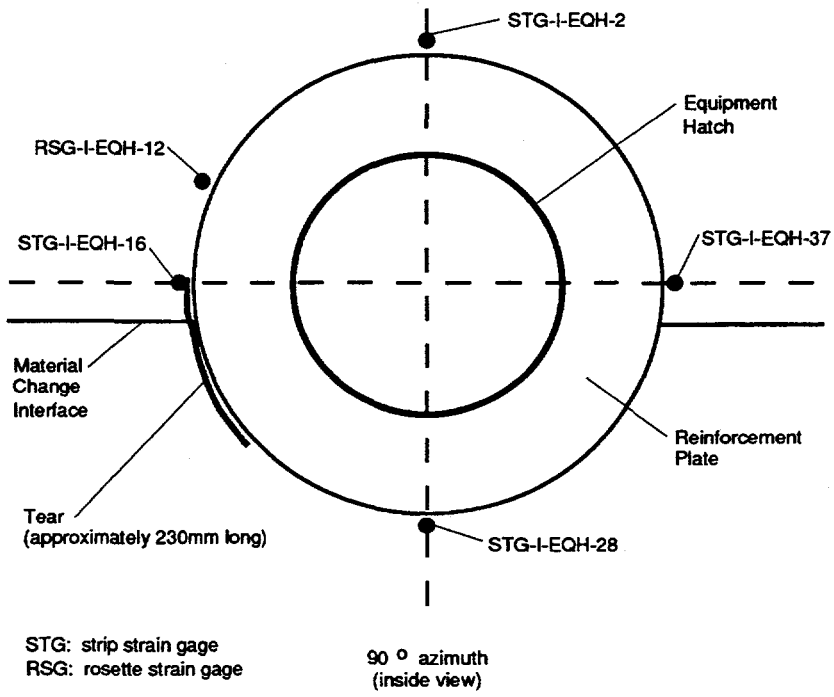

Fig. 1a Sketch of the equipment hatch from an interior view

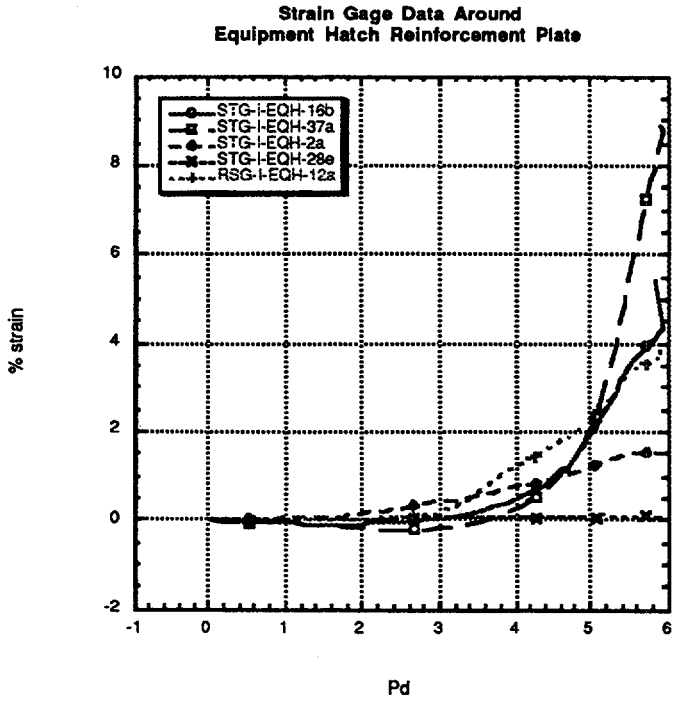

Fig. 1b Strain gage data around equipment hatch reinforcement plate

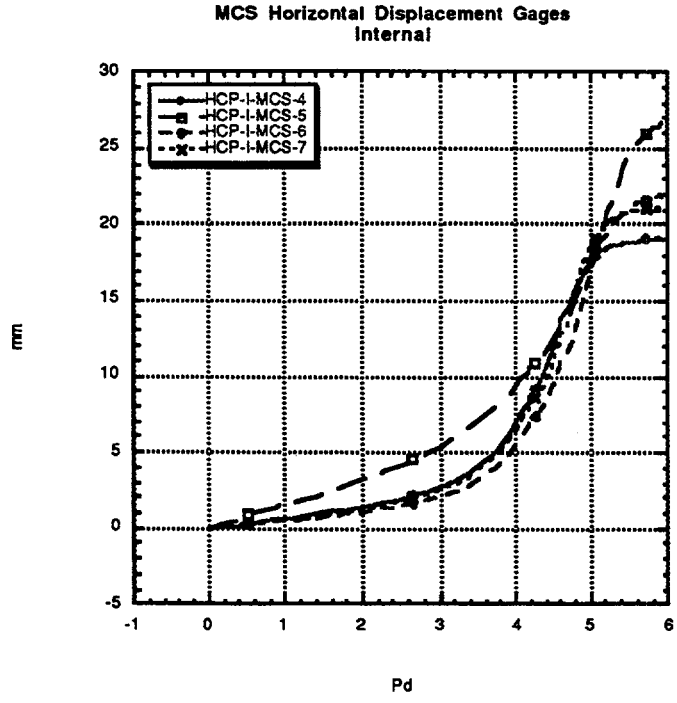

Fig. 2 Horizontal displacements recorded on four displacement transducers at the middle conical shell section, partitioned 90^0 apart

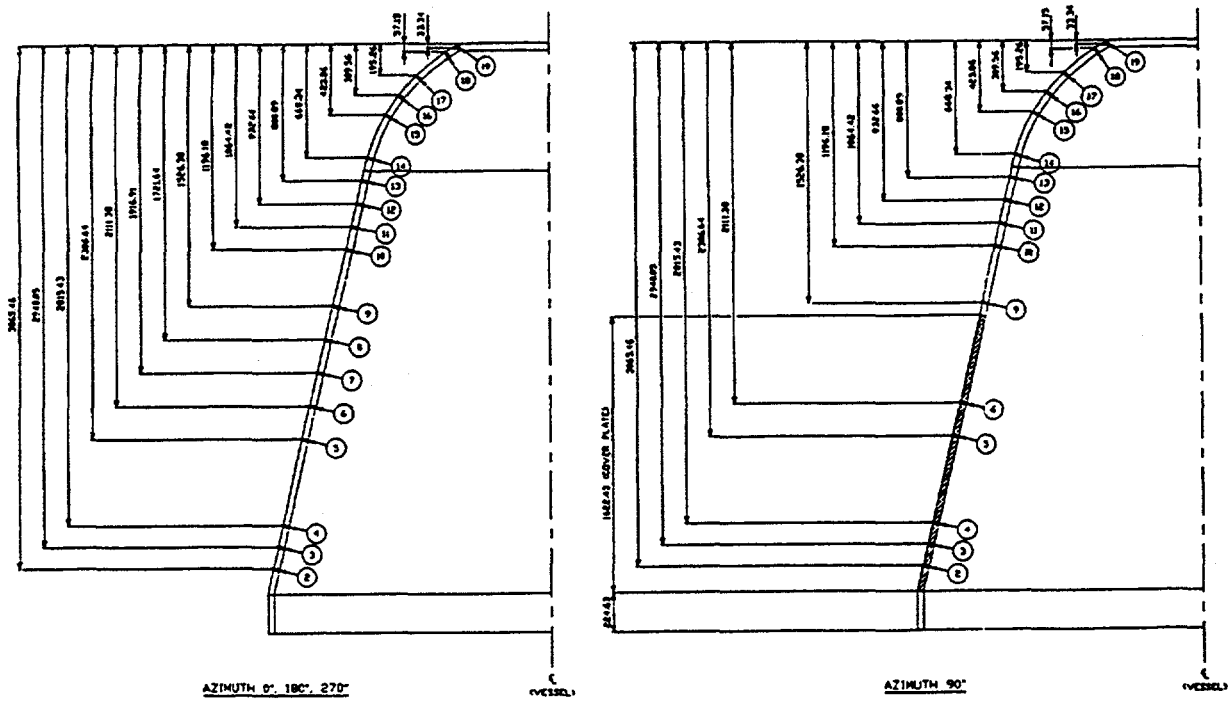

Fig. 3 Locations of measurement holes on the contact structure (dimensions in mm)

Table 1 Gap size measurements between SCV model and contact structure before and after the high pressure test

Measurement	0°		90°		180°		270°	
Hole #	A (mm)	B (mm)	A (mm)	B (mm)	A (mm)	B (mm)	A (mm)	B (mm)
2	130.71	130.20	124.38	123.75	136.88	136.73	140.13	140.06
3	99.29	98.68	94.26	92.99	104.91	104.29	108.31	105.16
4	69.62	69.39	66.15	65.05	74.45	73.66	77.47	76.50
5	19.05	17.45	13.36	9.65	22.00	21.03	24.61	23.06
6	18.39	15.60	20.37	7.47	20.55	18.34	22.99	20.19
7	18.80	11.28			21.11	13.31	22.73	13.49
8	20.98	2.62			22.81	3.51	23.77	4.01
9	19.81	2.08	29.39	3.43	21.64	1.50	22.43	3.33
10	20.17	4.32	24.71	5.89	23.27	5.38	23.80	6.30
11	22.35	2.59	23.47	3.15	22.96	2.92	23.54	4.57
12	22.48	3.07	20.65	3.02	24.33	3.48	22.25	3.30
13	21.28	6.68	19.38	7.21	24.00	7.92	22.78	7.11
14	25.42	20.09	18.24	14.15	24.18	18.39	23.62	17.98
15	22.63	23.19	19.63	19.20	22.23	22.40	21.31	21.21
16	20.14	20.50	18.23	17.81	19.76	19.99	18.49	18.34
17	19.69	20.19	17.12	16.97	18.01	18.44	17.10	17.15
18	19.66	12.37	15.78	10.06	16.03	11.73	15.39	10.46
19	24.77	1.28	27.18	1.66	27.69	1.91	24.00	1.81

Note: A = pretest gap size measurement B = post-test gap size measurement

TECHNICAL BASIS FOR ANCHORAGE TO CONCRETE IN NUCLEAR FACILITIES IN THE UNITED STATES OF AMERICA

Herman L. Graves, III[1] and Richard E. Klingner[2]

Abstract

In this paper, the background of the technical basis for anchorage to concrete in nuclear facilities in the USA is reviewed. The technical basis is currently being developed in the light of recent historical developments in the field of anchoring technology. To help provide data for that revision, the United States Nuclear Regulatory Commission (USNRC) has sponsored a testing program involving the behavior of anchors in cracked and uncracked concrete, under dynamic and static loads. Results of that testing program are summarized, and their significance is noted. The USNRC is now sponsoring the development of a resource document intended to transfer the results of testing (sponsored by the USNRC and others) in the form of recommendations for the design and evaluation of anchorage to concrete. Those recommendations are intended to form the technical basis for anchorage to concrete in nuclear facilities in the US.

BACKGROUND

Historical Development of Technical Basis in the USA

In December 1980, the US Nuclear Regulatory Commission (USNRC) designated "Seismic Qualification of Equipment in Operating Plants" as Unresolved Safety Issue (USI) A-46. The objective of USI A-46 is to develop alternative seismic qualification methods and acceptance criteria that can be used to assess the capability of mechanical and electrical equipment in operating nuclear power plants to perform their intended safety functions. Since equipment is usually anchored to concrete through anchor bolts, it is therefore necessary to ensure that the bolts are capable of resisting seismic loads.

In March 1988, it was reported, in accordance with the provisions of Title 10, Code of Federal Regulations, Part 21, that test of some expansive-type bolts had disclosed that the previously recommended minimum edge distance from an unsupported edge of five times the bolt diameter might be insufficient to develop 100 percent of the recommended anchor capacity. Since the disclosure of the edge distance problem to the NRC, the staff has embarked on an intensive program of collecting information pertinent to the issue at hand and assessment of the current situation with regard to the installation practices of expansion anchors. The issue of minimum edge distance was incorporated into the resolution of USI A-46.

The Seismic Qualification Utility Group (SQUG), a utility group, has developed a Generic Implementation Plan (GIP) including criteria and walkdown procedures that will be used to resolve the concerns of USI A-46. Following NRC approval of the GIP, each utility will conduct a walkdown of its nuclear facilities using the GIP criteria and procedures.

---

[1] United States Nuclear Regulatory Commission, Washington, DC, USA
[2] Phil M. Ferguson Professor in Civil Engineering, The University of Texas, Austin, Texas 78712, USA

The criteria and procedures specified for anchorage walkdown in the GIP contain specific information relating to bolt strength under dynamic conditions. The GIP, including criteria and walkdown procedures, has been reviewed and accepted by the NRC.

Motivation for Development of a New Technical Basis in the USA

Although the Generic Implementation Plan proposed by SQUG has been reviewed and accepted by the NRC, very little test data were available regarding the behavior and strength of anchor bolts under dynamic conditions (cyclic loads) to validate the criteria in the GIP. It was usually assumed that behavior and strength of anchor bolts under static loads did not differ much from that of earthquake conditions. The adequacy of this assumption had not been adequately verified.

To address that lack of information, in March 1991 the USNRC issued a nationwide RFP (Solicitation No. RS-NRR-91-029, "Anchor Bolt Behavior and Strength During Earthquakes"). The objective of this RFP was to obtain specialized technical assistance to verify, by testing, the adequacy of the assumption used in the U.S. nuclear power plant designs that the behavior and strength of anchor bolts (cast-in-place, expansion and bearing-type (undercut) and their supporting concrete under seismic loads do not differ significantly from those for static conditions.

DEVELOPMENT OF NRC-SPONSORED RESEARCH TO PROVIDE BACKGROUND INFORMATION ON ANCHOR BEHAVIOR

Testing Program (Objectives and Scope)

The experimental work described above was awarded to The University of Texas at Austin, under a contract entitled "Anchor Bolt Behavior and Strength during Earthquakes." Work began in the second half of 1993, and the results have been published in the form of theses, reports, and dissertations (Rodriguez 1994a, 1994b, 1995a, 1995b, Hallowell 1996, Lotze 1997, Zhang 1997, Graves 1997). The final report is being submitted to the NRC at this time, and refereed journal articles will then be written and submitted for review and possible publication. Material in this paper is taken from those references.

This research program addressed the behavior of cast-in-place and post-installed anchors in cracked and uncracked concrete, subjected to static and dynamic loading. The anchors tested were cast-in-place headed bolts (CIP), a conventional undercut anchor with large bearing area (UC1), another undercut anchor (UC2), a heavy-duty sleeve anchor with follow-up expansion capability (Sleeve), and two clip-type expansion anchors (EA and EAII). To systematically investigate and understand the effects of these various factors, the overall research program consisted of four tasks:

Task 1: Tensile behavior of single anchors under static and dynamic loading in uncracked and cracked concrete;

Task 2: Behavior of two-anchor connections under dynamic tensile loading and static eccentric shear, and behavior of single anchors under loading at various angles;

Task 3: Shear behavior of near-edge, single and double-anchor connections under static and dynamic loading in cracked and uncracked concrete, and the effects of hairpins on these near-edge connections; and

Task 4: Behavior of four-anchor connections under simulated seismic loads (eccentric shear loading) applied dynamically in repeated reversed cycles.

Resource Document

In July 1997, the USNRC announced its intention to sign a contract with The University of Texas at Austin, to obtain a comprehensive resource document that can be used to establish regulatory positions regarding anchorage to concrete. Existing information, including data from comprehensive testing conducted at The University of Texas at Austin, would be evaluated. Current and proposed approaches for the design, analysis and testing of anchorages to concrete would be reviewed. That work is now being conducted under the NRC research program, "Revision to Anchorage Criteria." Its progress is described briefly in a later section of this paper.

BASIC RESULTS FROM NRC-SPONSORED TESTING PROGRAM

Description of Single-Anchor Tension Tests in Uncracked and Cracked Concrete

Using the test setup shown in Figure 1, single-anchor tension tests were conducted in uncracked and cracked concrete. Most tests were conducted in concrete having a target compressive strength of 4700 psi (32.4 MPa), similar to that found in many operating nuclear power plants. To examine the effects of differences in concrete compressive strength, some tests were conducted in concrete with a target compressive strength of 3000 psi (20.7 MPa). Most concrete tested had river-gravel aggregate. To examine the effects of different aggregate types, some tests were conducted in concrete with a relatively soft limestone aggregate, and other tests in concrete with a relatively hard granite aggregate.

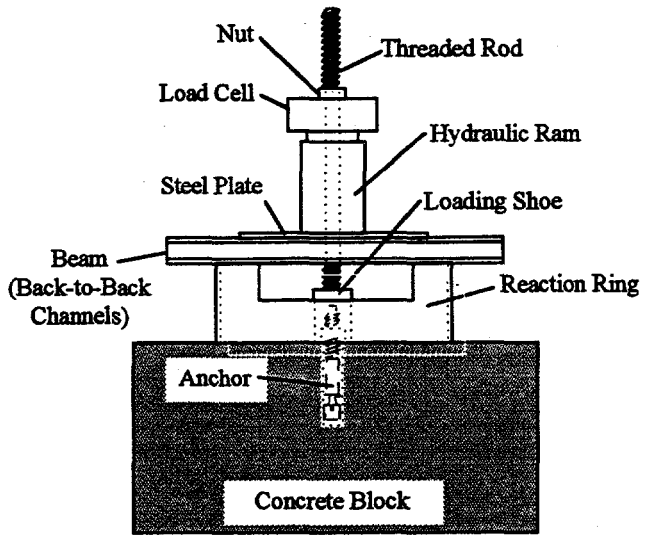

Figure 1 *Setup used for tension tests in uncracked and cracked concrete*

Cast-in-place headed bolts were tested, and also several types of post-installed anchors: a conventional undercut anchor, designated UC1; a different type of undercut anchor, based on a

different operating principle, and designated UC2; a heavy-duty sleeve anchor with follow-up expansion capability, designated Sleeve; a clip-type, torque-controlled expansion anchor, designated EA; and a later version of that same anchor, designated EAII. These anchors were selected because they are commonly found in nuclear power plants. For these tests, embedment depths were selected so that tensile failure would occur in some mode other than steel failure (that is, usually by concrete breakout, but sometimes by pullout or pull-through). Most anchors had a diameter of about 3/4 inches (19 mm), common for equipment-mounting applications in nuclear power plants. Some tests were conducted on anchors with a diameter of 3/8 inches (9.5 mm).

In the cracked-concrete tests, cracks were opened with wedges to an initial width of 0.3 mm, and their widths were monitored but not controlled during testing. This method of cracked-concrete testing is relatively simple and inexpensive to carry out, and is recommended for preliminary investigations of the behavior of different types of anchors in cracks.

The emphasis of these tests was to establish the tensile breakout behavior of anchors in uncracked and cracked concrete, under static and dynamic loads. For the latter case, a single ramp loading to failure was used, as shown in Figure 2. This ramp loading involved a loading rate (rise time) of 0.1 seconds, similar to that experienced by mounted equipment responding to seismic excitation.

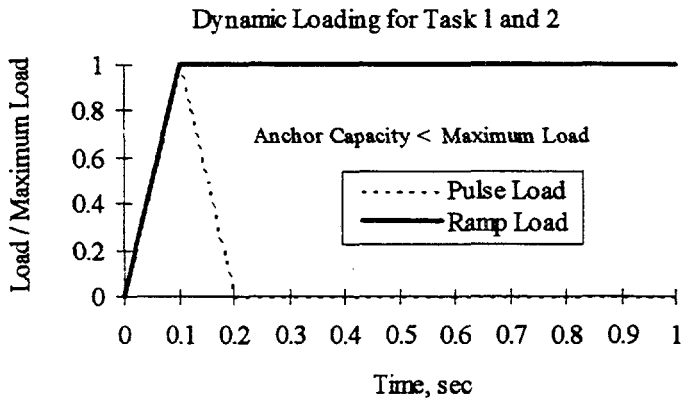

Figure 2 *Ramp-type loading used for dynamic tests of single anchors*

Conclusions from Single-Anchor Tension Tests in Cracked Concrete

The results of the single-anchor tension tests in cracked concrete were evaluated in terms of various expressions that have been proposed to predict anchor capacity. One of the most prevalent of these is the so-called "CC-Method" (Fuchs 1995), summarized in Appendix A of this paper.

The conclusions are all based on the averages of five replicate tests, all of which were designed to fail in concrete breakout. The capacity was presented in terms of mean normalization factors for the CC Method. In the dynamic tests, the connections were intended to fail in 0.1 second under monotonic, ramp-type dynamic loading.

1) Based on all the test results obtained from this testing program, which are presented and discussed in Sections 5.2 and 6.2 of Zhang (1997), and on the data from the tests of Rodriguez (1995) and Hallowell (1996), Table 1 summarizes the mean normalization coefficients obtained here for the CC Method (Fuchs 1995) for single anchors, using US customary units. Tensile breakout capacities are well described by the CC Method.

Table 1 *Mean normalization coefficients for tensile anchors in various conditions, obtained here for CC Method*

Anchor Type	Load Type and Concrete Condition			
	Static Uncracked	**Dynamic Uncracked**	**Static Cracked**	**Dynamic Cracked**
Cast-In-Place	41.6	53.9	36.2	52.3
Grouted	41.2	57.0	24.5	15.5
UC1, 3/8 in. (10 mm)	37.2	44.4	35.6	41.1
UC1, 3/4 in. (19 mm)	39.4	49.0	41.7	46.2
UC2, 3/4 in. (19 mm)	43.7	53.6	28.5	45.2
Sleeve, 10 mm	37.4	38.7	29.9	29.7
Sleeve, 20 mm	44.3	55.1	35.3	39.5
EA II	36.7	37.8	29.7	28.0

2) Table 2 shows ratios of static tensile breakout capacity (cracked concrete), dynamic capacity (uncracked concrete), and dynamic capacity (cracked concrete), all divided by static capacity in uncracked concrete. For the CIP and UC1 anchors, these ratios all exceed unity. For the UC2, Sleeve, and EAII anchors, the ratios are less than unity. For the grouted anchors, they are considerably less than unity. The tests of Rodriguez (1995) and Lotze (1997) show that the effects of anchor spacing and edge distance are essentially the same for dynamic as for static loading. The implications of Table 2 are clear. Anchors with capacity ratios (dynamic cracked / static uncracked) greater than 1.0, and designed for ductile behavior in uncracked concrete under static loading, will probably still behave in a ductile manner in cracked concrete under dynamic loading.

Table 2 *Ratios of tensile breakout capacities (static, cracked; dynamic, uncracked; and dynamic, cracked) to static tensile breakout capacities in uncracked concrete*

Anchor Type	Load Type and Concrete Condition		
	Static Cracked / Static Uncracked	Dynamic Uncracked / Static Uncracked	Dynamic Cracked / Static Uncracked
Cast-In-Place	0.87	1.30	1.26
Grouted	0.59	1.38	0.38
UC1, 3/8 in. (10 mm)	0.96	1.19	1.10
UC1, 3/4 in. (19 mm)	1.06	1.24	1.17
UC2, 3/4 in. (19 mm)	0.65	1.23	1.03
Sleeve, 10 mm	0.80	1.03	0.79
Sleeve, 20 mm	0.80	1.23	0.89
EA II	0.81	1.03	0.76

3) Based on all the test results obtained from this testing program, which are presented and discussed in Sections 5.2 and 6.2 of Zhang (1997), and on the data from the tests of Rodriguez (1995) and Hallowell (1996), Table 3 summarizes the average displacements at maximum load of the tested single anchors.

Table 3 *Average displacements at maximum load of single tensile anchors in various conditions*

Anchor Type	Load Type and Concrete Condition							
	Static Uncracked		Dynamic Uncracked		Static Cracked		Dynamic Cracked	
	in.	mm	in.	mm	in.	mm	in.	mm
Cast-In-Place	0.047	1.19	0.069	1.75	0.051	1.30	0.105	2.67
Grouted	0.043	1.09	0.074	1.88	0.032	.081	0.124	3.15
UC1, 3/8 in. (10 mm)	0.099	2.51	0.136	3.45	0.093	2.36	0.137	3.48
UC1, 3/4 in. (19 mm)	0.112	2.84	0.195	4.95	0.125	3.18	0.171	4.34
UC2, 3/4 in. (19 mm)	0.067	1.70	0.096	2.44	0.039	0.99	0.061	1.55
Sleeve, 10 mm	0.112	28.4	0.089	2.26	0.111	2.79	0.138	3.51
Sleeve, 20 mm	0.151	3.84	0.147	3.73	0.146	3.71	0.062	1.57
EA II	0.218	5.54	0.245	6.22	0.158	4.01	0.467	11.9

This table clearly shows that the clip-type expansion anchor tested here performs poorly in cracked concrete under dynamic loads. Its average displacement at maximum load is much greater in cracked than in uncracked concrete, indicating an increased tendency toward pullout and pull-through failure under those conditions.

4) As discussed in Sections 6.2.1 and 6.2.2 of Zhang (1997), under dynamic loading in cracked concrete, expansion anchors (Expansion Anchors II and Sleeve Anchors of 10 mm) have a greater tendency to pull out, due to the smaller dynamic friction coefficient. As a result, combined with the effect of concrete cracking, their dynamic capacity in cracked concrete decreased more than their static capacity in cracked concrete, but with a larger displacement, compared to their corresponding capacities in uncracked concrete. Their dynamic capacity in cracked concrete was also smaller than their static capacity in cracked concrete.

5) As discussed in Section 6.2.2 of Zhang (1997), in cracked concrete, the capacity of the 20-mm Sleeve Anchor decreased under both static and dynamic loading, compared to the corresponding tests in uncracked concrete. The increase in capacity due to dynamic loading is much higher in uncracked concrete than in cracked concrete. The step inside the expansion sleeve of this anchor, designed to limit its expansion force on surrounding concrete, affects its load-displacement behavior. When the cone touches the step, after being pulled farther into the expansion sleeve under tension, the friction between the expansion sleeve and the surrounding concrete determines the anchor behavior. Because of a smaller maximum clamping force between the cone and surrounding concrete due to a large gap caused by crack opening, and of a smaller dynamic friction coefficient, the friction between the expansion sleeve and surrounding concrete is smaller in cracked concrete than in uncracked concrete, resulting in more tests with pullout failure under dynamic loading than under static loading.

6) As discussed in Section 6.2.4 of Zhang (1997), compared to the corresponding tests in uncracked concrete, the capacity in cracked concrete of 3/8-inch (10-mm) Undercut Anchor 1 decreased slightly (less than 7%) under both static loading and dynamic loading. Its dynamic capacity in cracked concrete increased compared to its static capacity in cracked concrete, like its dynamic capacity in uncracked concrete.

7) As discussed in Section 6.2.4 of Zhang (1997), the effect of cracks on 3/4-inch (10-mm) Undercut Anchor 1 was also very small. However, the capacity of 3/4-inch (10-mm) Undercut Anchors 1 in cracked concrete increased under static loading, and decreased under dynamic loading, compared to its corresponding tests in uncracked concrete. In cracked concrete, the dynamic capacity exceeds the static capacity. The increase in static load capacity in cracked concrete was not expected. Nonetheless, considering the relatively small increase and the small scatter in the other capacities of this type of anchor, the test results are considered valid.

8) As discussed in Section 6.2.5 of Zhang (1997), compared to the corresponding tests in uncracked concrete, the capacity of Undercut Anchor 2 decreased in cracked concrete under both static and dynamic loading. Comparing the tests of UC2 in cracked concrete only, the dynamic capacity exceeds the static one. This increase is much higher than for the UC1 anchors. The installation procedure (fully pre-load of the anchor) eliminates the concrete plastic deformation under tension, and reduces the anchor displacement. As a result, the dynamic loading rate was increased at the ultimate load range, which increased the apparent dynamic capacity of UC2 more than that of UC1 anchors.

9) As discussed in Section 6.2.3 of Zhang (1997), the capacity of Grouted Anchors in cracked concrete decreased the most in all tested anchors under both static and dynamic loading. Their dynamic capacity in cracked concrete dropped dramatically, compared to their dynamic capacity in uncracked concrete, because of the loss of friction at the interface between the grout and the base concrete due to cracking.

10) As discussed in Section 6.2.6 of Zhang (1997), the additional crack openings measured in tests increased more rapidly than the applied load, due to the more rapid increase in the transverse deflection on the concrete surface of the breakout cones. The additional crack opening is a valid indicator of the expansion force exerted by an anchor head, especially in the low-load range.

11) In terms of the CC Method, and using the US customary units, the normalization coefficients listed in Table 4 are appropriate for estimating the capacity of single tensile anchors in various conditions.

Table 4 *Appropriate normalization coefficients (CC Method) for single tensile anchors in various conditions*

Anchor Type	Load Type and Concrete Condition			
	Static Uncracked	**Dynamic Uncracked**	**Static, Cracked**	**Dynamic, Cracked**
Cast-In-Place	41	50	35	50
Grouted	41	50	N/A	N/A
UC1, 3/8 in. (10 mm)	39	45	35	40
UC1, 3/4 in. (19 mm)	39	45	39	40
UC2, 3/4 in. (19 mm)	41	50	28	40
Sleeve, 10 mm	35	35	30	30
Sleeve, 20 mm	41	50	33	39
EA II	35	35	28	28

Description of Shear Tests on Two-Anchor Connections

Using the test setup shown in Figures 3 and 4, shear tests were conducted in uncracked and cracked concrete on two-anchor connections. The types of concrete used, and the types of anchors tested, were the same as discussed previously. The purpose of this loading arrangement was to permit measurement of the axial load in the baseplate, thereby permitting experimental observation of the amount of shear resisted by each anchor. Some of the near-edge shear anchors had supplementary "hairpins" reinforcement anchoring their shear breakout cones to the rest of the concrete.

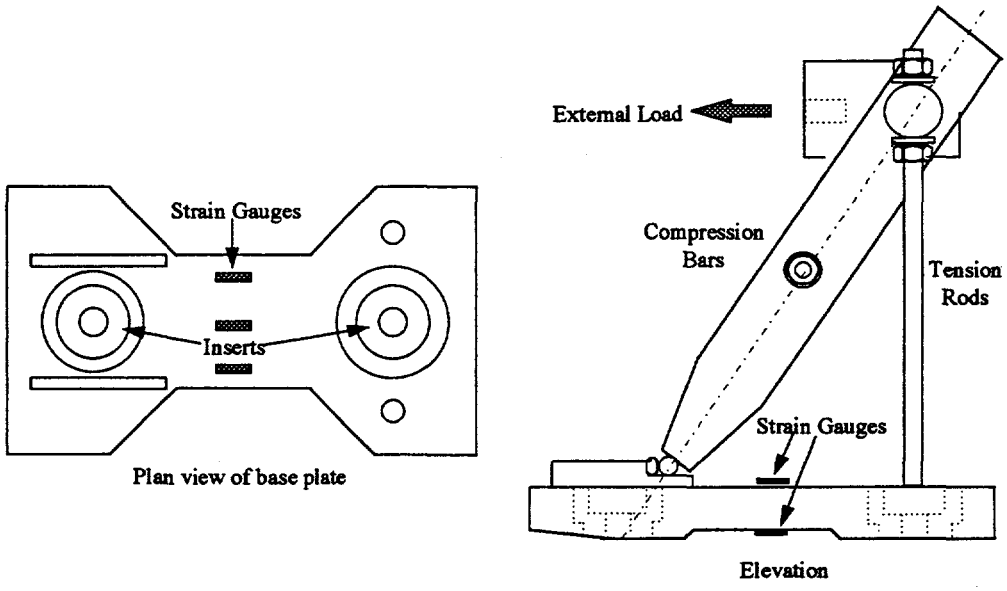

Figure 3 *Specially-machined baseplate for tests on two-anchor connections under shear*

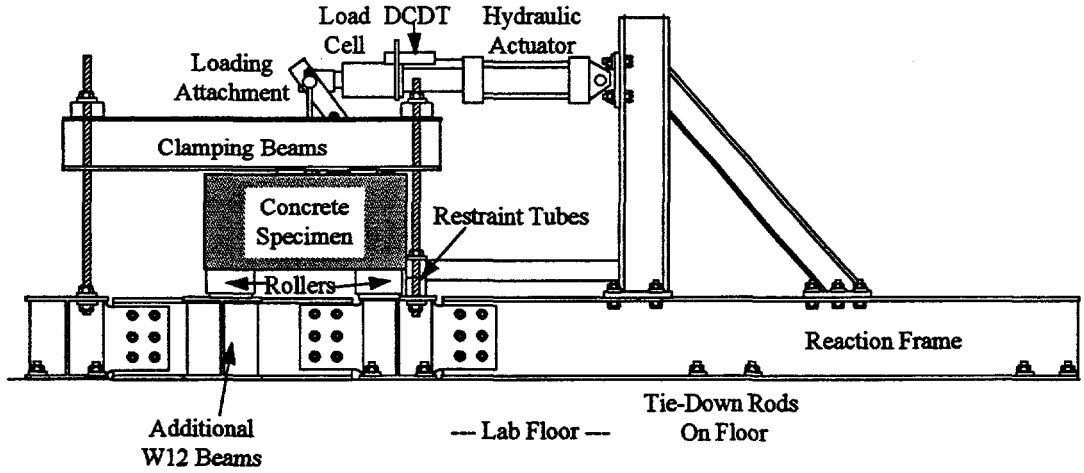

Figure 4 Setup for Tests on Two-Anchor Connections under Eccentric Shear

Conclusions from Shear Tests on Two-Anchor Connections

These conclusions are based on the discussions of Sections 6.3.2 and 6.3.3 of Zhang (1997), which were based on the averages of 5 replicates. The tested two-anchor connections failed by concrete breakout under shear at the front anchor and steel fracture of the back anchors. In the dynamic tests, the connections were intended to fail in about 0.1 second under the same ramp-type dynamic loading discussed previously.

The concrete breakout capacities of the anchors were compared with the predictions of the CC Method (Fuchs 1995), summarized in Appendix B.

1) The overall behavior of double-anchor shear connections is a combination of the behavior of the front (near-edge) anchor and the back anchor. The load-displacement curve is usually two-peaked, with the first peak corresponding to edge breakout of the front anchor, and the second peak corresponding to fracture of the back anchor. The maximum capacity is usually the fracture capacity of the back anchor, plus the residual capacity of the front anchor at the same displacement.

2) The maximum capacities of near-edge, two-anchor connections under ramp-type dynamic loading were higher than the corresponding static capacities. This increase is mainly attributed to the increased remaining shear force in the front anchors. The dynamic capacities at the concrete edge breakout were also higher than the corresponding static capacities, because of the increase in the concrete edge breakout capacity under dynamic loading. Reasons for these individual effects are discussed below. Their overall implication is that multiple-anchor shear connections, designed for ductile behavior in uncracked concrete under static loading, will probably still behave in a ductile manner in cracked concrete under dynamic loading.

3) The capacity of double-anchor shear connections was dominated by the behavior of the back anchor. This was essentially unaffected by concrete cracking, and was increased by about 25% to 30% by ramp-type dynamic loading.

4) The edge breakout capacity of the front anchor was about 20% less than predicted by the CC Method. Concrete cracking reduced this capacity by about 20%. Ramp-type dynamic loading increased this capacity by at least about 10%. Close hairpins increased this capacity by about 30%. The front-anchor shear necessary to produce concrete edge breakout was probably reduced by the simultaneous presence of baseplate shear and compression, on the concrete breakout body. This probably account for the over-prediction from the CC Method.

5) The most significant effect of close hairpins was to increase the sustained capacity of the front anchor after concrete edge breakout, and to permit the front anchor to form a flexural mechanism. Thereby, hairpins increased the capacity and ductility of near-edge shear connections.

6) The gap between the baseplate and anchors, and between anchors and the concrete, had little effect on the load capacities of two-anchor connections tested in this study.

Description of Seismic Tests of Multiple-Anchor Connections

Using the test setup shown in Figure 5, multiple-anchor connections were subjected to the displacement history shown in Figure 6. In some cases, the specimens were uncracked; in others, they were cracked. The purpose of these tests was to evaluate the seismic performance of multiple-anchor connections to concrete, and to see if this behavior was consistent with the behavior previously observed for single anchors.

Conclusions from Seismic Tests of Multiple-Anchor Connections

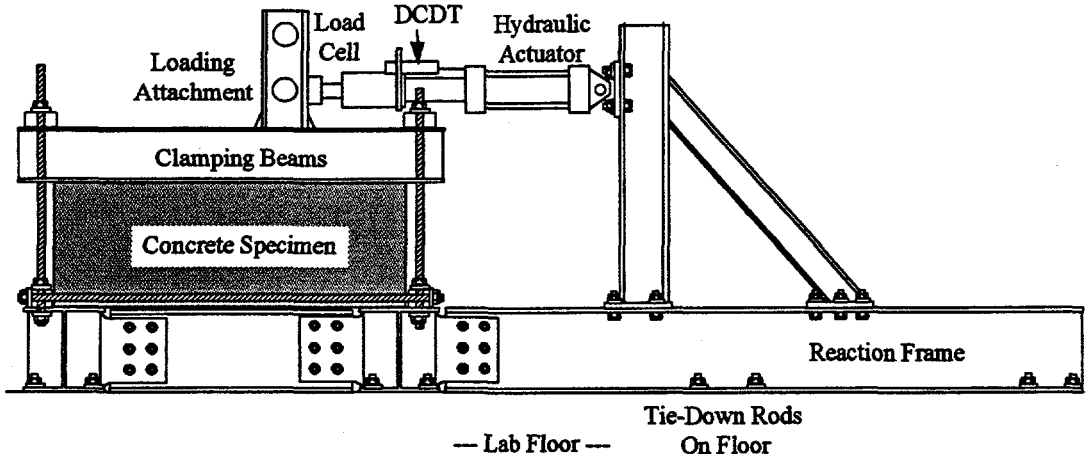

Figure 5 Test setup for seismic tests of multiple-anchor connections

Sample results from a seismic test on a multiple-anchor connection are shown in Figure 7.

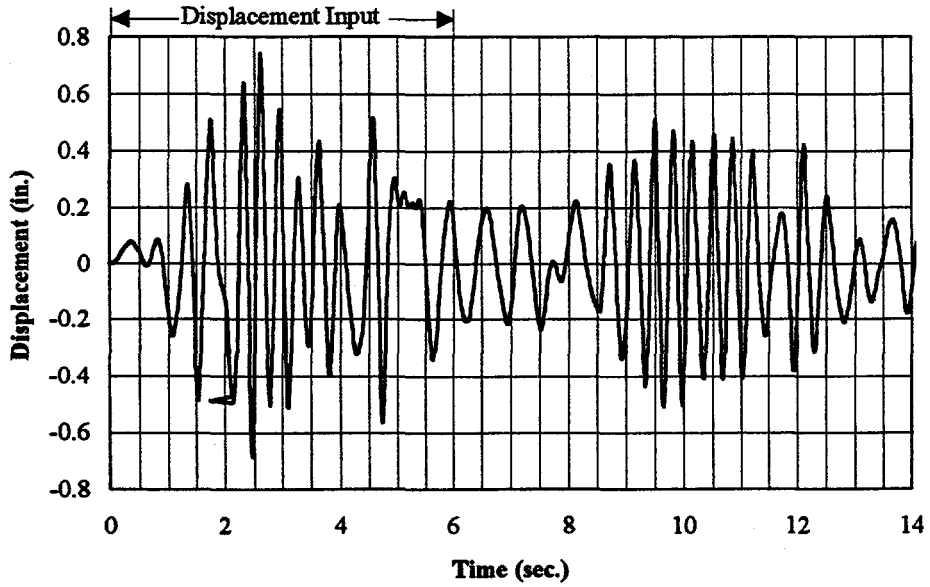

Figure 6 ***Time history of estimated attachment displacement used for seismic testing of multiple-anchor connections***

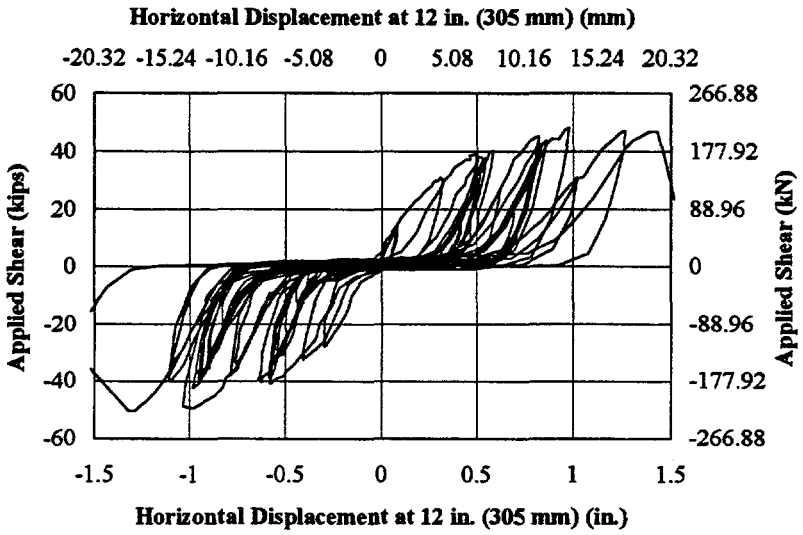

Figure 7 *Typical load-displacement curves of connection under seismic loading*

Based on the results of those tests, the following conclusions were drawn:

1) Multiple-anchor connections in uncracked or cracked concrete, with or without edge effect, and with or without hairpins, loaded dynamically under reversed cyclic loading histories representative of seismic response, behaved consistently with the results of previous single- and double-anchor tests of this study. Previous observations regarding the load-displacement behavior, and failure mechanisms of single and double anchors, were applicable in predicting the behavior of complex, multiple-anchor connections under simulated seismic loading. The implications of this are clear. Multiple-anchor connections designed for ductile behavior in uncracked concrete under static loading, will probably still behave in a ductile manner in cracked concrete under dynamic loading.

2) Anchors that show relatively good performance when tested individually in cracked concrete (CIP headed anchors, UC1, and 20-mm diameter Sleeve) would also be expected to show relatively good performance when used in multiple-anchor connections subjected to seismic loading. Anchors that show relatively poor performance when tested individually in cracked concrete (Grouted Anchor, EAII, and 10-mm diameter Sleeve) would also be expected to show relatively poor performance when used in multiple-anchor connections subjected to seismic loading.

3) Cyclic load-displacement behavior of multiple-anchor connections is accurately bounded by the corresponding static load-displacement envelope, and also by the static load-displacement envelope predicted by the BDA5 program. In other words, dynamic cycling does not significantly influence the fundamental load-displacement behavior of a multiple-anchor connections.

4) Under dynamic reversed cyclic loading in both uncracked and cracked concrete, the load-displacement curves of multiple-anchor connections with the UC1 Anchor basically follow the static ones in uncracked concrete over most displacements, differing only near the ultimate load. Dynamic reversed loading did not significantly affect the maximum dynamic capacity. In uncracked concrete, the connection had larger displacements under reversed dynamic than under static loading. Under dynamic reversed loading, connections in cracked concrete had slightly larger displacements than those in uncracked concrete.

5) Under dynamic reversed cyclic loading, multiple-anchor connections with Expansion Anchor II had very large displacements. In both uncracked and cracked concrete, the connections loaded at 12-inch (305-mm) eccentricity failed by steel fracture. The test in cracked concrete had a larger displacement and smaller capacity than that in uncracked concrete. The connection loaded at an 18-inch (457-mm) eccentricity experienced pullout failure.

6) Little effect of the baseplate flexibility was observed on the load-displacement behavior of multiple-anchor connections, even though the moment applied to the baseplate at the edge of the attached member (by the compression reaction of the concrete) exceeds the tested yield moment of the baseplate by about 25%.

7) The concrete edge breakout capacity remained almost constant for near-edge, multiple-anchor connections of UC1 Anchors with both eccentricities, under static loading without or with hairpins, and under dynamic reversed cyclic loading with hairpins. Due to gaps between the anchor shanks and the hairpins, the effect of hairpins on the concrete edge breakout capacity for undercut anchors is not as great as for cast-in-place anchors. Because of the smaller transient loading rate, the concrete edge breakout capacity did not increase as much under dynamic reversed loading as had been previously observed under dynamic ramp loading to failure.

8) As with the double-anchor shear connections, hairpins increased the ultimate capacity toward the edge, of near-edge, multiple-anchor connections. This capacity can be accurately predicted by assuming a flexural mechanism in the near-edge anchors. Hairpins also reduced the concrete edge breakout volume, and increased the lateral blowout capacity of near-edge anchors, and thereby increased the maximum capacity, for loading away from the edge, of those same connections.

9) As with the double-anchor shear connections, the forces induced by the baseplate on the edge breakout volume of near-edge, multiple-anchor connections significantly reduced the concrete edge breakout capacity.

Description of Finite Element Analysis

Behavior of single anchors in concrete was compared with the results of a nonlinear finite element analysis. The analytical approach used smeared cracks, with a fixed crack orientation, and is described further in Zhang (1997). Typical results are shown in Figure 8.

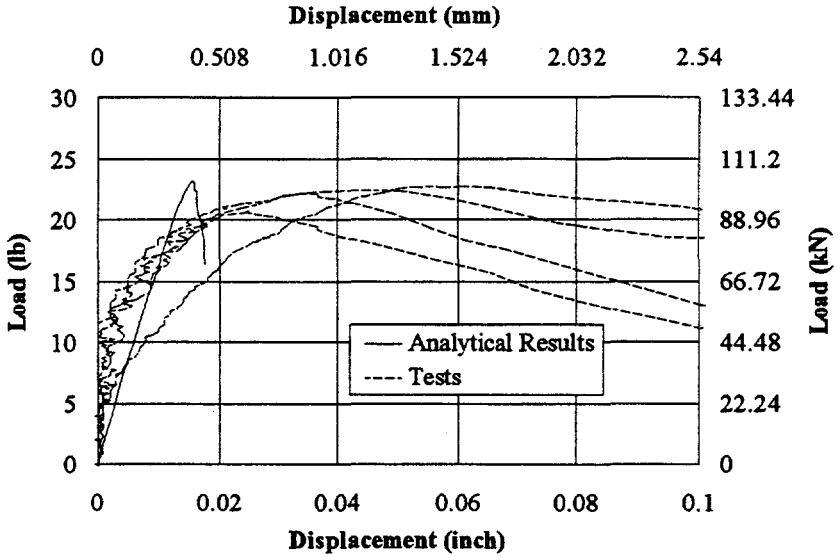

Figure 8 *Comparison of finite-element predictions with observed test results*

Conclusions Regarding Finite Element Analysis

1) The fixed smeared cracking approach used in Zhang (1997) can accurately predict the tensile capacity of anchors. The predicted crack path was close to the measured cone shapes. However, displacement behavior was not successfully modeled, due to the fact that concrete plastic deformation at the anchor head was ignored.

2) The maximum shear stress that can be transferred across a concrete crack has no significant effect on the load-displacement behavior of anchors in concrete, nor on the predicted crack path. Maximum predicted anchor breakout capacity increases with increasing cracked concrete shear capacity. However, the post-peak load-displacement behavior is affected by that maximum shear stress.

3) Change in the finite element mesh had no significant effect on the calculated capacity, nor on the predicted crack path. The equivalent crack width concept is therefore objective for this problem.

4) Computational time was dramatically reduced and computational stability dramatically increased, by permitting cracking only in element on or near the projected crack path, and

using a reduced number of integration points for those elements. However, this finite element approach would still be too complicated and time-consuming for use on multiple-anchor connections.

Description of BDA5 Program

The BDA5 program (Li 1994) is a macro-analysis package that uses experimentally obtained load-deformation behavior of individual anchors to predict the load displacement behavior of multiple-anchor connections. Results from the program were compared with the results of static tests, and also with the results of seismic tests. A typical comparison is shown in Figure 9.

Conclusions Regarding BDA5 Program

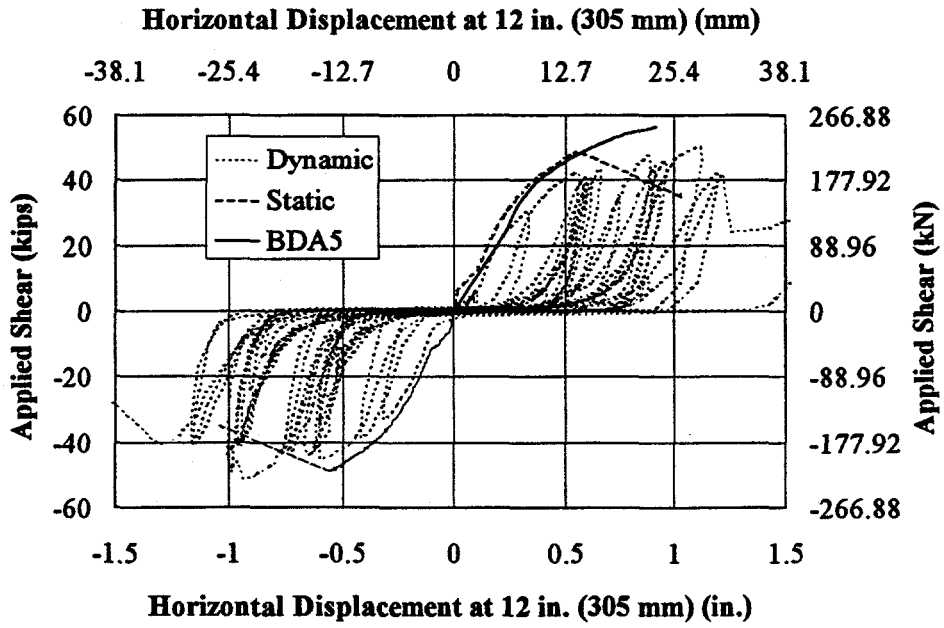

Figure 9 *Comparison of calculated results from BDA5 program with static and seismic test results of multiple-anchor connection with UC1 anchors, loaded in eccentric shear at 12 inches (305 mm)*

The BDA5 program is fast, and its predictions correlate reasonably well with experimental results. However, it relies heavily on the input data file of the load-displacement behavior of single anchors. To obtain this input file, many tests must be conducted. Since load-displacement behavior varies with anchor configuration (diameter and embedment), an enormous amount of work would be required to obtain a complete set of input files for different anchor configurations.

CURRENT STATUS OF RESOURCE DOCUMENT

At the present time, work on the resource document is addressing the following steps:

- Review the existing data base of tensile anchor test results. Correct internal inconsistencies in that data base. Check all formulas in the data base, and insert formulas where they are now missing. Include data from The University of Texas and elsewhere on behavior of anchors in cracked concrete, and behavior under dynamic loading.

- Use the augmented tensile data base to assess the consistency and reliability of different proposed design rules for tensile anchors in concrete. Evaluate probabilities of failure associated with different proposed design rules.

- Prepare a data base of shear anchor test results. Include data from The University of Texas and elsewhere on behavior of anchors in cracked concrete, and behavior under dynamic loading.

- Use the shear data base to assess the consistency and reliability of different proposed design rules for shear anchors in concrete. Evaluate probabilities of failure associated with different proposed design rules.

- Using the shear and tensile results, plus the behavioral conclusions from the previous University of Texas study, propose design procedures for single and multiple-anchor attachments to concrete.

The resource document is scheduled for completion in midyear 1998, and will be used to supplement the basis for future NRC licensing activities regarding anchorage to concrete.

SUMMARY

This paper has presented a summary of current research on anchorage to concrete in nuclear facilities in the US, and has reviewed current USNRC efforts to update the technical basis for design of such anchorage.

ACKNOWLEDGMENT AND DISCLAIMER

This paper presents results of a research program supported by U.S. Nuclear Regulatory Commission (NRC) under Contract No. NRC-03-92-05 ("Anchor Bolt Behavior and Strength during Earthquakes") and NRC Contract No. NRC-04-96-059 ("Revision to Anchorage Criteria"). The technical contact is Herman L. Graves III. The USNRC has neither approved nor disapproved the contents of this paper. The views and conclusions contained in this paper are those of the authors, and should not be interpreted as necessarily representing the official polices or recommendations of the USNRC.

REFERENCES

Fuchs 1995: Fuchs, W., Eligehausen and R. and Breen, J. E., "Concrete Capacity Design (CCD) Approach for Fastening to Concrete", *ACI Structural Journal*, Vol. 92, No. 1, January-February, 1995, pp. 73-94.

Graves, H. L., Klingner, R. E., Zhang, Y. and Hallowell, J. M., "Dynamic Behavior of Anchors in Cracked and Uncracked Concrete," *Proceedings*, 14th International Conference on Structural Mechanics in Reactor Technology (SMIRT), Lyon, France, August 17-22, 1997.

Hallowell 1996: Hallowell, Jennifer M., "Tensile and Shear Behavior of Anchors in Uncracked and Cracked Concrete under Static and Dynamic Loading," MS Thesis, Department of Civil Engineering, The University of Texas at Austin, December 1996.

Li 1994: Li, L., BDA: *Programm zur Berechnung des Trag- und Verformungsverhaltens von Gruppenbefestigungen unter kombinierter Schragzug- und Momentenbeanspruchung (Programmbeschreibung)*, The University of Stuttgart, June, 1994.

Lotze 1997: Lotze, D. and Klingner, R. E., Behavior of Multiple-Anchor Attachments to Concrete from the Perspective of Plastic Theory," *Report PMFSEL 96-4*, Ferguson Structural Engineering Laboratory, The University of Texas at Austin, March 1997.

Rodriguez 1994a: Rodriguez, M., Zhang, Y., Lotze, D., Graves III, H. L. and Klingner, R. E., "Dynamic Behavior of Anchors in Cracked and Uncracked Concrete: A Progress Report," *Proceedings*, 22nd Water Reactor Safety Information Meeting, Bethesda, Maryland, October 24-26, 1994.

Rodriguez 1994b: Rodriguez, M., Zhang, Y., Lotze, D., Graves III, H. L. and Klingner, R. E., "Dynamic Behavior of Anchors in Cracked and Uncracked Concrete: A Progress Report," *Proceedings*, 5th Symposium on Current Issues Related to Nuclear Power Plant Structures, Equipment and Piping, Lake Buena Vista, Florida, December 14-16, 1994.

Rodriguez 1995a: Rodriguez, Milton, "Behavior of Anchors in Uncracked Concrete under Static and Dynamic Tensile Loading," MS Thesis, Department of Civil Engineering, The University of Texas at Austin, August 1995.

Rodriguez 1995b: Rodriguez, M., Zhang, Y., Lotze, D., Graves III, H. L. and Klingner, R. E., "Dynamic Behavior of Anchors in Cracked and Uncracked Concrete: A Progress Report," *Nuclear Engineering and Design*, Stuttgart, Germany, November 1995. (approved for publication)

Zhang 1997: Zhang, Yong-gang, "Dynamic Behavior of Multiple-Anchor Connections in Cracked Concrete," Ph.D. Dissertation, Department of Civil Engineering, The University of Texas at Austin, August 1997.

APPENDIX A

SUMMARY OF THE CC METHOD FOR PREDICTING THE BREAKOUT CAPACITY OF TENSILE ANCHORS

According to the CC Method (Fuchs 1995), the concrete breakout capacity of a single tensile anchor far from edges is:

$$T_o = k\sqrt{f_c'}h_{ef}^{1.5} \qquad \text{(A-1)}$$

where: T_o = tension cone breakout capacity;

k = constant; for anchors in uncracked concrete the mean values originally proposed based on previous tests are: 35 for expansion and undercut anchors, 40 for headed anchors, in US units; or 15.5 for expansion and undercut anchors, 17 for headed anchors, in SI units;

f_c = specified concrete compressive strength (6 × 12 cylinder) (inch in US units, MPa in SI units.);

h_{ef} = effective embedment depth (inch in US unit, MPa in SI unit).

In design codes, different values for k, based on a 5% fractile, may be used.

In the CC Method, the breakout body is idealized as a pyramid with an inclination of about 35 degrees between the failure surface and the concrete member surface (Figure 10). As a result, the base of the pyramid measures $3h_{ef}$ by $3h_{ef}$.

If the failure pyramid is affected by edges or by other concrete pyramids, the concrete capacity is calculated according the following equation:

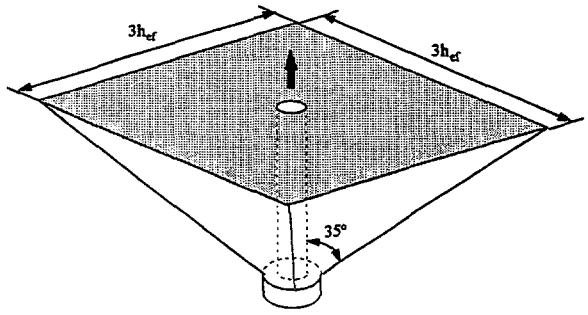

Figure 10 ***Tensile concrete breakout cone for single anchor as idealized in CC Method (Fuchs 1995)***

$$T_n = \frac{A_N}{A_{No}}\psi_2 T_{no} \qquad \text{(A-2)}$$

where: A_{No} = projected area of a single anchor at the concrete surface without edge influences or adjacent-anchor effects, idealizing the failure cone as a pyramid with a base length of $s_{cr} = 3h_{ef}$ ($A_{no} = 9\ h_{ef}^2$);

A_N = actual projected area at the concrete surface;

ψ_2 = tuning factor to consider disturbance of the radially symmetric stress distribution caused by an edge,

= 1, if $c_1 \geq 1.5h_{ef}$;

= $0.7 + 0.3\frac{c_1}{1.5h_{ef}}$, if $c_1 \leq 1.5h_{ef}$;

where:

c_1 = edge distance to the nearest edge.

APPENDIX B

SUMMARY OF THE CC METHOD FOR PREDICTING THE BREAKOUT CAPACITY OF SHEAR ANCHORS

According to Fuchs (1995), the shear breakout capacity of a single anchor, loaded toward a free edge, is given by:

$$V_{no} = 13\left(d_o f_c'\right)^{0.5}\left(l/d_o\right)^{0.2} c_1^{1.5} \qquad lb \qquad \text{(B-1)}$$

where: d_o = the outside diameter of the anchor (inch in US units, mm in SI units);

$$V_{no} = \left(d_o f_c'\right)^{0.5}\left(l/d_o\right)^{0.2} c_1^{1.5} \qquad N \qquad \text{(B-2)}$$

l = activated load-bearing length of fasteners, $\leq 8d_o$;
= h_{ef}, for fasteners with a constant overall stiffness;
= $2d_o$ for torque-controlled expansion anchors with spacing sleeve separated from the expansion sleeve;

f_c' = compressive strength of concrete; and

c_1 = edge distance in the direction of load.

This formula is valid for a member with a thickness of at least 1.4 h_{ef}. For anchors in a thin structural member or affected by the width of the member, by adjacent anchors, or both, a reduction must be made based on the idealized model of a half-pyramid measuring $1.5c_1$ by $3c_1$., as shown in Figures 11 and 12.

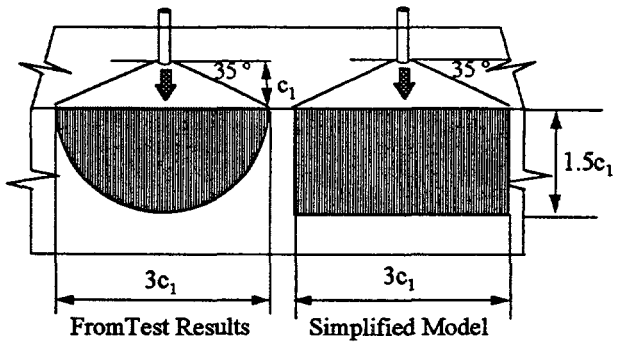

Figure 11 ***Idealized design model for single shear anchor, CC Method***

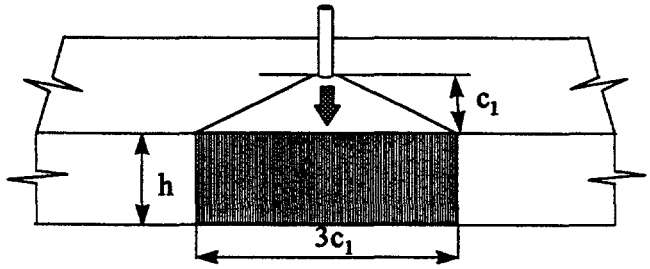

$A_V = 3.0c_1 h$
if $h \leq 1.5c_1$

Figure 12 ***Projected areas for shear anchors in thin members according to CC Method***

Taking into account the influence of adjacent anchors or thin members, the shear capacity is:

$$V_n = \frac{A_v}{A_{vo}} \psi_5 V_{no} \qquad \text{(B-3)}$$

where: A_v = actual projected area at the side of concrete member;

A_{vo} = projected area of one fastener in thick member without influence of spacing and member width, idealizing the shape of the projected fracture cone as a half-pyramid with side length of $1.5c_1$ and $3c_1$;

ψ_5 = reduction factor considering the disturbance of symmetric stress distribution caused by a corner;

= 1, if $c_2 \geq 1.5\ c_1$

= $0.7 + 0.3\frac{c_2}{1.5c_1}$, if $c_2 \leq 1.5\ c_1$;

where c_1 = edge distance in loading direction,

= max ($c_{2,max}/1.5$, h/1.5) for anchors in a thin and narrow member with $c_{2,max} < 1.5c_1$ and $h < 1.5c_1$;

where: h = thickness of concrete member;

c_2 = edge distance perpendicular to loading direction.